



**HAL**  
open science

# Biomimetic approach to decipher the mechanisms by which glycosaminoglycans regulate bone morphogenetic protein 2 (BMP2) signaling

Jean Le Pennec

► **To cite this version:**

Jean Le Pennec. Biomimetic approach to decipher the mechanisms by which glycosaminoglycans regulate bone morphogenetic protein 2 (BMP2) signaling. Structural Biology [q-bio.BM]. Université Grenoble Alpes [2020-..], 2023. English. NNT : 2023GRALV067 . tel-04762932

**HAL Id: tel-04762932**

**<https://theses.hal.science/tel-04762932v1>**

Submitted on 1 Nov 2024

**HAL** is a multi-disciplinary open access archive for the deposit and dissemination of scientific research documents, whether they are published or not. The documents may come from teaching and research institutions in France or abroad, or from public or private research centers.

L'archive ouverte pluridisciplinaire **HAL**, est destinée au dépôt et à la diffusion de documents scientifiques de niveau recherche, publiés ou non, émanant des établissements d'enseignement et de recherche français ou étrangers, des laboratoires publics ou privés.

THÈSE

Pour obtenir le grade de

## DOCTEUR DE L'UNIVERSITÉ GRENOBLE ALPES

École doctorale : CSV- Chimie et Sciences du Vivant

Spécialité : Biologie Structurale et Nanobiologie

Unité de recherche : Biologie et Biotechnologie pour la Santé

### Approche biomimétique pour déchiffrer les mécanismes de régulation de l'activité de la protéine-2 morphogénétique osseuse (BMP2) par les glycosaminoglycanes

### Biomimetic approach to decipher the mechanisms by which glycosaminoglycans regulate bone morphogenetic protein 2 (BMP2) signaling

Présentée par :

**Jean LE PENNEC**

#### Direction de thèse :

**Romain VIVES**

DIRECTEUR DE RECHERCHE, CNRS Alpes

**Elisa MIGLIORINI**

CHARGÉE DE RECHERCHE, CNRS Alpes

Directeur de thèse

Co-encadrante de thèse

#### Rapporteurs :

**Isabelle COMPAGNON**

MAITRESSE DE CONFÉRENCES HDR, Université de Lyon 1 - Claude Bernard

**Toril HOLIEN**

FULL PROFESSOR, Norges Teknisk - Naturvitenskapelige Universitet

#### Thèse soutenue publiquement le **20 octobre 2023**, devant le jury composé de :

**Romain VIVES**

DIRECTEUR DE RECHERCHE, CNRS délégation Alpes

Directeur de thèse

**Isabelle COMPAGNON**

MAITRESSE DE CONFÉRENCES HDR, Université de Lyon 1 - Claude Bernard

Rapporteuse

**Toril HOLIEN**

FULL PROFESSOR, Norges Teknisk - Naturvitenskapelige Universitet

Rapporteuse

**Douglas DYER**

DOCTEUR EN SCIENCES, University of Manchester

Examineur

**Franz BRUCKERT**

PROFESSEUR DES UNIVERSITÉS, Grenoble INP

Président

#### Invités :

**Elisa MIGLIORINI**

CHARGÉE DE RECHERCHE, CNRS Alpes





**Biomimetic approach to decipher the  
mechanisms by which glycosaminoglycans  
regulate bone morphogenetic protein 2  
(BMP2) signaling**



## Acknowledgements

This almost 4-year's PhD journey has been roller coaster of emotions with many hopes, failures, discoveries, and above all, much learning. While a PhD thesis is rather a personal experience, I had the incredible chance to be surrounded and supported along the way by many people who contributed one way or another to my achievements in this thesis, and whom I would like to thank.

First of all, I need to thank Elisa Migliorini and Romain Vivès, my two admirable mentors, for their continuous support. With your distinct scientific expertise, you two constituted a formidable supervision duo and complemented well each other for guiding me scientifically and managing to motivate me in difficult times. You are both remarkably kind and generous persons and I really appreciated that.

Elisa, many thanks for giving me the opportunity to work with you on this very interesting project. Despite my limited background in biology, you hired me for an M2 internship on a related but different topic, and then you gave me your trust for working on this new and challenging thesis project. Your mentorship and your dedication to teaching me new techniques were valuable. You provided me precious feedback to enhance both my oral communication and writing abilities. Even during your maternity leaves, you have always managed to maintain the link and keep some discussions and I want to thank you for that.

Romain, I did not know you before starting the PhD and it has really been a great surprise meeting you and working with you. You put a lot of commitment in this supervision, and at the same time you often brought an exterior point of view that gave stimulating and interesting ideas. Thank you for challenging me in improving my English writing style (that you liked to call “bof”) during the redaction of the review article, since I believe it has been very helpful later for the redaction of the thesis. Also, I would like to address many thanks to the other facet of yourself, the scuba-diving instructor, for this fantastic scuba-diving baptism in perfect conditions at the Lac du Bourget. The conference at the GRC with you was also a great moment. Your bollywood dance and our karaoke-like sessions will be remembered for long.

I am deeply appreciative of Dr. Douglas Dyer and Prof. Franz Bruckert for being part of my thesis committee. I thank in particular Prof. Toril Holien and Dr. Isabelle Compagnon for their contributions as thesis reviewers, providing precious feedback for improving my manuscript.

My gratitude extends to Marianne Weidenhaupt, Jérôme Dejeu, David Bonaffé, and Corinne Albigès-Rizo, my “CSI” supervising committee, for their stimulating scientific perspectives.

As I was doing my PhD thesis in cotutelle, I had the chance to be integrated in two proficient labs and two fantastic teams. I am thankful to the whole Biosanté lab at CEA for creating this friendly work environment. In particular, I would like to thank Cathy, Nicolas Lemaitre, Nicolas Ricard, Tala, Beatrice, Camille, Morgane, Valentin, Odile and Claude, Léa, Aude, Emma, Agnès, Claire, Louise, Laurent, Irinka, Constance, and Justine for their kindness, their help in the lab, and the nice chats we had. I feel very lucky having shared my office with wonderful persons. Lisa, it was great to be able to discuss with you of anything. Mohammad, I

am glad we were in the same boat for the thesis redaction. We supported each other in this difficult period, both for the writing and the struggle with French administration. Thanks also for our interesting discussions and your help in the lab. Laura (Fancello), we did not share the office for long but it was very enjoyable, you are a nice and supportive person.

I am deeply grateful to the BRM team, with whom I shared countless experiences, from lab outings and picnics to snow trips and bar sessions. Catherine, your human leadership, scientific expertise, and enthusiasm for science were inspiring. Thanks for your supervision during Elisa's maternity leaves.

Paul, you are the technical pillar of the team in the lab! Your technical expertise, your advices on my non-spe issue, and constant support in the lab were valuable. We had many nice times, I really enjoyed sharing some trail and bike sessions with you and I hope it will continue.

I have of course to thank Julius, my predecessor in doing a PhD with Elisa. You have set a great example for me with your motivation and dynamism. Thank you for teaching me many things at the lab, for your patience, our interesting discussions, and your great advices in presenting skills. You have set up many things that were useful then for my PhD project and I am grateful for that.

Irene, Elisa L, and Nathan, Adria and Valia, each of you helped me, supported me and made meaningful contributions. Thanks also for the nice talks and great times we had. Of course, I have thoughts for Joao, who is no longer with us but was a precious colleague.

I want to thank Bertin, Paola, and Amaury, whom I supervised during my thesis, for their involvement and commitment, and who contributed to several results my PhD project. Thanks also to the many other interns who joined the team and contributed to the nice atmosphere: Marie, Lisa, Aida-Naël, Bojana, Vincent, Cyril, Valentine, Maëlle, and Perrine.

Now, I need of course to acknowledge my second fantastic team, the SAGAG team at IBS. I consider myself very lucky having joined this dynamic team with an incredible cohesion. Although I was only part time present at IBS, I felt very comfortable and made strong bonds with each one of you. For all your support and our conviviality times, I address many thanks to Rabia, Rebecca-Joe, Rebekka, Francisco, Marie, Espérance, and Yara. In particular, I am very grateful to Evelyne, Mélanie, Catarina, and Sylvain for teaching me specific techniques and giving me precious advices.

Before the BRM team moved into the CEA, my PhD thesis actually started at the LMGP laboratory where I also did my M2 internship. I have great memories over there and I would like to acknowledge Dr. Carmen Jimenez at the direction for welcoming me at the lab at the beginning of my thesis. Thanks also to Prof. Franz Bruckert and Dr. Marianne Weidenhaupt for the scientific discussions and for letting me access to the DLS equipment after I moved at the CEA.

I have also to acknowledge the administrative support with Isabelle Zanotti, and Marie-Pierre Mendez at the CEA, and Michèle San Martin, Annie Ducher, and Josiane Viboud at LMGP.

My PhD project was initiated by a collaboration with the group of Andrea Vortkamp in Essen (UDE, Germany). I would like to thank her along with Velina Bachvarova, Ann-Christine Severmann, Fatima Asar, and Terrilyn Teichwart, for our stimulating discussions. I thank also

Jean-Baptiste Reiser and the ISBG platform for the use of the BLI equipment at IBS, and the PTA facility for the use of the evaporator equipment. I need to thank the various organizations that provided financial support to make this work possible: the ANR GlyCON [ANR-19-CE13-0031-01 PRCI], the “Investissements d’avenir” program Glyco@Alps, [ANR-15-IDEX-02], the CNRS GDR 2088 "BIOMIM”, the ANR-17-EURE-0003 and GRAL.

I had also much support from my friends and family outside the lab, whom I would like to thank. For this, I will switch to French.

De très bonnes amitiés ont débuté au LMGP avec quelques pauses (beaucoup !), des gâteaux du vendredi et des sessions billard, puis avec des bartarots, etc... Chachou, quelle chance j’ai eu que l’on fasse nos thèses quasiment en même temps ! Un grand merci de m’avoir écouté et soutenu dans les moments de stress, d’agacement, et autres... Guigui, le deuxième soleil du LMGP, merci pour ta grande empathie, merci pour tes précieux conseils et pour tout ton soutien. Étienne, c’est toujours super de faire des sorties avec toi ! Plein de courage pour la fin de ta thèse ! Laura, tu es passée d’une collègue de bureau à une bonne amie. Tu es une personne formidable avec une grande gentillesse.

Merci au Drômois Crew et en particulier Benjamin (et Marie), Pierre, Théo, Manon et Étienne, Virgil, et Alban pour tous ces bons moments depuis de très nombreuses années maintenant ! Merci aux amis du CPP Valence que je vois régulièrement à Grenoble: Laurie, Francesco, Pierrick, Clara. Merci en particulier à mes anciens colocs Gaël et Tim, pour votre soutien et nos longues discussions à la sortie du H2 ! Merci aux amis de Phelma : Thomas, Charles, Sandrine, Lucas et Xandre.

Merci à Camille, Totof, Fanf, Stéph’ et Nicole, pour tous ces bons moments et ces bons repas, et pour votre soutien.

Évidemment, un grand merci à ma famille d’être toujours là pour moi. Merci à mes grands-parents Guytou, Pierrot et Momo. Vous êtes une source d’inspiration au quotidien. Merci à aussi à Manou qui m’a toujours soutenu de manière inconditionnelle, et qui avait noté le titre de ma thèse pour se rappeler du nom un peu barbare de ces glycosaminoglycanes. Merci à Lucie ma sœur adorée ! Et bien sûr un grand merci à mes parents, pour votre soutien, et surtout pour l’éducation que vous nous avez prodiguée, ainsi que les opportunités que celle-ci nous offre chaque jour.

Lauriane, tu as été à mes côtés du début à la fin de ma thèse. Je ne saurais imaginer un meilleur soutien que celui que tu m’as offert, et je n’aurai sûrement pas aussi bien réussi sans toi. Merci infiniment d’avoir illuminé chacune de mes journées, et de m’avoir soutenu et supporté dans les périodes difficiles.

## List of abbreviations

<b>2OST:</b> 2-O sulfotransferase	<b>Hh:</b> Hedgehog
<b>3OSTs:</b> 3-O-sulfotransferases	<b>HME:</b> Hereditary Multiple Extostosis
<b>6OSTs:</b> 6-O-sulfotransferases	<b>HS:</b> Heparan sulfate
<b>aBMP2:</b> adsorbed BMP2	<b>HSPG:</b> Heparan sulfate proteoglycan
<b>ALK:</b> Activin receptor-like kinase	<b>HSulf1/2:</b> Human Sulf1 and Sulf2
<b>ALP:</b> Alkaline phosphatase	<b>IdoA:</b> L-iduronic acid
<b>AT III:</b> Antithrombin III	<b>IPR:</b> Ion pairing reagent
<b>bHS:</b> Biotinylated HS	<b>KI:</b> Knock-in
<b>BLI:</b> Biolayer Interferometry	<b>KO:</b> Knock-out
<b>BMPR:</b> BMP receptors	<b>k<sub>off</sub>:</b> Dissociation rate
<b>BMPs:</b> Bone Morphogenetic proteins	<b>k<sub>on</sub>:</b> Association rate
<b>botv:</b> <i>brother of tout-velu</i>	<b>KS:</b> Keratan Sulfate
<b>C4ST1,2,3:</b> Chondroitin 4-O-sulfotransferases	<b>Lbl:</b> Layer-by-layer
<b>C6ST1,2:</b> Chondroitin 6-O-sulfotransferases	<b>MMPs:</b> Matrix metalloproteinases
<b>ChGn-1/2:</b> Chondroitin GalNAcT-1/-2	<b>MSCs:</b> mesenchymal stem cells
<b>ChPF:</b> Chondroitin polymerizing factor	<b>NDST:</b> N-deacetylase/N-sulfotransferase
<b>ChSy-1/2/3:</b> Chondroitin synthase-1/-2/-3	<b>PAGE:</b> Polyacrylamide Gel Electrophoresis
<b>Co-SMAD:</b> Common mediator SMAD4	<b>PAPS:</b> 3'-phosphoadenosine 5'-phosphosulfate
<b>cRGD:</b> Cyclic RGD	<b>PG:</b> Proteoglycan
<b>CS:</b> Chondroitin Sulfate	<b>PLLgPEG:</b> poly(L-lysine)-graft-poly(ethylene glycol)
<b>csPG:</b> Cell surface PG	<b>pMad:</b> phosphorylated Mad
<b>D4ST1:</b> Dermatan 4-O-sulfotransferase 1	<b>QCM-D:</b> quartz crystal microbalance with dissipation monitoring
<b>dly:</b> <i>dally-like</i>	<b>RPIP-HPLC:</b> Reverse-phase ion-pair high-performance liquid chromatography
<b>Dpp:</b> Decapentaplegic	<b>SAM:</b> Self-assembled monolayer
<b>DS:</b> Dermatan Sulfate	<b>SAv:</b> Streptavidin
<b>DS-epi:</b> DS-epimerases	<b>sBMP2:</b> soluble BMP2
<b>ER:</b> Endoplasmic reticulum	<b>sfl:</b> <i>sulfateless</i>
<b>EXT1/2:</b> Exostosin-1/-2	<b>SHh:</b> Sonic Hedgehog
<b>FDA:</b> Food and drug administration	<b>SLRPs:</b> Small eucine-rich proteoglycans
<b>FGF:</b> Fibroblast growth factor	<b>SMAD:</b> Mothers against decapentaplegic
<b>GAGs:</b> Glycosaminoglycans	<b>sotv:</b> <i>sister of tout-velu</i>
<b>Gal:</b> Galactose	<b>SPR:</b> surface plasmon resonance
<b>GalNAc:</b> N-Acetyl galactosamine	<b>TGF-<math>\beta</math>:</b> transforming growth factor beta
<b>GalNAc4S-6ST:</b> GalNAc 4-sulfate 6-O-sulfotransferase	<b>ttv:</b> <i>tout-velu</i>
<b>GDFs:</b> Growth differentiation factors	<b>UDP:</b> uridine diphosphate
<b>GlcA:</b> D-glucuronic acid	<b>UST:</b> uronyl 2-O-sulfotransferase
<b>GlcNAc:</b> N-Acetyl glucosamine	<b>VEGF:</b> Vascular endothelial growth factor
<b>GlcNS:</b> N-sulfated glucosamine	<b>Xyl:</b> Xylose
<b>GPI:</b> Glycosyl-phosphatidyl-inositol	<b>XylT1 or XylT2:</b> Xylosyltransferase
<b>HA:</b> Hyaluronic Acid	
<b>Hep:</b> Heparin	
<b>HexA:</b> Hexuronic Acid	

## **Abstract (English)**

Glycosaminoglycans (GAGs) are involved in various biological functions, regulating tissue homeostasis and cellular differentiation in the human body. These long polysaccharide chains interact with a wide range of proteins that modulate the cellular behavior, including growth factors, chemokines, cytokines and morphogens. The interactions of GAGs with proteins mainly rely on negatively charged sulfate groups distributed along the polysaccharide chains, which bind to positively charged regions of proteins. Through these sulfation-dependent interactions, GAGs regulate the bioactivity and spatial distribution of proteins, thereby modulating their induced cellular responses. Among GAGs, heparan sulfate (HS) was reported to have a crucial role in regulating the bioactivity of bone morphogenetic proteins (BMPs), and in particular BMP2. As suggested by their name, BMPs are involved in the regulation of bone development. Interestingly, the deficiency of HS polymerization enzymes has been associated to an elevated BMP signaling and to a human disorder characterized by the formation of osteochondroma. In contrast to HS, the role of other GAGs in the regulation of BMP signaling has not been determined.

In this PhD thesis, we aimed at deciphering the role of the different GAGs in BMP signaling, including HS, chondroitin sulfate (CS), dermatan sulfate (DS), and hyaluronic acid (HA). To this end, we conducted molecular interaction studies and cellular studies, aiming to provide a comprehensive understanding of the interactions between GAGs and BMP2, and of their role in modulating the signaling. The binding affinities and kinetic properties of the GAG-BMP2 molecular interactions were investigated with biolayer interferometry (BLI). Our findings revealed a much stronger affinity of BMP2 for HS compared to the other GAGs, and differences were observed between CS types. Alongside, we investigated the effect of the interactions between GAGs and BMP2 on the cellular response using previously developed biomaterials, called biomimetic streptavidin platforms. Methodological developments have been achieved to allow a platform construction on glass substrates and the automation of the process permitting their functionalization in 96-well plates. Using these platforms, we explored the role of distinct GAGs on BMP signaling, but also of their localization (cell surface or extracellular), an aspect which has not been fully understood. Our results highlighted a distinct role of cell surface and extracellular GAGs, and distinct roles of HS and CS. Specifically, cell surface HS appeared to inhibit BMP2 signaling while cell surface CS promoted it. On the other hand, extracellular HS bound BMP2 and allowed its signaling, while CS had no observable effect.

The sulfation patterns of GAGs is key factor regulating the binding and bioactivity of proteins. In the literature, the extensively studied interactions of HS with antithrombin III and FGF1 are striking examples of how specific sulfation motifs and sequences are crucial for the bioactivity of proteins. We aimed to explore whether in a similar way the interaction of BMP2 with HS is dependent to specific sulfation motifs. To address this, we prepared a library of HS-oligosaccharides and we investigated the molecular interactions of the synthesized compounds with BMP2 using BLI technique. Our findings revealed a HS trisulfated disaccharide sequence (IdoA(2S)-GlcNS(6S)) that appeared to mediate high-affinity binding with BMP2. However, this sequence was not unique in mediating high-affinity binding and our data suggest that BMP2 exhibits some structural plasticity that allows its binding to various HS sulfation patterns. The multiple findings of this thesis constitute important bricks in the understanding of the complex interplay between GAGs and growth factors.

## Abstract (French)

Les glycosaminoglycanes (GAG) sont impliqués dans diverses fonctions biologiques, régulant l'homéostasie des tissus et la différenciation cellulaire dans le corps humain. Ces chaînes polysaccharidiques interagissent avec de nombreuses protéines qui modulent le comportement cellulaire, telles que les facteurs de croissance, les chimiokines, les cytokines, et les morphogènes. Les interactions GAGs-protéines reposent principalement sur des groupes sulfates chargés négativement, répartis le long de la chaîne polysaccharidique et se liant aux régions chargées positivement des protéines. Par ces interactions, les GAGs régulent la bioactivité et la localisation des protéines, modulant ainsi les réponses cellulaires induites par ces dernières. Parmi les GAGs, l'héparane sulfate (HS) joue un rôle crucial dans la régulation de la bioactivité des protéines morphogénétiques osseuses (BMPs), telles que BMP2, impliquées dans le développement osseux. La déficience d'enzymes de polymérisation de l'HS a notamment été reliée à une signalisation élevée des BMPs et à une maladie génétique caractérisée par la formation d'ostéochondromes. Cependant, le rôle d'autres GAGs dans la régulation de la signalisation des BMPs demeure énigmatique.

Cette thèse cherche à élucider le rôle de différents GAGs dans la signalisation de la BMP2, dont les chondroïtines sulfate (CS), les dermatanes sulfate (DS), les acides hyaluroniques (HA), et les HS. Pour cela, nous avons mené des études d'interactions moléculaires et des études cellulaires, pour comprendre de façon globale les interactions entre les GAG et la BMP2, et leur rôle dans la signalisation cellulaire. Les affinités de liaison et les propriétés cinétiques de ces interactions moléculaires ont été étudiées *via* une technique d'interférométrie optique (BLI). Les résultats ont révélé une affinité plus élevée de la BMP2 pour les HS que pour les autres GAGs, et des variations d'affinité entre différents types de CS. Parallèlement, l'effet des interactions entre les GAG et la BMP2 sur la réponse cellulaire a été exploré grâce à des biomatériaux appelés plateformes biomimétiques de streptavidine. Des développements méthodologiques ont permis la construction de ces plateformes sur des substrats en verre et l'automatisation de leur fonctionnalisation dans des plaques 96 puits. Utilisant ces plateformes, nous avons étudié le rôle de différents GAGs sur la signalisation BMP, mais aussi le rôle de leur localisation (surface cellulaire ou extracellulaire), un aspect peu exploré jusqu'à présent. Nos résultats ont mis en évidence un rôle distinct des GAGs de surface cellulaire et extracellulaires, ainsi que des rôles distincts des HS et des CS. Plus précisément, les HS de la surface cellulaire semblent inhiber la signalisation de la BMP2 alors que les CS de la surface

cellulaire la favorisent. D'autre part, les HS extracellulaires interagissent avec la BMP2 et permettent sa signalisation, tandis que les CS n'ont pas d'effet détectable.

Les motifs de sulfatation des GAG constituent un facteurs clé qui régule la liaison et la bioactivité de certaines protéines. Nous avons cherché à savoir si, de la même manière, l'interaction de la BMP2 avec les HS dépend de motifs de sulfatation spécifiques. Pour cela, nous avons préparé une librairie d'oligosaccharides d'HS et nous avons étudié les interactions moléculaires de ces composés avec la BMP2 par la technique BLI. Nos résultats ont révélé le rôle d'un motif disaccharidique trisulfaté d'HS (IdoA(2S)-GlcNS(6S)) qui semble promouvoir une affinité importante avec la BMP2. Cette séquence n'était cependant pas unique à promouvoir des interactions de haute affinité et nos données suggèrent que la BMP2 présente une certaine plasticité structurelle qui lui permet de se lier à divers motifs de sulfatation des HS. Les conclusions de cette thèse fournissent des éléments essentiels à la compréhension des interactions complexes entre les GAG et les facteurs de croissance.

# Table of contents

<b>Acknowledgements</b> .....	<b>5</b>
<b>List of abbreviations</b> .....	<b>8</b>
<b>Abstract (English)</b> .....	<b>9</b>
<b>Abstract (French)</b> .....	<b>11</b>
<b>Table of contents</b> .....	<b>13</b>
<b>Table of illustrations</b> .....	<b>15</b>
<b>Chapter I. Introduction</b> .....	<b>17</b>
I.A. Prolog .....	18
I.B. Proteoglycans and glycosaminoglycans .....	19
I.B.1. Classification of glycosaminoglycans (Review published in Advanced Materials, Annex) .....	19
I.B.2. Structure and classification of proteoglycans .....	23
I.B.3. Biosynthesis of proteoglycans .....	30
I.B.4. Proteoglycans post-synthesis regulation and turnover.....	36
I.B.5. Interactions with proteins and importance of sulfation.....	38
I.B.6. Strategies for synthesis of glycosaminoglycans (Review published in Advanced Materials, Annex) .....	42
I.C. Bone Morphogenetic proteins (BMPs) and osteogenesis.....	48
I.C.1. BMPs belong to the TGF- $\beta$ superfamily.....	48
I.C.2. The BMP family .....	49
I.C.3. The functional diversity of BMPs.....	50
I.C.4. Biosynthesis and structure of BMPs .....	52
I.C.5. BMP signaling and osteogenic differentiation.....	55
I.D. Interactions of glycosaminoglycans with BMPs .....	61
I.D.1. Structural basis of BMP-GAGs interactions .....	61
I.D.2. Physiological importance of the interactions.....	62
I.D.3. Influence of the GAG interactions on BMP signaling .....	64
I.D.4. Molecular interactions between GAGs and BMPs.....	69
I.E. Biomaterials to study GAGs .....	70
I.E.1. Use of biomaterials in medical applications (Review published in Advanced Materials, Annex) .....	70
I.E.2. Biomaterials to study GAGs (Review published in Advanced Materials, Annex).....	72
I.E.3. Biomimetic streptavidin platforms.....	76
<b>Chapter II. Objectives of the PhD thesis</b> .....	<b>83</b>
<b>Chapter III. Materials and methods</b> .....	<b>87</b>

<b>Chapter IV. Automated Fabrication of Streptavidin-Based Self-assembled Materials for High-Content Analysis of Cellular Response to Growth Factors .....</b>	<b>99</b>
IV.A. Article introduction .....	100
IV.B. Article .....	101
<b>Chapter V. Glycosaminoglycans exhibit distinct interactions and signaling with BMP2 according to their nature and localization .....</b>	<b>115</b>
V.A. Article introduction.....	116
V.B. Article.....	119
<b>Chapter VI. BMP2 binds non-specifically to PEG-passivated biomaterials and induces substantial signaling .....</b>	<b>173</b>
VI.A. Article introduction .....	174
VI.B. Article .....	176
<b>Chapter VII. Discussion and perspectives .....</b>	<b>195</b>
<b>Chapter VIII. Conclusion .....</b>	<b>207</b>
<b>References .....</b>	<b>211</b>
<b>Annex.....</b>	<b>224</b>

## Table of illustrations

Figure 1. Distribution of sulfates in different CS types. ....	23
Figure 2. Schematic representation of various PGs .....	24
Figure 3. Classification of PGs based on their location characteristics .....	25
Figure 4. Biosynthesis of the GAG tetrasaccharide linker .....	30
Figure 5. Elongation and maturation steps in the biosynthesis of HS/Hep chains.....	33
Figure 6. Maturation step in the biosynthesis of CS/DS chains.....	35
Figure 7. Mechanisms involved in the post-synthesis regulation and turnover of PGs .....	36
Figure 8. PG functions regulating the cellular response .....	38
Figure 9. Key HS sequences for specific interactions with proteins.....	39
Figure 10. Structures of GAG-binding sites present in proteins .....	41
Figure 11. Methods for preparing structurally defined GAG compounds .....	42
Figure 12. Classification of the TGF- $\beta$ superfamily .....	49
Figure 13. Functional diversity of BMPs and implications in diseases .....	51
Figure 14. Schematic representation of BMP biosynthesis and maturation .....	53
Figure 15. Structural representations of the BMP2 homodimer protein .....	55
Figure 16. BMP signaling via SMAD pathway and osteogenic differentiation.....	56
Figure 17. Specificities of interactions between BMP ligands and its receptors. ....	58
Figure 18. Structural domains in proteins of the SMAD family .....	60
Figure 19. BMP2 dimer exhibits a double-sided electropositive surface potential .....	62
Figure 20. Influence of GAG/PG defects on the shape of morphogen gradients.....	64
Figure 21. Models of PGs regulation of BMP signaling.....	68
Figure 22. Natural variation of GAG in animal tissues or cell cultures.....	74
Figure 23. Modulation of specific GAG parameters in biomaterials.....	76
Figure 24. Schematic representation of biomimetic SA <sub>v</sub> platforms .....	77
Figure 25. Sequential buildup of the SA <sub>v</sub> biomimetic platform on gold substrates .....	78
Figure 26. Strategies for building SAMs on optically transparent substrates .....	80
Figure 27. Automation of Lbl functionalization by a liquid-handling robot .....	81
Figure 28. Preparation of gold-sputtered surfaces .....	88
Figure 29. Chromatography methods for HS-oligosaccharide separation. ....	90
Figure 30. Scheme of molecular interactions within the RPIP-HPLC.....	91
Figure 31. Experimental setup of the RPIP-HPLC system .....	92
Figure 32. Reaction of 2-cyanoacetamide with glucose .....	92

Figure 33. Elution of HS-disaccharide standards with RPIP-HPLC.....	93
Figure 34. Principle of QCM-D technique.....	94
Figure 35. QCM-D characterization of SAV biomimetic platforms functionalization .....	95
Figure 36. Experimental setup of BLI technique .....	96
Figure 37. Biophysical principle of BLI technique.....	96
Figure 38. Kinetic sensorgram of HS/BMP2 interactions.....	97
Figure 39. Pipeline of pSMAD1/5/9 fluorescence intensity analysis. ....	98
Figure 40. Characterization of the oligosaccharide library .....	224
Table 1. Structure, location, and biological functions of the different GAGs .....	20
Table 2. Comparison of methods for production of defined GAG compounds.....	48
Table 3. Literature review about the effects of GAGs in the BMP signaling .....	67
Table 4. Affinities between different GAGs and BMPs determined in the literature .....	69
Table 5. Biomaterial applications of the different GAGs .....	72

# **Chapter I. Introduction**

## I.A. Prolog

Bones are essential tissues of our body, providing structural support, allowing motor capability and protecting vital organs<sup>[1]</sup>. In bone and other tissues, glycosaminoglycans (GAGs) play a crucial role in the development and homeostasis, by regulating the activity and diffusion of bioactive molecules<sup>[2]</sup>. Incorporating GAGs into biomaterials has emerged as a widely adopted strategy in medical applications due to their biocompatibility and ability to control the release of bioactive molecules<sup>[3]</sup>. The use of GAG-based biomaterials is broadly investigated for bone repair clinical applications to deliver bone morphogenetic proteins (BMPs), which exhibit a strong potential in inducing bone formation<sup>[3,4]</sup>. In particular, the bone morphogenetic protein 2 (BMP2) is widely employed since it has been approved for clinical use by the Food and Drug Administration (FDA)<sup>[5]</sup>.

GAGs are known to modulate the BMP cell signaling *in vivo* and their absence leads to skeletal defects, highlighting their role in the regulation of bone development<sup>[6]</sup>. However, the precise role of GAGs in BMP signaling remains unclear. The interplay between GAGs and BMP holds significant importance for the design of BMP-delivering GAG-based biomaterials, and therefore, the effect of these interactions at the cellular level should be better understood to enable their safe use in clinics. The main objective of this thesis was precisely to decipher the effects of the interplay between BMP2 and different GAGs, to provide fundamental knowledge for the development of future applications. Specifically, we sought to compare the modulation of BMP2 signaling exerted by different GAGs, in particular heparan sulfate (HS) and chondroitin sulfate (CS).

The following chapters introduce the context of GAGs, BMPs, and their interactions. Furthermore, we present the development of biomaterials for investigating the role of GAGs in a biomimetic context and we provide novel insights about the regulation of BMP2 signaling mediated by GAGs. During my PhD, I have written a review about GAG-based biomaterials (Annex information) that we submitted to *Advanced Materials*. Some sections of this review were extracted and appropriately inserted into the introduction of this thesis.

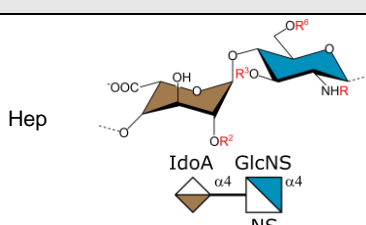
## I.B. Proteoglycans and glycosaminoglycans

### I.B.1. Classification of glycosaminoglycans (*Review published in Advanced Materials, Annex*)

#### I.B.1.a. Heparin

Glycosaminoglycans (GAGs) are the most abundant polysaccharides in the human body. The GAG family includes Heparin (Hep), Heparan Sulfate (HS), Chondroitin Sulfate (CS), Dermatan Sulfate (DS), Keratan Sulfate (KS) and Hyaluronic Acid (HA) (**Table 1**).

Every GAG is constituted by the repetition of a disaccharide unit, forming linear and negatively charged chains. Except for HA, these chains are covalently linked on a protein core to form a proteoglycan (PG) in a well-defined manner. The most important modifications of GAG chains are the transfer of sulfate groups at specific positions of the disaccharide units, which are catalyzed by various sulfotransferase enzymes. By precisely controlling the positions of sulfate groups all along the GAG chain, these sulfation enzymes can generate many different sulfated saccharide sequences, leading to a tremendous structural diversity. These different combinations of highly negatively charged sulfate groups mediate the interactions with a myriad of proteins. A recent extensive literature research revealed the existence of more than 3400 distinct GAG-binding proteins<sup>[7]</sup>. By interacting with proteins, GAGs can regulate their activity, their structural conformation, their interaction with cell receptors and their spatial distribution<sup>[8,9]</sup>. Through these interactions, GAGs govern a large number of biological functions in the organism<sup>[2]</sup>. Mutations of the genes associated to GAG biosynthesis are often related to phenotypical defects<sup>[10]</sup>. It suggests that the GAG biosynthesis is highly regulated and some evidence indicate the existence of compensation effects between GAGs. Indeed, alterations of both HS length or sulfation in chondrocytes have been correlated with a strong increase of CS content<sup>[11,12]</sup>. Due to their negative charge, the GAG chains adopt an extended conformation in aqueous solutions.

Disaccharide unit	Tissue prevalence	Biological functions
 <p>Hep</p>	Intracellular granules of mast cells <sup>[13]</sup> Lung arteries Liver and skin Bipotential glial progenitor cells	Anti-coagulation Anti-inflammation Anti-proliferation Anti-metastatic

<p>HS</p> <p>GlcA <math>\beta</math>4 GlcNAc</p>	<p>Basement membranes</p> <p>Cell surface of all cell types</p> <p>ECM of all tissues</p>	<p>Cell differentiation and proliferation</p> <p>Cell-cell interactions</p> <p>Tissue morphogenesis and organ function</p> <p>Interactions with GFs, cytokines and cell adhesion molecules</p> <p>Inflammation</p>
<p>HA</p> <p>GlcA <math>\beta</math>3 GlcNAc</p>	<p>Synovial fluid</p> <p>Articular cartilage</p> <p>Skin</p> <p>Vitreous humor</p> <p>ECM of loose connective tissues</p> <p>Umbilical cord</p>	<p>ECM assembly<sup>[14-16]</sup></p> <p>Resilience to compression</p> <p>Molecular weight dependent:</p> <ul style="list-style-type: none"> <li>▪ pro/anti-cancerous<sup>[17]</sup></li> <li>▪ pro/anti-inflammatory<sup>[17]</sup></li> <li>▪ pro/anti-angiogenic<sup>[17]</sup></li> <li>▪ pro/anti-proliferation<sup>[17]</sup></li> </ul>
<p>KS</p> <p>Gal <math>\beta</math>4 GlcNAc</p>	<p>Cornea</p> <p>Bone</p> <p>Cartilage</p> <p>Central and peripheral nervous system</p>	<p>Corneal ECM assembly for light passage and hydration</p> <p>Resilience to compression</p> <p>Guidance of neural growth and regeneration</p>
<p>CS</p> <p>GlcA <math>\beta</math>3 GalNAc</p>	<p>Cartilage</p> <p>Bone</p> <p>Brain</p> <p>Heart valves</p>	<p>Elasticity and anti-inflammatory properties</p> <p>Guidance of neural growth and regeneration</p> <p>Angiogenesis (CS-E)</p>
<p>DS</p> <p>IdoA <math>\alpha</math>3 GalNAc</p>	<p>Skin</p> <p>Blood vessels</p> <p>Heart valves</p> <p>Cornea</p> <p>Tendons</p> <p>Lung</p>	<p>Wound repair</p> <p>ECM assembly with collagen</p> <p>Inflammation</p> <p>Anticoagulation</p> <p>Neural guidance and development</p> <p>Cell proliferation, invasion, and metastasis</p>

**Table 1. Structure, location, and biological functions of the different GAGs**

In the disaccharide unit column are presented both the chemical structure and the representation with the Symbol Nomenclature for Glycans (SNFG). R<sub>2</sub>, R<sub>3</sub>, R<sup>4</sup>, R<sup>6</sup>, R<sup>6'</sup> and R indicate H or SO<sub>3</sub><sup>-</sup> groups.

Heparin (Hep) was discovered in 1916. It was first extracted from the liver but it is also present in the intracellular granules of mast cells, lung arteries, skin and in the bipotential glial progenitor cells. L-iduronic acid (IdoA) and N-sulfated glucosamine (GlcNS) are the two major components of the Hep disaccharide unit. With a substantially lower proportion, some disaccharides can also be composed of a D-glucuronic (GlcA) and an N-Acetyl glucosamine (GlcNAc). Hep can be sulfated at the C-2 hydroxyl of the Hexuronic Acid (HexA), at the C-2 amine of the GlcNAc (which becomes GlcNS) and at the C-3 and C-6 hydroxyl of the GlcNAc or GlcNS. Hep exhibits the highest sulfation degree among GAGs, with approximately 1.6 to 3.0 sulfates per disaccharide unit<sup>[18,19]</sup>, which explains its high affinity for various proteins with electropositive surfaces. Hep is particularly recognized in the medical field for its exceptional anticoagulant properties, but it can also inhibit cell proliferation, inflammation and tumor metastasis<sup>[20]</sup>.

### *I.B.1.b. Heparan Sulfate*

Heparan sulfate (HS) is closely structurally related to Hep. Originally, the less sulfated HS was considered as a side product of Hep purification and attracted less attention<sup>[21,22]</sup>. It was discovered later that Hep and HS follow the same biosynthesis pathway but Hep undergoes more modification steps than HS (sulfation, epimerization of GlcA into IdoA). Therefore, the main disaccharide unit of HS comprises a D-glucuronic (GlcA) and an N-Acetyl glucosamine (GlcNAc), although the reality is more complex. HS chains are organized in a succession of relatively homogeneous, poorly sulfated and modified regions (NAc domains) alternating with highly sulfated domains (NS domains), which are more prone to epimerization of GlcA into IdoA<sup>[23]</sup>. As a result, the sulfation degree of HS chains is generally between 0.4 and 2.0 sulfates per disaccharide, even if it can be sulfated at the same positions as Hep<sup>[18,19]</sup>. Differently from Hep, HS is produced ubiquitously in the body at the cell-surface of virtually all cell-types, and is present in the ECM of all tissues, especially in basement membranes. HS is involved in wide range of functions such as cell differentiation, tissue morphogenesis, cell interactions and proliferation, and interaction with GFs, cytokines and cell adhesion molecules<sup>[24–33]</sup>.

### *I.B.1.c. Hyaluronic acid*

Hyaluronic acid (HA), or hyaluronan, was first discovered in 1934 by Karl Meyer and John Palmer<sup>[34]</sup>. It is abundantly found in soft tissues such as synovial fluid, articular cartilage, skin, vitreous humor, ECM of loose connective tissues and in the umbilical cord. HA is peculiar because it is the only GAG that is unsulfated and never linked to a PG. Its disaccharide unit is composed of a GlcA and a GlcNAc like HS/Hep but with  $\beta 1 \rightarrow 3$  and  $\beta 1 \rightarrow 4$  glycosidic bonds instead of  $\beta 1 \rightarrow 4$  and  $\alpha 1 \rightarrow 4$ , since the biosynthesis of HA is performed by different enzymes than for HS/Hep. Although not sulfated and thus interacting with fewer proteins than other GAGs, HA is playing key roles in the ECM of various tissues for hydration preservation and resilience to compression. In cartilage and brain tissues, it mediates the ECM assembly through binding with several chondroitin sulfate PGs (CSPGs) such as aggrecan, neurocan, versican and brevican<sup>[35]</sup>. It also regulates cell-adhesion and motility through its well-studied CD44 and RHAMM cell receptors<sup>[36,37]</sup>. Many studies have reported that HA plays different roles depending on its molecular weight<sup>[17]</sup>. Generally, high molecular weights HA (HMW HA) are related to tissue homeostasis with anti-inflammatory, anti-proliferative, anti-angiogenic and anti-metastatic effects. On the other hand, low molecular weight HA (LMW HA) are often considered as an alarm signal related to inflammation, angiogenesis and metastasis<sup>[17]</sup>. It is important to acknowledge that even though most studies support this view, there are several

opposing results indicating cancer-promoting effects of HMW HA, which could be related to differences of cancer types<sup>[17]</sup>.

#### *I.B.1.d. Keratan Sulfate*

Keratan Sulfate (KS) was initially identified in the cornea in 1939 by Suzuki *et al*<sup>[38]</sup>. Although having important functions in the cornea, central and peripheral nervous systems, cartilage and bone, it is probably the least studied GAG. The structure of KS is atypical compared to the other GAGs because its disaccharide unit does not feature a HexA (IdoA or GlcA). The disaccharide unit of KS is composed of Gal and GlcNAc residues that can be both sulfated at their C-6 hydroxyl groups. Generally, its overall sulfation degree is comprised between 0.9 and 1.8 sulfates per disaccharide<sup>[19]</sup>. As opposed to the other GAGs, KS is associated to its core proteins by a branched glycosylation linkage that is not always connected to serine residues but may instead be coupled to a threonine or asparagine<sup>[39]</sup>. Furthermore, the attachment to their protein core involves complex N-linked or O-linked glycans. A classification has been established to differentiate the various KS types depending on their structure and location. KS-I/-II/-III are respectively associated to the cornea, cartilage and brain tissues. KS has an essential function in the cornea for the organization of collagen fibers to allow proper light transmission. KS can also regulate bone mineralization and bone induction. Within cartilage, when combined with aggrecan, it provides hydration and elasticity characteristics to the tissue, enabling it to withstand compression and shocks<sup>[40]</sup>. And finally in the brain, it contributes to neural guidance, development and regeneration with notably involvement in the promotion of neuron-glia cells interactions, myelination and axonal repair<sup>[39]</sup>.

#### *I.B.1.e. Chondroitin Sulfate*

Chondroitin Sulfate (CS) was first isolated by Fisher and Boedecker in 1861<sup>[41]</sup>. Mainly located in cartilage tissues, CS is also present in bone, brain and heart valves in important proportions. Its disaccharide unit is composed of GlcA and N-Acetyl galactosamine (GalNAc). In human, its sulfation degree varies between 0.1 and 1.3 sulfates per disaccharide<sup>[10,19]</sup>. Natural sulfation can occur at the C-4 or C-6 hydroxyl of the GalNAc and at the C-2 and C-3 hydroxyl of the GlcA<sup>[42,43]</sup>. The different sulfation combinations for a disaccharide are classified as specific units (A, C, D, E, etc...), which are depicted in the **Figure 1**. In cartilage, the CS is mainly attached to aggrecan in very large number, which confers its elasticity and anti-inflammatory properties<sup>[44,45]</sup>. In the nervous system, CS chains behave as cues for the guidance of neural development and regeneration<sup>[46,47]</sup>. CS plays also roles in angiogenesis, in particular for the CS-E sulfation pattern<sup>[48]</sup>.

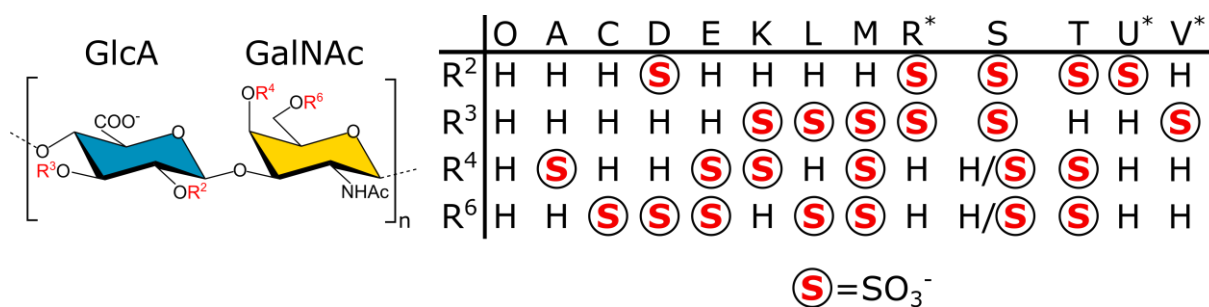


**Figure 1. Distribution of sulfates in different CS types.**

Here are represented the main *O*-, *A*-, *C*-, *D*-, *E*- units and the more rare *K*-<sup>[49,50]</sup>, *L*-<sup>[49]</sup>, *M*-<sup>[49,51]</sup>, *R*-<sup>[52]</sup>, *S*-<sup>[53]</sup>, *JT*-<sup>[54]</sup>, *U*-<sup>[55]</sup>, and *V*-<sup>[55]</sup> units. The star symbol \* indicates a unit that was synthesized but not identified nor extracted from natural source.

### *I.B.1.f. Dermatan Sulfate*

Dermatan sulfate (DS) was first extracted from skin by Karl Myer in 1941<sup>[56]</sup>. In addition, DS is also widely distributed in blood vessels, heart valves, cornea, tendons and lung. The disaccharide unit of DS is composed of IdoA and GalNAc. In old scientific publications, DS was referred as CS-B, before the classification changed. DS and CS can be distinguished by the presence of IdoA moieties in the former. DS can be sulfated at the C-4 or C-6 hydroxyl of the GalNAc and at C-2 hydroxyl of the IdoA, which results in a polysaccharide with a sulfation degree between 1 and 3 sulfates per disaccharide<sup>[10,19]</sup>. It is involved in various biological functions including wound repair, ECM assembly with collagen fibers, inflammation, anti-coagulation, neural guidance, cell proliferation, invasion and metastasis<sup>[56,57]</sup>.

### *I.B.2. Structure and classification of proteoglycans*

With the exception of HA, GAGs are found covalently linked on a protein core to form a proteoglycan (PG) in a well-defined manner. More than forty PGs have been identified and can be classified based on the sequence of their protein core, their location, or by their number and type of GAG chains<sup>[58]</sup>. The size of protein cores varies between 10 and 500 kDa and their amino acid sequence define the number and the positions of GAG linkages<sup>[59]</sup>. Depending on their protein core, PGs can carry between one to more than a hundred GAG chains of one or different GAG types<sup>[59]</sup>. PGs are present at different locations: in the ECM, at the cell surface, in the blood stream or even in intracellular vesicles. A few common PGs are schematically represented in the **Figure 2** to illustrate important structural properties including the number and the type of GAG chains, the size and conformation of the protein core and its possible linkage to the cell-surface. The location of these PGs is related to different biological functions, but several questions remain to be elucidated. In particular, it is not clear whether cell-surface and extracellular PGs have identical or distinct functions in cell signaling.

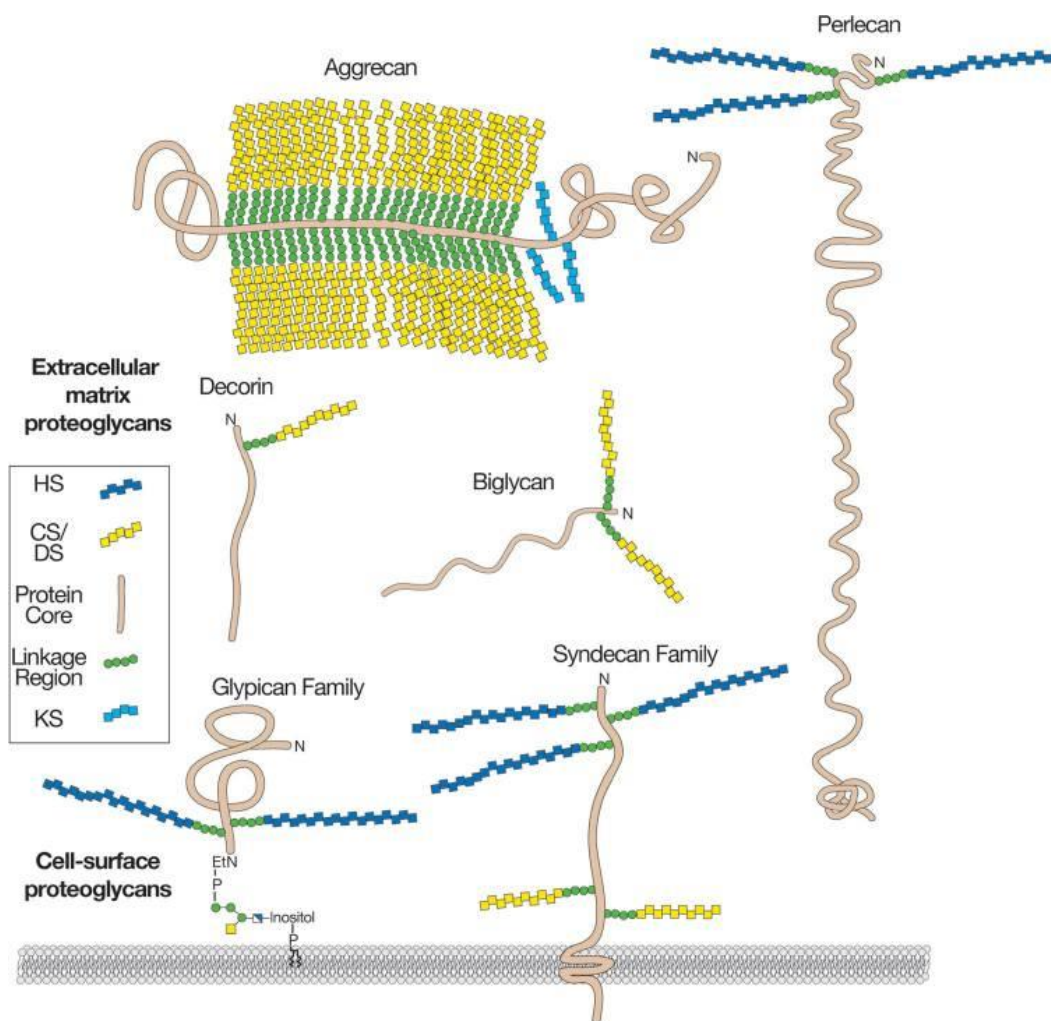


**Figure 2. Schematic representation of various PGs**

Cell-surface PGs correspond to glypican and syndecans that are attached to the cell membrane either by a GPI-anchor or by their transmembrane domain. Syndecans, among others, are hybrid PGs and may carry both HS and CS chains while glypicans carry exclusively HS chains. Aggrecan, perlecan, decorin and biglycan are extracellular matrix PGs secreted by the cells. They exhibit different core protein structures, carrying a highly variable number of GAG chains. Aggrecan is also able to bind HA via its N-terminal domain containing a G1 globular domain. Reproduced with permission<sup>[59]</sup>.

In 2015, Iozzo and Schaeffer proposed a novel and comprehensive classification of PGs, based on criteria of localization in the cell environment, overall gene/protein homology, and the presence of specific protein modules within their protein cores (**Figure 3**)<sup>[58]</sup>. PGs are classified within four major classes: intracellular, cell-surface, pericellular and extracellular. In this manuscript, we chose to detail only the cell-surface and extracellular PGs featuring HS, CS or DS chains. For extracellular PGs that are abundant, only the most relevant for bone tissues are presented<sup>[60]</sup>. Most functions of PGs are attributed to their GAG chains and have been described in the previous section. Therefore, the following description of PGs focuses on their protein core structures and associated specific functions.

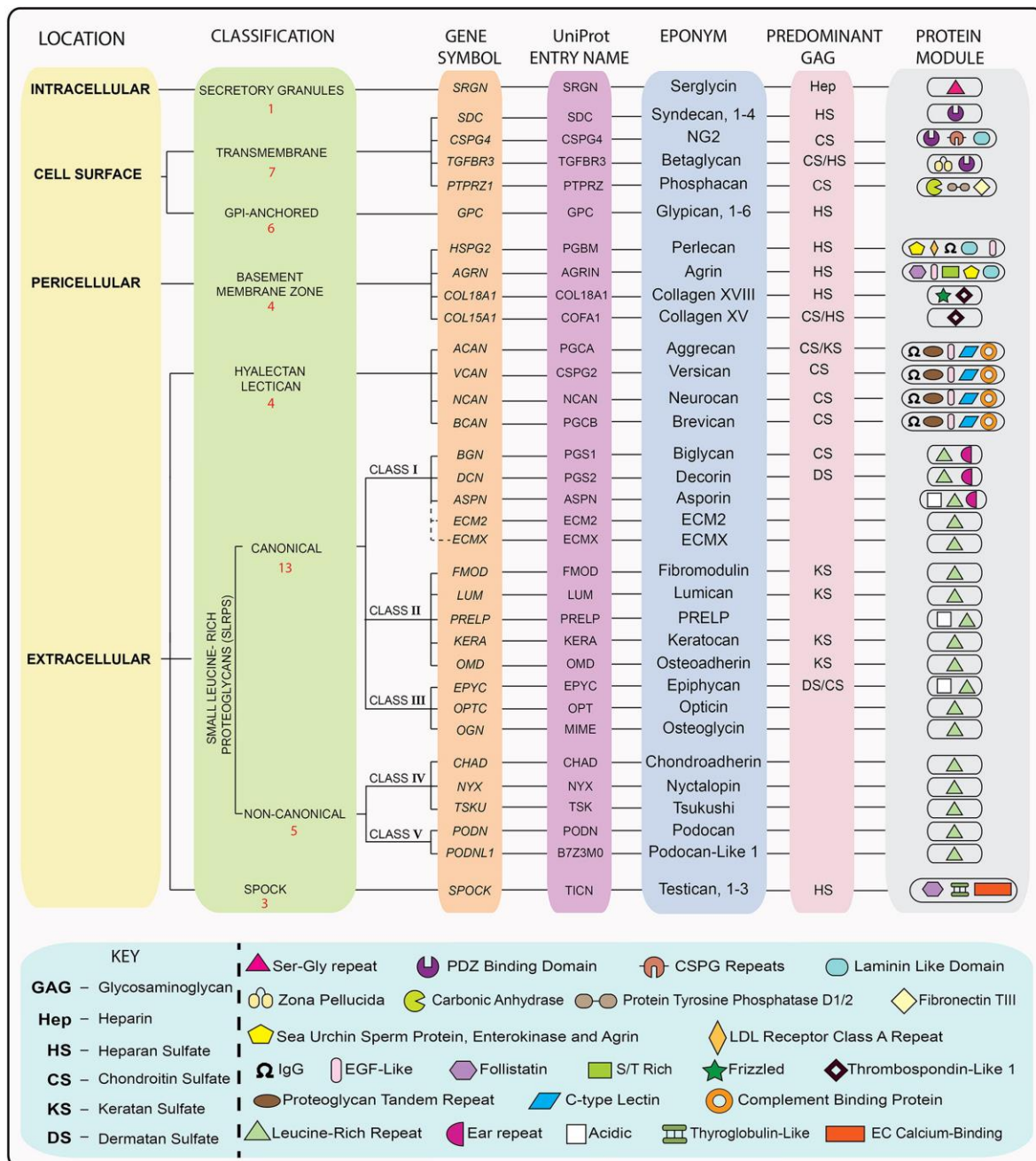


**Figure 3. Classification of PGs based on their location characteristics**  
 PGs are classified in four groups: intracellular, cell-surface, pericellular and extracellular. Further information about their GAG characteristics and specific modules of their protein cores are also depicted. Reproduced with permission under the terms of CC BY NC ND licence<sup>[58]</sup>. Copyright 2015, Iozzo and Schaefer, published by Elsevier.

### I.B.2.a. Cell-surface proteoglycans

Cell-surface PGs (csPGs) are associated with the plasma membranes of cells, either directly through an intercalated protein core or indirectly through a glycosyl-phosphatidyl-inositol (GPI) anchor. Transmembrane PGs are composed of syndecan 1-4, NG2, betaglycan and phosphacan, while GPI-anchored PGs correspond to the glypican family. The GAG chains exhibited by cell-surface PGs are limited to HS, CS and to a lesser extent DS.

### *GPI-anchored proteoglycans/Glypicans*

Glypicans are a family of PGs that are linked to the cell surface by a GPI anchor. Six members of this family (Glypican 1-6) have been identified in mammals and two in *Drosophila melanogaster* (Dally and Dlp)<sup>[61]</sup>. They are characterized by a protein core between 60 and 70 kDa with moderate homology among the family except for the conserved positions of 14 cysteine residues, suggesting that the three-dimensional structures of glypicans are similar. Another characteristic that is shared by all glypicans is the location of the linkage sites for the GAG chains, which seems to be restricted to the last 50 amino acids in the C-terminus, placing the chains close to the cell membrane. Glypicans carry from one to three GAG chains and are considered as strict heparan sulfate proteoglycans (HSPGs), although glypican-5 was reported to carry CS chains under specific conditions<sup>[62]</sup>. Even though these proteins lack transmembrane and cytoplasmic domains, it has been demonstrated that glypicans are involved in cellular response to various growth factors and morphogens<sup>[63-66]</sup>. A mutation in its gene has also been associated with Simpson-Golabi-Behmel overgrowth syndrome<sup>[59]</sup>. Finally, some biological properties of glypicans may be attributed to their GPI membrane anchoring, enabling their localization within specialized membrane microdomains called "lipid rafts", including or excluding specific cell-membrane receptors<sup>[67-69]</sup>.

### *Transmembrane proteoglycans*

- Syndecans

The syndecan family is composed of four members that all display an intracellular domain, a transmembrane domain and an ectodomain exhibiting GAG chains. The intracellular and transmembrane domains are rather conserved (60-70%) among syndecans, while their ectodomains have a low homology (10-20%). Short sequences at the N-terminal extremity of their ectodomains are however conserved in the four syndecans and correspond to attachment sites for HS chains. Syndecans -1 and -3 additionally present attachment sites for CS chains in the membrane-proximal region of the ectodomain. Syndecan-4 can carry CS chains as well, but their positions have not been elucidated<sup>[70]</sup>. Overall, syndecans are considered as hybrid HS/CS PGs and can carry up to four HS chains and two CS chains. The transmembrane domains of syndecans can form homodimers or heterodimers and this clustering could be of importance since antibody-induced dimerization of syndecans can trigger signaling<sup>[58,71]</sup>. Adding to the common role of PGs to interact with various growth factors, syndecans have a key role in cell adhesion mechanisms and cytoskeletal organization. Their intracellular domain contain an EFYA PDZ-binding site that plays a key role in their anchoring to cytoskeletal components.<sup>[58]</sup>

In relation with that, syndecan-4 activity is crucial to establish focal adhesion and depends on its multimerization<sup>[72,73]</sup>. Syndecans such as other PGs can be cleaved at specific sites close to the plasma membrane, releasing a part of their ectodomain in the extracellular domain. This naturally occurring process is called “shedding” and will be described further in the section “I.B.4. Proteoglycans post-synthesis regulation and turnover”.

- Betaglycan

Betaglycan, also called TGF- $\beta$  type III receptor, is a ubiquitously expressed transmembrane cell surface PG that acts as a co-receptor for protein members of the transforming growth factor beta (TGF- $\beta$ ) superfamily. Betaglycan can present up to two HS or CS chains. It was classified as part-time PG, since it can exist with or without a GAG chain<sup>[72]</sup>. Interestingly, betaglycan is able to bind its TGF- $\beta$  ligand with high affinity, independently of its GAG chains<sup>[74]</sup>. Its cytoplasmic domain is short and contains like syndecans a PDZ-binding domain.

- Phosphacan

Receptor protein tyrosine phosphatase zeta (RPTP $\zeta$ ) is a transmembrane CSPG that interacts with neurons and neural cell-adhesion molecules (N-CAM). Its gene (PTPRZ1) encodes a single-pass type I membrane protein with a relatively large ectodomain harboring a fibronectin type III domain commonly found in cell adhesion molecules. The ectodomain contains up to five GAG-binding sites for CS or DS chains that can be substituted in some cases with KS chains. The shed ectodomain of RPTP $\zeta$  corresponds to its extracellular isoform called Phosphacan. RPTP $\zeta$  and Phosphacan have been reported to bind with high affinity to neural cell adhesion molecule (N-CAM), neuron-glia cell adhesion molecule (Ng-CAM), and neuron-glia-related cell adhesion molecule (Nr-CAM), as well as other cell surface molecules like contactin<sup>[75]</sup>. Therefore, while RPTP $\zeta$  seems to promote neuronal adhesion and neurite outgrowth, Phosphacan seems to have the opposite effect<sup>[76,77]</sup>. It has been recently demonstrated that RPTP $\zeta$  act as structural regulators of perineuronal nets<sup>[75]</sup>. Furthermore, it has been suggested that Phosphacan, which is abundantly expressed in the neural stem cells niche, may help to create the favorable environment that supports self-renewal and maintenance of the cells<sup>[78]</sup>.

#### *Other cell-surface PGs*

There are other members of the cell-surface PG group. NG2 (also termed CSPG4) is a CSPG associated to melanoma and promotes tumor vascularization. Its ectodomain contains a D2 domain that exhibits attachment sites for the CS chains as well as a repetition of fifteen ‘CSPG’

motifs that binds directly to collagens V and VI and mediate cell-matrix interactions<sup>[58]</sup>. An isoform of the FGF2 receptor, FGFR2-IIIb, carries an HS chain increasing the affinity for its ligand<sup>[79]</sup>. Similarly, several members of the transmembrane hyaluronan cell-receptor CD44 family can carry HS or CS chains. Members of the CD44 family arise from alternative splicing of a single gene. The isoforms CD44H, CD44E and CD44 Epican can carry CS chains, but HS chains have only been identified on Epican<sup>[80]</sup>. Interestingly, while CD44 members are generally expressed on many epithelial, mesenchymal and hematopoietic cells, the expression of Epican is restricted to epithelial cells, mostly stratified squamous epithelial cells.

### *I.B.2.b. Extracellular proteoglycans*

In the **Figure 3** of Iozzo and Schaeffer, pericellular PGs are distinguished from extracellular PGs. The explanation is that agrin, perlecan, collagen XV and collagen XVIII are extracellular PGs generally in close vicinity to the plasma membranes of cells (pericellular). Another characteristic of this distinction is that pericellular PGs are prevalently HSPGs while extracellular PGs further to the cell membranes are essentially CS- or DS- carrying PGs. For simplification purpose, these two groups of PGs will be classified here as extracellular PGs.

Small Leucine-Rich Proteoglycans (SLRPs) are the most abundant PGs found in the bone mineralized matrix<sup>[60,81]</sup>. SLRPs represent a group of extracellular PGs characterized by their relatively small protein core with a molecular weight ranging from 36 to 42 kDa, and a central region composed of leucine-rich repeats. SLRPs share similar functions such as the stabilization and organization of collagen fibers, or other roles in innate immunity and regulation of growth factor signaling. In this family of PGs, biglycan and decorin, have important functions in the bone homeostasis<sup>[81]</sup>. Interestingly, decorin and biglycan are predominantly modified with CS chains within mineralized matrices, while they predominantly carry DS chains within soft connective tissues<sup>[81]</sup>.

- Biglycan

Biglycan is a class I SLRP containing two GAG chains, which are attached on amino acids 5 and 10 in humans. Biglycan-deficient mice develop age-dependent osteopenia and fail to achieve peak bone mass. These mice have a reduced number of bone marrow stromal cells, leading to lower osteoblast number and activity, increased osteoclast differentiation and activity, and reduced response to BMP2, BMP4 and TGF- $\beta$ <sup>[82]</sup>. Biglycan can interact with TGF- $\beta$  *via* its protein core such as other SLRPs like decorin<sup>[83]</sup>.

- Decorin

Decorin is also a class I SLRP. It contains only one GAG chain attached to a serine residue (Ser4). The interaction of decorin with TGF- $\beta$  increases the ligand affinity to its receptors and thus its activity. At the difference of biglycan, decorin-deficient mice display a fragile skin phenotype but without any apparent effect on bone mass or architecture. The structural similarity of decorin and biglycan suggests possible function redundancy, supported by overexpression of one due to ablation of the other. Double-deficient mice support this hypothesis with a more severe and premature skeletal phenotype with reduced cortical and trabecular bone mass<sup>[81]</sup>.

- Perlecan

Perlecan is an extracellular/pericellular strict HSPG and a major component of all basement membranes. Its large protein core of 400-500 kDa is composed of five domains with homology to N-CAM and laminin, therefore playing a role in cell adhesion<sup>[58,84]</sup>. The C-terminal domain is essential for supramolecular assembly of the basement membranes<sup>[81]</sup>. When cleaved by enzymes, this domain called Endorepellin is released in the ECM where it appears to exhibit anti-angiogenic properties<sup>[85]</sup>. On the other side, the N-terminal domain carries three HS chains that can interact with various components of the ECM, including osteogenic growth factors. Mutations in the human perlecan gene result in two rare diseases, namely Silverman-Handmaker-type dyssegmental dysplasia and Schwartz-Jampel syndrome type 1. These conditions are characterized by various clinical features, including short-limbed dwarfism, myotonic myopathy, dystrophy of epiphyseal cartilages, and joint contractures<sup>[81]</sup>.

- Aggrecan

Aggrecan is a main component of cartilage tissues and brain tissues. It is the largest form of PG identified and it belongs to the hyalectan family of PGs that bind HA. The protein core of 208-220 kDa is not the largest, but it carries about one hundred of CS chains and twenty KS chains. It features a G1 domain and a link module that interact with hyaluronan to form a very stable network, contributing to the mechanical properties of cartilage<sup>[58]</sup>. The important number of GAG chains provides a prodigious capacity of water retention that contributes to the resilience property of cartilage upon compression and shocks. Moreover, the G3 domain of aggrecan interacts with tenascins, fibulins and sulfated glycolipids, connecting various elements of the extracellular matrix. In the brain, aggrecan is primarily expressed in perineuronal nets. Mutations in the human aggrecan gene lead to conditions characterized by short stature and skeletal abnormalities, specifically chondrodysplasia and spondyloepiphyseal dysplasia<sup>[81]</sup>.

### I.B.3. Biosynthesis of proteoglycans

The PG protein core is initially produced within the rough endoplasmic reticulum (ER), after which it undergoes glycosylation modifications in the different compartments of the Golgi apparatus. The first step initiating the GAG chain synthesis consists in the addition of a Xyl-Gal-Gal-GlcA tetrasaccharide linker to the protein core (**Figure 4**). The formation of the tetrasaccharide begins with a xylosyltransferase (XylT1 or XylT2) that transfers a xylose (Xyl) residue to a serine residue of the protein core, generally juxtaposed to a glycine residue<sup>[86]</sup>. This step occurs in the ER or in the cis-Golgi compartment depending on the cell type. The xylosylation process is not necessarily exhaustive, which may explain why PGs with multiple potential attachment sites exhibit a variable number of GAG chains in different cells<sup>[59]</sup>. Next, in the cis-Golgi and the medial-Golgi compartments, two galactose (Gal) residues are transferred successively by GalT-1 and GalT-2 enzymes. The tetrasaccharide linker formation is completed in the medial- or the trans-Golgi with the transfer of a glucuronic acid (GlcA) residue by the GlcAT-1 enzyme. Alternatively, as previously mentioned, KS chains are linked to asparagine, serine, or threonine residues of the protein core *via* complex N-linked or O-linked glycans<sup>[87]</sup>. The different biosynthesis of KS PGs is not detailed here but it has been reviewed previously<sup>[87]</sup>.

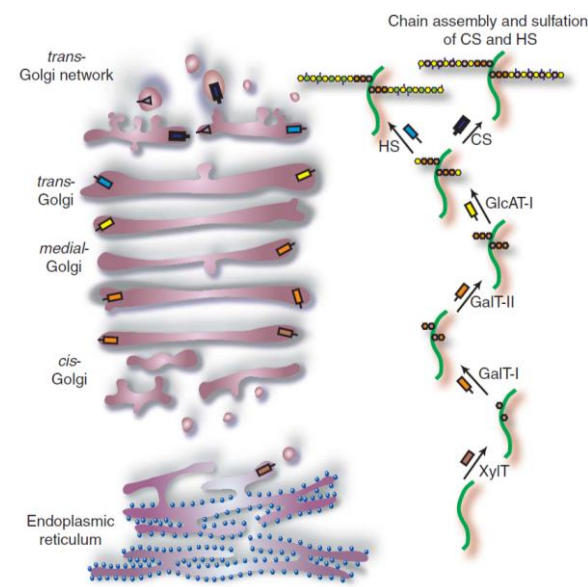


**Figure 4. Biosynthesis of the GAG tetrasaccharide linker**

*Transmembrane glycosyltransferases catalyzing the transfer of monosaccharide residues to the protein core of PGs are represented in the intracellular space of the Golgi/ER compartments. The residue catalyzed after the tetrasaccharide linker constitutes the divergence point in HS and CS biosynthesis. Reproduced with permission<sup>[88]</sup>.*

The addition of the next residue to the tetrasaccharide linker determines the nature of the synthesized GAG chains. The transfer of a GlcNAc residue leads to the synthesis of HS chains, while the transfer of a GalNAc residue is associated to the synthesis of CS/DS chains. The

regulation mechanisms of this determinant step remain unclear. Several potential mechanisms have been previously reviewed, including modification of the linker residues such as the sulfation of Gal residues that would promote CS/DS synthesis, and the 3-O sulfation of the GlcA linker that would prevent CS/DS synthesis in some cases<sup>[89]</sup>. The acidic and hydrophobic characteristics of the polypeptide sequence in proximity to the serine attachment site may also have an influence<sup>[90]</sup>. Several enzymes appear to be involved in this crucial step.

For the synthesis of HS/Hep, EXTL2 and EXTL3 glycosyltransferases of the exostosin family exhibit GlcNAcT-I activity that catalyzes the transfer of a GlcNAc upon the tetrasaccharide linkage<sup>[91]</sup>. EXTL3 exhibits both GlcNAcT-I (transfer of GlcNAc to the tetrasaccharide linker) and GlcNAcT-II (chain polymerization) activities and is therefore involved in both HS initiation and polymerization. EXTL2 appears to be involved in the termination of GAG chain biosynthesis by catalyzing either a GlcNAc to a Xyl-phosphorylated tetrasaccharide linker<sup>[92]</sup>, or a GalNAc to the tetrasaccharide linker, but with an unusual  $\alpha(1-4)$  glycosidic linkage<sup>[93]</sup>. Both activities terminate the GAG chain elongation by preventing the additional transfer of residues<sup>[93,94]</sup>. Alternatively, for the synthesis of CS/DS chains, GalNAcT-1 and GalNAcT-2 enzymes catalyze the transfer of a GalNAc to the tetrasaccharide linker<sup>[44,95]</sup>.

The GAG linkers are then elongated by several biosynthesis enzymes coupled to sugar donors (UDP-GlcNAc, UDP-GalNAc, UDP-GlcA, etc...) in the medial-, trans-Golgi and trans-Golgi network compartments<sup>[10,23,44,95-98]</sup>.

The elongation of HS/Hep chains is achieved by the alternating transfer of GlcA and GlcNAc residues, mediated by other glycosyltransferases of the exostosin family (EXT1, EXT2). In the Golgi, EXT1 and EXT2 proteins form a hetero-dimeric complex harboring four glycosyltransferase domains with both GlcNAc and GlcA transferase activities. Interestingly, recent studies indicate that the EXT2 pseudo-GlcA-T domain lacks catalytic activity and propose that GlcA transfer is exclusively performed by EXT1<sup>[99]</sup>. The EXTL1 and EXTL3 glycosyltransferases also possess GlcNAcT-II activity that catalyzes GlcNAc transfer for chain polymerization, even though their contribution remains unclear. EXTL1 exhibits a striking structural similarity to EXT1 and EXT2, but its absence in species such as *C. elegans* and *D. melanogaster* suggests that it may not be an essential component of the HS biosynthetic machinery<sup>[91]</sup>.

The elongation of CS/DS chains is performed by the combination of several enzymes, namely chondroitin synthase-1, -2 and -3 (ChSy-1, -2, -3), chondroitin polymerizing factor (ChPF), and chondroitin GalNAcT-1 and -2 (also referred as ChGn-1,-2). The former three enzymes ChSy-

1, 2 and -3, show dual GlcAT-II and GalNAcT-II glycosyltransferase activities, but cannot polymerize CS chains by themselves. They apparently need to form hetero-dimeric enzyme complexes composed of any combinations of ChSy-1, ChSy-2, ChSy-3, and ChPF to exhibit strong CS polymerase activity<sup>[100]</sup>. The other GalNAcT-1 and GalNAcT-2 glycosyltransferases also exhibit GalNAcT-I (CS initiation) and GalNAcT-II (CS elongation) activities. Their contribution to the CS elongation process is not clear, but some evidence suggests they could cooperate with sulfotransferases to control the chain length and number<sup>[100]</sup>.

The final step of PG biosynthesis is the maturation of the GAG chains, performed by several sulfotransferases that transfer sulfate groups at specific positions and epimerases that modify the stereoisomeric conformation of HexA moieties. The activity of sulfotransferases requires the presence of a sulfate donor molecule called 3'-phosphoadenosine 5'-phosphosulfate (PAPS), synthesized in the cytosol before its translocation to the Golgi.

The maturation of HS/Hep starts with the N-deacetylation/N-sulfation of glucosamines performed by bifunctional N-deacetylase/N-sulfotransferase (NDST) enzymes (four isoforms). This step is responsible for generating the alternation between low-sulfated domains and high-sulfated domains along the HS chain, termed NAc and NS domains, respectively. Especially, the NDST-1 has a critical role since it processes the substrate chain sequentially from the non-reducing end toward the reducing end until it finds a previously sulfated glucosamine, thereby generating an NS domain<sup>[101]</sup>. This step is considered the divergence point in the biosynthesis of HS and Hep since NS domains greatly influence the subsequent sulfation and modification steps of the maturation. In mast cells producing mainly Hep, NDST-2 enzymes acting principally on low-sulfated regions are highly expressed and may play a role in extending NS domains<sup>[102]</sup>. Supporting this idea, NDST-2 deficient mice are unable to synthesize sulfated Hep<sup>[103]</sup>. Next, the C5-epimerase enzyme (also called Hsepi) may convert D-GlcA residues into L-iduronic acid residues. To catalyze this process, the C5-epimerase requires the presence of an adjacent GlcNS residue towards the non-reducing end of its substrate<sup>[104–106]</sup>. This process is reversible *in vitro*, yielding a 2:1 ratio of GlcA and IdoA but it was identified as irreversible in cellular systems. Further analysis of the modified HS chains revealed that most IdoA units were also 2-O sulfated, likely blocking the back-epimerization. Since the HS 2-O sulfotransferase (2OST) has a strong substrate preference for IdoA compared to GlcA<sup>[107,108]</sup> and that 2-O sulfation is irreversible, the proportion of IdoA residues in NS domains of HS/Hep is favored compared to GlcA. It was later found that C5-epimerase associates *in vitro* with 2OST, thereby generating contiguous epimerized and 2-O-sulfated HS domains<sup>[109]</sup>. Additionally, the physical

interaction of C5-epimerase and 2OST is required *in vivo* for their translocation from the ER to the Golgi compartments<sup>[110]</sup>, suggesting they naturally work together. The final modifications of HS/Hep chains correspond to the 6-O sulfation and the 3-O sulfation of glucosamine residues, catalyzed by 6-O-sulfotransferases (6OSTs, 3 isoforms) and 3-O-sulfotransferases (3OSTs, 7 isoforms). The activity of 6OSTs seems to be less preferential for NS domains and targets low-sulfated NAc domains as well. The different 6OST isoforms were shown to have similar substrate specificities, with only minor differences linked to the presence of nearby 2-O sulfated IdoA residues<sup>[111,112]</sup>. Finally, 3OSTs have been extensively studied, because of their contribution to the formation of 3-O sulfated sequences involved in the binding of antithrombin III (AT III, **Section I.B.5**). Among the seven 3OST isoforms, only 3OST1 and 3OST5 are involved in the formation of the specific AT III binding sequence, while other isoforms show different substrate specificities. Remarkably, except for the 3OST1 isoform that is also secreted in the ECM, all the enzymes involved in HS biosynthesis are single-pass transmembrane type II proteins associated with the Golgi or the ER membranes.

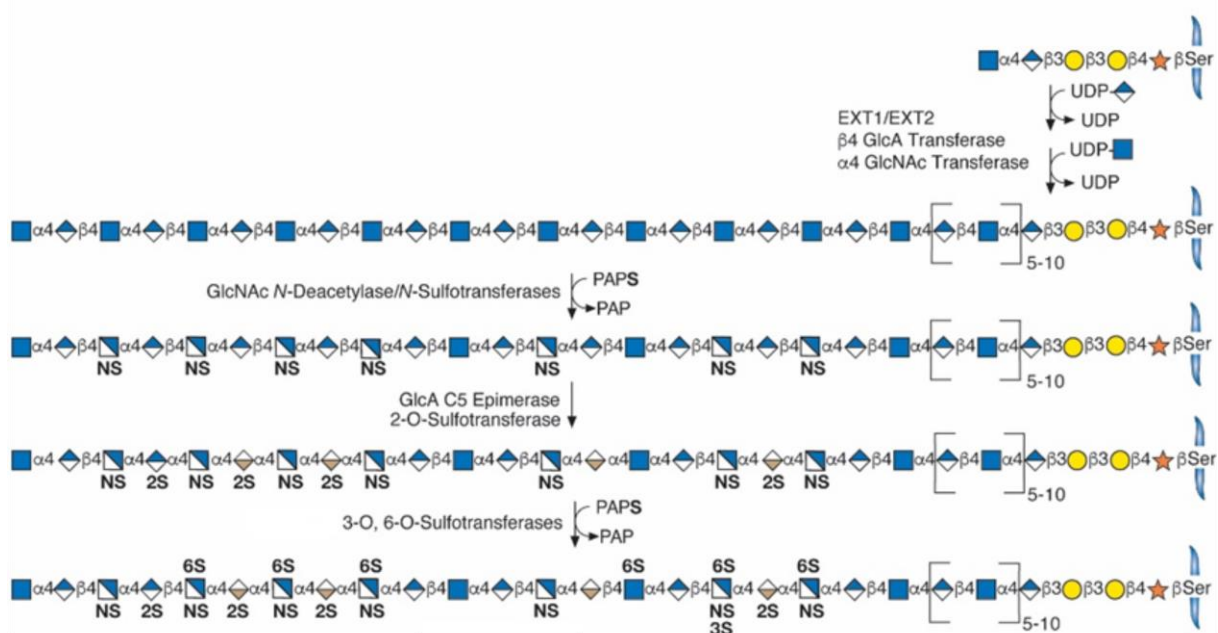


**Figure 5. Elongation and maturation steps in the biosynthesis of HS/Hep chains**

*EXT1* and *EXT2* are the main enzymes that polymerize the chains. Next *NDSTs* catalyze the deacetylation and *N*-sulfation of glucosamines generating *NS* and *NAc* domains. Then, the *C5*-epimerase and *2-O* sulfotransferases act in association principally within *NS* domains to generate stable *IdoA* residues with *2-O* sulfates, *IdoA* or more rarely *GlcA2S* residues. Finally, *3-O*- and *6-O*-sulfotransferases catalyze the transfer of additional sulfate groups. Reproduced under the terms of the *CC BY-NC-ND 4.0 licence*<sup>[59]</sup>.

The maturation of CS/DS chains involves several sulfotransferases and two epimerases. The two DS-epimerases (DS-epi1 and DS-epi2) convert the GlcA residues of CS chains into *IdoA* residues characteristic of DS disaccharide units (i0-iE, **Figure 6**). The proportion of

epimerization from GlcA to IdoA can vary significantly, with the IdoA content ranging from a single IdoA residue per chain to nearly 100%. The hybrid nature of these galactosaminoglycan chains is defined by the term CS/DS. IdoA can be distributed in different patterns, such as continuous blocks, alternating structures of IdoA and GlcA, or isolated IdoA dispersed among unmodified GlcA residues. DS-epi1 activity *in vitro* generates structures with only a few adjacent IdoA units, while the formation of long IdoA blocks is more common *in vivo*. Interestingly, the *in vivo* 4-O sulfation of adjacent GalNAc residues catalyzed by the dermatan 4-O-sulfotransferase 1 (D4ST1) facilitates the activity of DS-epi1 and the formation of contiguous IdoA-containing blocks with iA units<sup>[113]</sup>. Studies showed that DS-epi1 and D4ST1 colocalize in the Golgi and that they can form homomeric and heteromeric complexes with DS-epi2<sup>[113]</sup>.

Three isoforms of 4-O-sulfotransferases (C4ST1,2,3) are responsible for catalyzing the 4-O-sulfation of GalNAc residues, thus generating CS-A units. These enzymes show a preference for GlcA-rich regions. An intriguing observation is that C4ST1 works in conjunction with ChSy-2 to facilitate the elongation of CS chains<sup>[114]</sup>. Alternatively, 2 isoforms of 6-O-sulfotransferases (C6ST1,2) can catalyze the 6-O sulfation of GalNAc residues to generate CS-C or iC units. The modification of CS/DS chains may continue to synthesize di-sulfated units with the activity of two distinct sulfotransferases: uronyl 2-O-sulfotransferase (UST) and GalNAc 4-sulfate 6-O-sulfotransferase (GalNAc4S-6ST). GalNAc4S-6ST transfers sulfate to the C-6 position of preexisting 4-O-sulfated GalNAc (A/iA units) to generate E or iE units. On the other hand, UST is responsible for catalyzing the 2-O-sulfation of the GlcA residues of CS-C units to form disulfated D units (GlcA2S-GalNAc6S). UST might also be implicated in the formation of CS-B units (GlcA2S-GalNAc4S) but *in vitro* assays demonstrated no 2-O-sulfotransferase activity of the enzyme on chondroitin and CS-A substrates<sup>[115]</sup> and CS-B are very uncommon *in vivo*. However, it displays a strong activity on IdoA-GalNAc4S units (iA, **Figure 6**) to form IdoA2S-GalNAc4S units (iB). After completing their biosynthesis, PGs can be transported to the cell membranes or secreted to the extracellular space *via* extracellular vesicles<sup>[98]</sup>.

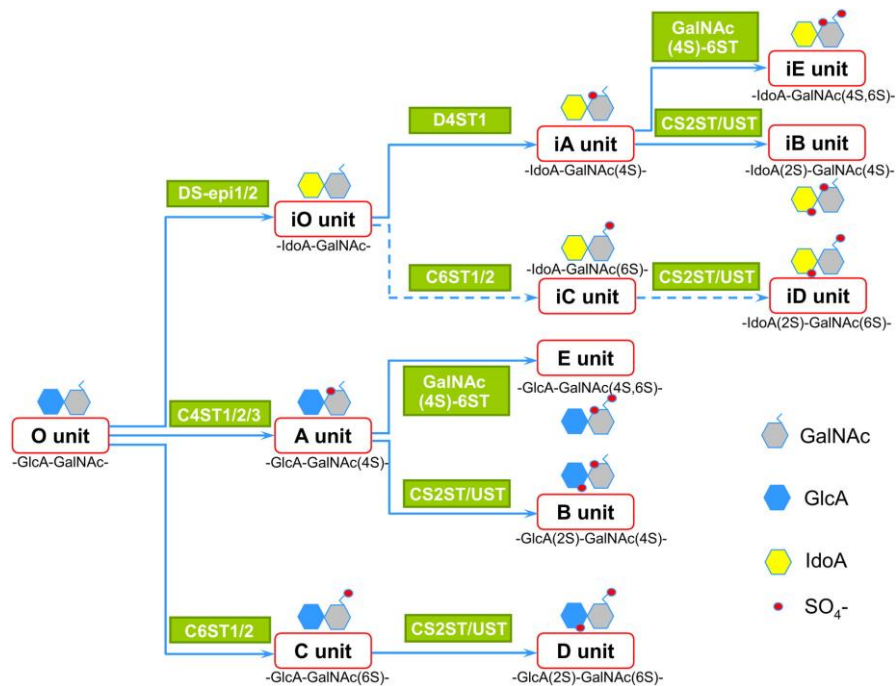


**Figure 6. Maturation step in the biosynthesis of CS/DS chains**

The DS and CS units are described with the terms 0-E for CS (HexA: GlcA) and i0-iE for DS (HexA: IdoA). Dotted lines indicate putative pathways because iC and iD unit formation has not been clarified yet. Reproduced with permission<sup>[116]</sup>.

Overall, the variable expression in different cell types and tissues of the GAG biosynthesis enzymes and their isoforms with distinct substrate preferences certainly contributes to the precise temporal and spatial regulation of specific GAG structures. This finely tuned GAG environment thereby regulates the spatial distribution and bioactivity of various proteins and growth factors, and plays a key role in embryogenesis and tissue homeostasis. In agreement with this, mutations of several GAG biosynthesis enzymes in different animals are associated with diseases and abnormal development<sup>[88]</sup>. Mutations in both EXT1 and EXT2 HS-elongating enzymes are responsible for the Hereditary Multiple Extostosis (HME) disease in humans. Most HME patients exhibit genetic mutations in EXT1 (60-70%), which are distributed throughout the entire gene, and in EXT2 (30-40%), with a more precise localization in the N-terminal domain<sup>[117]</sup>. In a minority of cases, mutations in the EXT3 genetic locus could also be associated with HME<sup>[118,119]</sup>. Interestingly, EXT-like genes (EXTL1, EXTL2, and EXTL3) of the exostosin family were not linked to HME. In drosophila, EXT1 and EXT2 (*ttv* and *sotv*) mutations were associated with developmental defects and alterations of hedgehog (Hh), wingless (Wg, homolog of Wnt-1) and decapentaplegic (Dpp, BMP2/4 ortholog). In mice, NDST-1, 2OST, and HS C5-epimerase knockouts lead to neonatal death, with skeletal defects for 2OST and C5-epimerase mutants. The reduction of drosophila 6OST activity causes embryonic lethality and a significant reduction of fibroblast growth factor (FGF) signaling. In

mice, C4ST-1 mutation is linked to a chondrodysplasia skeletal phenotype. In humans, GalT-I, C6ST-1, Glypican-3 and Perlecan mutations are related respectively to Ehlers–Danlos syndrome, Spondyloepiphyseal dysplasia, Simpson–Golabi–Behmel syndrome and Schwartz–Jampel syndrome, which are all associated with developmental or skeletal defects.

#### *I.B.4. Proteoglycans post-synthesis regulation and turnover*

After the controlled biosynthesis and transport of PGs to the cell surface or the extracellular matrix, other regulation mechanisms are involved in the continuous remodeling of PG content and structure of the cellular environment. In particular, extracellular lyases, sheddases and sulfatases play key roles in addition to the natural catabolism of PGs (**Figure 7**).

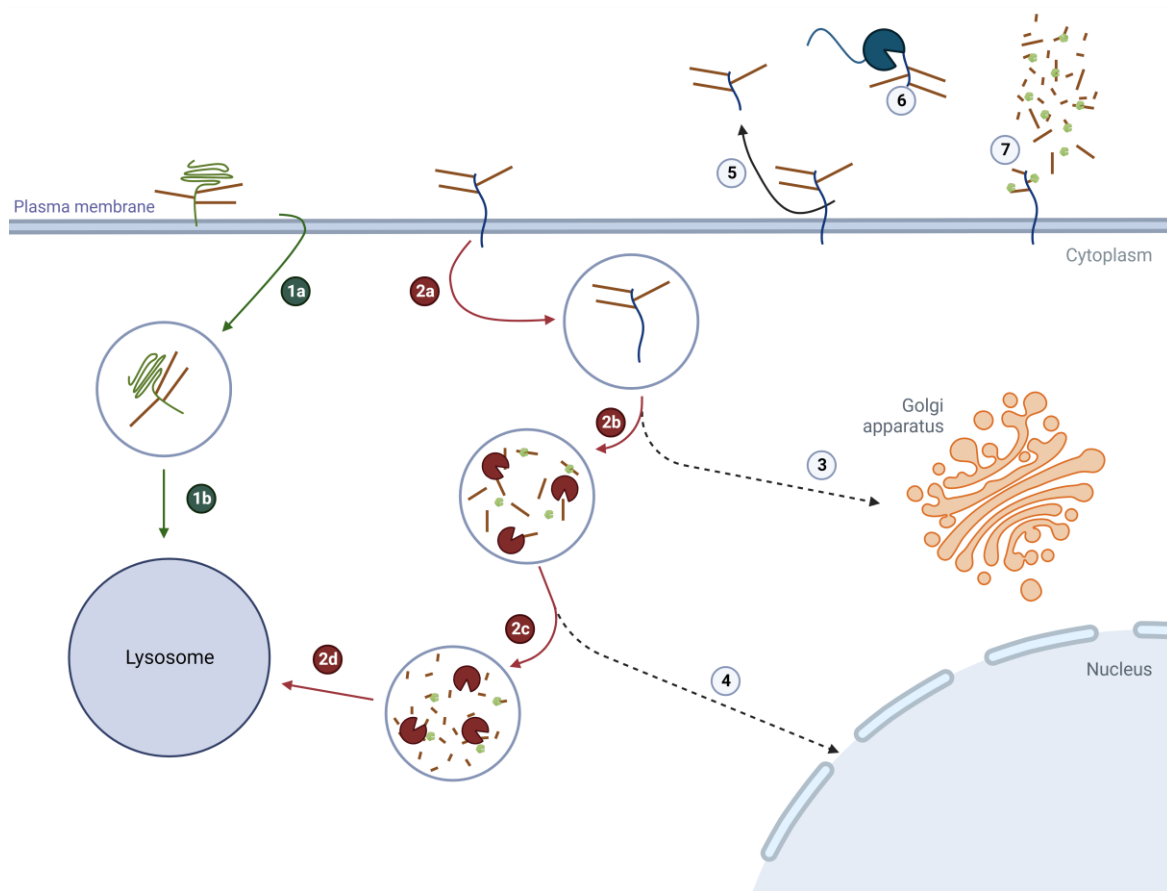


**Figure 7. Mechanisms involved in the post-synthesis regulation and turnover of PGs**

**1** Glypicans undergo a fast lysosomal degradation, while **2** transmembrane PGs undergo a stepwise lysosomal degradation including repetitive actions of lyases (green) to cleave the GAG chains and sulfatases (red) to cleave sulfate groups. In this stepwise degradation, PGs or GAG fragments may be transferred to **3** the Golgi or to **4** the nucleus. **5** Ectodomains of cell-surface PGs can be shedded by cleavage of matrix metalloproteinases (MMPs) and released in the ECM. **6** Sulfatases are extracellular sulfatases that can remodel the cell-surface and ECM by removing 6-O sulfate groups of HS/Hep chains. **7** Lyases can also be secreted to cleave GAG chains in the extracellular space. Created with Biorender.

Cell surface HSPGs have half-lives about 3-20 hours on the cell surface<sup>[120]</sup>. They are removed from the cell surface mainly by endocytosis prior to lysosomal degradation. The mechanisms involved in the endocytosis of HSPG appear to differ, whether they are attached to the cell

surface *via* a GPI-anchor or a transmembrane domain, but also depending on cell type. GPI-anchored PGs seem to be directly transferred to lysosomes and degraded within 30 minutes (**Figure 7.1**). In contrast, transmembrane HSPGs follow a stepwise degradation during endocytosis transfer to lysosomes, involving an endo- $\beta$ -glycosidase (heparanase) that cleaves HS chains in smaller fragments and sulfatases that cleave sulfate groups (**Figure 7.2**). CS/DS PGs follow a similar endocytic route<sup>[59]</sup>. However, several other mechanisms were reported such as the transfer of HSPGs to the Golgi for reutilization or to the nucleus to regulate cell proliferation<sup>[120]</sup> (**Figure 7.3-4**).

Matrix metalloproteinases (MMPs) cleave proteolytically the protein core of PGs, releasing them in the ECM<sup>[121]</sup> (**Figure 7.5**). This mechanism called “shedding” has been particularly studied for syndecans<sup>[122]</sup> but exist also for other PGs, such as TGF- $\beta$  type III receptor and its released ectodomain named betaglycan. Importantly, the growth of myeloma tumors *in vivo* is significantly stimulated by soluble syndecan-1. This stimulation, due to the shedding of syndecan-1, is further intensified by heparanase activity<sup>[58]</sup>.

Sulfatases catalyze the desulfation of GAGs or other sulfated compounds (**Figure 7.6**). In eukaryotes, several types of sulfatases exist and exhibit different properties. Among them, arylsulfatases (ARS) can be located in the Golgi, the ER, or in the lysosomes for GAG degradation. Lysosomal sulfatases targeting GAGs include N-acetylgalactosamine-4-sulfatase (ARSB, Uniprot P15848), N-sulfoglucosamine-3-sulfatase (ARSG, Uniprot Q96EG1), N-acetylglucosamine-6-sulfatase Glucosamine-6-sulfatase (G6S, Uniprot P15586), N-sulfoglucosamine sulfohydrolase (SGSH, Uniprot P51688), Glucuronate-2-sulfatase (ARSK, Uniprot Q6UWY0) and Iduronate 2-sulfatase (IDS, Uniprot P22304). It is worth noting that these sulfatases are only active at the non-reducing end of GAGs and probably act in a stepwise manner in concert with lyases to achieve the lysosomal degradation of GAGs. Other sulfatases can be secreted in the extracellular space and belong to the Sulfs family. In humans, HSulf1 and HSulf2 are the only identified members of this family and target 6-O sulfate groups of HS/Hep chains, especially trisulfated disaccharides HexA2S-GlcNS6S<sup>[123,124]</sup>. Interestingly, they are also the only eukaryotic sulfatases that exhibit an endosulfatase activity (intrachain, not only extremities). It was recently demonstrated that HSulf2 harbors a CS/DS chain, classifying it as a PG<sup>[125]</sup>. The activity of Sulfs is a unique post-synthetic mechanism that remodels the 6-O-sulfation patterns of cell surface and extracellular matrix HS, which modulates the signaling of several growth factors and morphogens such as Wnt, BMP and Sonic Hedgehog (SHh)<sup>[126]</sup>. Through these mechanisms, they constitute key regulators of tissue

development, in particular for neuronal and skeletal development. Additionally, they exhibit either pro- or anti-oncogenic properties in cancer<sup>[127]</sup>.

Lyase enzymes catalyze the cleavage of GAG glycosidic bonds, either intracellularly or in the extracellular environment. In humans, cells secrete heparanase which selectively cleaves HS chains, leading to the release of growth factors and chemokines bound to HSPGs on cell surfaces and in the ECM<sup>[128]</sup> (**Figure 7.7**). Likewise, hyaluronidase enzymes cleave both HA and CS chains into smaller fragments<sup>[129]</sup>. The release of high levels GAGs in solution, triggered by these lyase enzymes, is generally correlated with specific processes such as inflammation, sepsis and intoxication responses<sup>[130,131]</sup>. High levels of degraded soluble GAGs fragments but also PGs are considered as biomarkers of several diseases<sup>[132,133]</sup>.

### *I.B.5. Interactions with proteins and importance of sulfation*

#### *I.B.5.a. Functional view of GAG-protein interactions*

GAGs are negatively charged molecules, which enables the binding of proteins, growth factors, cytokines, and chemokines through electrostatic interactions<sup>[8,9,26]</sup>. The charge along the GAG chains varies locally, contributing to the specificity of the interactions with proteins. Upon binding, GAGs can trigger different mechanisms regulating the cellular response: organization and assembly of the ECM by interacting with extracellular components, sequestration and protection of protein ligands from degradation, establishment of morphogen gradients, and regulation of ligand-receptor binding by inducing ligand conformational change activating the protein function, or by forming complexes with cellular receptors (**Figure 8**).

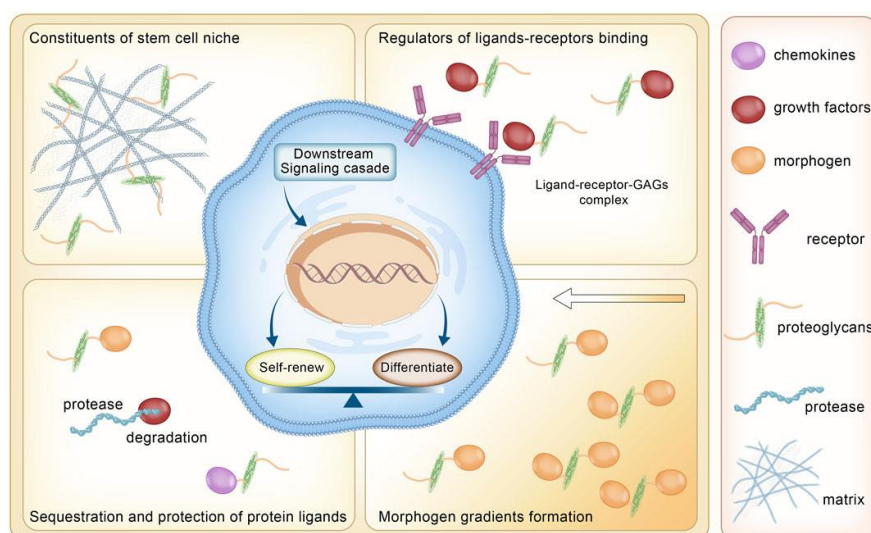


**Figure 8. PG functions regulating the cellular response**

Reproduced with permission under the terms of CC BY 4.0 licence<sup>[58]</sup>. Copyright 2021, Chen et al., published by Frontiers.

The most documented example of GAG effect on proteins is the role of Hep on the activation of AT III by inducing a conformational change of the protein<sup>[134]</sup>. There has been a global effort to investigate which sulfation motif of Hep has the highest affinity for AT III. It was found that the AT III bio-activation is highly specific of Hep pentasaccharide sequences featuring a central 3-O sulfated glucosamine (**Figure 9**)<sup>[135–137]</sup>. Compounds exhibiting this sulfation motif are therefore interesting for their anticoagulation properties.

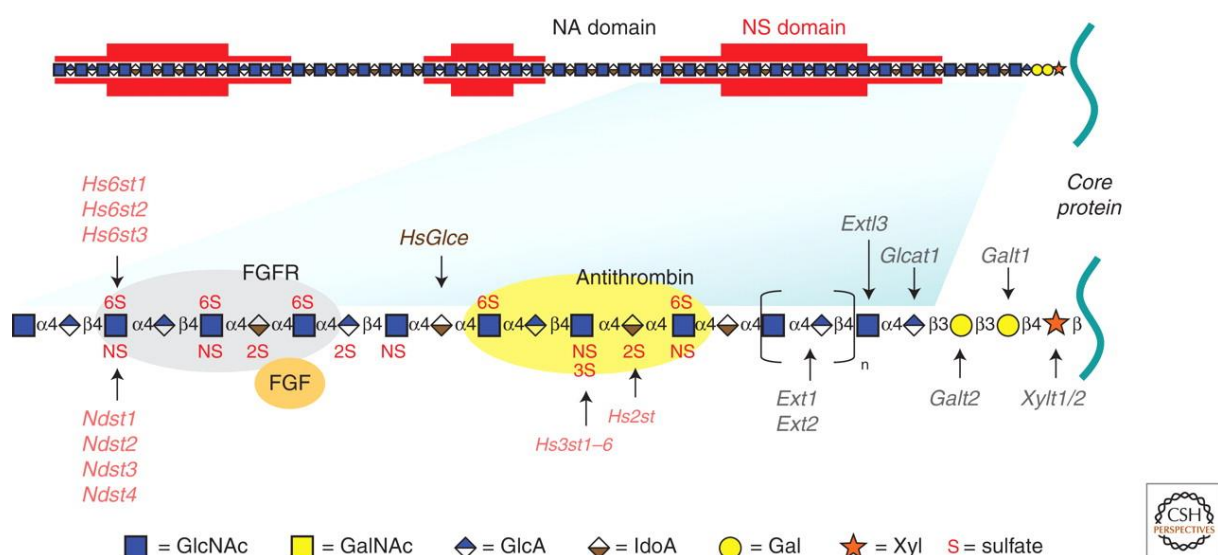


**Figure 9. Key HS sequences for specific interactions with proteins**

HS features specific sulfation patterns implicated in the high affinity interactions with AT III or for the formation of ligand-receptor-HS complex with FGF and FGF receptor. Reproduced from Sarrazin et al., 2011<sup>[72]</sup>.

Interactions of HS with members of the fibroblast growth factor (FGF) family, especially FGF1 and FGF2, have also been extensively studied. In 1991, two research groups independently showed that cell-surface HS is a co-receptor of FGF2 and is required for the growth factor biological activity<sup>[138,139]</sup>. Since then, extensive studies highlighted distinct structural features for the binding to these growth factors. The interaction between FGFs and HS requires saccharide motifs similar in size (5-6 sugar units) and saccharide content (need for GlcNS and IdoA,2S residues, **Figure 9**)<sup>[140,141]</sup>. However, 6-O-sulfates were found essential for binding to FGF1, but not necessary for the interaction with FGF2<sup>[142,143]</sup>. Surprisingly, studies highlighted different structural requirements for the promotion of FGF2 biological response, thereby providing the first evidence of an uncoupling between HS binding properties and ligand-promoting activities. Indeed the induction of FGF2 activity required longer saccharide fragments (10-12 sugar units) and the presence of 6-O-sulfates<sup>[144]</sup>. Resolution of the FGF/FGFR/HS complex structure by X-ray crystallography showed that 6-O-sulfates contributed to the stabilization of the ternary complex by establishing contacts with the FGFR<sup>[145]</sup>. Other studies provided further evidence of distinct structural requirements for the

binding and/or activation of other FGFs<sup>[126]</sup>. However, despite an increasing interest, the tremendous structural heterogeneity of GAGs and the lack of dedicated tools have constituted severe limitations that have hampered progress in the structural and functional characterization of GAGs and GAG/protein interactions<sup>[146]</sup>.

#### *I.B.5.b. Structural view of GAG-protein interactions*

Interactions between GAGs and proteins arise mainly from ionic interactions between the highly acidic sulfate groups and the basic side chains of arginine, lysine and, to a lesser extent, histidine<sup>[8]</sup>. Other interactions such as Van der Waals forces, hydrogen bonds and hydrophobic interactions with the carbohydrate backbone may also be involved. The pioneering study of Cardin and Weintraub formulated two consensus GAG-binding sequences known as [XBBXBX] and [XBBBXXBX], where **B** is a basic residue (Arg or Lys) and X is a non-charged residue<sup>[147]</sup>. Depending on the secondary structure of the protein, very few residues in these consensus sequences may actually participate in GAG binding<sup>[8]</sup>. GAG-binding sites are often found along one exposed face of a protein.

Molecular modeling indicated that when the [XBBXBX] sequence adopts a  $\beta$ -strand conformation, the basic amino acids align along one side of the  $\beta$ -strand, while the hydrophobic amino acids are oriented towards the interior of the protein core. Similarly, if the [XBBBXXBX] sequence is folded in an  $\alpha$ -helix, then the basic amino acids would be aligned on a specific side of the helix, mediating interactions with GAGs, while hydrophobic residues would be oriented towards the protein core (**Figure 10A**)<sup>[148]</sup>. In another study, Margalit *et al.* examined linear and contiguous protein binding sites known to interact with Hep. They observed that a ~20 Å distance between basic amino acids promotes the protein interaction with Hep (**Figure 10B**).

Two additional consensus sequences were proposed in other studies. First, by analysis of several GAG-binding proteins, the sequence [XBBXXBBBXXBBX] was proposed, where B represent a cationic residue (Arg, Lys, His) and X any other residue<sup>[149]</sup>. This led to the identification of the GAG-binding site in the protein von Willebrand factor. Then, the consensus sequence [TXXBXXTBXXXTBB] was proposed by Hileman and coworkers, where **T** defines a turn, **B** a basic amino acid (Arg, Lys) and X a hydrophobic residue<sup>[148]</sup>.

Not all GAG binding proteins contain binding sites that can be defined by linear contiguous sequences. AT III is known to contain a linear contiguous Hep-binding domain responsible for interaction with a specific Hep pentasaccharide binding site. Upon the folding of AT III,

additional remote basic residues (distant chain) are brought into close spatial proximity to participate in the interaction (**Figure 10C**).

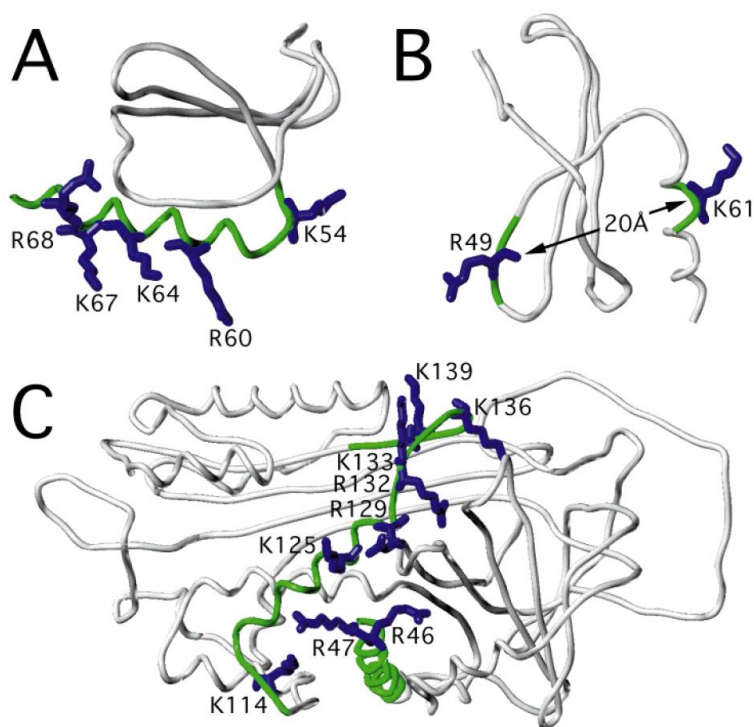


**Figure 10. Structures of GAG-binding sites present in proteins**

**A.** Linear XBBBXXBX sequence within an  $\alpha$ -helix of interleukin-8. Basic residues (blue) are oriented on one surface of the helix (green, residues 53–72). **B.** A linear motif of platelet factor-4 having two basic residues (blue) separated of a critical 20 Å linear distance, located on opposite surfaces (green, residues 48–50 and 60–62). **C.** Example of a higher order GAG-binding motif in AT III. The binding domain is comprised of two linearly contiguous domains (green, residues 46–65 and 113–140) brought spatially close through folding of the protein (white) with basic arginine and lysine residues (blue). Reproduced with permission<sup>[148]</sup>.

Overall, GAG binding sites are complex and often not conserved between proteins<sup>[8]</sup>. Moreover, there has been limited investigation into the influence of the structural variability of GAGs regarding their interactions with these consensus binding sequences. Historically, the exploration of protein-GAG interactions has primarily concentrated on the interactions with Hep or HS. Therefore, although the interactions of proteins with CS/DS can generally occur through the same consensus sequences with lower affinity, it is unclear whether proteins interacting specifically with other GAGs (CS, DS, KS or HA) feature distinct GAG binding sequences. Additionally, the role of specific sulfations in the GAG-protein interactions has only been investigated for few proteins. To facilitate these investigations for other proteins, methods for the synthesis of GAG compounds with defined structure and sulfation pattern are needed.



### *I.B.6.a. Specific desulfation*

Methods for specific desulfation of sulfated carbohydrates can use different chemistry strategies, including acid-catalyzed desulfation, solvolytic desulfation, alkali-catalyzed desulfation, and desulfation mediated by silylating reagents<sup>[13,150–152]</sup>.

For Hep and HS, chemical treatment for specific 2-O, 6-O, or N-desulfation have been developed and are now commonly used<sup>[153–159]</sup>. N-desulfation is usually performed by solvolytic desulfation with dimethyl sulfoxide containing methanol, without depolymerization of HS chains and very low O-desulfation<sup>[160]</sup>. Specific 2-O desulfation is generally achieved using sodium hydroxide treatment<sup>[156]</sup>. Under this treatment, Hep other sulfation motifs were not altered. However its chains were affected by depolymerization with a 2.5 kDa reduction, starting from an initial mean molecular weight of 9 kDa<sup>[156]</sup>. The 6-O specific desulfation is generally performed using N-methyl-N-(trimethylsilyl)-trifluoro acetamide (MTSTFA) silylating reagent allowing control of the desulfation degree by the temperature and reaction time<sup>[161,162]</sup>. For complete 6-O desulfation of Hep, a loss of ~20% of 2-O sulfate groups was reported but without any other structural alteration or depolymerization<sup>[163]</sup>. In contrast, the specific removal of 3-O sulfate groups cannot be achieved without affecting other sulfation sites. Lyophilization of Hep under extreme alkaline conditions induce selective loss of 2-O and 3-O sulfates, leaving intact 6-O and N-sulfation<sup>[164]</sup>. These strategies are adapted to study the overall importance of one type of sulfation, but do not allow the study of precise sulfation sequences. Another strategy for the selective desulfation of HS is to perform digestion of HS or Hep by sulfatase enzymes<sup>[123]</sup>. Human Sulf1 and Sulf2 (HSulf1 and HSulf2) are the only known extracellular post-synthetic HS modifying enzyme with a substrate specificity for 6-O sulfation motifs. More precisely, it seems that HSulf2 essentially targets HexA(2S)-GlcNS(6S) trisulfated disaccharides, which are then converted into HexA(2S)-GlcNS disaccharides. HSulf2 was shown to reduce dramatically the FGF1/FGF2-induced proliferation of FGFR1-IIIc-transfected BaF32 cells<sup>[124]</sup>. This result supports further the previously reported requirement of HS 6-O sulfation for promoting the bioactivity of these growth factors<sup>[144,165]</sup>. In addition, the authors showed that HSulf2 differentially regulated FGF1 and FGF2, thereby highlighting the involvement of specific 6-O sulfation pattern in these mechanisms<sup>[124]</sup> The approach of enzymatic desulfation is limited by the lack of sulfatases with other substrate specificities. The discovery of other enzymes may trigger the development of new strategies for preparation of GAGs compounds.

Chondroitin, the non-sulfated version of CS can be obtained from the reaction of CS with acidic methanol<sup>[166,167]</sup>, or in dimethyl sulfoxide (DMSO) with a small amount of methanol<sup>[168]</sup>. These desulfation methods can also be used for other GAGs such as DS or KS<sup>[157]</sup>. For CS, regioselective methods for 4-O and 6-O desulfation have been established<sup>[169]</sup>. The 6-O desulfated CS can be obtained with MTSTFA agent without any depolymerization. A DMSO/methanol-based method was recently reported as an efficient regioselective method for the preparation of 4-O desulfated CS, albeit with some depolymerization. Surprisingly, the conditions used are very similar to the method of Nagasawa *et al.* for the preparation of chondroitin *via* global 4-O and 6-O desulfation of CS<sup>[168]</sup>, suggesting that minor protocol modifications may affect the reaction.

#### *I.B.6.b. Specific sulfation*

Another approach for studying sulfation of GAGs is to perform sulfation of non-sulfated precursors such as HA, heparosan (non-sulfated HS) or chondroitin (non-sulfated CS).

For CS, the use of SO<sub>3</sub><sup>-</sup>-pyridine complex in dimethylformamide (DMF) at 0 °C, allows regioselective sulfation at the C-6 hydroxyl of the GalNAc with limited sulfation at the C-2 hydroxyl of the GlcA<sup>[170,171]</sup>.

For HS, chemically sulfated GAGs can be obtained from sulfation of heparosan. O-sulfation is not effective prior N-sulfation of the heparosan chain. First, heparosan must be N-deacetylated with NaOH before N-sulfation in Na<sub>2</sub>CO<sub>3</sub> at 40-50 °C with SO<sub>3</sub><sup>-</sup>-pyridine complex or SO<sub>3</sub><sup>-</sup>-trimethylamine complex. The N-sulfated HS can further be O-sulfated with regioselective sulfation at the C-6 hydroxyl of the GlcNS with some sulfation at the C-2 or C-3 hydroxyls of the GlcA<sup>[150]</sup>. Several studies have used the same approach for sulfation of HA with apparently similar regioselectivity of the C-6 hydroxyl of the GlcNAc followed by sulfation at the C-4 of the GlcNAc and at the C-2 and C-3 of the GlcA<sup>[172-174]</sup>.

#### *I.B.6.c. Cell-based biosynthesis*

Due to the complexity of GAG structures, recent research has focused on producing GAGs using genetically modified cells to avoid complex chemistry or chemo-enzymatic steps. After a first success to genetically modify the production of GAGs in CHO-K1 cells by Dr Jeffrey Esko in the 1980s, the way was open to constitute a larger cell library with specific knock-in (KI) and knock-out (KO) of GAG biosynthesis enzymes. Such a library called the GAGome has been recently developed by Chen *et al.* and comprises various cell lines with distinct CS/DS and HS biosynthetic capabilities<sup>[175]</sup>. In total, 28 different genes of biosynthesis enzymes have

been targeted to generate cell-lines displaying unique GAG structural features. The recovery of GAGs from the cell lysates is possible but the purity of the samples obtained is certainly limited by undesired components. Additionally, GAG-biosynthesis enzymes unlikely catalyze structural modifications on every available substrates, yielding intra-variation of GAG chains with enzyme-processed and -unprocessed domains. However, this genetic approach is very versatile (Table 2) and hold huge potential because it enables to perform directly cell-based assays, or to synthesize entire PGs and xyloside-primed GAG chains that can be used in microarrays.

#### *I.B.6.d. Preparation of well-defined GAG oligosaccharides*

Three other methods are more adapted to the synthesis of defined oligosaccharides with control of length and sulfation patterns: the purification, the chemo-enzymatic synthesis and the chemical synthesis. Arising from the development of these methods, commercial GAG compound libraries constitute an alternative option.

##### *Purification*

GAGs extracted from natural sources have a large structural diversity and are by definition physiologically relevant. Natural GAGs can be directly used as they stand, but they will exhibit a strong level of structural heterogeneity. Alternatively, libraries of oligosaccharides with defined size and charges can be generated using a combination of different depolymerization and purification strategies. For this, a first step of digestion is performed to fragment the GAG chains in smallest oligosaccharides. Different enzymes can be used to obtain different fragment structures. As an example, the use of Heparinase III enzyme will cleave HS/Hep mostly in the low-sulfated NAc domains, yielding highly sulfated fragments from the NS domains. GAG samples are then purified by size-exclusion chromatography to separate them by their polymerization degree (dp2, dp4...). The collected oligosaccharides can be further separated according to charge by several chromatography techniques, such as anion-exchange chromatography or reverse-phase ion pair liquid chromatography, to isolate fractions with distinct sulfation patterns. These purification strategies have been already reviewed<sup>[176-178]</sup>. However, due to the charge heterogeneity of related oligosaccharides, it is likely to collect fractions with co-eluting compounds. To improve the resolution of separation, columns modified with cetyltrimethylammonium salts (CTA-SAX) were used in combination with volatile ammonium bicarbonate salt to distinguish Hep hexasaccharides isomeric structures, which was not possible with traditional methods<sup>[179]</sup>. Another advantage is that the volatile ammonium salt allows evaporation of the produced samples instead of a dialysis desalting step,

reducing considerable sample loss and enabling more effective subsequent mass spectrometry analysis. Polyacrylamide Gel Electrophoresis (PAGE) has also shown the ability to separate compounds that cannot be differentiated with traditional chromatography methods. Oligosaccharide co-eluting species obtained with strong-anion exchange high-performance liquid chromatography could be further separated with PAGE to obtain pure compounds<sup>[180]</sup>. The preparation of oligosaccharide libraries using purification methods is time-consuming and requires some expertise, but it is more straightforward and accessible compared to the other oligosaccharide synthesis methods (Table 2). However, the control of oligosaccharide structures is limited to naturally occurring structures in GAG extracts and by the limitation to separate closely related structures with chromatography technique, especially challenging for large oligosaccharides. The quantities obtained depend on the amount of the starting material, but are mainly limited by the scale-up capabilities of preparative chromatography<sup>[181]</sup>. Another general limitation is that selective depolymerization enzymes are available for HS but not for CS. It is therefore more complex to prepare CS oligosaccharide libraries with purification methods.

#### *Chemo-enzymatic synthesis*

The chemo-enzymatic synthesis combines chemical reactions with the use of natural GAG-biosynthesis enzymes to elongate the oligosaccharide chain or for sulfate transfer. With the unique capabilities of these enzymes, this approach circumvents the technical difficulties of chemical synthesis (see next section) such as regio- and stereo-selectivity, and prevents numerous steps of group protection and de-protection for the transfer of sulfate groups at specific positions.

The action and functional specificities of a large number of GAG biosynthesis enzymes are well characterized, facilitating their use for the production of defined oligosaccharides. Elongation enzymes catalyze the transfer of monosaccharide compounds with the adequate glycosidic linkage. These enzymes rely on the presence of uridine diphosphate (UDP) sugar donors such as UDP-GlcNAc, UDP-GlcA, UDP-Glc, UDP-Gal or UDP-GalNAc. Sulfation enzymes transfer sulfate groups at specific position with the assistance of the 3'-phosphoadenosine-5'-phosphosulfate (PAPS) sulfate donor. The exceptional abilities of these various enzymes reduce considerably the number of reaction steps needed for the oligosaccharide synthesis. The successive reactions and their order of execution must be carefully designed to be compatible with the substrate specificities of the enzymes and to improve the reactions yields. Various reviews about chemo-enzymatic synthesis provide more

in-depth information about the different aspects of the approach<sup>[182–185]</sup>. The chemo-enzymatic strategy is complex and needs a strong expertise and knowledge in the production of recombinant biosynthesis enzymes, their roles and substrate specificities. The preparation of defined oligosaccharides requires the availability to various enzymes, and a large quantity of various sugar and sulfate donors, which represents a considerable initial investment. Chemo-enzymatic synthesis of oligosaccharides have a good performance regarding the purity and the control of oligosaccharide structure, but it is complex and time-consuming. Quantities obtained with this method are compatible for translation to *in vivo* assays and therefore account for its versatility potential in Table 2. The enzymatic approach may also be employed for sulfation of large GAG polysaccharide chains starting from non-sulfated heparosan or chondroitin, or to increase specifically the content of some sulfation types of natural GAG samples<sup>[186,187]</sup>.

#### *Chemical synthesis*

The chemical synthesis of GAG oligosaccharides requires the use of monosaccharides or disaccharides building blocks with protection groups in well-defined positions. The chain elongation is achieved by assembling these building blocks controlling the stereochemistry of the glycosidic bonds formation. The sulfation of the oligosaccharides at specific positions is then performed after initial de-protection of the targeted groups. The introduction of HexA moieties is an additional difficulty due to their low reactivity. The chemical synthesis can be carried-out either in solution-phase or on-resin (automated solid-phase synthesis) to facilitate the removal of side products after each reaction. More details of the different strategies of chemical GAG oligosaccharide synthesis have been reviewed elsewhere<sup>[188–190]</sup>. The control of the different steps of the process is very challenging and requires strong chemistry expertise to design properly the successive reactions. Only a few research groups have the equipment and skills to achieve the chemical synthesis of large oligosaccharides libraries. However, the purity and the structural control of the chemically synthesized oligosaccharides are excellent<sup>[191]</sup>. Similarly, as chemo-enzymatic synthesis, quantities obtained can be important and are therefore compatible with *in vivo* assays.

#### *Commercial GAG-oligosaccharide libraries*

Thanks to the development of the above-mentioned techniques, various GAG compounds and oligosaccharides of defined length and sulfation pattern are available commercially (Biosynth, Creative Biolabs, Glycan Therapeutics, Iduron...). Since most compounds commercially available are produced with chemical, chemo-enzymatic and to a lesser extent purification approaches, commercial libraries obviously facilitate strongly the access to defined

oligosaccharide structures with high purity. Although the structural diversity is limited to the available compounds, the number of available structures is increasing with time and some companies provide custom synthesis service that may circumvent this problem. Furthermore, the cost of oligosaccharide compounds is relatively low compared to the time and effort required for self-preparation of oligosaccharide libraries.

	Simplicity	Time saving	Purity	Control of GAG structure	Versatility
Chemical desulfation	++	++	-	-	-
Chemical sulfation	++	++	-	-	-
Cell-based biosynthesis	-	-	-	+	++
Chemical synthesis	-	-	+++	+++	+
Chemo-enzymatic synthesis	-	-	+++	+++	+
Purification	+/-	+/-	+	++	+/-
Commercial libraries	+++	+++	+++	+	-

**Table 2. Comparison of methods for production of defined GAG compounds**

Comparison is based on various criteria: simplicity to establish the technique in your own laboratory, time saving characteristics, purity of the produced materials and the ability to control precisely the structure of the GAG materials produced regarding their sulfation and length. The methods are also compared upon a versatility criterion that represents their potential of use in other experimental contexts, such as cell-based assays, entire PG synthesis or in vivo assays. The two methods with a light brown font correspond to rather simple chemical methods generally used for sulfation modification of large GAG chains. The cell-based biosynthesis method, as the only genetics-based method, is represented with a blue font. The three methods with a purple font are particularly adapted for the synthesis of GAG-oligosaccharides. Commercial libraries, represented with a black font, arose from the development of the other methods.

## I.C. Bone Morphogenetic proteins (BMPs) and osteogenesis

### I.C.1. BMPs belong to the TGF- $\beta$ superfamily

Bone morphogenetic proteins (BMPs) are protein members of the vast transforming growth factor beta (TGF- $\beta$ ) superfamily. The TGF- $\beta$  superfamily comprises 33 identified protein members in humans, involved in the control of development, differentiation, proliferation and tissue homeostasis<sup>[192]</sup>. As depicted in **Figure 12**, the TGF- $\beta$  superfamily can be classified into three different subfamilies: the TGF- $\beta$  subgroup (three isoforms: TGF- $\beta$ 1, TGF- $\beta$ 2, and TGF- $\beta$ 3), the subgroup composed of BMPs and growth differentiation factors (GDFs), the group composed of activins, inhibins and anti-Müllerian hormone (AMH, also termed MIS for Müllerian-inhibiting substance). Finally, there is a last group composed of glial cell line-derived neurotrophic factors (GDNFs), considered as distant members of the family<sup>[193,194]</sup>. Due to the evolution of naming conventions, the initial nomenclature for each growth factor may not always accurately reflect their structural homology, which could lead to some confusion. A

striking example is BMP1, which was initially associated with the TGF- $\beta$  superfamily and has been subsequently reclassified as a member of the astacin family of metalloproteinases<sup>[195]</sup>. Members of the TGF- $\beta$  superfamily are structurally related and all comprise a central “cystine knot” motif, which stabilizes the protein structure<sup>[196,197]</sup>. Moreover, except for GDNFs, all proteins signal through similar mechanisms involving their interaction with a receptor complex, composed of two type I, and two type II receptors (**section I.C.5**).

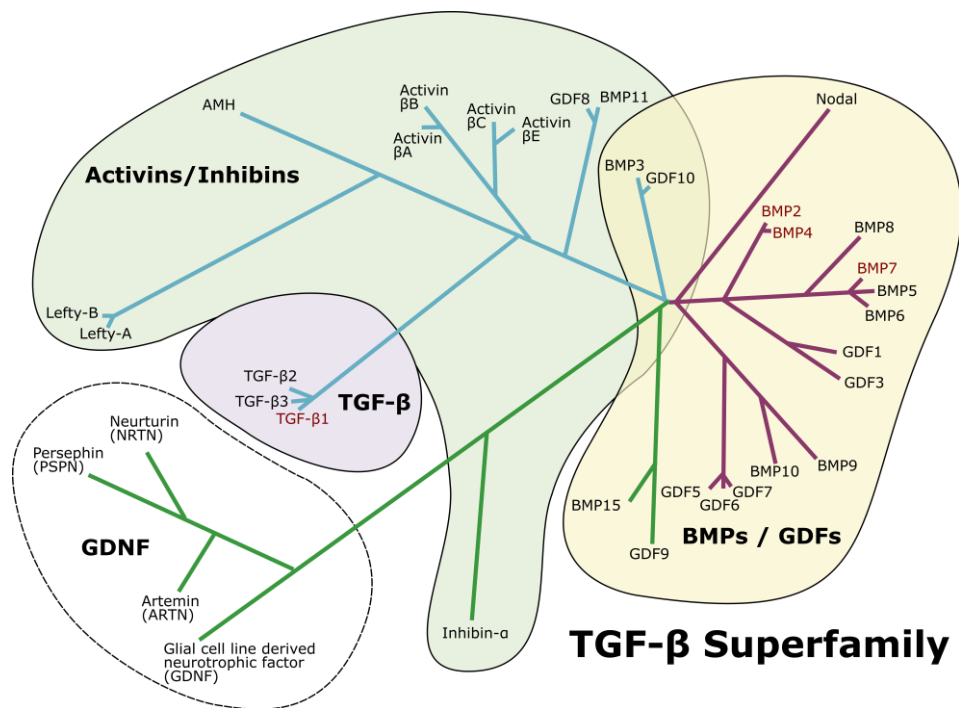


**Figure 12. Classification of the TGF- $\beta$  superfamily**

Protein members of the TGF- $\beta$  superfamily are classified in four different subgroups: TGF- $\beta$ , BMP/GDF, Activins/Inhibins/AMH, and the distant GDNF. Inspired from <sup>[198]</sup>.

### I.C.2. The BMP family

BMPs were initially discovered in the 1960s, when Dr. Urist identified a substance responsible for the induction of bone formation<sup>[199]</sup>. Few years later, he introduced the name of BMP to describe the discovered proteins<sup>[200]</sup>. In 1988, two BMPs were cloned for the first time. Termed at this time BMP2A and BMP3, these proteins were recognized as members of the TGF- $\beta$  superfamily<sup>[201]</sup>. Since then, more than a dozen members of the BMP family have been identified in humans<sup>[202]</sup>.

The homology in the polypeptide sequences of BMPs allows refining their classification within different subgroups. This classification is based on phylogenetic trees established by different studies<sup>[203,204]</sup>. First, a group composed of BMP2 and BMP4 arose from a single ancestral gene and exhibits more than 80 % homology<sup>[205]</sup>. The *decapentaplegic* BMP-gene identified in *Drosophila* is also related to this family, sharing more than 75 % identity with the human

BMP2/4<sup>[206]</sup>. A second group is composed of BMP5, BMP6, BMP7 (also termed OP-1), and BMP8 (also termed OP-2)<sup>[207]</sup>. Two BMP-genes in drosophila are also linked to this family: first, the gene *screw* showing similarities to human BMP5/6/7/8, and secondly, *glass bottom boat* (gbb or 60A), the orthologue of BMP7 sharing more than 70 % homology with human BMP5/6/7<sup>[206]</sup>. A third group composed of BMP9 and BMP10 group exhibits a good degree of similarity, with 65% amino acid homology<sup>[208]</sup>. Finally, additional proteins within the BMP family can be classified into distinct groups, including GDF1/3 group, GDF5/6/7 group (also known as BMP12/13/14), and GDF9/15, BMP15 and Nodal group. A subgroup of the TGF- $\beta$  superfamily composed of BMP3 and GDF10 is inconsistently classified, either in the activin/inhibin family or in the BMP family. Classification differences observed in various studies may arise from the use of different polypeptide sequence (prodomain included or not) to perform phylogenetic analysis. The most extensively studied members of the BMP family include BMP2, BMP4, BMP6, BMP7, BMP9<sup>[192]</sup>.

### *I.C.3. The functional diversity of BMPs*

As suggested by their name, BMPs play a crucial role in bone development. The osteogenic role of 14 human members of the BMP family was previously compared with C3H10T1/2, C2C12 and TE-85 cells *in vitro*, and *in vivo* using an athymic mice model<sup>[209,210]</sup>. These findings demonstrated the important osteogenic role of BMP2, 6, and 9 and to a lesser extent, of BMP4 and 7. In contrast, BMP3 was identified as negative modulator of osteogenic differentiation, and acting as an antagonist of BMP2 signaling<sup>[211]</sup>. This mechanism was suggested to occur through signaling *via* distinct BMP cell receptors (activin receptors). Intriguingly, within the study of Kang *et al.*, BMP9 was the only BMP member inducing bone differentiation that was not inhibited by BMP3, in contrast to BMP2, 6 and 7<sup>[210]</sup>. Although BMP5 has been scarcely studied, it was reported to contribute to sternal and rib development, acting in synergy with GDF5<sup>[212,213]</sup>. Despite the osteogenic potential of other BMPs, BMP2 and 7 are the most studied for bone repair applications, since they have both been approved by the FDA<sup>[214]</sup>. The use of BMP2 is approved for spine fusion, open tibial fractures and craniomaxillofacial surgery applications, and BMP2 has also been used “off-label” for treating large segmental defects<sup>[215]</sup>. In contrast, the approved BMP7 is no longer used, since its production was discontinued by the manufacturer.

As shown in **Figure 13**, although the term BMP refers only to bone tissues, a striking particularity of BMPs is their involvement in a wide variety of functions and in many different organs. It was thus suggested by Obradovic Wagner and coworkers that BMPs should be called

instead body morphogenetic proteins<sup>[216]</sup>. Since the roles of BMPs in different organs is too broad to be covered in this thesis, only few key aspects are discussed here to provide a general overview of their functional diversity. Several reviews on the subject may provide additional information to the interested reader<sup>[202–204]</sup>.

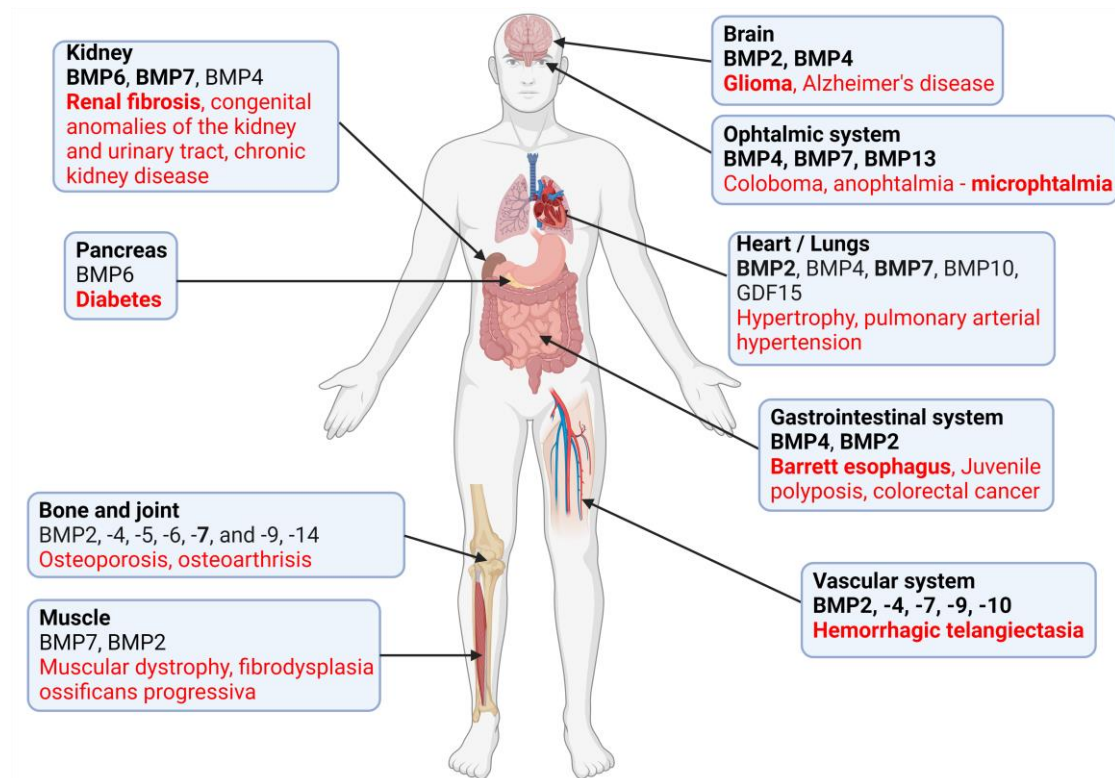


**Figure 13. Functional diversity of BMPs and implications in diseases**

Various organs in which BMPs are involved and the related disorders caused by their dysregulation. Alterations of BMP activity in these organs can lead to pathologies, depicted by the red markings in the diagram. Created in BioRender.com, adapted with permission from previous works<sup>[202,216,217]</sup>.

BMP2 is involved throughout the whole body. Besides its roles in bone tissues, it has been implicated in cartilage, brain, heart, muscle, pulmonary artery, and gastrointestinal tract<sup>[216]</sup>. BMP2 has a crucial role in chondrocyte proliferation and maturation during endochondral bone development<sup>[218]</sup> and appears to be connected to cartilage remodeling and osteoarthritis disease<sup>[219,220]</sup>. Additionally, BMP2 contributes to angiogenesis, as reported with human endothelial progenitor cells<sup>[221]</sup>. In the heart, BMP2 has an effect in the regulation of cardiomyocyte contractility<sup>[222]</sup>. In the brain, the neurogenesis is controlled by inhibition of BMP2/4 signaling mediated by histone deacetylases<sup>[223]</sup>. In line with this, the aberrant expression of BMP2 in the brain was correlated with poor prognosis for human glioma patients<sup>[224]</sup>. Furthermore, mutations in BMP2 are responsible to the brachydactyly type A2 disease (“short finger” disease), associated to congenital limb malformation<sup>[204]</sup>.

BMP4 is reported to be upregulated in the gastrointestinal system, where it has an essential role in the development of Barrett esophagus (BE) disease<sup>[225]</sup>. The selective inhibition of BMP2 and BMP4 was reported to repress the development of BE<sup>[226]</sup>. Genetic mutation of BMP4 is responsible for microphthalmia disease associated to eye, brain and digital anomalies<sup>[227]</sup>

BMP6 is highly expressed in the kidney, adipose tissues, and female tissues such as ovary and placenta (source: Human protein atlas). It appears to be very important for iron metabolism and for the regulation of hepcidin expression<sup>[228,229]</sup>. Its role in the kidney seems to prevent renal fibrosis<sup>[230,231]</sup>. BMP6 also was studied for its promoting role in female fertility<sup>[232,233]</sup>. Recently, it was reported that BMP6 also has a role in glucose homeostasis, improving the glycaemia in type 2 diabetes<sup>[234]</sup>.

BMP7 gene is abundantly expressed in human kidney and heart<sup>[235]</sup>. The protein was reported to be essential during the mammalian development, especially for kidneys and eyes<sup>[236]</sup>. Furthermore, BMP7 is important in skeletal development, as evidenced by the presence of skeletal patterning defects in the rib cage, skull, and hind limbs of BMP7-deficient mice.

BMP8 has a demonstrated role in spermatogenesis, while BMP12 is needed for seminal vesicle development and tenocyte differentiation<sup>[202,237]</sup>. BMP13 plays a modulatory role in the eyes development, and BMP15 is classically associated with ovarian function<sup>[202]</sup>.

BMP9 and BMP10 are particularly associated with angiogenesis. They have been proposed as crucial circulating factors for the adulthood endothelium quiescence<sup>[238]</sup>. The balance between pro- and anti-angiogenic factors is essential to maintain the endothelium quiescence. While vascular endothelial growth factor (VEGF) promotes endothelial proliferation, BMP9 and 10 are necessary to stabilize the newly formed vessels<sup>[239]</sup>. Interestingly, BMP9 mutations have recently been linked to a vascular anomaly syndrome that has phenotypic similarities with hemorrhagic telangiectasia (HHT), a disorder linked to mutations in a BMP9 specific cell receptor<sup>[240]</sup>. It appears that BMP2, 4 and 7 have pro- and antiangiogenic roles while BMP9 and 10 have anti-angiogenic roles instead<sup>[241]</sup>.

Many BMPs have also been linked to adipose tissues, including the different subgroups BMP2/4, BMP9/10, BMP5/6/7/8, and BMP3<sup>[242]</sup>.

#### *I.C.4. Biosynthesis and structure of BMPs*

BMPs, as other members of the TGF- $\beta$  superfamily are synthesized in the endoplasmic reticulum as a precursor containing a signal peptide, a large prodomain of 200 to 300 residues and a mature signaling domain of about 115 residues (**Figure 14**)<sup>[243]</sup>. After removal of the

signal peptide, the precursor is further processed through furin protease cleavage at basic residues, thus separating the prodomain from the mature signaling polypeptide, which remain associated through non-covalent interactions. Subsequently, glycosylation and disulfide-linked dimerization of the mature polypeptides lead to the mature homodimeric or heterodimeric complexes<sup>[244]</sup>.

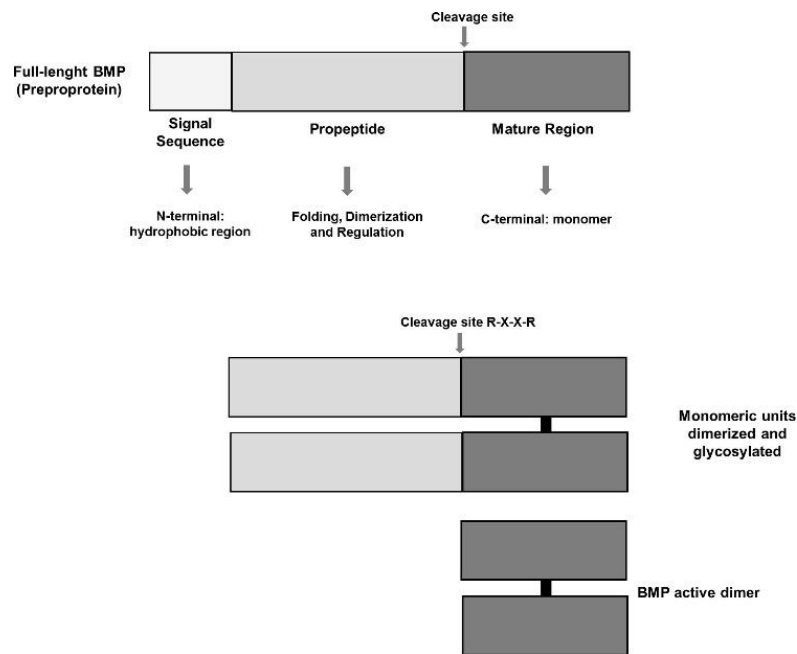


**Figure 14. Schematic representation of BMP biosynthesis and maturation**

Full-length BMP pre-pro-protein includes a signal peptide at the N-terminal domain for its secretion, a long prodomain (or propeptide), and a C-terminal mature region responsible for signaling. After release of the signal peptide, dimerization and glycosylation take place, prior to cleavage of the prodomain, and secretion. Reproduced with permission<sup>[245]</sup>.

While the association of TGF- $\beta$  proteins with their prodomains have been well-studied, very little is known about the interactions of BMPs and their prodomains<sup>[243,246]</sup>. For the majority of BMPs, whether they are secreted with or without their prodomain is not known. Some studies reported that BMP7 and BMP9 are naturally secreted in the ECM with their prodomains, which mediate their interaction with ECM components such as fibrillin microfibrils<sup>[247,248]</sup>. Their prodomains however do not block their bioactivity, in contrast to GDF-11 and myostatin members of the TGF- $\beta$  superfamily which are inactive when associated with their prodomains<sup>[246]</sup>. Moreover, it was demonstrated that the interaction of prodomain-BMP7 or prodomain-BMP9 with fibrillin modified their conformation into an inactive form<sup>[249]</sup>. Alternatively, their interactions with Hep/HS spatially concentrate the complexes into a bioactive form. Another finding highlighted that BMP cell receptors compete with and displace the BMP7 prodomain to bind the BMP7 protein<sup>[250]</sup>. For BMP2, the interaction with its prodomains appears to be significantly less stable than for other BMPs<sup>[248]</sup>, which suggest that

studying BMP2 bioactivity in absence of its prodomain may be still physiologically relevant. The prodomain of BMP2 appears to be involved in the secretion of the mature part<sup>[251]</sup> and it also alters the signaling by modulating the ability of the mature part to interact with the receptors<sup>[252]</sup>.

BMPs have been mostly characterized without their prodomains, as homodimers or heterodimers formed by a single disulfide-bridge within the mature polypeptide chains<sup>[197,253]</sup>. Most studies focus on homodimers assuming these are physiologically formed, but few evidence suggest that natural secretion as heterodimers also occurs<sup>[254–256]</sup>. In particular, it was shown that both BMP2/BMP7 heterodimers and BMP2 and BMP7 homodimers are expressed in *zebrafish*, but that only the heterodimer is able to induce BMP signaling in the early embryo<sup>[257]</sup>.

The structures of mature BMP homodimers have been well characterized. In particular, the structures of BMP2, 3, 6, 7 and 9 have been determined by X-ray crystallography<sup>[253,258–261]</sup>. The mature BMP monomers comprise seven cysteine residues, with six forming three intramolecular disulfide bonds. The remaining seventh cysteine residue is involved in the dimerization with another BMP monomer through a covalent disulfide bond, resulting in a biologically active dimeric ligand for BMP receptor activation<sup>[262]</sup>.

BMPs are often described as a “butterfly-shaped” dimer, as illustrated by the structure of BMP2 in **Figure 15A**. Each monomer is formed by two antiparallel  $\beta$ -sheets and a four-turn  $\alpha$ -helix perpendicular to the strands. This folding structure has also been compared to two hands joined palm to palm, with the  $\beta$ -sheets corresponding to “fingers” 1 and 2, the  $\alpha$ -helix and the dimer interface forming the “palm”, and the N-terminus described as “thumb”. At the cell surface, BMPs interact with a tetrameric complex formed of two type I and two type II kinase receptors. The binding sites for the receptors are highlighted in **Figure 15B**.

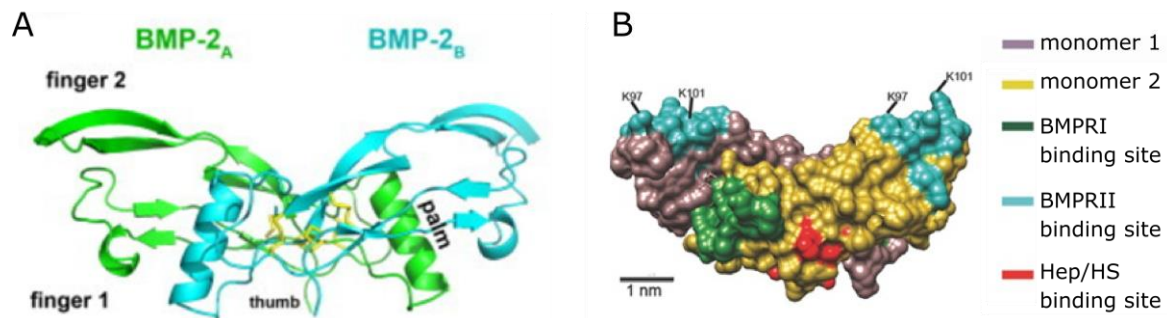


**Figure 15. Structural representations of the BMP2 homodimer protein**

**A.** Ribbon representation of BMP2 dimer with each monomer represented in green and blue. Disulfide bridges are represented in yellow. The denoted “thumb” part corresponds to the N-terminal domains of each monomer. Reproduced with permission<sup>[263]</sup>. **B.** Spacing-filling sphere model representation of BMP2 dimer, colored by monomer units and domains for BMP receptors and GAG (annotated here Hep/HS) binding sites. Reproduced with permission<sup>[264]</sup>.

To focus on BMP2, it is synthesized as a pre-pro-peptide chain of 396 amino acids with an N-terminal signal peptide of 23 amino acids (1-23) and a long prodomain (amino acids 24-282). It contains five glycosylation sites, four of which are in the prodomain sequence, and the last one (Asn338) is located on the mature chain. The mature monomer chain is composed of 114 amino acids, yielding a dimer of 26 kDa with an isoelectric point of  $8.2 \pm 0.4$ . Therefore, BMP2 is positively charged at physiological pH, which enables its binding to negatively charged GAGs. The binding of BMP2 of GAGs is believed to occur mainly through its N-terminal domain, termed “thumb” domain in **Figure 15A** and corresponding to the amino acids colored in red in **Figure 15B** (Hep/HS binding site). The structural details about the interaction between BMP2 and GAGs are described in the **section I.D.1**.

#### *I.C.5. BMP signaling and osteogenic differentiation*

As previously mentioned, BMPs possess binding sites mediating their interaction with cell membrane receptors. Upon the interaction of the dimeric BMP ligand with a tetrameric complex composed of two type I and two type II serine/threonine kinase receptors, the BMP signaling cascade is triggered (**Figure 16A**), of which the key steps are described below. The interaction between BMP and its receptors leads to the activation by phosphorylation of the type I receptors, which then bind, phosphorylate and activate a group of transcription factors proteins known as R-SMADs, belonging to the Mothers against decapentaplegic (SMAD) family. The R-SMADs recruited in the BMP pathway by type I receptors consist mainly in SMAD1, SMAD5 and SMAD9 (also referred to as SMAD8). Upon phosphorylation in the C-terminus domain, these factors hetero-oligomerize with the common mediator SMAD4 (Co-SMAD), often as a trimer. The constituted complex next translocates into the nucleus, where it associates to DNA with co-factors to regulate the expression of BMP responsive genes. Through this

signaling, the exposition of mesenchymal stem cells to potent osteogenic BMPs such as BMP2 can drive their differentiation toward the osteoblast lineage (**Figure 16B**). This is achieved by suppressing the adipogenic, myogenic, chondrogenic and other related transcription factors, while inducing the expression of osteogenic transcription factors RUNX2 and Osterix. This leads to the cell transition into an immature osteoblast, which expresses alkaline phosphatase and synthesizes type I collagen. Differentiation to the non-proliferating mature osteoblast that actively mineralizes bone matrix is dependent on the transcription factor Osterix. Matrix maturation is associated with increased expression of alkaline phosphatase, osteocalcin, osteopontin, and bone sialoprotein. Mineralization of bone is completed by the incorporation of hydroxyapatite into the matrix along with the differentiation into osteocyte.

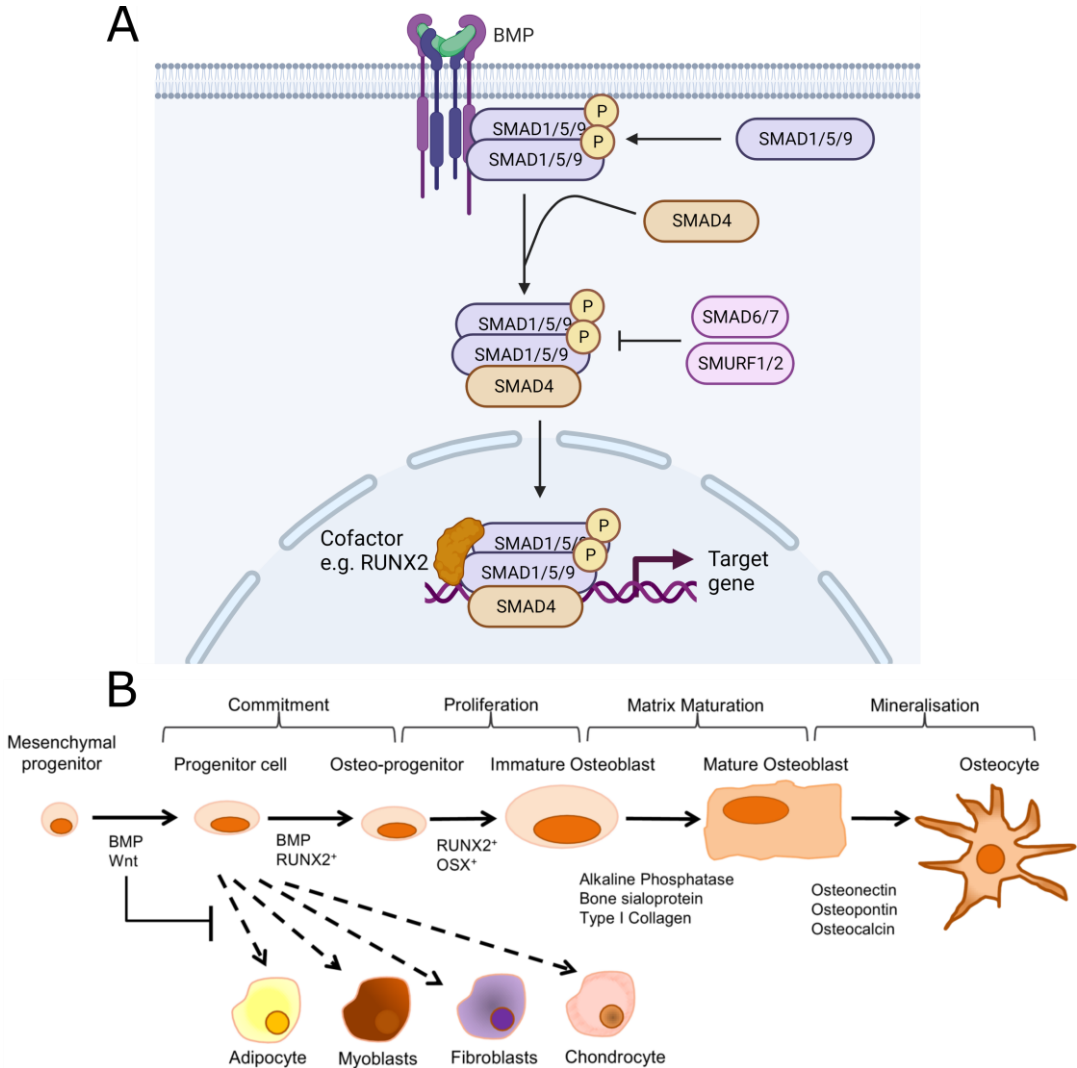


**Figure 16. BMP signaling via SMAD pathway and osteogenic differentiation**  
**A.** Schematic representation of BMP signaling via the canonical SMAD pathway. Created in BioRender.com. **B.** Osteogenic differentiation of mesenchymal progenitors triggered by BMPs or other osteogenic factors such as Wnt. Reproduced with permission<sup>[265]</sup>.

### *I.C.5.a. BMP cell-surface receptors*

In humans, four type-I BMP receptors (BMPR) have been identified, namely ALK1 (Activin receptor-like kinase 1), ALK2 (or Activin A receptor type I, ACVR1), ALK3 (or BMPR type IA, BMPR-IA), ALK6 (or BMPR type IB, BMPR-IB). The type I receptors comprise key cytoplasmic structural domains essential for their function. A glycine-serine rich region termed GS domain is highly conserved and constitutes the phosphorylation site activated by type II receptors and mediating the recruitment of R-SMADs. A L45-loop within the serine/threonine kinase domain is critical regarding this event, mediating the binding selectivity and phosphorylation of R-SMADs. It has been reported in particular that swapping the L-45 domain of different type-I receptors modified their binding preferences<sup>[266]</sup>.

Three type-II receptors have been identified, named BMPR-II, activin receptor 2A (ACTR-IIA) and activin receptor 2B (ACTR-IIB). Once forming a complex with the BMP ligand and BMP receptors type I, the type II receptors initiate the signaling process by phosphorylating the GS domain of the type I receptor, which triggers a signaling cascade. The receptors-BMP complex formation has been described to occur by two distinct binding models. First, the “preformed complex” (PFC) binding model was described to involve the binding of a BMP ligand to naturally occurring complexes of type I and type II receptors at the cell surface<sup>[267]</sup>. A second binding model was described as “BMP-induced signaling complexes” (BISC) where BMPs bind first to one receptor, triggering the recruitment of additional receptors to form the signaling complex<sup>[267]</sup>. BMP2 and BMP4 exhibit a stronger affinity for type I receptors compared to type II receptors, leading to stable ligand-type I receptor complexes with half-lives of several minutes instead of few seconds with type II receptors<sup>[268]</sup>. Based on these differences, it is assumed that for the BISC binding model, BMP2 first binds to its type I receptor prior to recruiting type II receptors<sup>[269]</sup>. Interestingly, the PFC or BISC binding models appear to activate different signaling mechanism, with SMAD1/5/9 phosphorylation for PFC model and SMAD-independent pathways (**section I.C.5.c**) for BISC model<sup>[270]</sup>.

The interactions between BMP ligands and BMP receptors exhibit some specificities depicted in **Figure 17**. ALK1 was reported to bind preferentially BMP9/10, while ALK2 binds both the BMP9/10 and BMP5/6/7 subgroups. ALK3 is more affine to the BMP2/4 and ALK-6 binds both BMP2/4 and BMP5/6/7 subgroups. In contrast to the type I receptors, no obvious ligand specificities were identified for the type II receptors.

A recent study in our group provided new insights into these interactions<sup>[271]</sup>. In particular, the ALK5 receptor, classically related to TGF- $\beta$  proteins, has been shown to also interact with all

BMPs studied (BMP2,4,7,9). Although type II receptors interacted with all BMPs, they showed a preference for interacting with BMP9. Additionally, some interaction specificities were identified between BMP2 and BMP4, despite belonging to the same subgroup.

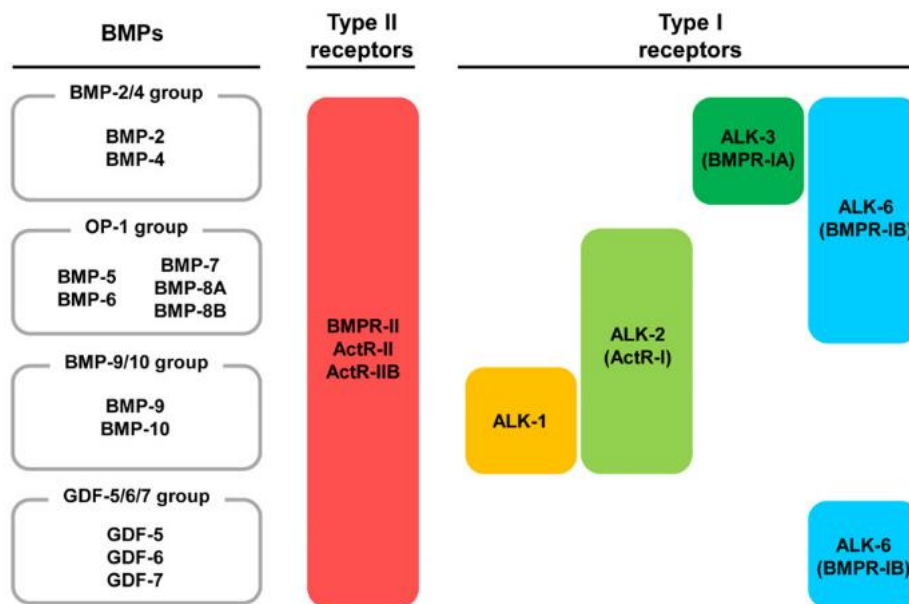


**Figure 17. Specificities of interactions between BMP ligands and its receptors.**

The different BMP subgroups all bind type II receptors but exhibit more specificities towards type I receptors. Reproduced with permission<sup>[272]</sup>.

As for BMP proteins, mutations in several BMP receptors are associated with human disorders<sup>[202,204]</sup>, and some of them are listed here. Regarding type I receptors, mutations in the ACVRL1 gene coding for the receptor ALK1 are related to a genetic vascular disorder named hemorrhagic telangiectasia (HHT)<sup>[239]</sup>. Due to the specificity of the BMP9/10 subgroup for ALK1, the role of these BMPs has been particularly studied in this pathological context<sup>[239,240]</sup>. ALK2 is related to fibrodysplasia ossificans progressiva, ALK3 to juvenile polyposis syndrome, ALK5 to Loeys–Dietz syndrome type 1 and ALK6 to brachydactyly type A2. Regarding type II receptors, mutations in genes encoding for BMPRII are associated to pulmonary arterial hypertension (PAH) and for ACVR2B are related to heterotaxy-4.

#### *I.C.5.b. The SMAD transcription factors*

SMADs are key transcription factors that mediate BMP signaling from the membrane receptors to the nucleus, targeting DNA. The SMAD family includes receptor-regulated R-SMADs (SMAD1/5/9 and SMAD2/3), one common mediator Co-SMAD corresponding to SMAD4, and two inhibitory I-SMADs (SMAD6/7). All members of this family contain an MH1 and an MH2 domain (MAD homology 1/2) except for I-SMADs, which do not feature the MH1 domain<sup>[273]</sup>. While there is an established divergence between TGF- $\beta$  and BMP signaling

involving SMAD2/3 or SMAD1/5/9 respectively (**Figure 18**), some findings highlighted that BMPs can also signal through SMAD2/3<sup>[274]</sup>.

The MH2 domain mediates the interactions with several protein partners. In particular, it facilitates the binding of R-SMADs to type I receptors, leading to their phosphorylation (into pR-SMADs) and activation. This phosphorylation allows the subsequent binding of SMAD4<sup>[275]</sup>, forming a free heterotrimeric R-SMAD/R-SMAD/SMAD4 complex able to translocate to the cell nucleus. The MH2 domain is also responsible for facilitating the interaction with proteins such as SMAD partners and transcription cofactors associated with DNA. Except for SMAD2, the MH1 domain of R-SMAD or Co-SMAD mediates the interaction with DNA and can bind directly to it. Some characteristic DNA binding sequences of SMADs have been identified, such as the so-called SMAD-binding elements (SBEs; AGAC or GTCT sequence) interacting with SMAD4 and SMAD3. The best-defined SMAD1/5-binding site is GGCGCC, which is present in the enhancers of well-characterized BMP-responsive genes, such as the Id genes<sup>[276]</sup>.

The direct affinity of SMADs for DNA is however relatively low to induce effective signaling ( $K_D \sim 100$  nM). Thus, high-affinity and high-specificity recruitment of SMADs to DNA usually requires additional transcription cofactors. Such cofactors bind to both DNA and SMAD oligomeric complexes, thereby increasing the specificity of the interactions at transcription sites. The expression of these cofactors probably contributes to the selectivity of the further expressed genes. Cofactors involved in BMP signaling include the RUNX family and several others previously reviewed<sup>[273,277]</sup>. Interestingly, SMAD complexes activate the expression of RUNX2 gene and subsequently associate with the synthesized RUNX2 protein, which acts itself as a cofactor to regulate the expression of genes involved in osteoblastogenesis<sup>[278]</sup>.

Since I-SMADs do not have an MH1 domain, they cannot bind DNA. However, through their MH2 domain, they still can bind R-SMADs, SMAD4, type I receptors and DNA-binding cofactors, thus exhibiting an inhibiting effect by preventing the formation of bioactive signaling complexes (**Figure 18**).

Within R-SMADs, the linker region located between the MH1 and MH2 domains plays an additional role in BMP signaling regulation. This region contains specific sites that serve as binding sites for Smad ubiquitination-related factor (Smurf) ubiquitin ligases, facilitating the process of ubiquitination. Although generally linked to protein degradation, the effects of the

ubiquitination process are not limited to that and include regulation of substrate localization, protein–protein interactions and activity<sup>[279,280]</sup>.

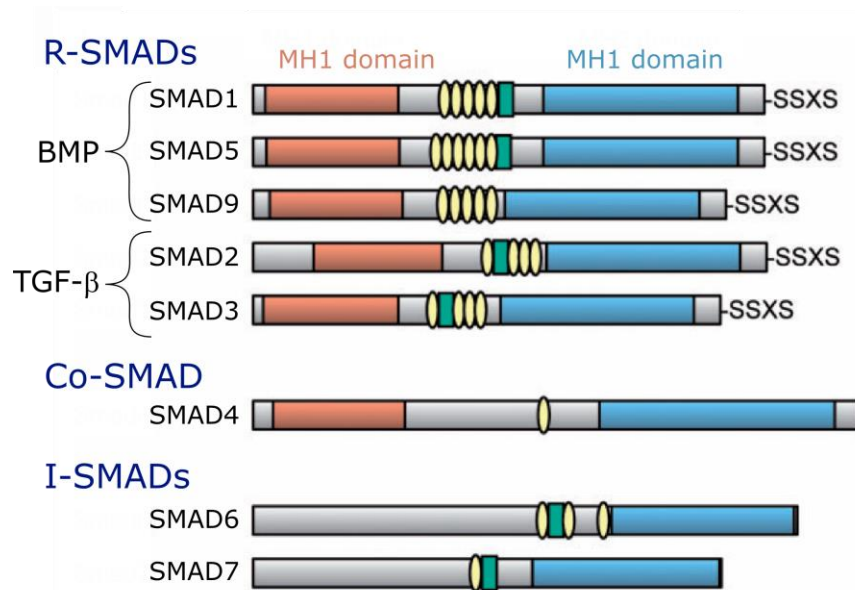


**Figure 18. Structural domains in proteins of the SMAD family**  
*Circles and green squares in the middle linker region indicate motifs potentially phosphorylated by MAP kinases.*  
*Adapted with permission<sup>[281]</sup>.*

#### *I.C.5.c. Other protagonists of BMP signaling*

Despite its complexity, the SMAD canonical pathway has been intensively studied and is now rather well understood. However, BMPs were also demonstrated to signal through several non-canonical pathways, reviewed elsewhere<sup>[243]</sup>. These pathways, not detailed here, include the ERK MAP kinase pathway, the activation of p38 MAPK and JNK pathway signaling through TAK1, the PI3K-AKT–mTOR signaling pathway, and the JAK-STAT activation.

Additionally, several other factors are involved in BMP signaling, such as interactions with BMP co-receptors or cross-talk with other cell-surface receptors<sup>[282]</sup>. As an example, a cross-talk mechanism was identified between BMP2 and integrins (cell adhesion receptors)<sup>[283]</sup>. This effect is characterized by a mutual positive dependency of BMP2 and integrins, where BMP2 binding to its receptor induces integrin-mediated adhesion, and activation of integrins up-regulates BMP2 signaling. Moreover, several ECM components regulate the availability, spatial distribution, and bioactivity of BMPs<sup>[246]</sup>. First, a large number of antagonists bind BMPs with very high affinity and prevent the interaction of BMPs with their receptors<sup>[284]</sup>. For instance, Noggin, the most characterized antagonist of BMPs, binds to BMP4 with a  $K_D$  in the picomolar range ( $\sim 19$  pM)<sup>[285]</sup>, while the interactions between BMPs and BMPRs are generally within the nanomolar range<sup>[271]</sup>. Finally, several major ECM components bind to BMPs with

low or high affinities, such as fibrillins, collagen, possibly fibronectin, and PGs<sup>[282]</sup>. The interaction of BMPs with PGs occurs through their GAG chains and is crucial for the BMP spatial distribution and signaling regulation<sup>[27,244,246,286]</sup>, as discussed in the next sections of this introduction.

## I.D. Interactions of glycosaminoglycans with BMPs

### I.D.1. Structural basis of BMP-GAGs interactions

BMP2 and BMP4 interact with GAGs through their N-terminal domains. Both exhibit typical Cardin-Weintraub sequences<sup>[147]</sup> in their N-terminal region, with [XBBXBX] and [XBBBXXBX] arrangements, respectively (B: basic residue; X: non-charged residue). These motifs are well conserved from *Xenopus* to humans. Ruppert *et al.* demonstrated that a BMP2 variant, where the N-terminal residues 1-12 have been substituted by a dummy sequence, exhibited a negligible interaction with Hep<sup>[287]</sup>. In contrast, they proved that the wild type BMP2 bound Hep with a high affinity, characterized by a  $K_D$  of 20 nM. The competition of BMP2 with a BMP2 N-terminal peptide (amino acids 1-17) increased BMP2 activity by about fivefold, probably by restraining its interaction with GAGs and thus facilitating the binding to cell surface receptors. Therefore, the N-terminal domain, represented in red in **Figure 15B** was highlighted as the region containing the Cardin-Weintraub sequence responsible for GAG binding, identified as QAKHKQRKRLKSSCKRH (1-17)<sup>[288]</sup>. However, the precise contribution of each amino acid in this sequence has not been investigated yet. Billings and coworkers recently performed a sequence analysis of the N-terminal domain in different BMPs<sup>[288]</sup>. Their N-terminal sequences exhibited a significant degree of conservation across different species, despite being highly variable from one BMP to another. Interestingly, HS binding appeared to involve domains at opposite ends for different BMPs: at the N-terminal domain of BMP2/4 versus the C-terminal domain of BMP5/6/7. Several elements about the interaction of BMP2 with GAGs remain unclear in the literature. First, it has not been clarified whether the two N-terminal domains of each monomer constitute two independent binding sites with identical affinity, or if they associate to form a large single binding domain. Secondly, the BMP2 structure is composed of two electropositive areas on opposite sides (**Figure 19**)<sup>[289]</sup>. The basic residues in the N-terminal domain modelled by Gandhi and Mancera conferred an electropositive nature to both sides<sup>[289]</sup>. It was suggested that these two surfaces could constitute a Hep-binding site for long oligosaccharides, while the two N-terminals could form two independent binding sites for binding short oligosaccharides. Although supported by a

biosensor assay indicating two distinct fast and slow phases of BMP2 association with Hep<sup>[287]</sup>, these hypotheses remain largely speculative and should be further explored. It is noteworthy that the highly flexible N-terminal domain of BMP2 greatly influences molecular simulation studies. Therefore, the combination of molecular dynamics with experimental techniques such as NMR will be required to account for the flexibility in the interactions between BMP2 and GAGs<sup>[289]</sup>.

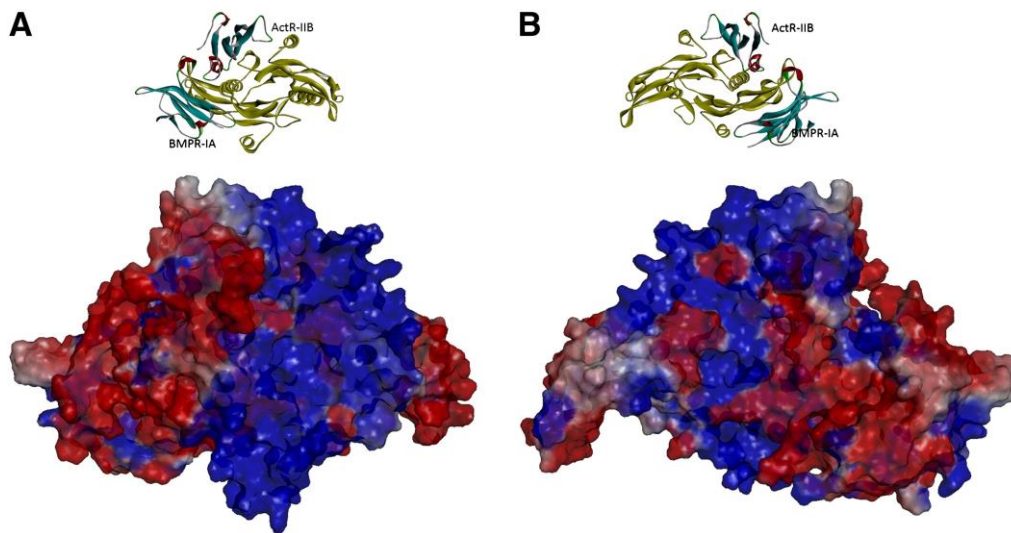


**Figure 19. BMP2 dimer exhibits a double-sided electropositive surface potential**  
Surfaces are colored by electrostatic potential on the accessible surface on a scale of  $-10$  to  $+10$   $k_B T/e_c$  (red to blue i.e. negatively to positively charged). For visualization of the protein orientation, the BMP2 dimer is shown as yellow ribbons with its two receptors colored according to their secondary structures (blue and red). **A** BMP2 protein surface is shown in an orientation facing the residues Lys73, Lys76, His44 and His17. **B** The second electropositive region (including Arg114) is shown upon rotation by  $180^\circ$ . Reproduced with permission<sup>[289]</sup>.

#### *I.D.2. Physiological importance of the interactions*

As previously mentioned, mutations in the PG/GAG biosynthesis are often related to skeletal human disorders, such as HME for EXT1/2 mutations<sup>[290]</sup>, skeletal dysplasia for CHST3 mutations<sup>[291]</sup>, and others for GalT-I, C6ST-1, 2OST, C5-epimerase, glypican-3 and perlecan mutations<sup>[88]</sup>. In mice models, heterozygote mutants of EXT2 develop exostoses (like in HME) and homozygote mutants of EXT1 and EXT2 fail to gastrulate<sup>[292,293]</sup>.

One well-investigated hypothesis to explain the link between GAGs and these diseases is the involvement of GAGs in finely regulating the signaling and the spatial distribution of morphogens involved in the skeletal developments such as hedgehogs (Hh), Wntless-related integration site (Wnt), fibroblast growth factors (FGF) and BMPs.

BMPs are believed to act as morphogens in organisms regulating the development of tissues<sup>[244]</sup>. The precise definition of a morphogen consists of locally synthesized signaling molecules that

diffuse and act over long distances to induce cellular responses and control growth and pattern throughout a tissue region<sup>[294]</sup>. At the production site, morphogen levels are elevated and decrease progressively further away in the tissues. Consequently, morphogens are spatially distributed according to concentration gradients during embryonic development. In the absence of other regulators, the signaling intensity downstream of the morphogen is assumed to be directly linked to the morphogen concentration. The BMP gradients have been nicely studied in drosophila embryonic development, by exploring the distribution of the Dpp BMP2/4 orthologue, in particular in the wing imaginal disc. The visualization of the gradient has commonly been achieved either directly with fluorescently labelled Dpp, or indirectly by observing the intensity of fluorescently labelled phosphorylated Mad (pMad), a readout of Dpp signaling (analogue to pSMAD). While studies in drosophila show indeed the morphogen diffusion of the fluorescently labelled Dpp to some extent, studies in vertebrates use fluorescent gene reporters revealing gradient-like expression of BMPs, but do not provide information on their diffusion<sup>[244]</sup>.

Interestingly, a wealth of studies in drosophila demonstrated the presence of Hh, Wingless (Wg, homolog of Wnt-1), and Dpp signaling defects in mutants for several elongation or sulfation PG/GAG biosynthesis enzymes<sup>[88,295-300]</sup>. These defects include spatial alteration of signaling within tissues and alteration of signaling levels, leading to developmental defects. For instance, it was demonstrated that the pMad signaling gradient was altered with a restricted diffusion in the wing discs of drosophila *dally* mutants compared to wild types, as illustrated in **Figure 20A**. Belenkaya and coworkers demonstrated that the diffusion of extracellular GFP-Dpp fails to move across cells mutant for *dally* and *dally-like* (*dly*), two drosophila glypicans<sup>[296]</sup>. Consequently, the pMad signaling was abolished in the same area, as illustrated in the **Figure 20B**. These effects were also verified for mutants of *sulfateless* (*sfl*), which encodes for an NDST enzyme. Apart from HSPGs, the aggrecan CSPG has also been implicated in the gradient distribution of morphogens such as BMP<sup>[301]</sup>.

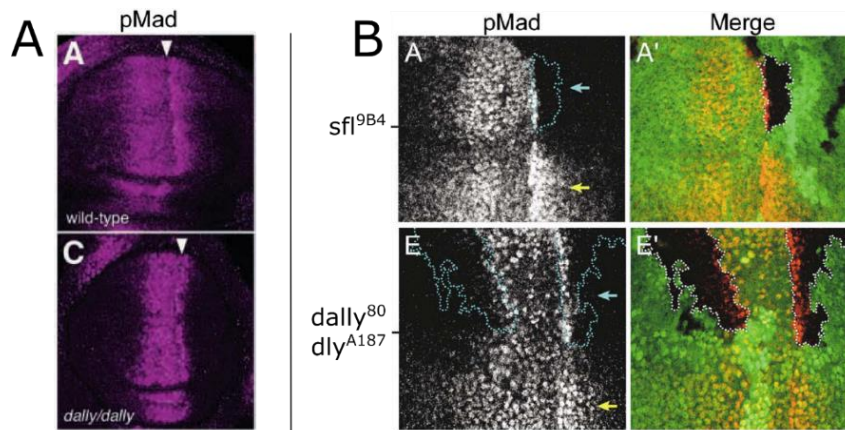


**Figure 20. Influence of GAG/PG defects on the shape of morphogen gradients**

**A** pMad staining (pink) in the wing disc of *drosophila* either wild type or homozygote mutants for *dally* hypomorphic alleles. Adapted with permission<sup>[295]</sup>. **B** pMad levels in the wing imaginal disc of *drosophila*. On the left is pMad fluorescence and area delimited by blue dots correspond to mutant cells for *sbl* or *dally* and *dly*. On the right is the merge of the pMad signal (orange) and the GFP signal (green) to visualize mutant and non-mutant clones (mutants are localized in unstained areas). Adapted with permission<sup>[296]</sup>.

Overall, PGs are believed to regulate the signaling by controlling BMP diffusion to shape morphogen gradients and control the development and tissue homeostasis<sup>[302]</sup>. This mechanism appears to occur through their GAG chains since the sulfation of GAGs also contributes to the controlled diffusion of BMPs. Therefore, the fine-tuning of sulfation patterns on the GAG chains of cell-surface and extracellular PGs could contribute to regulate precisely the different stages of development. Noteworthy, PGs have the potential to collaborate with additional extracellular proteins, including BMP antagonists, in order to govern the signaling process<sup>[244]</sup>. In particular, various BMP antagonists are also believed to play a role in shaping the gradients of morphogens<sup>[303]</sup>. This process seems to rely also on their interactions with PGs, which create an antagonist counter-gradient to that of the morphogen. In *drosophila*, the Dpp gradient is also regulated by an inverse gradient of one antagonist termed Short gastrulation<sup>[27]</sup>.

### I.D.3. Influence of the GAG interactions on BMP signaling

Apart from their role in shaping morphogen gradients, GAGs have been investigated for their direct effect on BMP signaling, to determine whether they positively or negatively regulate the signaling. As depicted in **Table 3**, the role of GAGs in BMP signaling has been intensively investigated, using several strategies such as mutating GAG biosynthesis enzymes *in vivo* or *in vitro*, interfering with GAG function, or treatments with exogenous GAGs. However, it seems that the action of GAGs on the signaling is highly complex and context-dependent, as observed by the many discrepancies in the literature. Studies in *drosophila* are rather in good agreement, indicating that PGs, their GAG chains and their sulfation positively influence Dpp diffusion and subsequent pMad signaling. Few studies not included in **Table 3** show that Dpp signaling in dorsoventral patterning during embryogenesis is not defective in fly embryos mutant for HS

biosynthesis enzymes, in contrast to signaling in the wing discs<sup>[27]</sup> (**Table 3**). One explanation suggested by Lin and coworkers is that Dpp is highly expressed in the dorsal half of embryos, where its activity gradient is regulated by an inverse gradient of its antagonist Short gastrulation, whereas Dpp forms concentration gradients in the wing discs to transduce its signaling<sup>[27]</sup>. Mutations of GAG biosynthesis enzymes in other species generally disagree with the observed findings in drosophila. In mice, EXT1 mutants develop osteochondromas, reminiscent of the HME disease. EXT1 cell mutants exhibit an increased BMP2-induced signaling and chondrogenic differentiation<sup>[6,304]</sup>. Interestingly, treating EXT1 mutant mice with LDN-193189, a BMP type I receptor inhibitor, suppresses osteochondroma formation<sup>[304]</sup>. In zebrafish, the overexpression of the 6-O endosulfatase Sulf1 led to phenotypic defect of the myoseptum and an increased SMAD1/5/9 phosphorylation, showing that reduced HS sulfation aberrantly potentiates the signaling. In a similar way as described before, treating the mutants the LDN-193189 drug rescued both the phenotype and the SMAD phosphorylation to a normal state<sup>[305]</sup>. The effect of *in vitro* treatments interfering with the GAG functions has also been subject to several contradictions in the literature. Common treatments include lyase treatment to degrade GAG chains, surfen treatment to inhibit protein binding to GAGs, and chlorate treatment to reduce the sulfation of GAG chains synthesized by the cells. Heparinase and chlorate treatment demonstrated to reduce the signaling induced by either BMP2 or BMP7 in mice and rat cell lines<sup>[306,307]</sup>, while increasing the BMP2-induced signaling in C2C12 or mice limb bud mesenchymal stem cells (MSCs)<sup>[6,308]</sup>.

When treating cells with exogenous GAGs and BMPs, there seems to be a clearer trend that it promotes BMP signaling. Only a few studies contradict this trend, such as Jiao *et al.*<sup>[308]</sup>, who showed that ALP signaling at 6 days was reduced with BMP2 and Hep compared to BMP2 alone. This difference could be explained by the experimental design, where media was changed every two days with fresh BMP2. Therefore, the effect of exogenous Hep in protecting the BMP2 degradation and sustaining its release in the long term would be countered by the addition of new BMP2 in conditions without Hep.

It is noteworthy that some of these studies also implicated the role of HS in recruiting type II BMP receptors to the complex of BMP2 and type I receptors, unraveling another mechanism by which GAGs can modulate the BMP signaling<sup>[306,309]</sup>.

### Mutations in GAG biosynthesis

Growth factor	Genetic modification	Drug	Study model	Animal	Effect	
[300]	Dpp	<i>Dally</i> mutant	In vivo	Drosophila	Reduced Dpp target genes expression	
[296]	Dpp	<i>Dally /Dly</i> mutant <i>Sulfateless</i> mutant	In vivo	Drosophila	Restricted diffusion of Dpp and disrupted signaling across mutants	
[297]	Dpp	<i>ttv, sotv</i> mutants	In vivo	Drosophila	Reduced pMad signaling	
[298]	Dpp	<i>ttv, sotv, botv</i> mutants	In vivo	Drosophila	Reduced pMad signaling and altered gradient across mutants	
[299]	Dpp	<i>ttv, sotv, botv</i> mutants	In vivo	Drosophila	Restricted diffusion of Dpp and disrupted signaling across mutants	
[295]	Dpp	<i>Dally</i> overexpression	In vivo	Drosophila	Increased pMad in mutant cells / Altered signalling and protein gradients	
[310]	ΔN-Ter BMP4		In vivo	Xenopus laevis	Increased diffusion of ΔN-Ter BMP4 compared to BMP4	
[311]	BMP4 mRNA	XtSulf1 overexpression	Ex vivo	Xenopus	Reduced SMAD1 phosphorylation / Inhibit binding of BMP to its receptors	
[305]	-	Sulf1 overexpression	In vivo	Zebrafish	Increased SMAD1/5/8 phosphorylation and loss of the myoseptum	
		Sulf1 overexpression	LDN-193189	In vivo	Zebrafish	Rescued SMAD1/5/8 phosphorylation and myoseptum
[312]	BMP4	Syndecan-1 overexpression	In vivo	Xenopus	Reduced BMP signaling (gene expression reporter)	
	BMP4	Syndecan-1 silencing	In vivo	Xenopus	Concentration-dependent effect; high levels block and low levels enhance BMP signaling	
	BMP4	Syndecan-1 silencing	C2C12	Mice	Increased BMP signaling (gene expression reporter)	
[313]	BMP2	Syndecan-3 overexpression	limb bud MSCs	Chick	Reduced SMAD phosphorylation and impaired cartilage differentiation	
[6]	-	EXT1 flox/flox	In vivo	Mice	Ectopic bone formation	
[6]	BMP2	EXT1 flox/flox	limb bud MSC	Mice	Increased ectopic SMAD1/5/8 phosphorylation and chondrogenic genes levels	
[304]	-	EXT1 flox/flox	In vivo	Mice	Osteochondromagenesis	
	-	EXT1 flox/flox	LDN-193189	In vivo	Mice	Suppression of osteochondroma
	BMP2	EXT1 flox/flox	MSCs	Mice	Increased BMP signaling, increased chondrogenic differentiation	
[314]	-	C4st1 gt/gt	In vivo	Mice	Reduced SMAD1 phosphorylation in hypertrophic zone of embryonic growth plate	

### Interference with GAGs function

Growth factor	Treatment	Study model	Animal	Effect	
[6]	BMP2	Heparitinase I	limb bud MSC	Mice	Increased ectopic pSMAD 1/5/8 and chondrogenic genes levels
	BMP2	Chlorate	limb bud MSC	Mice	Increased ectopic pSMAD 1/5/8 and chondrogenic genes levels
	BMP2	Surfen	limb bud MSC	Mice	Increased ectopic pSMAD 1/5/8 and chondrogenic genes levels
[306]	BMP2/4	Heparitinase	C2C12/PC12	Mice	Reduced pSMAD1/5 levels and p38 activation
	BMP2/4	Chlorate	C2C12/PC12	Mice	Reduced pSMAD1/5 levels and p38 activation
	ΔN-Ter BMP2	Heparitinase	C2C12	Mice	No effect on SMAD1/5 with the DN-Ter BMP2
[313]	BMP2	Heparitinase	limb bud MSC	Chick	Increased BMP2-induced cartilage differentiation and related genes
[308]	BMP2	Heparinase III	C2C12	Mice	Increased ALP activity
	BMP2	Chlorate	C2C12	Mice	Increased ALP activity

[315]	BMP2/4	Heparitinase	C2C12	Mice	No effect of heparitinase
[307]	BMP7	Heparitinase	ROS 17/2.8	Rat	Reduced BMP7-induced pSMAD1/5/8
	BMP7	Chlorate	ROS 17/2.8	Rat	Reduced BMP7-induced pSMAD1/5/8
[11]	BMP2	Chondroitinase	Primary chondrocytes	Mice	Reduced BMP2-induced pSMAD1/5/9
<b>Exogenous GAG treatment</b>					
	Growth factor	Exogenous GAG	Study model	Animal	Effect
[313]	BMP2	HS	limb bud MSC	Chick	Increased BMP2-induced cartilage differentiation and related genes
[308]	BMP2	Hep	C2C12	Mice	Reduced ALP activity
[315]	BMP2/4	Hep	C2C12	Mice	Increased BMP2-induced pSMAD1/5/8 and ALP activity
	BMP2	Hep	In vivo	Mice	Increased amounts of mineralized bone tissue
[264]	BMP2	bHS	C2C12	Mice	Sustained signaling compared to soluble BMP2
[283]	BMP2	bHS	C2C12	Mice	Comparable/reduced pSMAD1/5/8 compared to soluble BMP2
	BMP2	bHS	hPDSC	Human	Increased pSMAD1/5/8 compared to soluble BMP2
[287]	BMP2	Hep	limb bud cells	Chick	Increased sulfated GAG synthesis after 6 days of culture
[316]	BMP2	Hep/HS	C2C12	Mice	Increased BMP2-induced osteogenic differentiation (RUX2, ALP, osteocalcin)
[317]	BMP4	CS-E	MC3T3-E1	Mice	Increased BMP4-induced ALP activity and mineralization
[318]	BMP4	Hep	SaOS-2	Human	Reduced pSMAD1 signaling
[307]	BMP7	Hep	ROS 17/2.8	Rat	Reduced BMP7-induced pSMAD1/5/8

**Table 3. Literature review about the effects of GAGs in the BMP signaling**

The different studies are classified within three different groups: Mutations in GAG biosynthesis, interference with GAG function, or exogenous GAG treatment. The effects observed in each study are depicted in green or red when GAGs or their sulfation positively or negatively influences the BMP signaling, respectively.  $\Delta N$ -Ter indicate a protein that has been mutated at its N-terminal domain (GAG-binding site for BMP2/4). MSC: Mesenchymal stem cells. dly: dally-like. tv (tout-velu), sotv (sister of tout-velu) and botv (brother of toutvelu) are homologues of EXT1, EXT2 and EXTL3, respectively. LDN-193189 is a type I BMP receptor inhibitor.

The role of GAGs in the regulation of BMP signaling appears to be very complex and context-dependent. The localization of GAGs at the cell surface or in the ECM could potentially contribute to different roles in cell signaling and dynamics of interactions with cell-surface receptors. Additionally, the presentation of GAGs in solution may not be physiologically relevant since GAGs are generally attached to their protein core on PGs, themselves frequently linked to other matrix components such as HA. Therefore, future studies should focus on the aforementioned aspects that might clarify the ambiguous role of GAGs in the signaling of several proteins, including BMPs. Furthermore, the role of the PG protein core may also be of importance, although not explored in this thesis. Miguez and coworkers showed in the C2C12 cell line that BMP2-induced ALP activity was increased by biglycan PG, but even more by the deglycanated biglycan deprived of its GAG chains<sup>[319]</sup>, indicating a suppressor role of GAG chains in the biglycan-assisted BMP activity. This is in line with the previously mentioned

ability of biglycan to bind TGF- $\beta$ . As suggested previously, the role of GAGs appears to be tissue-dependent (i.e. wing discs versus dorsal half of drosophila). This tissue dependency might be linked to differences in growth factor concentrations, where GAGs would increase the signal with low concentrations by catching the ligands whereas they would reduce the signal by sequestering ligands at high concentrations.

In the **Figure 21** are depicted several models about the potential different roles of PGs in regulating BMP signaling.

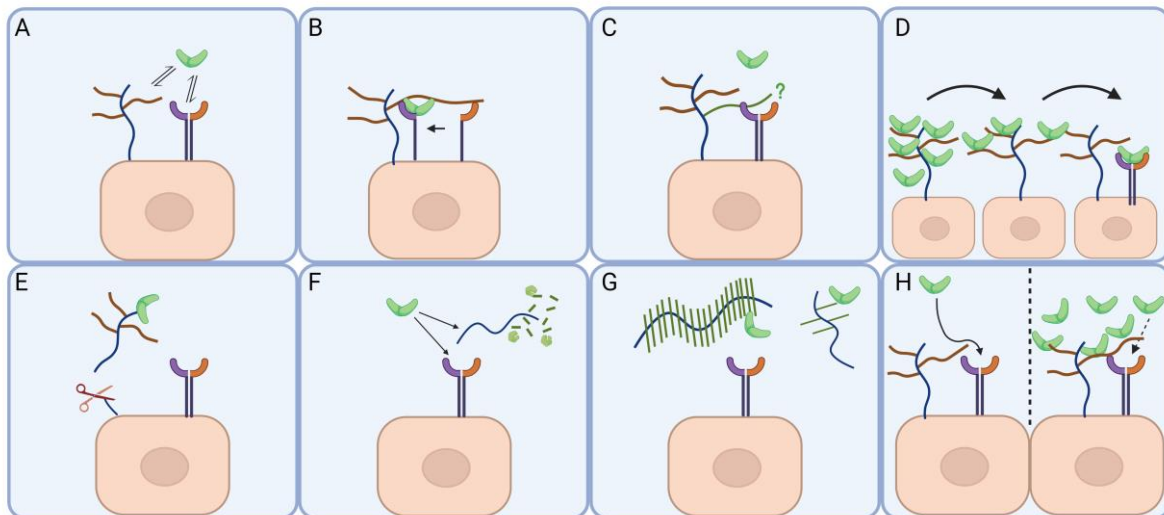


**Figure 21. Models of PGs regulation of BMP signaling**

**A.** Competitive interactions of BMP2 with PGs or with BMP receptors. **B.** HSPGs facilitate the recruitment of type II receptors to the complex of BMP2 and type I receptors. **C.** The role of CS chains in PGs remains unexplored but it could modulate the dynamics of BMP interactions with its receptors. **D.** Cell-surface PGs mediate the restricted diffusion of BMP from BMP-expressing cells to BMP-receiving cells, forming a morphogen gradient. **E.** Shedding of cell-surface could also regulate BMP signaling by modifying the dynamics of BMP interactions with its receptors. **F.** Lyase degradation of GAG chains could modulate BMP signaling by releasing soluble GAG fragments and exposing the protein core of PGs binding BMPs such as biglycan. **G.** CSPGs in the extracellular matrix could be involved in the formation of BMP gradients. **H.** PGs could have opposite roles depending on the BMP concentration: with low concentration, PGs could attract distant BMP molecules to facilitate the binding to its receptor while at high concentration it would restrain the binding to its receptors by sequestering BMP molecules. Created with Biorender.

Recently, another intriguing model implicating the role of HS nanostructure was described by the research group of Prof. Kiessling for the regulation of FGF signaling<sup>[320]</sup>. In undifferentiated human pluripotent stem cells, the HS chains formed extended hair-like protrusion structures, while along the differentiation into motor neurons, HS chain morphology changed towards a dispersed punctate structure. This differentiation process was also associated with the loss of FGF binding to the neural cells and loss of signaling, suggesting a role of the HS nanostructure in the regulation of growth factor signaling.

#### I.D.4. Molecular interactions between GAGs and BMPs

A survey of the literature was conducted to provide a more comprehensive understanding of BMPs with GAGs. As depicted in **Table 4**, the molecular interactions of BMPs with GAGs have been mainly studied with Hep and HS. BMPs exhibit a high affinity for HS and Hep in the nanomolar range. However, the affinity values determined in the literature deserve to be clarified, since they are subject to variations of several orders of magnitude. In particular, for BMP2 which has been the most studied, the  $K_D$  values vary from 37 to 1600 nM for HS interaction<sup>[288,321,322]</sup>, and from 2.4 to 490 nM for interaction with Hep<sup>[6,287,323]</sup>. Such discrepancies could be related to different experimental setups or GAG sources. Furthermore, it was demonstrated that the minimal size of HS oligosaccharides to bind BMP2 is a hexasaccharide<sup>[324]</sup>.

The interactions of BMPs with other GAGs such as CS, DS, KS and HA remain rather unexplored and deserve to be investigated to bring new insights into their role in the regulation of BMP signaling.

$K_D$ [nM]	BMP2	BMP4	BMP5	BMP6	BMP7
HS	37 <sup>[288]</sup> 186±33 <sup>[321]</sup> 1600 <sup>[264]</sup>	4940-5450 <sup>[172]</sup>	16 <sup>[288]</sup>	56 <sup>[288]</sup>	40 <sup>[288]</sup> 7 <sup>[249]</sup>
Hep	20,0 <sup>[287]</sup> 2,4±0,3 <sup>[323]</sup> 490±20 <sup>[6]</sup>	69,4 <sup>[325]</sup>		6,3 <sup>[142]</sup>	
2O-ds-Hep				11 <sup>[142]</sup>	
6O-ds-Hep				15 <sup>[142]</sup>	
Hep dp6-n°1	24000 <sup>[326]</sup>				
Hep dp6-n°2	46000 <sup>[326]</sup>				
Hep dp6-n°3	34000 <sup>[326]</sup>			9000 <sup>[326]</sup>	
CS-E		30,0 <sup>[325]</sup>			
DS	20,0 <sup>[323]</sup>				
HA					
sHA (SD=1,0)		7,3-11,4 <sup>[172]</sup>			
sHA (SD=2,8)		0,013-0,020 <sup>[172]</sup>			

**Table 4. Affinities between different GAGs and BMPs determined in the literature**

The  $K_D$  values, corresponding to the inverse of the affinity, are indicated for each interaction. Hep dp6 n°1-3 indicate synthesized Hep-oligosaccharides.

Given the crucial role of specific HS sequences for protein binding and bioactivity of some growth factors (as demonstrated with FGF and AT III)<sup>[137,144,165]</sup>, it is plausible that essential HS structural features (sequences and sulfation patterns) are similarly crucial for the interactions with BMPs. Up to date, only a few studies have explored the role of GAG sulfation degree and sulfation patterns for their interaction with BMP2, focusing mainly on HS. Using desulfated Hep, Smith *et al.* found that N-sulfation played a crucial role in BMP2 binding,

surpassing the influence of 6-O sulfation, while 2-O sulfation had only a minor role<sup>[324]</sup>. However, these results contradicted the findings from Tellier and coworkers, which indicated a minor importance of N-sulfation and a clear importance of 6-O sulfation<sup>[327]</sup>. Another study conducted by Chopra *et al.* in 2021 investigated the interaction between HS and BMP2 using a microarray that exhibited rare 3-O sulfated hexasaccharides<sup>[328]</sup>. The authors demonstrated that oligosaccharides including a 3-O sulfate bound BMP2 with more affinity. In particular, oligosaccharides featuring a central IdoA(2S)-GlcNS(3S6S) disaccharide generally exhibited a high affinity for BMP2. The importance of 3-O sulfation in BMP signaling and organ function was also shown for other BMPs<sup>[2,329]</sup>. In contrast, in a microarray study, Söderlund and coworkers did not observe major modification of BMP interactions for five distinct oligosaccharides, with  $K_D$  values in the 100 nM range<sup>[330]</sup>. In particular, there was no significant effect on the binding using a HS dodecasaccharide that included a 3-O sulfated GlcNS(3S6S)-IdoA(2S) sequence, which is palindromic to the motif identified by Chopra *et al.*<sup>[328]</sup>.

## I.E. Biomaterials to study GAGs

### *I.E.1. Use of biomaterials in medical applications (Review published in Advanced Materials, Annex)*

The remarkable physical and biological properties of GAGs make them excellent candidates for biomaterial applications and particularly for tissue regeneration<sup>[3,46,331–336]</sup>. In this section, we provide an overview of the biomedical applications investigated using GAG-based biomaterials, for each type of GAG, summarized in the **Table 5**.

Because of its large binding properties, Hep has been incorporated in many biomaterials developed for biomedical applications, and especially tissue engineering. Various medical devices incorporating Hep for its anticoagulant properties have been successfully validated in clinical trials and are now commercially available. These devices include cardiopulmonary bypass devices, hemodialysis catheters, vascular and stent-grafts<sup>[337]</sup>. Due to its ability to bind growth factors that play key roles in various tissues, Hep-based biomaterials have also been developed for anti-inflammation<sup>[338–340]</sup>, bone repair<sup>[323,341–347]</sup>, wound healing<sup>[348,349]</sup>, cartilage repair<sup>[343,350,351]</sup>, vascular reconstruction<sup>[333,352–367]</sup>, tendon reconstruction<sup>[368–370]</sup>, nerve growth<sup>[371–373]</sup>, and cancer detection and apoptosis<sup>[374,375]</sup> (**Table 5**).

HS has been less studied than other GAGs and there is currently no HS-based biomaterial under clinical trial. However, *in vitro* and *in vivo* studies have investigated HS-based biomaterials for

bone repair<sup>[376]</sup>, cartilage repair<sup>[377–379]</sup>, angiogenesis<sup>[360,380–383]</sup>, wound healing<sup>[380]</sup>, and stem cell-therapy enhancement<sup>[384]</sup> (**Table 5**).

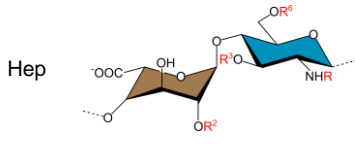
HA is certainly the most advanced GAG for biomaterial applications and commercial uses in medicine and cosmetics. It is commonly used in a wide range of cosmetics but also in clinical trials for wound repair in different biomaterials like HA-based sponges<sup>[385]</sup>, or HA-based dermal substitute membranes<sup>[386,387]</sup>. Some HA-based scaffolds have also been tested in clinics for cartilage repair<sup>[388–395]</sup>. In research, HA-based biomaterials are emerging for bone repair<sup>[343,396–401]</sup>, vascular reconstruction<sup>[402–404]</sup>, anti-inflammation<sup>[405,406]</sup>, vocal fold repair<sup>[407–409]</sup>, muscle regeneration<sup>[410,411]</sup>, lung tissue modelling<sup>[412]</sup>, tendon or ligament repair<sup>[413]</sup>, nerve growth<sup>[414]</sup>, and adipose tissue engineering<sup>[415]</sup> (**Table 5**).

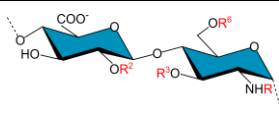
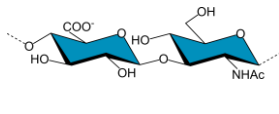
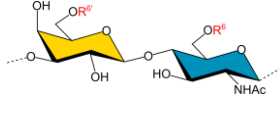
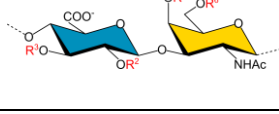
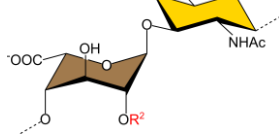
Even though KS seems to have a lot of potential for biomedical application, no KS-based biomaterial has been developed, to our knowledge.

Various CS-based biomaterials have been developed for a broad range of applications. Notably, a membrane made of bovine tendon collagen and CS-C has passed clinical trials and is now commercially available for skin repair of burn victims<sup>[416,417]</sup>. Other biomaterials with CS have been developed for bone repair<sup>[376,418–421]</sup>, nerve growth<sup>[422,423]</sup>, tendon regeneration<sup>[424,425]</sup> and vascular applications<sup>[381]</sup> (**Table 5**). For cartilage repair, CS has already been used in clinical trials and is commercially available, though not as a biomaterial. Instead, it was used as an intra-articular injectable solution<sup>[426]</sup>. Alongside, CS-based biomaterials such as hydrogels are currently being developed to repair damaged cartilage<sup>[392–395,427,428]</sup>.

The use of DS in biomaterials is progressing slowly compared to the other GAGs, but as depicted in **Table 5**, some applications are emerging for the reduction of biofilm deposition<sup>[429]</sup>, vascular application<sup>[430,431]</sup>, bone repair<sup>[323,432]</sup>, and wound healing<sup>[433]</sup>.

The ability of GAGs to interact with GFs and to regulate their bioactivity is attractive to design biomaterials. The combination of GAGs with GFs in biomaterials has been extensively investigated for biomedical applications, as shown in Table 1. However, up to date, the only GAG-biomaterials that reached clinics do not include GF, likely due to the increased biomaterial intricacy resulting from the addition of GF.

Disaccharide unit		Biomaterial applications
	Anti-coagulation <sup>[337]</sup>	Vascular reconstruction <sup>[333,352–367]</sup> – SDF-1 $\alpha$ <sup>[353,354]</sup> , VEGF <sup>[352,358–364]</sup> , FGF2 <sup>[365,366]</sup> , Shh+IL-10 <sup>[367]</sup>
	Anti-inflammation <sup>[338–340]</sup> – IL-4 <sup>[338,339]</sup> , IL-13 <sup>[340]</sup>	Tendon reconstruction <sup>[368–370]</sup> – PDGF-BB <sup>[368–370]</sup>
	Bone repair <sup>[323,341–347]</sup> – BMP2 <sup>[323,341–347]</sup>	Nerve growth <sup>[371–373]</sup> – GDNF <sup>[371]</sup> , NGF <sup>[371–373]</sup>
	Wound healing <sup>[348,349]</sup> – FGF2 <sup>[348]</sup> , HB-EGF <sup>[349]</sup>	Cancer detection and apoptosis <sup>[374,375]</sup>
	Cartilage repair <sup>[343,350,351]</sup> – BMP2 <sup>[343]</sup> , TGF- $\beta$ <sup>[350]</sup>	

HS		Bone repair [376] – <b>BMP2</b> [376] Cartilage repair [377–379] – <b>BMP2</b> [377–379] Vascular reconstruction [360,380–383] – <b>VEGF</b> [360,380], <b>FGF2</b> [382,383]	Wound healing [380] – <b>VEGF</b> [380] Stem cell therapy enhancement [384]
HA		<b>Wound healing</b> [385,434–436] – <b>HB-EGF</b> [436] <b>Cartilage repair</b> [388–395] Bone repair [396,343,397–401] – <b>BMP2</b> [343,396–398], <b>SV</b> [400], <b>FGF2</b> [401] Vascular reconstruction [402–404] Anti-inflammation [405,406] – <b>IL-10</b> [405]	Vocal fold repair [407–409] Muscle regeneration [410,411] Lung tissue model [412] – <b>FGF7+FGF10</b> [412] Tendon / ligament repair [413] Nerve growth [414] Adipose tissue engineering [415]
KS			
CS		<b>Wound healing</b> [348,417,437,438] – <b>FGF2</b> [348] <b>Cartilage repair</b> [392–395,427,428] Bone repair [376,418–421] – <b>BMP2</b> [376,418,419], <b>BMP4</b> [420], <b>PDGF-BB</b> [421]	Nerve growth [422,423] – <b>NGF</b> [422,423] Tendon regeneration [424,425] – <b>IGF-1/GDF-5</b> [425] Angiogenesis [381]
DS		Reduction of biofilm deposition [429] Vascular reconstruction [430,431]	Bone repair [323,432] – <b>BMP2</b> [323] Wound healing [433]

**Table 5. Biomaterial applications of the different GAGs**

In green, the biomaterials that have already been used in clinical trials for the mentioned application. In light brown, which bioactive molecules have been used in the biomaterials. **BMP2/4**: Bone Morphogenetic Protein 2/4; **FGF2**: Fibroblast Growth Factor 2; **GDNF**: Glial cell line-derived neurotrophic factor; **HB-EGF**: Heparin-Binding EGF-like Growth Factor; **IGF-1**: insulin-like growth factor-1; **IL-4/-10/-13**: Interleukin-4/-10/-13; **NGF**: Nerve Growth Factor; **PDGF-BB**: Platelet Derived Growth Factor –BB; **SDF-1 $\alpha$** : Stromal cell-Derived Factor 1-Alpha; **Shh**: Sonic Hedgehog; **SV**: Simvastatin; **TGF- $\beta$ 3**: Transforming Growth Factor Beta-3; **VEGF**: Vascular Endothelial Growth Factor

### I.E.2. Biomaterials to study GAGs (Review published in *Advanced Materials*, Annex)

Many GAG-based biomaterials have been developed for medical applications, tissue engineering, and GF delivery. The cytotoxicity and GF delivery of these biomaterials are widely studied, but the mechanisms by which the biomaterials regulate GF signaling depending on GAG type are generally less considered. A majority of studies on GAG-mediated regulation of growth factor signaling have been using GAGs in their soluble form<sup>[29,308,324,439]</sup>. However, the release of GAGs or PGs in solution is generally correlated with specific processes such as inflammation, sepsis, and intoxication responses. High levels of degraded soluble GAG fragments are considered as biomarkers of several diseases<sup>[132,133]</sup>. For *in vitro* studies, treating cells with GFs bound to soluble or immobilized GAGs (most GAGs are bound at the cell surface or the ECM) may therefore induce a different response. For example, contradictory roles of HS have been reported for BMP2 growth factor signaling, depending on whether HS was presented in a soluble form or bound at the cell surface. In particular, it has been shown that HS promotes

the BMP2-mediated SMAD 1/5/9 pathway (early effectors of BMP signaling) when added in solution to cells<sup>[316,440]</sup>. On the contrary, conditional KO mice for Ext1 HS elongation enzyme showed an improved SMAD1/5/9 phosphorylation, thereby suggesting that cell-surface HS inhibits BMP signaling<sup>[6,309]</sup>. Biomaterials developed for clinical applications are often presenting immobilized GAGs, which may have a different role with respect to soluble and cell-surface GAGs. It is therefore important to determine the effects of immobilized GAGs in simple experimental *in vitro* conditions before using GAG-based biomaterials in clinics. It is noteworthy that the immobilization strategy can also have an impact. A study of protein-Hep interactions demonstrated that immobilizing Hep to a surface *via* intra-chain modifications negatively affects the protein binding compared to Hep biotinylated at the reducing end<sup>[441]</sup>. Therefore, reducing-end functionalization of GAG chains is certainly a more biomimetic approach, mimicking better the natural PG structure and enabling efficient interactions with proteins<sup>[442]</sup>.

Additionally, the modulation of some GAG properties (i.e. type, density, length, and sulfation) directly affects the interactions with bioactive molecules and consequently modifies the cellular response. Therefore, they have to be considered in the design of GAG-based materials. The fine-tuning of these parameters should be achieved to determine the best conditions for a specific medical application. Interestingly, these parameters are highly variable *in vivo* depending on the tissue, pathology or age. The variation of these parameters in tissues is summarized in the **Figure 22**. The panel A illustrates differences in GAG type distributions, as exemplified by distinct localizations of HS and CS mice eye sections during embryonic development. The panel B depicts variations in concentration of sulfated GAGs (sGAG), as in mice growth plate exhibiting well-defined areas with high (dark blue) or low (white) concentrations. The panel C highlights differences in GAG sulfation in tissues. This panel shows glycan fragments detected by MALDI-FT-ICR mass spectrometry in gastric cancer patients. Some glycans detected can be attributed to GAG structures. It is possible to identify a separation between an area with sulfated glycans and a non-sulfated area. Considering the natural variability of GAG type, density and sulfation distributions, a rational design of biomaterials in relation to the *in vivo* characteristics of the tissue targeted is critical for biomedical application. Obviously, the systematic evaluation of these characteristics in tissues for translation into biomaterials is a tremendous challenge and will require important technological developments.

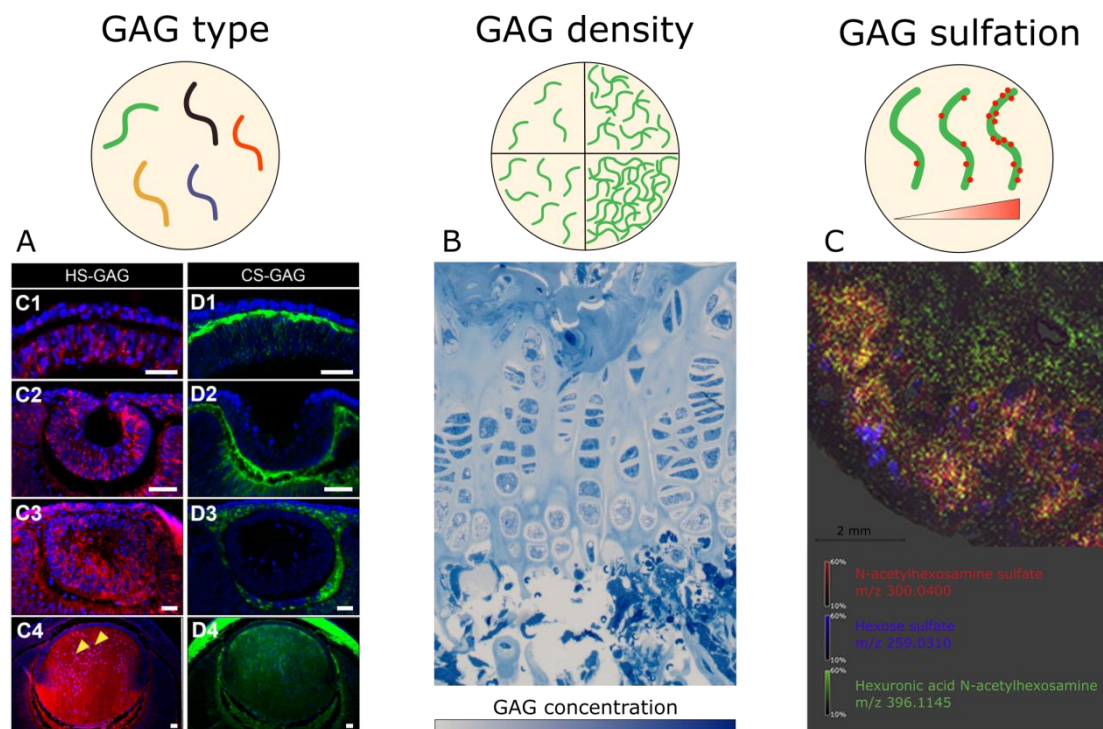


**Figure 22. Natural variation of GAG in animal tissues or cell cultures**

**A.** Immunocytochemical staining of HS and CS in mouse eye sections at embryonic days 9.5, 10.5, 11.5 and 14.5. Scale bars are 25  $\mu\text{m}$ . Adapted with permission under terms of the CC-BY license<sup>[443]</sup>. Copyright 2023, Wishart and Lovicu, published by MDPI. **B.** Toluidine Blue staining representing the density variation of sulfated GAGs in growth plate of wild type mice. Adapted with permission<sup>[444]</sup>. Copyright 2017, Elsevier. **C.** Ion map of N-acetylhexosamine sulphate, hexose sulfate, and hexuronic acid N-acetylhexosamine glycan fragments detected by MALDI-FT-ICR mass spectrometry in whole tissue sections from a gastric cancer patient shows a separation between areas with sulfated glycans (red and blue) and without non-sulfated area (green). Adapted with permission under terms of the CC-BY license<sup>[445]</sup>. Copyright 2017, Kunzke et al., published by Oncotarget

We present in this section several biomaterials designed for modulating the aforementioned parameters and investigating their role in the cellular response. The incorporation of GAGs into biomaterials alters their effect on stem cell fate, either directly by activating some specific cell response, or indirectly by modulating the binding of GFs and their activity. Since the various GAGs interact with specific partners and with distinct affinities, it is not surprising that each GAG can differently modulate the cellular response when incorporated into a biomaterial (**Figure 23A**). Depending on the application, some GAGs may be more adapted to trigger the desired effects. Interestingly, only a few studies compared the effect of different GAGs on specific processes. Dewey *et al.* observed the effects of different GAG types incorporated in collagen scaffolds and showed that CS-C induced the greatest endothelial tube formation compared to Hep and CS-A scaffolds, and was also associated with the highest expression of VEGF<sup>[446]</sup>. All GAGs had anti-inflammatory effects, but CS-C scaffolds were the ones with the strongest influence to decrease IL6 levels and induce the M1 to M2 macrophage gene expression transition. In the same study, Hep showed the best potential to inhibit osteoclastogenesis.

In animal tissues, the density of GAGs varies depending on tissue type but also throughout lifetime<sup>[447,448]</sup>. Therefore, it is important, in the design of a biomaterial, to consider the GAG density of the targeted tissue since it may impact the behavior and the response of cells, ultimately affecting the tissue regeneration properties of a biomaterial. However, the determination of GAG density in tissues can be complex to assess and to relate with biomaterial fabrication. The determination of GAG concentrations in body fluids such as urine plasma and serum is the most straightforward and can be performed with ultra-high-performance liquid chromatography (UHPLC) eventually coupled with mass spectrometry systems<sup>[444,449,450]</sup>. In soft and solid tissues, the determination of GAG content is more complex and only a few quantitative values of tissue-specific GAG density are available in the literature, especially for human tissues. When designing a biomaterial, it might be possible to some extent to identify a range of GAG concentrations specific to a tissue type or age of the patient. With this information, the biomaterial can be modulated in GAG density to target the best tissue regeneration properties. Wang and Yang compared the incorporation of methacrylated HS and CS at different densities in hydrogels to induce chondrogenic differentiation of hMSCs<sup>[451]</sup>. In this study, different hydrogel stiffnesses were used, and the GAG concentration was tuned between 20 mg/mL to 100 mg/mL. They observed that chondrogenesis was enhanced with CS compared to HS, especially in soft (7.5 kPa) hydrogels. The highest amount of collagen types I and II and sulfated GAGs neocartilage deposition was obtained for intermediate CS density (50 mg/mL), suggesting that GAG density has to be well regulated in tissues to induce specific cellular response (**Figure 23B**).

Several evidence demonstrated the importance of sulfation degree and specific sulfation motifs in various biological contexts. They regulate the formation of morphogen gradients (hedgehogs, BMP, Wnt), particularly important in early development<sup>[27,439,452–454]</sup>. As previously mentioned, they are also key factors for regulating the bioactivity of growth factors such as FGF, AT III or hepatocyte growth factor (HGF), VEGF, IGFs, and cell membrane receptors and coreceptors<sup>[2,134]</sup>. Therefore, the control of sulfation degree and patterns in a biomaterial has a determinant role on its properties. In the study of Tellier *et al.*, microparticles were coated with either Hep, N- or N,6-O-desulfated Hep or fully desulfated Hep to assess how Hep sulfation pattern regulates BMP2-induced ALP expression in C2C12 cells (**Figure 23C**)<sup>[327]</sup>. The microparticles coated with the most sulfated compounds (Hep and N-desulfated Hep) combined with BMP2 enhanced ALP expression compared to soluble BMP2. Microparticles carrying N,6-O-desulfated Hep and fully desulfated Hep with BMP2 were not able to promote ALP expression. This suggested that N-sulfation is not essential for efficient Hep-mediated BMP2

bioactivity, although this result was not supported by another study as previously mentioned<sup>[324]</sup>.

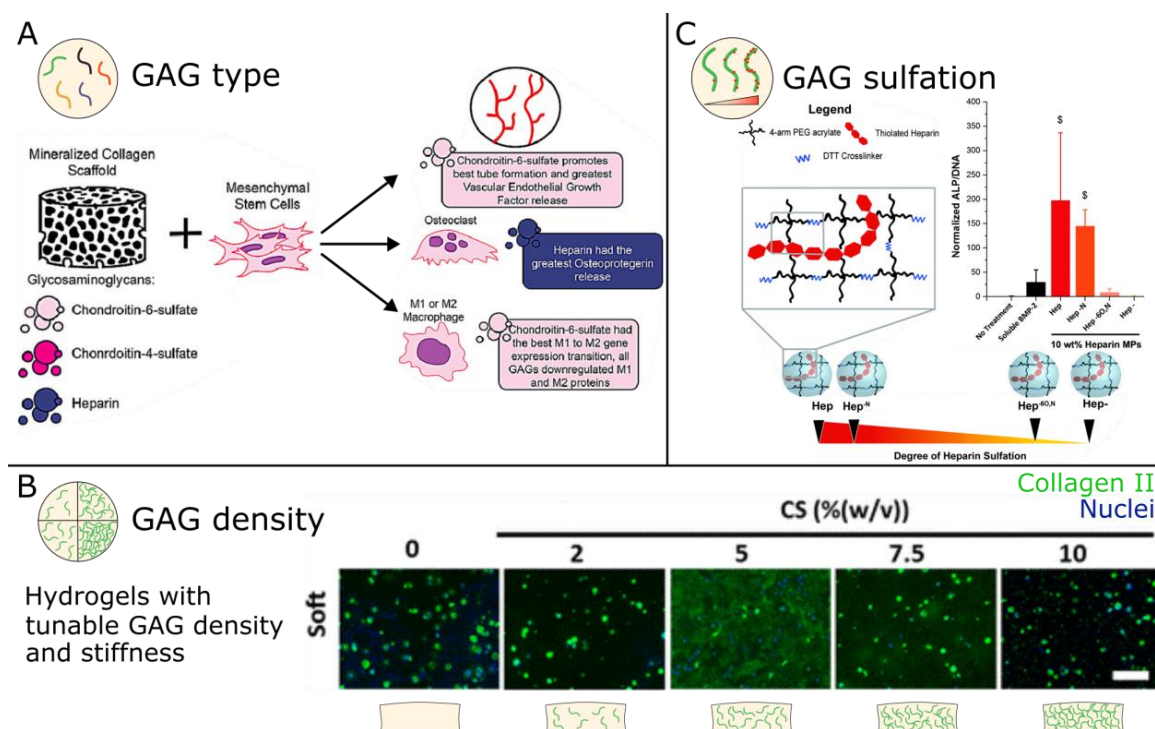


**Figure 23. Modulation of specific GAG parameters in biomaterials**

**A.** Modulation of GAG type in collagen-GAG scaffolds induces distinct differentiation pathways. Adapted with permission<sup>[446]</sup>. Copyright 2021, Elsevier. **B.** Modulation of GAG density in hydrogels induces a stronger chondrogenic response for intermediate concentrations of CS, with a more important deposition of collagen II. Scale bar is 200  $\mu\text{m}$ . Adapted under terms of the CC-BY license<sup>[451]</sup>. Copyright 2017, Wang et Yang, published by Springer Nature. **C.** Modulation of GAG sulfation degree/pattern in microparticles with BMP2 induce sulfation-dependent alkaline phosphatase (ALP) expression. Adapted with permission<sup>[327]</sup>. Copyright 2015, The Royal Society of Chemistry.

The previously presented biomaterial constructions all constitute sophisticated approaches to investigate the interplay between GAGs and growth factors within a cellular environment, each carrying its advantages and drawbacks depending on the scientific question addressed. Within the context of this thesis, we made the strategic choice of using biomimetic streptavidin (SAV) platforms, described in the following section, and offering several benefits to address our scientific aims.

### *I.E.3. Biomimetic streptavidin platforms*

An additional challenge in the design of biomaterials is to present GAGs in an oriented manner such as in the ECM, side-specifically attached to their protein core. To achieve this, Migliorini and coworkers developed a two-dimensional SAV-based biomaterial allowing the immobilization of biotinylated compounds in a controlled way (**Figure 24**)<sup>[264]</sup>. They studied

the role of HS in the regulation of BMP2 signaling by comparing the effect of soluble BMP2 (sBMP2) and HS-adsorbed BMP2 (aBMP2). Interestingly, they demonstrated that HS sustained the BMP2-induced signaling. Indeed the pSMAD1/5/9 protein content decreased over time with sBMP2, reaching a significantly lower level than with immobilized HS after 3 hours of culture. In our research group, Sefkow-Werner and coworkers also used the same biomaterial to explore the interplay between integrins and GF receptors, showing the bidirectional property of a crosstalk between these receptors<sup>[283]</sup>. Few other research groups also investigated similar SAV-based biomaterial systems, but not necessarily for cellular studies<sup>[455–457]</sup>.

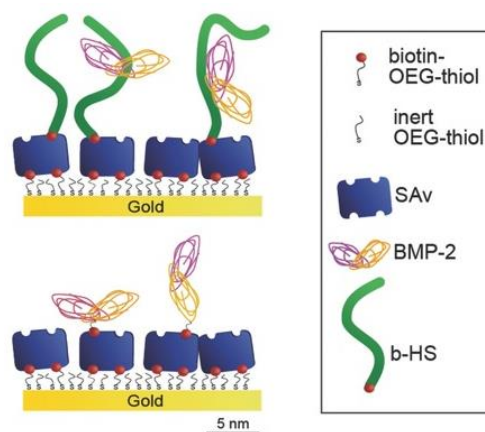


**Figure 24. Schematic representation of biomimetic SAV platforms**

SAV monolayer is functionalized on a gold substrate via a mix of thiol-PEG-biotin and inert thiol-PEG. Biotinylated molecules were next immobilized on the platform. BMP2 was adsorbed onto oriented iHS and compared to immobilized BMP2.

The concept of the biomimetic SAV platforms is to enable the binding of molecules of interest from the ECM in a controlled way for presenting them to cells. In this project, we used biomimetic SAV platforms to address the role of various GAGs in the regulation of BMP2 signaling. The biomimetic SAV platform, introduced above, is functionalized on a gold substrate using a sequential buildup with successive binding of molecules, as depicted in **Figure 25**. To functionalize the SAV monolayer, a thiol-conjugated biotinylated linker is coupled to the gold substrate.

Gold exhibits strong interactions with thiol groups following oxygen plasma or UV/Ozone activation, making it a widely used strategy for constructing self-assembled monolayers (SAMs)<sup>[458–460]</sup>. Migliorini *et al.* used a blend comprising thiol-conjugated PEG and PEG-biotin to establish a SAM on gold substrates, with a specific 95:5 molar providing the optimal amount of biotins that ensure the availability of biotin-binding sites facing upwards the protein<sup>[461]</sup>. Furthermore, the incorporation of PEG chains into biomaterials is known to reduce effectively undesired protein adsorption, especially in SAMs<sup>[462,463]</sup>.

The functionalized SAV monolayer next serves as a molecular breadboard for the attachment of various biotinylated ligands. The interaction between SAV and biotin is extremely affine. With a  $K_D$  estimated to  $10^{-15}$  M, it constitutes one of the strongest interactions occurring in nature<sup>[464]</sup>, thereby providing a robust functionalization strategy for biomaterials. From previous works using similar constructs, we can estimate an average binding of 1.68 to 1.95 biotinylated compounds per SAV molecule<sup>[456]</sup>.

A further development of the biomimetic SAV platforms is the co-functionalization of two different biotinylated molecules on the same SAV monolayer. This approach has been employed to improve the cell adhesion properties of the platforms using biotinylated cell adhesion molecules such as intercellular adhesion molecule 1 (ICAM-1)<sup>[461]</sup> or cyclic RGD (cRGD) integrin ligand<sup>[465]</sup>. Sefkow-Werner and coworkers co-functionalized the cRGD peptide in combination with HS<sup>[283]</sup>. Using a technique called quartz crystal microbalance with dissipation monitoring (QCM-D), they could determine concentrations and incubation times to perform a partial functionalization of the SAV, preventing the saturation of all biotin-binding sites and allowing subsequent binding of the second molecule of interest.

In addition to biotinylated molecules, biomimetic SAV platforms can also be employed to investigate interactions with non-biotinylated substrate molecules. As an example, Migliorini *et al.* previously used biomimetic platforms functionalized with BMP2 adsorbed to HS<sup>[264]</sup>. Unlike the SAV-biotin interaction, this type of interaction is partly reversible, depending on its affinity. The interaction of BMP2 with HS seemed rather stable, since it sustained the signaling for up to three days, as measured with an ALP assay.

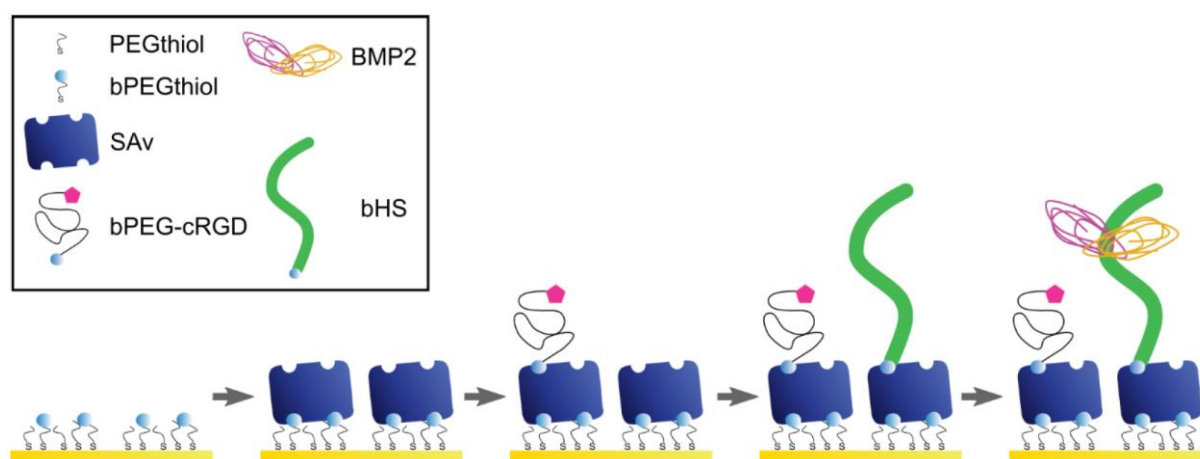


**Figure 25. Sequential buildup of the SAV biomimetic platform on gold substrates**

Molecules in solution are incubated with the gold substrate to form a SAM of SAV allowing the binding of biotinylated compounds such as cRGD and HS. In the case of cRGD co-functionalization with HS, the cRGD incubation is stopped before saturation of the biotin-binding sites of SAV, to allow subsequent binding of biotinylated HS (bHS) on the remaining available binding sites<sup>[283]</sup>.

### *I.E.3.a. Advantages and opportunities for development*

The biomimetic SAV platforms exhibit several advantages but also carry opportunities for further developments to improve their potential.

The biomimetic platform being founded on the key SAV-biotin interactions, their design offers great flexibility in tailoring the platform construction to specific needs. Indeed, any molecules of interest can be biotinylated and immobilized on the platforms to be investigated in association with one or a few other co-functionalized compounds. For instance, the co-functionalization of GAGs with adhesion peptides offers enhanced cellular adhesion properties for cellular assays. Furthermore, the platforms are compatible with commonly used biophysical techniques such as QCM-D, enabling convenient *ex situ* characterization of newly made design adaptations. The platforms also appear to be suited for modulating molecular surface density, by determining the adequate concentration and incubation time to occupy the biotin-binding sites of SAV to the desired extent. This property could be particularly interesting to investigate the role of GAG density in the binding of proteins and in the induced cellular response.

For cellular studies, the experimental setup of Migliorini *et al.* is based on gold-sputtered 2.4 cm x 2.4 cm glass coverslips, which remain compatible with optical and fluorescence microscopy due to the thin layer of 1.5 nm Cr and 8 nm Au<sup>[264]</sup>. Sefkow-Werner *et al.* next improved the system by gluing the PEG-passivated gold surfaces to standardized bottomless 96-well plates, thereby dividing the surface into 4 different wells that increase the number of conditions achievable within an experiment and reduce the sample quantity required for functionalization<sup>[283]</sup>. Lastly, the previous use of the platforms for studying the interplay between BMP2 and HS highlights its potential for investigating GAG-BMP2 interactions in a broader context.

Apart from these advantages, this experimental setup carries potential to be further developed. The use of gold-sputtering equipment to prepare gold surfaces is time-consuming and requires an expensive access to a clean-room facility. Moreover, such surfaces need to be manually glued to bottomless 96-well plate using a double-sided tape, which represents a delicate step. The successive steps of the functionalization being performed with manual pipetting, it is also extensively time-consuming. Although optically transparent, the gold-sputtered surfaces require the use of high-power excitation sources to be compatible with fluorescence microscopy and may generate diffraction artifacts. In the absence of a direct characterization method for the functionalized platforms intended for cellular studies, the characterization is performed *ex situ*

using QCM-D. Therefore, we have to assume there is no significant difference between the QCM-D crystals and the functionalized platforms for cellular studies.

Other strategies have been developed to prepare SAMs on negatively charged glass or metal oxide surfaces, which are optically transparent (**Figure 26**). These strategies include the functionalization of a lipid-supported bilayer (**Figure 26A**)<sup>[461]</sup> or covalent silane-PEG molecules (**Figure 26B**)<sup>[466]</sup>, or more recently to silicon oxide by electrostatic and covalent immobilization of a complex polymer termed PAcrAmTM-g-(PEG,NH<sub>2</sub>, Si) (**Figure 26C**)<sup>[467]</sup>. For the latter, stability is conferred through covalent siloxane binding to the silicon oxide surface, while additional electrostatic binding ensures resilience and allows achieving an optimal packing of the macromolecule on the surface<sup>[467]</sup>. The most commonly employed strategy is the electrostatic adsorption of poly(L-lysine)-graft-poly(ethylene glycol) (PLLgPEG) and several studies have investigated the influence of PEG grafting ratio (g) and chain length on the polymer architecture in liquid and its anti-fouling properties (**Figure 26D**)<sup>[468–470]</sup>. Such strategies may be interesting for future improvements. In particular, it would allow the functionalization of biomimetic platforms on commercial 96-well plates, ruling out the necessity of gold-sputtering and gluing surfaces, and providing a more adequate substrate for optical and fluorescence microscopy.

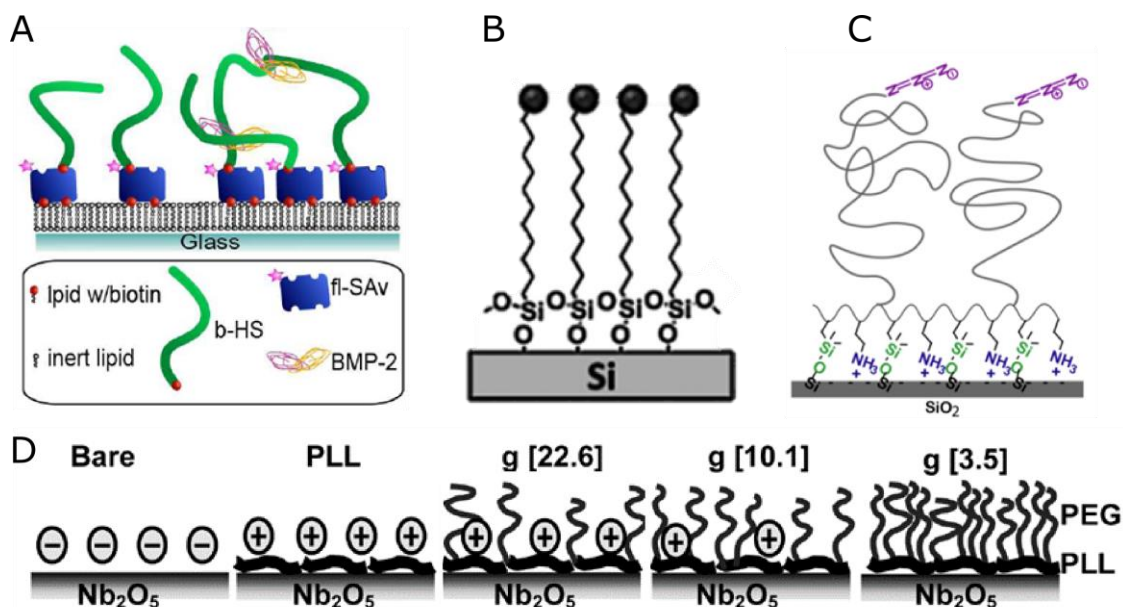


**Figure 26. Strategies for building SAMs on optically transparent substrates**

**A.** Supported lipid bilayer with SAv functionalization Adapted with permission<sup>[264]</sup>. **B.** Silane-PEG covalent immobilization. Adapted with permission under the terms CC BY-NC 3.0.<sup>[471]</sup> **C.** PAcrAmTM-g-(PEG,NH<sub>2</sub>, Si) bi-covalent-electrostatic functionalization. Adapted with permission under the terms CC BY<sup>[467]</sup>. **D.** PLLgPEG electrostatic functionalization on negatively charged surface. The grafting ratio (number of lysine monomers to PEG chains) is indicated as g [x]. Adapted with permission<sup>[470]</sup>.

As previously mentioned, the functionalization process of biomimetic platforms is manual, time-consuming, and prone to errors. In our team, Machillot *et al.* previously developed a liquid-handling robot system to automate the functionalization of layer-by-layer (Lbl) films in 96-well plates, previously performed manually, with alternative deposition of twelve PLL and HA layers<sup>[472]</sup> (**Figure 27**). In particular, they implemented an automated plate tilting that allowed complete aspiration of the liquid in microwells to perform efficiently the rinsing steps between each molecule deposition.

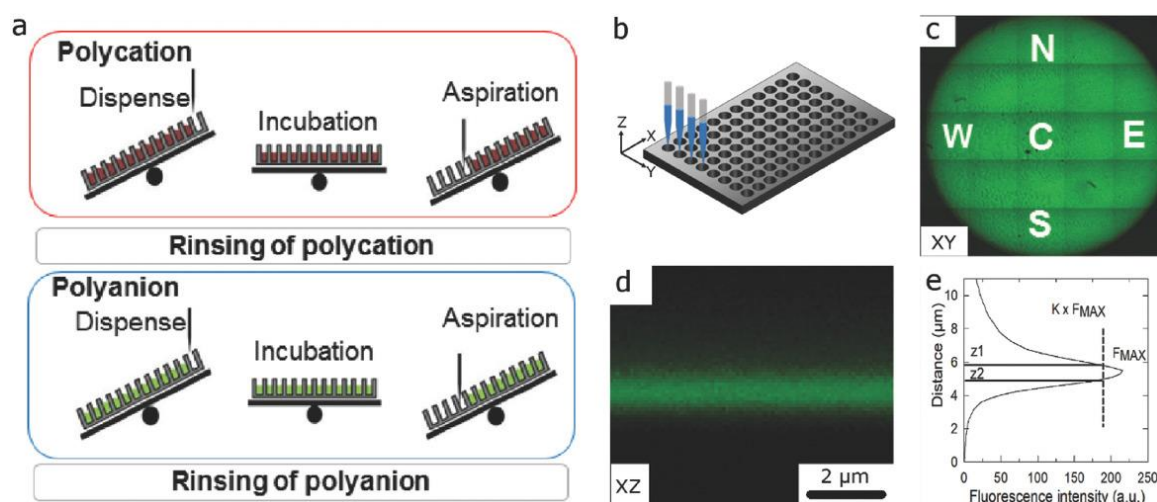


**Figure 27. Automation of Lbl functionalization by a liquid-handling robot**

**a.** Lbl fabrication process by successive incubation and rinsing of PLL polycation and HA polyanion. The 96-well plate is tilted for dispensing and aspirating the solutions deposited in 96-well plates. **b.** Scheme of the liquid-handling robot functionalization. **c.** Fluorescently-labelled Lbl film homogeneity in a microwell tile-scan. **d.** Lbl film thickness visualized by z-stacks images **e.** Quantification of LBL film thickness based on the z-stack. Reproduced with permission<sup>[472]</sup>.

This new setup improved greatly the homogeneity and the reproducibility of the produced Lbl films, also saving precious time for the researcher. Few experimental parameters could be easily changed (number of multilayers or the choice of wells) but the process was developed to achieve a single task: performing the highly repetitive incubation and rinsing steps of these two molecules, after depositing a base layer of polyethyleneimine (PEI). Therefore, this process is not yet adapted for the versatile functionalization of biomimetic SAV platforms including several different molecules but it represents a great potential for future developments.



## **Chapter II. Objectives of the PhD thesis**

As previously introduced, the role of GAGs in the regulation of BMP signaling remains unclear, even for HS and Hep, which have been extensively studied. While a consensus seems established regarding the contribution of GAGs in the formation of BMP gradients, the direct influence of GAGs on BMP signaling is subject to many controversies, thus requiring further investigation. In particular, the role of GAGs besides HS and Hep has been so far disregarded, leaving unexplored the effects of CS, DS, HA, and KS in the BMP signaling. Additionally, we speculate that GAGs may elicit different signaling mechanisms when located at the cell surface or in the extracellular matrix, thereby contributing to the observed discrepancies in the literature. Specific sulfation motifs of Hep have been demonstrated to have different roles for the binding of BMP2 and its signaling, with N- and 6O- sulfates appearing to be the two most important motifs<sup>[324,327]</sup>. Nevertheless, it has not been elucidated whether the BMP2 interaction with HS is responsive to specific sequences with key sulfation patterns.

The first objective of my PhD thesis consisted in methodological development to pave the way for investigating the role of various GAG compounds in the presentation and signaling of BMP2. To conduct these experiments, it was necessary to explore a wide range of conditions, which required high levels of parallelization and automation. Regarding molecular interactions, the BLI technique is particularly adapted to investigate many conditions since it has a higher throughput than surface plasmon resonance (SPR). In contrast, the cellular experiments on biomimetic SAV platforms exhibited a restricted parallelization capacity. Indeed, the requirement of gold surfaces limited the number of conditions in a 96-well plate and the multi-step build-up process was time-consuming, involving gold sputtering, gluing surfaces on bottomless plates, and manual pipetting. Therefore, we aimed to develop a new approach for building biomimetic SAV platforms on standardized 96-well plates. Furthermore, to increase the parallelization degree of our experimental setup, we inspected the possibilities of implementing new functionalities to a liquid-handling robot available in the team for automating the SAV platform functionalization.

The second and main objective of my PhD was to decipher the role of the type and the localization of GAGs in BMP2 binding and signaling. In this context, we first aimed to explore the molecular interactions between BMP2 and diverse GAGs. Using the biolayer interferometry (BLI) technique, we sought to provide in-depth information about the molecular dynamics between BMP2 and GAGs compounds, such as affinity, association and dissociation rates. Alongside, our strategy was to prepare and use a library of structurally defined HS-oligosaccharides to investigate whether specific sulfation patterns within HS sequences have a

crucial influence on the BMP2 interaction. Furthermore, we planned to investigate the interplay between GAGs and BMP2 in a cellular context using biomimetic SAV platforms, to provide novel insights about the type, sulfation, and localization of GAGs. We intend to correlate these findings with molecular interaction data obtained from the BLI studies.

In the frame of achieving this objective, we identified that the biomimetic SAV platforms in their existing state were unsuitable for our investigations due to BMP2 non-specific adsorption. A limited amount of BMP2 non-specific attachment on components of the platforms, besides GAGs, induced significant BMP2 signaling and hampered the use of the platforms for our purposes. Therefore, we explored various options aimed at improving their anti-fouling properties.

Overall, the work achieved during my PhD is divided into three chapters written in the form of articles, which are summarized below.

**Chapter III:** Biomimetic SAV platforms were newly constructed on glass with a PLLgPEG-biotin linker. The surfaces were characterized *ex situ* with QCM-D and spectroscopic ellipsometry as well as *in situ* through photobleaching image correlation spectroscopy. Tools were developed to enable the automated functionalization procedure of up to 96 distinct biomimetic SAV platforms within a standardized glass-bottom 96-well plate.

**Chapter IV:** The molecular interactions between HS, HA, DS, and various CS types (-A, -D, -E) were investigated with BLI. Biomimetic SAV platforms with reduced non-specific BMP2 adsorption were characterized extensively for performing cellular experiments to investigate the role of extracellular GAGs in BMP2 signaling. The effects of cell-surface GAGs were explored by employing CHO cell mutants for GAG biosynthesis. The requirement of specific HS sulfation patterns for the interaction with BMP2 was examined with BLI employing a library of HS-derived oligosaccharides.

**Chapter V:** A limited non-specific adsorption of BMP2 on biomimetic SAV platforms induced significant signaling to the cells. Several control experiments have been performed to understand the origins of this non-specific adsorption and various condition optimizations have been undertaken to reduce this phenomenon, thereby allowing the study of GAGs with the biomimetic platforms (**Chapter IV**).



## **Chapter III. Materials and methods**

In this chapter, I have chosen to highlight the preparation of specific materials and the most specific methods employed in this thesis, providing a description of their operation principles, important for the understanding of the following chapters. Additional information about the experimental conditions adopted for each measurement, or about other methods not detailed here, are described within the material and methods section of each article.

## Materials

### Functionalization of biomimetic SAv platforms for cellular studies

The fabrication of biomimetic SAv platforms built on gold substrates requires the initial preparation of gold-sputtered surfaces. To this end, glass coverslips (24×24 mm; Menzel Gläser) were first cleaned in acetone and isopropanol baths with sonication, before being gold-sputtered (1.5 nm Cr and 8 nm Au) in a clean room with a Plassys™ evaporating machine (**Figure 28A**). Gold-sputtered surfaces were activated with UV/Ozone Procleaner™ (BioForce Nanosciences) for 10 min, functionalized with mPEG-Thiol and biotin-PEG-Thiol, and immersed overnight in an ethanol solution with 0.95 mM mPEG-thiol and 0.05 mM biotin-PEG-thiol, before blow-drying the surfaces with nitrogen. When preparing samples for automated immunofluorescence analysis, gold-coated surfaces were attached to the bottom side of a bottomless 96-well plate (Greiner Bio-one) using double-sided adhesive tape (FRAP Sandwich set, Paul Marienfeld), dividing one surface into four wells (**Figure 28B**).

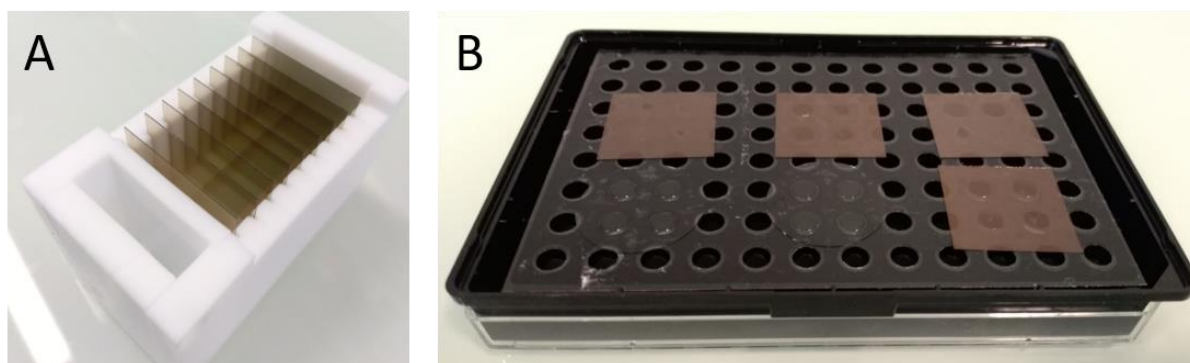


**Figure 28. Preparation of gold-sputtered surfaces**

*A. The surfaces after gold sputtering with the evaporating machine in the clean room*

*B. Four square gold surfaces glued on bottomless 96-well plate. In comparison, two round glass surfaces were also glued.*

Next, the assembly of SAv platforms was achieved by a liquid-handling robot executing the incubation of all molecules (SAv, cRGD, biotinylated GAGs and BMP2) and rinsing steps as described in previous work<sup>[47]</sup> and in the introduction of this thesis.

## Library of HS-oligosaccharides

The preparation of our library of HS-derived oligosaccharides was achieved in three main steps described below:

- Digestion of native HS

First, 8 g of native HS from porcine intestinal mucosa (Celsus Laboratories, 12 kDa average, polydispersity of 1.59) were exhaustively digested with heparinase III at 37°C in heparinase buffer: 100 mM sodium acetate and 0.5 mM CaCl<sub>2</sub> buffer at pH 7.1. The substrate specificity of heparinase III allows generating fragments from highly sulfated domains (NS domains). The enzyme cleavage generates unsaturated bonds at the non-reducing end of oligosaccharides, absorbing at 232 nm. The digestion was monitored for 6 days by absorbance measurements at 232 nm with a NanoDrop™ 2000. The content of the digestion was then stored at -20 °C in eight fractions of 1 g.

- Size-exclusion chromatography (SEC)

The digested HS was next separated by size using SEC, a robust chromatography technique commonly employed for the separation of macromolecules based on their hydrodynamic volume<sup>[178]</sup>. The working principle of SEC relies on the ability of compounds to enter the pores of beads constituting the stationary phase of the column. Depending on their hydrodynamic volume, the analyte will enter a different number of pores, modulating their elution time. Smaller molecules will enter to more pores, thus moving slower in the column than larger molecules (**Figure 29**). The use of mobile phases with high ionic strength allows reducing unwanted electrostatic interactions of analytes with the stationary phase. In our case, we used a Vantage® L VL44 x 1000 column, extended with a Vantage extension kit (Merck-Millipore), and packed with Bio-Gel® P-10 Gel resin (Bio-Rad), equilibrated in 0.2 M NaCl buffer at a flow rate of 0.5 mL/min. Fractions of 15 mL were collected, and the absorbance at 232 nm was measured for all fractions to identify the peaks corresponding to oligosaccharides of different sizes, which were then pooled, dialyzed against water, and lyophilized.

- Strong anion exchange high-performance liquid chromatography (SAX-HPLC)

The tetrasaccharides (polymerization degree: dp4) and hexasaccharides (polymerization degree: dp6) collected with SEC were then separated according to their charge by SAX-HPLC. SAX-HPLC is a widely used chromatography technique for separating analytes based on their charge, and is “the approved method for FDA-approved quality control of pharmaceutical Hep”<sup>[178]</sup>. This method relies on a column stationary phase composed of positively charged groups like quarternary amines. Negatively charged analytes, such as GAG compounds, interact

with the stationary phase and are retained in the column under low ionic conditions (**Figure 29**). Gradually increasing the ionic strength of the mobile phase allows achieving the separation of anionic compounds based on their charge. For small GAG oligosaccharides with identical number of sulfates, there is a significant degree of separation based on the presence of 2OS, 6OS, and NS groups, but this resolution decreases with larger oligosaccharides. In our case, HS-dp4 and HS-dp6 were separated using a ProPac PA1 preparative column (ThermoFisher Scientific) composed of quarternary amines. The salt gradient was optimized to resolve the different oligosaccharide species out of the column and each sample injection in the column used 5 mg of oligosaccharides, for a total of ~65 mg of each dp4 and dp6 oligosaccharides.

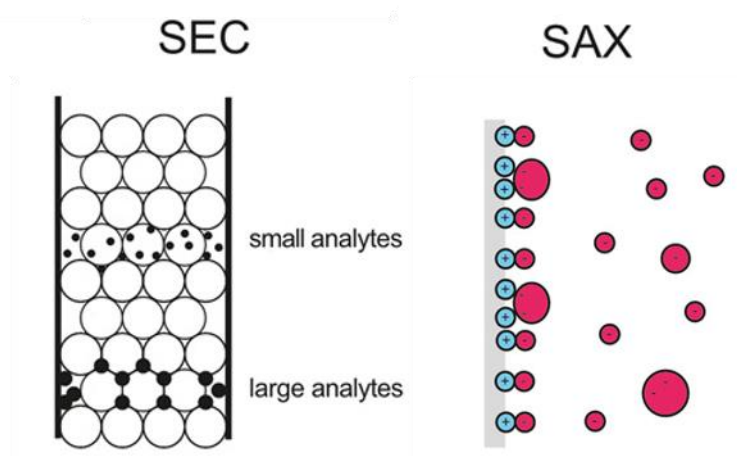


**Figure 29. Chromatography methods for HS-oligosaccharide separation.**  
*Reproduced with permission<sup>[178]</sup>.*

### **Biotinylation of GAGs and oligosaccharides**

For functionalization on biomimetic platforms and molecular interaction studies, GAGs and HS-oligosaccharides were biotinylated at their reducing-end through oxime ligation that yields a more stable product than biotinylation through hydrazine linkage<sup>[442]</sup>. GAGs or HS-oligosaccharides were incubated for 24 h at 37°C at 5 mg/mL concentration in 100 nM sodium acetate, 12.5 nM EZ-Link Alkoxyamine-PEG4-biotin (ThermoFisher Scientific), and 10 mM aniline (Sigma-Aldrich) to achieve coupling with the biotinylated linker. Double HiTrap® Desalting columns (GE29-0486-84, Sigma-Aldrich) coupled to AKTA Pure equipment (GE Healthcare) were used to identify and recover the fractions of desalted biotinylated GAGs. The compounds were next concentrated by freeze-drying.

## Methods

### Reverse-phase ion pair high-performance liquid chromatography

Reverse-phase ion-pair high-performance liquid chromatography (RPIP-HPLC) is a common method for the separation of di- and oligo-saccharides and is particularly used for full disaccharide compositional analysis<sup>[473]</sup>. In our case, we used RPIP-HPLC for disaccharide analysis of our HS-derived oligosaccharides library.

This liquid chromatography technique involves a hydrophobic stationary phase (reverse phase column) and an (essentially) aqueous mobile phase including an ion pairing reagent (IPR). The IPR features a hydrophobic moiety and an ionic group that has the opposite charge of the studied analyte. Through its hydrophobic part, the IPR binds and covers the reverse phase column surface, thereby displaying a charged surface to the mobile phase, allowing binding of the analyte. The elution of the analyte is achieved by applying a salt gradient to the column, which reduces the stability of analyte-IPR complexes and thereby disrupts the analyte interaction with the stationary phase. In our case, the experimental setup used a reverse-phase column packed with octadecyl (C18)-coated silica particles (Luna 5  $\mu\text{m}$  C18, 4.6 x 300 mm, Phenomenex) and tetra-N-butylammonium hydrogen sulfate (TBA) as IPR (**Figure 30**).

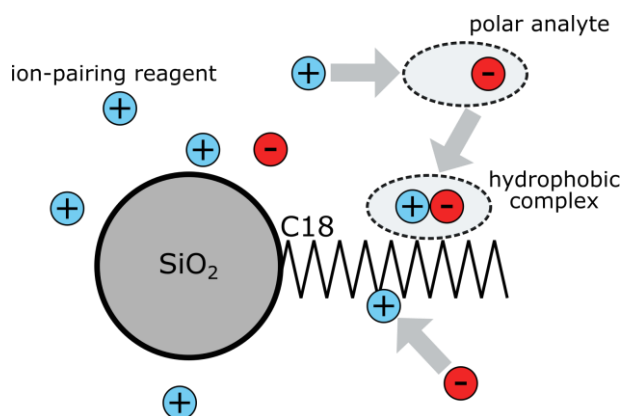


**Figure 30. Scheme of molecular interactions within the RPIP-HPLC**

The ion-pairing reagent (blue) binds the polar analyte (GAG) to form a neutral hydrophobic complex that interacts with the hydrophobic stationary phase (C18-coated silica particles). Simultaneously, it also binds through its hydrophobic domain to the stationary phase prior to being joined by the polar analyte. Inspired from <sup>[178]</sup>.

The elution of unsaturated HS disaccharides (obtained with heparinase I/II/III digestion) was performed at 0.5 mL/min in 1.2 mM tetra-N-butylammonium hydrogen sulfate (TBA), pH 3.15 with 8.5% (v/v) acetonitrile and using a NaCl gradient generated by a first set of pumps (Pump 1, **Figure 31A-B**) and calibrated with HS disaccharide standards.

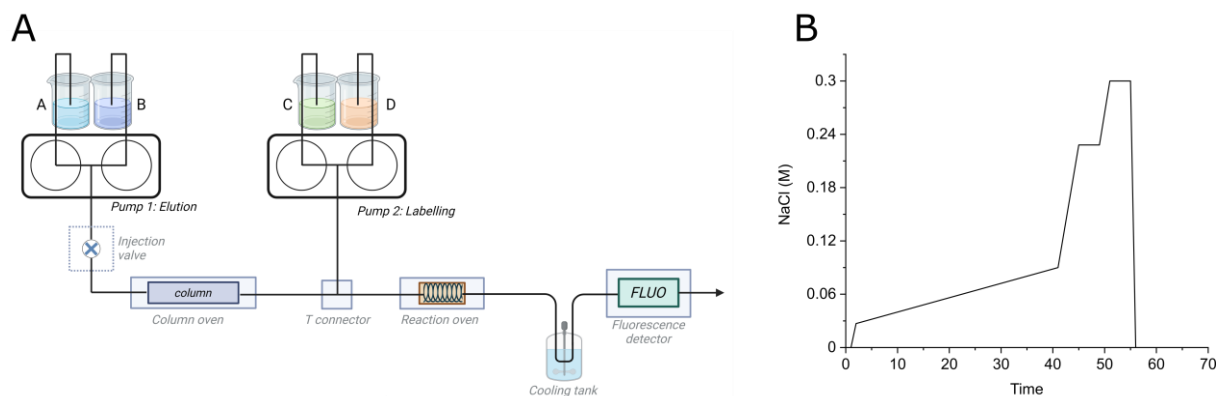


**Figure 31. Experimental setup of the RPIP-HPLC system**

**A.** Scheme of the RPIP-HPLC setup. Created with Biorender. **B.** NaCl gradient applied for the elution of HS-disaccharides.

In addition, a second set of pumps (Pump 2, **Figure 31**) adds 0.25% 2-cyanoacetamide and 1% NaOH at 0.16 mL/min to the column eluents, to allow the fluorescence labelling of the resolved disaccharides through a passage in a 130°C-heated reaction oven. The reaction mechanism of 2-cyanoacetamide with carbohydrates in weakly alkaline conditions is complex, as illustrated by the reaction with glucose in **Figure 32**<sup>[474]</sup>.

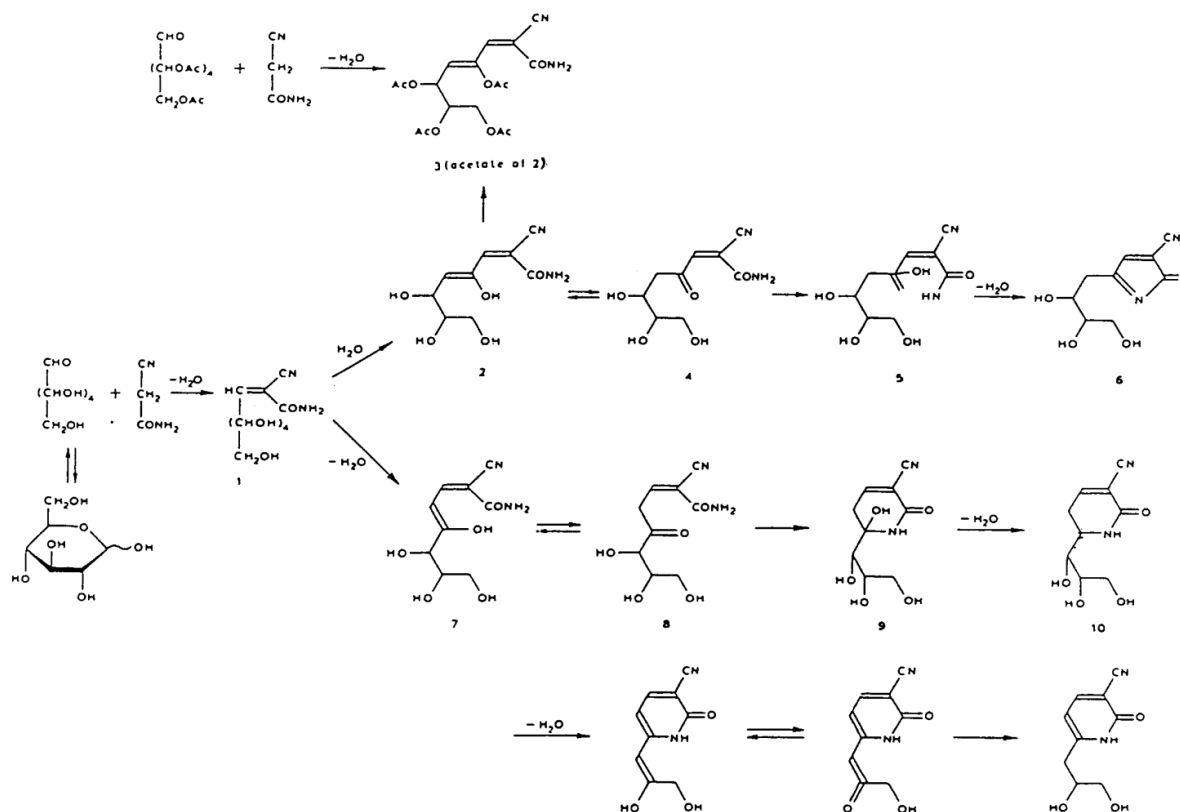


**Figure 32. Reaction of 2-cyanoacetamide with glucose**

The compounds 6 and 13 are considered the fluorescence-generating entities of the reaction. Reproduced with permission<sup>[475]</sup>.

The reaction has been adapted for the detection of unsaturated GAGs disaccharides<sup>[476,477]</sup>, where the labelled disaccharides are detected by the 410 nm fluorescence emission after

excitation at 346 nm, in contrast to neutral sugars that exhibit maximum fluorescence intensity with 331 nm excitation and 383 nm emission wavelengths. It is worth noting that the fluorescence formation is restricted to reducing carbohydrates<sup>[474]</sup>, which has important implications to determine the reducing end of oligosaccharides.

Disaccharide composition was attributed by comparison to the elution of standard unsaturated HS disaccharides (**Figure 33**) (Iduron, Alreley Edge, UK:  $\Delta$ UA–GlcNAc/ $\Delta$ UA–GlcNS / $\Delta$ UA–GlcNAc6S / $\Delta$ UA2S – GlcNAc / $\Delta$ UA – GlcNS6S / $\Delta$ UA,2S – GlcNS / $\Delta$ UA,2S – GlcNAc,6S / $\Delta$ UA2S – GlcNS6S). By integrating the area of disaccharide peaks and applying signal / mass ratio corrections, we could determine the quantities generated for the entire oligosaccharide library.

To determine the sequence of HS oligosaccharides, a second analysis was undertaken with an initial reduction step performed overnight at 37°C with 50 mM NaOH and 150 mM NaBH<sub>4</sub>, prior to digesting oligosaccharides. Consequently, the reducing-end disaccharide was excluded from the labelling procedure, allowing to identify it by comparison of the two analysis RPIP-HPLC profiles.

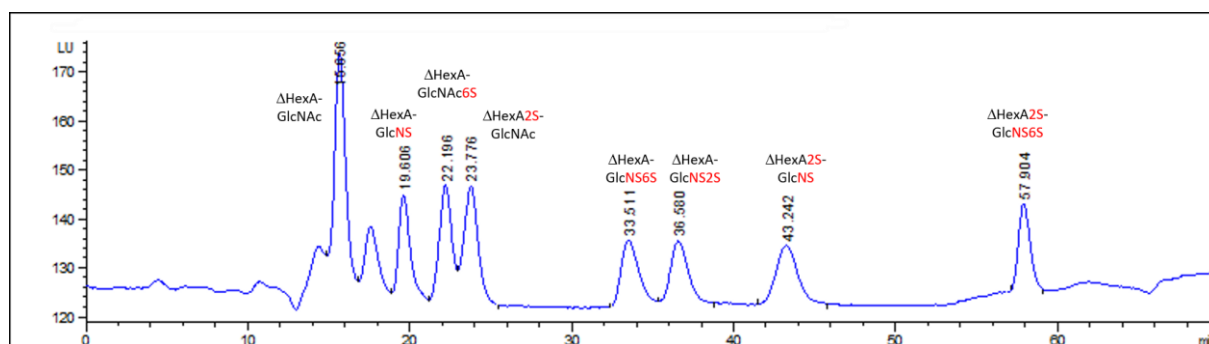


**Figure 33.** Elution of HS-disaccharide standards with RPIP-HPLC

The elution of the unsaturated ( $\Delta$ ) HS disaccharide standards from the reverse phase column is detected by fluorescence detection for 70 minutes.

## QCM-D

Quartz Crystal Microbalance with Dissipation Monitoring (QCM-D) is a technique used to characterize molecular interactions at surfaces<sup>[478,479]</sup>. A piezoelectric quartz crystal (**Figure 34A**) connected to electrodes serves as a substrate to detect the binding of molecules. Commercial quartz crystals are available with a wide range of coatings such as gold or SiO<sub>2</sub>. Quartz being a piezoelectric material, the mechanical constraints are converted in electric signals and inversely. Therefore, when an oscillating voltage is applied to the crystal, the crystal resonates at a specific resonance frequency (**Figure 34B-C**). Upon adsorption of molecules at

the surface, the oscillation frequency of the crystal decreases, which is detected by the QCM-D setup as a shift in the voltage oscillation frequency. When operating in liquid conditions, the QCM-D devices provide an additional readout compared to standard QCM, which is the dissipation monitoring. The dissipation measurement is obtained by monitoring the decay in the signal amplitude after the drive potential has been switched off<sup>[480]</sup>. The rate of decay is fitted to an exponential curve from the moment when the drive potential is switched off (**Figure 34C**). The dissipation parameter corresponds to a coefficient of the fitted exponential curve, indicating a loss of energy. The dissipation therefore reflects the rigidity of the adsorbed film; *i.e.*: high dissipation meaning a soft film and low dissipation a rigid film.

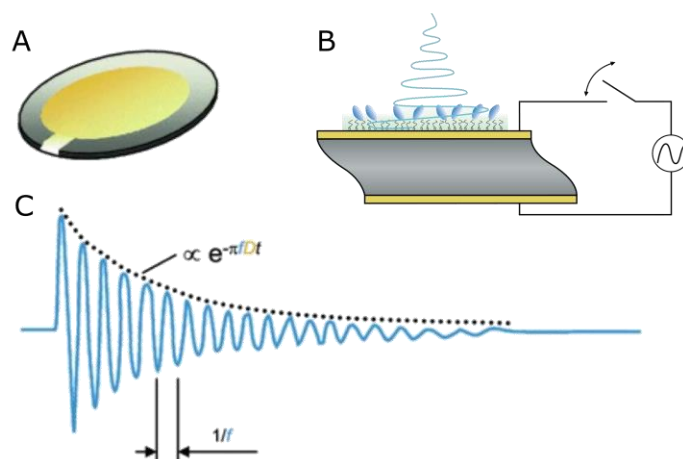


**Figure 34. Principle of QCM-D technique**

**A.** Quartz crystal with gold surface for molecule deposition. **B.** Oscillation of the crystal induced by applying a driving electric potential. **C.** Exponential decay of the signal amplitude over time ( $t$ ) after switching off the driving potential.  $f$ : resonance frequency;  $D$ : dissipation parameter. Adapted with permission<sup>[479,481]</sup>.

Both frequency and dissipation are measured by the QCM-D at multiple overtones of the resonance frequency ( $n$ ), typically 1, 3, 5, 7, 9, 11, and 13. As the overtone number increases, there is a reduction in the penetration depth, enabling to determine information at specific layers within the deposited film. Rigid films exhibit no strong variations among overtones, whereas viscoelastic films display varying frequency or dissipation signals depending on the overtone. In rigid films, mostly encountered when measurements are performed in air, the Sauerbray equation (**Equation 1**) enables to determine the molecule surface concentration<sup>[482]</sup>:

$$\Delta m = -\frac{C}{n} \Delta f \quad (1)$$

$C = 18 \text{ ng} \cdot \text{cm}^{-2} \cdot \text{Hz}^{-1}$  where  $C$  is the mass sensitivity constant

The Sauerbrey equation may be used in liquid conditions if the dissipation shift is small ( $\Delta D \sim 0$ ). More precisely, it was determined that it could be applied under the following conditions (**Equation 2**), where  $n$  corresponds to the overtone number<sup>[482]</sup>:

$$\frac{-\Delta D_n}{\Delta f_n/n} \ll 0.4 \cdot 10^{-6} \text{ Hz} \quad (2)$$

Even in the case of rigid films (Equation 2), the Sauerbrey equation is always a measurement of the hydrated mass adsorbed on the surface (mass of the molecules + the solvent around them). The QCM-D technique is particularly adapted to follow the sequential buildup of biomaterials. In the **Figure 35** is depicted the QCM-D monitoring of the functionalization of SAV biomimetic platforms. Upon binding of SAV, biotinylated HS (bHS), and BMP2, the frequency gradually decreases, confirming the functionalization of these molecules. The dissipation increases mostly during the binding of bHS, while it decreases for BMP2 binding. As previously shown, this indicates that BMP2 rigidifies the molecule film by crosslinking the HS chains<sup>[264]</sup>.

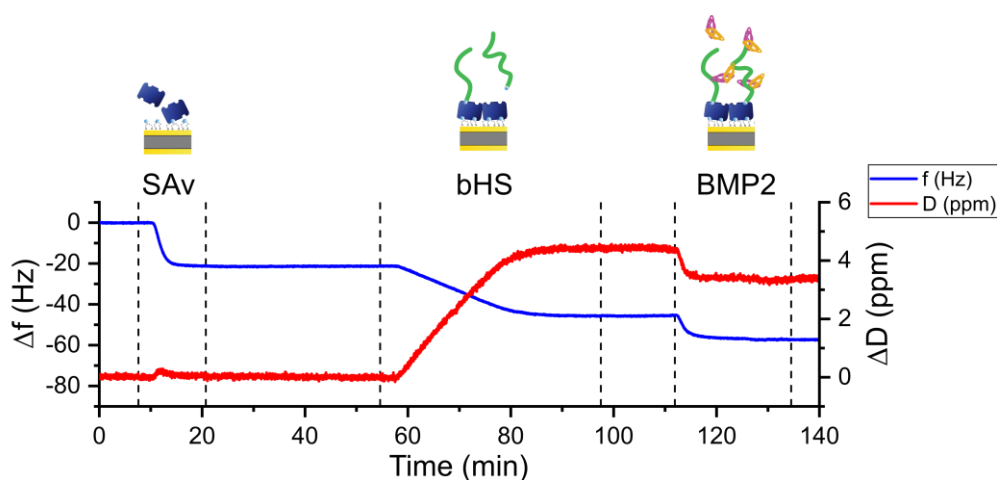


**Figure 35. QCM-D characterization of SAV biomimetic platforms functionalization**  
 $\Delta f$  and  $\Delta D$  corresponds to the shifts in frequency and dissipation shown for the third overtones ( $n=3$ ).

### Bilayer Interferometry

Bilayer interferometry (BLI) is a biophysical technique that enables the investigation of molecular interactions. It shares many similarities with surface plasmon resonance (SPR), as they are both label-free optical techniques allowing the determination of interaction kinetic parameters ( $k_{on}$ ,  $k_{off}$ ,  $K_D$ ). Despite that, the working principles of the two techniques are rather different. BLI instruments (**Figure 36A**) are based on reflectometry interference spectroscopy and use disposable glass fiber tips (biosensors) that are successively dipped into solutions disposed in 96-well plates, maintained at constant agitation (**Figure 36B**). The biosensors can be functionalized with a ligand to detect the binding of an analyte molecule. To facilitate the immobilization of ligands, BLI biosensors are commercially available with various base coatings such as anti-Fc, anti-Fab, Amine Reactive 2G, protein A/L/G, aminopropylsilane, anti-His and Ni-NTA biosensors. In our studies, we used an OctetRED96e BLI instrument and commercial SAV pre-coated biosensors allowing efficient binding of biotinylated GAG ligands.

A



B



**Figure 36. Experimental setup of BLI technique**

**A.** The OctetRED96e BLI instrument. **B.** BLI biosensor tips are moved by an automated system to the wells of a 96-well plate containing ligand, analyte, buffer or any other solution. Reproduced with permission<sup>[483]</sup>.

The principle of the binding detection relies on an incident white light travelling through the sensor and being reflected in different wavelengths at various interfaces: the internal reference interface and the interface of bound molecules on the surface of the biosensors (**Figure 37**). Upon analyte binding, the optical thickness perceived by the biosensor changes, shifting the interference pattern detected<sup>[484]</sup>. After detection, the signals are processed to compute a wavelength shift (or spectral shift,  $\Delta\lambda$  [nm], **Figure 37**) that is proportional to the binding of molecules.

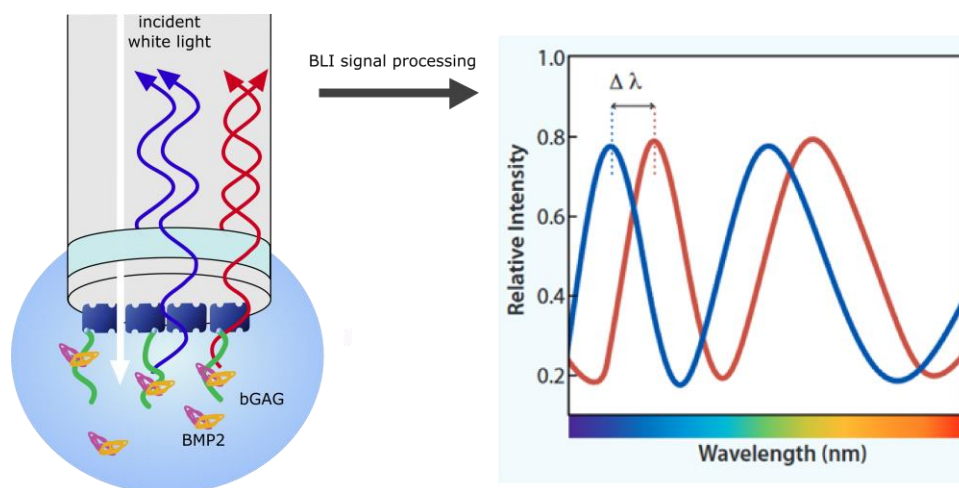


**Figure 37. Biophysical principle of BLI technique**

An incident white light is reflected in different wavelengths at the internal reference interface of the biosensor and at the interface of bound molecules at the surface. The interference pattern detected from the reflected wavelengths is processed to determine a spectral shift ( $\Delta\lambda$ ) that is correlated to the binding of molecules.

The typical process to determine kinetic parameters of a molecular interaction consists in immobilizing the ligand and then measuring the analyte association and dissociation at different concentrations, ideally covering the concentration range from  $0.1 K_D$  and  $10 K_D$  (**Figure 38**). Short NaCl pulses can also be used before analyte association or after to dissociate the analyte

from the biosensors and regenerate them for reuse. For interactions of proteins with GAGs, the GAG ligand immobilization level should be very low to avoid mass transport and steric hindrance effects that are facilitated with large chains.

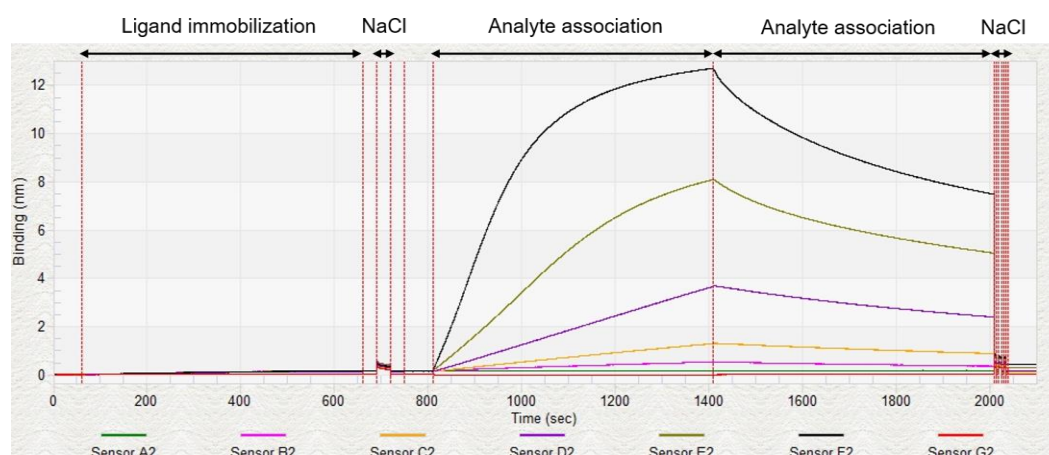


**Figure 38. Kinetic sensorgram of HS/BMP2 interactions**

The different steps of the sensorgram include baselines, immobilization of the ligand (here biotinylated HS), analyte association (here with BMP2) and dissociation steps, NaCl pulses for disrupting protein interactions and sensor regeneration. Sensors are incubated with increasing analyte (BMP2) concentrations.

Next, the kinetic data were fitted with a 1:1 Langmuir model and kinetic constants such as association rate ( $k_{on}$ ) and dissociation rate ( $k_{off}$ ) were determined. The  $K_D$  equilibrium binding constant, known as the inverse of the affinity, was obtained by the analysis software using the equation  $K_D = k_{off} / k_{on}$ .

### Evaluation of BMP signaling in cellular assays

The BMP signaling of cells seeded on biomimetic SA<sub>v</sub> platforms was quantified by immunofluorescence staining and analysis of nuclear pSMAD1/5/9 a few hours after BMP stimulation (generally 1h30).

Immunofluorescence is a technique employing antibody/antigen interactions to detect and locate target molecules. Fluorescently labeled antibodies attach to the target molecules, enabling their visualization under a fluorescence microscope. This method is often performed with an indirect configuration using an unlabeled antibody binding the antigen, followed by a secondary fluorescent antibody binding to the primary one. In our case, we used indirect immunofluorescence where a rabbit anti-pSMAD1/5/9 primary antibody binds to pSMAD1/5/9 and a goat anti-rabbit Alexa Fluor 488 binds to the primary antibody, enabling its detection. A robust high-content imaging and analyzing system was previously developed in the team, allowing the subsequent quantitative analysis of nuclear markers such as pSMAD1/5/9 for a large number of conditions performed in 96-well plates<sup>[485]</sup> (**Figure 39**).

To describe the protocol in details, cells were fixed after using pre-fixation and fixation steps with 2% paraformaldehyde (PFA) for 5 min and 4% PFA for 20 min, respectively. Fixed cells were first permeabilized with 0.2% Triton X-100 (w/v) in PBS for 3 min and blocked for 1 h with 3% BSA at RT. Primary rabbit anti-pSMAD1/5/9 (Cell Signaling Technology) was diluted at 1:400 in PBS with 3% BSA and incubated overnight at 4°C. The goat anti-rabbit Alexa Fluor 488 secondary antibody (1:500, ThermoFischer Scientific), as well as rhodamine phalloidin (1:1000, ThermoFischer Scientific) and DAPI (1:1000, Sigma-Aldrich) were incubated for one hour at RT in PBS with 3% BSA. The immunofluorescence assay is concluded with three rinsing steps with PBS prior to image acquisition and data analysis.

Each condition was performed in technical duplicates and cells were imaged using InCell Analyzer 2500 high-content microscope using the 20x objective on three channels (red, green, and blue), acquiring 20 fields of view for each well. Images were further analyzed with the automated image analysis software InCarta (Molecular Devices), as previously described<sup>[47,48]</sup>.



**Figure 39. Pipeline of pSMAD1/5/9 fluorescence intensity analysis.**

Segmentation of cells and their nuclei were achieved using the phalloidin-rhodamine and DAPI images. The pSMAD1/5/9 intensity was measured only inside the nucleus under a mask defined by the DAPI signal and background-subtracted for at least 100 cells/well. Mean nuclear area was calculated by the InCarta software. For comparing conditions with identical nuclear area, the mean intensity was calculated. In contrast, the total intensity in the nuclei was plotted for conditions exhibiting differences in nuclear area. After analysis, we obtain data are presented in excel files with data per cell, field of view or well. We then analyze the data per well by taking the nuclei intensity subtracted from background and do the mean and standard deviation for each condition.

**Chapter IV. Automated Fabrication of  
Streptavidin-Based Self-assembled Materials  
for High-Content Analysis of Cellular Response  
to Growth Factors**

## IV.A. Article introduction

The previously developed streptavidin biomimetic platforms are sophisticated biomaterials that enable the study of the complex ECM environment by co-presenting several molecules and investigating their effects on the cellular response<sup>[264]</sup>. A first improvement of the platforms was implemented by Sefkow-Werner *et al.*, which allowed their functionalization on gold-sputtered surfaces that could be glued on bottomless 96-well plates, dividing each surface into 4 wells<sup>[283]</sup>. This development enhanced the throughput of both the platform functionalization and cellular experiments by increasing the number of conditions and reducing the amount of samples needed for functionalizing each condition. Despite that, the necessity of using and gluing gold-sputtered surfaces represents a delicate and time-consuming manual procedure that limits the number of conditions to 48 wells within a 96-well plate, and limits the quality of microscopy images due optical absorption of the gold layer.

In this article, we identified a PLLgPEG-biotin molecule as a compatible linker for building streptavidin biomimetic platforms on standardized glass 96-well plates, thereby reducing the cost and duration of fabrication, enhancing the throughput of the experiments and increasing the quality of fluorescence microscopy images. The platforms built with this new linker were extensively characterized by QCM-D and spectroscopic ellipsometry (SE) *ex situ* techniques, but also with a novel *in situ* photo bleaching image correlation spectroscopy (pbICS). The quantifications of bound fluorescently tagged SA<sub>v</sub> with SE and pbICS were in agreement, confirming that the *in situ* and *ex situ* functionalization are comparable.

Furthermore, we developed a software enabling to perform the functionalization of the platforms with a liquid-handling robot. This software allowed a fully automated and versatile workflow to functionalize 96-well plates (glass or gold substrates) by choosing the number of solutions and selecting the wells to be incubated for each solution. To demonstrate the potential of this automated setup, we functionalized an entire 96-well plate with HS and aBMP2, aBMP4, aBMP6, and aBMP7 at various concentrations to study the short-term BMP signaling *via* SMAD1/5/9 phosphorylation.

We demonstrated the compatibility of the novel platform construction with cellular assays, by showing that C2C12 cells homogeneously adhered over the entire surface and responded to the different BMPs presented via immobilized HS. Using adjusted concentration ranges of BMP2, BMP4, BMP6, and BMP7, we could identify EC<sub>50</sub> values for all BMPs adsorbed to iHS (aBMPs) based on their bioactivity. Our findings highlighted that BMP2 was about 10-fold more bioactive than BMP4, BMP6, and BMP7, regarding the induced SMAD1/5/9

phosphorylation.

In this highly collaborative work, Julius Sefkow-Werner, a former doctoral student of our team, was the main contributor. He performed the QCM-D, SE experiments and pbICS experiments in collaboration with the Liphy laboratory (Antoine Delon, Irene Wang). As for me, I was in charge of the development of the software to control the liquid-handling robot to automate the functionalization of the biomimetic platforms and for the supervision of the student performing the cellular experiment in the 96-well plates. My contributions in this article extended as well to experimental design, preliminary experiments for the high-throughput proof of concept experiment, and revisions of the article draft. I also trained and supervised Bertin Ndayishimiye, the M2 student who performed this high-content experiment (Figure 6 of the article). The software developments in this study took inspiration from previous developments in the team<sup>[472]</sup>. The software consists in a graphical user interface created with Visual Basic 6, enabling users to define conveniently the parameters of the functionalization in order to generate worklists compatible with the liquid-handling robot. This interface allows in particular the selection of the total number of solutions, the position of the solution in the robot worktable, the wells to be incubated for each solution, the volume of solution per well, the type of tips (volume capacity), the incubation time for each solution and the number of rinsing steps. An option was implemented to enable the functionalization of several molecules in parallel to prevent successive incubations and reduce the functionalization time (i.e. several BMPs or several GAGs simultaneously in different wells instead of one by one). The robot can functionalize up to three plates simultaneously, and developments were carried out to allow the distinct functionalization of each plate, and the use of distinct plate formats (12-, 24-, 48- or 96-well plates). Additionally, I improved the ergonomics of the interface in several aspects, especially for the selection of the well to be functionalized and of the solution's positions on the robot worktable. In the frame of data management guidelines, a saving option was also added to allow the storage of the generated worklists transmitted to the liquid-handling robot. These developments in the automation of the biomimetic platform functionalization opened the path for further studies. Indeed, developing such an automated system was a fundamental achievement to investigate the role of many diverse GAGs or HS-derived oligosaccharides in BMP signaling.

## **IV.B. Article**

→ Next page

# Automated Fabrication of Streptavidin-Based Self-assembled Materials for High-Content Analysis of Cellular Response to Growth Factors

Julius Sefkow-Werner, Jean Le Pennec, Paul Machillot, Bertin Ndayishimiye, Elaine Castro-Ramirez, João Lopes, Christophe Licitra, Irene Wang, Antoine Delon, Catherine Picart,\* and Elisa Migliorini\*



Cite This: *ACS Appl. Mater. Interfaces* 2022, 14, 34113–34125



Read Online

ACCESS |



Metrics & More



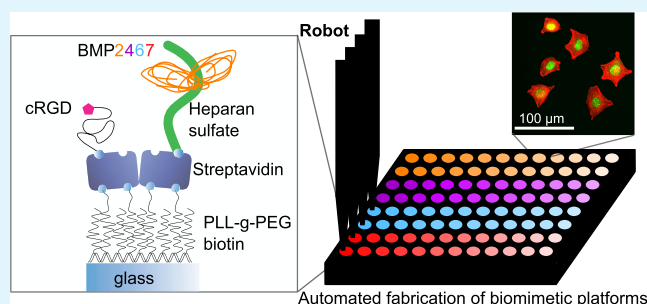
Article Recommendations



Supporting Information

**ABSTRACT:** The automation of liquid-handling routines offers great potential for fast, reproducible, and labor-reduced biomaterial fabrication but also requires the development of special protocols. Competitive systems demand for a high degree in miniaturization and parallelization while maintaining flexibility regarding the experimental design. Today, there are only a few possibilities for automated fabrication of biomaterials inside multiwell plates. We have previously demonstrated that streptavidin-based biomimetic platforms can be employed to study cellular behaviors on biomimetic surfaces. So far, these self-assembled materials were made by stepwise assembly of the components using manual pipetting. In this work, we introduce for the first time a fully automated and adaptable workflow to functionalize glass-bottom multiwell plates with customized biomimetic platforms deposited in single wells using a liquid-handling robot. We then characterize the cell response using automated image acquisition and subsequent analysis. Furthermore, the molecular surface density of the biomimetic platforms was characterized *in situ* using fluorescence-based image correlation spectroscopy. These measurements were in agreement with standard *ex situ* spectroscopic ellipsometry measurements. Due to automation, we could do a proof of concept to study the effect of heparan sulfate on the bioactivity of bone morphogenetic proteins on myoblast cells, using four different bone morphogenetic proteins (BMPs) (2, 4, 6, and 7) in parallel, at five increasing concentrations. Using such an automated self-assembly of biomimetic materials, it may be envisioned to further investigate the role of a large variety of extracellular matrix (ECM) components and growth factors on cell signaling.

**KEYWORDS:** automation, biomaterials, biomimicry, growth factors, BMP, glycosaminoglycans, high-content studies



Automated fabrication of biomimetic platforms

## INTRODUCTION

Biomimetic approaches gain influence in the design and fabrication of biomaterials for biomedical applications such as tissue repair and drug screening or in fundamental research when studying the interface between cells and their surrounding extracellular matrix (ECM).<sup>1,2</sup> Biomimetics in cellular studies means to model the natural environment of cells as precisely as possible, notably mimicking their surrounding ECM in terms of molecular composition<sup>3</sup> and physical properties.<sup>4,5</sup> These models help for example to reveal synergies between the ECM components such as glycosaminoglycans (GAGs) and growth factors (GFs), which influence cellular fate.<sup>6,7</sup> Also spatial proximity between cellular adhesion ligands and GFs<sup>8</sup> as well as matrix elasticity or topography<sup>9</sup> play a role in cell signaling. Various biomaterials to study these parameters in two-dimensional (2D) and three-dimensional (3D) were extensively reviewed and each of them helps to respond to a specific need.<sup>8,10–12</sup>

Due to the high chemical, mechanical, and structural complexity of the ECM models and the need for flexibility in biomaterial design for fundamental research, most of the workflow from fabrication to data analysis is manual and thus time-consuming.<sup>13</sup> This makes these approaches less suitable for high-content studies, which gain popularity to test different functionalities of biomaterials. Vasilevich et al. predicted a rising involvement of robotics and automation covering almost the integral workflow of an experiment.<sup>14</sup> The researcher would formulate a precise question, later recover the desired biomaterial, and present data to the scientific community, while the central robot takes over the experimental design, biomaterial fabrication, cell culture, and data analysis. A recent review summarizes the implementation of automation in research laboratories related to biomimetic modeling of

Received: May 10, 2022

Accepted: July 5, 2022

Published: July 18, 2022

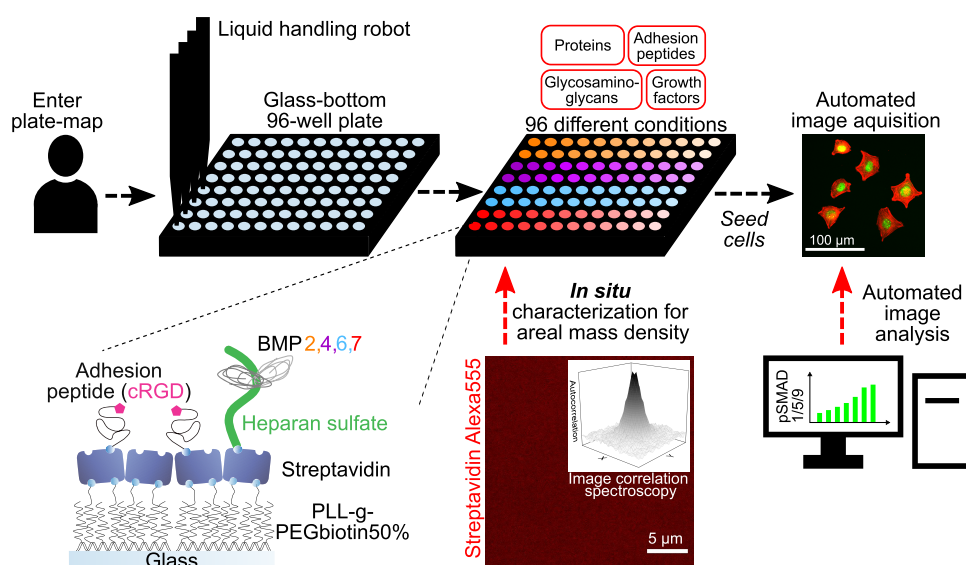


**Figure 1.** Schematic of automated platform fabrication, surface characterization, and cellular studies. A user communicates the plate-map corresponding to the experimental plan to the liquid-handling robot. Glass-bottom 96-well plates are then automatically functionalized with different biomimetic platforms co-presenting cellular adhesion ligands, glycosaminoglycans, and growth factors. In this work, streptavidin binds to the linker poly(L-lysine)-g-poly(ethylene glycol)biotin(3.4)50% (PLL-g-PEGbiotin50%). Then, biotinylated cRGD and biotinylated heparan sulfate bind to streptavidin and BMP2, 4, 6, or 7 adsorbs to heparan sulfate. The areal mass density of fluorescence-labeled molecules such as Streptavidin Alexa555 is characterized in situ using image correlation spectroscopy. Cells are seeded on the platforms for biophysical assays using automated image acquisition and automated image analysis to quantify for example BMP-mediated SMAD1/5/9 phosphorylation inside the nucleus.

diseases and thus enabling high-content studies.<sup>15</sup> Notably, manual pipetting can be replaced by automation, with the advantage of saving labor time. Indeed, recent studies showed that manual pipetting accuracy depends on the individual operator and thus decreases data reproducibility.<sup>16,17</sup> Soft lithography or microcontact printing was already shown to be well suited for a high degree of parallelization and miniaturization by creating poly(dimethylsiloxane) (PDMS) microwells,<sup>18</sup> which can further include bioactive compounds.<sup>19</sup> However, the degree of flexibility is limited due to time-consuming design and the need for fabrication of new masks. Other techniques are adapted to build high-complexity assemblies or human tissues, including bioprinters to produce spatially controlled 3D tissues<sup>20</sup> and liquid-handling robots to produce thin films.<sup>17</sup>

Standardized multiwell plates with for example 96 wells offer a degree of miniaturization, which reduces the amount of precious cells like stem cells and expensive molecules like growth factors and chemokines while still providing sufficient sample volume and thus are adapted for automated biomaterial fabrication.<sup>15</sup> They are commercially available in different versions with different substrates, mostly plastic and glass, and are compatible with common laboratory equipment, including liquid-handling robots, microplate readers, and high-content screening microscopes. This makes them candidates for automation over the whole experimental workflow from fabrication, cell seeding, sample preparation, data acquisition, and post-treatment.<sup>17,21–23</sup> Examples of liquid-handling robots in industry<sup>24</sup> or of automated cell cultures<sup>25</sup> demonstrate the broad application potential and interest of automation. Regarding biomaterial fabrication, Brooks et al. described the fabrication of 2D and 3D hydrogels on glass using a liquid-handling robot inside 96-well plates and further immobilized ECM proteins.<sup>22</sup> In a previous work by our team, Machillot et al. built up a polyelectrolyte multilayer film inside 96-well plates for cellular studies by executing iterative cycles of

incubation and rinsing of the three involved electrolytes using a liquid-handling robot.<sup>17</sup> This ensured high reproducibility between the equally functionalized wells and plates but the loading of bone morphogenetic proteins (BMPs) at different concentrations was still done by hand. Sales et al. further automated the workflow of this system by applying automated microscopy and automated image analysis to perform a high-content screening of cell adhesion and early cell differentiation to four BMPs simultaneously.<sup>21</sup> Eggert et al. recently developed the automated fabrication of hydrogels at the single-well level.<sup>23</sup> To our knowledge, this approach has never been applied to self-assembled materials made of several combinations of deposited layers.

Another challenge relies on the precise characterization of the functionalization of biomaterials inside the 96-well plates, *i.e.*, *in situ*. For thin assemblies, surface-sensitive techniques like quartz crystal microbalance with dissipation monitoring (QCM-D) or spectroscopic ellipsometry (SE), among others, enable to follow binding events and to quantify the surface density of molecules built-up on model substrates.<sup>26–29</sup> However, to date, these techniques are barely adapted to the 96-well plate format. Thus, there is a need to use other quantitative characterization methods that can be performed *in situ*.

Fluorescence microscopy reveals only relative intensity changes between different conditions based on labeled molecules of interest.<sup>30,31</sup> Our group recently further developed image correlation spectroscopy (ICS) to precisely measure the number of labeled molecules on 2D biomaterials.<sup>32</sup> The spatial autocorrelation of confocal images reveals intensity fluctuations and its amplitude indicates the number of molecules per point spread function (PSF), and ICS is thus a suitable tool to characterize 2D biomaterials.

In terms of the type of biomaterials, thin films or assemblies are often used to biofunctionalize surfaces. Notably, the layer-by-layer technique<sup>33</sup> and the streptavidin-based platforms<sup>28</sup>

Table 1. Molecule Concentrations and Incubation Times Based on QCM-D Measurements

compound	abbreviation	concentration ( $\mu\text{g/mL}$ )	incubation time for surface saturation (min)
PLL(20)-g[3.5]-PEG(2)/PEGbiotin(3.4)50%	PLL-g-PEGbiotin50%	10	45
streptavidin	SAv	10	30
streptavidin alexa555	SAvAlexa	10	30
biotinylated cyclic arginylglycylaspartic acid	cRGD	0.25	4 min (partly saturated)
SAv/cRGDmix in molar ratio 3:4	SAv/cRGDmix	10 (SAv) + 1 (cRGD)	30 for pre-coupling, then 45 for saturation
SAvAlexa/cRGDmix in molar ratio 3:4	SAvAlexa/cRGDmix	10 (SAvAlexa) + 1 (cRGD)	30 for pre-coupling, then 45 for saturation
biotinylated Atto565	bAtto	10	30
biotinylated heparan sulfate	iHS	10	30
adsorbed BMP2, 4, 6, and 7 on iHS	aBMP2, 4, 6, and 7	0.01–10	90–130
soluble BMP2, 4, 6, and 7	sBMP2, 4, 6, and 7	0.005–5	until cell fixation

can provide a high degree of versatility in experimental conditions. Our team previously developed a biomimetic platform based on a streptavidin (SAv) monolayer, built on gold-sputtered glass surfaces.<sup>6,28,34–36</sup> SAv is commonly used for analytical assays or as an antibody conjugate and for biochemical studies of molecular interactions.<sup>37</sup> The high affinity and specificity between SAv and biotin permits to immobilize biotinylated molecules of interest in a highly controlled manner to reveal their specific role in cell fate. We recently used such streptavidin platforms to study the synergy between integrins, the GAG heparan sulfate (iHS), and BMP2 adsorbed on iHS, by quantifying cell adhesion and BMP2 signaling (*i.e.*, the phosphorylation of the SMAD1/5/9 proteins is an early effector of BMP2 interaction with BMP receptors).<sup>38</sup> To date, comparable data for the role of HS on BMP4, 6, and 7-mediated SMAD signaling is not available.

In this work, we present for the first time the automated fabrication of customized biomimetic SAv platforms on glass-bottom 96-well plates to study cellular responses to GF presented *via* iHS. The entire workflow from discrete functionalization of every single well of a 96-well plate to subsequent analysis of cellular readouts was fully automated using a liquid-handling robot, automated image acquisition and analysis (Figure 1). To this end, a custom-made graphical user interface was designed to allow the operator to individually assign different biomimetic SAv platforms to discrete wells selected by the user and to define experimental parameters in minutes. As a proof of concept, we co-immobilized the adhesion peptide cRGD together with HS to promote cellular adhesion and to present GFs *via* its natural ligand HS. Using ICS, we quantified *in situ*, inside 96-well plates, the molecular surface density and homogeneity of the self-assembled material. Using the automated approach, we simultaneously studied increasing concentrations of BMP2, BMP4, BMP6, and BMP7 adsorbed on HS and compared them to the presentation in solution. We selected these BMPs in view of their role in various biological processes throughout the body.<sup>39</sup> BMP2 is mainly involved in the development of the musculoskeletal system, BMP4 regulates cancer, BMP6 takes part in the ion metabolism, and BMP7 participates in fat cell differentiation.<sup>7</sup> We quantified SMAD1/5/9 phosphorylation in BMP-responsive C2C12 mouse myoblasts.<sup>21,40,41</sup>

## METHODS

**Buffers and Molecules.** 10 mM *N*-(2-hydroxyethyl)piperazine-*N'*-ethanesulfonic acid (Hepes) and 150 mM NaCl buffer (Sigma-Aldrich, Saint-Quentin Fallavier, France), pH 7.2, named hereafter Hepes, was used for dilution and rinsing of all molecules if not further specified. PLL(20)-g[3.5]-PEG(2)/PEGbiotin(3.4)50% (PLL-g-PEG-biotin50%, ~107 kDa, SuSoS AG, Dübendorf, Switzerland) consists

of a poly(L-lysine) backbone (~20 kDa, ~100 monomers) with one PEG chain (2 kDa) or one PEGbiotin chain (3.4 kDa) grafted to one of 3.5 PLL monomers in a 50% ratio. Stock solution (10  $\mu\text{M}$ ) was stored at 4 °C for up to 2 months and diluted to 100 nM upon use. Details for SAv (SAv, 55 kDa, Sigma-Aldrich, Saint-Quentin Fallavier, France), biotinylated cyclic arginylglycylaspartic acid (RGD) pentapeptide (cRGD, 3.9 kDa), and biotinylated HS (iHS, 12 kDa) can be found in previous works.<sup>36,38</sup> Biotinylated Atto565 (bAtto, 922 Da, Sigma-Aldrich, Saint-Quentin Fallavier, France) and streptavidin Alexa Fluor 555 conjugate (SAvAlexa, ~55 kDa, Molecular probes, Eugene, Oregon) were used for ICS studies and homogeneity analysis. For some conditions, SAv or SAvAlexa was pre-bound to cRGD at a molar ratio of 3:4 and incubated for 30 min before binding to PLL-g-PEGbiotin50% on the surface. BMP2 (26 kDa, R&D Systems Inc., Minneapolis, Minnesota), BMP4 (24 kDa, Peprotech, Neuilly-Sur-Seine, France), BMP6 (30 kDa, R&D Systems Inc., Minneapolis, Minnesota), and BMP7 (26 kDa, Olympus Biotech, Lyon, France) were serial-diluted to reach the concentrations to bind to iHS or to be added to the cell media.

**Surface Functionalization.** For *ex situ* characterization, biomimetic platforms were built on silicon dioxide (SiO<sub>2</sub>) crystals (QX 303, Biolin Scientific, Västra Frölunda, Sweden) for QCM-D measurements and on thermally oxidized silicon wafers coated with a 60 nm thick SiO<sub>2</sub> layer for SE analysis. For *in situ* characterization and cellular studies, glass-bottom 96-well plates (Greiner bio-one, Les Ulis, France) were used. Substrates were activated using UV/Ozone (ProCleaner Plus, Bioforce Nanosciences, Virginia Beach, Virginia) for 10 min to clean and charge the surface. Molecules were pumped inside a liquid chamber for crystals (QCM-D) and wafers (SE) or pipetted by the liquid-handling robot (Evo 100, Tecan, Männedorf, Switzerland) in the case of 96-well plates with the concentrations mentioned in Table 1.

**Ex Situ Characterization with Quartz Crystal Microbalance with Dissipation Monitoring (QCM-D).** To assess the effective deposit on the self-assembled streptavidin-based platform on glass, we used QCM-D (QSense Analyzer, Biolin Scientific, Västra Frölunda, Sweden), which allows to follow binding events of the sequential buildup of the biomimetic platform, using SiO<sub>2</sub>-coated QCM-D crystals.

Dissolved molecules in the concentrations stated in Table 1 passed through the liquid chamber *via* a peristaltic pump with 15  $\mu\text{L}/\text{min}$  (IPC4, Ismatec, Wertheim, Germany) followed by rinsing with Hepes as described in more detail elsewhere.<sup>28</sup> The measured time for a molecule to saturate on the surfaces indicates the incubation time used for each molecule when building up the biomimetic platforms inside 96-well plates.

**Ex Situ Characterization with Spectroscopic Ellipsometry (SE).** We used SE (RC2, J.A. Woollam, Lincoln, New England) complementary to QCM-D to measure the mass of molecules bound to the biomimetic platform *ex situ* on silicon wafers covered with a 60 nm-thick thermal SiO<sub>2</sub> layer. Due to optical constraints, it was not possible to use amorphous glass surfaces as in 96-well plates. A peristaltic pump (IPC4, Ismatec, Wertheim, Germany) pumped the molecules or the rinsing buffer Hepes at 100  $\mu\text{L}/\text{min}$  into the 500  $\mu\text{L}$

liquid chamber (J.A. Woollam, Lincoln, New England), which was tightly screwed on the wafer.

SE measures the change of the ellipsometric angles  $\Psi$  and  $\Delta$  of polarized light upon changes in the refractive index and thicknesses of optical layers.<sup>42</sup> We measured the SiO<sub>2</sub> layer in buffer and fitted its thickness and the angle of incidence offset based on the known optical properties of thermal SiO<sub>2</sub> with the J.A. Woollam model SIO2\_JAW3 on a fixed 1 nm Intr\_JAW3 layer to account for the SiO<sub>2</sub>/Si interfacial layer.<sup>43</sup> The refractive index for the Hepes buffer was modeled with a Cauchy dispersion law with parameters A set to 1.324, B set to 0.00322, and C set to 0.<sup>44</sup> Molecular adsorption to this base substrate was then modeled using a Cauchy layer where thickness and parameter A were fitted. B was set to 0.00322 and C to 0.<sup>45</sup> The areal mass density was calculated using the De Feijter eq 1

$$M = d_A \frac{A_A - A_C}{dn/dc} \quad (1)$$

with  $d_A$  is the fitted thickness of the adsorbed layer,  $A_A$  its fitted Cauchy parameter,  $A$  and  $A_C$  are the Cauchy parameter of the ambient buffer.<sup>46</sup> The corresponding refractive index increments  $dn/dc$  relative to water for each molecule were 0.18 (SAv, SAvAlexa, SAvRGDmix) and 0.158 (PLL-g-PEGbiotin50%, bHS).<sup>47</sup>

**Automated Liquid Handling.** The liquid-handling robot was used to fabricate different biomimetic platforms at the bottom of the wells of a 96-well plate. First, the user entered the experimental design of the 96-well plate into a custom-made graphical user interface, defining the corresponding wells and incubation time for each molecule and their position in the compound rack. Each well can thus represent a different biomimetic platform or replicates of those. Then, molecule solutions, in their adjusted concentrations (Table 1) based on QCM-D measurements, and rinsing buffer were placed into racks and up to three UV/ozone-activated 96-well plates were put on the plate carrier. The operating software of the liquid-handling robot executed a custom-made script with the user-entered parameters' well selection, and incubation time, for each molecule  $n$  as the input. For each of the defined molecules, an iterative cycle was run:

1. Aspiration of storage buffer from wells, to empty the wells
2. Aspiration of solution, from compound rack position, and dispense of 60  $\mu$ L inside well selection,
3. Waiting for incubation time,
4. Rinsing wells, via five loops of dispense and aspiration of rinsing buffer

With the five rinsing loops, we achieved a dilution of  $\sim$ 1000 times the initial compound, which was enough to interrupt the binding to the previous molecule. PLL-g-PEGbiotin50% and biotinylated molecules were incubated much longer than measured since incubation inside wells was static and not under flow as in QCM-D. BMP was incubated as long as measured in QCM-D. Plates were then ready for cellular studies and were always used the same day.

**In Situ Characterization Inside 96-Well Plates with Optical Fluorescence Microscopy and ICS.** A fluorescence-based approach was used to quantify the homogeneity of glass-bottom 96-well plates functionalized by the robot as well as to measure the areal mass density of different components of the biomimetic platform. SAvAlexa replaced SAv and bAtto served as a representative molecule for the binding of functional biotinylated molecules to SAv.

Wells were functionalized by the robot with PLL-g-PEGbiotin50% followed by either SAvAlexa, SAvAlexa/cRGDmix, or SAv and subsequently bAtto in the latter case. The plate was imaged *in situ* with an automated image acquisition system (InCell Analyzer 2500, 20 $\times$ , Molecular Devices, San Jose, California) for qualitative defect characterization on the macroscale. These immunofluorescence images of the whole well were further treated to remove artifacts due to uneven illumination or optical constraints. An average image based on at least 20 images not touching the well's border was calculated to represent the acquisition bias. All images of this well were then divided by this average image and in the next step stitched together for a 96-well montage. Intensities were analyzed along a vertical and horizontal line.

To quantify the areal mass density of SAvAlexa and bAtto, a series of 10 acquisitions at five different positions throughout the well were taken with a Leica SP8 confocal microscope (Leica, Wetzlar, Germany) using an HC PL APO 63 $\times$ /1.2 water-immersion objective. The focal plane was identified at maximum intensity and stabilized with automated focus control, and a field of 25  $\mu$ m  $\times$  25  $\mu$ m with a 512  $\times$  512 pixels was imaged with 1% laser intensity at 561 nm and 1.2  $\mu$ s pixel dwell time. Images were then analyzed using the principle of ICS as described elsewhere.<sup>32,48</sup> In summary, the confocal images were split up into 64 subimages and the spatial autocorrelation function (ACF) was calculated for each subimage. This ACF reveals intensity fluctuations and its amplitude is inversely proportional to the number of molecules in the observation area.<sup>49</sup> The observation area is defined by the waist of the point spread function specific for each microscope and the used objective and ranges around 230 nm. An additional photobleaching routine revealed the average number and distribution of fluorophores per molecule and was used to correct the number of molecules by the factor 1.2 for SAvAlexa and 1.09 for bAtto. Representative 63 $\times$  images were equally contrast treated to retain relative intensity differences.

**Cell Culture.** To study the cellular compatibility of PLL-g-PEGbiotin50%-based biomimetic platforms, C2C12 mouse myoblasts (CRL-1772, ATCC, Manassas, Virginia) were chosen as BMP-responsive reference cells.<sup>41</sup> They were cultured on tissue-treated polystyrene cell culture flasks in Dulbecco's modified Eagle's growth medium (DMEM, Gibco, Illkirch, France) supplemented with 10% heat-deactivated fetal bovine serum (FBS, PAA Laboratories, Toronto, Canada) and antibiotic-antimycotic (1%, Gibco, Illkirch, France) at 37  $^{\circ}$ C and 5% CO<sub>2</sub>. Cells were passed at subconfluency with Trypsin EDTA (Gibco, Illkirch, France) and discarded after 12 passages. Four hours prior to manual seeding onto biomimetic platforms inside 96-well plates, cells were serum-starved with FBS-free growth media and then detached from the flask with Accutase (Sigma-Aldrich, Saint-Quentin Fallavier, France) and resuspended in FBS-free growth media.

**C2C12 Cell Adhesion and Differentiation for Microcopy Analysis.** To study cellular adhesion on biomimetic platforms, 31 000 serum-starved C2C12 cells per cm<sup>2</sup> were plated on functionalized 96-well plates, incubated (37  $^{\circ}$ C, 5% CO<sub>2</sub>), and stained with 10 ng/mL Hoechst after 1 h. Cells were imaged using a Zeiss Axio Observer 7 epifluorescence microscope (Carl Zeiss Sas, Le Pecq, France) and then rinsed with phosphate-buffered saline (PBS) to remove nonadherent cells before again imaging the remaining cells at the same position. Nuclei were counted using an ImageJ plugin to calculate the percentage of adherent cells.

For the quantification of the cellular area and the phosphorylation of SMAD1/5/9 translocated into the nucleus upon BMP2 stimulation, 31 000 serum-starved cells per cm<sup>2</sup> were plated on functionalized surfaces, and sBMPs2, 4, 6, and 7 was added into the cell media at increasing concentrations. Cells were incubated (37  $^{\circ}$ C, 5% CO<sub>2</sub>), rinsed after 1 h 30 min with PBS, and fixed with 4% paraformaldehyde. Cell membranes were permeabilized with 0.2% (w/v) Triton X-100 (Sigma-Aldrich, Saint-Quentin Fallavier, France) for 3 min and blocked with 3% bovine serum albumin (BSA) for 1 h. Primary rabbit anti-pSMAD1/5/9 (Cell Signaling Technology, Danvers, Massachusetts) diluted 1:400 in PBS and 3% BSA was incubated overnight at 4  $^{\circ}$ C. After rinsing, secondary goat anti-rat/rabbit Alexa Fluor 488 (Thermo Fischer Scientific, Illkirch, France), 1:500, F-actin phalloidin-rhodamine (Sigma-Aldrich), 1:1000, and 4',6-diamidino-2-phenylindole (DAPI), 1:1000, were incubated for 60 min in PBS and 3% BSA at RT. 2.5% (w/v) Dapco (Sigma-Aldrich, Saint-Quentin Fallavier, France) in PBS at pH = 7.8 was used as antifade. Cells were imaged using InCell Analyzer 2500 using the 20 $\times$  objective on three channels. Images were further analyzed with the automated image analysis software InCarta (Molecular Devices, San Jose, California), as previously described.<sup>21</sup> pSMAD1/5/9 intensity was measured only inside the nucleus under a mask defined by the DAPI signal and background-subtracted for at least 50 cells/well.

**Statistical Analysis and Data Treatment.** For cell experiments, each condition was prepared as a technical duplicate in two different

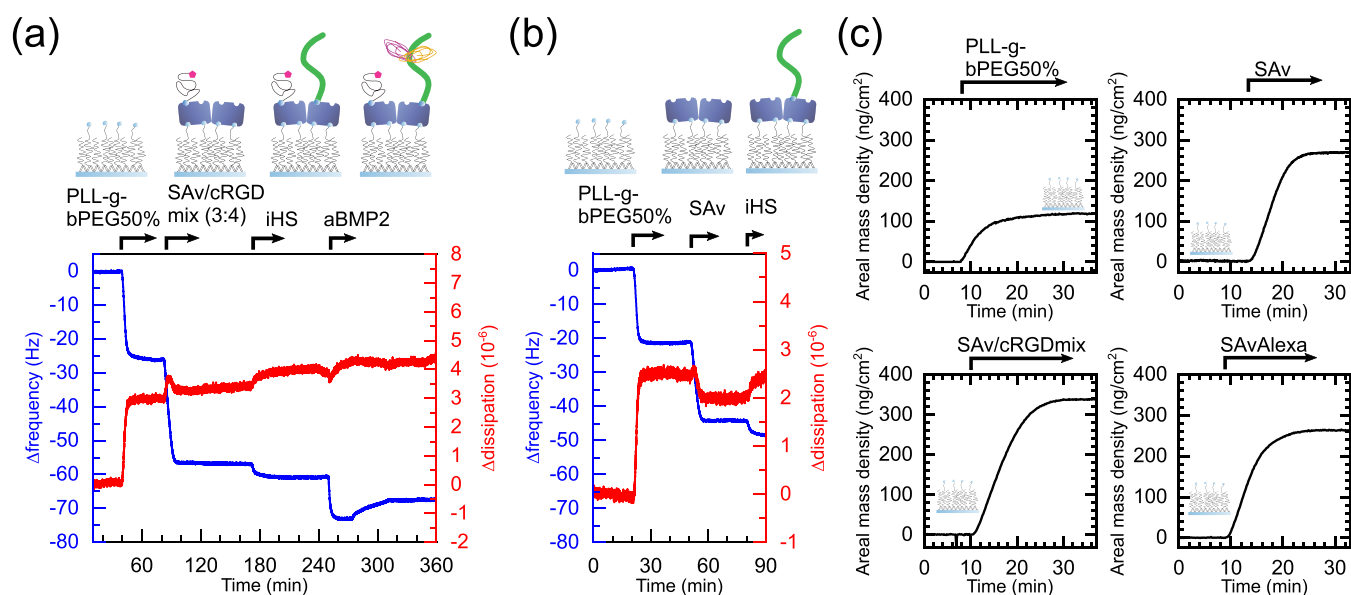


**Figure 2.** *Ex situ* QCM-D and SE characterization of the sequential functionalization of the biomimetic platform (a) QCM-D graph showing the frequency change and dissipation change upon the sequential buildup of a biomimetic platform on plasma-activated SiO<sub>2</sub> crystals. SAV and cRGD were precoupled in solution with a molar ratio of 3:4 before binding to the PLL-g-PEGbiotin50% layer. Black arrows indicate periods of incubation followed by rinsing with buffer. (b) Graph showing the change in frequency by SAV binding to PLL-g-PEGbiotin50% and iHS occupying the remaining biotin-binding sites measured with QCM-D. (c) Graph showing the change of the areal mass density of PLL-g-PEGbiotin50% binding to plasma-activated SiO<sub>2</sub> wafers measured with SE (c, top left). Black arrows indicate the time of incubation followed by rinsing with buffer. Areal mass density was calculated using the de Feijter (eq 1) equation based on the measured  $\Delta$ thickness and  $\Delta$ refractive index. The other three panels show SAV, SAV/cRGDmix, and SAVAlexa binding to PLL-g-PEGbiotin50%.

wells, and experiments were repeated in three biological replicates. Means were tested for statistical significance between different conditions with the nonparametric Mann–Whitney test with  $p \leq 0.05$  and based on at least three biological replicates. To calculate the half-maximal effective concentration (EC<sub>50</sub>), data was fitted with Origin using the dose response curve (four-parameter logistic model<sup>50</sup>). For the negative control, we assigned a BMP concentration 10<sup>-4</sup> times lower than the lowest BMP concentration instead of zero. The coefficient of variation (CV) was used as a measure for the overall homogeneity of stitched full-well immunofluorescence images by dividing the standard deviation of its intensity by its mean intensity. Then, the homogeneity is expressed by the mean and standard deviation of the CV over three wells. To assess the reproducibility of the functionalization, the CV of the mean intensity of five confocal images per well of three wells and two independent plates was calculated.

## RESULTS

**Ex Situ Characterization of Biomimetic Platforms on QCM-D Crystals and SiO<sub>2</sub>-Coated Wafers.** To establish the streptavidin-based self-assembled material on glass surfaces, we studied *ex situ* the step-by-step buildup using QCM-D and SE with silica-coated crystals and wafers.

PLL-g-PEGbiotin50% saturated the surface after 30 min with an average frequency shift of  $-23.4 \pm 2.9$  Hz (Figure 2a). A positive shift in dissipation of  $2.8 \pm 0.3 \times 10^{-6}$  indicated the deposition of a soft layer. SAV precoupled in solution with the cellular adhesion peptide cRGD at the molar ratio 3:4 saturated after 30 min, decreasing the frequency further by  $-31.1 \pm 2.6$  Hz. The study of Zhen et al.<sup>51</sup> showed that the number of available biotin-binding sites increased when SAV was prelinked with a biotinylated molecule, probably due to improved layer organization. iHS bound to the remaining biotin-binding sites with  $-4.6 \pm 1.3$  Hz and BMP2 (192 nM) adsorbed specifically to iHS with  $-11.7 \pm 2.8$  Hz. About 50%

of BMP2 was partly removed from iHS when rinsed until equilibrium was reached and we further measured that BMP2 bound only marginally and reversibly to the SAV/cRGDmix (Figure S1a). BSA bound nonspecifically to SiO<sub>2</sub> with 2.5 Hz but the passivation with PLL-g-PEGbiotin50% led to non-measurable BSA binding after all incubation steps (Figure S1b,c). Biotinylated molecules bound as well to a plain SAV layer as seen *via* the example of iHS (Figure 2a), and also a sequential functionalization of cRGD, iHS, and aBMP2 was feasible but more difficult to control (Figure S1d).

We further observed that SiO<sub>2</sub> crystals aged from their third regeneration cycle, which lead to up to 25% higher molecule adsorption starting with PLL-g-PEGbiotin50% and propagating through the consecutive compounds (Figure S1c,e). Data in Figure 2 was acquired on new crystals, while experiments in Figure S1 were conducted on crystals regenerated at least 3 times.

We conclude that the SAV/cRGDmix has the highest potential to bind further functional molecules and is the most practical and straightforward approach for automated platform fabrication since it is more simple than incubating SAV and cRGD sequentially. Table 1 lists the concentrations and incubation times based on the results obtained using QCM-D. These conditions will be used for *in situ* functionalizations of the 96-well plates using the liquid-handling robot.

We then characterized these platforms with SE on SiO<sub>2</sub>-coated wafers to measure adsorbed “dry” mass of the immobilized compounds. PLL-g-PEGbiotin50% bound to glass with  $119 \pm 9$  ng/cm<sup>2</sup>, SAV then with  $264 \pm 6$  ng/cm<sup>2</sup>, and SAV/cRGDmix with  $343 \pm 25$  ng/cm<sup>2</sup> (Figure 2c). To characterize the amount of SAV inside the 96-well plates, we used the *in situ* ICS technique. We first verified if SAVAlexa binds similarly to SAV to PLL-g-PEGbiotin50% by QCM-D

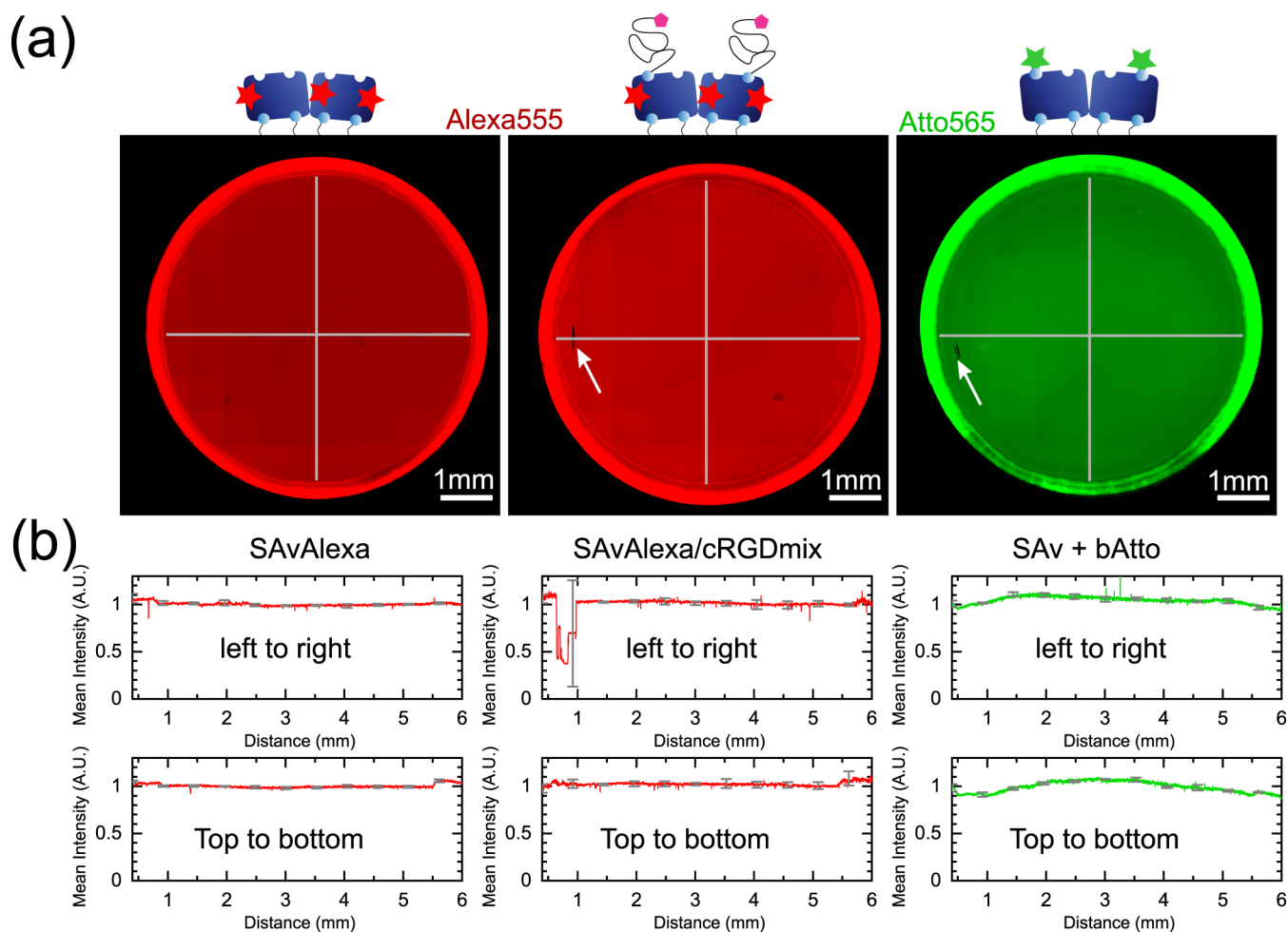


**Figure 3.** Homogeneity analysis of individual wells of a 96-well plate functionalized using the robot with PLL-g-PEGbiotin50%, SAvAlexa, and bAtto (a) Representative stitched and shading-corrected 20 $\times$  IF images of the whole wells presenting different surface functionalization. White arrows indicate the presence of artifacts due to pipetting tips touching the surface. (b) Graphs showing the intensity quantification of stitched 96-well images along a line from left to right and top to bottom ( $n =$  three independent wells, error bars = standard deviation (SD)).

(Figure S1f). We measured that SAvAlexa bound with a frequency shift of  $-18.6 \pm 0.7$  Hz to the PLL-g-PEGbiotin50% layer, which is about 25% less than that of unlabeled SAv ( $-24.7 \pm 2.2$  Hz); on the other hand, we observed a higher decrease in dissipation. Plotting both binding curves normalized to the time we observed that molecules saturated after an equivalent time. We thus chose SAvAlexa as a suitable molecule to study the SAv-base-layer homogeneity. We also performed SE to calculate the dry mass adsorption of SAvAlexa and SAvAlexa/cRGDmix, which are bound to PLL-g-PEGbiotin(50%) with  $253 \pm 31$  ng/cm<sup>2</sup> (Figure 2c) and  $315 \pm 6$  ng/cm<sup>2</sup> (Figure S2a), respectively.

We demonstrated that it is possible to fabricate complex biomimetic surfaces presenting three different functional molecules on glass surfaces.

**In Situ Characterization of Biomimetic Platforms Fabricated Using a Liquid-Handling Robot.** Biomimetic platforms were fabricated inside glass-bottom 96-well plates using a liquid-handling robot, as described above (Figure 1). To characterize surface homogeneity and areal mass density *in situ* with fluorescent-based approaches, SAvAlexa was immobilized on PLL-g-PEGbiotin50%. The homogeneity of biotinylated molecules binding to SAv was quantified by immobilizing bAtto on unlabeled SAv in a second incubation

step and bAtto binding to the free biotin pockets on SAv. As a third condition, we tested SAvAlexa bound to cRGD with the molar ratio of 3:4 before binding to PLL-g-PEGbiotin50%.

Stitched and shading-corrected 20 $\times$  fluorescent images of wells acquired with the automated microscope show the global appearance of wells functionalized with the liquid-handling robot (Figure 3a). The wells only presented few minor defects. However, in some cases, artifacts were present, such as sickle-shaped black spots (white arrows) at the same place where the tips of the liquid-handling robot touched the surface. These were present close to the border of the well. Intensity measurements along a line from left to right and from top to bottom enabled us to visualize that SAvAlexa, SAvAlexa/cRGDmix, and SAv + bAtto surfaces were globally uniform and reproducible over three different wells (Figure 3b). Tight histograms of the montage of the stitched and shading-corrected images further show the uniformity of the wells and their reproducibility (Figure S3a). The CV based on intensity distribution of the full-well images is on average  $3.5 \pm 0.7\%$  for SAvAlexa,  $6.2 \pm 1.7\%$  for SAvAlexa/cRGDmix, and  $7.3 \pm 1.1\%$  SAv + bAtto. We demonstrated that the 96-well plates were homogeneously functionalized with self-assembled streptavidin platforms using the liquid-handling robot.

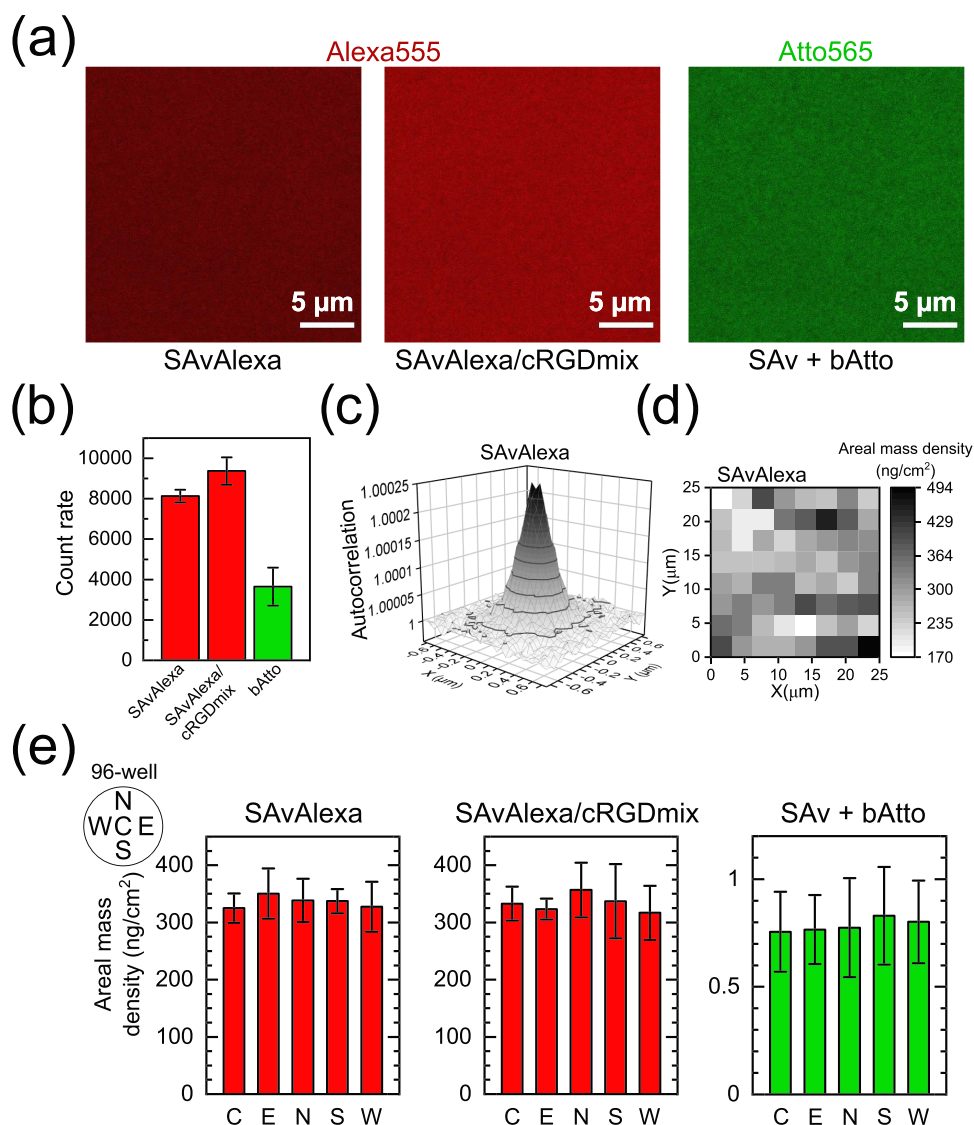


**Figure 4.** *In situ* characterization for areal mass density of SAvAlexa, SAvAlexa/cRGDmix, and SAvAlexa + bAtto. (a) Representative 63 $\times$  confocal images were taken inside a single well. (b) Graph showing the count rate quantification of 63 $\times$  confocal images acquired at five positions inside each well ( $n =$  three wells, error bars = SD). (c) Exemplary spatial autocorrelation function calculated from the whole image to deduce the number of molecules *via* its amplitude. (d) Representative grayscale map visualizing the areal mass density per subimage (3.1  $\mu\text{m} \times$  3.1  $\mu\text{m}$ ) measured *via* ICS. (e) Graphs showing the areal mass density *via* ICS at the five different positions: center (C), east (E), north (N), south (S), and west (W) per well ( $n =$  three wells, two replicates, error bars = SD).

Confocal images were acquired to quantify the mass density *in situ* using ICS (Figure 4). Representative 63 $\times$  confocal images showed no systematic defect at the microscale, which is the size of a typical spread cell (Figure 4a). The grain-like structure was then compared to a simulated image based on the random placement of SAvAlexa-like fluorescence emitting entities, which had a similar morphology (Figure S4a).

The count rate, which is the measure of mean intensity over three independent wells, revealed a 15% higher signal of SAvAlexa/cRGDmix compared to SAvAlexa (Figure 4b). The bAtto signal could not be directly compared due to the different fluorophore. The CV based on average intensities was 4% for SAvAlexa, 7% for SAvAlexa/cRGDmix, and 25% for bAtto.

The areal mass density of SAvAlexa and bAtto molecules was quantified *in situ* at five different positions. Figure 4c gives an example of an ACF over the entire SAvAlexa image. The 25  $\mu\text{m} \times$  25  $\mu\text{m}$  grayscale map exemplarily represents the areal

mass densities of 64 subimages for the SAvAlexa sample deduced from the corresponding autocorrelation functions (Figure 4d). We applied ICS on the above-mentioned simulated image, which presents a similar theoretical molecular density and equal image size (Figure S4b–e). We showed that fluctuations between the subimages were similar to the simulated image by comparing their CV (Figure S4e).

The absolute quantification of the adsorbed mass with ICS *in situ* at five different positions of the well indicated a homogeneous functionalization of SAvAlexa, SAvAlexa/cRGDmix, and SAv + bAtto (Figure 4e). SAvAlexa saturated the surface on average with  $336 \pm 34$  ng/cm<sup>2</sup> and the SAvAlexa/cRGDmix condition presented an average of  $334 \pm 45$  ng/cm<sup>2</sup>. Then,  $0.79 \pm 0.19$  ng/cm<sup>2</sup> bAtto bound to SAV. To note: bAtto binding could not be measured by QCM-D and neither SE probably due to its low molecular weight and hence low adsorbed mass.

Compared to simple intensity measurements, ICS further revealed information about the fluorescence intensity per molecule, which indicated that SAvAlexa molecules bound to cRGD were brighter than plain SAvAlexa molecules. This might be explained by the different spatial organization of these molecules on the surface with an impact on fluorophore efficiency, which did not influence ICS analysis but biased relative intensity comparison between both conditions.

With ICS studies, we succeeded to measure the areal mass density of large and small labeled molecules *in situ*.

ICS-derived areal mass densities were compared to complementary SE measurements summarized in Table 2.

**Table 2. Comparison of SE and ICS to Measure the Areal Mass Density *Ex Situ* and *In Situ*<sup>a</sup>**

compound	molecular weight (kDa)	mass SE (ng/cm <sup>2</sup> )	mass ICS (ng/cm <sup>2</sup> )
PLL-g-PEGbiotin50%	107	120 ± 8.7	N.A.
SAv	55	263 ± 6	N.A.
SAvAlexa	55	253 ± 33	336 ± 34
SAv/cRGDmix 3:4	N.A.	343 ± 25	N.A.
SAvAlexa/cRGDmix 3:4	N.A.	315 ± 6	334 ± 45
bAtto	0.922	N.A.	0.79 ± 0.19

<sup>a</sup>The measured mass of SAvAlexa/cRGDmix for ICS presents only the SAvAlexa part, whereas for SE, the mass of the whole complex is measured. Values are given as mean and SD. ICS measurements were not possible on unlabeled molecules and SE was not sensitive enough to measure bAtto binding. Values are given as mean ± SD over at least three replicates.

The mass of SAvAlexa is the only one directly comparable between both ICS and SE. ICS is the only technique to measure molecular densities *in situ* inside 96-well plates without passing *via* auxiliary substrates as needed for SE or QCM-D. It is further sufficiently sensitive to measure very small densities as seen with bAtto.

**Cellular Adhesion and BMP2 Signaling on Biomimetic Platforms in 96-Well Plates.** To study BMP2-mediated cellular responses on C2C12 skeletal myoblasts, we studied the cellular responses on streptavidin-based biomimetic platforms fabricated using the liquid-handling robot. We quantified the homogeneity of cell adhesion onto cRGD and also the homogeneity of BMP2 signaling.

While 86.6 ± 4.2% of cells adhered to saturated cRGD and spread well, only 10.0 ± 0.1% remained on bPEG-functionalized surfaces and with round shape (Figure 5a). A comparison of cellular adhesion between different positions throughout the well revealed no significant difference (Figure 5b). We showed that C2C12 cells adhered specifically to cRGD and homogeneously over the whole surface (Figure 5b).

Platforms functionalized with a submonolayer of cRGD and co-functionalized with iHS and aBMP2 (2.5 μg/mL for 90 min) were fabricated, and sBMP2 at 100 ng/mL was used as a control. Seeded cells were fixed after 1.5 h, and F-actin, nucleus, and pSMAD1/5/9 were stained to quantify BMP2 signaling. Cells still spread on platforms with the subsaturated layer of cRGD with an area of 951 ± 9 μm<sup>2</sup> and slightly more on the co-functionalized platform with 1009 ± 17 μm<sup>2</sup>.

We quantified the homogeneity of BMP2 response by analyzing pSMAD1/5/9 intensity at five positions throughout the surface (Figure 5c). sBMP2 and aBMP2 equally induced

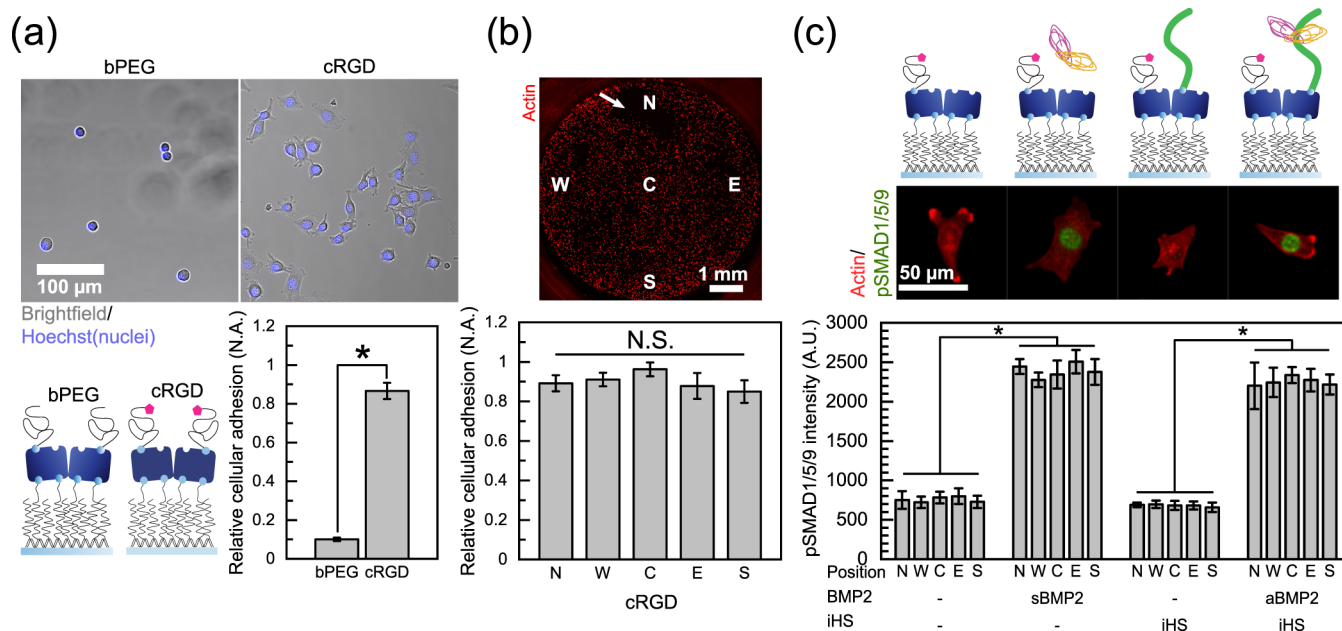


**Figure 5.** C2C12 cell adhesion to cRGD and BMP2-induced pSMAD1/5/9 signaling (a) Representative bright-field images of C2C12 cells adhering to bPEG and cRGD with the graph showing the corresponding quantification of relative cellular adhesion after rinsing. (b) Representative stitched 10× immunofluorescence image of fixed and actin-labeled C2C12 cells adhering throughout the whole well at the five positions: center (C), east (E), north (N), south (S), and west (W). The white arrow indicates rinsing artifacts during staining. Below, a graph shows the quantification of relative cellular adhesion of C2C12 cells on saturated cRGD platforms at five positions throughout the well. (c) Automatically acquired representative immunofluorescence images of C2C12 cells on cRGD and/or BMP2-presenting platforms stained for actin and pSMAD1/5/9. Below is a graph showing the pSMAD1/5/9 intensity quantification at five positions throughout the well and processed using an automated image analysis software. All experiments were repeated at least 3 times, error bars = standard error of the mean (SEM), and significance was tested with the Mann–Whitney test for  $p \leq 0.05$ .

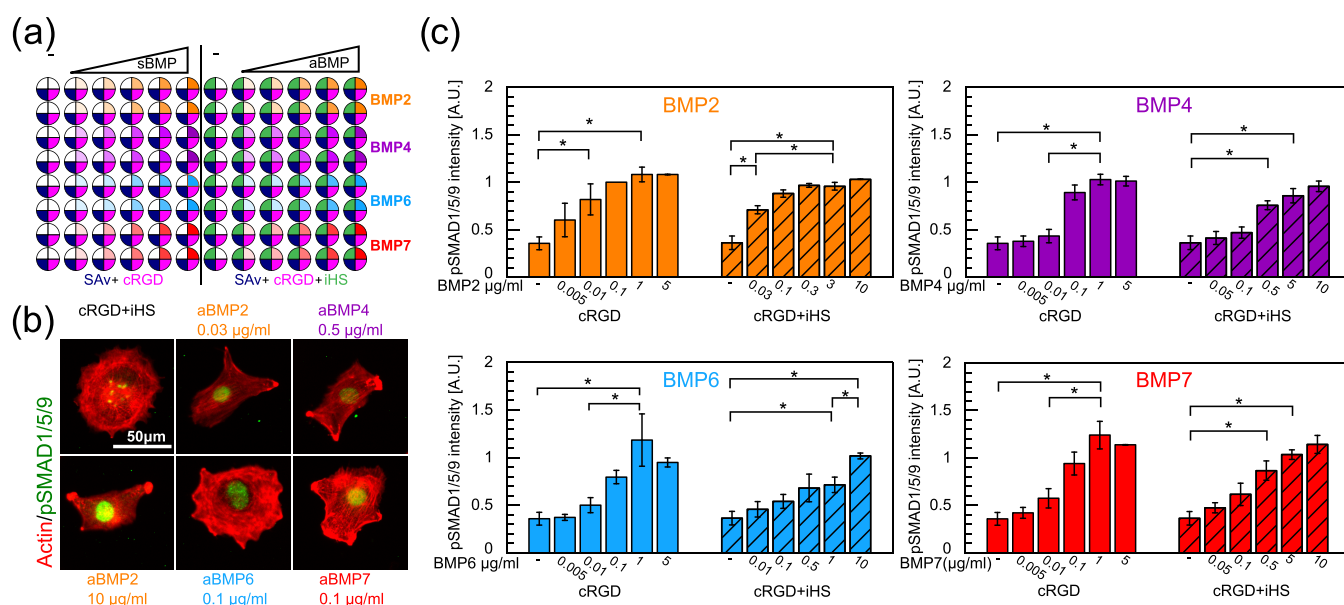


**Figure 6.** Automated high-content study of the C2C12 cell response to sBMP2, 4, 6, and 7 and aBMP2, 4, 6, and 7. (a) Schematic of a 96-well plate with 42 different conditions in duplicates fully functionalized by the robot. sBMP2, 4, 6, and 7 in different concentrations were added by hand into the cell media when cells were plated. (b) Representative and equally treated images of C2C12 cells plated inside the 96-well plate were functionalized by the robot, fixed after 90 min, and labeled for actin, and pSMAD1/5/9 was translocated into the nucleus. BMP concentrations were chosen to represent a condition close to the  $EC_{50}$  concentration. (c) Graphs show the quantification of pSMAD1/5/9 translocated into the nucleus. Values were normalized to the sBMP2 condition at 0.1  $\mu\text{g}/\text{mL}$ . Each experiment was the average of two wells and the error bars represent the SEM. Significance was tested with the Mann–Whitney test and  $p < 0.05$  for  $n = 3$ . The aBMP2, 4, 6, and 7 concentrations represent the concentrations used for the incubation on iHS and do not permit a quantitative conclusion on the amount of aBMP2/4/6/7 eventually adsorbed on iHS.

**Table 3.**  $EC_{50}$  Values for sBMP2, 4, 6, and 7 and aBMP2, 4, 6, and 7 on cRGD Platforms Compared to Values of a Similar Study with C2C12 Cells on Tissue Culture Plates<sup>52 a</sup>

	$EC_{50}$ ( $\mu\text{g}/\text{mL}$ )		$EC_{50}$ (nM)		$EC_{50}$ (nM)
	sBMP	aBMP	sBMP	aBMP	sBMP <sup>52</sup>
BMP2 (26 kDa)	0.007 $\pm$ 0.001	0.028 $\pm$ 0.007	0.269 $\pm$ 0.038	1.08 $\pm$ 0.27	0.033 $\pm$ 0.002
BMP4 (24 kDa)	0.027 $\pm$ 0.003	0.227 $\pm$ 0.033	1.13 $\pm$ 0.13	9.46 $\pm$ 1.38	0.010 $\pm$ 0.0004
BMP6 (30 kDa)	0.035 $\pm$ 0.022	fit failed	1.12 $\pm$ 0.73	fit failed	1.3 $\pm$ 0.032
BMP7 (26 kDa)	0.042 $\pm$ 0.011	0.294 $\pm$ 0.150	1.62 $\pm$ 0.42	11.3 $\pm$ 5.77	5.9 $\pm$ 0.22

<sup>a</sup>Values are given as mean  $\pm$  SD over three replicates.

SMAD1/5/9 phosphorylation with significant difference from the negative controls, and the signal was evenly intense at the five different positions.

We conclude that C2C12 adhesion on PLL-g-PEGbio-tin50%-based platforms is specific to cRGD and that platforms are sequentially built up by the robot and presenting the functional molecules cRGD, bHS, and aBMP2 are homogeneous over the entire well.

**C2C12 Dose Response to sBMP2, 4, 6, and 7 or aBMP2, 4, 6, and 7.** We took advantage of the high-content fabrication protocol to study the dose response of C2C12 cells to four different BMPs in parallel by comparing the  $EC_{50}$  values. We further studied the effect of HS on BMP signaling. With the liquid-handling robot, we functionalized a 96-well plate with 42 different conditions in technical duplicates presenting the BMPs either in solution (sBMP2, 4, 6, and 7) or adsorbed on iHS (aBMP2, 4, 6, and 7) for 130 min. This approach is easy to use for the experimentalist, with a trained user taking only 15 min to enter the experimental parameters via the custom-made graphical user interface. We quantified

SMAD1/5/9 phosphorylation with automated microscopy and image analysis (Figure 6a).

We identified initial aBMP2, 4, 6, and 7 concentrations in a way that all BMPs bound with comparable frequency shifts to iHS before rinsing using QCM-D (Figure S5a). These concentrations were high, in the range of 1–10  $\mu\text{g}/\text{mL}$ , to induce maximal SMAD1/5/9 phosphorylation. From this BMP2, 4, 6, and 7 specific base concentration, we chose a stepwise 100-fold dilution and also added a 10  $\mu\text{g}/\text{mL}$  common upper concentration.

The robot functionalized this specific whole plate in 6 h of which roughly 4 h were waiting time for molecule incubation and 2 h liquid-handling operations. Automated image acquisition and analysis took 1 h each with additional 15 min user interaction for both steps to set up the microscope and calibrate the image analysis software.

Representative single-cell images of the negative control, an intermediate BMP concentration, and a plateau condition show the presence of pSMAD1/5/9 in the nucleus (Figure 6b). For all sBMP2, 4, 6, and 7 and aBMP2, 4, 6, and 7 conditions, we observed a BMP dose-dependent response in

C2C12 cells (Figure 6c). The sBMP2, 4, 6, and 7 concentration of 1  $\mu\text{g}/\text{mL}$ , which in all cases represented an upper plateau pSMAD1/5/9 signal, was significantly higher than the negative control. Also, when comparing the aBMP2, 4, 6, and 7 conditions, the comparable concentration of 3, 5, 10, and 5  $\mu\text{g}/\text{mL}$  respectively induced a plateau pSMAD1/5/9 signal, which was significantly higher than the negative control and comparable to the plateau induced by corresponding sBMP2, 4, 6, and 7. Statistical significance between intermediate concentrations and the negative control and either sBMP2, 4, 6, and 7 at 1  $\mu\text{g}/\text{mL}$  or aBMP2, 4, 6, and 7 at 3, 5, 10, or 5  $\mu\text{g}/\text{mL}$  was tested.

$\text{EC}_{50}$  was calculated from these curves, which corresponds to the BMP concentration for which the pSMAD1/5/9 signal is about 50% of the plateau value (Figure S5b). The results of the fits are summarized in Table 3. sBMP2 thus was more potent to induce SMAD1/5/9 phosphorylation than sBMP4, 6, and 7, which were comparable to each other. In addition, aBMP2 was more bioactive than aBMP4 and aBMP7 but for aBMP6 the fit for the dose response curve failed because at high aBMP6 concentrations the plateau of the pSMAD1/5/9 response was not reached. In a similar experiment with soluble BMPs, Hammers et al. measured  $\text{EC}_{50}$  values for sBMP2, 4, 6, and 7 (Table 3<sup>52</sup>).

Thus, using the robot, many different conditions could be studied in parallel to user demand. Together with automated image acquisition and analysis, the workflow appears to be fast and reproducible for high-content studies with a customized biomaterial. Here, we were able to identify sBMP2, 4, 6, and 7 and aBMP2, 4, 6, and 7 concentrations in the dynamic range of induced SMAD1/5/9 phosphorylation, which allows direct comparison of the BMP bioactivity. These so-called critical concentrations may further be used to measure the influence of other factors on SMAD1/5/9 phosphorylation, including gene mutations, drugs, receptors, or molecules from the extracellular matrix.

## DISCUSSION

Here, we presented for the first time the automated functionalization of SAV biomimetic platforms built-up on glass-bottom 96-well plates for cellular studies. To this end, we developed an automated experimental workflow to fabricate on-demand biomimetic platforms using custom-made software, a liquid-handling robot, and automated image acquisition and analysis. C2C12 cells responded to co-presented cRGD and iHS-adsorbed aBMP2, 4, 6, and 7 *via* specific adhesion and SMAD1/5/9 phosphorylation.

Automated liquid-handling protocols for self-assembled materials directly inside multiwell plates have been rarely developed before,<sup>17</sup> and the previous study did not address single-well customization with a large choice of different solutions. The originality here relies on the possibility to assign complex and independent experimental conditions to each individual well. Moreover, it is possible to choose between using few wells only or the plate as a whole, resulting in optimized material consumption and allowing low-content preliminary studies. In addition, the number of replicates is flexible, which is important if different cell types are studied in parallel on identical conditions or if different readouts on the same condition are desired. Finally, the advantage of using SAV as a base opens this system to a vast field of applications due to its specific affinity to biotin.

By transferring all liquid-handling operations to the robot, the user participation in the experiment was reduced by hours depending on the complexity of the experimental plan and a source for human errors was eliminated.<sup>16</sup> Adaptation to other glass-bottom multiwell supports is possible due to the large range of compatible pipetting hardware offered by TECAN but would also come along with further development of the graphical user interface. In addition, cell seeding and adding soluble factors to the media would be feasible with this setup under the condition that the system is placed under a sterile environment.

Here, we applied ICS for the first time to quantify molecular densities in fluorescence confocal images acquired *in situ* in the context of surface characterization of biofilms where this technique is not common.<sup>29</sup> Functionalized surfaces were characterized *in situ* using ICS and compared to results obtained in *ex situ* measurements on model silica substrates using QCM-D and SE.

The calculated number of molecules per observation area translated into mass per area allow direct comparison to measurements acquired with SE (Table 2). With SE, we were not able to detect the small-molecule bAtto binding to SAV, whereas with ICS, we reproducibly measured  $0.79 \pm 0.19 \text{ ng}/\text{cm}^2$ . The SE measurements for SAV and SAVAlexa were comparable to each other, while the SAVcRGDmix bound with an increase of  $80 \text{ ng}/\text{cm}^2$ . Since ICS measurements suggest that the amount of SAVAlexa on the surface in its pure version or coupled to cRGD is similar, the additional mass describes mostly the amount of cRGD on the surface. Interestingly, the amount of bAtto bound on the SAV layer is more than an order of magnitude lower than the amount of cRGD precoupled with SAVAlexa.<sup>32</sup> This may indicate that when we premixed SAV and cRGD we avoided the long PLL-g-PEGbiotin chains from occupying the biotin pockets available on streptavidin, in line with Zhen et al.<sup>51</sup>

ICS-derived areal mass densities were comparable to the ones measured with SE with a difference of 32% for SAVAlexa, while the standard deviation between replicates ranges around 10–20% for both approaches. We thus validated ICS as a suitable technique to characterize biomimetic SAV platforms *in situ*. One source for this difference can originate from the two different substrates used, glass for ICS and thermal  $\text{SiO}_2$  for SE. With SE, we measured  $120.2 \pm 8.7 \text{ ng}/\text{cm}^2$  PLL-g-PEGbiotin50% and  $253.2 \pm 32.8 \text{ ng}/\text{cm}^2$  SAVAlexa. Indeed, other studies show that the binding of PLL-g-PEGbiotin depends on the substrate.<sup>53</sup> Huang et al. show that PLL-g-PEGbiotin with different percentages of grafted biotin binds all similar with  $2.5 \text{ pmol}/\text{cm}^2$  ( $268 \text{ ng}/\text{cm}^2$  for PLL-g-PEGbiotin50%) to  $\text{NbO}_2$  to which SAV adsorbed with  $369 \text{ ng}/\text{cm}^2$ .<sup>2,47</sup> Städler et al. however measured on the same substrate  $218 \pm 16 \text{ ng}/\text{cm}^2$  of PLL-g-PEGbiotin with 350  $\text{ng}/\text{cm}^2$  neutravidin adsorption.<sup>54</sup> But experiments on  $\text{SiO}_2$  show  $145 \text{ ng}/\text{cm}^2$  for a PLL-g-PEGbiotin layer and subsequent SAV binding of only  $120 \text{ ng}/\text{cm}^2$ .<sup>55</sup>

While ICS avoids passing *via* tools with different substrates such as QCM-D, SE, OWLS, or *via* indirect measurements ( $\mu\text{BCA}$ ), it has other constraints: Compounds need to be labeled with a fluorophore, which might alter molecular binding properties and also leads to negligence of unlabeled molecules.<sup>56</sup> While confocal microscopes are abundant in research facilities, specific analysis software to calculate the ACF and deduce the number of molecules per observation area is scarcely available and analysis relies on custom-made tools,

extensions, and experienced users. Nevertheless, we proved that this method is more accurate to characterize biomaterials *in situ* than a simple relative intensity comparison done with any fluorescent microscopy due to artifacts from varying fluorophore efficiency between samples probably related to quenching (Figure 4b,e).<sup>57</sup>

As proof of concept of our functionalization workflow, we studied the dose–response of C2C12 cells to different concentrations of BMP2, 4, 6, and 7 in parallel adsorbed to iHS or in soluble conditions. The calculated EC<sub>50</sub> values proved that BMP2 is the most potent among the four studied GFs in the soluble form and adsorbed on HS because it already induced SMAD1/5/9 phosphorylation at lower concentrations. Hammers et al. measured one and two orders of magnitude lower EC<sub>50</sub> values for sBMP2 and sBMP4, respectively, whereas sBMP6 and sBMP7 were comparable.<sup>52</sup> Their use of typical tissue culture plates compared to our cRGD platforms could explain these differences. Sales et al. also compared concentrations of matrix-bound BMP2, 4, and 7 to each other and found higher SMAD1/5/9 phosphorylation induced by BMP2 compared to BMP4 and BMP7 at low concentrations.<sup>21</sup> However, at higher concentrations, BMP7 was inducing the highest signal among all. Due to the novel workflow here reported, it will be possible to perform a systematic study of the effect of different GFs and different GAGs on cellular signaling.

## CONCLUSIONS

We presented an automated workflow for the functionalization at the single-well level of a biomimetic self-assembled material inside glass-bottom 96-well plates. With a graphical user interface, we empowered the user to enter a complex experimental setup in minutes, presenting a maximum of 96 different conditions on the same plate for up to three identical plates in parallel. A custom-made software translated this plan into liquid-handling commands, which were executed by a liquid-handling robot in a reproducible and homogeneous way. By characterizing the wells with image correlation spectroscopy, we measured the molecular density of biomimetic surfaces *in situ*. We did a proof of concept and studied the effect of BMP-mediated cell signaling on streptavidin platforms presenting heparan sulfate and four different BMPs. Cell adhesion and BMP2-mediated signaling were followed using automated image acquisition and subsequent high-content analysis. We found that BMP2, 4, 6, and 7 adsorbed at very low concentrations to immobilized heparan sulfate and could induce SMAD1/5/9 phosphorylation, BMP2 being the most effective. Due to this automated workflow, it may be considered to custom-design any type of multiwell plate made of biological or nonbiological self-assembled materials and to perform parallel studies in the same experimental conditions. Such fabrication methods may be used by other researchers to study the synergies between matrix components and growth factors in cellular processes.

## ASSOCIATED CONTENT

### Supporting Information

The Supporting Information is available free of charge at <https://pubs.acs.org/doi/10.1021/acsami.2c08272>.

QCM-D measurements of the sequential co-functionalization and nonspecific BSA binding to the platforms (Figure S1); binding of SAvAlexa/cRGDmix measured

with spectroscopic ellipsometry (Figure S2); reproducibility of surface functionalization (Figure S3); homogeneous binding of SAvAlexa to the platforms, confocal vs simulated images (Figure S4); and binding kinetics of different BMPs to iHS and fitted curves for the calculation of EC<sub>50</sub> values (Figure S5) (PDF)

## AUTHOR INFORMATION

### Corresponding Authors

**Catherine Picart** – Univ. Grenoble Alpes, CNRS, Grenoble INP\*\*, LMGP, 38000 Grenoble, France; Univ. Grenoble Alpes, CEA, INSERM, U1292 Biosanté, CNRS EMR 5000 BRM, 38000 Grenoble, France; [orcid.org/0000-0003-0130-1000](https://orcid.org/0000-0003-0130-1000); Phone: (33)-04 56 52 93 24; Email: [catherine.picart@cea.fr](mailto:catherine.picart@cea.fr)

**Elisa Migliorini** – Univ. Grenoble Alpes, CNRS, Grenoble INP\*\*, LMGP, 38000 Grenoble, France; Univ. Grenoble Alpes, CEA, INSERM, U1292 Biosanté, CNRS EMR 5000 BRM, 38000 Grenoble, France; [orcid.org/0000-0003-3264-2027](https://orcid.org/0000-0003-3264-2027); Email: [elisa.migliorini@cea.fr](mailto:elisa.migliorini@cea.fr)

### Authors

**Julius Sefkow-Werner** – Univ. Grenoble Alpes, CNRS, Grenoble INP\*\*, LMGP, 38000 Grenoble, France; Univ. Grenoble Alpes, CEA, INSERM, U1292 Biosanté, CNRS EMR 5000 BRM, 38000 Grenoble, France

**Jean Le Pennec** – Univ. Grenoble Alpes, CEA, INSERM, U1292 Biosanté, CNRS EMR 5000 BRM, 38000 Grenoble, France

**Paul Machillot** – Univ. Grenoble Alpes, CEA, INSERM, U1292 Biosanté, CNRS EMR 5000 BRM, 38000 Grenoble, France

**Bertin Ndayishimiye** – Univ. Grenoble Alpes, CEA, INSERM, U1292 Biosanté, CNRS EMR 5000 BRM, 38000 Grenoble, France

**Elaine Castro-Ramirez** – Univ. Grenoble Alpes, CEA, INSERM, U1292 Biosanté, CNRS EMR 5000 BRM, 38000 Grenoble, France

**João Lopes** – Univ. Grenoble Alpes, CEA, INSERM, U1292 Biosanté, CNRS EMR 5000 BRM, 38000 Grenoble, France

**Christophe Licitra** – Univ. Grenoble Alpes, CEA, Leti, F-38000 Grenoble, France

**Irene Wang** – Univ. Grenoble Alpes, CNRS, LiPhy, 38000 Grenoble, France

**Antoine Delon** – Univ. Grenoble Alpes, CNRS, LiPhy, 38000 Grenoble, France; [orcid.org/0000-0001-9533-4529](https://orcid.org/0000-0001-9533-4529)

Complete contact information is available at: <https://pubs.acs.org/doi/10.1021/acsami.2c08272>

### Notes

The authors declare no competing financial interest.

## ACKNOWLEDGMENTS

The authors acknowledge Dr. Didier Boturyn and Remy Lartia from DCM in Grenoble for the synthesis of the cRGD peptide. For fruitful discussions, the authors thank Prof. Ralf Richter (University of Leeds), Dr. Liliane Guerente (DCM Grenoble), and Dr. Elisabetta Ada Cavalcanti-Adam (MPI Heidelberg) as well as the members of their group BRM at CEA. Hajar Ajiyel, Marie Dutoit, Samy Idelcadi, and Julia Levy from Grenoble INP further contributed to software development. This project received funding from Fondation Recherche Médicale (No.

DEQ20170336746 and No. PLP20201012457), ANR CODE-CIDE (No. ANR-17-CE13-022), ANR GlyCON (No. ANR-19-CE13-0031-01 PRCI), and the Initiative de Recherche Stratégique, University Grenoble Alpes (IDEX- IRS 2018–2021). This work has been supported by CNRS GDR 2088 “BIOMIM”, ANR-17-EURE-0003, GRAL, ERC POC BIO-ACTIVECOATINGS 2015 (GA692924), and TEC21 Labex. C.P. is a senior member of the “Institut Universitaire de France”.

## REFERENCES

- (1) Mano, J. F.; Choi, I. S.; Khademhosseini, A. Biomimetic Interfaces in Biomedical Devices. *Adv. Healthcare Mater.* **2017**, *6*, No. 1700761.
- (2) Curry, A. S.; Pensa, N. W.; Barlow, A. M.; Bellis, S. L. Taking Cues from the Extracellular Matrix to Design Bone-Mimetic Regenerative Scaffolds. *Matrix Biol.* **2016**, *52–54*, 397–412.
- (3) Hynes, R. O. The Extracellular Matrix: Not Just Pretty Fibrils. *Science* **2009**, *326*, 1216–1219.
- (4) Engler, A. J.; Sen, S.; Sweeney, H. L.; Discher, D. E. Matrix Elasticity Directs Stem Cell Lineage Specification. *Cell* **2006**, *126*, 677–689.
- (5) Migliorini, E.; Ban, J.; Greci, G.; Andolfi, L.; Pozzato, A.; Tormen, M.; Torre, V.; Lazzarino, M. Nanomechanics Controls Neuronal Precursors Adhesion and Differentiation. *Biotechnol. Bioeng.* **2013**, *110*, 2301–10.
- (6) Migliorini, E.; Horn, P.; Haraszti, T.; Wegner, S.; Hiepen, C.; Knaus, P.; Richter, P.; Cavalcanti-Adam, E. Enhanced Biological Activity of Bmp-2 Bound to Surface-Grafted Heparan Sulfate. *Adv. Biosyst.* **2017**, *1*, No. 1600041.
- (7) Migliorini, E.; Guevara-Garcia, A.; Albiges-Rizo, C.; Picart, C. Learning from Bmps and Their Biophysical Extracellular Matrix Microenvironment for Biomaterial Design. *Bone* **2020**, *141*, No. 115540.
- (8) Monteiro, A. I.; Kollmetz, T.; Malmstrom, J. Engineered Systems to Study the Synergistic Signaling between Integrin-Mediated Mechanotransduction and Growth Factors (Review). *Biointerphases* **2018**, *13*, No. 06D302.
- (9) Vassey, M. J.; Figueredo, G. P.; Scurr, D. J.; Vasilevich, A. S.; Vermeulen, S.; Carlier, A.; Luckett, J.; Beijer, N. R. M.; Williams, P.; Winkler, D. A.; de Boer, J.; Ghaemmaghami, A. M.; Alexander, M. R. Immune Modulation by Design: Using Topography to Control Human Monocyte Attachment and Macrophage Differentiation. *Adv. Sci.* **2020**, *7*, No. 1903392.
- (10) Nicolas, J.; Magli, S.; Rabbachin, L.; Sampaoli, S.; Nicotra, F.; Russo, L. 3d Extracellular Matrix Mimics: Fundamental Concepts and Role of Materials Chemistry to Influence Stem Cell Fate. *Biomacromolecules* **2020**, *21*, 1968–1994.
- (11) Pagel, M.; Beck-Sickinger, A. G. Multifunctional Biomaterial Coatings: Synthetic Challenges and Biological Activity. *Biol. Chem.* **2017**, *398*, 3–22.
- (12) He, W.; Reaume, M.; Hennenfent, M.; Lee, B. P.; Rajachar, R. Biomimetic Hydrogels with Spatial- and Temporal-Controlled Chemical Cues for Tissue Engineering. *Biomater. Sci.* **2020**, *8*, 3248–3269.
- (13) Eggert, S.; Huttmacher, D. W. In Vitro Disease Models 4.0 Via Automation and High-Throughput Processing. *Biofabrication* **2019**, *11*, No. 043002.
- (14) Vasilevich, A.; de Boer, J. Robot-Scientists Will Lead Tomorrow's Biomaterials Discovery. *Curr. Opin. Biomed. Eng.* **2018**, *6*, 74–80.
- (15) Grubb, M. L.; Caliani, S. R. Fabrication Approaches for High-Throughput and Biomimetic Disease Modeling. *Acta Biomater.* **2021**, *132*, 52–82.
- (16) Lippi, G.; Lima-Oliveira, G.; Brocco, G.; Bassi, A.; Salvagno, G. L. Estimating the Intra- and Inter-Individual Imprecision of Manual Pipetting. *Clin. Chem. Lab. Med.* **2017**, *55*, 962–966.
- (17) Machillot, P.; Quintal, C.; Dalonneau, F.; Hermant, L.; Monnot, P.; Matthews, K.; Fitzpatrick, V.; Liu, J.; Pignot-Paintrand, I.; Picart, C. Automated Buildup of Biomimetic Films in Cell Culture Microplates for High-Throughput Screening of Cellular Behaviors. *Adv. Mater.* **2018**, *30*, No. 1801097.
- (18) Afshar, M. E.; Abraha, H. Y.; Bakooshli, M. A.; Davoudi, S.; Thavandiran, N.; Tung, K.; Ahn, H.; Ginsberg, H. J.; Zandstra, P. W.; Gilbert, P. M. A 96-Well Culture Platform Enables Longitudinal Analyses of Engineered Human Skeletal Muscle Microtissue Strength. *Sci. Rep.* **2020**, *10*, No. 6918.
- (19) Kaufmann, T.; Ravoo, B. J. Stamps, Inks and Substrates: Polymers in Microcontact Printing. *Polym. Chem.* **2010**, *1*, 371–387.
- (20) Murphy, S. V.; Atala, A. 3d Bioprinting of Tissues and Organs. *Nat. Biotechnol.* **2014**, *32*, 773–785.
- (21) Sales, A.; Khodr, V.; Machillot, P.; Chaar, L.; Fourel, L.; Guevara-Garcia, A.; Migliorini, E.; Albiges-Rizo, C.; Picart, C. Differential Bioactivity of Four Bmp-Family Members as Function of Biomaterial Stiffness. *Biomaterials* **2022**, *281*, No. 121363.
- (22) Brooks, E. A.; Jansen, L. E.; Gencoglu, M. F.; Yurkevich, A. M.; Peyton, S. R. Complementary, Semiautomated Methods for Creating Multidimensional Peg-Based Biomaterials. *ACS Biomater. Sci. Eng.* **2018**, *4*, 707–718.
- (23) Eggert, S.; Kahl, M.; Bock, N.; Meinert, C.; Friedrich, O.; Huttmacher, D. W. An Open-Source Technology Platform to Increase Reproducibility and Enable High-Throughput Production of Tailorable Gelatin Methacryloyl (Gelma) - Based Hydrogels. *Mater. Des.* **2021**, *204*, No. 109619.
- (24) Zeng, W.; Guo, L.; Xu, S.; Chen, J.; Zhou, J. High-Throughput Screening Technology in Industrial Biotechnology. *Trends Biotechnol.* **2020**, *38*, 888–906.
- (25) Kletzmayer, A.; Clement Frey, F.; Zimmermann, M.; Eberli, D.; Millan, C. An Automatable Hydrogel Culture Platform for Evaluating Efficacy of Antibody-Based Therapeutics in Overcoming Chemoresistance. *Biotechnol. J.* **2020**, *15*, No. 1900439.
- (26) Reviakine, I.; Johannsmann, D.; Richter, R. P. Hearing What You Cannot See and Visualizing What You Hear. *Anal. Chem.* **2011**, *83*, 8838–8848.
- (27) Dubacheva, G. V.; Araya-Callis, C.; Geert Volbeda, A.; Fairhead, M.; Codée, J.; Howarth, M.; Richter, R. P. Controlling Multivalent Binding through Surface Chemistry: Model Study on Streptavidin. *J. Am. Chem. Soc.* **2017**, *139*, 4157–4167.
- (28) Migliorini, E.; Thakar, D.; Sadir, R.; Pleiner, T.; Baleux, F.; Lortat-Jacob, H.; Coche-Guerente, L.; Richter, R. P. Well-Defined Biomimetic Surfaces to Characterize Glycosaminoglycan-Mediated Interactions on the Molecular, Supramolecular and Cellular Levels. *Biomaterials* **2014**, *35*, 8903–8915.
- (29) Migliorini, E.; Weidenhaupt, M.; Picart, C. Practical Guide to Characterize Biomolecule Adsorption on Solid Surfaces (Review). *Biointerphases* **2018**, *13*, No. 06D303.
- (30) Waters, J. C.; Wittmann, T. *Concepts in Quantitative Fluorescence Microscopy*, Waters, J. C.; Wittman, T., Eds.; Academic Press, 2014; Vol. 123, pp 1–18.
- (31) Galush, W. J.; Nye, J. A.; Groves, J. T. Quantitative Fluorescence Microscopy Using Supported Lipid Bilayer Standards. *Biophys. J.* **2008**, *95*, 2512–2519.
- (32) Sefkow-Werner, J.; Migliorini, E.; Picart, C.; Wahyuni, D.; Wang, I.; Delon, A. Combining Fluorescence Fluctuations and Photobleaching to Quantify Surface Density. *Anal. Chem.* **2022**, *94*, 6521–6528.
- (33) Gribova, V.; Auzely-Velty, R.; Picart, C. Polyelectrolyte Multilayer Assemblies on Materials Surfaces: From Cell Adhesion to Tissue Engineering. *Chem. Mater.* **2012**, *24*, 854–869.
- (34) Migliorini, E.; Thakar, D.; Kuhnle, J.; Sadir, R.; Dyer, D. P.; Li, Y.; Sun, C.; Volkman, B. F.; Handel, T. M.; Coche-Guerente, L.; Fernig, D. G.; Lortat-Jacob, H.; Richter, R. P. Cytokines and Growth Factors Cross-Link Heparan Sulfate. *Open Biol.* **2015**, *5*, No. 150046.
- (35) Amin, L.; Ercolini, E.; Shahapure, R.; Migliorini, E.; Torre, V. The Role of Membrane Stiffness and Actin Turnover on the Force Exerted by Drg Lamellipodia. *Biophys. J.* **2012**, *102*, 2451–2460.

- (36) Thakar, D.; Dalonneau, F.; Migliorini, E.; Lortat-Jacob, H.; Boturyn, D.; Albiges-Rizo, C.; Coche-Guerente, L.; Picart, C.; Richter, R. P. Binding of the Chemokine Cxcl12alpha to Its Natural Extracellular Matrix Ligand Heparan Sulfate Enables Myoblast Adhesion and Facilitates Cell Motility. *Biomaterials* **2017**, *123*, 24–38.
- (37) Nguyen, B.; Tanious, F. A.; Wilson, W. D. Biosensor-Surface Plasmon Resonance: Quantitative Analysis of Small Molecule-Nucleic Acid Interactions. *Methods* **2007**, *42*, 150–161.
- (38) Sefkow-Werner, J.; Machillot, P.; Sales, A.; Castro-Ramirez, E.; Degardin, M.; Boturyn, D.; Cavalcanti-Adam, E.-A.; Albiges-Rizo, C.; Picart, C.; Migliorini, E. Heparan Sulfate Co-Immobilized with Crgd Ligands and Bmp2 on Biomimetic Platforms Promotes Bmp2-Mediated Osteogenic Differentiation. *Acta Biomater.* **2020**, *114*, 90–103.
- (39) Salazar, V. S.; Gamer, L. W.; Rosen, V. Bmp Signalling in Skeletal Development, Disease and Repair. *Nat. Rev. Endocrinol.* **2016**, *12*, 203–221.
- (40) Sieber, C.; Kopf, J.; Hiepen, C.; Knaus, P. Recent Advances in Bmp Receptor Signaling. *Cytokine Growth Factor Rev.* **2009**, *20*, 343–355.
- (41) Katagiri, T.; Yamaguchi, A.; Komaki, M.; Abe, E.; Takahashi, N.; Ikeda, T.; Rosen, V.; Wozney, J. M.; Fujisawa-Sehara, A.; Suda, T. Bone Morphogenetic Protein-2 Converts the Differentiation Pathway of C2c12 Myoblasts into the Osteoblast Lineage. *J. Cell Biol.* **1994**, *127*, 1755–1766.
- (42) Richter, R. P.; Rodenhausen, K. B.; Eisele, N. B.; Schubert, M. *Coupling Spectroscopic Ellipsometry and Quartz Crystal Microbalance to Study Organic Films at the Solid-Liquid Interface*, Hinrichs, K.; Eichhorn, K.-J., Eds.; Springer International Publishing: Cham, 2018; pp 391–417.
- (43) Herzinger, C. M.; Johs, B.; McGahan, W. A.; Woollam, J. A.; Paulson, W. Ellipsometric Determination of Optical Constants for Silicon and Thermally Grown Silicon Dioxide Via a Multi-Sample, Multi-Wavelength, Multi-Angle Investigation. *J. Appl. Phys.* **1998**, *83*, 3323–3336.
- (44) Carton, I.; Brisson, A. R.; Richter, R. P. Label-Free Detection of Clustering of Membrane-Bound Proteins. *Anal. Chem.* **2010**, *82*, 9275–9281.
- (45) Cauchy, A. L. *Mémoire Sur La Dispersion De La Lumière*; Chez J. G. Calve: Prague, 1836; Vol. IV, p 236.
- (46) De Feijter, J. A.; Benjamins, J.; Veer, F. A. Ellipsometry as a Tool to Study the Adsorption Behavior of Synthetic and Biopolymers at the Air-Water Interface. *Biopolymers* **1978**, *17*, 1759–1772.
- (47) Huang, N.-P.; Vörös, J.; De Paul, S. M.; Textor, M.; Spencer, N. D. Biotin-Derivatized Poly(L-Lysine)-G-Poly(Ethylene Glycol): A Novel Polymeric Interface for Bioaffinity Sensing. *Langmuir* **2002**, *18*, 220–230.
- (48) Mets, R. D.; Wang, I.; Gallagher, J.; Destaing, O.; Baland, M.; Delon, A. In *Determination of Protein Concentration on Substrates Using Fluorescence Fluctuation Microscopy*, SPIE Proceedings, March 3, 2014.
- (49) Petersen, N. O.; Höddelius, P. L.; Wiseman, P. W.; Seger, O.; Magnusson, K. E. Quantitation of Membrane Receptor Distributions by Image Correlation Spectroscopy: Concept and Application. *Biophys. J.* **1993**, *65*, 1135–1146.
- (50) Sebaugh, J. L. Guidelines for Accurate Ec50/Ic50 Estimation. *Pharm. Stat.* **2011**, *10*, 128–134.
- (51) Zhen, G.; Eggl, V.; Vörös, J.; Zammaretti, P.; Textor, M.; Glockshuber, R.; Kuennemann, E. Immobilization of the Enzyme B-Lactamase on Biotin-Derivatized Poly(L-Lysine)-G-Poly(Ethylene Glycol)-Coated Sensor Chips: A Study on Oriented Attachment and Surface Activity by Enzyme Kinetics and in Situ Optical Sensing. *Langmuir* **2004**, *20*, 10464–10473.
- (52) Hammers, D. W.; Merscham-Banda, M.; Hsiao, J. Y.; Engst, S.; Hartman, J. J.; Sweeney, H. L. Supraphysiological Levels of Gdf 11 Induce Striated Muscle Atrophy. *EMBO Mol. Med.* **2017**, *9*, 531–544.
- (53) Kenausis, G. L.; Vörös, J.; Elbert, D. L.; Huang, N.; Hofer, R.; Ruiz-Taylor, L.; Textor, M.; Hubbell, J. A.; Spencer, N. D. Poly(L-Lysine)-G-Poly(Ethylene Glycol) Layers on Metal Oxide Surfaces: Attachment Mechanism and Effects of Polymer Architecture on

Resistance to Protein Adsorption. *J. Phys. Chem. B* **2000**, *104*, 3298–3309.

(54) Städler, B.; Falconnet, D.; Pfeiffer, I.; Höök, F.; Vörös, J. Micropatterning of DNA-Tagged Vesicles. *Langmuir* **2004**, *20*, 11348–11354.

(55) Marie, R.; Dahlin, A. B.; Tegenfeldt, J. O.; Höök, F. Generic Surface Modification Strategy for Sensing Applications Based on Au/Sio 2 Nanostructures. *Biointerphases* **2007**, *2*, 49–55.

(56) Cooper, M. *Label-Free Biosensors: Techniques and Applications*; Cambridge University Press: Cambridge, 2009.

(57) Bae, W.; Yoon, T. Y.; Jeong, C. Direct Evaluation of Self-Quenching Behavior of Fluorophores at High Concentrations Using an Evanescent Field. *PLoS One* **2021**, *16*, No. e0247326.

## Recommended by ACS

### Programmable DNA Nanodevices for Applications in Neuroscience

Pravin Hivare, Dhiraj Bhatia, *et al.*

JANUARY 12, 2021  
ACS CHEMICAL NEUROSCIENCE

READ 

### Nanoenabled Bioelectrical Modulation

Aleksander Prominski, Bozhi Tian, *et al.*

AUGUST 30, 2021  
ACCOUNTS OF MATERIALS RESEARCH

READ 

### Printed-Circuit-Board-Based Two-Electrode System for Electronic Characterization of Proteins

Sara Talebi, Vengadesh Periasamy, *et al.*

APRIL 01, 2020  
ACS OMEGA

READ 

### Ultrasensitive and Selective Field-Effect Transistor-Based Biosensor Created by Rings of MoS<sub>2</sub> Nanopores

Heekyeong Park, Sunkook Kim, *et al.*

DECEMBER 29, 2021  
ACS NANO

READ 

Get More Suggestions >

**Chapter V. Glycosaminoglycans exhibit distinct interactions and signaling with BMP2 according to their nature and localization**

## V.A. Article introduction

Past investigations into the role of GAGs in the regulation of BMP signaling have focused essentially on HS and Hep. In line with this, the molecular interactions between BMP2 and GAGs have only been explored for HS and Hep. Although few findings suggested an influence of CS and its sulfation in upregulating the SMAD1/5/9 phosphorylation<sup>[11,314]</sup>, the role of CS, DS, HA, and KS in the regulation of BMP2 signaling has been scarcely explored. In addition, several contradictory findings obscure the precise role of HS and Hep in the regulation of BMP2 signaling. We suspect that the type of GAGs and their location at the cell membrane or in the extracellular matrix may elicit different BMP2 signaling dynamics, thereby complicating the comparison of various studies and obscuring our understanding of their roles.

In this article, we aimed to compare within a single study the molecular interactions of different GAGs with BMP2. To address this, we used the BLI optical technique to perform kinetics studies and determine interaction kinetic parameters with a higher throughput than the standard surface plasmon resonance technique. We next explored how these interactions modulate BMP2 signaling, depending on the localization of GAGs. We used well-characterized biomimetic SA<sub>v</sub> platforms to investigate the role of GAGs when presented in the extracellular matrix. Alternatively, we employed Chinese hamster ovary (CHO) cell mutants that synthesize distinct GAG repertoires to explore the role of cell-surface GAGs. The BMP2 signaling was studied using a robust high-content imaging and analysis system developed in the team to evaluate the fluorescence nuclear intensity of SMAD1//5/9 phosphorylation. Our findings highlighted a potential distinct role of cell-surface and extracellular GAGs, as well as a distinct effect of CS compared to HS at both sites. Specifically, HS was the only extracellular GAG significantly enhancing SMAD1/5/9 phosphorylation. For cell-surface GAGs, we unraveled a role of CS that increased BMP2 signaling in comparison to HS that seemed to inhibit it, as previously observed in the literature using EXT1 mutant cells. These results regarding the role of cell-surface GAGs have also been confirmed using Western Blot.

Specific HS sulfation patterns have been demonstrated to be crucial for FGF and AT III binding and bioactivity, which questions whether similar sulfation specificity may also exist for BMP2. Since previous studies demonstrated the distinct contributions of different HS sulfation types (N-,6O, 2-O)<sup>[324,327]</sup> for the binding to BMP2, we sought to refine these identified HS structural preferences using a library of HS-derived oligosaccharides to explore their molecular interactions with BMP2. Smith and coworkers previously reported that the minimal size of HS oligosaccharides to bind BMP2 was a hexasaccharide<sup>[324]</sup>. However, preliminary

QCM-D experiments in the team showed the binding of BMP2 on tetrasaccharides. Therefore, we chose to generate a library of both HS-derived tetrasaccharides and hexasaccharides for our investigations. Several strategies exist to generate structurally defined GAG oligosaccharides, such as chemical synthesis, chemo-enzymatic synthesis, and purification method, which have been detailed and compared in the review article provided in Annex information. Despite their efficacy, all these strategies are highly time-consuming. In our case, we used the purification strategy, benefiting from the strong expertise of Romain Vivès in this approach. We started by digesting native heparan sulfate (HS) to retrieve smaller fragments. These fragments were initially separated using size-exclusion chromatography and subsequently by charge using strong anion exchange HPLC (SAX-HPLC). The oligosaccharide amounts produced and their structural features for the whole library are detailed in the Annex information. Among the oligosaccharides generated, some were selected based on their purity and structural features to be further biotinylated for molecular studies. Molecular interaction studies with BLI enabled the identification of HS structural features that modulate the binding to BMP2. In particular, a central trisulfated disaccharide in HS-dp6 compounds appeared to enable high-affinity binding with BMP2. It is worth noting that these interesting experimental data will be further consolidated with molecular modeling of the interactions thanks to an ongoing collaboration with Dr. Olga Makshakova and Dr. Serge Pérez (CERMAV, Grenoble).

In this study, we intended to employ the new construction of biomimetic SA<sub>v</sub> platforms on glass substrates to compare several conditions in parallel. However, initial experiments revealed a strong non-specific signal due to the adsorption of BMP2 on other platform components than GAGs, thus preventing the interpretation of our results. The SA<sub>v</sub> platforms on gold substrates were also affected by this problem. Significant work was achieved to establish conditions that allowed the distinction between the non-specific signal and the signal induced by GAG-bound BMP2 (**Chapter VI**). These conditions consisted in adding a blocking step with a mix of BSA and trehalose, which was more effective on gold platforms than on glass platforms. Additional investigations will be needed to further the background signal for applications with the library of HS-oligosaccharides.

Moreover, we have needed to readapt the co-functionalization protocol used in the team since only a few cells adhered to on gold platforms presenting CS, DS, and HA, which had never been tested before. Indeed the CS, DS, and HA chains are longer than the HS chains and therefore hid the cRGD peptides needed for cell adhesion (data not shown). By QCM-D followed by cellular experiments, we defined a new protocol for platform functionalization by increasing the time of injection of cRGD peptide and therefore decreasing the amount of GAGs

on the surface. This increased the space between them and permitted the access of integrins to the cRGD peptides to obtain a comparable cellular adhesion between the different platforms.

We intend to publish this original article in a peer-reviewed journal with interests in the biology of the extracellular matrix or more specifically in the biological functions of carbohydrates. I was the main contributor of this article by preparing the oligosaccharide library, performing nearly all experiments, analyzing data, preparing figures, writing the entire manuscript, and revising it with my supervisors. Additionally, I supervised Paola Nevola, an M2 foreign student, training her in conducting cellular experiments related to cell-surface GAGs and QCM-D experiments for co-functionalization with RGD and GAGs. Other contributors to the article provided essential technical support such as preparation of common reagents, or scientific support and supervision, and funding acquisition. They also assisted in revising the manuscript and improving the overall quality of the article.

## V.B. Article

### **Glycosaminoglycans exhibit distinct interactions and signaling with BMP2 according to their nature and localization**

Jean Le Pennec<sup>1</sup>, Paola Nevola<sup>1,2</sup>, Evelyne Gout<sup>3</sup>, Paul Machillot<sup>1</sup>, Mélanie Friedel-Arboleas<sup>3</sup>, Catherine Picart<sup>1</sup>, Andrea Vortkamp<sup>4</sup>, Romain R. Vivès<sup>3\*</sup>, Elisa Migliorini<sup>1\*</sup>

<sup>1</sup>Univ. Grenoble Alpes, INSERM, CEA, CNRS, U1292 Biosanté, EMR 5000, Grenoble, France

<sup>2</sup>Dipartimento di Ingegneria Chimica e dei Materiali e della Produzione Industriale, University of Naples Federico II, Napoli, Italy.

<sup>3</sup>Univ. Grenoble Alpes, CNRS, CEA, IBS, Grenoble, France

<sup>4</sup>Developmental Biology, Centre for Medical Biotechnology, University Duisburg-Essen, Essen, Germany.

\*Co-Corresponding authors

Migliorini Elisa (E.M.): [elisa.migliorini@cea.fr](mailto:elisa.migliorini@cea.fr)

Romain Vivès (R.R.V.): [romain.vives@ibs.fr](mailto:romain.vives@ibs.fr)

#### **Abstract**

The role of glycosaminoglycans (GAGs) in the regulation of bone morphogenetic protein (BMP) signaling appears to be very complex and context-dependent. Indeed, several studies indicate either a positive or a negative effect on the BMP signaling or in the establishment of BMP gradients, and tissue-dependent effects. It remains unclear whether these effects depend on the localization of the GAGs (at the cell surface or in the extracellular matrix) or on the type of GAG. Furthermore, the molecular interactions between BMP2 and different GAGs, including chondroitin sulfate (CS) and dermatan sulfate (DS), have not been investigated up to date. Moreover, the importance of heparan sulfate (HS) sulfation patterns for the binding to BMP2 has not been deciphered. In this study, we show that BMP2 binds preferentially to heparan sulfate (HS) in comparison to differently sulfated CS, DS, and the unsulfated hyaluronic acid (HA). Next, using well-characterized biomaterials for cellular studies, we investigated the role of GAGs by distinguishing the effects of extracellular GAGs and cell-surface GAGs. Extracellular GAGs were presented by the biomaterials in an immobilized manner and the role of cell-surface GAGs was explored using Chinese hamster ovary (CHO) cell mutants for GAG biosynthesis enzymes. Our findings unveil novel perspectives in the regulation of BMP signaling where cell-surface CS appears to enhance the BMP2 bioactivity. Alternatively, the extracellular HS immobilized on our biomaterials increased the BMP2 signaling compared to CS, DS, and HA, in a mechanism that seems related to its BMP2 binding

properties. Our study clarifies the role of HS in BMP signaling and highlights distinct roles depending on its localization.

To elucidate the structural properties of HS that are responsible for the high affinity binding to BMP2, we prepared a library of HS-derived oligosaccharides to explore the role of specific sulfation patterns. Interestingly, we observed that BMP2 could bind to HS compounds as short as tetrasaccharides and that a central IdoA(2S)-GlcNS(6S) tri-sulfated motif in hexasaccharides appeared to increase significantly the binding. Generally, BMP2 exhibited a certain plasticity for different HS sulfation types and sequences and our results do not suggest the existence of a unique sequence required for BMP2 high affinity binding.

## Introduction

Glycosaminoglycans (GAGs) are linear polysaccharides, which are major components of the extracellular matrix. They include Heparan Sulfate (HS), Heparin (Hep), Chondroitin Sulfate (CS), Dermatan Sulfate (DS), Hyaluronic Acid (HA) and Keratan Sulfate (KS). With the exception of HA, GAG chains are found attached to a protein core to form a proteoglycan (PG). GAGs exhibit a wide range of interactions with proteins, growth factors, cytokines, and chemokines, facilitated by electrostatic forces influenced by sulfation patterns along their chains. Sulfation patterns of GAGs are not genetically encoded but are regulated by the spatiotemporally controlled expression of enzymes involved in the GAG biosynthesis machinery, including glycosyltransferases, sulfotransferases, and epimerases<sup>[5]</sup>. As a result, GAGs modulate diverse biological processes and contribute significantly to tissue homeostasis<sup>[6-11]</sup>. Bone Morphogenetic Protein 2 (BMP2) is a protein member of the transforming growth factor beta superfamily (TGF $\beta$ ) and is a potent osteogenic growth factor, classified also as a morphogen. The transmission of BMP signals from receptors on the plasma membrane to the nucleus occurs either *via* the canonical SMAD pathway or *via* several non-canonical pathways such as the p38 mitogen-activated protein kinase pathway<sup>[12]</sup>. The BMP signaling cascade is regulated by various endogenous and exogenous molecular factors at different spatiotemporal scales, which can exert either positive or negative effects<sup>[13,14]</sup>.

The interaction of GAGs with BMP2 is particularly important for bone development<sup>[1,15-17]</sup>. Alterations in the biosynthesis of HS are responsible for Hereditary Multiple Osteochondromas (HMO, previously Hereditary Multiple Exostoses)<sup>[18]</sup>, a skeletal disease in humans highly correlated to an altered BMP2 signaling<sup>[19,20]</sup>. CSPGs may also contribute to bone tissue homeostasis by regulating BMP2 signaling. Although there is limited research on the involvement of CS in BMP signaling, it has been demonstrated that the introduction in mice

of a gene trap mutation in the gene chondroitin-4-sulfotransferase 1 (*C4st1*), responsible for the transfer of a sulfate group to the 4-O-position in CS, results in a severe chondrodysplasia<sup>[1]</sup>. This mutation also leads to a significant increase of TGF $\beta$  signaling, while simultaneously decreasing BMP signaling.

Several studies focused on the role of Hep and HS in the regulation of BMP2 signaling. While the lack of HS is clearly dysregulating embryonic development and BMP signaling, several contradictory findings have obscured its precise role as a promoter or inhibitor of signaling. First, the alteration of GAG biosynthesis in *Ext1* or *Ext2* (glycosyltransferases responsible for elongation of HS chains) mutant mice causes the disruption of gastrulation<sup>[21]</sup>. In *Drosophila*, the mutation of *tout-velu* (*ttv*), homolog of the human *EXT1* gene, leads to defective *decapentaplegic* (Dpp, orthologue of BMP2/4) signaling activity and morphogen distribution<sup>[16]</sup>. During *Drosophila* embryogenesis, HSPGs are crucial regulators of Dpp (a BMP2/4 ortholog) signaling by mediating the formation of gradients, which is a characteristic of morphogens<sup>[16,22]</sup>. Takei and coworkers showed that the signaling of hedgehog (Hh), Dpp, and wingless (Wg) morphogens are reduced in mutant cells for homologs of EXT genes, indicating a positive role of HS in these signaling pathways<sup>[22]</sup>. In agreement with this, another study showed that a pre-treatment of C2C12 and PC12 cells with heparinase III before exposure to BMP2 led to a decreased SMAD1/5/9 phosphorylation and p38 activation<sup>[23]</sup>. Several studies contradict these results and report a negative role of HS in BMP signaling<sup>[19,20,24,25]</sup>. Huegel and coworkers showed that reducing EXT1 expression or interfering with HS function by heparinase I or Surfen treatment stimulated the chondrogenesis *in vivo*, with an increase of pSMAD1/5/9 protein levels and Runx2/Sox9 gene expression<sup>[19]</sup>. This increase of pSMAD1/5/9 was reproduced by the same research group in Ad-293 and C3H/10T1/2 cells upon Surfen treatment<sup>[24]</sup>. Another study showed that the pretreatment of limb mesenchymal cells in micromass culture with Hep III also enhanced the chondrogenic activity of BMP2<sup>[25]</sup>. Recently, Inubushi and coworkers demonstrated that the enhancement of BMP2 signaling in EXT1 mutant mice is the primary signaling defect that leads to osteochondroma formation, suggesting the possibility of targeted treatment of HME with BMP inhibitors<sup>[20]</sup>. In addition, the comparison of several studies suggests that cell-surface<sup>[17,25–27]</sup> and extracellular GAGs<sup>[25,28–31]</sup> exhibit different functions. The comparison of these studies is complicated by several factors that may influence the effect of GAGs, such as their location (extracellular/cell-surface), the presentation mode (solution/immobilized), the assay duration (short-term/long-term), or even the concentrations of growth factor or GAG used<sup>[32]</sup>. The precise role of GAGs in BMP signaling therefore remains unclear.

The understanding of GAGs-protein interactions is a key step to comprehending the full picture of the GAG-mediated regulation of protein bioactivity. Regarding BMP2, it exhibits a well-demonstrated high affinity for HS<sup>[33–35]</sup> and Hep<sup>[19,33,36]</sup>, which might be related to the important functions of HSPGs in the regulation of bone development *in vivo*. However, the affinity values described in the literature deserve to be clarified since they are subject to variations of several orders of magnitude, likely related to different experimental setups or GAG sources. The sulfation degree and sulfation patterns of HS are key structural features driving the high affinity of HS for various proteins. For some proteins like antithrombin III and FGF1, specific sulfation motifs and/or sulfation sequences of HS are particularly important for their interaction and their bioactivity<sup>[37–39]</sup>. In the case of BMP2, few studies investigated the HS sulfation motifs or sequences required for the interaction. Using desulfated Hep, Smith *et al.* demonstrated that N-sulfation was more important for BMP2 binding compared to 6-O sulfation, and 2-O sulfation which had a minor contribution<sup>[3]</sup>. This trend is however in contradiction with *in vitro* assays of Tellier and coworkers, who showed a minor importance of N-sulfation and a role of 6-O sulfation using desulfated Hep immobilized on microparticles. Chopra and coworkers also studied the HS-BMP2 interaction with a microarray displaying 3-O sulfated hexasaccharides. The authors demonstrated that BMP2 bound more strongly on oligosaccharides including a 3-O sulfate. They noticed generally a high affinity of several proteins to oligosaccharides with a central IdoA(2S)-GlcNS(3S6S) disaccharide<sup>[40]</sup>. In zebrafish, 3-O sulfation was demonstrated to contribute to the spatial restriction of BMP signaling away from ventricular myocytes, thereby promoting the cardiac contractile function<sup>[41]</sup>. In contrast, in a microarray study, Söderlund and coworkers did not observe major modification of BMP interactions for five distinct oligosaccharides, with  $K_D$  values in the 100 nM range. In particular, an HS dodecasaccharide including a 3-O sulfated GlcNS(3S6S)-IdoA(2S) sequence did not have a particular effect.

In this study, we have examined the molecular interactions between various GAGs and BMP2, yielding novel insights into their affinity and kinetics parameters. To investigate the involvement of GAGs in mediating BMP2 signaling as extracellular components, we employed biomimetic streptavidin (SAv) platforms, previously developed to support cell adhesion and present immobilized GAGs in a manner resembling the natural extracellular matrix<sup>[30,31]</sup>. These platforms have been thoroughly characterized regarding the binding of GAGs and BMP2 and the co-functionalization with cRGD peptides. To explore the role of cell-surface GAGs, we employed different CHO cellular models, including mutations of GAG biosynthesis enzymes. In particular, we unveil novel perspectives about the distinct contributions of cell-surface HS

and cell-surface CS in BMP2 signaling. Finally, we generated a library of HS tetrasaccharides and hexasaccharides to investigate the structural specificities of BMP2-HS binding and the significance of specific HS sulfation motifs and sequences. Moreover, to gain a deeper understanding of these interactions, we performed 3D molecular reconstruction and molecular dynamics simulations.

## **Materials and methods**

### **Buffers and Molecules**

A solution called Hepes, with a composition of 10 mM Hepes and 150 mM NaCl (Sigma-Aldrich) at pH 7.4, was used for diluting and rinsing all molecules unless otherwise specified. To prepare biomimetic SA<sub>v</sub> platforms, mPEG-Thiol and biotin-PEG-Thiol (11156-0695 and 41156-1095, Polypure) were functionalized on gold substrate, and further conjugated with streptavidin (SA<sub>v</sub>, Sigma-Aldrich). For information on the biotinylated cyclic arginyl-glycyl-aspartic acid (cRGD), refer to previous works<sup>[31,42]</sup>. Heparan sulfate (HS) sourced from porcine intestinal mucosa was acquired from Celsus Laboratories. It has an average molecular weight of 12 kDa and a polydispersity of 1.59<sup>[43]</sup>. Chondroitin Sulfate A (C9819, CS-A, bovine trachea, average molecular mass 28 kDa<sup>[44]</sup>), and Dermatan Sulfate (C3788, DS/CS-B, porcine intestinal mucosa) were purchased from Sigma-Aldrich. Chondroitin Sulfate D (400676, CS-D, shark cartilage, average molecular mass of 38 kDa<sup>[45]</sup>) was acquired from Seikagaku. Chondroitin Sulfate E (CS-E) and Hyaluronic Acid (HA) were a gift from Kawthar Bouchemal. BSA was purchased from ThermoFisher Scientific (BP9703-100) and D-(+)-Trehalose was acquired from ThermoFisher Scientific (A19434.14). BMP2 produced in CHO cells was obtained from Medtronic (26 kDa, InductOs). Heparinase I, II and III were acquired from GrampEnz (GE-H0001, GE-H0002, GE-H0003). Filtered phosphate buffered saline (PBS, without MgCl<sub>2</sub> and CaCl<sub>2</sub>, Gibco™, ThermoFisher Scientific) was used in all the rinsing steps related to the cells.

### **Generation of HS-oligosaccharide libraries**

An HS-oligosaccharide library was generated as previously described<sup>[38]</sup>. 8 g of HS were exhaustively digested with heparinase III at 37°C in heparinase buffer: 100 mM sodium acetate and 0.5 mM CaCl<sub>2</sub> buffer at pH 7.1. The digestion was monitored for 6 days by absorbance measurements at 232 nm with a NanoDrop™ 2000. The content of the digestion was then stored at -20 °C in eight fractions of 1 g. The fractions were separated by size one by one with a Vantage® L VL44 x 1000 size-exclusion chromatography (SEC) column, extended with a Vantage extension kit (Merck-Millipore), and packed with Bio-Gel® P-10 Gel resin (Bio-Rad),

equilibrated in 0.2 M NaCl buffer at a flow rate of 0.5 mL/min. Fractions of 15 mL were collected, and the absorbance at 232 nm was measured for all fractions to identify the peaks corresponding to oligosaccharides of different sizes, which were then pooled, dialyzed against water, and lyophilized. The dp4- and dp6- oligosaccharides were then separated according to their charge by strong anion exchange (SAX)-HPLC (5 mg of oligosaccharides per injection, for a total of ~65 mg of each dp4 and dp6 oligosaccharides) using a ProPac PA1 preparative column (ThermoFisher Scientific). The salt gradient was optimized to resolve the different oligosaccharide species out of the column.

### **Analysis and characterization of HS-oligosaccharides**

The generated HS-oligosaccharides were characterized with reverse phase ion pair (RPIP)-HPLC disaccharide analysis. First, oligosaccharides (1-2 µg) were cleaved into disaccharides with 10 mU of each heparinase I, II and III in heparinase buffer for 48 h at 37 °C. Samples were boiled at 100 °C for 10 min, and the supernatant was recovered after centrifugation at 13200 rpm to remove the enzymes. The RPIP-HPLC experimental setup has been described in previous work<sup>[46]</sup>. Briefly, the different HS disaccharides were resolved from a C18 reversed-phase column (Luna 5 µm C18, 4.6 x 300 mm, Phenomenex), using a NaCl gradient in 1.2 mM tetra-N-butylammonium hydrogen sulfate (TBA), pH 3.15, 8.5% (v/v) acetonitrile. The post-column labelling was performed in a 130 °C heated reaction with a second pump mixing the HS disaccharides with 0.125% 2-cyanoacetamide and 0.5% NaOH. After passing through a cooling tank, the disaccharides were detected by the 410 nm fluorescence emission of 2-cyanoacetamide after excitation at 346 nm. Disaccharide composition was attributed by comparison to the elution of standard unsaturated HS disaccharides (Iduron, Alreley Edge, UK: ΔUA–GlcNAc/ΔUA–GlcNS /ΔUA– GlcNAc6S /ΔUA2S – GlcNAc /ΔUA – GlcNS6S /ΔUA,2S – GlcNS /ΔUA,2S – GlcNAc,6S /ΔUA2S – GlcNS6S). By integrating the area of disaccharide peaks and applying signal / mass ratio corrections, we could determine the quantities generated for the entire oligosaccharide library. The analysis was repeated with NaBH<sub>4</sub> reduction to determine the reducing-end disaccharide of oligosaccharides, which could not be detected anymore after treatment. Oligosaccharides were reduced with 50 mM NaOH and 150 mM NaBH<sub>4</sub> (Sigma-Aldrich) overnight at 37 °C and the pH was neutralized with acetic acid (Sigma-Aldrich) prior to heparinase digestion.

### **Biotinylation of GAGs and oligosaccharides**

Glycosaminoglycans or oligosaccharides were incubated for 24 h at 37°C at 5 mg/mL concentration in 100 nM sodium acetate, 12.5 nM EZ-Link Alkoxyamine-PEG4-biotin (ThermoFisher Scientific), and 10 mM aniline (Sigma-Aldrich) to achieve coupling with the biotinylated linker. Double HiTrap® Desalting columns (GE29-0486-84, Sigma-Aldrich) coupled to AKTA Pure equipment (GE Healthcare) were used to identify and recover the fractions of desalted biotinylated GAGs. The compounds were next concentrated by freeze-drying.

### **Biolayer interferometry (BLI) measurements**

BLI studies were performed with an OctetRED96e instrument (Pall/FortéBio), using the manufacturer's software (Data Acquisition v11.11) to record the data. All molecules were dissolved in PBS-T, a PBS buffer (Euromedex) containing 0.02% Tween® 20 (Sigma-Aldrich). Samples were deposited in the wells of black 96-plates (Nunc F96 MicroWell, ThermoFisher Scientific), kept at a constant temperature of 25°C while being stirred at 1000 rpm throughout the experiments. All biosensors were pre-wetted in 200 µL of PBS-T for 10 min before each test, after which the equilibration was monitored for 60 s. SAV-coated biosensors (FortéBio) were loaded with each biotinylated GAG ligand for 600 s. The concentrations used for immobilization were as follows: 0.06 µg/mL and 0.12 µg/mL for HS and CS/DS/HA, respectively. The concentrations used were 0.075 µg/mL and 0.04 µg/mL for dp4 and dp6 ligands, respectively. Association and dissociation phases were monitored during 200 s. Identical procedures were followed on non-functionalized reference biosensors to assess and monitor BMP2 non-specific binding. All measurements were performed in three independent experiments with new sensors, and newly prepared sample solutions.

Kinetics data were analyzed using the manufacturer software (Data analysis HT v11.1). The non-specific signals on reference biosensors were subtracted from the signals obtained on GAGs-functionalized biosensors for each BMP2 analyte concentration. The kinetic signals were then fitted using a global method with a 1:1 Langmuir model. Dissociation on several GAG ligands was composed of a rapid phase and a slow phase close to the baseline. Therefore, only the first 40 s of dissociation were included in the fitting. Affinity constants were calculated from the ratio of  $k_{off}/k_{on}$  values. The reported values are plotted as mean ± SEM obtained from independent experiments.

### **Biomimetic streptavidin platforms surface functionalization**

Glass coverslips (24×24 mm; Menzel Gläser) were gold-sputtered (1.5 nm Cr and 8 nm Au) in a clean room with a Plassys™ evaporating machine and constituted the base substrates for biomimetic platforms functionalization. Gold-sputtered surfaces were activated with UV/Ozone Procleaner™ (BioForce Nanosciences) for 10 min, functionalized with mPEG-Thiol and biotin-PEG-Thiol, and immersed overnight in an ethanol solution with 0.95 mM mPEG-thiol and 0.05 mM biotin-PEG-thiol, before blow-drying the surfaces with nitrogen. When preparing samples for automated immunofluorescence (IF) analysis, gold-coated surfaces were attached to the bottom side of a bottomless 96-well plate (Greiner Bio-one) using double-sided adhesive tape (FRAP Sandwich set, Paul Marienfeld), dividing one surface into four wells. For Western blot experiments requiring significant amounts of samples, whole surfaces were put in a UV-sterilized polycarbonate dish.

Next, the assembly of SA<sub>v</sub> platforms was achieved by a liquid-handling robot executing all the incubation and rinsing steps as described in previous work<sup>[47]</sup>. SA<sub>v</sub> was incubated at 10 µg/mL for 30 min to construct a monolayer and a 2-hour blocking with 10% BSA and 0.6 M of D-(+)-Trehalose was achieved to reduce non-specific binding of BMP2. Then, co-functionalization of cRGD and GAGs was performed with a 10-minute incubation of biotinylated cRGD at 1.2 µg/mL prior to saturation of SA<sub>v</sub> binding sites with biotinylated GAGs at 10 µg/mL for 40 min. BMP2 was allowed to bind to GAGs with a 90-minute incubation step at 0.02 µg/mL (0.768 nM) in Hepes supplemented with 0.02% Tween® 20 (Hepes-T) to prevent aggregation at physiological pH during the process. To remove the non-adsorbed BMP2, two rinsing steps were performed in Hepes-T followed by three rinsing in Hepes prior to cell seeding.

### ***Ex Situ* Characterization with Quartz Crystal Microbalance with Dissipation Monitoring (QCM-D)**

We measured with QCM-D (QSense Analyzer, Biolin Scientific) the shifts in resonance frequency ( $\Delta f$  in Hz) and energy dissipation ( $\Delta D$  in dissipation units, ppm=10<sup>-6</sup>) to characterize binding events in the biomimetic platforms sequential buildup. Experiments were performed at 24°C and  $\Delta f$  and  $\Delta D$  were measured at six overtones ( $i = 3, 5, \dots, 13$ )<sup>[30]</sup>. In this article, only dissipation and normalized frequency of the third overtone ( $i = 3$ ) are presented. Frequency measurements are related to the hydrated mass bound on the surface, while dissipation measurements are related to the rigidity of the adsorbed film. With the exception of BMP2, all surface functionalization steps were carried out using the concentrations indicated above for biomimetic platforms surface functionalization. To enable adequate signal detection for

comparing its binding on various GAGs, BMP2 was injected at a concentration of 5 µg/mL. Molecules were injected into the liquid chamber with a peristaltic pump (IPC4, Ismatec) imposing a flow rate of 15 µL/min until saturation (except for cRGD and BMP2), followed by rinsing with Hepes at the same flow rate. For cRGD and BMP2, we used a “fast injection” procedure to mimic the functionalization performed by the liquid-handling robot. The solutions of cRGD and BMP2 were injected at a high flow rate of 100 µL/min until the liquid chamber was filled. At this moment, the flow was stopped to let the molecules bind in a static regime. All measurements of frequency and dissipation shifts were performed after stabilization of the signal. For co-functionalization of cRGD with GAGs, the frequency shift of -4.7 Hz obtained for a 10 min static incubation at 1.2 µg/mL was reproduced using 0.5 µg/mL of cRGD to allow a better control.

### **Cell Culture**

CHO cell lines (CHO-K1: CCL-61<sup>TM</sup>; pgsD-677 : CRL-2244<sup>TM</sup>; pgsA-745 : CRL-2242<sup>TM</sup>) were a gift from Andrea Vortkamp. The cell lines were cultured below confluence in polystyrene cell culture flasks (Falcon®, Corning) using growth medium composed of Dulbecco's modified Eagle's medium (DMEM/F-12 GlutaMAX, 10565018, Gibco<sup>TM</sup>), supplemented with 10% heat-inactivated fetal bovine serum (FBS, 10270-106, Gibco<sup>TM</sup>), and 1% of antibiotic-antimycotic (15240062, Gibco<sup>TM</sup>). Cells were cultured at 37°C under a 5% CO<sub>2</sub> atmosphere until they were discarded upon reaching a passage number of 12. Before any experiment, cells were serum-starved for 4 hours. Accutase (A6964, Sigma-Aldrich) was used to detach the cells from the culture flasks, and they were seeded on functionalized surfaces in growth medium without FBS. Throughout the experiment, the seeded cells were maintained at 37 °C with 5% CO<sub>2</sub>.

### **Cellular assays on biomimetic platforms**

For each condition, 10000 starved cells were seeded in 96-well plates functionalized with biomimetic platforms. The soluble BMP2 (sBMP2) positive control consisted in seeding cells with 0.1 µg/mL BMP2 on platforms with cRGD. For other conditions, we focused on the role of adsorbed BMP2 on the GAGs by rinsing the unbound BMP2 prior to seeding cells. Cells were fixed after 90 min with pre-fixation and fixation steps using 2% PFA for 5 min and 4% PFA for 20 min, respectively. Each condition was assessed with intra-experimental technical duplicates and at least biological triplicate.

To quantify pSMAD1/5/9 *via* IF, we adapted already published protocols<sup>[31,47,48]</sup>. Briefly, fixed cells were first permeabilized with 0.2% Triton X-100 (Sigma-Aldrich) (w/v) in PBS for 3 min and blocked for 1 h with 3% BSA (Sigma-Aldrich) at RT. Primary rabbit anti-pSMAD1/5/9 (Cell Signaling Technology) was diluted at 1:400 in PBS with 3% BSA and incubated overnight at 4°C. A secondary antibody (1:500, goat anti-rabbit Alexa Fluor 488, ThermoFischer Scientific), as well as rhodamine phalloidin (1:1000, ThermoFischer Scientific) and DAPI (1:1000, Sigma-Aldrich) were incubated for one hour at RT in PBS with 3% BSA. Cells were imaged using InCell Analyzer 2500 using the 20x objective on three channels. Images were further analyzed with the automated image analysis software InCarta (Molecular Devices), as previously described<sup>[47,48]</sup>: pSMAD1/5/9 intensity was measured only inside the nucleus under a mask defined by the DAPI signal and background-subtracted for at least 100 cells/well. Mean nuclear area was calculated by the InCarta software. For comparing conditions with identical nuclear areas, the mean intensity was calculated. In contrast, the total intensity in the nuclei was plotted for conditions exhibiting differences in nuclear area.

### **Western Blot**

800 000 serum-starved cells were seeded onto 24x24 mm gold surfaces, functionalized with biomimetic platforms as previously described, disposed in wells of 6-well plates (Corning), and incubated for 90 min at 37°C and 5% CO<sub>2</sub>. Then they were rinsed with ice-cold PBS, and lysed with RIPA lysis buffer (Sigma-Aldrich) and scraped. The samples were centrifuged at 1600 rpm for 20 min at 4°C. The proteins were quantified using BCA assay (Sigma-Aldrich). Laemmli SDS sample buffer 4X (ThermoFisher Scientific) was added to the samples. For each sample, 8 µg of total protein was loaded in precast polyacrylamide gel (4561023, Bio-Rad) and protein migration was achieved by electrophoresis with Mini-PROTEAN Tetra Cell (Bio-Rad) in running buffer (25 mM Tris, 190 mM glycine, 0.1% (v/v) SDS in MilliQ water) according to standard protocols.

The proteins were then transferred to a PVDF (polyvinylidene difluoride) membrane using iBlot™ 2 Dry Blotting System (Bio-Rad Laboratories), rinsed with TBS-T (20 mM Trizma® base, 150 mM NaCl and 0.1% (v/v) Tween-20 at pH 7.5), blocked with 5% BSA in TBS-T and kept in constant agitation for 1 hour. Blocked membrane was probed with rabbit anti-pSMAD1/5/9 (1:1000 Cell Signaling Technology) and rabbit anti-GADPH (1:2000, Cell Signaling Technology) as a reference in 3% BSA in TBS-T and kept on constant agitation overnight at 4°C. Immunological detection was achieved with anti-rabbit HRP-conjugated secondary antibody (1:5000, ThermoFisher Scientific). The proteins were visualized by

chemiluminescence on an iBRIGHT FL1000 Imaging System (ThermoFisher Scientific) using a Clarity™ Western ECL Substrate (Bio-Rad Laboratories). pSMAD1/5/9 was quantified with ImageJ and was normalized by GAPDH control.

### **Separation of glycosaminoglycan with PAGE**

The separation of GAGs based on their size was achieved with polyacrylamide gel electrophoresis (PAGE)<sup>[49]</sup>. Initially, 10 µg of samples diluted in 20% glycerol were run through a 1.5 cm stacking gel (1 M Tris/HCl, pH 6.8, 5% acrylamide, 2% cross-linker) at a constant voltage of 150 V for 1 h in running buffer (Tris-HCl 2.5 mM, glycine 20 mM). Then samples were passed through the resolving gel (1.5 M Tris/HCl at pH 8.8, 25% acrylamide and 5% cross-linker) with a constant current of 25 mA for 3 h (maximum voltage of 1000 V). A mixture of Xylene Cyanole, Bromophenol Blue and Phenol Red in 20% glycerol was used in a separate lane as electrophoresis markers. After electrophoresis, GAG bands were visualized by staining with 0.08% aqueous Azure A for 10 min under constant agitation. The gel was washed twice in water for 5 min to remove the excess of dye.

### **Statistical Analysis and Data Treatment**

To compare independent experiments, the values were possibly normalized to a positive control, the mean was calculated and the SEM was used for the error bars in the figures and in the text (mean ± SEM). For cell experiments, intra-experimental technical duplicates were used to calculate the mean of biological replicates for each condition. Significance between two conditions was tested with the non-parametric Mann-Whitney test and represented in the graphs with \* for  $p \leq 0.05$ .

## **Results**

### **BMP2 exhibits higher binding affinity for HS compared to CS, DS, and HA**

In the literature, the binding affinities between BMP2 and GAGs are highly variable and have never been compared within the same study. Here, we have investigated the dynamics of the interactions between BMP2 and different GAGs (HS, HA, CS-A, -D, -E and DS), using the BLI biophysical characterization technique. As depicted in **Fig. 1A-E** and **Supplementary Fig. S1**, the binding of BMP2 was detected on all the different GAGs except the non-sulfated HA (data not shown). While BMP2 bound to HS at concentrations as low as 10 nM, the binding to CS or DS required concentrations above 200 nM to trigger a detectable signal. CS-A exhibited the lowest binding affinity to BMP2, requiring concentrations greater than 600 nM. We determined

binding affinities ( $K_D$ ) and the kinetics parameters  $k_{on}$  and  $k_{off}$  for the tested GAGs by fitting the binding curves with a 1:1 binding model (**Fig. 1F** and **Supplementary Table 1**). BMP2 bound to HS with the highest affinity ( $K_D$  of  $57 \pm 7$  nM) followed by CS-D ( $K_D$  of  $400 \pm 43$  nM). The other CS types and DS exhibited affinities in the low  $\mu$ M range ( $2.5 \pm 0.4$  and  $1.4 \pm 0.4$   $\mu$ M for CS-E and DS, respectively), or above 70  $\mu$ M for CS-A. Of note, the concentration range used for the BLI analysis is suitable for  $K_D$  values found for HS and CS-D, but is not optimal for  $K_D$  values found for CS-A, -E, and DS interactions with BMP2. Therefore, the determination of  $K_D$  values for CS-E, DS and CS-A may not be as accurate.

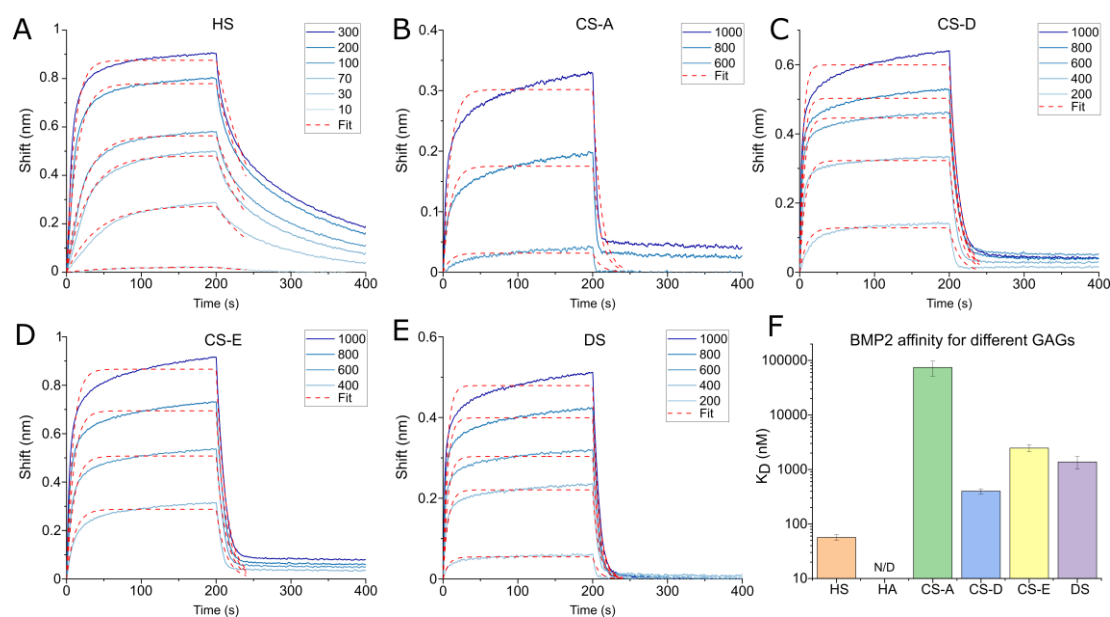


**Fig. 1. Biolayer Interferometry (BLI) kinetics assays of BMP2 binding on different GAGs: A. HS; B. CS-A; C. CS-D; D. CS-E; E. DS.** The phases of BMP2 association and dissociation were measured for 200 s each at different concentrations indicated at the bottom of each graph (nM). The curves were fitted with a 1:1 Langmuir binding model on the full association and 40 s of the dissociation (red curves) to obtain the kinetics parameters of the interactions. **F.**  $K_D$  values of BMP2 interactions for the different GAGs, representing the inverse of the affinity, are plotted on a logarithmic scale.

### Design of well-characterized biomaterials for cellular assays

Once the BMP2 affinity for different GAGs was determined, we sought to investigate the role of GAGs in BMP signaling, which has been the subject of conflicting studies<sup>[19–25]</sup>. These discrepancies may be attributed to differences in GAG presentation mode (in solution or bound to a biomaterial) and their location (cell-surface or extracellular). To address this, we adapted our previously developed biomimetic SA<sub>v</sub> platforms, which enable the presentation of GAGs as extracellular components mediating the BMP2 cellular response<sup>[30,31,50]</sup>. Gold has been chosen as support on which a SA<sub>v</sub> monolayer is bound by a biotin-PEG-thiol linker. Biotinylated GAGs are then immobilized on SA<sub>v</sub>, and BMP2 is adsorbed onto the GAG films. The functionalization process was characterized *ex situ* with QCM-D to evaluate the binding of

each GAG and BMP2 to the platforms, as exemplified for HS and CS-D in **Fig. 2A-B**. The binding of the SAV monolayer was homogeneous in all experiments, with an average shift around  $-24.3 \pm 1.3$  Hz. The immobilization of GAGs (at  $10 \mu\text{g/mL}$ ) on the SAV monolayer generates important positive shifts in dissipation, indicating an increased softness of the platforms, and strong negative frequency shifts due to the high hydration of the GAG layer<sup>[50]</sup>. The immobilization of HA yielded the largest frequency shift (thus the heaviest hydrated mass on the QCM-D crystals), CS/DS compounds yielded intermediate shifts and HS the smallest shift (**Fig. 2C, E**). This trend was also observed in the analysis of GAGs by acrylamide gel electrophoresis (**Supplementary Fig. S2**), confirming the distinct molecular weights of these GAGs.

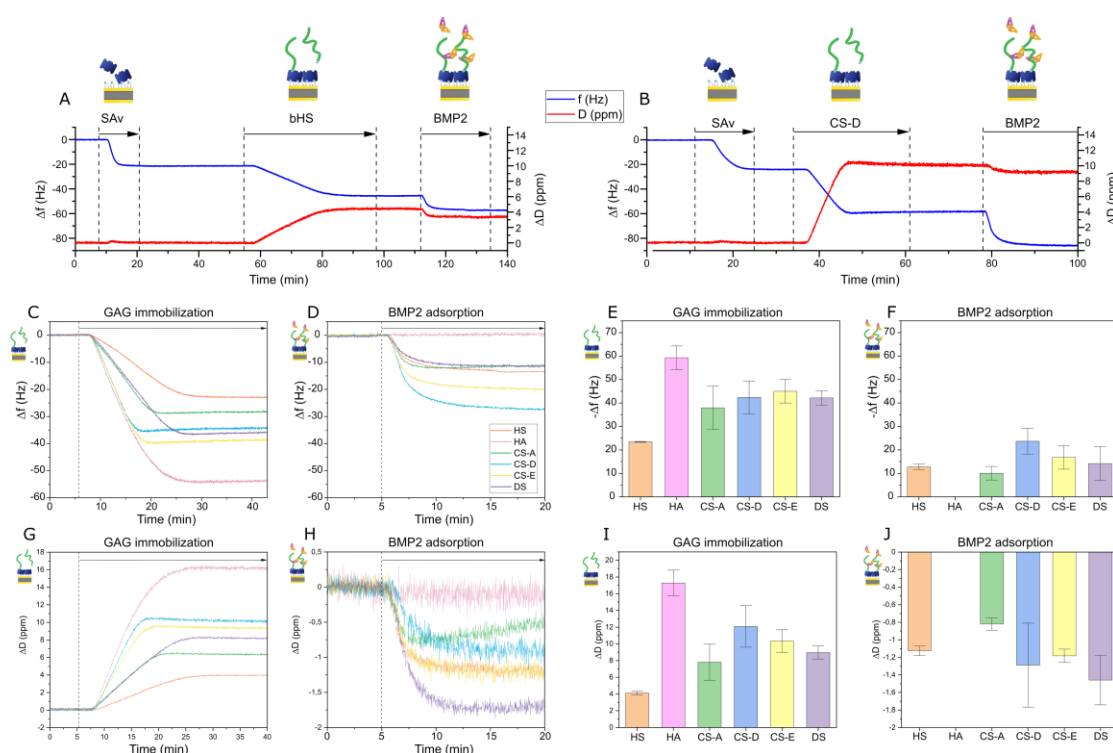


**Fig. 2. Characterization of the sequential buildup of the biomimetic platform by QCM-D.** Example of platform buildup characterized by QCM-D for **A. HS** and **B. CS-D**. Black arrows represent injection of molecules, SAV, biotinylated GAGs and BMP2, alternating with Hepes rinsing. The third overtones of frequency and dissipation shifts are depicted in blue and red, respectively. **C-H** Representative QCM-D raw data to compare the **C. frequency** and **G. dissipation** shifts of different GAGs on SAV monolayer, and similarly, we compared the **D. frequency** and **H. dissipation** curves upon binding of BMP2 on the different GAGs. The experiments were performed at least in duplicate for each GAG and we quantified the mean of frequency shifts (**E-F**) and dissipation shifts (**I-J**) for GAG immobilization (**E, I**) and BMP2 binding (**F, J**). Data are plotted as mean  $\pm$  SEM. As previously observed, the binding of BMP2 to HS triggered a negative shift of the dissipation, likely indicating a cross-linking of HS chains mediated by the growth factor<sup>[30,51]</sup>. We show that BMP2 binding on CS and DS triggers the same effect, characterized by a negative dissipation shift measured via QCM-D. The dissipation shift was the highest for DS followed by CS-D, CS-E and HS in a comparable manner, and finally CS-A (**Fig. 2H, J**).

Subsequently, the binding of BMP2 at  $5 \mu\text{g/mL}$  was varying depending on the GAGs, as indicated by the distinct frequency shifts (**Fig. 2D, F**). BMP2 bound stronger to CS-D followed by CS-E, with frequency shifts of  $23.7 \pm 3.9$  Hz and  $16.9 \pm 3.6$  Hz, respectively. The frequency

shift for DS was larger than for HS and CS-A, with values of  $14.2 \pm 4.2$  Hz,  $12.8 \pm 0.7$  Hz, and  $10.1 \pm 2.1$  Hz, respectively. On the contrary, BMP2 did not bind to the non-sulfated HA. Interestingly, the binding of BMP2 on CS-A seems less stable, since some BMP2 dissociated during the incubation step. By plotting  $\Delta f$  versus  $\Delta D$ , we can relate the levels of BMP2 binding ( $\Delta f$ ) to the rigidification of the GAG film ( $\Delta D$ ). As shown in **Supplementary Fig. S3.**, we observed that for similar  $\Delta f$  induced by BMP2, the cross-linking is stronger for HS and DS, followed by CS-E and CS-A, and finally CS-D. For cellular assays, the biomimetic platforms were co-functionalized with cRGD peptide to mediate a similar cell adhesion for the different GAG conditions. The co-functionalization process of cRGD with HS, CS-A, or CS-D was also characterized *via* QCM-D as shown in **Supplementary Fig. S4.** In comparison to the platform without cRGD, the frequency shift upon BMP2 binding was increased on HS and CS-D while it was reduced on the CS-A platform. With the co-functionalization procedure, the number of available biotin binding sites for the GAGs was decreased by about 65-75%. The reduced GAG density on the platforms may modify the binding dynamics by reducing cross-linking and facilitating the BMP2 binding to intra-chain regions. Overall, the binding of BMP2 detected *via* QCM-D on the biomimetic platforms was stronger on CS-D and CS-E than on DS, HS, and CS-A. In conclusion, we obtained well-characterized platforms binding and presenting BMP2 for cellular studies.

### **Role of extracellular and cell-surface GAGs in BMP2 signaling**

To explore the potential functional differences between cell-surface (csGAGs) and extracellular GAGs in BMP2 signaling, we seeded CHO cells on characterized biomimetic SAV platforms, either wild type (WT) or mutant cells presenting an altered repertoire of cell surface GAGs. We first investigated the role of extracellular GAGs on BMP2 bioactivity. CHO WT cells were cultured on biomimetic platforms for 90 min, fixed and the nuclear pSMAD1/5/9 was measured by IF (**Fig. 3A**). The mean nuclear intensity of pSMAD1/5/9 is plotted in **Fig. 3B**. We show that only HS significantly increased the amount of pSMAD1/5/9 above the control. CS-D seemed to generate a more pronounced signal than DS and the other CS types, but these differences were not significant. These data correlate well with the affinity measured by the BLI experiment: the higher the binding affinity, the stronger the BMP-induced SMAD1/5/9 phosphorylation. During method development, we first noticed significant non-specific binding of BMP2 to the platforms. This non-specific binding was not strongly detected in QCM-D<sup>[30]</sup>, suggesting that only a small amount of BMP2 binds non-specifically to the platforms. Nevertheless, even these small amounts can trigger SMAD1/5/9 phosphorylation, therefore

complicating the interpretation of the results. In the following experiments, we succeeded in reducing the non-specific binding, through blocking of the substrate with BSA and trehalose (Chapter VI).

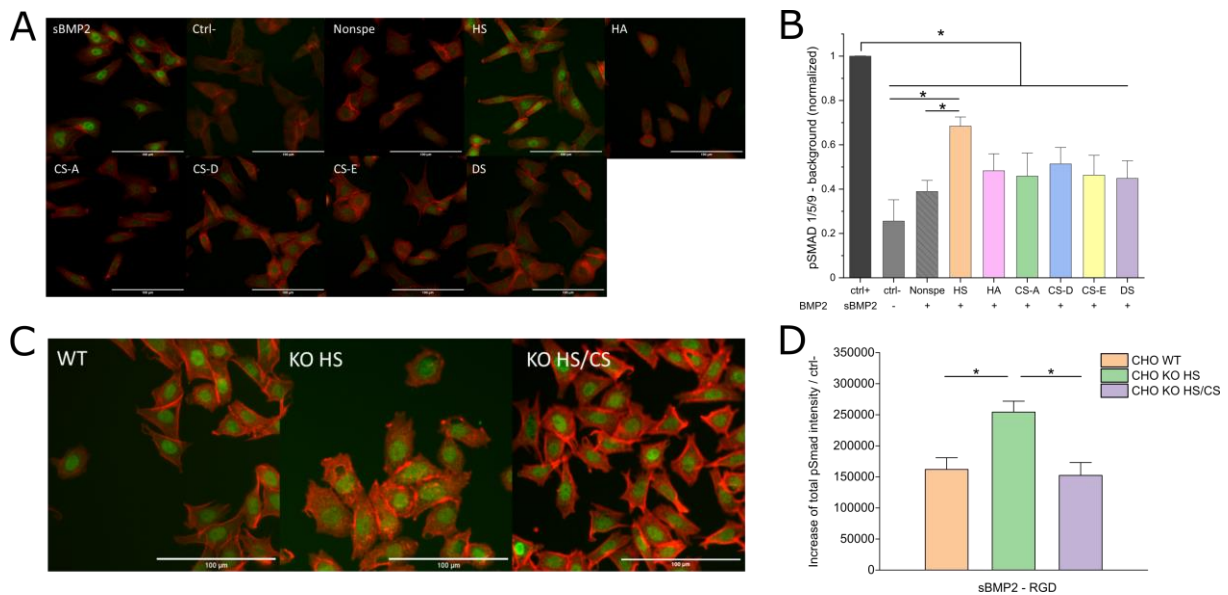


**Fig. 3. Extracellular HS enhances while cell-surface HS regulates pSMAD1/5/9 levels and csCS promotes short-term signaling.**

**A.** Representative IF images of wild type CHO cells after a 90-minute culture on the biomimetic platforms functionalized with different GAGs (extracellular) and BMP2, and stained for actin (red) and pSMAD1/5/9 (green). Scale bar is 100  $\mu$ m. Positive and negative controls correspond to cRGD functionalized platforms (without GAGs) exposed to soluble BMP2 at 0.1  $\mu$ g/mL (sBMP2) or not (ctrl-). The platforms harboring GAGs were incubated with 0.02  $\mu$ g/mL BMP2, which was rinsed before cell seeding. cRGD platforms without GAGs followed the same procedure, as a control of BMP2 non-specific binding (Nonspe). **B.** Corresponding mean fluorescence intensity of nuclear pSMAD1/5/9 in wild type CHO cells. Values were normalized by the positive sBMP2 positive control (n=4).

**C.** Representative IF images of CHO WT, KO HS, and KO HS/CS cells cultured for 90 min on cRGD biomimetic platforms with or without sBMP2 at 0.1  $\mu$ g/mL, and stained for actin (red) and pSMAD1/5/9 (green). Scale bar is 100  $\mu$ m. **D.** Corresponding total fluorescence intensity of nuclear pSMAD1/5/9 in CHO WT, KO HS, and KO HS/CS cells. For each cell type, the intensity value was plotted after subtraction of the negative control without BMP2 (n=4). Statistical significance between two conditions was tested with Mann-Whitney test and is represented with \* for  $p \leq 0.05$ .

To test the role of the csGAGs, we analyzed CHO with defects in the GAG synthesis. We either used the wild type CHO-K1 and mutant CHO pgsD-677 and pgsA-745 cell lines previously characterized. Wild type CHO-K1 (CHO WT) cells produce about 70% HS and 30% CS<sup>[52]</sup>, whereas CHO pgsD-677 cells (CHO KO HS) contain mutations in the gene encoding EXT1, an enzyme responsible for HS chain elongation<sup>[53]</sup>. It has been shown that these cells produce 3-to 4-fold more csCS than the wild type cells<sup>[52]</sup>. CHO-pgsA-745 cells (CHO KO HS/CS) completely lack csHS and csCS since they are deprived of xylotransferase responsible for the catalysis of the first sugar transfer in GAG synthesis<sup>[52,54,55]</sup>. In **Fig. 3C-D**, the total pSMAD1/5/9 levels induced by soluble BMP2 treatment were evaluated for the three CHO variants exhibiting distinct cell-surface GAGs. As previously shown<sup>[19,20]</sup>, we noticed increased

SMAD1/5/9 phosphorylation for the CHO KO HS compared to the wild type. Interestingly, the CHO KO HS/CS cells deprived of csGAGs exhibited a pSMAD1/5/9 level similar to the wild type cells. These results obtained with IF were also confirmed by Western Blot (**Supplementary Fig. S5A-B**). Overall, HS mutant cells exhibit an increased pSMAD1/5/9 level while HS/CS mutants display a reduced signaling. We conclude that csCS promotes BMP2 signaling while csHS may have an inhibitory effect. On the contrary, extracellular HS enhances the most pSMAD1/5/9 levels compared to HA, CS and DS.

### **Heparan Sulfate structural requirements for BMP2 binding**

HS is the most potent extracellular GAG to induce the BMP-mediated SMAD1/5/9 phosphorylation and is therefore an attractive target for regenerative medicine. However, potential applications require the determination of the minimal HS structural requirements for binding to BMP2. We therefore sought to define the specific HS sulfation pattern responsible for the binding of BMP2, as previously shown for other growth factors<sup>[37–39]</sup>. To investigate this, we generated a library of HS tetrasaccharides (dp4) and hexasaccharides (dp6) from porcine intestinal mucosa HS as starting material. After depolymerization with heparinase III, the cleaved fragments were separated by size to obtain pure samples of HS-dp4 and-dp6 (**Supplementary Fig. S6A**). The isolated oligosaccharides were further separated by charge to isolate compounds with distinct sulfation patterns. The elution of the generated HS-hexasaccharides in SAX-HPLC is shown in **Fig. 4A** (or **Supplementary Fig. S6B** for tetrasaccharides). Disaccharide analysis of the obtained oligosaccharides was then performed by RPIP-HPLC (**Supplementary Fig. S7**). For the most abundant species, the oligosaccharides were biotinylated and their interactions with BMP2 were analyzed using the BLI technique to determine the  $K_D$  parameters. The raw data of the BLI experiment are provided in **Supplementary Fig. S8**. Disaccharide analysis was also performed with  $\text{NaBH}_4$  oligosaccharide reduction (**Supplementary Fig. S9**) to identify the disaccharide reducing end (blocked by the reduction), thereby allowing to determine their sequences with high confidence, as shown in **Fig. 4C**.

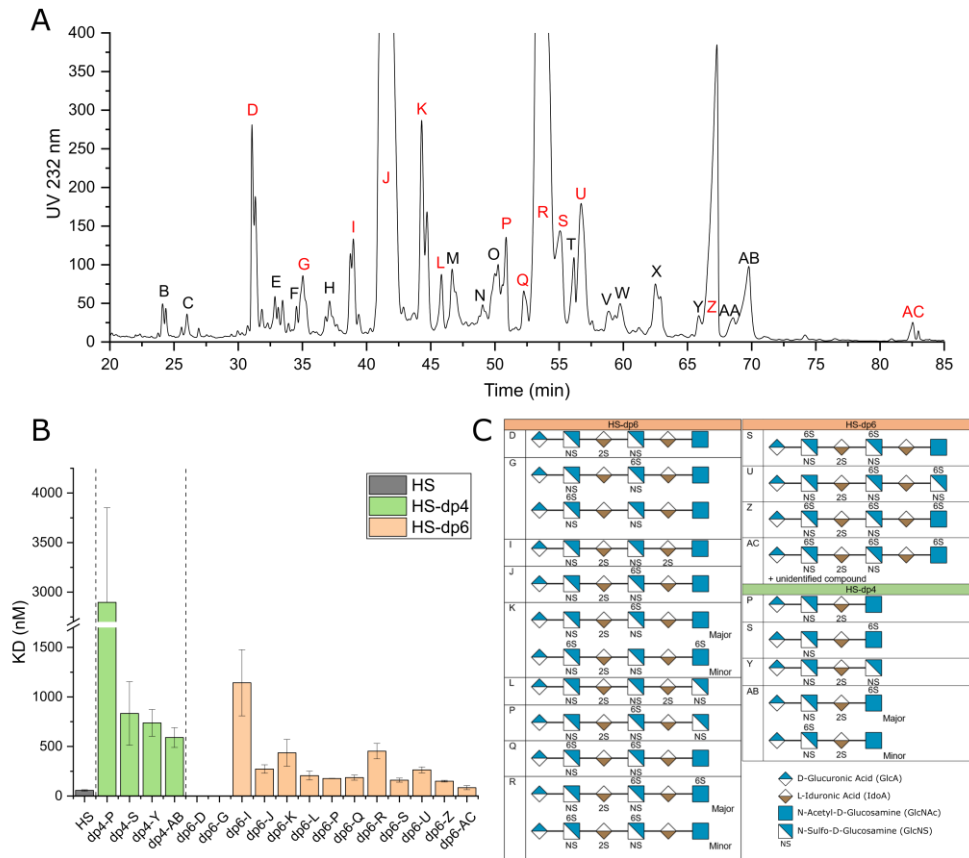


**Fig. 4.** Characterization of BMP2 binding on HS-oligosaccharides with defined structures.

**A.** Absorbance measurement detecting the elution of HS hexasaccharides from SAX-HPLC. The absorbance at 232 nm detects the unsaturated bonds generated by heparinase III cleavage. The different peaks represented by letters (B to AC) were collected and their disaccharide composition was determined by RPIP-HPLC. Letters in red represent the selected oligosaccharides that were biotinylated to perform kinetics analysis with BMP2. **B.** Comparison of the  $K_D$  values of BMP2 interactions with the selected oligosaccharides. For each oligosaccharide, the  $K_D$  value was measured with BLI at least in duplicate in independent experiments with a 1:1 Langmuir model on the 200 s association phase and the first 40 s of the dissociation phase. **C.** Structure of selected oligosaccharides, depicted according to the Symbol Nomenclature for Glycans (SNFG, Version 1.5). Legend for symbols is represented on the bottom right. Few compounds correspond to a mixture of co-eluting species the major and minor components are depicted. For dp6-G, two alternative structures are possible, while there was an unidentified compound in dp6-AC (potentially 3-O sulfated).

Oligosaccharides tested in BLI comprised between 3 and 6 sulfate groups for hexasaccharides, and between 2 and 3 for tetrasaccharides. Some of the isolated compounds clearly corresponded to a mix of two co-eluting species, which could be individually identified (dp4-AB, dp6-K, -R and -AC, see **Fig. 4C**). For dp6-G, the relative position of the identified disaccharides could not be ascertained, and the two possible sequences are shown in **Fig. 4C**. We show for the first time that BMP2 is able to bind to different HS-dp4 with a moderate affinity (**Fig. 4B**), in the same range or better than full chains of DS or CS-A,-E. Indeed, the  $K_D$  of dp4-S, -Y and -AB compounds for BMP2 was between 500 nM and 1  $\mu$ M and the  $K_D$  of dp4-P was about 3  $\mu$ M. We also show that the affinity for HS-dp6 oligosaccharides is generally better than for HS-dp4, with some potent BMP2-binding compounds (dp6-Z, -AC) exhibiting an affinity relatively

close to that of full chains of HS. By studying more precisely the variation in affinity in relation to the oligosaccharide structures, some binding characteristics could be identified. The dp6-D, -I and -L only differ by the addition of one consecutive sulfate. While the tri-sulfated dp6-D binding was too weak to measure an affinity, a low affinity was measured on the dp6-I ( $K_D=1143\pm 472$  nM) showing one additional 2-O sulfate group and a high affinity was determined for the dp6-L ( $K_D=206\pm 64$  nM) featuring five consecutive sulfate groups (additional 2-O and N- sulfates). These data support the idea that the sulfation degree increases the binding affinity for BMP2. Interestingly, dp6-J had a 4-fold better affinity ( $K_D = 273\pm 61$  nM) than the structurally close dp6-I exhibiting the same sulfate number, indicating that sulfation patterns are also important for the binding. While dp6-I is composed of four mono-sulfated monosaccharides, dp6-J differs by featuring a central tri-sulfated disaccharide IdoA(2S)-GlcNS(6S) that may play a role in high-affinity binding of BMP2. This central tri-sulfated disaccharide was common with other hexasaccharides exhibiting a high affinity for BMP2 such as dp6-P, -S, -U, -Z, and -AC. The study of dp6-K, composed of two co-eluting oligosaccharides, is very interesting. The major component of dp6-K is identical to dp6-J, but it is also composed of a minor oligosaccharide with one more sulfate, which however reduced the affinity compared to dp6-J only. Essentially, the central part of the minor compound is inversed compared to dp6-J with a disaccharide GlcNS(6S)-IdoA(2S) and the N-terminus features a GlcNAc(6S). This suggests either that the structurally inversed central part was less favorable for the binding of BMP2 or that the additional 6-O sulfate on the reducing GlcNAc was somehow destabilizing the high-affinity binding to the central part. A similar effect seemed to occur with dp6-R. In this compound, a high-affinity sequence GlcA-GlcNS(6S)-IdoA(2S)-GlcNS(6S)-IdoA-GlcNAc corresponding to dp6-S is present in minority. Here again, the major component GlcA-GlcNS-IdoA(2S)-GlcNS(6S)-IdoA-GlcNAc(6S) may have decreased the overall binding affinity of dp6-R, with an isolated GlcNAc(6S) at the reducing end that could destabilize the high-affinity domain in the central region. This effect was however not observed in the dp6-Z compound with an isolated GlcNAc(6S), maybe related to a higher sulfation in its central domain. Also, in the dp6-P, the isolated GlcNS at the reducing end seemed to have rather a positive effect, by comparison with the similar dp6-J without this additional sulfate. This would suggest that the differences in spatial positioning of the isolated N- and 6-O sulfate groups positively or negatively influence the binding of BMP2. The use of molecular modelling is needed to better understand the molecular dynamics of BMP2 binding to these oligosaccharides. Overall, our data do not point to a highly specific saccharide structure required for BMP2 binding, but indicate that sulfation types and/or distribution may drastically

improve binding, at least within the structures tested. BMP2 seems to show a certain binding plasticity regarding the sulfation types and sequences, with no striking binding differences between various HS oligosaccharides. Globally, we identified a positive role of sulfation levels, with high affinity binding achievable through locally highly sulfated motifs (such as IdoA(2S)-GlcNS(6S)), or through a lower sulfation degree on more extended domains (dp6-L).

## Discussion

In this manuscript, we explored the molecular interactions of BMP2 with various GAGs and investigated the role of GAGs as either extracellular or cell-surface components in the regulation of BMP2 signaling. While csCS may enhance short-term BMP2 signaling and csHS is a regulator of BMP2 bioactivity, HS presented by the platforms (extracellular HS) is the most potent to trigger BMP2 signaling. To better understand the molecular interactions between HS and BMP2, we generated a library of HS oligosaccharides. With that, we aimed at exploring the specific HS sulfation patterns that are responsible for the high-affinity binding with BMP2. We demonstrated for the first time that the minimal length of HS oligosaccharides able to bind BMP2 is a tetrasaccharide (dp4), contrary to what had been previously reported<sup>[3]</sup>. BMP2 binds to dp4 with a moderate affinity and hexasaccharides with a good affinity, comparable to that of full-length HS chains. We also show that BMP2 exhibits some structural plasticity for its binding to various HS sulfation patterns, with high affinity binding achievable through locally high sulfated domains such as (IdoA(2S)-GlcNS(6S)) or through a lower sulfation degree on more extended domains (dp6-L).

Although the affinity of BMP2 for HS and Hep has been already explored, to our knowledge the interactions with other GAGs have never been investigated and the affinities for HS and Hep remained unclear, due to important variations of  $K_D$  values reported in the literature. Indeed,  $K_D$  of HS for BMP2 was measured at 37 nM<sup>[35]</sup> or 1.6  $\mu$ M<sup>[30]</sup>, while that of Hep ranged from 2.4 nM to 490 nM<sup>[19,33,36]</sup>. Such differences likely arise from different experimental conditions, since the Hep source was identical (Sigma-Aldrich, porcine intestinal mucosa) and a SPR setup was used in all these studies. In our case, we performed several tests to identify an optimal ligand concentration for the immobilization, to avoid mass transport and steric hindrance effects. We established the  $K_D$  of BMP2 interactions with HS and CS-D at 57 nM and 400 nM respectively. However, the  $K_D$  values determined for CS-A, -E, and DS were out of the concentration range tested and should be considered with caution. The affinities of these GAGs for BMP2 are relatively low, with a  $K_D$  in the  $\mu$ M range, but this does not preclude the possible physiological importance of these interactions *in vivo*. Indeed, as an example, the

interaction of CS-E with Contactin-1 in the nervous system with a  $K_D$  of 1.4  $\mu\text{M}$  is required for CS-mediated neurogenesis in N2A cells<sup>[56]</sup>. The high affinity observed for CS-D may be linked to its higher sulfation level with disulfated D units. The CS-E, exhibiting disulfated E units, however showed a moderate affinity, which may be linked to the slightly lower number of disulfated units within its chains (**Supplementary Table 2**), or a less affine E-unit sulfation pattern compared to the D unit. Although the fitting of the binding curves to a 1:1 binding model is not ideal, it remains the most appropriate option, given the structural heterogeneity of the GAG ligands. Furthermore, applying a more intricate model to account for this heterogeneity could introduce further bias.

When characterizing the biomimetic platforms with QCM-D, we observed different trends of binding compared to BLI. The binding of BMP2 was in this case more important on CS-D and CS-E, followed by HS, CS-B, and CS-A. Two main reasons can explain these differences. First, the density of GAGs is much lower in the BLI setup compared to QCM-D, where GAGs saturate all the binding sites of the SA<sub>v</sub> monolayer. Despite low affinity for BMP2, CS chains may sequester the protein more efficiently at high chain density. Secondly, the frequency shift upon BMP2 binding was measured with QCM-D at the end of the association phase, not accounting for the dissociation of the protein that is important in the  $K_D$  measurements with BLI.

We also observed with QCM-D that for similar  $\Delta f$  levels upon BMP2 binding, the  $\Delta D$  negative shifts were more important for DS and HS, followed by CS-A and CS-E and finally CS-D, suggesting cross-linking differences depending on the GAG chains. Since BMP2 exhibits a preferential affinity for HS and CS-D, these differences in crosslinking might be related to the percentage variability of sulfated units in GAG chains.

Thereafter, the biomimetic platforms were used as a support for cellular assays to study the roles of extracellular and cell-surface GAGs in BMP2 signaling. In the literature, the role of GAGs in BMP interactions and signaling regulation has only been explored for HS and Hep, neglecting the potential roles of other GAGs such as CS and DS. We first showed that extracellular HS is more potent in inducing SMAD1/5/9 phosphorylation compared to CS, DS, and HA. This result is consistent with the affinity measurement, suggesting that a higher affinity of extracellular GAGs leads to increased signaling, likely due to an increased amount of BMP2 sequestered and later delivered to the cells. Supporting this idea, we also observed a small increase of pSMAD1/5/9 level with CS-D, although not statistically significant. Using CHO cells variants mutated for GAG biosynthesis, we showed that both cell-surface and extracellular GAGs are not essential to trigger SMAD1/5/9 phosphorylation, as observed with the culture of

KO HS/CS cells on biomimetic platforms with cRGD only. In agreement with that, it was previously suggested that HSPGs are not essential for triggering Dpp signaling, at least in tissues where Dpp is strongly expressed<sup>[27]</sup>. However, proper signaling in *Drosophila* wing development requires HSPGs for the spatial distribution of the morphogen and generation of gradients<sup>[22,57]</sup>. We also showed that the EXT1 mutation in CHO pgsD-677 (KO HS) cells results in an increased pSMAD1/5/9 level, as observed in the literature in other cellular or mice models<sup>[19,20]</sup>. Interestingly, this increase has only been related to the lack of HS in these cells. Here, we show for the first time that this increase is related to the presence of CS chains at the cell surface. Indeed, the signaling in KO HS/CS mutant cells was reduced in comparison to the HS mutants, returning to the same level as the wild type. While the role of CS in promoting signaling is evident, the influence of HS is not entirely clear. Since the number of CS chains is upregulated in KO HS (pgsD-677) compared to the wild type cells, the pSMAD1/5/9 reduction in these cells could be attributed either to an inhibitory effect of HS or to the increased availability of CS chains at the cell surface. Interestingly, the same trend was observed in the basal SMAD1/5/9 phosphorylation without BMP2 (**Supplementary Fig. S5C**). These effects could be related to GAGs regulating the bioactivity of endogenous BMPs or to BMP-independent mechanisms.

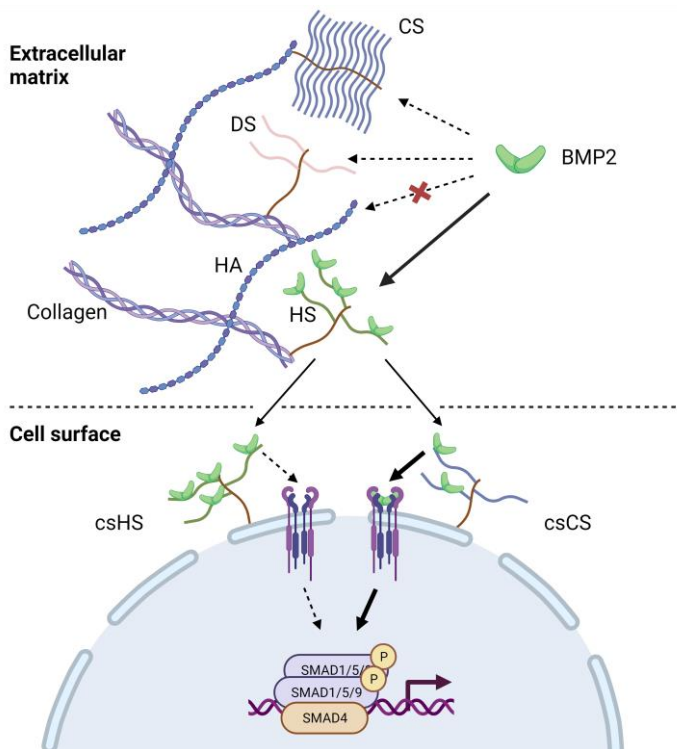


**Fig. 5.** Model of BMP2 interactions with extracellular and cell-surface GAGs modulating the BMP2 signaling. Figure created with BioRender.com.

Our findings about how cell-surface and extracellular GAGs modulate the BMP2 signaling are illustrated by the model depicted in **Fig. 5**. BMP2 secreted by cells in the extracellular matrix interact mainly with HS, while interactions with CS and DS are less important, or null in the case of HA without an additional partner. When getting near the cell surface, BMP2 from the extracellular matrix or bound to GAGs can interact with either csHS, csCS, or potentially directly with BMP receptors. When BMP2 binds csHS, it appears that SMAD1/5/9 phosphorylation is hindered, potentially by restraining interactions of BMP2 with its receptors.

In contrast, the interactions between BMP2 and csCS promote SMAD1/5/9 phosphorylation, likely due to their transient nature that does not retain BMP2 as strongly as csHS, but rather deliver it to BMP receptors.

We speculate that csCS would promote the short-term BMP2 signaling, while csHS would slow down the signaling but sustain it in the long term. In line with this, the relatively low BMP2 affinity for csCS could promote transient interactions, governed by fast kinetics of BMP2 binding/unbinding along the CS chains. This mechanism may facilitate the BMP2 binding to cell-surface BMP receptors. For HS, due to higher affinity, this process would occur at slower dynamics, resulting in a lower but sustained BMP signaling. Cell response to BMP2 exposition would therefore be finely tuned by the balance of fast/transient csCS and slow/sustained csHS promoting signaling. In agreement with this, Bachvarova and coworkers demonstrated that a chondroitinase treatment reduced pSMAD1/5/9 levels in chondrocytes<sup>[2]</sup>. In another study, unlike Hep, incubation of BMP4 with various concentrations of CS was not able to trigger significant ALP signaling<sup>[32]</sup>, which is consistent since the secretion of ALP requires sustained BMP exposition and corresponds to long-term signaling compared to pSMAD1/5/9. We therefore believe that the temporal dynamics of BMP signaling induced by HS or CS chains should be the object of future studies, to explore the validity of the mentioned hypotheses.

Subsequently, we investigated whether the ability of HS to bind to BMP2 required specific sulfation patterns. To this end, a library of tetrasaccharides and hexasaccharides was generated from a natural source of HS. The use of Hep III digestion allowed the recovery of oligosaccharides originating mostly from highly sulfated NS domains. The preparation of defined and highly pure oligosaccharides remains a time-consuming and technical challenge. Consequently, although the library comprised many compounds, only the few that exhibited sufficient purity levels were selected for structural and functional characterization. For structural analysis of oligosaccharides, we first performed a disaccharide analysis to determine their disaccharide content. Further information about their saccharide sequence was deduced from the substrate specificity of Hep III for GlcNAc $\pm$ 6S-GlcA and GlcNS $\pm$ 6S-GlcA linkages, and disaccharide analysis of the NaBH<sub>4</sub>-treated oligosaccharides, which enabled unambiguous determination of the reducing end disaccharide. BMP2 binding properties of oligosaccharides were then assessed using the BLI technique. We demonstrated for the first time that BMP2 could bind to HS tetrasaccharides with a moderate affinity, and bound to HS hexasaccharides with an affinity close to that of intact HS chains for some of the tested species. In a previous study, Smith *et al.* did not detect binding of BMP2 on HS tetrasaccharides, probably related to the use of less sensitive, indirect SPR competition assays, or less sulfated oligosaccharides<sup>[3]</sup>.

Here, we immobilized HS oligosaccharides onto BLI sensors to monitor binding to BMP2 directly. Furthermore, we did not find any binding with the least sulfated species of our HS hexasaccharide library. For species interacting with BMP2, although we found a positive correlation between binding and global sulfation degree, striking differences in affinity were observed for oligosaccharides exhibiting the same sulfate number, thus highlighting the importance of sulfation pattern for the interaction. Further analysis of structure/binding relationships did not reveal an obvious specific sequence required for the interaction with BMP2, except for a central IdoA(2S)-GlcNS(6S) tri-sulfated disaccharide shared by several high-affinity binding oligosaccharides. Overall, we identified a positive role of sulfation level, with high affinity binding achievable through locally highly sulfated motifs such as (IdoA(2S)-GlcNS(6S)), or through more extended domains with a lower sulfation degree (dp6-L). It is also noteworthy that, due to the absence of commercial standards, we could not identify 3-O sulfates in our oligosaccharide library, except for the dp6-AC compound that comprised a non-identified peak. Indeed it was previously shown that 3-O sulfated tetrasaccharides are lyase-resistant<sup>[40,58]</sup>. An oligosaccharide microarray study reported that BMP2 has some dependence on 3-O sulfate modified HS, showing especially a high binding on hexasaccharides containing a IdoA(2S)-GlcNS(3S6S)<sup>[40]</sup>. Compounds featuring a central GlcNS(3S6S) generally bound better than with a GlcNS(3S), followed by compounds with a central GlcNS(6S). In the presence of two IdoA(2S) bridging moieties, the compounds including a GlcNS(3S) or a GlcNS(6S) however exhibited identical binding levels of BMP2, suggesting a positive effect of the flexible IdoA(2S) moieties. Another study showed that 2-O-sulfation was the least critical in BMP2 binding, compared to 6-O and the utmost important N-sulfation, but still had a positive effect on the BMP2 binding, stabilization, and induced SMAD1/5/9 phosphorylation<sup>[3]</sup>. If GlcNS(3S6S)-containing compounds are binding BMP2 efficiently, 3-O sulfation does not mediate the binding by itself. Several compounds containing 3-O sulfates and other sulfates did not bind BMP2<sup>[40]</sup>. The additional 3-O sulfate in IdoA(2S)-GlcNS(3S6S) moieties could contribute to increasing locally the negative charge and thus stabilize the interaction. Regarding our data, it also seems unlikely that the presence of 3-O sulfate would play a major role in BMP2 binding since the affinity of many hexasaccharides is already rather close to that of full-length HS. More generally, it seems that BMP2 exhibits a certain plasticity for different HS sulfation types or sequences. This plasticity could be a common feature of morphogens that require GAGs to regulate their spatial distribution and establish concentration gradients. Specifically, GAGs could establish gradients of BMP2 from tissues with elevated endogenous BMP2 production to other tissues producing less BMP2, such as in the wing disc of *Drosophila*<sup>[27]</sup>. For future studies,

it would be particularly interesting to observe whether the sulfation patterns and the expression of GAG biosynthesis enzymes are correlated *in vivo* with the gradient of morphogens such as BMP2.

## Acknowledgments

This work used the platforms of the Grenoble Instruct-ERIC center (ISBG; UAR 3518 CNRS-CEA-UGA-EMBL) within the Grenoble Partnership for Structural Biology (PSB), supported by FRISBI (ANR-10-INBS-0005-02) and GRAL, financed within the University Grenoble Alpes graduate school (Ecoles Universitaires de Recherche) CBH-EUR-GS (ANR-17-EURE-0003). Authors acknowledge the BLI platform scientific responsible, Jean-Baptiste REISER Ph.D., for its help and assistance. We would like to acknowledge the PTA facility, Upstream Technological Platform, for the use of the evaporator equipment. This work was funded by the ANR (GlyCON, grant number [ANR-19-CE13-0031-01 PRCI] and by the “Investissements d’avenir” program Glyco@Alps, grant number [ANR-15-IDEX-02]. This work has been supported by CNRS GDR 2088 "BIOMIM”, ANR-17-EURE-0003 and GRAL. IBS (Institut de Biologie Structurale) acknowledges integration into the IRIG (CEA).

- [1] M. Klüppel, T. N. Wight, C. Chan, A. Hinek, J. L. Wrana, *Dev. Camb. Engl.* **2005**, *132*, 3989.
- [2] V. Bachvarova, T. Dierker, J. Esko, D. Hoffmann, L. Kjellen, A. Vortkamp, *Matrix Biol.* **2020**, DOI 10.1016/j.matbio.2020.03.006.
- [3] R. A. A. Smith, S. Murali, B. Rai, X. Lu, Z. X. H. Lim, J. J. L. Lee, V. Nurcombe, S. M. Cool, *Biomaterials* **2018**, *184*, 41.
- [4] L. E. Tellier, T. Miller, T. C. McDevitt, J. S. Temenoff, *J. Mater. Chem. B* **2015**, *3*, 8001.
- [5] T. Annaval, R. Wild, Y. Créton, R. Sadir, R. R. Vivès, H. Lortat-Jacob, *Mol. Basel Switz.* **2020**, *25*, DOI 10.3390/molecules25184215.
- [6] D. Soares da Costa, R. L. Reis, I. Pashkuleva, *Annu. Rev. Biomed. Eng.* **2017**, *19*, 1.
- [7] A. L. Gray, R. Karlsson, A. R. E. Roberts, A. J. L. Ridley, N. Pun, B. Khan, C. Lawless, R. Luís, M. Szpakowska, A. Chevné, C. E. Hughes, L. Medina-Ruiz, H. L. Birchenough, I. Z. Mulholland, C. L. Salanga, E. A. Yates, J. E. Turnbull, T. M. Handel, G. J. Graham, T. A. Jowitt, I. Schiessl, R. P. Richter, R. L. Miller, D. P. Dyer, *Cell Rep.* **2023**, *42*, 111930.
- [8] L. E. Collins, L. Troeberg, *J. Leukoc. Biol.* **2019**, *105*, 81.
- [9] J. Chen, T. Sun, Y. You, B. Wu, X. Wang, J. Wu, *Front. Cell Dev. Biol.* **2021**, *9*, 760532.
- [10] N. K. Karamanos, Z. Piperigkou, A. D. Theocharis, H. Watanabe, M. Franchi, S. Baud, S. Brézillon, M. Götte, A. Passi, D. Vigetti, S. Ricard-Blum, R. D. Sanderson, T. Neill, R. V. Iozzo, *Chem. Rev.* **2018**, *118*, 9152.
- [11] R. El Masri, A. Seffouh, H. Lortat-Jacob, R. R. Vivès, *Glycoconj. J.* **2017**, *34*, 285.
- [12] R. Derynck, E. H. Budi, *Sci. Signal.* **2019**, *12*, eaav5183.
- [13] M.-C. Ramel, C. S. Hill, *FEBS Lett.* **2012**, *586*, 1929.

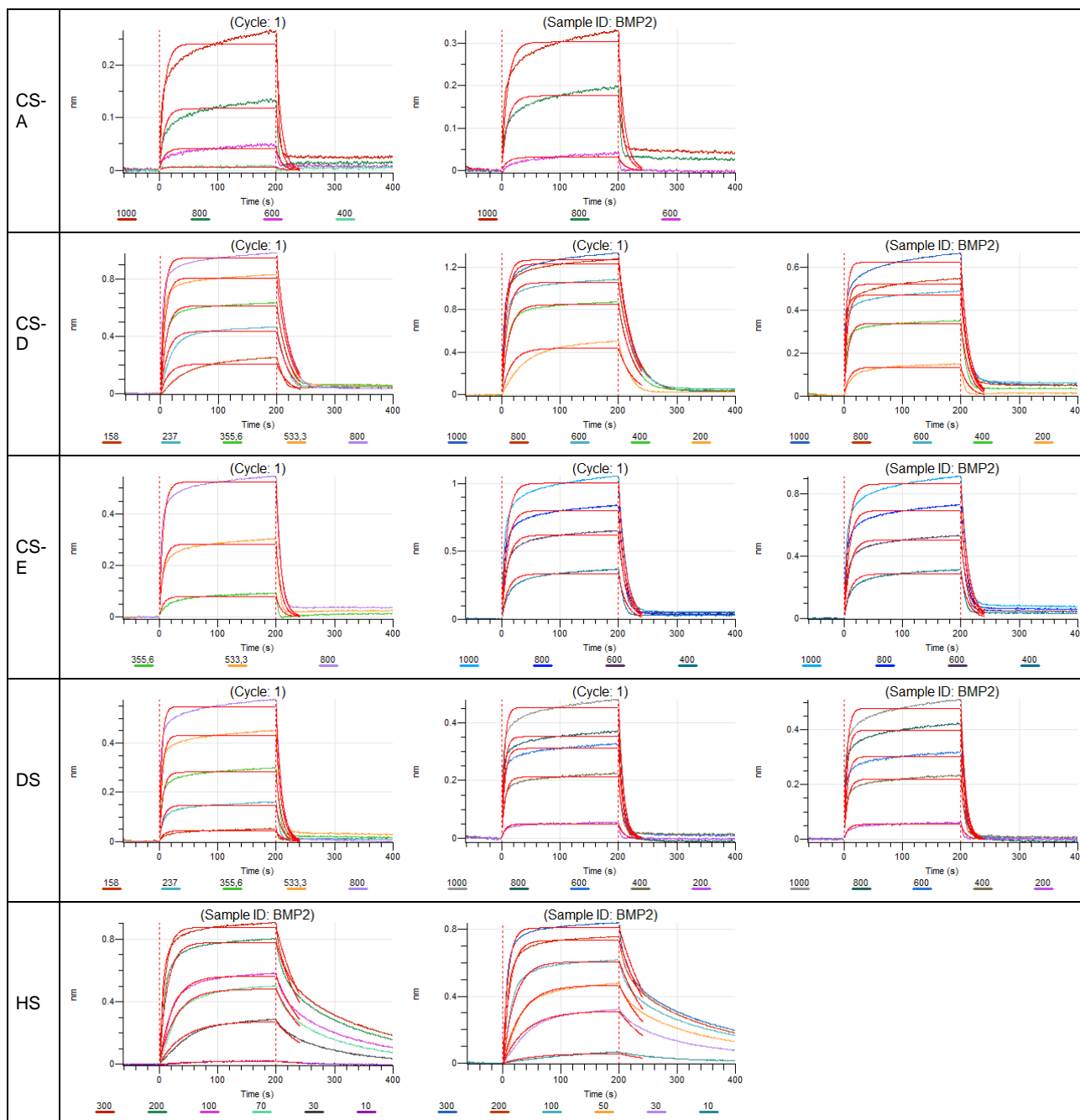
- [14] D. Umulis, M. B. O'Connor, S. S. Blair, *Development* **2009**, *136*, 3715.
- [15] M. Pacifici, *Matrix Biol.* **2018**, *71–72*, 28.
- [16] C. Han, T. Y. Belenkaya, M. Khodoun, M. Tauchi, X. Lin, X. Lin, *Development* **2004**, *131*, 1563.
- [17] S. M. Jackson, H. Nakato, M. Sugiura, A. Jannuzi, R. Oakes, V. Kaluza, C. Golden, S. B. Selleck, *Development* **1997**, *124*, 4113.
- [18] W. Wuyts, G. A. Schmale, H. A. Chansky, W. H. Raskind, in *GeneReviews®* (Eds.: M. P. Adam, G. M. Mirzaa, R. A. Pagon, S. E. Wallace, L. J. Bean, K. W. Gripp, A. Amemiya), University Of Washington, Seattle, Seattle (WA), **1993**.
- [19] J. Huegel, C. Mundy, F. Sgariglia, P. Nygren, P. C. Billings, Y. Yamaguchi, E. Koyama, M. Pacifici, *Dev. Biol.* **2013**, *377*, 100.
- [20] T. Inubushi, S. Nozawa, K. Matsumoto, F. Irie, Y. Yamaguchi, *JCI Insight n.d.*, *2*, e90049.
- [21] X. Lin, G. Wei, Z. Shi, L. Dryer, J. D. Esko, D. E. Wells, M. M. Matzuk, *Dev. Biol.* **2000**, *224*, 299.
- [22] Y. Takei, Y. Ozawa, M. Sato, A. Watanabe, T. Tabata, *Development* **2004**, *131*, 73.
- [23] W.-J. Kuo, M. A. Digman, A. D. Lander, *Mol. Biol. Cell* **2010**, *21*, 4028.
- [24] C. Mundy, E. Yang, H. Takano, P. C. Billings, M. Pacifici, *J. Biol. Chem.* **2018**, *293*, 7703.
- [25] M. C. Fisher, Y. Li, M. R. Seghatoleslami, C. N. Dealy, R. A. Kosher, *Matrix Biol.* **2006**, *25*, 27.
- [26] S. Paine-Saunders, B. L. Viviano, A. N. Economides, S. Saunders, *J. Biol. Chem.* **2002**, *277*, 2089.
- [27] X. Lin, *Development* **2004**, *131*, 6009.
- [28] X. Jiao, P. C. Billings, M. P. O'Connell, F. S. Kaplan, E. M. Shore, D. L. Glaser, *J. Biol. Chem.* **2007**, *282*, 1080.
- [29] B. Zhao, T. Katagiri, H. Toyoda, T. Takada, T. Yanai, T. Fukuda, U. Chung, T. Koike, K. Takaoka, R. Kamijo, *J. Biol. Chem.* **2006**, *281*, 23246.
- [30] E. Migliorini, P. Horn, T. Haraszti, S. V. Wegner, C. Hiepen, P. Knaus, R. P. Richter, E. A. Cavalcanti-Adam, *Adv. Biosyst.* **2017**, *1*, 1600041.
- [31] J. Sefkow-Werner, P. Machillot, A. Sales, E. Castro-Ramirez, M. Degardin, D. Boturnyn, E. A. Cavalcanti-Adam, C. Albiges-Rizo, C. Picart, E. Migliorini, *Acta Biomater.* **2020**, DOI 10.1016/j.actbio.2020.07.015.
- [32] S. Chasan, E. Hesse, P. Atallah, M. Gerstner, S. Diederichs, A. Schenker, K. Grobe, C. Werner, W. Richter, *Adv. Funct. Mater.* **2022**, *32*, 2109176.
- [33] M. Kisiel, A. S. Klar, M. Ventura, J. Buijs, M.-K. Mafina, S. M. Cool, J. Hilborn, *PLoS ONE* **2013**, *8*, e78551.
- [34] E. Migliorini, J. Ban, G. Greci, L. Andolfi, A. Pozzato, M. Tormen, V. Torre, M. Lazzarino, *Biotechnol. Bioeng.* **2013**, *110*, 2301.
- [35] P. C. Billings, E. Yang, C. Mundy, M. Pacifici, *J. Biol. Chem.* **2018**, *293*, 14371.
- [36] R. Ruppert, E. Hoffmann, W. Sebald, *Eur. J. Biochem.* **1996**, *237*, 295.
- [37] B. Richard, R. Swanson, S. T. Olson, *J. Biol. Chem.* **2009**, *284*, 27054.
- [38] D. A. Pye, R. R. Vives, J. E. Turnbull, P. Hyde, J. T. Gallagher, *J. Biol. Chem.* **1998**, *273*, 22936.
- [39] D. A. Pye, R. R. Vivès, P. Hyde, J. T. Gallagher, *Glycobiology* **2000**, *10*, 1183.
- [40] P. Chopra, A. Joshi, J. Wu, W. Lu, T. Yadavalli, M. A. Wolfert, D. Shukla, J. Zaia, G.-J. Boons, *Proc. Natl. Acad. Sci.* **2021**, *118*, DOI 10.1073/pnas.2012935118.
- [41] S. C. Samson, T. Ferrer, C. J. Jou, F. B. Sachse, S. S. Shankaran, R. M. Shaw, N. C. Chi, M. Tristani-Firouzi, H. J. Yost, *PLOS Biol.* **2013**, *11*, e1001727.

- [42] D. Thakar, F. Dalonneau, E. Migliorini, H. Lortat-Jacob, D. Boturyn, C. Albiges-Rizo, L. Coche-Guerente, C. Picart, R. P. Richter, *Biomaterials* **2017**, *123*, 24.
- [43] B. Mulloy, C. Gee, S. F. Wheeler, R. Wait, E. Gray, T. W. Barrowcliffe, *Thromb. Haemost.* **1997**, *77*, 668.
- [44] O. A. Hamad, K. N. Ekdahl, P. H. Nilsson, J. Andersson, P. Magotti, J. D. Lambris, B. Nilsson, *J. Thromb. Haemost.* **2008**, *6*, 1413.
- [45] L. Djerbal, R. Vivès, C. Lopin-Bon, R. Richter, J. C. F. Kwok, H. Lortat-Jacob, **2020**, DOI 10.1101/851121.
- [46] C. Laguri, R. Sadir, E. Gout, R. R. Vivès, H. Lortat-Jacob, in *Glycosaminoglycans Methods Protoc.* (Eds.: K. Balagurunathan, H. Nakato, U. Desai, Y. Saijoh), Springer US, New York, NY, **2022**, pp. 121–137.
- [47] J. Sefkow-Werner, J. Le Pennec, P. Machillot, B. Ndayishimiye, E. Castro-Ramirez, J. Lopes, C. Licitra, I. Wang, A. Delon, C. Picart, E. Migliorini, *ACS Appl. Mater. Interfaces* **2022**, *14*, 34113.
- [48] A. Sales, V. Khodr, P. Machillot, L. Chaar, L. Fourel, A. Guevara-Garcia, E. Migliorini, C. Albigès-Rizo, C. Picart, *Biomaterials* **2022**, 121363.
- [49] R. R. Vivès, S. Goodger, D. A. Pye, *Biochem. J.* **2001**, *354*, 141.
- [50] E. Migliorini, D. Thakar, R. Sadir, T. Pleiner, F. Baleux, H. Lortat-Jacob, L. Coche-Guerente, R. P. Richter, *Biomaterials* **2014**, *35*, 8903.
- [51] E. Migliorini, D. Thakar, J. Kühnle, R. Sadir, D. P. Dyer, Y. Li, C. Sun, B. F. Volkman, T. M. Handel, L. Coche-Guerente, D. G. Fernig, H. Lortat-Jacob, R. P. Richter, *Open Biol.* **n.d.**, *5*, 150046.
- [52] K. Lidholt, J. L. Weinke, C. S. Kiser, F. N. Lugemwa, K. J. Bame, S. Cheifetz, J. Massagué, U. Lindahl, J. D. Esko, *Proc. Natl. Acad. Sci. U. S. A.* **1992**, *89*, 2267.
- [53] G. Wei, X. Bai, M. M. G. Gabb, K. J. Bame, T. I. Koshy, P. G. Spear, J. D. Esko, *J. Biol. Chem.* **2000**, *275*, 27733.
- [54] J. D. Esko, T. E. Stewart, W. H. Taylor, *Proc. Natl. Acad. Sci. U. S. A.* **1985**, *82*, 3197.
- [55] J. D. Esko, K. S. Rostand, J. L. Weinke, *Science* **1988**, *241*, 1092.
- [56] T. Mikami, D. Yasunaga, H. Kitagawa, *J. Biol. Chem.* **2009**, *284*, 4494.
- [57] T. Y. Belenkaya, C. Han, D. Yan, R. J. Opoka, M. Khodoun, H. Liu, X. Lin, *Cell* **2004**, *119*, 231.
- [58] J. Liu, L. C. Pedersen, *Am. J. Physiol. Cell Physiol.* **2022**, DOI 10.1152/ajpcell.00110.2022.

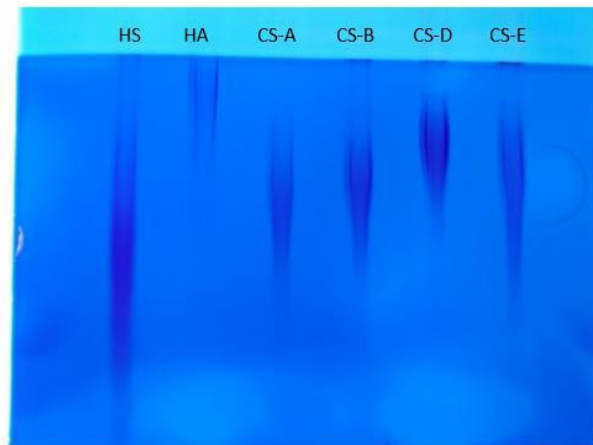
## Supporting information

	K <sub>D</sub> (μM)	k <sub>on</sub> (1/Ms) (10 <sup>3</sup> )	k <sub>off</sub> (1/s) (10 <sup>-2</sup> )
HS	0.057±0.007	300±33	2±0.01
HA			
CS-A	74±23	1±0.7	10±4
CS-D	0.40±0.04	134±18	5±1
CS-E	2.5±0.4	37±3	9±1
DS	1.4±0.4	97±24	12±1

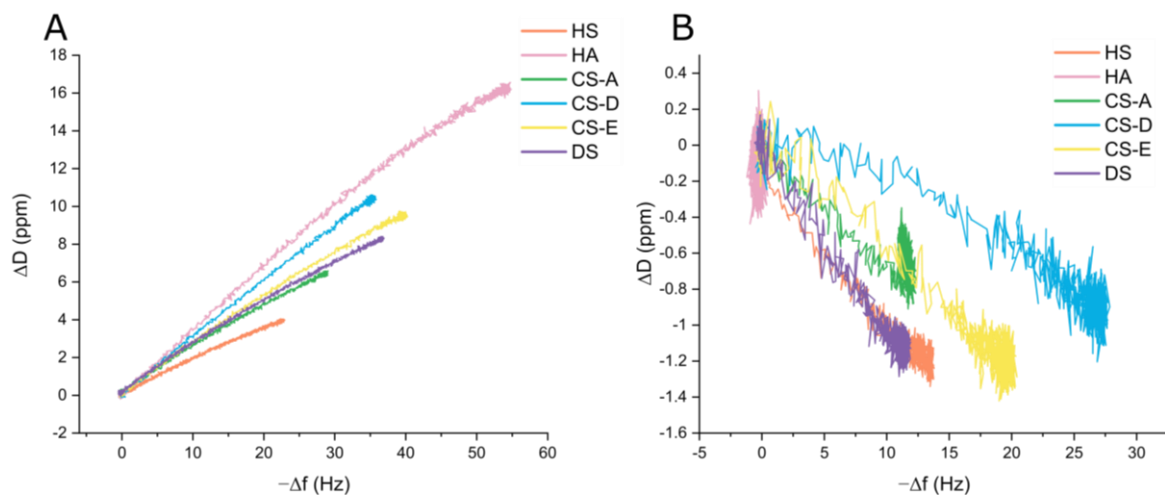
**Supplementary Table 1.** Kinetics parameters determined via BLI for the interactions of BMP2 with various GAGs. Background in darker blue indicates a stronger interaction. Data are represented as mean ± SEM for at least two independent experiments.



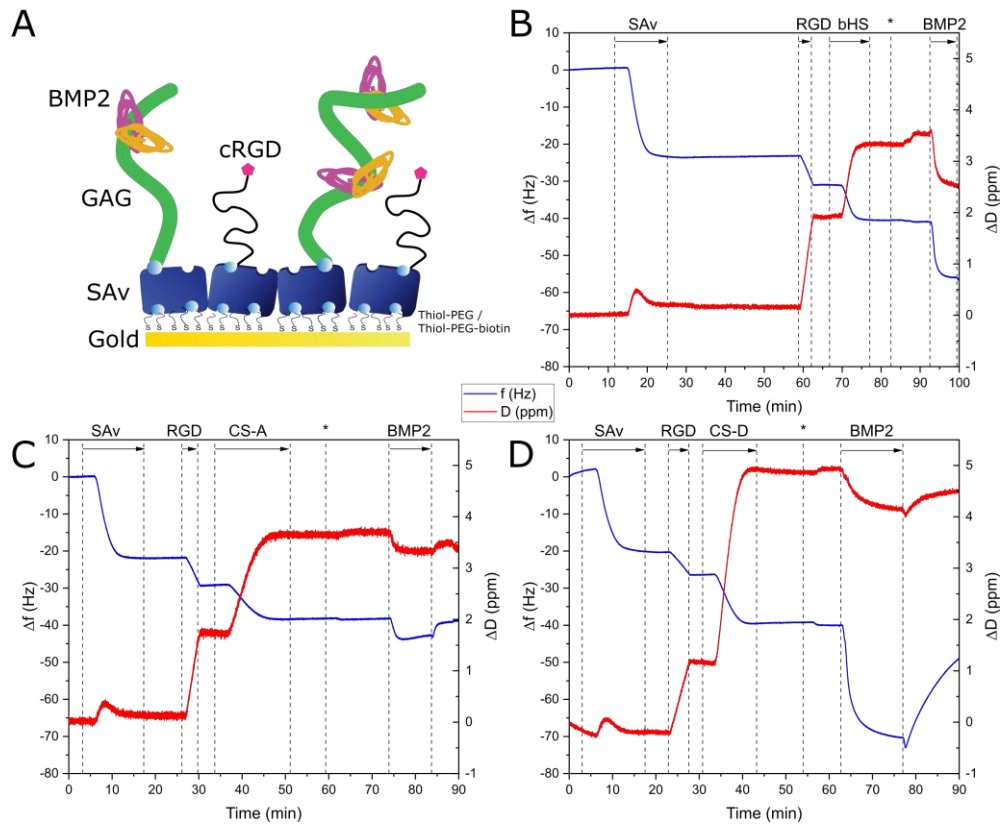
**Supplementary Fig. S1.** Raw data for all replicates of BLI kinetics assays of BMP2 binding on different GAGs: CS-A, CS-D, CS-E, DS, HS and HA (binding not detected). The phases of BMP2 association and dissociation were measured for 200s each at different concentrations indicated at the bottom of each graph (nM). The curves were fitted with a 1:1 Langmuir binding model on the full association and 40 s of the dissociation (red curves) to obtain the kinetics parameters of the interactions.



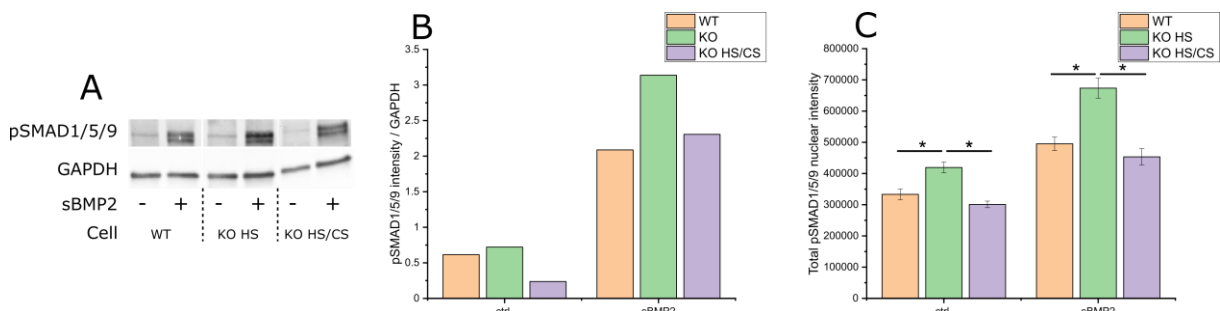
**Supplementary Fig. S2.** Acrylamide gel electrophoresis of the different GAGs for relative comparison of molecular weights (with the approximation of the global charge impact).



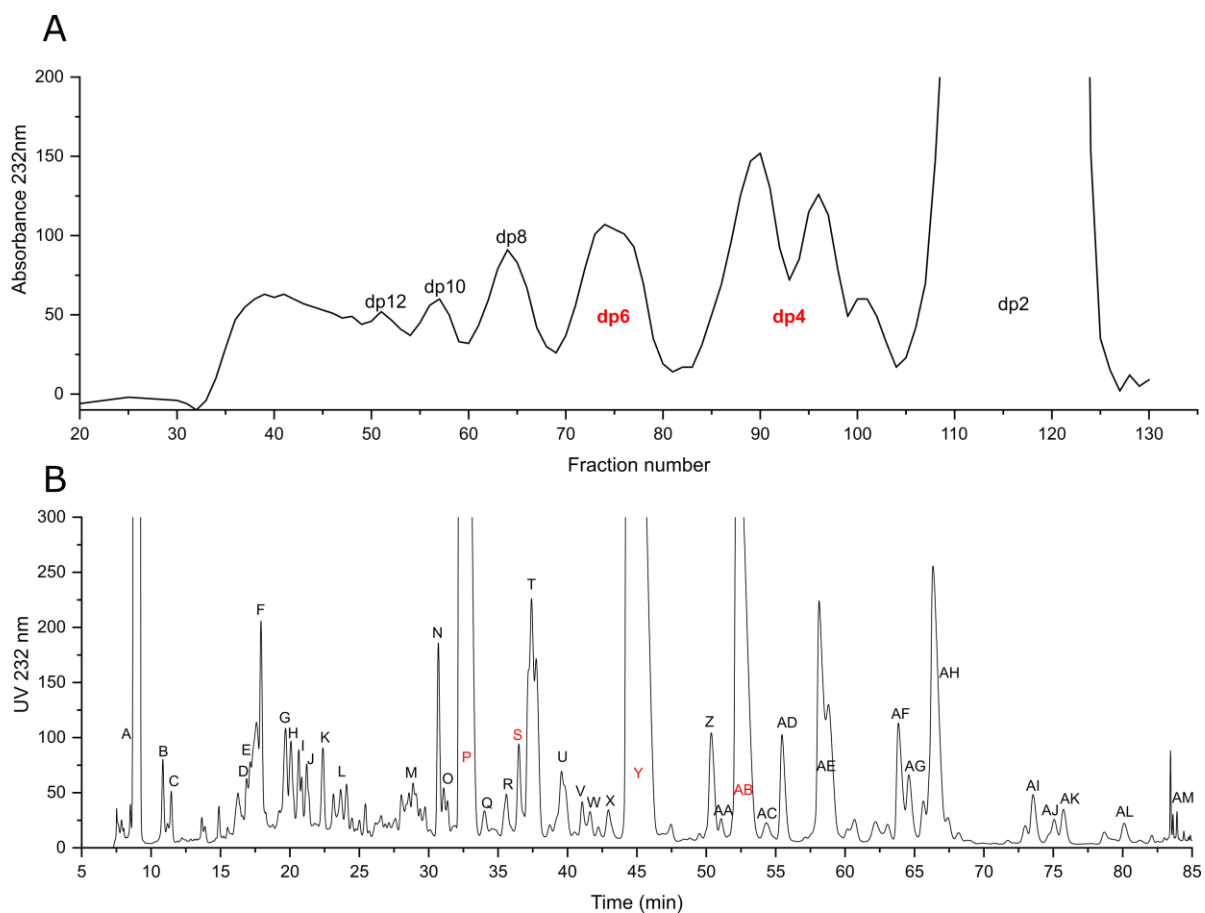
**Supplementary Fig. S3.** Plots of  $\Delta D$  versus  $-\Delta f$  for the **A.** immobilization of GAGs on SAV and **B.** binding of BMP2 on the different GAGs.  $-\Delta f$  corresponds to the hydrated mass bound on the surface and  $\Delta D$  corresponds to the mechanical properties of the deposited molecule film (rigidity, crosslinking). We notice that the mechanical properties of the different GAGs are not comparable upon binding of BMP2. BMP2 increased more the rigidity of the HS and DS films compared to the other GAGs, in particular CS-D.



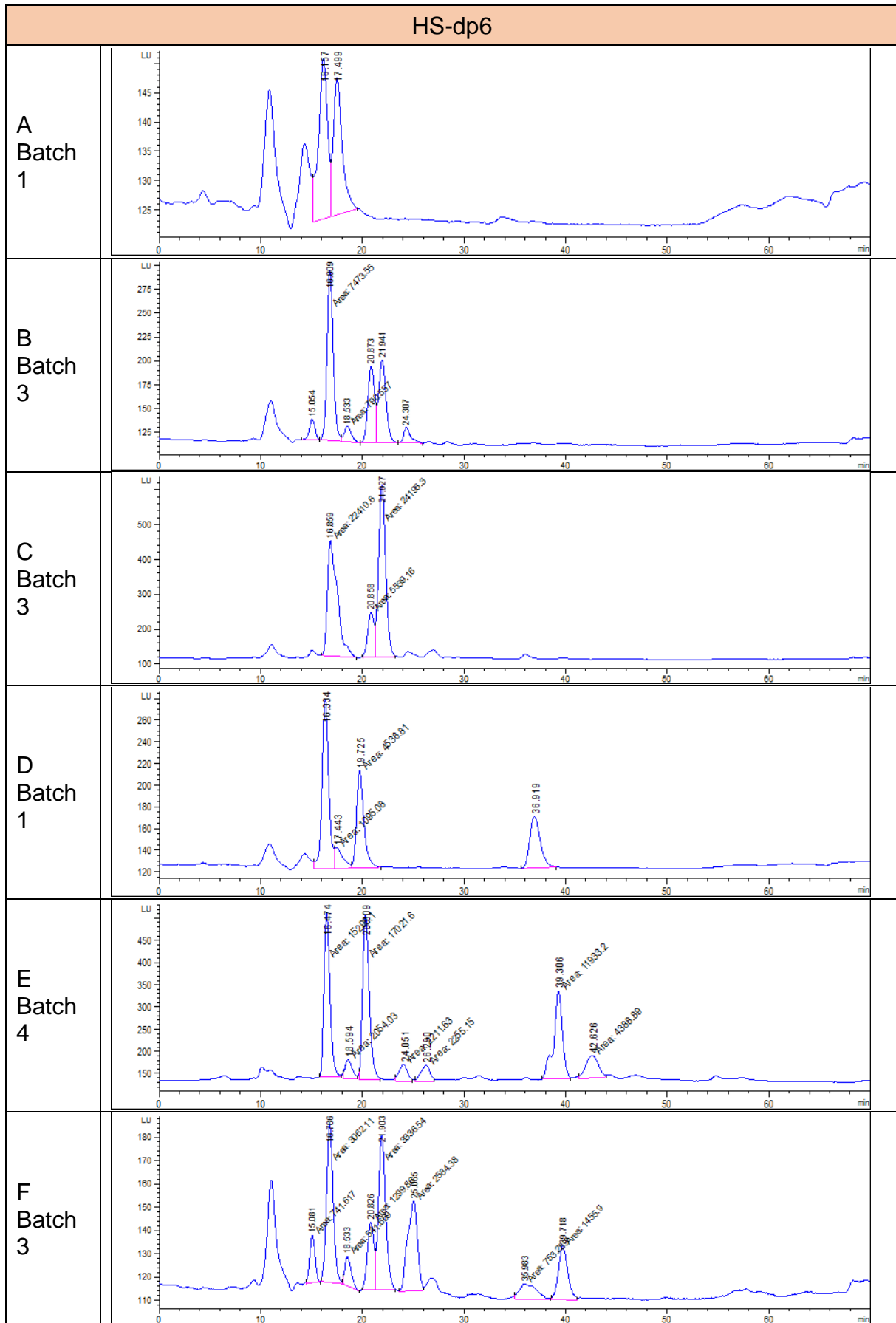
**Supplementary Fig. S4.** Co-functionalization process to build biomimetic platforms presenting cRGD peptides, GAGs and BMP2 for cellular assays. **A.** Schematic representation of the biomimetic platforms presenting cRGD, GAGs and BMP2. The sequential buildup of the platforms was characterized via QCM-D for **B. HS**, **C. CS-A** and **D. CS-D**. The cRGD peptide was injected at 0.5  $\mu\text{g/mL}$  at 100  $\mu\text{L/min}$  until reaching a frequency shift of -4.7 Hz. This shift was determined by mimicking the liquid-handling robot functionalization with a “fast injection” procedure at 100  $\mu\text{L/min}$  followed by 10 min static incubation. Since the follow-up rinsing always led to additional binding of cRGD remaining in the tubing, we chose this lower concentration of 0.5  $\mu\text{g/mL}$  with respect to the 1.2  $\mu\text{g/mL}$  used for the liquid-handling robot to allow a better control. The \* symbol corresponds to a transition in Hepes-T before the BMP2 injection at 5  $\mu\text{g/mL}$ .

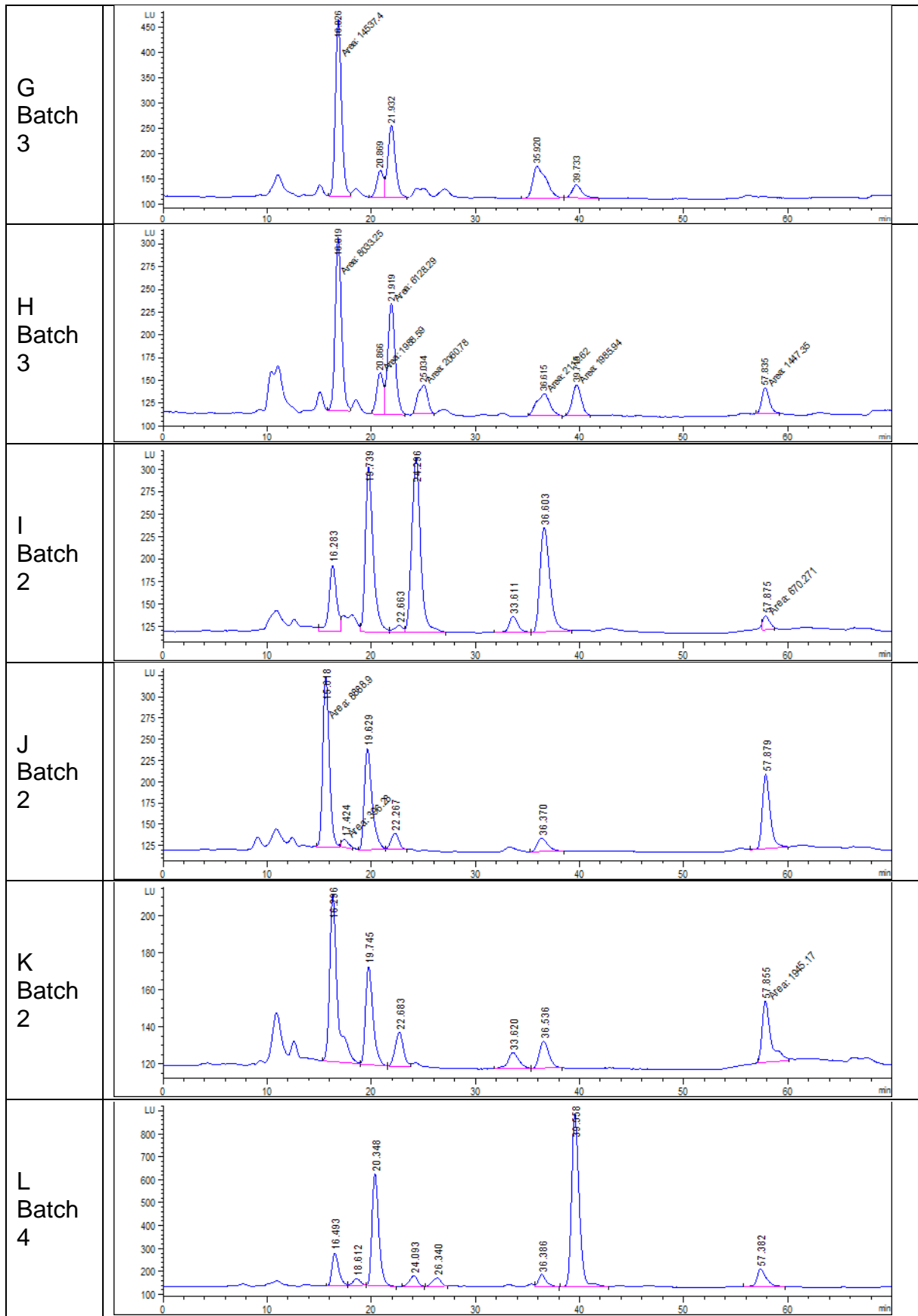


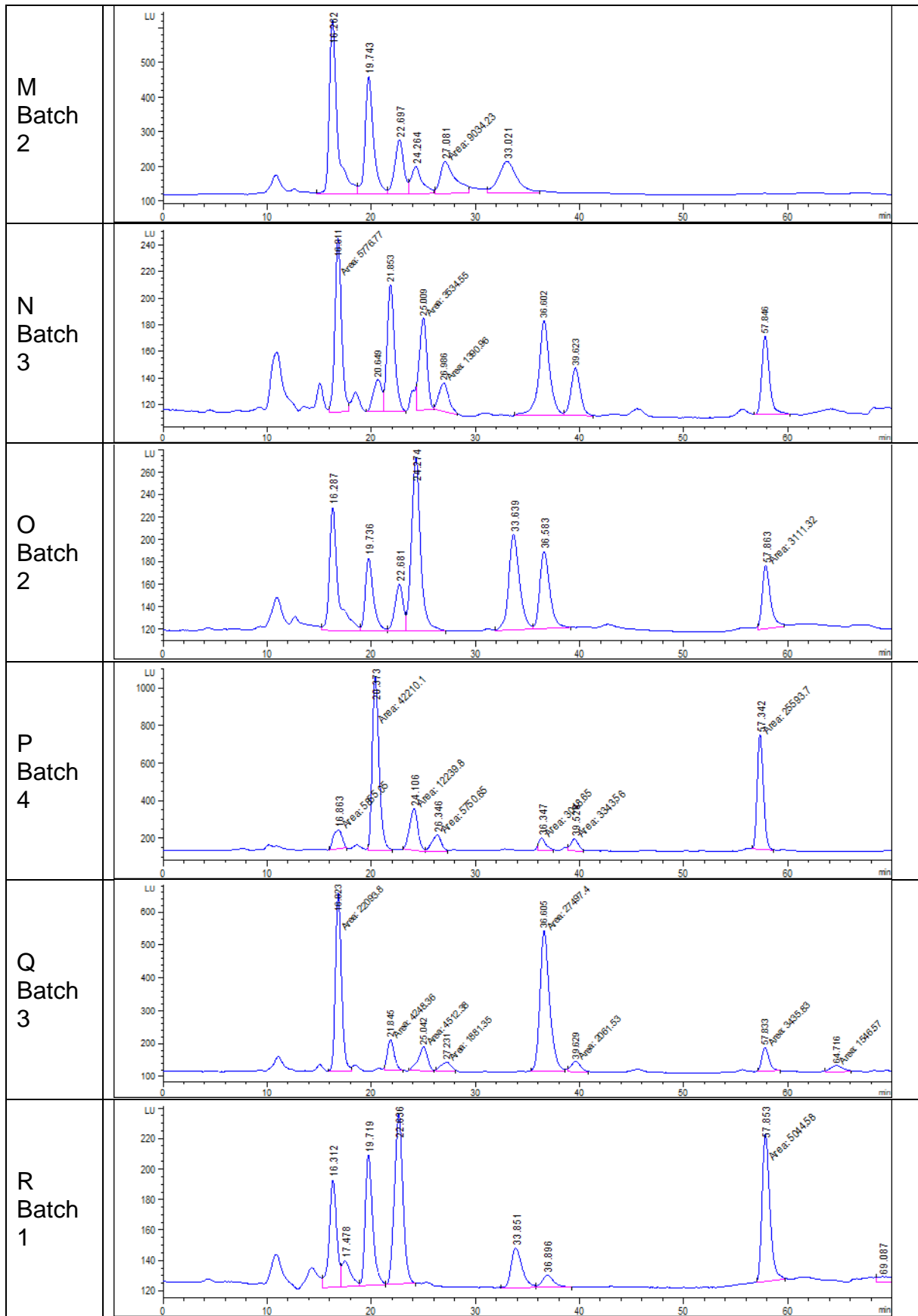
**Supplementary Fig. S5. A.** Western blot of pSMAD1/5/9 levels of CHO WT and the mutants KO HS and KO HS/CS cells cultured for 90 min on cRGD biomimetic platforms with or without sBMP2 at 0.1  $\mu\text{g/mL}$ . **B.** Quantification of the Western Blot bands. pSMAD1/5/9 was normalized by GAPDH. **C.** Quantification of the mean immunofluorescence intensity of pSMAD1/5/9 translocated in the nuclei of CHO wild type and mutants in identical experiment. Values were normalized by the positive sBMP2 positive control ( $n=4$ ). Statistical significance between two conditions was tested with Mann-Whitney test and was represented with \* for  $p \leq 0.05$ .

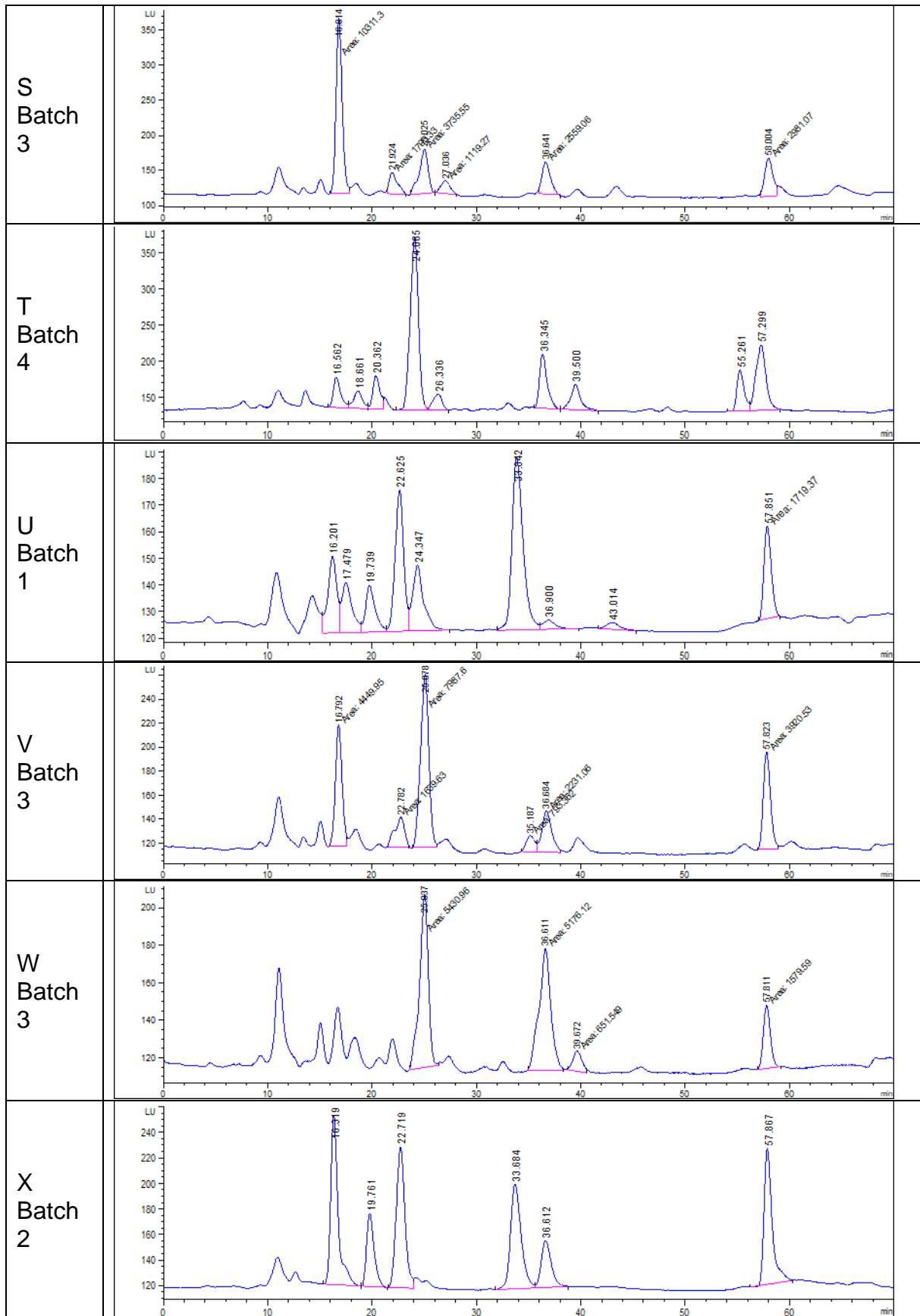


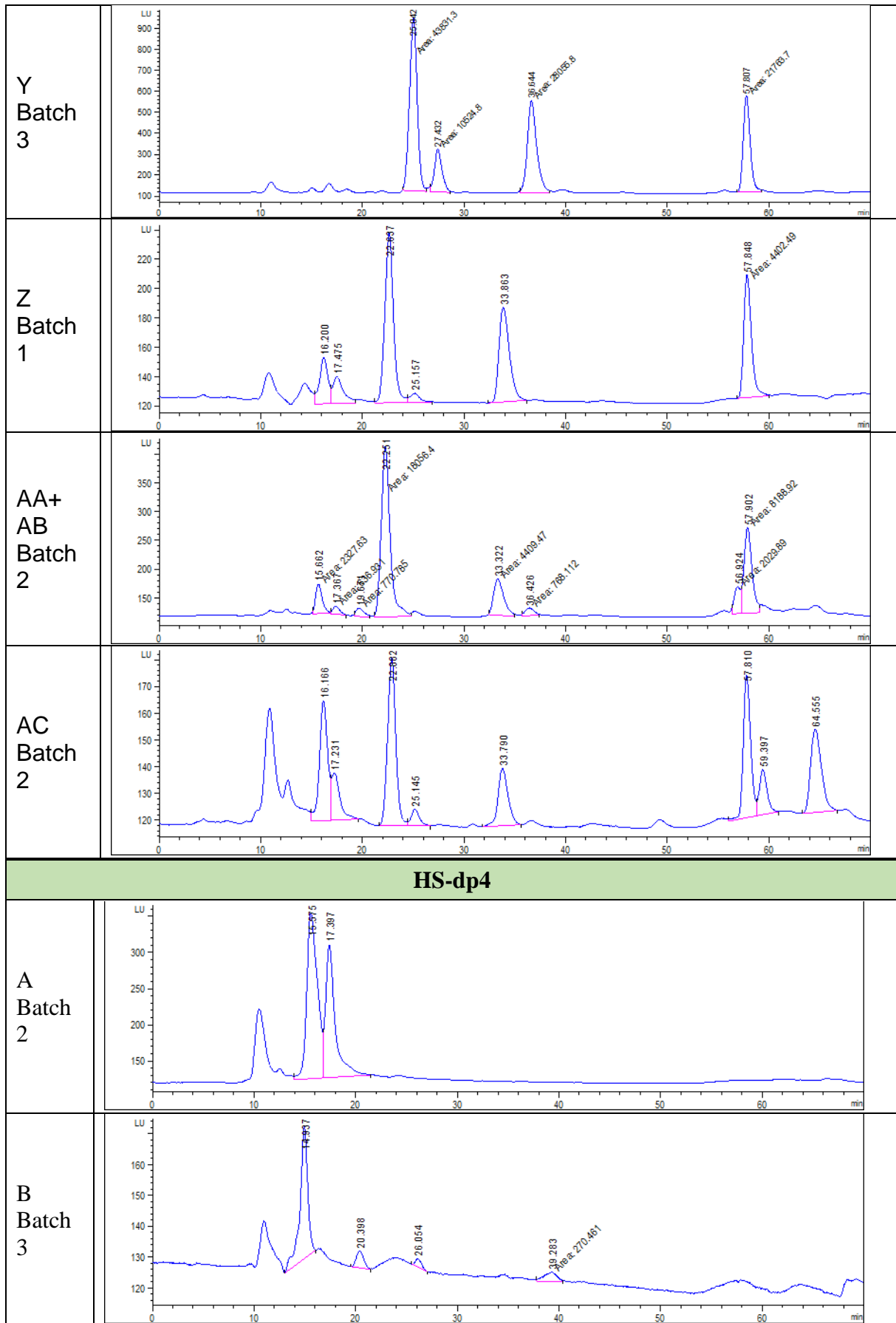
**Supplementary Fig. S6.** Generation of the HS-oligosaccharide library. **A.** Size exclusion chromatography of HS fragmented by heparinase III digestion. The absorbance at 232 nm detects the unsaturated bonds generated by heparinase III cleavage. Collected tetrasaccharides and hexasaccharides are represented in red. **B.** Absorbance measurement to detect the elution and separation of HS tetrasaccharides by SAX-HPLC. The different peaks represented by letters (B to AC) were collected and their disaccharide composition was determined by RPIP-HPLC. Letters in red represent the selected oligosaccharides that were biotinylated to perform binding analysis with BMP2.

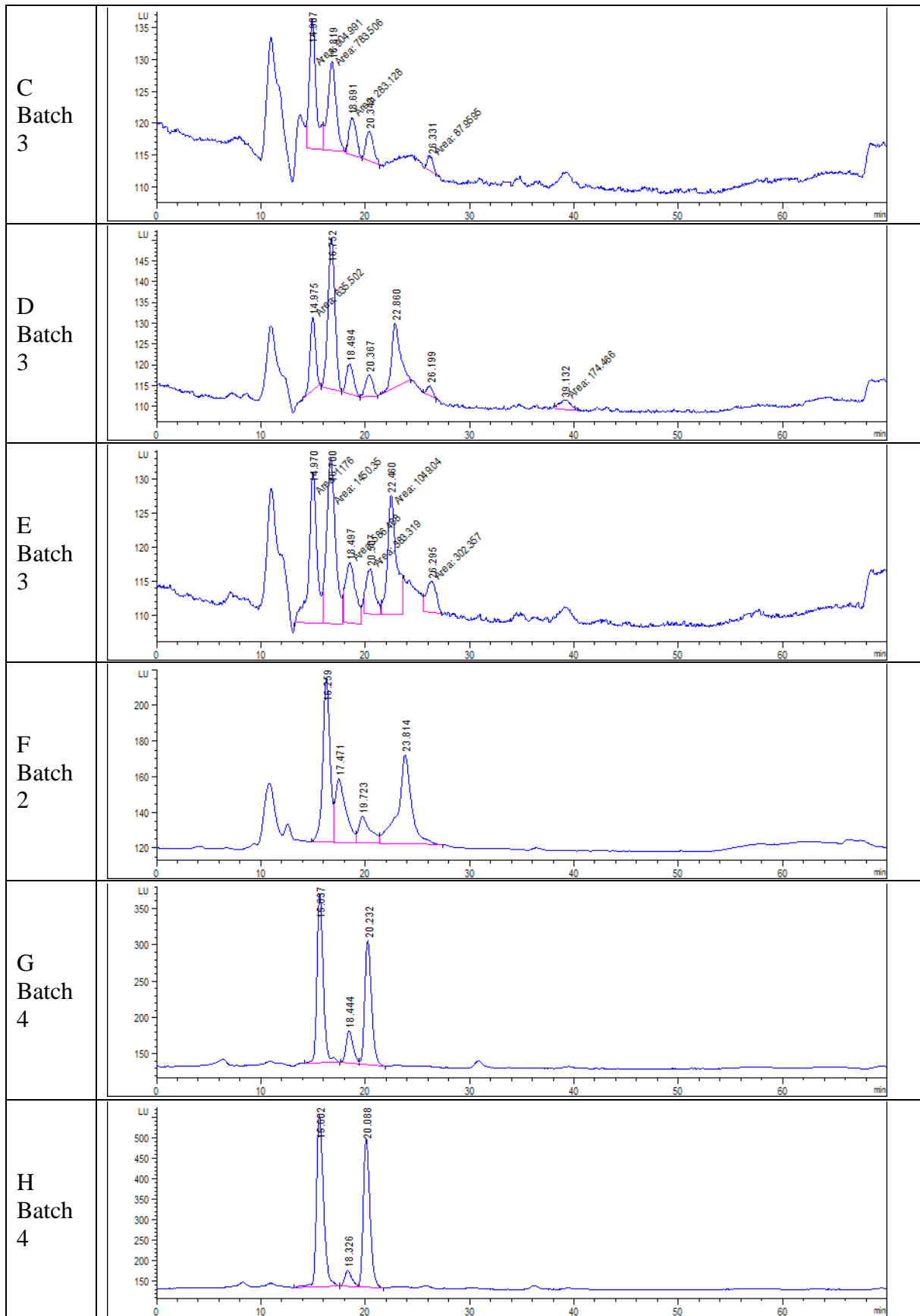


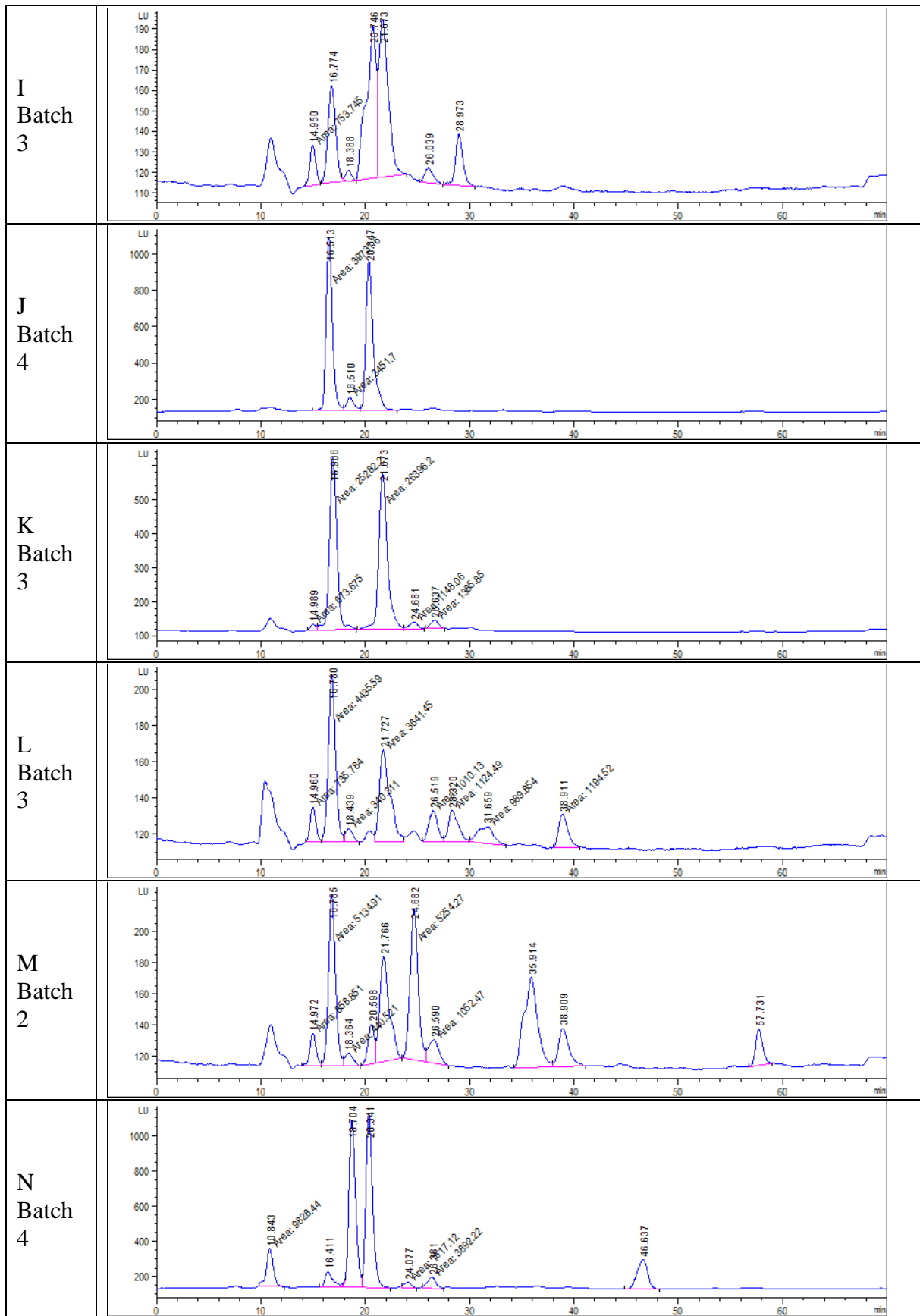


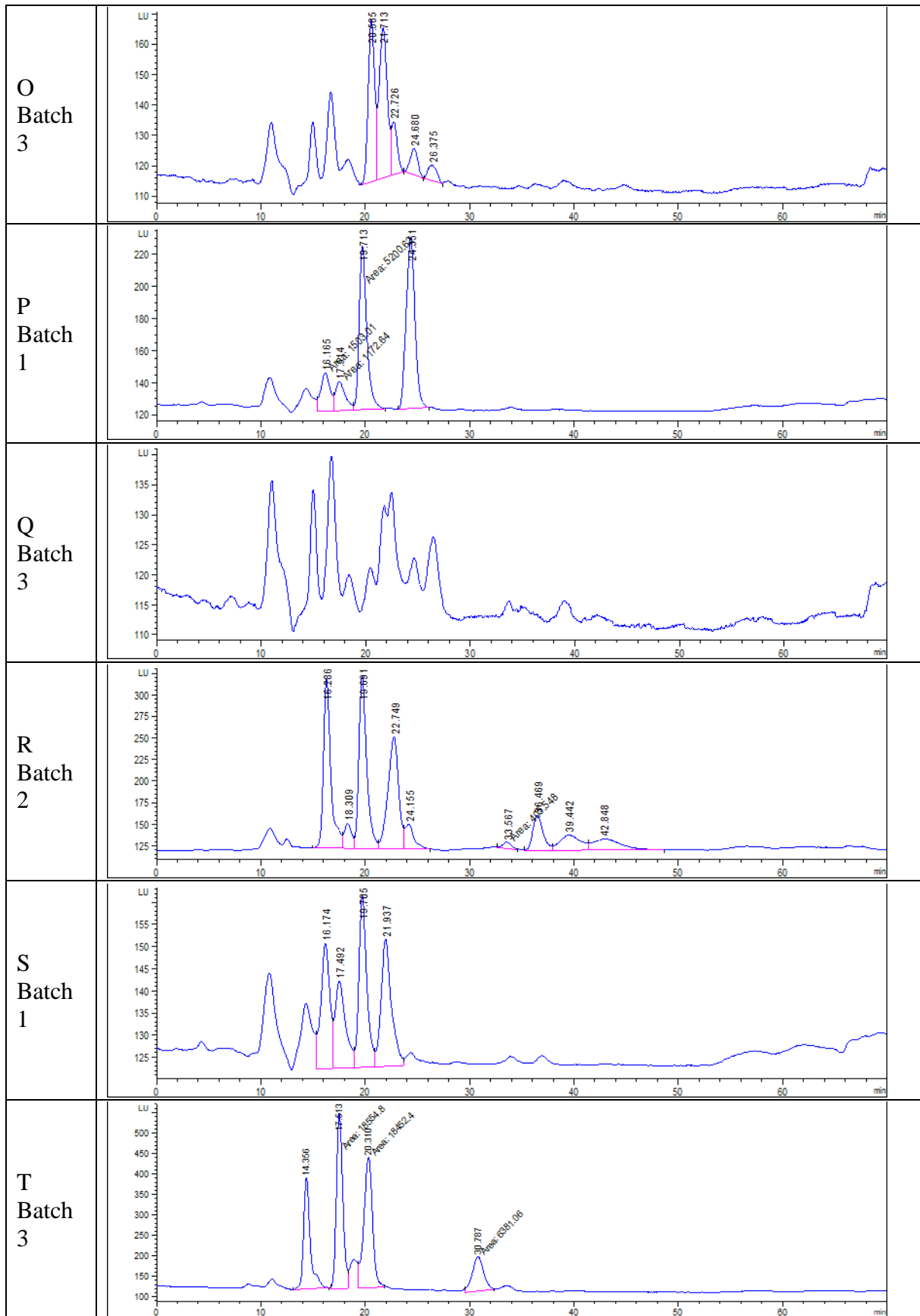


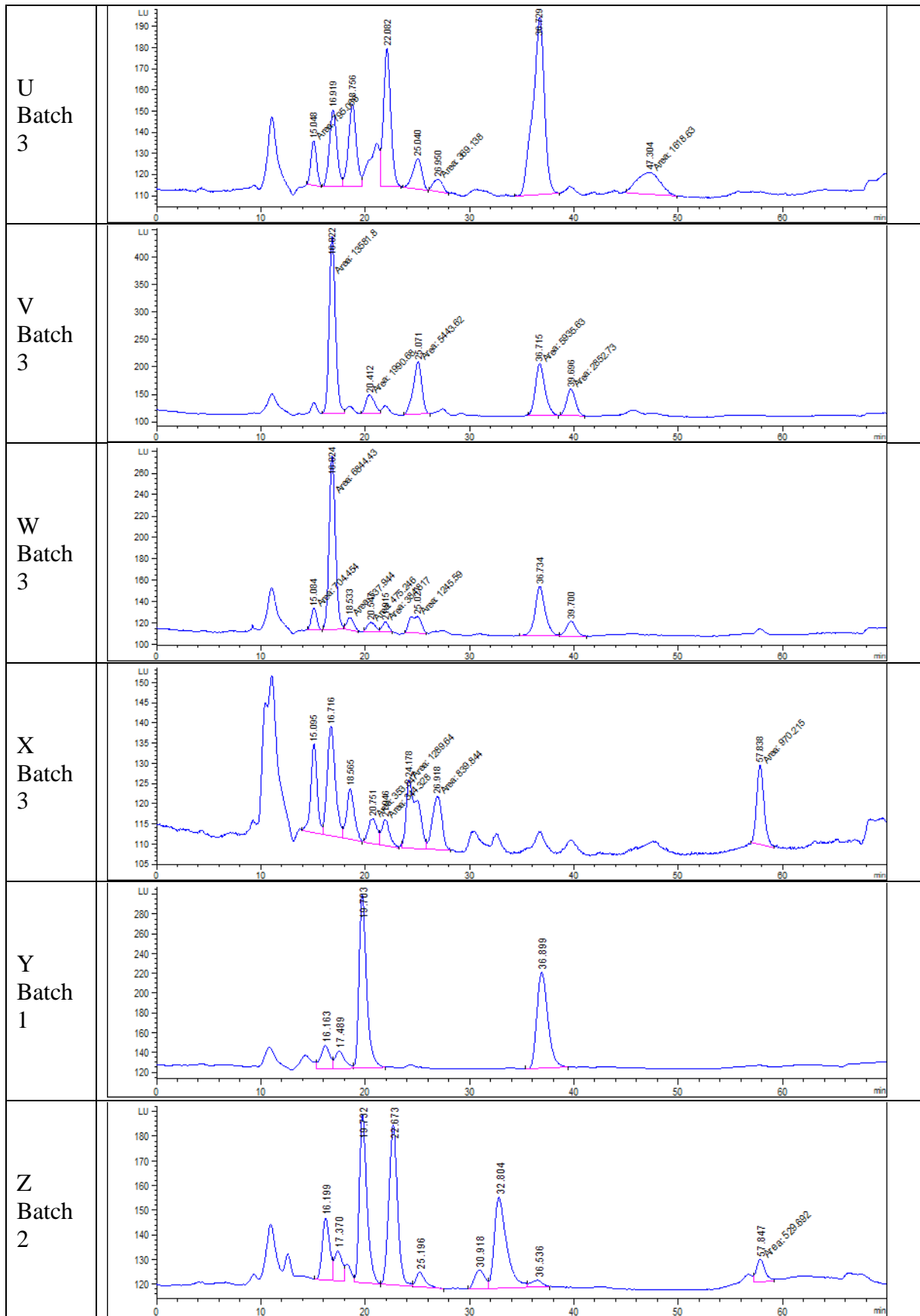


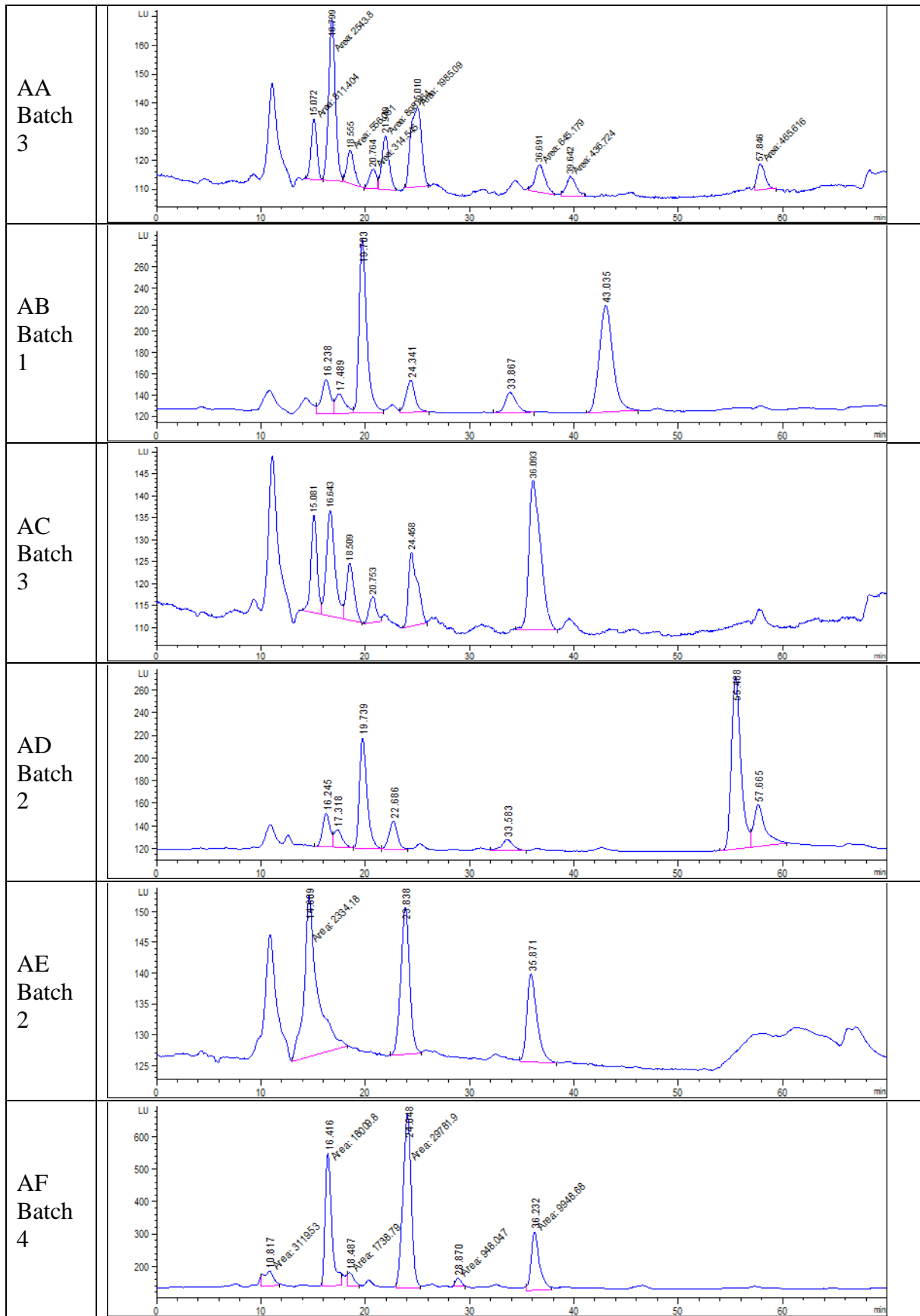


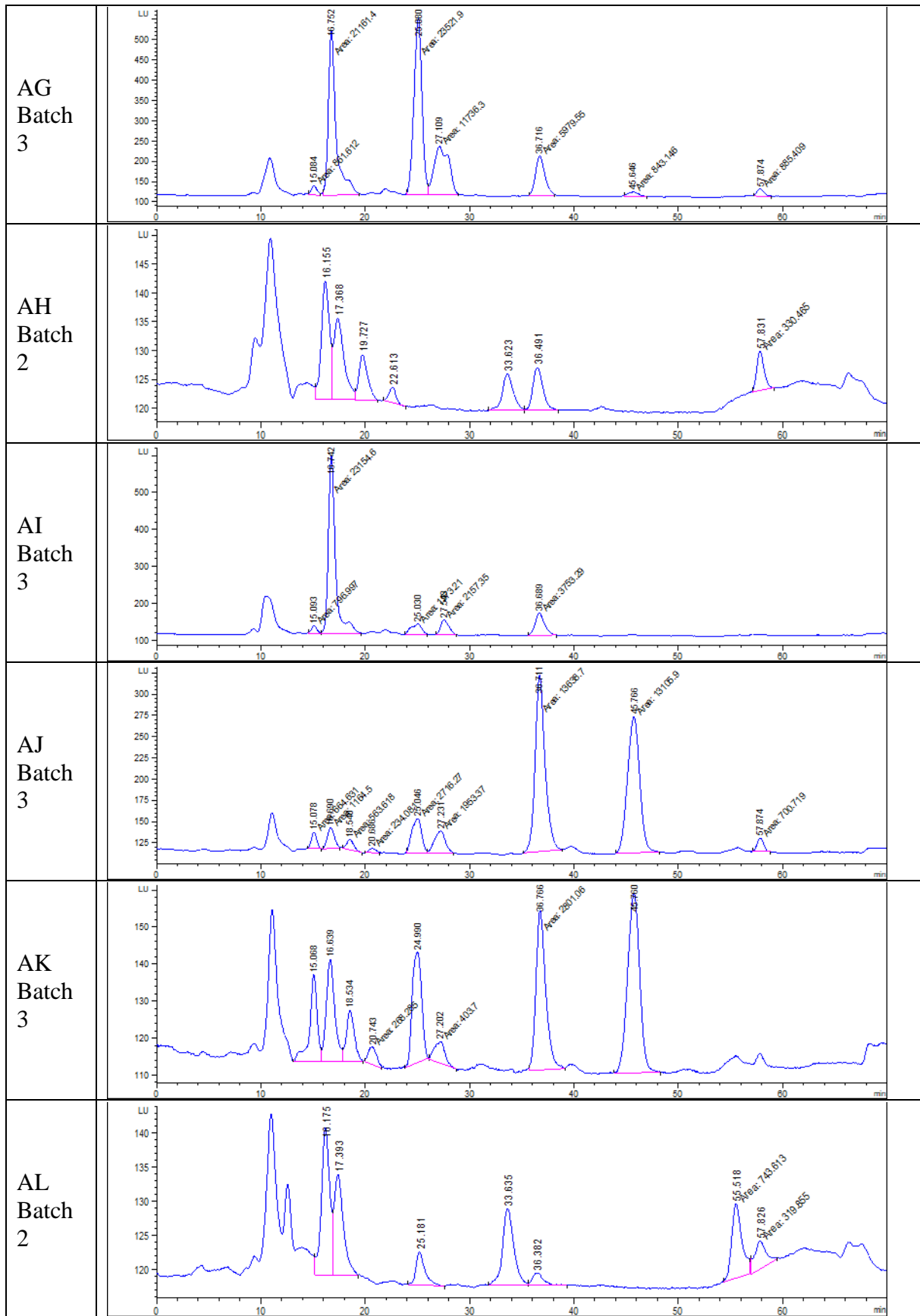


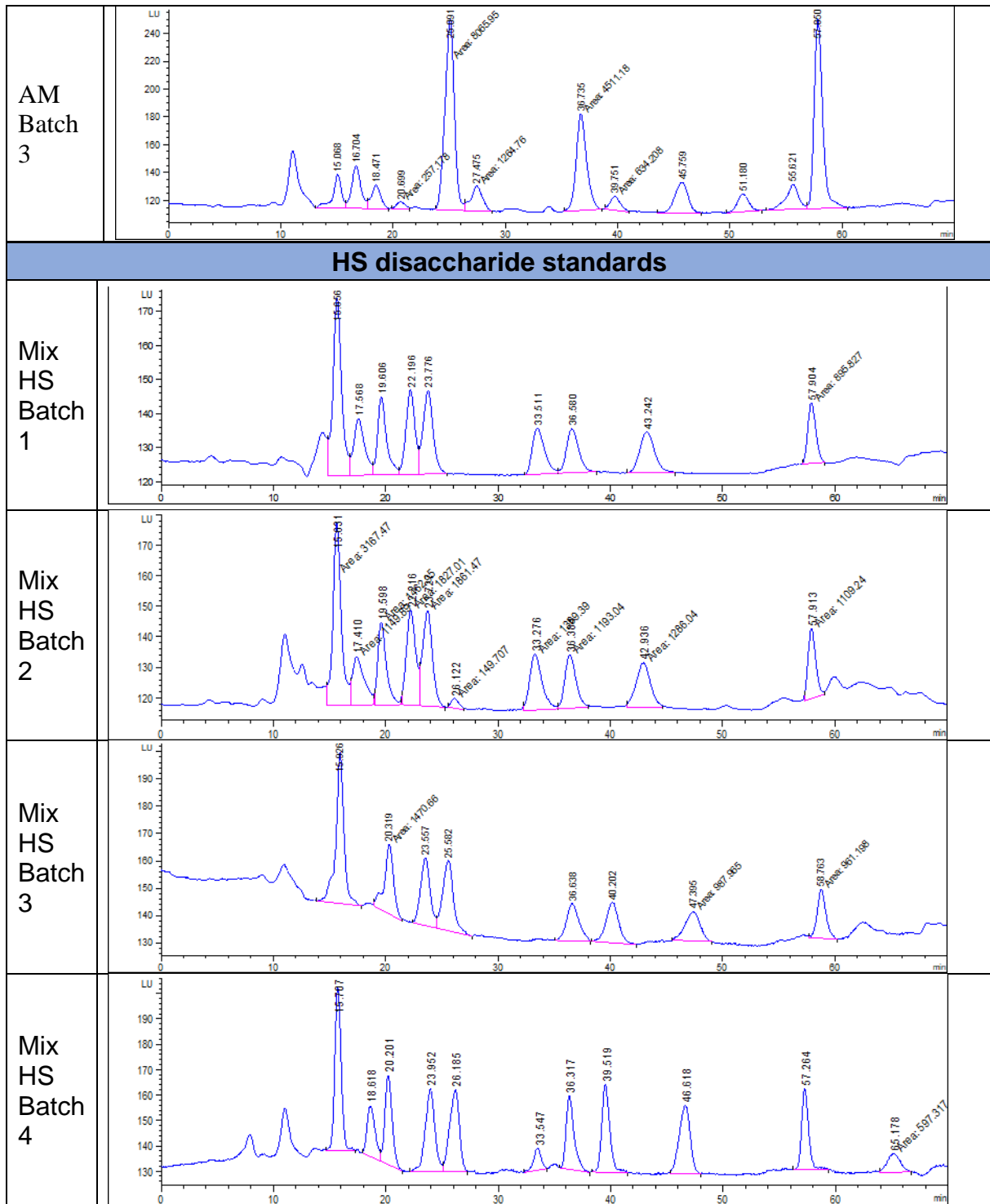








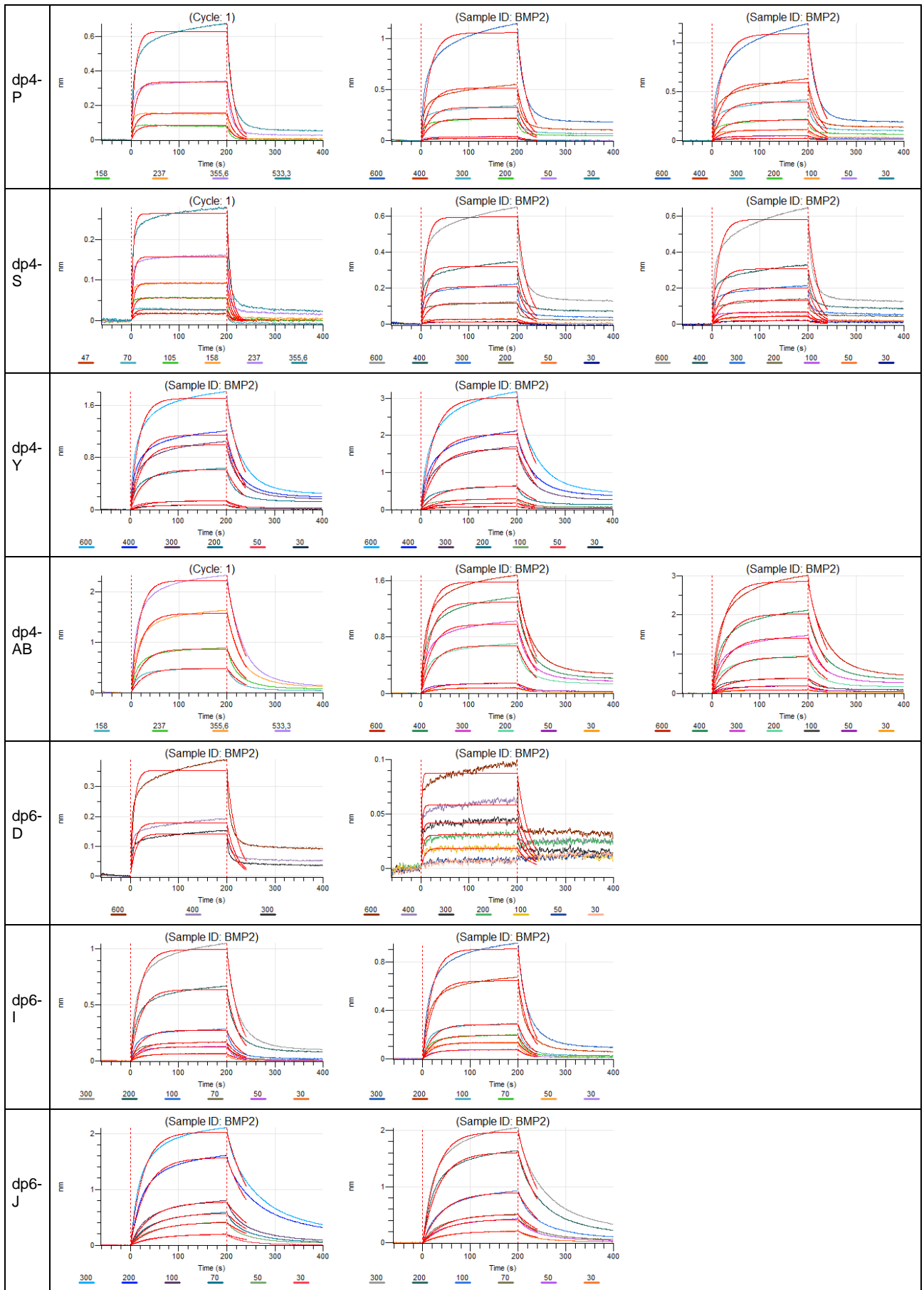


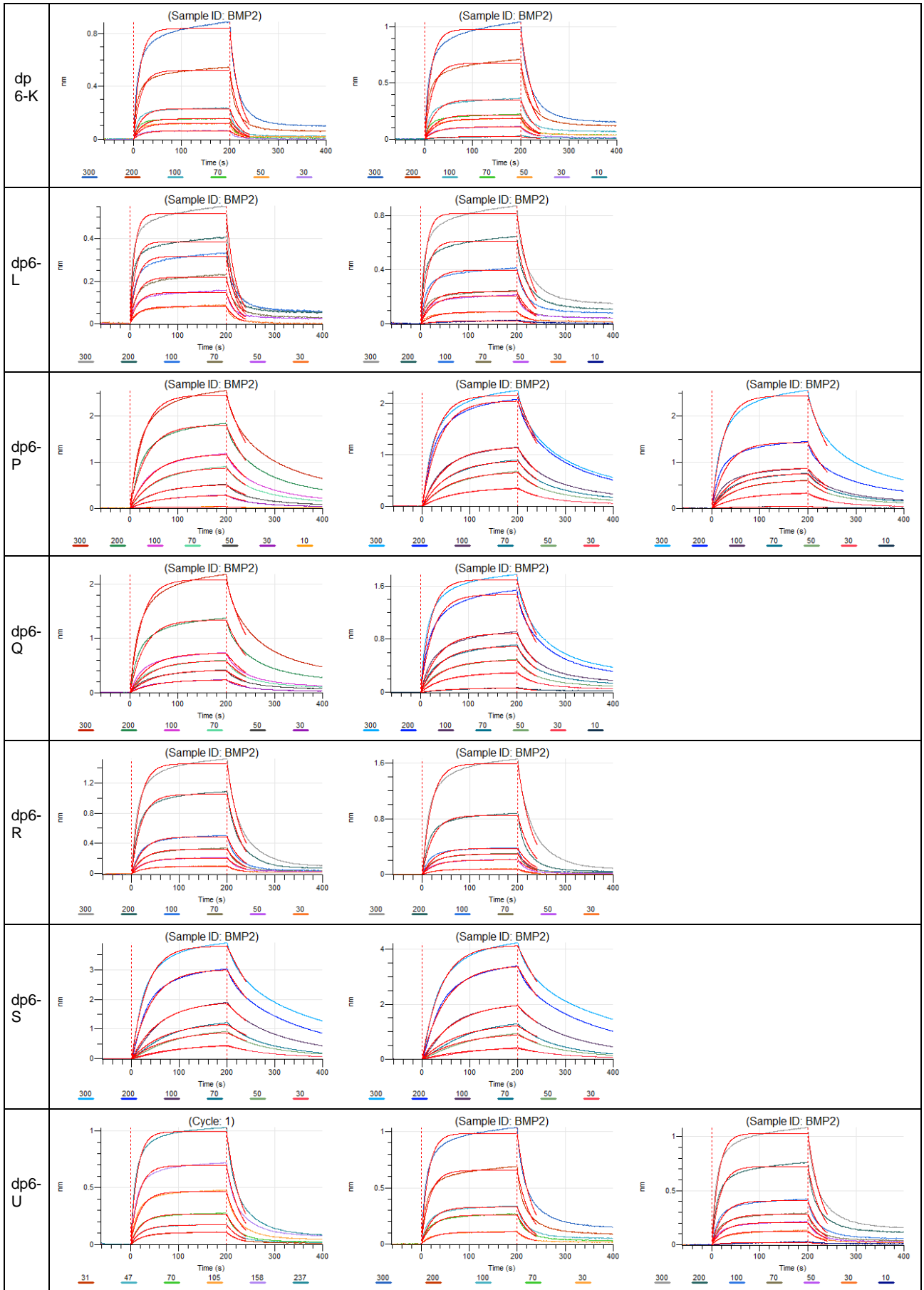


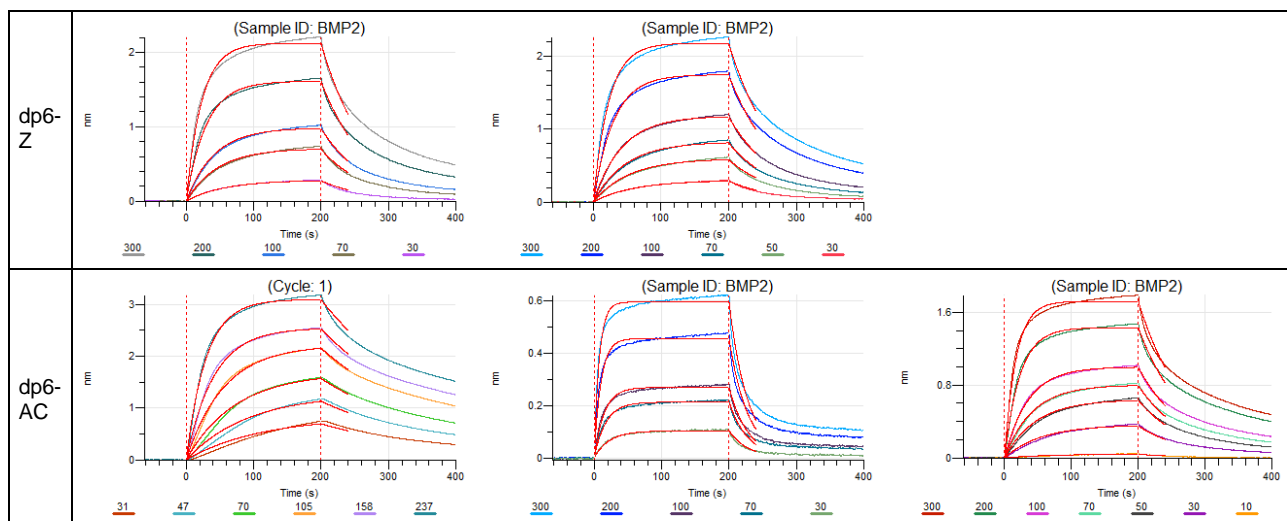
**Supplementary Fig. S7.** Disaccharide composition profile of the entire oligosaccharide library. After digestion with a cocktail of heparinase I, II and III, the oligosaccharides are cleaved into disaccharides that are separated, labelled and detected using a RPIP-HPLC setup, calibrated with HS disaccharide standards to identify detected disaccharide structures. For each experiment (called batch), at least one sample composed of standard disaccharides was injected (see above). It is common to observe a peak at 17' that might correspond to an isomeric structure of  $\Delta$ UA–GlcNS disaccharide but the unambiguous elution times of standard disaccharides are as follows:

16'	20'	22'-24'	24'-26'	33'-36'	36'-40'	43'-47'	~57'
$\Delta$ UA–GlcNAc	$\Delta$ UA–GlcNS	$\Delta$ UA–GlcNAc6S	$\Delta$ UA2S–GlcNAc	$\Delta$ UA–GlcNS6S	$\Delta$ UA,2S–GlcNS	$\Delta$ UA,2S–GlcNAc,6S	$\Delta$ UA2S–GlcNS6S

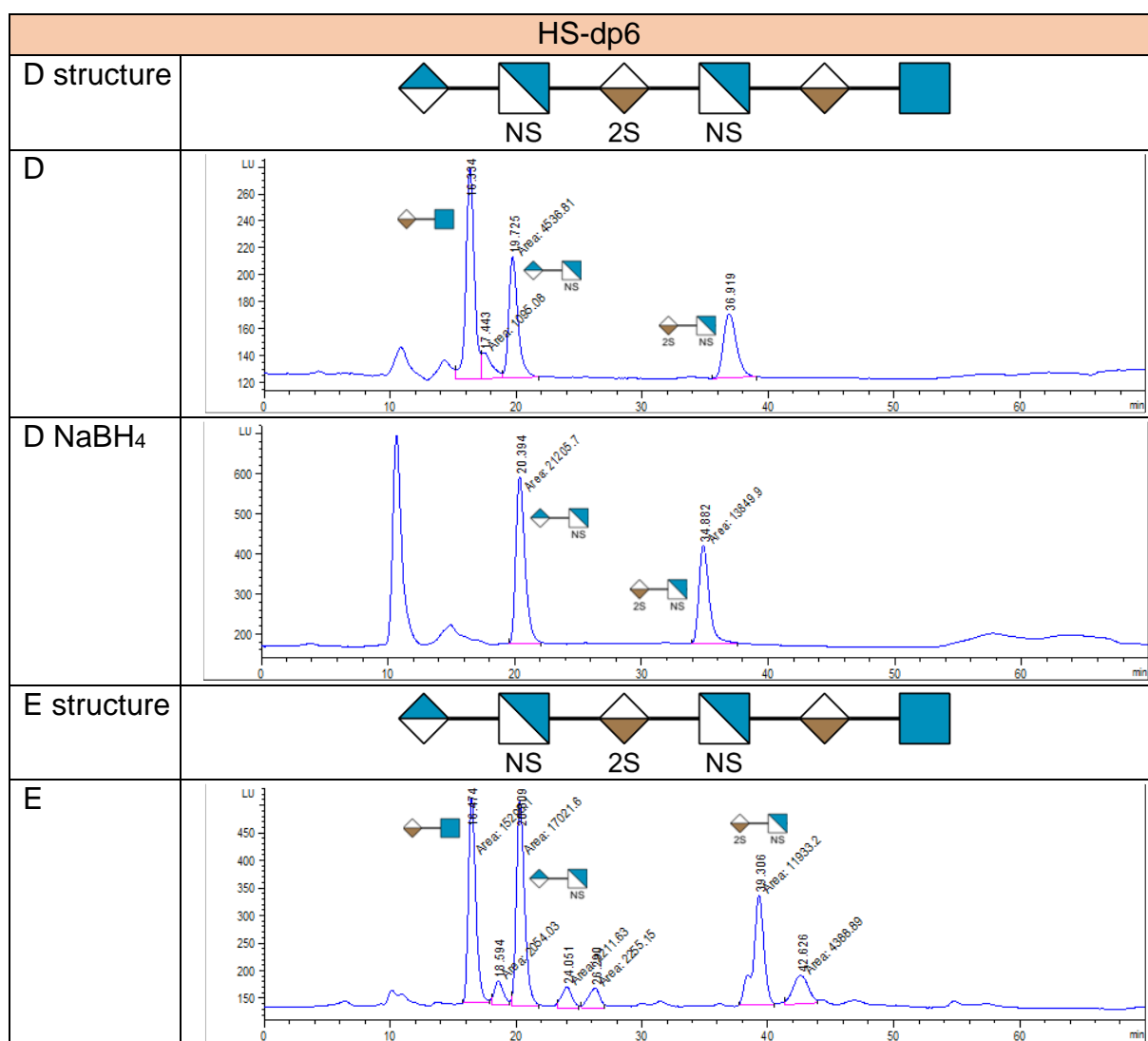
The different peaks were integrated and signal / mass ratio corrections were applied to determine the amounts of each disaccharide. By summing the amounts of disaccharide components for each oligosaccharide, we could determine the quantities produced for the entire oligosaccharide library.

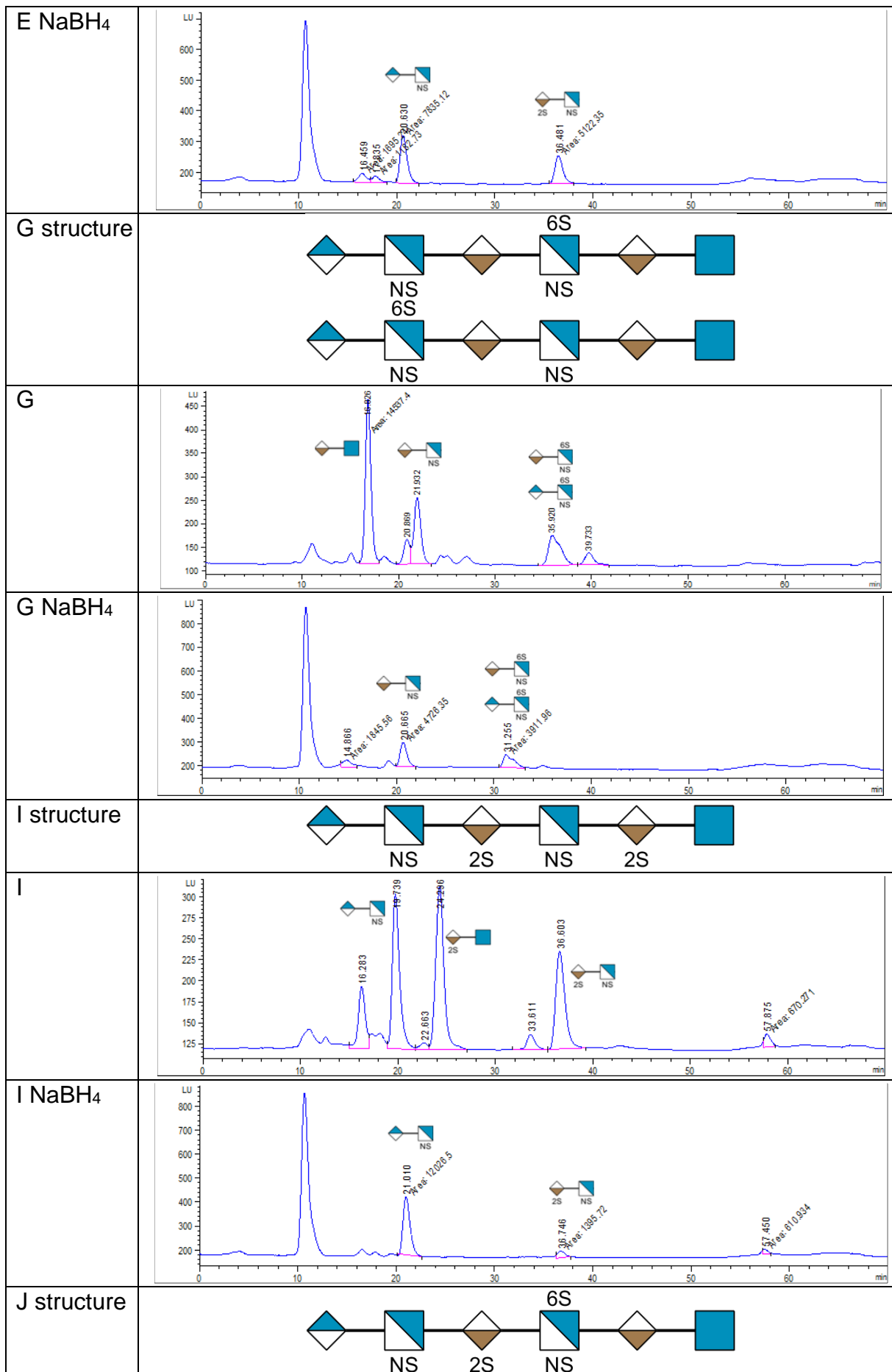


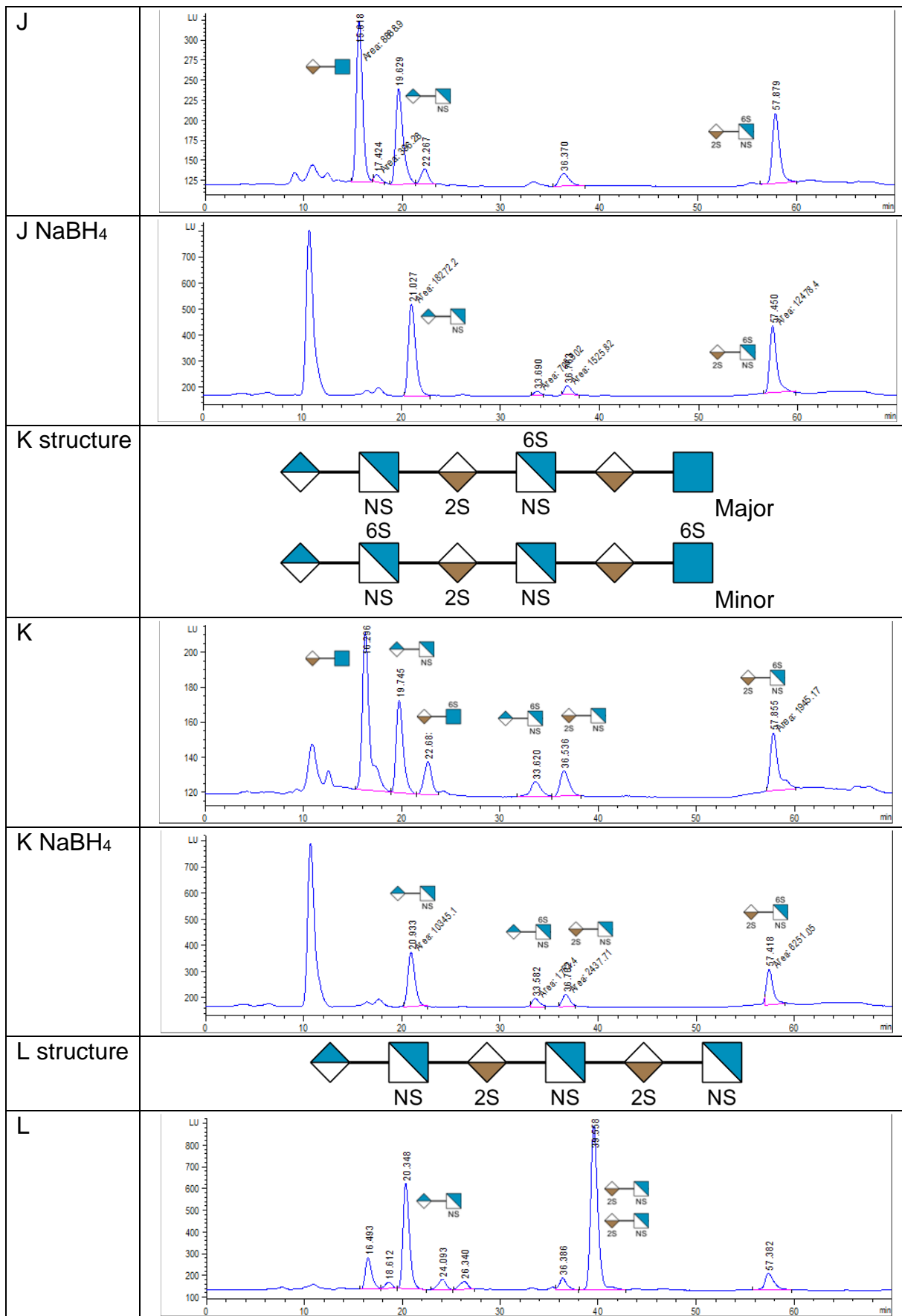


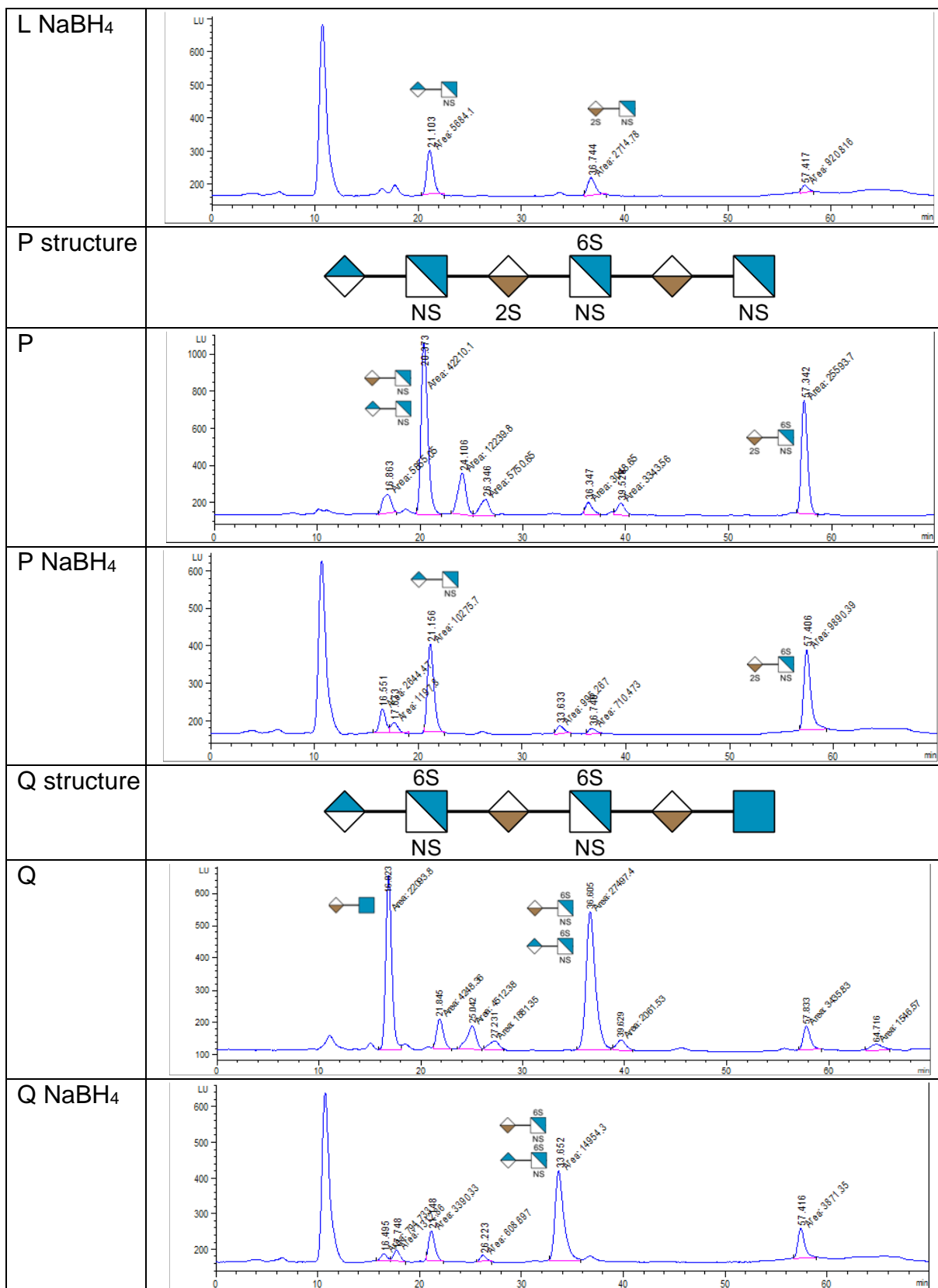


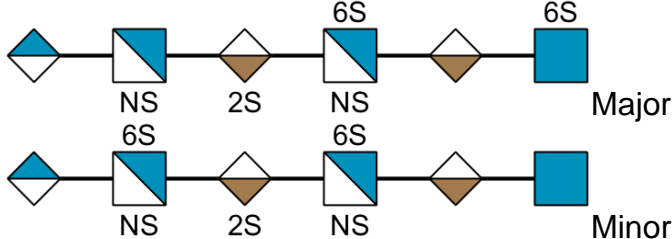
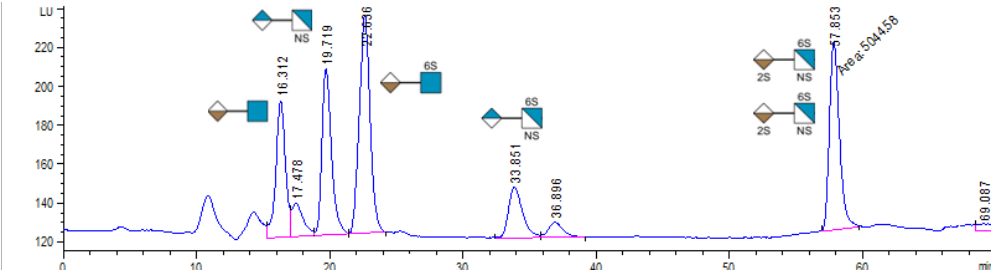
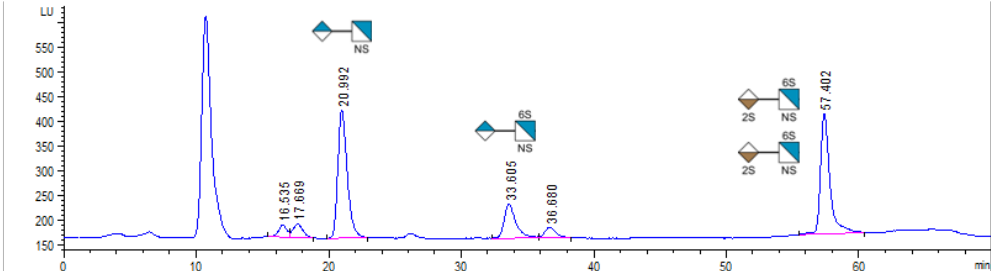
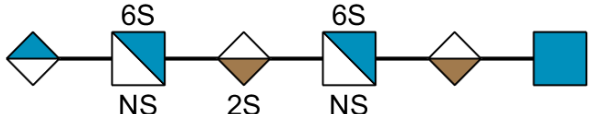
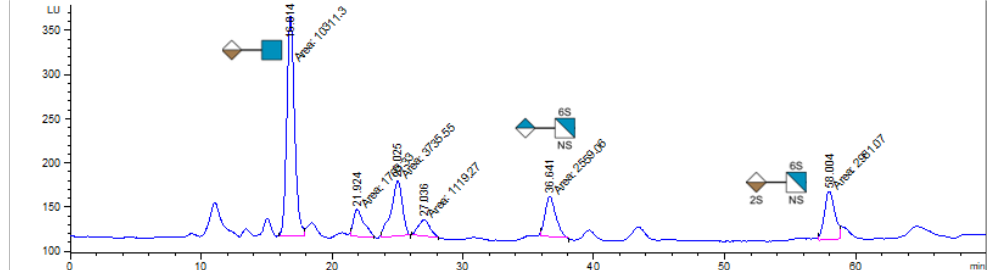
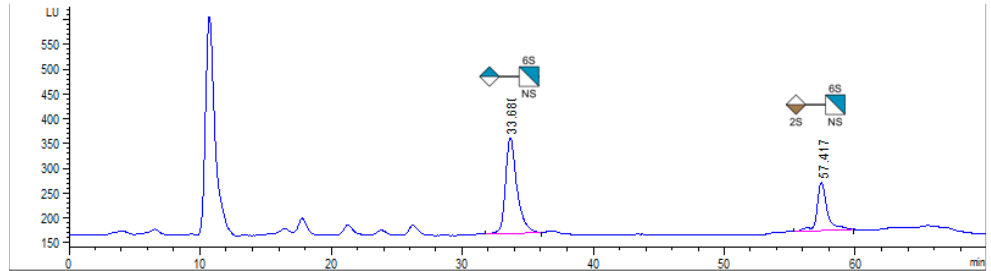
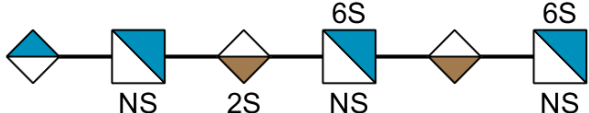
**Supplementary Fig. S8.** Raw data for all replicates of BLI kinetics assays of BMP2 binding on different HS oligosaccharides. The phases of BMP2 association and dissociation were measured for 200 s each at different concentrations indicated at the bottom of each graph (nM). The curves were fitted with a 1:1 Langmuir binding model on the full association and 40 s of the dissociation (red curves) to obtain the kinetics parameters of the interactions.

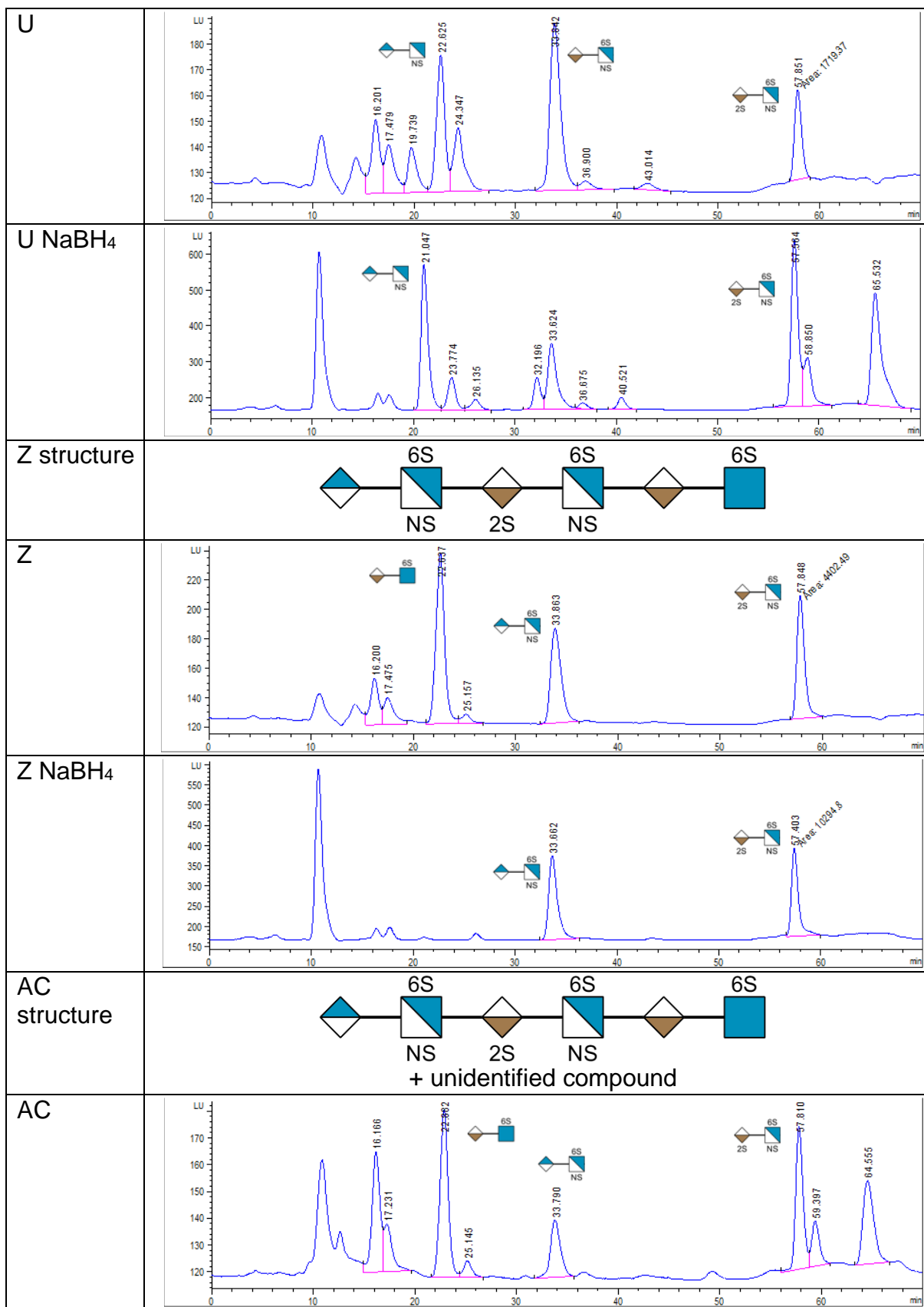


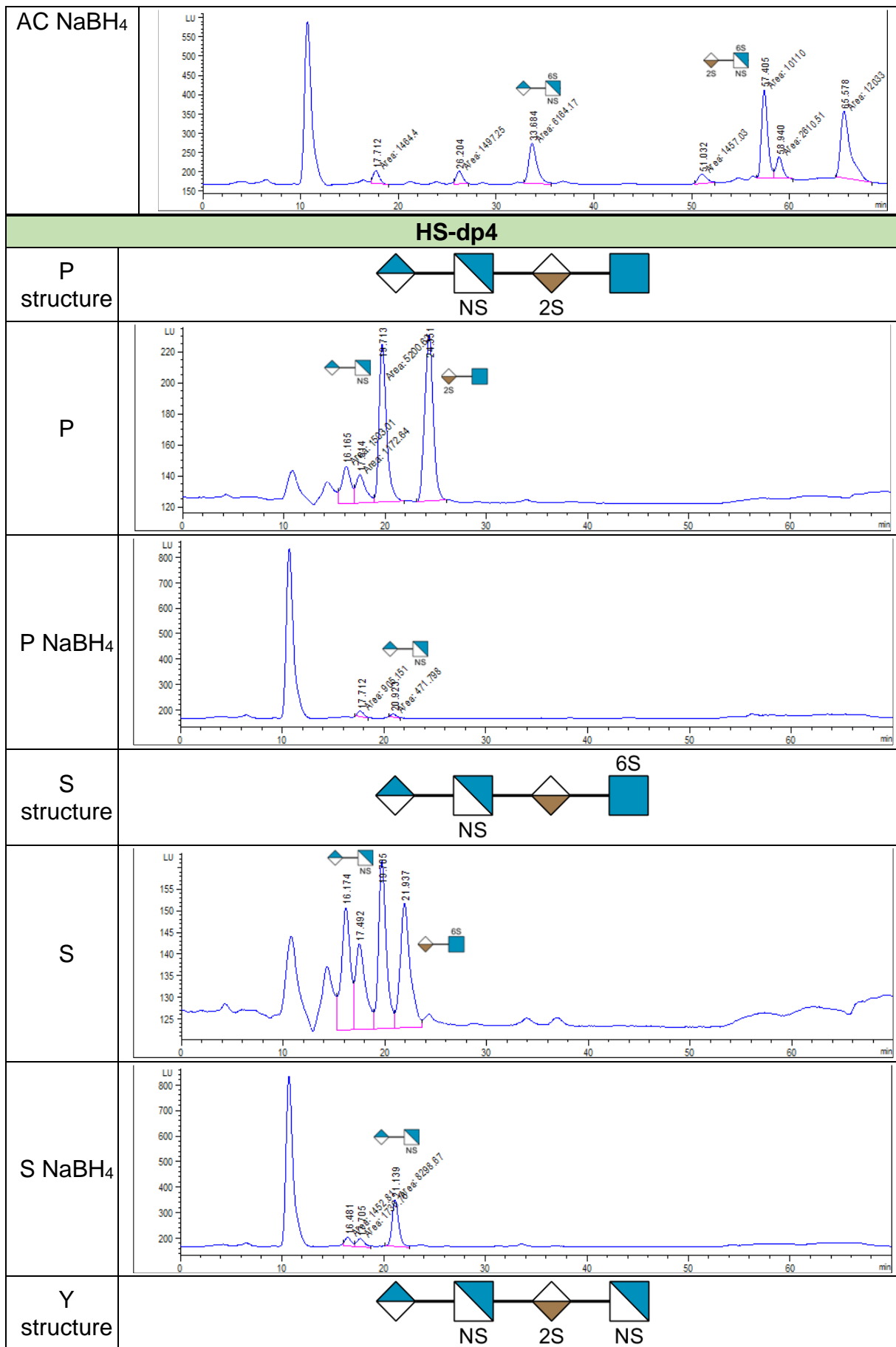


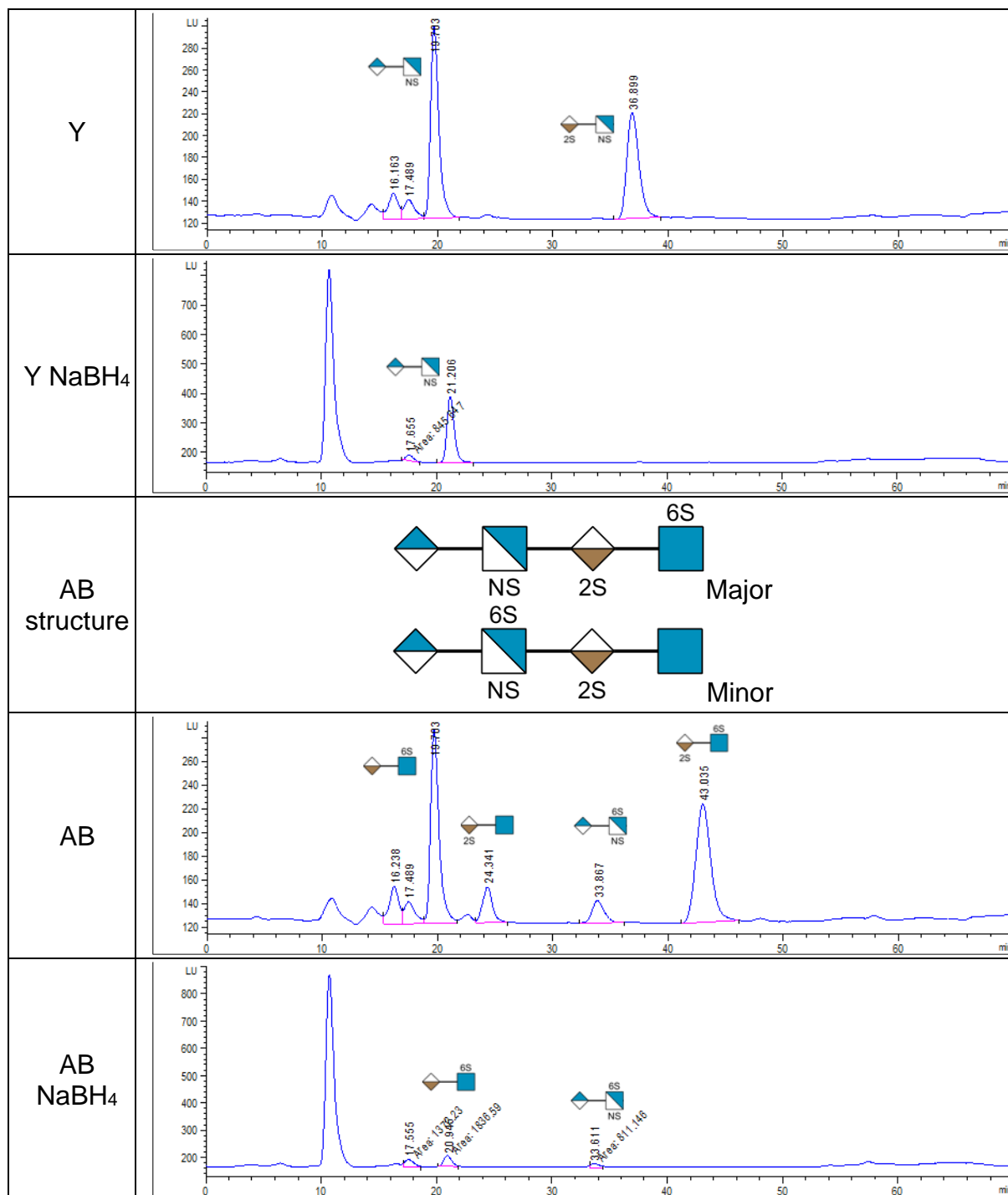




R structure	 <p>Major</p> <p>Minor</p>
R	
R NaBH <sub>4</sub>	
S structure	
S	
S NaBH <sub>4</sub>	
U structure	







**Supplementary Fig. S9.** RPIP-HPLC disaccharide analysis of oligosaccharides with or without NaBH<sub>4</sub> reduction. The comparison of both analyses allow determining the reducing end of the oligosaccharides (lacking in the analysis with NaBH<sub>4</sub>). Generally, the sequence of the different oligosaccharides could be determined from the substrate specificities of heparinase III for GlcNAc±6S-GlcA and GlcNS±6S-GlcA linkages. For each compound, the determined structure is first depicted, then the disaccharide analysis of the oligosaccharide, and finally the disaccharide analysis of the oligosaccharide reduced with NaBH<sub>4</sub>. The disaccharides corresponding to detected peaks are depicted in the HPLC profiles with the Symbol Nomenclature for Glycans (SNFG, Version 1.5).

	CS-A	CS-D	CS-E
0S (0/i0)	8,7	18,1	4,2
4S (A/iA)	63,6	19,7	20,0
6S (C/iC)	27,7	33,0	56,3
2S (U/iU)	0,0	0,0	0,0
6S4S (E/iE)	0,0	0,0	19,5
4S2S	0,0	0,0	0,0
6S2S (D/iD)	0,0	29,2	0,0
2S4S6S (T/iT)	0,0	0,0	0,0

**Supplementary Table 2.** *Composition of the different GAG chains determined by RPIP-HPLC disaccharide analysis.*



**Chapter VI. BMP2 binds non-specifically to  
PEG-passivated biomaterials and induces  
substantial signaling**

## VI.A. Article introduction

Non-specific adsorption of proteins is a frequent and challenging issue for biomaterial studies. In the case of our biomimetic SA<sub>v</sub> platforms, we normally expect the binding of BMP2 to occur only on GAGs and not on any other components of the platforms (non-specific binding), in order to study specifically the effect of GAG-bound BMP2. Previous QCM-D data demonstrated a significantly lower BMP2 non-specific attachment on glass biomimetic SA<sub>v</sub> platforms compared to its binding onto HS-functionalized platforms<sup>[486]</sup>. However, we show in this manuscript that the contribution of this limited non-specific BMP2 attachment to BMP signaling is not negligible. This phenomenon has represented the major issue of my PhD project, hampering the acquisition of unbiased findings about the role of GAGs in the BMP2 signaling. This manuscript, in the form of an article, intends to share the significant work achieved to address this issue of non-specific signaling, from its discovery to the investigations to circumvent it.

The non-specific BMP2 signaling was studied by comparing the level of SMAD1/5/9 phosphorylation on platforms with or without GAGs, using immunofluorescence and high-content imaging and analysis. For both glass-based and gold-based SA<sub>v</sub> platforms, we found that non-specific BMP2 signaling fell within the same range as BMP2 signaling mediated by GAGs, preventing to distinguish their specific effects. The non-specific BMP2 signaling was dose-dependent and was observed up to three days by analyzing the expression of ALP, a marker of osteogenic differentiation. Other BMP proteins than BMP2 (BMP4, BMP7) were also subject to strong non-specific signaling.

We used dynamic light scattering (DLS) technique to analyze the aggregation of BMP2, potentially involved in its non-specific adsorption. Different buffers were tested and we observed that BMP2 aggregates at neutral pH and that it could be reduced by the addition of Tween-20 surfactant or by decreasing the pH.

To facilitate our investigations for reducing the BMP2 non-specific adsorption, we employed a fluorescent plate reader to measure the binding of BMP2 (with a specific anti-BMP2 antibody) or a fluorescently tagged BMP2. Several blocking strategies were tested and a combination of highly concentrated bovine serum albumin (BSA) and trehalose had the strongest effect in reducing the non-specific BMP2 binding. This combination was applied to the studies of the article presented in **Chapter V** and enabled to distinguish different effects of distinct extracellular GAGs in BMP signaling.

The investigations conducted in this work were performed mainly with the glass biomimetic platforms because of the higher throughput, simplicity, and convenience of the fluorescence readout with the glass substrate. However, gold streptavidin biomimetic platforms were also employed in some cases. We explored mainly the cellular response of C2C12 cells, which are a standard model for studying the bone differentiation induced by BMPs. Additionally, we extended our investigations to Chinese hamster ovary (CHO) wild type cells, as the availability of CHO mutants for GAG biosynthesis enzymes represents an attractive opportunity to investigate the role of GAGs. As the initial objective of these investigations was not to publish an article but to find rapidly a solution, some experiments were not sufficiently replicated for statistical analysis. We therefore intend to publish this article in an open archive (such as bioRxiv) as a methodological development to explain and support the use of BSA trehalose combination in the **Chapter V** article for blocking BMP2 non-specific binding. It is worth noting that for logical purposes, this manuscript does not encompass all experiments conducted within the scope of our investigation.

I was the main contributor of this article by performing about 90% of experiments, analyzing data, preparing figures, writing the entire manuscript, and revising it with my supervisors. I also supervised Amaury Guibert, an apprenticeship student (L2 equivalent), and trained him in conducting immunofluorescence assays to measure the non-specific binding of BMP2 in various conditions. Other authors of the article provided essential scientific support and supervision, and contributed to the funding acquisition and manuscript revision.

## VI.B. Article

### **BMP2 binds non-specifically to PEG-passivated biomaterials and induces substantial signaling**

Jean Le Pennec<sup>1</sup>, Amaury Guibert<sup>1</sup>, Romain R. Vivès<sup>2\*</sup>, Elisa Migliorini<sup>1\*</sup>

<sup>1</sup>Univ. Grenoble Alpes, INSERM, CEA, CNRS, U1292 Biosanté, EMR 5000, Grenoble, France

<sup>2</sup>Univ. Grenoble Alpes, CNRS, CEA, IBS, Grenoble, France

\*Co-Corresponding authors

Migliorini Elisa (E.M.): [elisa.migliorini@cea.fr](mailto:elisa.migliorini@cea.fr)

Romain Vivès (R.R.V.): [romain.vives@ibs.fr](mailto:romain.vives@ibs.fr)

#### **Abstract**

Biomaterials are widely employed across diverse biomedical applications and represent an attractive strategy to explore in a physiological manner how extracellular matrix components influence the cellular response. In this study, we aimed to employ previously developed biomimetic streptavidin platforms to investigate the role of glycosaminoglycans (GAGs) in bone morphogenetic protein 2 (BMP2) signaling. However, we observed that the interpretation of our findings was skewed due to the GAG-unrelated non-specific adsorption of BMP2 on components of our biomaterials, beyond GAGs. Non-specific adsorption of proteins is a recurrent and challenging issue for biomaterial studies. Despite the initial incorporation of anti-fouling poly(ethylene glycol) (PEG) chains within our biomaterials, the residual non-specific BMP2 adsorption still triggered BMP2 signaling within the same range as our conditions of interest. To tackle this issue, we explored in this study a wide range of options to prevent BMP2 non-specific adsorption. Specifically, we tested alternative constructions of our biomaterials, either on gold or glass substrate, using distinct PEG-based linkers. We identified the aggregation of BMP2 at neutral pH as a potential cause of non-specific adsorption and thus we determined specific buffer conditions to prevent it. We also investigated the induced BMP2 signaling over different culture periods. Nevertheless, none of these options resulted in a viable suitable solution to reduce the non-specific BMP2 signaling.

Next, we studied the effect of various blocking strategies and we identified a blocking condition involving a combination of bovine serum albumin and trehalose that successfully reduced the unspecific attachment of BMP2 and the non-specific signaling. Furthermore, the effect of this blocking step was improved when using gold platforms instead of glass, in particular with Chinese hamster ovary (CHO) cells that seemed less responsive to non-specifically bound BMP2 in comparison with C2C12 cells.

## Introduction

Biomaterials are commonly used for a wide range of applications, including biosensors, encompassing biosensors, drug delivery systems, biomedical implants, and the exploration of cellular responses in a more physiological environment than classically used plastic substrates. In this context, the non-specific adsorption of molecules or bacteria constitutes a major issue hampering the development of new applications<sup>[2,3]</sup>. The underlying mechanisms of protein non-specific binding predominantly entail interactions between hydrophobic domains and surfaces, potentially augmented by electrostatic interactions<sup>[4]</sup>. To tackle this issue, common anti-fouling strategies include the functionalization at surfaces of highly hydrophilic components with a neutral charge, providing a barrier to protein adsorption<sup>[5-7]</sup>. In particular, poly-ethylene glycols (PEG) synthetic polymers are commonly employed for this purpose<sup>[6,8]</sup>. The reduction of protein adsorption exerted by PEGs can be explained physically by the generated steric hindrance between the protein and the surface, and chemically by the strong interaction between the PEG ether linkage and water molecules, which can hardly be overcome by proteins, thereby reducing their adsorption on surfaces. The PEG grafting density and polymer length also modify the conformation of the coating, but with an unclear role in its anti-fouling performance<sup>[9-11]</sup>. Despite having a well-established role in reducing non-specific protein adsorption, common coating strategies including PEGs are not entirely satisfying and their performance are protein-dependent<sup>[10]</sup>.

In previous studies, we developed PEG-based biomaterials (streptavidin biomimetic platforms) to facilitate the investigation of the roles of extracellular matrix components in cellular responses under physiological conditions<sup>[12-14]</sup>. In particular, we have been interested in investigating the roles of different glycosaminoglycans (GAGs) in the regulation of bone morphogenetic protein 2 (BMP2) signaling<sup>[13]</sup>. Developments were realized to functionalize the biomimetic platforms on glass or gold substrates either with PLL-g-PEG-biotin or thiol-PEG-biotin linkers ensuring a certain surface passivation. These biomaterials were also designed to be compatible with a microscopy readout developed for high-content applications<sup>[1,15]</sup>. We have commonly assessed the non-specific adsorption of BMP2 (on other components than GAGs) *ex-situ* with quartz crystal microbalance (QCM) monitoring technique, revealing relatively low measurements in comparison to specific binding on GAGs<sup>[1]</sup>.

Existing studies on BMP2 adsorption have predominantly focused on hydrophobic substrates utilized in biomedical implant applications. These investigations have primarily examined the ability to bind and release BMP2, while preventing protein unfolding that could hinder its

bioactivity<sup>[16–21]</sup>. To the best of our knowledge, concerns regarding non-specific BMP2 adsorption have not emerged, as long as bioactivity is maintained for biomedical applications. In this study, we underscore that even negligible amounts of non-specifically adsorbed proteins can induce a significant cellular response, complicating the interpretation of experimental outcomes *in vitro*. Specifically, the non-specific adsorption of BMP2 hindered our ability to elucidate the distinctive roles of various GAGs in the modulation of BMP2 signaling. We examined the effects of BMP2 adsorption on gold or glass biomaterials, at different time points, and with other proteins of the BMP family (BMP4 and BMP7). To circumvent this adsorption issue, we investigated the aggregation of BMP2 in different buffers that potentially could be involved in these adsorption mechanisms. The quantification of BMP2 adsorption onto distinct components of our biomaterials enabled us to determine whether this adsorption was specific to these elements. Finally, we explored various blocking strategies to reduce BMP2 adsorption and the associated non-specific signaling in two different cell lines, either on gold or glass platforms with the aim of identifying specific conditions compatible for our *in vitro* cellular studies.

## **Material and methods**

### **Buffers and Molecules**

Unless stated otherwise, a solution termed Hepes, containing 10 mM Hepes and 150 mM NaCl (Sigma-Aldrich) at pH 7.4, was utilized for dilution and rinsing of samples. Phosphate buffer saline (PBS, Sigma-Aldrich) was adjusted at pH 7.4 if necessary and a sodium acetate (Sigma-Aldrich) buffer was prepared at 10 mM with a pH of 4.2. All buffers supplemented with 0.02% Tween-20 are consistently termed with the -T suffix (Hepes-T, PBS-T, Acetate-T). Biomimetic platforms were prepared by functionalizing mPEG-Thiol and biotin-PEG-Thiol (Polypure) on a gold substrate, or PLL(20)-g[3.5]-PEG(2)/PEGbiotin(3.4)50% linker (PLLgPEG, SuSoS AG) for glass substrates. Platforms were further conjugated with streptavidin (SA<sub>v</sub>, 55 kDa, Sigma-Aldrich). Details about biotinylated cyclic arginyl-glycyl-aspartic acid (RGD, 3.9 kDa) can be found in prior works<sup>[14,22]</sup>. GAGs were obtained from different sources as described elsewhere (**Chapter V**). BMP2 produced was acquired from Medtronic (26 kDa, InductOs). BMP4 and BMP7 were both purchased from R&D.

### **Dynamic light scattering BMP2 size measurement**

The size distribution by volume of BMP2 aggregates in different media was determined by dynamic light scattering (DLS; Zetasizer Ultra, Malvern Panalytical, Worcestershire, United

Kingdom). Light scattering was measured in a low-volume disposable sizing cell (ZSU1002, Malvern) at 25°C after an equilibration time of 300 s. The DLS size distribution was calculated from the autocorrelation curves applying the protein analysis algorithm (“general purpose” option) of the Zetasizer Software 7.11 (Malvern). A refractive index (RI) of 1.45 and an absorption coefficient of 0.001 were defined for BMP2, using the RI of water as solvent (RI: 1.33). Before measurement, BMP2 was stocked at 1 mg/mL in HCl 1mM (pH 3.0). The stock aliquot was centrifuged for 10 min at 13200 rpm preceding its dilution at 100 µg/mL with different buffers in low-binding tubes. Samples were briefly centrifuged for 1 min 30 before being placed in measurement cuvettes. Triplicate measurements were performed for each sample. In case of “weak scattering” indication provided by the software data quality guidance, measurements were removed from the analysis.

### **Biomimetic platform surface functionalization**

Glass coverslips (24×24 mm; Menzel Gläser) underwent a gold-sputtering process (1.5 nm Cr and 8 nm Au) using a Plassys™ evaporating machine in a clean room, constituting the base substrate of gold biomimetic platforms. The gold-sputtered surfaces were activated with UV/Ozone Procleaner™ (BioForce Nanosciences) for 10 min, and immersed overnight in an ethanol solution with 0.95 mM mPEG-thiol and 0.05 mM biotin-PEG-thiol, before blow-drying the surfaces with nitrogen. SAV, cRGD, HS, and BMP2 were incubated sequentially by a liquid-handling robot (Evo 100, Tecan) performing as well the intermediate rinsing steps<sup>[1]</sup>. Concentrations and durations used for incubation steps are described in previous work (**Chapter V**). When preparing samples for automated immunofluorescence (IF) analysis, gold-coated surfaces were attached to the bottom side of a bottomless 96-well plate (Greiner Bio-one) using double-sided adhesive tape (FRAP Sandwich set, Paul Marienfeld), dividing one surface into four wells.

Glass biomimetic surfaces were built on glass-bottom 96-well plates (Greiner Bio-One) *via* a PLL(20)-g[3.5]-PEG(2)/PEGbiotin(3.4)50% linker (PLLgPEG, SuSoS AG). As previously described, SAV and cRGD were premixed (molar ratio 3:4) before incubation on the linker to leave an increased number of available biotin binding sites for the subsequent functionalization of GAGs<sup>[1]</sup>.

For both gold and glass platforms, BMP2 was finally incubated by the robot with adequate buffer and concentrations indicated for each experiment. BMP2 was incubated between 30 and 90 min for cell experiments and 30 min for BMP2 immunofluorescence assays. When using

0.02% Tween-20 for BMP2 incubation, the unbound BMP2 was rinsed twice in Hepes-T followed by three rinsing in Hepes prior to cell seeding.

### **Blocking step on biomimetic platforms**

A 2-hour blocking step was possibly performed to prevent BMP2 non-specific adsorption. The blocking was performed after SAV functionalization for gold platforms, and after either PLLgPEG or SAV-RGD functionalization for glass platforms. The blocking step was performed using one of the following conditions: bovine serum albumin (BSA) at 3%, 5% or 10% (BP9703, ThermoFisher Scientific), D-(+)-Trehalose at 0.6 M (A19434.14, ThermoFisher Scientific), BSA/Trehalose mix (10%/0.6M), myoglobin at 1 mg/mL (M1882, Sigma-Aldrich), m-PEG2-NHS ester (284BP-23656, Tebubio), imidazole at 50mM (Sigma-Aldrich), glycine at 0.2 M (Sigma-Aldrich), and arginine at 0.2 M (Sigma-Aldrich). After blocking, the biomimetic platforms were rinsed 5 times with Hepes.

### ***Ex situ* characterization of BMP2 binding with quartz crystal microbalance**

We measured with quartz crystal microbalance with dissipation monitoring (QCM-D, QSense Analyzer, Biolin Scientific) the shifts in resonance frequency ( $\Delta f$  in Hz) and energy dissipation ( $\Delta D$  in dissipation units, ppm= $10^{-6}$ ) to characterize binding events in the biomimetic platforms sequential buildup. Experiments were performed at 24°C and  $\Delta f$  and  $\Delta D$  were measured at six overtones ( $i = 3, 5, \dots, 13$ )<sup>[13]</sup>. Only dissipation and normalized frequency of the third overtone ( $i = 3$ ) are presented. Frequency measurements are related to the hydrated mass bound on the surface, while dissipation measurements are related to the rigidity of the deposited molecule film. Platforms were functionalized on silicon dioxide (SiO<sub>2</sub>) crystals (QSX303, Biolin Scientific) as previously described<sup>[1]</sup>. BMP2 was injected at a concentration of 5 µg/mL in Hepes buffer on crystals functionalized with SAV and cRGD, with or without HS. For BMP2, we used a “fast injection” procedure to mimic the functionalization performed by our liquid-handling robot. The solution of BMP2 was injected at a high flowrate of 100 µL/min until the liquid chamber was filled. At this moment, the flow was stopped to let the molecules bind in a static regime. All measurements of frequency and dissipation shifts were performed after signal stabilization.

### **Cellular assays**

C2C12 cells were acquired from the ATCC (CRL1772) and cultured in DMEM with high glucose, pyruvate, and GlutaMAX™ Supplement (cat. 10569010, Gibco™). Wild type CHO-K1 cell lines (CHO-K1: CCL-61™) were culture in DMEM/F-12 GlutaMAX, (cat. 10565018,

Gibco™). Both cell lines were cultured below confluence, at 37°C under a 5% CO<sub>2</sub> atmosphere, in polystyrene cell culture flasks (Falcon®, Corning) using the previously indicated media supplemented with 10% heat-inactivated fetal bovine serum (FBS, cat. 10270-106, Gibco™), and 1% of antibiotic-antimycotic (cat. 15240062, Gibco™). Cells were discarded after reaching a passage number of 12. Cells were serum-starved for 4 hours, detached with Accutase (A6964, Sigma-Aldrich), and plated on functionalized surfaces in 96-well plates. Each condition involved seeding 10,000 cells in coated wells of the 96-well plates that were maintained at 37°C with 5% CO<sub>2</sub>. Positive control and negative control correspond to cRGD platforms with or without 0.1 µg/mL of soluble BMP2 (sBMP2). The effect of BMP2 adsorbed on GAGs or non-specifically was studied by rinsing unbound BMP2 before cell seeding. Cells were fixed after 90 min using 2% PFA for 5 min, then 4% PFA for 20 min. Each condition was assessed with intra-experimental technical duplicates.

### **Immunofluorescence assays on biomimetic platforms**

A standard ELISA assay was performed to detect the binding of BMP2 on the platforms. After a 1-hour blocking step with 3% BSA in PBS, a polyclonal anti-BMP2/BMP4 primary antibody (AF355, R&D Systems) was incubated at 10 µg/mL for 2 h with 3% BSA in PBS at room temperature. Samples were then washed with PBS, incubated with a secondary Cy3-conjugated donkey anti-mouse antibody (Jackson ImmunoResearch) for 1 h in 3% BSA and finally washed. Mean fluorescence intensity at 595±35 nm was measured with a spectrophotometer microplate reader (Spark®, Tecan) with 535±25 nm wavelength excitation. Measurements of technical duplicates were plotted as mean ± standard deviation (SD).

For cellular assays, we adapted existing protocols already published to quantify the nuclear translocation of pSMAD1/5/9 via immunofluorescence (IF)<sup>[1,14,15]</sup>. Briefly, fixed cells were first permeabilized with 0.2% Triton X-100 (Sigma-Aldrich) (w/v) before following the same steps as indicated above (blocking, primary antibody, fluorescent-conjugated secondary antibody). Primary rabbit anti-pSMAD1/5/9 (Cell Signaling Technology) was diluted at 1:400 and the secondary antibody (1:500, goat anti-rabbit Alexa Fluor 488, ThermoFischer Scientific), was incubated simultaneously with rhodamine-phalloidin (1:1000, ThermoFischer Scientific) and DAPI (1:1000, Sigma-Aldrich). Cell imaging was performed utilizing the InCell Analyzer 2500 (GE Healthcare) microscope with the 20x objective across three channels. Subsequent image analysis was conducted using the automated software InCarta (Molecular Devices), following established protocols<sup>[1,15]</sup>. Intensity of pSMAD1/5/9 was evaluated exclusively within the

nucleus, employing a mask derived from the DAPI signal, and the measurements were background-corrected for a minimum of 100 cells per well.

### **Alkaline phosphatase staining**

For ALP staining, we used fast blue RR salt (Sigma-Aldrich) within a 0.01% (w/v) naphthol AS-MX solution (Sigma Aldrich), following the manufacturer's guidelines. The quantification of ALP staining was conducted under liquid conditions by capturing images of the 96-well plate with the 4x objective of InCell Analyzer 2500 microscope in brightfield mode. The acquired brightfield images were processed using ImageJ, wherein a low-intensity threshold was applied to assess the positive ALP area per well.

## **Results**

### **Low BMP2 non-specific binding on the biomimetic SA<sub>v</sub> platforms induces a strong cell signaling**

Previous studies demonstrated with QCM-D that gold-based biomimetic SA<sub>v</sub> platforms were well passivated against the non-specific binding of BMP2<sup>[13]</sup>. Therefore, we employed them to investigate the influence of GAGs on BMP signaling by evaluating the nuclear translocation of pSMAD1/5/9 in C2C12 cells seeded on gold biomimetic platforms. We adsorbed BMP2 at a concentration of 0.1 µg/mL to different GAGs and we rinsed the unbound proteins before seeding cells. Following a 90-minute incubation period on the platforms, we quantified pSMAD1/5/9 within cell nuclei *via* high-content immunofluorescence analysis. Strikingly, as illustrated in **Fig 1.A**, the adsorbed BMP2 led to similar increases in pSMAD1/5/9 regardless of the immobilized GAG on the platform. This outcome was unexpected, given the significant differences in affinity we have previously observed for BMP2 interactions with distinct GAGs (**Chapter V**). In light of this, we conducted a control cellular experiment, comparing the effects of BMP2 incubation on RGD-functionalized gold biomimetic platforms with and without heparan sulfate (HS), a GAG exhibiting a high affinity for BMP2 (**Fig 1.B**). This experiment revealed a slightly higher pSMAD1/5/9 level on platforms lacking HS, indicating that even the relatively small amount of non-specifically bound BMP2, as determined by QCM, exhibited significant bioactivity. This observation may explain why the signaling observed in **Fig 1.A** was comparable across different GAGs, as the non-specific signaling falls within the same range as the specific signaling induced by HS-bound BMP2.

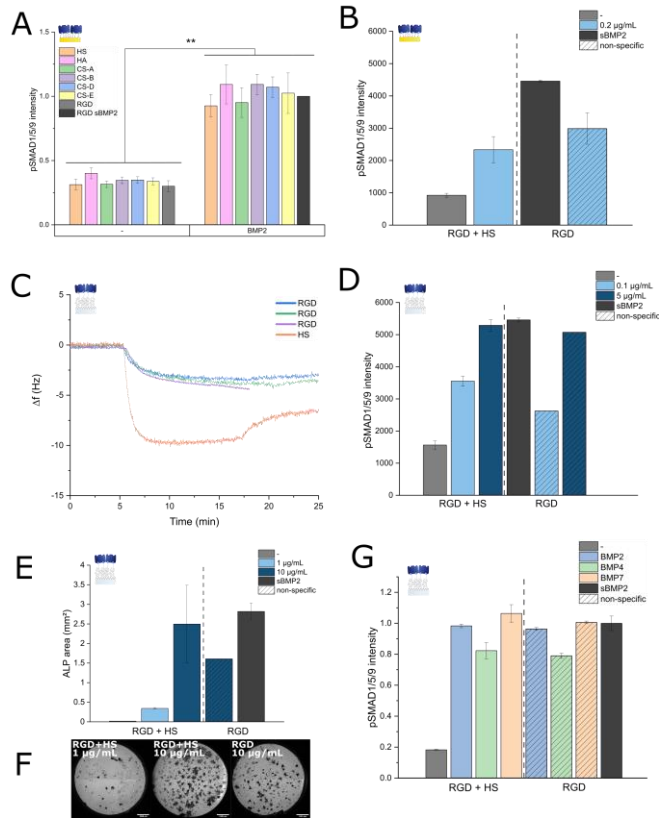


**Fig 1.** For graphs **A**, **B**, **D**, **E**, **G**, positive (black) and negative (gray) controls correspond to cRGD functionalized platforms (without HS) exposed to soluble BMP2 at  $0.1\mu\text{g/mL}$  or not.

**A.** Mean fluorescence intensity of nuclear pSMAD1/5/9 in C2C12 cells after a 90-minute culture on gold biomimetic platforms with or without BMP2. BMP2 was either incubated at  $0.2\mu\text{g/mL}$  with GAGs, or added directly in solution with cells at  $0.1\mu\text{g/mL}$  (sBMP2). Mean values were normalized by the positive sBMP2 positive control  $\pm$  SEM ( $n=3$ ).

**B. D.** Mean fluorescence intensity of nuclear pSMAD1/5/9 in C2C12 cells after a 90-minute culture on **B.** gold or **D.** glass biomimetic platforms with or without BMP2. The HS platforms were incubated with  $0.1$ ,  $0.2$  or  $5.0\mu\text{g/mL}$  BMP2. cRGD platforms without GAGs correspond to the non-specific cellular response. Mean fluorescence values are plotted  $\pm$  SD

**C.** Frequency shifts measured via QCM-D upon binding of BMP2 at  $5\mu\text{g/mL}$  on glass biomimetic platforms, specifically on HS, or non-specifically on platforms with PLLgPEG, SAv and RGD only.

**E.** Alkaline phosphatase (ALP) positive area after 3 days of culture on glass biomimetic platforms. The platforms harboring HS were incubated with  $1$  (light blue) or  $10\mu\text{g/mL}$  (dark blue) BMP2. Cellular response induced by BMP2 non-specific binding is represented with diagonal stripes. Mean ALP positive surface is plotted  $\pm$  SD. **F.** Brightfield images of the entire wells with ALP accumulation in black. Scale bar is  $1000\mu\text{m}$ .

**G.** Mean fluorescence intensity of nuclear pSMAD1/5/9 in C2C12 cells after a 90-minute culture on glass biomimetic platforms, with or without BMPs: BMP2 (blue), BMP4 (green) and BMP7 (beige). All BMPs were incubated at  $1.0\mu\text{g/mL}$ . Data are plotted as normalized mean fluorescence intensity  $\pm$  SD.

We next investigated if the non-specific binding of BMP2 remained an issue with the alternative construction of biomimetic platforms on glass substrates. We first characterized *via* QCM-D the binding of BMP2 on glass biomimetic platforms, as depicted in **Fig 1C**. Our results indicated that specific binding on HS was approximately threefold greater than non-specific binding on RGD-functionalized platforms. However, dissociation from HS platforms seemed quicker than from RGD platforms, suggesting that non-specific binding was relatively stable. We then plated C2C12 cells on glass biomimetic platforms to assess the impact of non-specific binding on RGD-functionalized platforms on pSMAD1/5/9 cellular response. In **Fig 1D**, we show that similarly to gold substrate platforms, the non-specific signaling is in the same range as the signaling mediated by HS-bound BMP2. Furthermore, we tested two different BMP2 concentrations and showed that the non-specific signaling is also dose-dependent, probably due to increased BMP2 adsorption at higher concentrations. The pSMAD1/5/9 level being an early marker of osteogenic differentiation, we then explored whether the non-specific

binding of BMP2 also influenced cellular signaling over an extended culture period. C2C12 cells were cultured on glass biomimetic platforms for 3 days before comparing their expression of alkaline phosphatase (ALP) as a marker of bone differentiation. We show in **Fig 1.E-F** that for 10  $\mu\text{g/mL}$  BMP2 concentration, the ALP expression was slightly lower on the RGD platform, yet remaining comparable to the ALP expression on HS platforms.

To explore if this non-specific binding was a unique feature of BMP2, we conducted a cellular experiment with IF analysis of nuclear pSMAD1/5/9 with other protein members of the BMP family, namely BMP4 and BMP7. As shown in **Fig 1.G**, for all BMPs, the non-specific signal induced by BMPs adsorbed on RGD-functionalized glass platforms was always comparable to the signal on HS-functionalized platforms. Of note, BMP2 purchased from another provider (R&D Systems) also induced non-specific signaling (data not shown).

Overall, the non-specific binding of BMP2 on glass or gold biomimetic platforms triggers an important signaling response, even if lower than on HS. The non-specific signal induced by adsorbed BMP2 was also found to be dose-dependent and was sustained for at least up to three days, as observed with ALP staining. The non-specific binding of BMP2 appears to be a characteristic shared with other members of the BMP family, such as BMP4 and BMP7.

### **BMP2 aggregates at physiological pH but native state can be rescued by Tween-20**

We noticed from the literature that BMP2 tends to aggregate under physiological pH conditions<sup>[23]</sup>. Considering that aggregation may contribute to significant non-specific binding, we explored whether the use of adequate buffer conditions to avoid BMP2 aggregation could prevent its non-specific adsorption. Given the isoelectric point (pI) of BMP2 is  $8.2 \pm 0.4$ , its solubility is greatly improved at acidic pH. To allow its interaction with negatively charged sulfate groups of GAGs, the pH must be below the pI where BMP2 is positively charged. In our research of BMP2 aggregation-free conditions, we used dynamic light scattering (DLS) to measure the size distribution of BMP2 particles in different buffers (**Fig 2.A-F**). In the recommended HCl stock buffer at pH 3.0, the mean particle size (hydrodynamic diameter) measured  $5.56 \pm 1.39$  nm, close to previously reported values for BMP2 in MES buffer at pH 5.0 with a diameter of  $7.8 \pm 0.7$  nm<sup>[23]</sup>. In contrast, as expected, BMP2 formed aggregates in Hepes and PBS buffers at pH 7.4, larger than 100 nm or 500 nm for Hepes and PBS, respectively. Interestingly, the addition of Tween-20 surfactant into the buffers rescued the native state of BMP2 observed in HCl buffer, with a mean particle size of  $7.62 \pm 0.4$  nm and  $6.87 \pm 0.67$  nm in Hepes-T and PBS-T, respectively. Alternatively, the use of below-neutral pH at 4.2 with an acetate buffer also conserved the initial state of BMP2 with a particle size of 5.24

$\pm 0.12$  nm. Hence, both pH adjustments and the use of Tween-20 surfactants preserve the native state of BMP2 and prevent its aggregation. It is worth noting that the use of HEPES buffer without salt also improved the BMP2 solubility, with a monitored particle size of  $13.3 \pm 1.7$  nm, which could be explained by complex salting-in and salting-out effects dependent on the salt concentration, as previously observed<sup>[24]</sup>. With the new conditions found to avoid BMP aggregation, we performed a cellular experiment on glass biomimetic platforms to investigate their effect on the non-specific BMP2 signaling. Unfortunately, the pSMAD1/5/9 level of C2C12 cells was still the same between HS and the non-specific conditions, both with HEPES-T or Acetate-T buffers, indicating that the BMP2 adsorption on platforms was not exclusively due to protein aggregation (**Fig 2.G**). Nevertheless, in subsequent experiments, we consistently included 0.02% Tween-20 in buffers to prevent BMP2 aggregation.

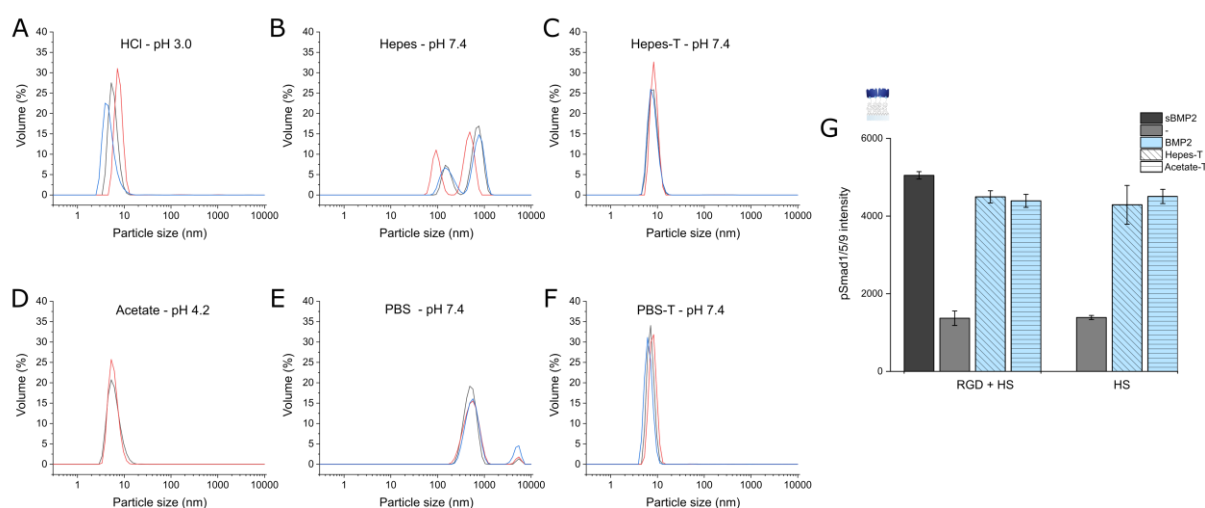


**Fig 2. DLS size distribution by volume of BMP2 at 100µg/mL in different buffers. A.** HCl 1mM, pH 3.0; **B.** HEPES, pH 7.4; **C.** HEPES-T, pH 7.4; **D.** Sodium acetate, pH 4.2; **E.** PBS, pH 7.4; **F.** PBS-T, pH 7.4. Triplicate measurements are represented in blue, black, and orange. **G.** Mean fluorescence intensity of nuclear pSMAD1/5/9 in C2C12 cells after a 90-minute culture on glass biomimetic platforms, with or without BMP2. BMP2 was incubated at 1 µg/mL either in HEPES-T (diagonal stripes) or acetate-T buffer (horizontal stripes). Mean fluorescence values are plotted  $\pm$  SD.

### BMP2 mainly binds non-specifically to the base substrate of biomimetic platforms

Given that BMP2 aggregation was not the primary reason for its non-specific adsorption, we next explored whether it could involve non-specific interactions with one of the components forming the biomimetic platforms. To this end, we assessed the BMP2 adsorption at different stages of the glass biomimetic platform construction using either a fluorescently labelled BMP2 (BMP2-rhodamine) or a specific polyclonal anti-BMP2 antibody (for the latter, microscopy images are shown in **Fig 3.A**).

The protein adsorption was quantified with a fluorescence plate reader, which highlighted that the binding of both BMP2 and BMP2-rhodamine was most pronounced on the bare glass

substrate (**Fig 3.B**). The functionalization with PLL or PLLgPEG significantly reduced the binding, although not to the extent of the negative control. The functionalization with SAV yielded no change in binding, and neither did RGD except for a slight change detected with the BMP2 antibody. However, further analysis with BLI revealed that there was no specific binding of BMP2 onto RGD (data not shown), suggesting that the observed variation was negligible. BMP2 bound effectively to HS, showing that even after rinsing steps, the amount of BMP2 seems to remain more important on the HS platforms than when non-specifically bound to the platforms.

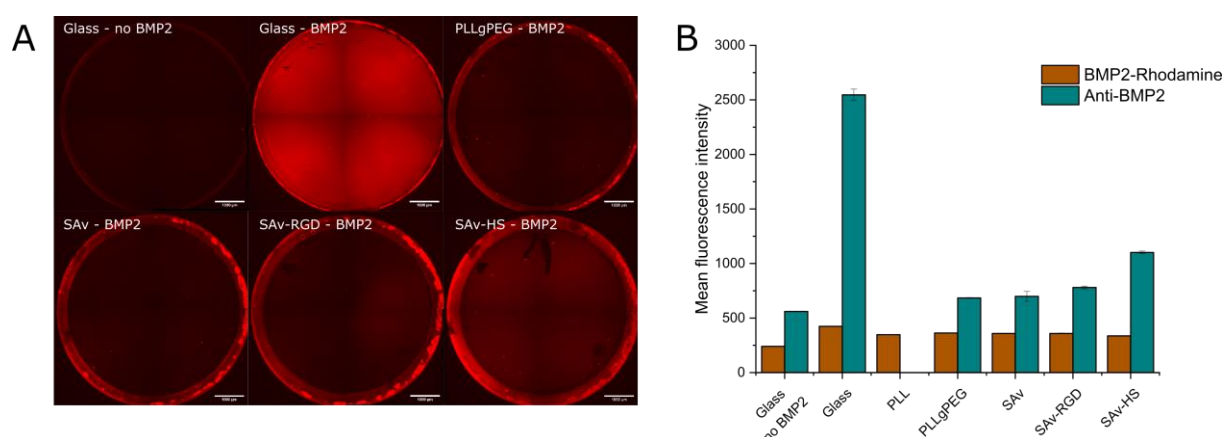


**Fig 3. A.** Representative fluorescence images of BMP2 binding detected via the anti-BMP2 antibody. **B.** Mean fluorescence intensity BMP2-Rhodamine or BMP2 detected with a specific antibody on glass biomimetic platforms after each functionalization step. Mean fluorescence values are plotted  $\pm$  SD.

In contrast to BMP2, the modified BMP2-rhodamine did not bind to HS, and even showed a slightly reduced fluorescence potentially related to the steric hindrance of HS chains. We indeed showed *via* QCM-D that the tagged BMP2 did not bind to HS (data not shown), certainly due to the labelling procedure primarily affecting the amine groups of lysine residues, some of which are present in the N-terminal BMP2 domain responsible for HS interaction<sup>[25]</sup>. Although the experiment was not conducted on gold platforms, the observed non-specific binding of BMP2 appears disconnected from the constituents of the platform (SAV, RGD). This implies that the predominant influence of non-specific BMP2 binding arises from the underlying substrate (glass or gold), which is insufficiently shielded by the PEG linkers. Increasing the grafting density of PEG chains should theoretically further reduce the binding. However, higher grafting densities of PEG on PLLgPEG copolymer products are not commercially available.

### **Non-specific binding is electrostatic and can be reduced to some extent by several blocking strategies**

Since the BMP2 adsorption arises from the underlying substrate of the biomimetic platforms (glass or gold), we attempted to reduce it by employing different blocking strategies to passivate the surfaces. We first tested in a cell experiment the effect of various blocking molecules after the functionalization of SAV and RGD, ensuring no interference with the initial steps of platform construction. As shown in **Fig 4.A**, we blocked the glass biomimetic platforms with either 3% BSA, 1 mg/mL myoglobin or m-PEG2-NHS-Ester. While BSA is a common choice, we also assessed myoglobin, which is approximately fourfold smaller (16 kDa, approximately the size of BMP2) and could potentially infiltrate PEG films more easily to bind to non-specific sites on the glass surface. To make sure that BMP2 did not bind onto the PLL, we employed an m-PEG2-NHS-Ester linker to react with amine groups of PLL lysine residues. This approach could also provide a way to increase the PEG density, potentially enhancing the platform anti-fouling properties.

However, none of these options reduced sufficiently the non-specific binding, since the pSMAD1/5/9 level was even higher than on HS signaling platforms. Comparable outcomes were observed when using Poloxamer 188 (also known as Pluronic<sup>®</sup> F-108), a non-ionic surfactant frequently employed in biological formulations. Poloxamer 188 is a tri-block copolymer of the form polyethylene oxide – polypropylene oxide – polyethylene oxide (PEO–PPO–PEO). It normally binds surfaces through its central PPO hydrophobic part, while the two PEO hydrophilic tails extend in solution. Self-assembled monolayers of Poloxamer 188 have demonstrated good anti-fouling properties<sup>[26]</sup>. However, probably due to restrained surfactant adsorption influenced by PEG chains on the platforms (QCM-D data not shown), the surfactant showed no effect on the non-specific signaling in our cellular assay.

For the following tests, we investigated with the anti-BMP2 antibody the efficacy of various conditions for passivating the surfaces; indeed SMAD1/5/9 is rapidly phosphorylated in the presence of a minimal amount of BMP2, preventing to be sensitive to small improvements of the passivation. As shown in **Fig 4.B**, we next tested an expanded range of reagents at high concentrations to prevent the binding of BMP2 on the platforms. Each reagent was used both in the blocking step and in the BMP2 incubation buffer. The binding was quantified *via* IF by the anti-BMP2 antibody. Remarkably, we observed that the non-specific binding was significantly reduced using 1 M of NaCl, indicating that it relies, at least in part, on electrostatic interactions. However, the use of high salt in our experimental setup could not be considered, as the binding of BMP2 to GAGs also involves electrostatic interactions. We also showed that

increasing the BSA concentration to 10% reduced the non-specific binding by about 80%, similarly to the 1 M NaCl condition. Trehalose, imidazole, glycine, and arginine were other compounds tested for blocking non-specific binding. All exhibited a moderately positive effect, reducing BMP2 adsorption on PLLgPEG by approximately 50%. Among these, trehalose displayed a slightly better effect than the other molecules and was thus used in combination with 10% BSA for the blocking step.

As shown in **Fig 4.C**, performing a blocking step with 10% BSA/0.6 M trehalose reduced the non-specific binding of BMP2 on PLLgPEG without affecting its binding to HS. The comparably lesser effect of the BSA and trehalose combination compared to the experiment shown in **Fig 4.B** could be attributed to inherent variability in non-specific binding across different experiments. In contrast, the combination of the blocking step with incubation of BMP2 in a HEPES-T buffer containing 10% BSA and 0.6 M trehalose further reduced the non-specific binding but also concurrently lowered the specific binding to HS. Overall, the precise contributions of BSA and trehalose in the blocking step or within the BMP2 incubation buffer remain unclear but their combination as blocking agents undoubtedly reduced the non-specific binding.

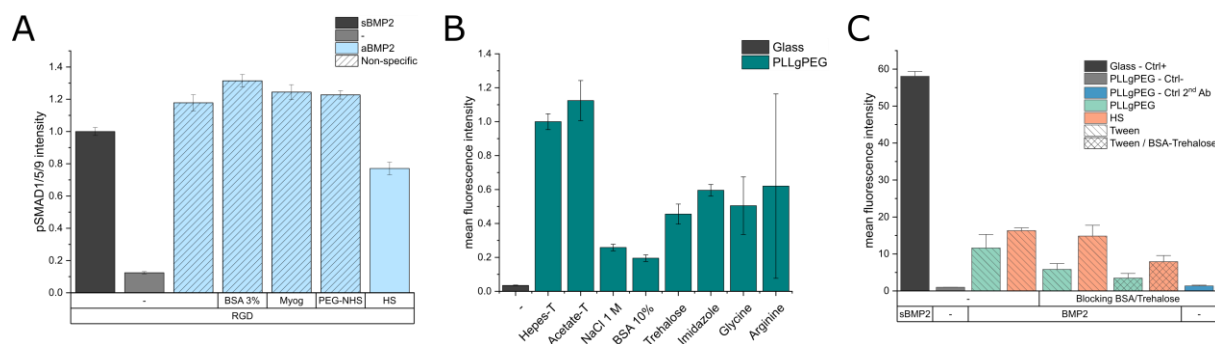


**Fig 4. A.** Mean fluorescence intensity of nuclear pSMAD1/5/9 in C2C12 cells after a 90-minute culture on glass biomimetic platforms, including a blocking step with either 3% BSA, 1 mg/mL myoglobin or m-PEG2-NHS-Ester. BMP2 was incubated at 1  $\mu$ g/mL in HEPES-T. Mean fluorescence values are plotted  $\pm$  SD.

**B.** Mean fluorescence intensity of BMP2 detected with a specific antibody on PLLgPEG-functionalized glass, using different reagents for blocking step and supplemented with Tween-20 for BMP2 incubation buffer. Negative control without BMP2 on glass is in gray. Means fluorescence values were normalized to the HEPES-T condition on PLLgPEG and plotted  $\pm$  SD.

**C.** Mean fluorescence intensity of BMP2 detected with a specific antibody. Intensity comparison on glass biomimetic platforms with or without HS, with different combinations of blocking and BMP2 incubation buffers: 1) No blocking and BMP2 in HEPES-T; 2) BSA/Trehalose blocking and BMP2 in HEPES-T; 3) BSA/Trehalose blocking and BMP2 in HEPES-T with BSA/Trehalose. BMP2 was incubated on platforms at 5  $\mu$ g/mL. A secondary antibody control on BSA-Trehalose blocked platforms was included (blue). Mean fluorescence values are plotted  $\pm$  SEM for at least two experiments.

## Gold-based biomimetic platforms prevent better BMP2 non-specific signal with respect to glass-based platforms

To explore the effects of BSA and trehalose in reducing the BMP2 non-specific signaling, we performed cellular experiments on gold and glass platforms with C2C12 and CHO cells, using two different blocking formulations: either 5% BSA alone or 10% BSA with 0.6 M trehalose. We show in A-B the comparison of the mean nuclear pSMAD1/5/9 intensity between the non-specific signal (RGD) and the signal mediated by HS platforms (RGD+HS), considering distinct platform substrates and passivation conditions. If the basal non-specific signaling seemed to be reduced for CHO cells compared to C2C12 cells, there was a consistent reduction of non-specific signaling on gold platforms compared to glass platforms, for both cell types. Indeed, while the surface passivation with 5% BSA on glass platform only slightly reduced the non-specific signal, the reduction amounted to approximately 50% on gold platforms. In comparison to BSA at 5%, the application of the BSA/trehalose mix reduced slightly more the C2C12 non-specific signal on glass platforms (**Fig 5.A**) and reduced it importantly on gold platforms for CHO cells (**Fig 5.B**). Surprisingly, BSA/trehalose blocking on gold platforms with C2C12 cells led to a strikingly elevated pSMAD1/5/9 intensity. Overall, the gold platforms seem to provide better anti-fouling properties compared to glass platforms, probably due to a more organized layer or PEG chains. Additionally, CHO cells apparently displayed reduced responsiveness to non-specifically bound BMP2 in comparison to C2C12 cells, making them potentially more appropriate cellular models for limiting the impact of non-specific signaling.

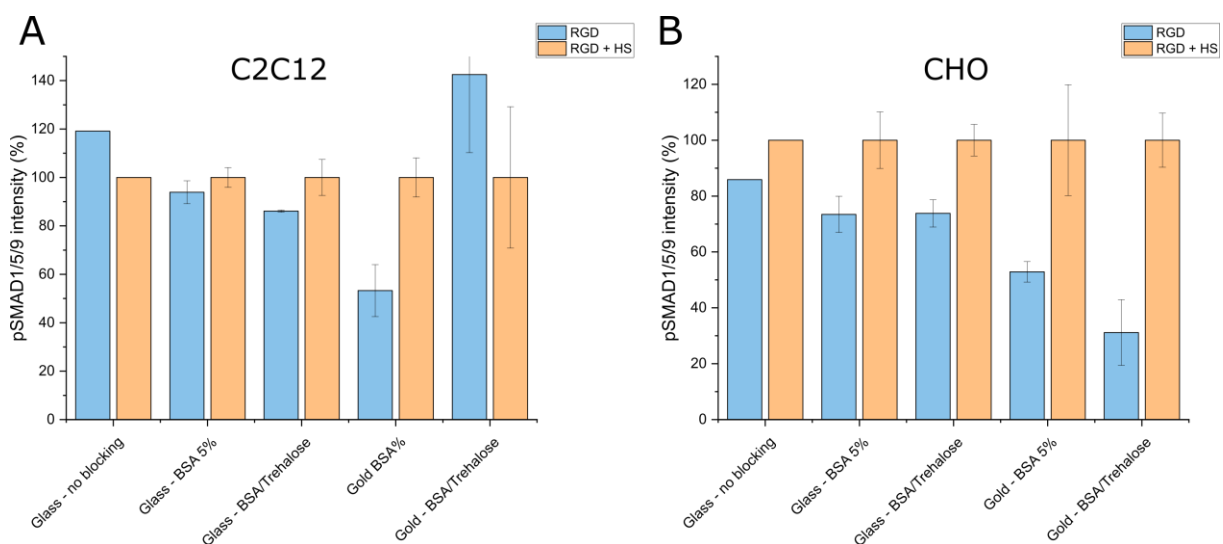


**Fig 5.** Mean fluorescence intensity of nuclear pSMAD1/5/9 in **A.** C2C12 or **B.** CHO cells after a 90-minute culture on glass or gold biomimetic platforms functionalized, including a blocking step with 5% BSA or BSA/Trehalose (10%/0.6M) before BMP2 incubation. Mean fluorescence values are normalized to each HS condition  $\pm$  SD.

## Discussion

In summary, our study highlights that moderate protein non-specific binding on biomaterials (here BMP2 on biomimetic platforms) can trigger an important cell signaling response. The non-specific binding of proteins on biomaterials should be considered in their design and for applications – both *in vitro* and *in vivo* – to correctly interpret the effect of biomaterials on the bioactivity of proteins. During our investigations, the BMP2-induced non-specific signaling initially prevented us from elucidating the distinct roles of GAGs in BMP2 signaling regulation. We established that this non-specific adsorption (and signaling) was dose-dependent, relatively stable, bioactive for up to three days, and was present independently of the biomimetic platform substrate (glass or gold). This issue was also extended to other BMP family proteins, including BMP4 and BMP7. We determined that the primary cause of non-specific binding is the platform's underlying substrate (glass or gold), rather than its constituents like SA<sub>v</sub> or RGD. To tackle this issue, we next explored conditions susceptible to reducing the non-specific signaling. Addressing this challenge was complex, with the objectives of retaining the GAG-binding capacity of BMP2, preserving the substrate transparency for high-throughput microscopy, and avoiding interference with the platform construction.

We investigated the BMP2 aggregation in different media and confirmed that BMP2 aggregates at physiological pH but can be solubilized with acidic pH buffers<sup>[23]</sup>. Remarkably, we discovered that the addition of surfactants such as Tween-20 could prevent BMP2 aggregation, even at neutral pH. Of note, the use of Hepes buffer without salt also enhanced BMP2 stability, likely due to complex “salting-out” and “salting-in” effects. As previously observed, the addition of NaCl in MES buffer (pH 5) was demonstrated to cause BMP2 precipitation at concentrations of only 80 mM NaCl (salting-out)<sup>[24]</sup>. Further increasing the NaCl concentration above 0.3 M increased the solubility (salting-in) until decreasing again above 1 M.

Our research revealed that BMP2 non-specific adsorption relies on electrostatic interactions that could be disrupted with high salt concentrations, though not compatible with GAG-BMP2 interactions. We then showed that some blocking reagents at high concentrations, in particular BSA and trehalose, could reduce the BMP2 non-specific binding by 50 % to 80 %. Although this study did not focus on clarifying the specific contributions of BSA and trehalose as blocking agents or additives in the BMP2 buffer formulation, their combined use as blocking agents unequivocally led to an important reduction of the non-specific binding.

While BSA is commonly used in immunofluorescence both for the blocking step and as an additive in the incubation of antibodies, the use of trehalose has been primarily in biological formulations<sup>[27,28]</sup>. Trehalose, recognized for preventing protein aggregation, has been studied

in particular for treating neurodegenerative diseases, such as Alzheimer and Huntington<sup>[29]</sup>. It also showed some interesting properties in biolayer interferometry studies as an additive for reducing non-specific binding<sup>[30]</sup>. Interestingly, a patent described the use of 5% trehalose to block functionalized surfaces, resulting in reduced serum protein adsorption<sup>[31]</sup>.

Our findings suggested that CHO cells might be less sensitive to non-specifically bound BMP2 than C2C12 cells. We also determined that under identical blocking conditions, gold platforms exhibited superior anti-fouling properties compared to glass. The distinct PEG-based linkers for the different substrates may contribute to these differences. Therefore, out of the scope of this study, another option to reduce the non-specific signaling could be to design alternative constructions of the platforms with improved anti-fouling properties. Potential strategies include the functionalization of poloxamers conjugated with an appropriate amount of biotin to build the streptavidin monolayer. Other strategies inspired by cell membrane properties could be considered, such as the functionalization of phosphorylcholines (PC) exhibiting non-fouling properties<sup>[32,33]</sup>. Studies on protein adsorption with PC phospholipid films underscored their strong resistance to protein adsorption<sup>[34–36]</sup>. Preferably, platform development should be achieved on optical transparent surfaces for compatibility with established high-throughput functionalization and readout strategies. Improving coating stability for long-term cellular culture involves employing covalent or nearly covalent immobilization strategies to withstand cell traction forces<sup>[37]</sup>.

Although some residual non-specific signaling persisted under the established blocking conditions (BSA/Trehalose), it was reduced enough to investigate a biological outcome, highlighting the potent role of HS as an extracellular GAG in mediating BMP2 signaling (**Chapter V**). However, minor effects of other GAGs may remain undetected due to the significant residual non-specific signaling. Thorough investigations of a broader range of blocking or formulation agents could potentially reveal more relevant conditions to reduce the BMP2 non-specific adsorption. Moreover, exploring their contribution in the blocking step or as additives during the incubation process may provide interesting insights.

In summary, the findings of this study have implications for the design of biomaterials intended for investigating cellular responses upon bound proteins. Despite a relatively low non-specific protein binding detected *via* biophysical surface characterization techniques, it does not exclude a potentially significant impact at the cellular level. This study also provides new information about BMP2 aggregation and adsorption at surfaces. We show in particular that the combination of BSA and trehalose exhibits good performance as a blocking agent. Although the significant bioactivity of non-specifically bound BMP2 was an issue in our case, this study demonstrated

the potential of biomaterials with bare glass in effectively retaining and delivering biologically active BMP2, as previously investigated<sup>[38]</sup>.

## Acknowledgments

We would like to thank Marianne Weidenhaupt and Franz Bruckert for fruitful discussions and the use of the DLS equipment at the LMGP Grenoble. We would like to acknowledge the PTA facility, Upstream Technological Platform, for the use of the evaporator equipment. This work used the platforms of the Grenoble Instruct-ERIC center (ISBG; UAR 3518 CNRS-CEA-UGA-EMBL) within the Grenoble Partnership for Structural Biology (PSB), supported by FRISBI (ANR-10-INBS-0005-02) and GRAL, financed within the University Grenoble Alpes graduate school (Ecoles Universitaires de Recherche) CBH-EUR-GS (ANR-17-EURE-0003). Authors acknowledge the BLI platform scientific responsible, Jean-Baptiste REISER Ph.D., for its help and assistance. This work was funded by the ANR (GlyCON, grant number [ANR-19-CE13-0031-01 PRCI] and by the “Investissements d’avenir” program Glyco@Alps, grant number [ANR-15-IDEX-02]. This work has been supported by CNRS GDR 2088 “BIOMIM”, ANR-17-EURE-0003 and GRAL. IBS (Institut de Biologie Structurale) acknowledges integration into the IRIG (CEA).

## References

- [1] J. Sefkow-Werner, J. Le Pennec, P. Machillot, B. Ndayishimiye, E. Castro-Ramirez, J. Lopes, C. Licitra, I. Wang, A. Delon, C. Picart, E. Migliorini, *ACS Appl. Mater. Interfaces* **2022**, *14*, 34113.
- [2] P. Silva-Bermudez, S. E. Rodil, *Surf. Coat. Technol.* **2013**, *233*, 147.
- [3] J. Y. Lichtenberg, Y. Ling, S. Kim, *Sensors* **2019**, *19*, 2488.
- [4] J. D. Andrade, V. Hlady, in *Biopolym.-Exclusion HPLC*, Springer, Berlin, Heidelberg, **1986**, pp. 1–63.
- [5] J. B. Schlenoff, *Langmuir* **2014**, *30*, 9625.
- [6] H. Otsuka, Y. Nagasaki, K. Kataoka, *Curr. Opin. Colloid Interface Sci.* **2001**, *6*, 3.
- [7] B. K. D. Ngo, M. A. Grunlan, *ACS Macro Lett.* **2017**, *6*, 992.
- [8] S. Lowe, N. M. O’Brien-Simpson, L. A. Connal, *Polym. Chem.* **2014**, *6*, 198.
- [9] X.-F. Xiao, X.-Q. Jiang, L.-J. Zhou, *Chin. J. Anal. Chem.* **2013**, *41*, 445.
- [10] R. Michel, S. Pasche, M. Textor, D. G. Castner, *Langmuir ACS J. Surf. Colloids* **2005**, *21*, 12327.
- [11] L. Li, S. Chen, S. Jiang, *J. Biomater. Sci. Polym. Ed.* **2007**, *18*, 1415.
- [12] E. Migliorini, D. Thakar, R. Sadir, T. Pleiner, F. Baleux, H. Lortat-Jacob, L. Coche-Guerente, R. P. Richter, *Biomaterials* **2014**, *35*, 8903.
- [13] E. Migliorini, P. Horn, T. Haraszti, S. V. Wegner, C. Hiepen, P. Knaus, R. P. Richter, E. A. Cavalcanti-Adam, *Adv. Biosyst.* **2017**, *1*, 1600041.
- [14] J. Sefkow-Werner, P. Machillot, A. Sales, E. Castro-Ramirez, M. Degardin, D. Boturyn, E. A. Cavalcanti-Adam, C. Albiges-Rizo, C. Picart, E. Migliorini, *Acta Biomater.* **2020**, DOI 10.1016/j.actbio.2020.07.015.

- [15] A. Sales, V. Khodr, P. Machillot, L. Chaar, L. Fourel, A. Guevara-Garcia, E. Migliorini, C. Albigès-Rizo, C. Picart, *Biomaterials* **2022**, 121363.
- [16] I. Marquetti, S. Desai, *Int. J. Mol. Sci.* **2022**, *23*, 2432.
- [17] I. Marquetti, S. Desai, *Chem. Phys. Lett.* **2018**, *706*, 285.
- [18] B. Huang, *Mater. Today Commun.* **2023**, *34*, 105307.
- [19] T. Utesch, G. Daminelli, M. A. Mroginski, *Langmuir* **2011**, *27*, 13144.
- [20] A. F. Oliveira, S. Gemming, G. Seifert, *Mater. Werkst.* **2010**, *41*, 1048.
- [21] X. Dong, Q. Wang, T. Wu, H. Pan, *Biophys. J.* **2007**, *93*, 750.
- [22] D. Thakar, F. Dalonneau, E. Migliorini, H. Lortat-Jacob, D. Boturyn, C. Albigès-Rizo, L. Coche-Guerente, C. Picart, R. P. Richter, *Biomaterials* **2017**, *123*, 24.
- [23] J. Sundermann, H. Zagst, J. Kuntsche, H. Wätzig, H. Bunjes, *Pharmaceutics* **2020**, *12*, E1143.
- [24] B. Quaas, L. Burmeister, Z. Li, A. Satalov, P. Behrens, A. Hoffmann, U. Rinas, *Pharm. Res.* **2019**, *36*, 184.
- [25] P. C. Billings, E. Yang, C. Mundy, M. Pacifici, *J. Biol. Chem.* **2018**, *293*, 14371.
- [26] Y. Chang, W.-L. Chu, W.-Y. Chen, J. Zheng, L. Liu, R.-C. Ruaan, A. Higuchi, *J. Biomed. Mater. Res. A* **2010**, *93A*, 400.
- [27] N. K. Jain, I. Roy, *Protein Sci. Publ. Protein Soc.* **2009**, *18*, 24.
- [28] J. K. Kaushik, R. Bhat, *J. Biol. Chem.* **2003**, *278*, 26458.
- [29] M. Khalifeh, G. E. Barreto, A. Sahebkar, *Neural Regen. Res.* **2021**, *16*, 2026.
- [30] A. Dubrow, B. Zuniga, E. Topo, J.-H. Cho, *ACS Omega* **2022**, *7*, 9206.
- [31] G. Jogikalmath, *Method for Blocking Non-Specific Protein Binding on a Functionalized Surface*, **2008**, WO2008055080A2.
- [32] S. Chen, J. Zheng, L. Li, S. Jiang, *J. Am. Chem. Soc.* **2005**, *127*, 14473.
- [33] V. A. Tegoulia, W. Rao, A. T. Kalambur, J. F. Rabolt, S. L. Cooper, *Langmuir* **2001**, *17*, 4396.
- [34] R. Richter, A. Mukhopadhyay, A. Brisson, *Biophys. J.* **2003**, *85*, 3035.
- [35] E. Migliorini, D. Thakar, J. Kühnle, R. Sadir, D. P. Dyer, Y. Li, C. Sun, B. F. Volkman, T. M. Handel, L. Coche-Guerente, D. G. Fernig, H. Lortat-Jacob, R. P. Richter, *Open Biol.* **n.d.**, *5*, 150046.
- [36] P. Vermette, V. Gauvreau, M. Pézolet, G. Laroche, *Colloids Surf. B Biointerfaces* **2003**, *29*, 285.
- [37] C. Jurchenko, Y. Chang, Y. Narui, Y. Zhang, K. S. Salaita, *Biophys. J.* **2014**, *106*, 1436.
- [38] B. Huang, Y. Yuan, C. Liu, *Appl. Mater. Today* **2020**, *19*, 100599.



## **Chapter VII. Discussion and perspectives**

Along the years spent on this PhD work and while redacting the thesis, several questions and perspectives for future research have emerged. These elements are discussed in the following section.

### **Automation of biomaterial functionalization**

The automation of the biomimetic SA<sub>v</sub> platform functionalization paves the way for future research, allowing the investigation of a wide range of conditions. Furthermore, this automated setup could be applied to any other biomaterial to functionalize various conditions with multiple peptides, GAGs, or growth factors, in a single experiment. Combined with a high-content fluorescence readout developed in the team, the experimental setup is particularly adapted to explore the levels of signaling markers that are translocated in the nuclei of cells, such as pSMAD1/5/9, RUNX2 or Osterix for BMP signaling. Moreover, it allows quantifying the cell area, cell morphology parameters, and the cytoplasmic expression of some markers. However, improvements will be necessary to employ high-resolution imaging, qPCR, and WB as readouts since they are so far not compatible with high-throughput analysis.

### **Reduction of the BMP2 non-specific adsorption**

Significant time and effort were spent to address the issue of the unexpected non-specific binding of BMP2 on the biomimetic SA<sub>v</sub> platforms. We managed to optimize the experimental conditions, leading to a strong reduction of this signal and allowing the successful study into the role of GAGs in BMP signaling. However, the anti-fouling properties of the SA<sub>v</sub> platforms are not yet entirely satisfactory. Indeed, the BMP2-induced non-specific signaling remained too high to identify distinct effects between HA, DS, and different CS. More importantly, the non-specifically bound BMP2 hindered our investigation of BMP2 signaling regulation mediated by HS-oligosaccharides from our homemade library. Nevertheless, the technical developments achieved opened perspectives for further reducing the non-specific signaling.

First, tools have been developed in the lab for investigating the amount of non-specific BMP2 adsorption. QCM-D measurements lacked the necessary sensitivity to detect the importance of non-specific adsorption, whereas the highly sensitive cellular experiments were regrettably highly time-consuming. We identified a commercial anti-BMP2 antibody that proved to be sensitive enough to detect and compare the amount of BMP2 adsorption in various conditions, with a shorter experimentation time compared to cellular experiments.

Since future applications of the biomimetic SA<sub>v</sub> platforms may be hampered by non-specific BMP2 adsorption, this antibody provides a good tool for performing an extensive screening of

blocking reagents that may reduce it. Such screening could investigate the effects of a wide range of compounds both for the blocking step and as additives in the BMP2 incubation buffer, and possibly for the rinsing step. Common blocking reagents that were not tested during this thesis could be included, such as casein or glucose. Although powdered milk and serum are commonly employed blocking reagents, their use may generate additional problems since they contain growth factors that could have consequences on the BMP or other signaling pathways. The use of more stringent rinsing of BMP2 after incubation on the platforms could also be investigated. In our study, we found that a 1 M NaCl concentration reduced strongly the BMP2 non-specific adsorption, but a previous study showed that BMP2 elutes from a Hep-Sepharose column at already ~580 mM NaCl<sup>[487]</sup>. Concentrations of NaCl below this threshold might have a positive influence, but it certainly constitutes a delicate compromise between disrupting non-specific interactions while maintaining GAG-BMP2 interactions.

Our findings revealed that the addition of 0.02% Tween-20, such as in BLI experiments, prevented the aggregation of BMP2, even at unfavorable neutral pH. We subsequently used 0.02% Tween-20 for the incubation of BMP2 on the biomimetic platforms. We have not explored whether the presence of Tween-20 could influence the blocking capacity of BSA and trehalose passivation. However, both Tween-20 and Tween-80 surfactants have been previously demonstrated to improve the passivation of PEG-coated glass substrate, when used at concentrations of 1-5 % (v/v) in a blocking step<sup>[488]</sup>. Therefore, the use of higher concentrations of Tween-20 in the BMP2 incubation buffer but also in the blocking step may further reduce the non-specific binding. Since Tween-20 molecules form micelles when above their critical micelle concentration ( $\sim 0.06 \cdot 10^{-3}$  M,  $\sim 0.007$  % (v/v)), BMP2 molecules might be trapped into the micelles which could prevent the non-specific interactions but it might also affect the interactions with GAGs. Consequently, the use of low Tween-20 concentrations may be preferable for the incubation with BMP2 to prevent its aggregation while high concentrations may be appropriate for the blocking step. In a review about Tween surfactants, the time to establish equilibrium at the interface was reported as a potential factor of importance regarding their ability to prevent protein adsorption<sup>[489]</sup>.

In addition to these strategies, the non-specific adsorption of BMP2 could be reduced by using alternative designs for constructing the biomimetic SA<sub>v</sub> platforms (see below).

## Development of the biomimetic SA<sub>v</sub> platforms

As mentioned in the introduction, several strategies have been proposed for building biomaterials with a SAM of SA<sub>v</sub>.

The construction of SAMs on oxide-free metal substrates (like gold) *via* thiols and dithiols is probably the most characterized<sup>[459]</sup>. SAMs built on gold planar surfaces are generally sketched as a perfect monolayer, but can in fact be affected by several types of defects, such as vacancy islands or disordered regions. This can be partially explained by structural defects in the gold layer itself, like steps and dislocations<sup>[459]</sup>. In our case, defects in the SAM of thiol-PEG and thiol PEG-biotin may arise from imperfections from the gold-sputtering process performed in a clean room with evaporator equipment. To maintain the transparency of the SA<sub>v</sub> platforms, only a thin gold layer of 8 nm is deposited on top of a chromium adhesion layer of 1.5 nm on a glass coverslip. In comparison, QCM-D crystals exhibit a gold thickness of more than 100 nm<sup>[490]</sup>. We can reasonably question whether the *ex situ* QCM-D characterization exactly matches the *in situ* functionalization process on a gold-sputtered surface. The particularly low BMP2 non-specific adsorption detected *via* QCM-D could be true for crystals with a thick gold layer, but not necessarily on more disordered gold surfaces. The *in situ* photobleaching ICS characterization method developed for glass biomimetic platforms could be particularly useful to examine this, but diffraction artifacts due to the gold layer may affect the analysis. Although it would prevent the use of high-content microscopy readout, we could prepare biomimetic platforms with increased gold thickness to evaluate if they prevent more efficiently non-specific adsorption. BMP2 adsorption could therefore be quantified by immunofluorescence with a top reading microplate reader, and BMP signaling could be quantified by Western Blot, qPCR, or ALP colorimetric staining, as alternatives to the IF analysis of nuclear pSMAD1/5/9.

As for glass platforms built with a PLLgPEG(biotin50%) linker, they come with great advantages of fabrication simplicity, allowing high-throughput and optical transparency. Glass constitutes a material of choice for building biomimetic platforms with the commercial availability of high-capacity glass-bottom plates (96-well, 384-well, and more). However, the glass-based platform construction with PLLgPEG(biotin50%) linker presents lower anti-fouling properties compared to gold-based platforms with thiol-PEG and thiol-PEG-biotin. The binding of PLLgPEG on the glass surface requires a surface activation step. Both UV/Ozone and plasma O<sub>2</sub> treatment are reported as suitable methods for surface activation, and we adopted the UV/Ozone method. The literature states that UV/Ozone activation is softer than plasma-based methods causing fewer cracking failures, but it is more time-consuming with increased

exposition times<sup>[491,492]</sup>. QCM-D experiment could explore whether the two activation methods lead to similar platform construction by comparing the frequency shift obtained upon PLLgPEG, SAV-RGD, and GAG binding. Furthermore, the BMP2 non-specific binding should be tested with an anti-BMP2 antibody since it might be possible that the two activation methods induce different conformations in the binding of the PLLgPEG, leading to altered anti-fouling properties. Anyway, the PLLgPEG linker appears not to be the most appropriate for long-term cellular culture, as observed with increased cellular detachment and clustering at 2-3 days of culture in comparison to the gold-based platforms<sup>[283]</sup>. This phenomenon could derive from the traction forces exerted by adhering cells that may disrupt the electrostatic interactions of PLLgPEG. For investigating the BMP signaling mediated by GAGs in the late stages of BMP signaling such as ALP readout at 3 days or even other applications requiring long-term cultures, the cellular detachment could constitute an issue. Therefore, the development of other platform construction strategies with covalent linkages to the glass substrate should be considered.

Commercial SAV-coated BLI biosensors are also based on a glass substrate and patents from ForteBio company suggest that these sensors are functionalized either with biotin-conjugated silane or lipid molecules<sup>[493,494]</sup>. Since the non-specific binding of BMP2 detected on BLI biosensors is extremely low, both functionalization strategies could have potential for the design of novel biomimetic SAV platforms on glass substrates.

Previously, biomimetic SAV platforms have been constructed on a lipid bilayer to form an SAV monolayer<sup>[461]</sup>. Nevertheless, there were reasonable concerns regarding the platform stability and whether the lipid bilayer could withstand the mechanical forces exerted by adhering cells.

The most common functionalization approach for glass substrate is the silanization of glass surfaces, which is generally achieved via oxysilane precursors, providing a covalent linkage. Previous investigations in the team using this strategy however faced high levels of BSA non-specific adsorption in comparison to gold platforms, which later oriented our choice towards PLLgPEG linkers. However, the good antifouling performance of SAV-coated BLI biosensors suggests that alternative silane molecules could be used to optimize the functionalization of SAV platforms. The stable covalent bond could provide better support for long-term cultures, provided that biotin-SAV linkages are sufficiently stable to withstand cell adhesion<sup>[495]</sup>.

Alternatively, an option that we have not yet explored is the recently developed graft copolymer PAcrAm<sup>TM</sup>-g-PEG presenting a polyacrylamide backbone, a silane group for covalent binding with the silicon oxide, an amine group for electrostatic binding to the surface, and an N3 group

to allow functionalization of bio-functional groups such as biotin. This copolymer has been shown to confer resistance to protein adsorption and was suitable for cellular studies with the functionalization of RGD peptides<sup>[467]</sup>.

Finally, the platform construction could also be inspired by polyelectrolyte multilayers. Boulmedais and coworkers prepared films made of PLL/poly(1-glutamic acid) (PLL/PGA) multilayers, ending with several PLL/PGA-g-PEG bilayers that provide protein and bacterial adhesion resistance<sup>[496]</sup>. A similar design with biotin-conjugated PEG chains (PLL/PGA-g-PEG-biotin or PLLgPEG-biotin/PGA bilayers) could be an interesting strategy for building SAv platforms. However, some concerns about the SAv molecular organization can be raised due to the uncontrolled conformation of the adsorbed polyelectrolytes.

Overall, it is uncertain if a single design of biomimetic SAv platforms could be adapted to all desired applications (optical transparency, long-term culture, antifouling properties, etc...) and the development of several design alternatives could provide a panel of different biomaterial constructions each more adapted for specific purposes.

### **The role of GAGs in BMP signaling**

The role of GAGs in BMP signaling appears to be dependent on several factors, which will be discussed here. Of significant importance, GAGs or PGs may exhibit distinct regulatory functions on BMP signaling depending on their localization. This aspect is not fully understood since it is practically complex to distinguish the role of cell-surface GAGs from the one of extracellular GAGs.

### **The role of cell-surface GAGs**

Our BLI experiments revealed that CS and DS have a much lower affinity for BMP2 than HS, with a slower association and a faster dissociation of BMP2. These findings indicate a transient nature of CS-BMP2 interactions, which could explain the positive role of cell-surface CS on SMAD1/5/9 phosphorylation that we observed with soluble BMP2. We speculate that the transient nature of these interactions facilitates the binding of BMP2 to its receptors, potentially by attracting BMP2 close to the cell surface where it dissociates quickly from CS to interact with BMP receptors. In contrast, the role of cell-surface HS is not entirely clear in our results but it is more in favor of an inhibitory effect of HS on SMAD1/5/9 phosphorylation, such as previously observed in the literature<sup>[6,304]</sup>. In this study, we assume that the extracellular GAGs synthesized by cells have only a minor effect and that the observed differences are mainly due to the cell-surface GAGs, due to the short experiment time and the simultaneous incubation of

CHO cells with sBMP2. It is worth noting that our experiments were performed with a relatively high concentration of soluble BMP2 (0.1  $\mu\text{g/mL}$ ) and were focused on early BMP signaling with the SMAD1/5/9 phosphorylation after 90 minutes of culture. Future studies could investigate whether these findings are reproducible at different concentrations or different stages of BMP signaling, up to several days of culture, since GAGs may temporally alter BMP signaling.

### **The role of extracellular GAGs**

In contrast to cell-surface HS, our findings suggest that extracellular HS would promote SMAD1/5/9 phosphorylation by binding and delivering BMP2 to the cells. The SMAD1/5/9 phosphorylation being an early readout of BMP signaling, the effect of HS in later steps of BMP signaling could be different. However, several studies highlight the role of extracellular HS in sustaining the BMP signaling longer than without GAGs<sup>[264,283]</sup>, and many *in vivo* studies reported that BMP-delivery biomaterials achieve better bone regeneration when incorporating HS or Hep<sup>[315,316,344,347,497]</sup>. These studies also indicate that HS/Hep modulate the release of BMP2 with a reduced initial burst and a more sustained delivery. Overall, our results and most findings in the literature (**Table 3**) suggest that extracellular HS in the presence of exogenous BMP positively influences the signaling by binding BMP2 and sustaining its delivery to the cells.

In contrast, our results did not demonstrate a significant role of extracellular CS, DS, or HA in mediating BMP2 signaling. This finding probably reflects the lower BMP2 binding capacity of these GAGs, with probably more protein washed away from the platforms during the incubation of rinsing steps of the functionalization, as suggested by our results from BLI and QCM-D. *In vivo*, CS hydrogels were demonstrated to be as performant as collagen sponges to trigger BMP2-induced bone formation in a critical-size femoral defect in rats<sup>[419]</sup>. However, it is now well established that collagen sponges have low affinity for BMP2 which triggers an initial burst release, and retaining only 5% of the protein after 14 days<sup>[498]</sup>. In another study, CS was unable to increase the ALP activity induced by BMP4 in C2C12 cells despite the very high concentrations tested (from 2 to 2800  $\mu\text{g/mL}$ )<sup>[499]</sup>, which is consistent with our data on the role of CS.

### **The effect of the GAG density**

In the aforementioned study, Hep strongly enhanced the ALP activity, in contrast to CS. Interestingly this effect was modulated by its concentration. Indeed, low concentration (2

$\mu\text{g/mL}$ ) enhanced slightly the ALP activity, intermediate concentrations (5-50  $\mu\text{g/mL}$ ) increased it strongly, while it gradually decreased with concentrations above 50  $\mu\text{g/mL}$  until abolishing completely the BMP4-induced ALP activity (700-2800  $\mu\text{g/mL}$ ). These data nicely illustrate a model where extracellular Hep/HS promotes BMP signaling at low concentrations by protecting it from degradation and the action of inhibitors, while it inhibits BMP signaling at high concentrations because of hampered BMP interaction with cell receptors due to rebinding on Hep/HS. Wang and Yang compared the incorporation of methacrylated HS and CS at different densities in hydrogels to induce chondrogenic differentiation of human MSCs. The GAG concentration was tuned between 20 mg/mL and 100 mg/mL and they observed that the highest amount of collagen types I and II and sulfated GAG neocartilage deposition was obtained for intermediate CS density (50 mg/mL). These findings indicate that GAG density has to be well regulated in tissues to induce a specific cellular response. Furthermore, the latter study was performed without additional BMP, suggesting that CS can induce chondrogenic differentiation in a BMP-independent manner. From a molecular point of view, increased densities of GAGs may trigger stronger BMP2 binding as previously shown by the cross-linking of HS chains<sup>[264]</sup>.

Overall, the above-mentioned effects of GAG concentration on the regulation of signaling suggest that the density of GAGs is an important parameter, as indicated in our review published in *Advanced Materials* (**Annex**).

To address the role of GAG density in BMP signaling, the SA<sub>v</sub> biomimetic platforms could be quite easily adapted to present different GAG densities on the SA<sub>v</sub> monolayer. After the functionalization of RGD on the platforms, the density of GAGs can be controlled by incubating biotinylated GAGs combined with other inert biotinylated molecules (biotin, biotin-PEG, or else) at well-controlled ratios. Since GAG chains would be more spaced with increased amounts of inert biotinylated molecules, we expect reduced cross-linking effects of BMP2 and a decreased binding capacity. The effect of adsorbed BMP2 on GAGs would be likely negatively correlated with the GAG density. However, the effect of soluble BMP2 may be more complex since it would provide insights into the BMP2 binding competition with BMP receptors and extracellular GAGs at different densities.

### **The role of distinct GAGs**

This modulatory role of HS appears to be crucial *in vivo* for ensuring bone tissue homeostasis *via* regulating BMP signaling, as observed with the increased BMP signaling and the formation

of exostoses in mice models upon ablation of EXT1 glycosyltransferase. Interestingly, it was reported in primary mice chondrocyte cultures that both a reduced HS synthesis and an altered HS sulfation lead to increased levels of CS, potentially linked to the increased aggrecan expression observed<sup>[11]</sup>. These findings suggest a compensation mechanism where cells sense the HS deficiency and balance it by an increased CS production.

While altered expression of CS sulfation enzymes has been associated with skeletal disorders (C4st1: mice chondrodysplasia; C6ST-1: Spondyloepiphyseal dysplasia), the link of CS with BMP signaling is less clear. So far, only the observed reduction of SMAD1/5/9 phosphorylation upon CS alteration in a few studies, including ours, indicate a role of CS in BMP signaling<sup>[11,314]</sup>. The role of CS in skeletal disorders may be attributed as well to the deregulation of other growth factor signaling pathways involved in cartilage and bone homeostasis, such as iHh (indian hedgehog), Wnt, or others<sup>[439,500–502]</sup>.

In our studies, HA did not trigger significant BMP2 signaling, which was consistent with the fact that BMP2 did not bind HA. However, previous findings highlighted that BMP7 signaling could be potentiated by HA in a way dependent on the CD44 cell-surface HA receptor<sup>[503]</sup>.

Although the role of KS has not been explored during this thesis, fibromodulin and mimecan KS PGs have been reported to be involved in bone development. Fibromodulin is expressed during fetal endochondral and intramembranous ossification and fibromodulin-deficient mice develop ectopic bone in tendon<sup>[504]</sup>. The binding of mimecan to BMP2 and BMP3 was shown to induce osteoinductive activity<sup>[39]</sup>. Therefore, future studies could explore whether KS plays a key role in BMP signaling.

### **Spatial regulation of BMP signaling mediated by GAGs**

It is now well established that GAGs play a significant role in the PG-mediated formation of BMP gradients. Studies in drosophila illustrate nicely this effect, which has also been observed in other species such as zebrafish and xenopus. In drosophila, sulfation of HS chains appeared essential for the establishment of these gradients, as shown by the alteration of pMAD signaling gradients across *sfl* (NDST enzyme encoding gene) mutant cells. It has been shown that cell-surface PGs (*Dally*, *Dly*) contribute to the gradient formation but the role of extracellular PGs is unclear. To our knowledge, the aggrecan hybrid KS/CS PG is the only extracellular PG that has been reported to contribute to the BMP gradient distribution<sup>[301]</sup>.

Lin and coworkers underscored in a review that the role of HSPGs in establishing BMP gradients appears to be tissue-dependent. This effect was highlighted in drosophila where the

embryonic dorsoventral patterning controlled by Dpp signaling was not defective in *sfl*, *ttv*, *sotv* and *botv* HSPG mutant cells, in contrast to the wing disc tissue where HSPGs are essential. They suggested that HSPGs would not be essential in tissues where BMP is abundant.

To explore this, the biomimetic SA<sub>v</sub> platforms could be employed with different sBMP2 concentrations to investigate whether extracellular GAGs modulate BMP signaling in a concentration-dependent manner. Furthermore, it could be interesting to perform a similar study with CHO mutants for GAG biosynthesis enzymes to explore if the effect of cell-surface GAGs is also dependent on the BMP2 concentration. At low soluble BMP2 concentrations, csHS might improve the signaling by attracting BMP2 near cell receptors while at high concentrations, csHS might inhibit signaling by slowing down the interaction of BMPs with receptors. To investigate the formation of gradients by GAG chains, ongoing developments to construct the biomimetic SA<sub>v</sub> platforms into microfluidic chips could provide a technical solution. After the functionalization of GAG chains in a compartment of the chip, we could investigate the restricted diffusion of BMP2 from its injection channel *via* a specific antibody or fluorescently labelled BMP2 (not affected in the HS-binding site). Furthermore, the signaling single-cell analysis of cells seeded onto this SA<sub>v</sub> platform could be correlated with the observed BMP2 gradient.

The variable expression of HS in tissues appears to control BMP signaling locally. This was observed in the perichondrium cells of mice long bones, which highly express HS, and where *Ext1* ablation led to increased BMP signaling and ectopic bone formation<sup>[6,304]</sup>. In this context, HS was suggested to exert a boundary role along the chondro-perichondrial border, where it would prevent excessive and ectopic BMP signaling.

Since the spatial distribution of morphogens such as BMP must be tightly controlled during embryonic development, one could wonder whether the variable expression of GAG modification enzymes (epimerase, sulfotransferases, sulfatases) in cells contributes to the finely controlled BMP gradients. So far, the visualization of sulfation patterns in tissues remains very complex, but the development of techniques such as MALDI-FT-ICR mass spectrometry (described in the review article in Annex) may provide a solution.

### **HS sulfation patterns for BMP2 binding and bioactivity**

This thesis explored whether BMP2 responds particularly to specific sulfation patterns as shown for other growth factors (AT III, FGF). Such features would be of utmost importance for the bioactivity of BMP2. Previous findings indicated that sulfation motifs exhibit distinct

importance for binding and bioactivity of BMP2, with a main role of N- and 6O-sulfates in comparison to 2O-sulfates. Using a library of oligosaccharides, we observed that high-affinity binding of BMP2 on HS-dp6 was achievable through locally high sulfated domains such as (IdoA(2S)-GlcNS(6S)). A few additional structural features of oligosaccharides were suggested to modulate as well the BMP2 binding. Molecular modeling will be performed by collaborators to correlate these experimental data with structural insights.

Furthermore, we intended to investigate the effects of the prepared HS-oligosaccharides in cellular studies with the biomimetic platforms. Unfortunately, preliminary results with the oligosaccharides were affected by the non-specific binding of BMP2 to some extent, even after optimization of the conditions to reduce the background. Our data suggests that the oligosaccharides were able to induce SMAD1/5/9 phosphorylation but within a close range to the non-specific signal. Therefore, we preferred to conserve these valuable HS-oligosaccharide materials for further studies, when the background signal will be sufficiently reduced. It will be particularly interesting to analyze how the cellular response induced by BMP2 on these oligosaccharides relates to our molecular interaction data.

In summary, many aspects regarding the involvement of GAGs in BMP signaling hold mysteries that could constitute the foundation of future research. The presented PhD work contributes to the comprehensive understanding of these intricate interactions by providing several novel insights. These achievements, among others of this thesis, are detailed in the following conclusion chapter.



## **Chapter VIII. Conclusion**

GAGs are known to modulate the BMP cell signaling *in vivo* and *in vitro* and their absence leads to skeletal defects, highlighting their role in the regulation of bone development. However, the precise role of GAGs in the regulation of BMP signaling remains unclear, even for HS and Hep, which have been extensively studied. The role of other GAGs in BMP signaling has been practically unexplored, leaving open questions about their role in this context. The interplay between GAGs and BMP holds significant importance for the design of BMP-delivering GAG-based biomaterials, and therefore, the effect of these interactions at the cellular level should be better understood to enable their safe use in clinics. All these different elements have been well explained in the introduction chapter of this thesis. Noteworthy, some sections of a review I have written about GAG-based biomaterials (Annex information, published in *Advanced Materials*) were integrated into this introduction.

The main objective of this thesis was precisely to decipher the effects of the interplay between BMP2 and various GAGs, aiming to provide fundamental knowledge for future applications.

We hypothesized that different GAGs may be involved in the regulation of BMP signaling, potentially in different manners. Therefore, we sought to compare the modulation of BMP2 signaling exerted by different GAGs, such as DS, HA and in particular, HS and CS. Additionally, we speculated that GAGs might elicit different signaling mechanisms when located at the cell surface or in the extracellular matrix, thereby contributing to the observed discrepancies in the literature. Specific sulfation motifs of Hep have been demonstrated to have different roles for the binding of BMP2 and its signaling, with N- and 6O- sulfates appearing to be the two most important motifs<sup>[324,327]</sup>. However, it remains unclear whether BMP2 interaction with HS is influenced by specific HS sequences characterized by key sulfation patterns. One approach for exploring that is to study the interactions of BMP2 with various oligosaccharides exhibiting specific sulfation patterns. To address that, I aimed to prepare a library of structurally defined HS-oligosaccharides.

### **Automated fabrication of biomimetic streptavidin platforms**

One main objective of my PhD project was to study the effect of GAGs and various oligosaccharides from this library in BMP signaling, performing cellular assays with biomimetic SAV platforms developed in the team. Due to the elevated number of conditions to test, we first aimed to automate and parallelize the fabrication of biomimetic SAV platforms. The developments achieved in this context have been the subject of a publication to ACS

Applied Materials & Interfaces, which I signed as second author. In particular, a novel construction of the platform on glass substrate using a PLLgPEG(biotin50%) allowed their fabrication in commercial 96-well plates, increasing as intended the throughput of our experimental setup. This approach circumvented the need to prepare gold-sputtered surfaces, a costly and time-consuming process. Simultaneously, the glass allowed high-resolution imaging, quantification of the molecular distribution homogeneity and the SAv layer molecular surface density. To automate their fabrication, I developed a new software (i.e. graphical user interface for parameters input) that enabled a fully automated and versatile workflow to functionalize up to three multiple-well plates in parallel (96-well, 48-well, 24-well, 12-wells, with glass or gold substrates). Administrative procedures are currently carried out for protecting the intellectual property of this process. Each well of the plate can correspond to a unique condition defined by the user with a graphical interface, involving up to 48 different solutions. In combination with a high-content imaging acquisition and analysis, the versatility of this setup provides a good tool to investigate a wide number of conditions with GAG compounds, peptides and growth factors.

### **Reduction of BMP2 non-specific adsorption**

We next intended to use this automated experimental setup for studying the effects of different GAGs in BMP signaling. Achieving this objective was rapidly hampered upon the discovery of the strong influence of moderate non-specific BMP2 adsorption on BMP signaling. A big amount of work was achieved to understand this non-specific adsorption and to reduce it. We determined that Tween-20, added to the running buffer, prevented BMP2 aggregation at neutral pH. We established the partly electrostatic nature of the BMP2 non-specific adsorption to the substrate, and we found that a combination of BSA and trehalose prevented it sufficiently to allow analysis of specifically GAG-bound BMP2 on the signaling. The efficacy of this blockage was improved when using SAv platforms built on gold compared to glass. This work was described in a manuscript that we intend to publish in an open archive (such as bioRxiv). Furthermore, I identified during this work an anti-BMP2 antibody with good specificity that was particularly useful for quantifying BMP2 amounts and investigating conditions to reduce BMP2 non-specific adsorption. This work has several implications for future studies with the SAv platforms. In particular, the control of non-specific signaling will be systematically tested and the blocking with BSA and trehalose will constitute a new step of the functionalization protocol.

## Role of GAGs in BMP2 signaling

This last part of my work signaling will constitute an article that provides novel insights about the role of GAGs in BMP2 signaling. With BLI technique, I succeeded in characterizing the molecular interactions between BMP2 and distinct GAGs. Among them, HS had a significantly higher affinity for BMP2 compared to CS, DS, and HA which did not bind to it. As expected, distinct types of CS (-A, -D, -E) bound differently to BMP2, with CS-D exhibiting a strong binding and CS-A a very weak binding. We highlighted that GAGs appear to have distinct roles when presented at the cell surface or in the ECM. The BSA-trehalose condition determined to reduce non-specific BMP2 adsorption have been employed to distinguish different effects of extracellular GAGs in BMP signaling. When BMP2 was presented to cells by extracellular GAGs using biomimetic SA<sub>v</sub> platforms, only HS was able to induce a significant signaling response. By employing CHO cell mutants for GAG biosynthesis enzymes, we could explore the effect of cell-surface GAGs. When located at the cell surface, we highlighted that HS appears to have rather a negative regulatory role on BMP signaling, while CS promotes short-term BMP signaling (pSMAD1/5/9). Finally, we explored the role of HS sulfation patterns in the binding of BMP2 by investigating with BLI the molecular interactions between BMP2 and a home-made library of 39 HS-tetrasaccharides and 28 HS-hexasaccharides that were prepared with a high level of purity and structurally characterized. We identified that a central trisulfated disaccharide motif (IdoA(2S)-GlcNS(6S)) within HS hexasaccharides improves BMP2 binding affinity, although BMP2 seemed to display a certain plasticity for different HS sulfation types and sequences. Due to the remaining level of non-specific BMP2 signaling on the SA<sub>v</sub> platforms, we could not perform cellular assays with the HS-oligosaccharides library. Nevertheless, this library constitute rare and valuable samples that could be used for future studies.

Part of the work for this article has been communicated in several conferences or meetings (**Poster** at GDR BIOMIM, October 2020; Prize of best **graphical abstract** EDCSV PhD day, June 2021; **Poster** at Proteoglycans Gordon Research Conference and Seminar, July 2022; **Presentation** at Glyco@Alps kickoff meeting, November 2022). We intend to publish this original article in a peer-reviewed journal with interests in the biology of the extracellular matrix or more specifically in the biological functions of carbohydrates.

# References

- [1] P. T. Cowan, P. Kahai, in *StatPearls*, StatPearls Publishing, Treasure Island (FL), **2023**.
- [2] R. A. Townley, H. E. Bülow, *Current Opinion in Structural Biology* **2018**, *50*, 144.
- [3] D. Hachim, T. E. Whittaker, H. Kim, M. M. Stevens, *Journal of Controlled Release* **2019**, *313*, 131.
- [4] Z. Sheikh, M. A. Javaid, N. Hamdan, R. Hashmi, *Materials (Basel)* **2015**, *8*, 1778.
- [5] B. Huang, Y. Yuan, C. Liu, *Applied Materials Today* **2020**, *19*, 100599.
- [6] J. Huegel, C. Mundy, F. Sgariglia, P. Nygren, P. C. Billings, Y. Yamaguchi, E. Koyama, M. Pacifici, *Dev Biol* **2013**, *377*, 100.
- [7] S. D. Vallet, C. Berthollier, S. Ricard-Blum, *Am J Physiol Cell Physiol* **2022**, *322*, C1271.
- [8] N. S. Gandhi, R. L. Mancera, *Chemical Biology & Drug Design* **2008**, *72*, 455.
- [9] L. Kjellén, U. Lindahl, *Current Opinion in Structural Biology* **2018**, *50*, 101.
- [10] D. Soares da Costa, R. L. Reis, I. Pashkuleva, *Annu Rev Biomed Eng* **2017**, *19*, 1.
- [11] V. Bachvarova, T. Dierker, J. Esko, D. Hoffmann, L. Kjellen, A. Vortkamp, *Matrix Biology* **2020**, DOI 10.1016/j.matbio.2020.03.006.
- [12] K. Lidholt, J. L. Weinke, C. S. Kiser, F. N. Lugemwa, K. J. Bame, S. Cheifetz, J. Massagué, U. Lindahl, J. D. Esko, *Proc Natl Acad Sci U S A* **1992**, *89*, 2267.
- [13] E. Bedini, A. Laezza, A. Iadonisi, *European Journal of Organic Chemistry* **2016**, *2016*, 3018.
- [14] H. Jiang, R. S. Peterson, W. Wang, E. Bartnik, C. B. Knudson, W. Knudson, *Journal of Biological Chemistry* **2002**, *277*, 10531.
- [15] M. Assunção, C. H. K. Yiu, H.-Y. Wan, D. Wang, D. F. E. Ker, R. S. Tuan, A. Blocki, *J. Mater. Chem. B* **2021**, *9*, 7205.
- [16] C. B. Knudson, *Birth Defects Research Part C: Embryo Today: Reviews* **2003**, *69*, 174.
- [17] L. Bohaumilitzky, A.-K. Huber, E. M. Stork, S. Wengert, F. Woelfl, H. Boehm, *Front Oncol* **2017**, *7*, 242.
- [18] L. O. Sampaio, I. L. S. Tersariol, C. C. Lopes, R. I. Bouças, F. D. Nascimento, H. A. O. Rocha, H. B. Nader, *Insights into Carbohydrate Structure and Biological Function, Transworld Research Network, Kerala* **2006**, *37*, 1.
- [19] U. Lindahl, M. Hook, *Annual Review of Biochemistry* **1978**, *47*, 385.
- [20] P. Wang, L. Chi, Z. Zhang, H. Zhao, F. Zhang, R. J. Linhardt, *Carbohydrate Polymers* **2022**, *295*, 119818.
- [21] J. E. Jorpes, S. Gardell, *Journal of Biological Chemistry* **1948**, *176*, 267.
- [22] A. Linker, P. Hoffman, P. Sampson, K. Meyer, *Biochimica et Biophysica Acta* **1958**, *29*, 443.
- [23] T. Annal, R. Wild, Y. Créton, R. Sadir, R. R. Vivès, H. Lortat-Jacob, *Molecules* **2020**, *25*, DOI 10.3390/molecules25184215.
- [24] A. L. Gray, R. Karlsson, A. R. E. Roberts, A. J. L. Ridley, N. Pun, B. Khan, C. Lawless, R. Luís, M. Szpakowska, A. Chevigné, C. E. Hughes, L. Medina-Ruiz, H. L. Birchenough, I. Z. Mulholland, C. L. Salanga, E. A. Yates, J. E. Turnbull, T. M. Handel, G. J. Graham, T. A. Jowitt, I. Schiessl, R. P. Richter, R. L. Miller, D. P. Dyer, *Cell Rep* **2023**, *42*, 111930.
- [25] L. E. Collins, L. Troeberg, *Journal of Leukocyte Biology* **2019**, *105*, 81.
- [26] J. Gallagher, *International Journal of Experimental Pathology* **2015**, *96*, 203.
- [27] X. Lin, *Development* **2004**, *131*, 6009.
- [28] D. Papy-Garcia, P. Albanese, *Glycoconj J* **2017**, *34*, 377.
- [29] M. Grünert, V. Nurcombe, S. M. Cool, *Curr Stem Cell Res Ther* **2008**, *3*, 1.
- [30] B. L. Farrugia, M. S. Lord, J. Melrose, J. M. Whitelock, *J Histochem Cytochem* **2018**, *66*, 321.
- [31] J. L. Dreyfuss, C. V. Regatieri, T. R. Jarrouge, R. P. Cavalheiro, L. O. Sampaio, H. B. Nader, *An. Acad. Bras. Ciênc.* **2009**, *81*, 409.
- [32] P. C. Billings, M. Pacifici, *Connect Tissue Res* **2015**, *56*, 272.
- [33] F. Gude, J. Froese, D. Manikowski, D. Di Iorio, J.-N. Grad, S. Wegner, D. Hoffmann, M. Kennedy, R. P. Richter, G. Steffes, K. Grobe, *Nat Commun* **2023**, *14*, 758.
- [34] In *Hyaluronic Acid*, John Wiley & Sons, Ltd, **2015**, pp. 1–8.
- [35] D. Jiang, J. Liang, P. W. Noble, *Physiological Reviews* **2011**, *91*, 221.
- [36] L. Sherman, J. Sleeman, P. Herrlich, H. Ponta, *Curr Opin Cell Biol* **1994**, *6*, 726.
- [37] D. Vigetti, E. Karousou, M. Viola, S. Deleonibus, G. De Luca, A. Passi, *Biochimica et Biophysica Acta (BBA) - General Subjects* **2014**, *1840*, 2452.
- [38] M. Suzuki, *The Journal of Biochemistry* **1939**, *30*, 185.
- [39] B. Catterson, J. Melrose, *Glycobiology* **2018**, *28*, 182.
- [40] V. H. Pomin, *International Journal of Biological Macromolecules* **2015**, *72*, 282.
- [41] L. Djerbal, H. Lortat-Jacob, J. Kwok, *Glycoconj J* **2017**, *34*, 363.
- [42] C. Malavaki, S. Mizumoto, N. Karamanos, K. Sugahara, *Connective Tissue Research* **2008**, *49*, 133.
- [43] F. N. Lamari, N. K. Karamanos, in *Advances in Pharmacology*, Academic Press, **2006**, pp. 33–48.

- [44] E. Bedini, M. M. Corsaro, A. Fernández-Mayoralas, A. Iadonisi, **2019**, DOI 10.13039/501100003329.
- [45] J. Martel-Pelletier, S. Kwan Tat, J.-P. Pelletier, *Osteoarthritis and Cartilage* **2010**, *18*, S7.
- [46] R. Menezes, R. Vincent, L. Osorno, P. Hu, T. L. Arinzeh, *Acta Biomaterialia* **2022**, DOI 10.1016/j.actbio.2022.09.064.
- [47] C. P. Mencio, R. K. Hussein, P. Yu, H. M. Geller, *J Histochem Cytochem*. **2021**, *69*, 61.
- [48] P. Kastana, E. Choleva, E. Poimenidi, N. Karamanos, K. Sugahara, E. Papadimitriou, *The FEBS Journal* **2019**, *286*, 2921.
- [49] A. Kinoshita, S. Yamada, S. M. Haslam, H. R. Morris, A. Dell, K. Sugahara, *Biochemistry* **2001**, *40*, 12654.
- [50] K. Higashi, Y. Okamoto, A. Mukuno, J. Wakai, S. Hosoyama, R. J. Linhardt, T. Toida, *Carbohydrate Polymers* **2015**, *134*, 557.
- [51] A. K. Shetty, T. Kobayashi, S. Mizumoto, M. Narumi, Y. Kudo, S. Yamada, K. Sugahara, *Carbohydr Res* **2009**, *344*, 1526.
- [52] C. I. Gama, S. E. Tully, N. Sotogaku, P. M. Clark, M. Rawat, N. Vaidehi, W. A. Goddard, A. Nishi, L. C. Hsieh-Wilson, *Nat Chem Biol* **2006**, *2*, 467.
- [53] R. S. Cavalcante, A. S. Brito, L. C. G. F. Palhares, M. A. Lima, R. P. Cavalheiro, H. B. Nader, G. L. Sasaki, S. F. Chavante, *Carbohydrate Polymers* **2018**, *183*, 192.
- [54] N. K. Karamanos, A. Syrokou, P. Vanky, M. Nurminen, A. Hjerpe, *Analytical Biochemistry* **1994**, *221*, 189.
- [55] G. Vessella, S. Traboni, D. Cimini, A. Iadonisi, C. Schiraldi, E. Bedini, *Biomacromolecules* **2019**, *20*, 3021.
- [56] S. Mizumoto, S. Yamada, *International Journal of Molecular Sciences* **2022**, *23*, 7485.
- [57] J. M. Trowbridge, R. L. Gallo, *Glycobiology* **2002**, *12*, 117R.
- [58] R. V. Iozzo, L. Schaefer, *Matrix Biology* **2015**, *42*, 11.
- [59] C. L. R. Merry, U. Lindahl, J. Couchman, J. D. Esko, in *Essentials of Glycobiology* (Eds.: A. Varki, R. D. Cummings, J. D. Esko, P. Stanley, G. W. Hart, M. Aebi, D. Mohnen, T. Kinoshita, N. H. Packer, J. H. Prestegard, R. L. Schnaar, P. H. Seeberger), Cold Spring Harbor Laboratory Press, Cold Spring Harbor (NY), **2022**.
- [60] F. Lamoureux, M. Baud'huin, L. Duplomb, D. Heymann, F. Rédini, *BioEssays* **2007**, *29*, 758.
- [61] J. Filmus, M. Capurro, J. Rast, *Genome Biology* **2008**, *9*, 224.
- [62] S. Saunders, S. Paine-Saunders, A. D. Lander, *Developmental Biology* **1997**, *190*, 78.
- [63] B. Hu, J. J. Rodriguez, A. Kakkerla Balaraju, Y. Gao, N. T. Nguyen, H. Steen, S. Suhaib, S. Chen, F. Lin, *J Cell Biol* **2021**, *220*, e202009082.
- [64] J. Ouchida, T. Ozaki, N. Segi, Y. Suzuki, S. Imagama, K. Kadomatsu, K. Sakamoto, *Exp Neurol* **2023**, *366*, 114444.
- [65] S. Paine-Saunders, B. L. Viviano, J. Zupicich, W. C. Skarnes, S. Saunders, *Developmental Biology* **2000**, *225*, 179.
- [66] Y. C. Liu, B. M. Wierbowski, A. Salic, *J Cell Sci* **2022**, jcs. 259297.
- [67] J. Gutiérrez, E. Brandan, *Molecular and Cellular Biology* **2010**, *30*, 1634.
- [68] K. Simons, D. Toomre, *Nat Rev Mol Cell Biol* **2000**, *1*, 31.
- [69] D. R. Taylor, I. J. Whitehouse, N. M. Hooper, *PLOS Pathogens* **2009**, *5*, e1000666.
- [70] S. S. Deepa, S. Yamada, M. Zako, O. Goldberger, K. Sugahara, *J Biol Chem* **2004**, *279*, 37368.
- [71] A. Yoneda, J. R. Couchman, *Matrix Biology* **2003**, *22*, 25.
- [72] S. Sarrazin, W. C. Lamanna, J. D. Esko, *Cold Spring Harb Perspect Biol* **2011**, *3*, a004952.
- [73] R. Zimmermann, C. Werner, J. Sterling, *Polymers (Basel)* **2018**, *10*, E1376.
- [74] J. L. Andres, L. Rönnstrand, S. Cheifetz, J. Massagué, *Journal of Biological Chemistry* **1991**, *266*, 23282.
- [75] G. J. Eill, A. Sinha, M. Morawski, M. S. Viapiano, R. T. Matthews, *Journal of Biological Chemistry* **2020**, *295*, 955.
- [76] J. Garwood, N. Heck, F. Reichardt, A. Faissner, *Journal of Biological Chemistry* **2003**, *278*, 24164.
- [77] S. Lamprianou, E. Chatzopoulou, J.-L. Thomas, S. Bouyain, S. Harroch, *Proceedings of the National Academy of Sciences* **2011**, *108*, 17498.
- [78] U. Theocharidis, K. Long, C. ffrench-Constant, A. Faissner, in *Progress in Brain Research* (Eds.: A. Dityatev, B. Wehrle-Haller, A. Pitkänen), Elsevier, **2014**, pp. 3–28.
- [79] R. Vivès, Héparanes Sulfate : Structure, Fonctions, Régulation, HDR, **2011**.
- [80] L. M. Milstone, L. Hough-Monroe, L. C. Kugelmann, J. R. Bender, J. G. Haggerty, *Journal of Cell Science* **1994**, *107*, 3183.
- [81] V. Kram, M. F. Young, in *Osteogenesis Imperfecta* (Eds.: J. R. Shapiro, P. H. Byers, F. H. Glorieux, P. D. Sponseller), Academic Press, San Diego, **2014**, pp. 85–95.
- [82] V. Kram, R. Shainer, P. Jani, J. A. N. Meester, B. Loeys, M. F. Young, *J Histochem Cytochem* **2020**, *68*, 747.

- [83] A. Hildebrand, M. Romarís, L. M. Rasmussen, D. Heinegård, D. R. Twardzik, W. A. Border, E. Ruoslahti, *Biochemical Journal* **1994**, *302*, 527.
- [84] A. J. Hayes, B. L. Farrugia, I. J. Biose, G. J. Bix, J. Melrose, *Frontiers in Cell and Developmental Biology* **2022**, *10*.
- [85] S. Douglass, A. Goyal, R. V. Iozzo, *Connective Tissue Research* **2015**, *56*, 381.
- [86] J. E. Silbert, G. Sugumaran, *Biochimica et Biophysica Acta (BBA) - Reviews on Biomembranes* **1995**, *1241*, 371.
- [87] J. L. Funderburgh, *IUBMB Life* **2002**, *54*, 187.
- [88] T. Uyama, H. Kitagawa, K. Sugahara, in *Comprehensive Glycoscience* (Ed.: H. Kamerling), Elsevier, Oxford, **2007**, pp. 79–104.
- [89] K. Prydz, *Biomolecules* **2015**, *5*, 2003.
- [90] L. Zhang, G. David, J. D. Esko, *Journal of Biological Chemistry* **1995**, *270*, 27127.
- [91] H. Kitagawa, S. Nadanaka, in *Handbook of Glycosyltransferases and Related Genes* (Eds.: N. Taniguchi, K. Honke, M. Fukuda, H. Narimatsu, Y. Yamaguchi, T. Angata), Springer Japan, Tokyo, **2014**, pp. 885–903.
- [92] S. Nadanaka, S. Zhou, S. Kagiya, N. Shoji, K. Sugahara, K. Sugihara, M. Asano, H. Kitagawa, *Journal of Biological Chemistry* **2013**, *288*, 9321.
- [93] H. Kitagawa, H. Shimakawa, K. Sugahara, *Journal of Biological Chemistry* **1999**, *274*, 13933.
- [94] C. Marques, J. Poças, C. Gomes, I. Faria-Ramos, C. A. Reis, R. R. Vivès, A. Magalhães, *J Biol Chem* **2022**, *298*, 102546.
- [95] T. Uyama, H. Kitagawa, K. Sugahara, in *Comprehensive Glycoscience* (Ed.: H. Kamerling), Elsevier, Oxford, **2007**, pp. 79–104.
- [96] M. Kusche-Gullberg, L. Kjellén, *Current Opinion in Structural Biology* **2003**, *13*, 605.
- [97] N. B. Schwartz, N. R. Smalheiser, in *Neurobiology of Glycoconjugates* (Eds.: R. U. Margolis, R. K. Margolis), Springer US, Boston, MA, **1989**, pp. 151–186.
- [98] K. Prydz, K. Dalen, *Journal of cell science* **2000**, *113 Pt 2*, 193.
- [99] F. Leisico, J. Omeiri, C. Le Narvor, J. Beaudouin, M. Hons, D. Fenel, G. Schoehn, Y. Couté, D. Bonnaffé, R. Sadir, H. Lortat-Jacob, R. Wild, *Nat Commun* **2022**, *13*, 7110.
- [100] T. Mikami, D. Yasunaga, H. Kitagawa, *Journal of Biological Chemistry* **2009**, *284*, 4494.
- [101] J. Sheng, R. Liu, Y. Xu, J. Liu, *Journal of Biological Chemistry* **2011**, *286*, 19768.
- [102] J. Ledin, M. Ringvall, M. Thuveson, I. Eriksson, M. Wilén, M. Kusche-Gullberg, E. Forsberg, L. Kjellén, *Journal of Biological Chemistry* **2006**, *281*, 35727.
- [103] E. Forsberg, G. Pejler, M. Ringvall, C. Lunderius, B. Tomasini-Johansson, M. Kusche-Gullberg, I. Eriksson, J. Ledin, L. Hellman, L. Kjellén, *Nature* **1999**, *400*, 773.
- [104] Å. Hagner-McWhirter, J.-P. Li, S. Oscarson, U. Lindahl, *Journal of Biological Chemistry* **2004**, *279*, 14631.
- [105] C. Debarnot, Y. R. Monneau, V. Roig-Zamboni, V. Delauzun, C. Le Narvor, E. Richard, J. Hénault, A. Goulet, F. Fadel, R. R. Vivès, B. Priem, D. Bonnaffé, H. Lortat-Jacob, Y. Bourne, *Proceedings of the National Academy of Sciences* **2019**, *116*, 6760.
- [106] J. Sheng, Y. Xu, S. B. Dulaney, X. Huang, J. Liu, *Journal of Biological Chemistry* **2012**, *287*, 20996.
- [107] J. Rong, H. Habuchi, K. Kimata, U. Lindahl, M. Kusche-Gullberg, *Biochemistry* **2001**, *40*, 5548.
- [108] E. Smeds, A. Feta, M. Kusche-Gullberg, *Glycobiology* **2010**, *20*, 1274.
- [109] A. Préchoux, C. Halimi, J.-P. Simorre, H. Lortat-Jacob, C. Laguri, *ACS Chem Biol* **2015**, *10*, 1064.
- [110] M. A. S. Pinhal, B. Smith, S. Olson, J. Aikawa, K. Kimata, J. D. Esko, *Proceedings of the National Academy of Sciences* **2001**, *98*, 12984.
- [111] E. Smeds, H. Habuchi, A.-T. Do, E. Hjertson, H. Grundberg, K. Kimata, U. Lindahl, M. Kusche-Gullberg, *Biochem J* **2003**, *372*, 371.
- [112] P. Jemth, E. Smeds, A.-T. Do, H. Habuchi, K. Kimata, U. Lindahl, M. Kusche-Gullberg, *J Biol Chem* **2003**, *278*, 24371.
- [113] E. Tykesson, A. Hassinen, K. Zielinska, M. A. Thelin, G. Frati, U. Ellervik, G. Westergren-Thorsson, A. Malmström, S. Kellokumpu, M. Maccarana, *J Biol Chem* **2018**, *293*, 13725.
- [114] T. Izumikawa, Y. Okuura, T. Koike, N. Sakoda, H. Kitagawa, *Biochemical Journal* **2011**, *434*, 321.
- [115] J. E. Silbert, G. Sugumaran, *IUBMB Life* **2002**, *54*, 177.
- [116] A. Malmström, B. Bartolini, M. A. Thelin, B. Pacheco, M. Maccarana, *J Histochem Cytochem.* **2012**, *60*, 916.
- [117] W. Wuyts, W. Van Hul, *Human Mutation* **2000**, *15*, 220.
- [118] C. Francannet, A. Cohen-Tanugi, M. L. Merrer, A. Munnich, J. Bonaventure, L. Legeai-Mallet, *Journal of Medical Genetics* **2001**, *38*, 430.
- [119] L. Legeai-Mallet, P. Margaritte-Jeannin, M. Lemdani, M. L. Merrer, H. Plauchu, P. Maroteaux, A. Munnich, F. Clerget-Darpoux, *Hum Genet* **1997**, *99*, 298.

- [120] M. Yanagishita, *Trends in Glycoscience and Glycotechnology* **1998**, *10*, 57.
- [121] H. Stanton, J. Melrose, C. B. Little, A. J. Fosang, *Biochimica et Biophysica Acta (BBA) - Molecular Basis of Disease* **2011**, *1812*, 1616.
- [122] T. Manon-Jensen, Y. Itoh, J. R. Couchman, *The FEBS Journal* **2010**, *277*, 3876.
- [123] A. Seffouh, R. El Masri, O. Makshakova, E. Gout, Z. el O. Hassoun, J. Andrieu, H. Lortat-Jacob, R. R. Vivès, *Cell. Mol. Life Sci.* **2019**, *76*, 1807.
- [124] A. Seffouh, F. Milz, C. Przybylski, C. Laguri, A. Oosterhof, S. Bourcier, R. Sadir, E. Dutkowski, R. Daniel, T. H. van Kuppevelt, T. Dierks, H. Lortat-Jacob, R. R. Vivès, *The FASEB Journal* **2013**, *27*, 2431.
- [125] R. El Masri, A. Seffouh, C. Roelants, I. Seffouh, E. Gout, J. Pérard, F. Dalonneau, K. Nishitsuji, F. Noborn, M. Nikpour, G. Larson, Y. Créton, M. Friedel-Arboleas, K. Uchimura, R. Daniel, H. Lortat-Jacob, O. Filhol, R. R. Vivès, *Cell Rep* **2022**, *38*, 110516.
- [126] R. El Masri, A. Seffouh, H. Lortat-Jacob, R. R. Vivès, *Glycoconj J* **2017**, *34*, 285.
- [127] A. Khurana, D. Belefond, X. He, J. Chien, V. Shridhar, *Am J Cancer Res* **2013**, *3*, 34.
- [128] K. J. Bame, *Glycobiology* **2001**, *11*, 91R.
- [129] R. Stern, M. J. Jedrzejewski, *Chem Rev* **2006**, *106*, 818.
- [130] R. C. Sullivan, M. D. Rockstrom, E. P. Schmidt, J. A. Hippensteel, *Matrix Biol Plus* **2021**, *12*, 100094.
- [131] T. Pape, A. M. Hunkemöller, P. Kumpers, H. Haller, S. David, K. Stahl, *Matrix Biol Plus* **2021**, *12*, 100095.
- [132] D. Anand, S. Ray, L. M. Srivastava, S. Bhargava, *Clin Biochem* **2016**, *49*, 768.
- [133] K. Oshima, S. M. Haeger, J. A. Hippensteel, P. S. Herson, E. P. Schmidt, *Pulmonary Circulation* **2018**, *8*, 2045893217745786.
- [134] J. D. Esko, J. H. Prestegard, R. J. Linhardt, in *Essentials of Glycobiology* (Eds.: A. Varki, R. D. Cummings, J. D. Esko, P. Stanley, G. W. Hart, M. Aebi, A. G. Darvill, T. Kinoshita, N. H. Packer, J. H. Prestegard, R. L. Schnaar, P. H. Seeberger), Cold Spring Harbor Laboratory Press, Cold Spring Harbor (NY), **2015**.
- [135] M. Petitou, *Biochimie* **2003**, *85*, 83.
- [136] U. Lindahl, G. Bäckström, M. Höök, L. Thunberg, L. A. Fransson, A. Linker, *Proc Natl Acad Sci U S A* **1979**, *76*, 3198.
- [137] B. Richard, R. Swanson, S. T. Olson, *Journal of Biological Chemistry* **2009**, *284*, 27054.
- [138] A. C. Rapraeger, A. Krufka, B. B. Olwin, *Science* **1991**, *252*, 1705.
- [139] A. Yayon, M. Klagsbrun, *Cancer Metast Rev* **1990**, *9*, 191.
- [140] S. Faham, R. E. Hileman, J. R. Fromm, R. J. Linhardt, D. C. Rees, *Science* **1996**, *271*, 1116.
- [141] M. Maccarana, B. Casu, U. Lindahl, *J Biol Chem* **1993**, *268*, 23898.
- [142] S. Ashikari-Hada, H. Habuchi, Y. Kariya, N. Itoh, A. H. Reddi, K. Kimata, *J. Biol. Chem.* **2004**, *279*, 12346.
- [143] J. Kreuger, M. Salmivirta, L. Sturiale, G. Giménez-Gallego, U. Lindahl, *J Biol Chem* **2001**, *276*, 30744.
- [144] D. A. Pye, R. R. Vives, J. E. Turnbull, P. Hyde, J. T. Gallagher, *J. Biol. Chem.* **1998**, *273*, 22936.
- [145] J. Schlessinger, A. N. Plotnikov, O. A. Ibrahim, A. V. Eliseenkova, B. K. Yeh, A. Yayon, R. J. Linhardt, M. Mohammadi, *Mol Cell* **2000**, *6*, 743.
- [146] S. Perez, O. Makshakova, J. Angulo, E. Bedini, A. Bisio, J. L. de Paz, E. Fadda, M. Guerrini, M. Hricovini, M. Hricovini, F. Lisacek, P. M. Nieto, K. Pagel, G. Paiardi, R. Richter, S. A. Samsonov, R. R. Vivès, D. Nikitovic, S. Ricard Blum, *JACS Au* **2023**, *3*, 628.
- [147] Cardin A D, Weintraub H J, *Arteriosclerosis: An Official Journal of the American Heart Association, Inc.* **1989**, *9*, 21.
- [148] R. E. Hileman, J. R. Fromm, J. M. Weiler, R. J. Linhardt, *BioEssays* **1998**, *20*, 156.
- [149] M. Sobel, D. F. Soler, J. C. Kermode, R. B. Harris, *Journal of Biological Chemistry* **1992**, *267*, 8857.
- [150] E. Bedini, A. Laezza, M. Parrilli, A. Iadonisi, *Carbohydrate Polymers* **2017**, *174*, 1224.
- [151] L. C. G. F. Palhares, J. A. London, A. M. Kozłowski, E. Esposito, S. F. Chavante, M. Ni, E. A. Yates, *Molecules* **2021**, *26*, 5211.
- [152] R. Takano, *Trends in Glycoscience and Glycotechnology* **2002**, *14*, 343.
- [153] P. Atallah, L. Schirmer, M. Tsurkan, Y. D. Putra Limasale, R. Zimmermann, C. Werner, U. Freudenberg, *Biomaterials* **2018**, *181*, 227.
- [154] Q. Chen, F. Li, H. Wang, C. Bu, F. Shi, L. Jin, Q. Zhang, L. Chi, *Frontiers in Molecular Biosciences* **2022**, *9*.
- [155] S. Hara, K. Yoshida, M. Ishihara, *Process for Producing Desulfated Polysaccharide, and Desulfated Heparin*, **2004**, US6809086B2.
- [156] M. Jaseja, R. N. Rej, F. Sauriol, A. S. Perlin, *Can. J. Chem.* **1989**, *67*, 1449.
- [157] K. Nagasawa, Y. Inoue, T. Kamata, *Carbohydrate Research* **1977**, *58*, 47.
- [158] A. Naggi, B. Casu, M. Perez, G. Torri, G. Cassinelli, S. Penco, C. Pisano, G. Giannini, R. Ishai-Michaeli, I. Vlodayky, *J Biol Chem* **2005**, *280*, 12103.
- [159] Y. Peng, L. E. Tellier, J. S. Temenoff, *Biomater. Sci.* **2016**, *4*, 1371.
- [160] Y. Inoue, K. Nagasawa, *Carbohydrate Research* **1976**, *46*, 87.

- [161] M. Matsuo, R. Takano, K. Kamei-Hayashi, S. Hara, *Carbohydrate Research* **1993**, *241*, 209.
- [162] Z. Ye, R. Takano, K. Hayashi, T.-V. Ta, H. Kato, Y. Kamikubo, Y. Nakahara, K. Kumeda, S. Hara, *Thrombosis Research* **1998**, *89*, 263.
- [163] Y. Kariya, M. Kyogashima, K. Suzuki, T. Isomura, T. Sakamoto, K. Horie, M. Ishihara, R. Takano, K. Kamei, S. Hara, *Journal of Biological Chemistry* **2000**, *275*, 25949.
- [164] A. Fryer, Y.-C. Huang, G. Rao, D. Jacoby, E. Mancilla, R. Whorton, C. A. Piantadosi, T. Kennedy, J. Hoidal, *J Pharmacol Exp Ther* **1997**, *282*, 208.
- [165] D. A. Pye, R. R. Vivès, P. Hyde, J. T. Gallagher, *Glycobiology* **2000**, *10*, 1183.
- [166] T. G. Kantor, M. Schubert, *J. Am. Chem. Soc.* **1957**, *79*, 152.
- [167] J. J. Lim, J. S. Temenoff, *Biomaterials* **2013**, *34*, 5007.
- [168] K. Nagasawa, Y. Inoue, T. Tokuyasu, *The Journal of Biochemistry* **1979**, *86*, 1323.
- [169] W. Han, Q. Li, Y. Lv, Q. Wang, X. Zhao, *Carbohydr Res* **2018**, *460*, 8.
- [170] C. Cai, K. Solakyildirim, B. Yang, J. M. Beaudet, A. Weyer, R. J. Linhardt, F. Zhang, *Carbohydr Polym* **2012**, *87*, 822.
- [171] K. Nagasawa, H. Uchiyama, N. Wajima, *Carbohydrate Research* **1986**, *158*, 183.
- [172] V. Hintze, S. Moeller, M. Schnabelrauch, S. Bierbaum, M. Viola, H. Worch, D. Scharnweber, *Biomacromolecules* **2009**, *10*, 3290.
- [173] S. Vogel, S. Arnoldini, S. Möller, M. Schnabelrauch, U. Hempel, *Sci Rep* **2016**, *6*, 36418.
- [174] Q. Feng, S. Lin, K. Zhang, C. Dong, T. Wu, H. Huang, X. Yan, L. Zhang, G. Li, L. Bian, *Acta Biomaterialia* **2017**, *53*, 329.
- [175] Y.-H. Chen, Y. Narimatsu, T. M. Clausen, C. Gomes, R. Karlsson, C. Steentoft, C. B. Spliid, T. Gustavsson, A. Salanti, A. Persson, A. Malmström, D. Willén, U. Ellervik, E. P. Bennett, Y. Mao, H. Clausen, Z. Yang, *Nat Methods* **2018**, *15*, 881.
- [176] L. E. Pepi, P. Sanderson, M. Stickney, I. J. Amster, *Molecular & Cellular Proteomics* **2021**, *20*, DOI 10.1074/mcp.R120.002267.
- [177] J. M. Fasciano, N. D. Danielson, *Journal of Separation Science* **2016**, *39*, 1118.
- [178] A. Zappe, R. L. Miller, W. B. Struwe, K. Pagel, *Mass Spectrometry Reviews* **n.d.**, *n/a*, DOI 10.1002/mas.21737.
- [179] R. L. Miller, S. E. Guimond, M. Shivkumar, J. Blocksidge, J. A. Austin, J. A. Leary, J. E. Turnbull, *Anal. Chem.* **2016**, *88*, 11542.
- [180] R. R. Vivès, S. Goodger, D. A. Pye, *Biochem J* **2001**, *354*, 141.
- [181] K. Robards, D. Ryan, in *Principles and Practice of Modern Chromatographic Methods (Second Edition)* (Eds.: K. Robards, D. Ryan), Academic Press, **2022**, pp. 495–513.
- [182] P. L. DeAngelis, J. Liu, R. J. Linhardt, *Glycobiology* **2013**, *23*, 764.
- [183] J. Liu, R. J. Linhardt, *Nat. Prod. Rep.* **2014**, *31*, 1676.
- [184] X. Zhang, V. Pagadala, H. M. Jester, A. M. Lim, T. Q. Pham, A. M. P. Goulas, J. Liu, R. J. Linhardt, *Chem. Sci.* **2017**, *8*, 7932.
- [185] X. Zhang, L. Lin, H. Huang, R. J. Linhardt, *Acc. Chem. Res.* **2020**, *53*, 335.
- [186] X. Xi, L. Hu, H. Huang, Y. Wang, R. Xu, G. Du, J. Chen, Z. Kang, *Journal of Industrial Microbiology and Biotechnology* **2023**, *50*, kuad012.
- [187] Y. Zhang, Y. Wang, Z. Zhou, P. Wang, X. Xi, S. Hu, R. Xu, G. Du, J. Li, J. Chen, Z. Kang, *Green Chem.* **2022**, *24*, 3180.
- [188] N. Karst, R. Linhardt, *CMC* **2003**, *10*, 1993.
- [189] V. H. Pomin, X. Wang, *ChemMedChem* **2018**, *13*, 648.
- [190] M. Mende, C. Bednarek, M. Wawrzyszyn, P. Sauter, M. B. Biskup, U. Schepers, S. Bräse, *Chem. Rev.* **2016**, *116*, 8193.
- [191] L. Wang, A. W. Sorum, B.-S. Huang, M. K. Kern, G. Su, N. Pawar, X. Huang, J. Liu, N. L. B. Pohl, L. C. Hsieh-Wilson, *Nat. Chem.* **2023**, *1*.
- [192] C. J. David, J. Massagué, *Nat Rev Mol Cell Biol* **2018**, *19*, 419.
- [193] A. P. Hinck, *FEBS Lett* **2012**, *586*, 1860.
- [194] M. Morikawa, R. Derynck, K. Miyazono, *Cold Spring Harb Perspect Biol* **2016**, *8*, a021873.
- [195] M. P. Sarras, *Bioessays* **1996**, *18*, 439.
- [196] A. Galat, *Cell Mol Life Sci* **2011**, *68*, 3437.
- [197] E. J. Goebel, K. N. Hart, J. C. McCoy, T. B. Thompson, *Exp Biol Med (Maywood)* **2019**, *244*, 1530.
- [198] R. Weiskirchen, S. K. Meurer, O. A. Gressner, J. Herrmann, E. Borkham-Kamphorst, A. M. Gressner, *FBL* **2009**, *14*, 4992.
- [199] M. R. Urist, *Science* **1965**, *150*, 893.
- [200] M. R. Urist, B. S. Strates, *Journal of Dental Research* **1971**, *50*, 1392.
- [201] J. M. Wozney, V. Rosen, A. J. Celeste, L. M. Mitscock, M. J. Whitters, R. W. Kriz, R. M. Hewick, E. A. Wang, *Science* **1988**, *242*, 1528.

- [202] R. N. Wang, J. Green, Z. Wang, Y. Deng, M. Qiao, M. Peabody, Q. Zhang, J. Ye, Z. Yan, S. Denduluri, O. Idowu, M. Li, C. Shen, A. Hu, R. C. Haydon, R. Kang, J. Mok, M. J. Lee, H. L. Luu, L. L. Shi, *Genes & Diseases* **2014**, *1*, 87.
- [203] T. Katagiri, T. Watabe, *Cold Spring Harb Perspect Biol* **2016**, *8*, a021899.
- [204] V. S. Salazar, L. W. Gamer, V. Rosen, *Nat Rev Endocrinol* **2016**, *12*, 203.
- [205] D. C. Goldman, N. Donley, J. L. Christian, *Mech Dev* **2009**, *126*, 117.
- [206] T. K. Sampath, K. E. Rashka, J. S. Doctor, R. F. Tucker, F. M. Hoffmann, *Proc Natl Acad Sci U S A* **1993**, *90*, 6004.
- [207] K. Miyazono, S. Maeda, T. Imamura, *Cytokine & Growth Factor Reviews* **2005**, *16*, 251.
- [208] L. David, C. Mallet, S. Mazerbourg, J.-J. Feige, S. Bailly, *Blood* **2006**, *109*, 1953.
- [209] H. Cheng, W. Jiang, F. M. Phillips, R. C. Haydon, Y. Peng, L. Zhou, H. H. Luu, N. An, B. Breyer, P. Vanichakarn, J. P. Szatkowski, J. Y. Park, T.-C. He, *JBJS* **2003**, *85*, 1544.
- [210] Q. Kang, M. H. Sun, H. Cheng, Y. Peng, A. G. Montag, A. T. Deyrup, W. Jiang, H. H. Luu, J. Luo, J. P. Szatkowski, P. Vanichakarn, J. Y. Park, Y. Li, R. C. Haydon, T.-C. He, *Gene Ther* **2004**, *11*, 1312.
- [211] A. Daluiski, T. Engstrand, M. E. Bahamonde, L. W. Gamer, E. Agius, S. L. Stevenson, K. Cox, V. Rosen, K. M. Lyons, *Nat Genet* **2001**, *27*, 84.
- [212] A. Vortkamp, *Current Biology* **1997**, *7*, R104.
- [213] E. E. Storm, D. M. Kingsley, *Development* **1996**, *122*, 3969.
- [214] G. S. Krishnakumar, A. Roffi, D. Reale, E. Kon, G. Filardo, *International Orthopaedics (SICOT)* **2017**, *41*, 1073.
- [215] L. P. Hatt, K. Thompson, J. A. Helms, M. J. Stoddart, A. R. Armiento, *Clinical and Translational Medicine* **2022**, *12*, e690.
- [216] D. Obradovic Wagner, C. Sieber, R. Bhushan, J. H. Börgermann, D. Graf, P. Knaus, *Science Signaling* **2010**, *3*, mr1.
- [217] C. Garot, Dispositifs Médicaux Bioactifs Pour La Réparation Osseuse, These de doctorat, Université Grenoble Alpes, **2022**.
- [218] B. Shu, M. Zhang, R. Xie, M. Wang, H. Jin, W. Hou, D. Tang, S. E. Harris, Y. Mishina, R. J. O'Keefe, M. J. Hilton, Y. Wang, D. Chen, *Journal of Cell Science* **2011**, *124*, 3428.
- [219] E. N. Blaney Davidson, E. L. Vitters, P. L. E. M. van Lent, F. A. J. van de Loo, W. B. van den Berg, P. M. van der Kraan, *Arthritis Res Ther* **2007**, *9*, R102.
- [220] Y. Liu, R. Hou, R. Yin, W. Yin, *Med Sci Monit* **2015**, *21*, 363.
- [221] W.-C. Chen, C.-H. Chung, Y.-C. Lu, M.-H. Wu, P.-H. Chou, J.-Y. Yen, Y.-W. Lai, G.-S. Wang, S.-C. Liu, J.-K. Cheng, Y.-J. Wu, H.-I. Yeh, L.-Y. Wang, S.-W. Wang, *Biochemical Pharmacology* **2018**, *150*, 256.
- [222] N. Ghosh-Choudhury, S. L. Abboud, B. Chandrasekar, G. Ghosh Choudhury, *FEBS Lett* **2003**, *544*, 181.
- [223] M. Shakèd, K. Weissmüller, H. Svoboda, P. Hortschansky, N. Nishino, S. Wölfl, K. L. Tucker, *PLOS ONE* **2008**, *3*, e2668.
- [224] C. Liu, G. Tian, Y. Tu, J. Fu, C. Lan, N. Wu, *Japanese Journal of Clinical Oncology* **2009**, *39*, 625.
- [225] C. Kestens, P. D. Siersema, G. J. A. Offerhaus, J. W. P. M. van Baal, *PLOS ONE* **2016**, *11*, e0155754.
- [226] A. C. P. Correia, D. Straub, M. Read, S. J. M. Hoefnagel, S. Romero-Pinedo, A. C. Abadía-Molina, N. J. Clemons, K. Wang, S. Calpe, W. Phillips, K. K. Krishnadath, *Cell Mol Gastroenterol Hepatol* **2023**, *15*, 1199.
- [227] P. R. Blackburn, C. J. Zepeda-Mendoza, T. M. Kruisselbrink, L. A. Schimmenti, S. García-Miñaur, M. Palomares, J. Nevado, M. A. Mori, G. Le Meur, E. W. Klee, C. Le Caignec, P. Lapunzina, B. Isidor, D. Babovic-Vuksanovic, *Eur J Hum Genet* **2019**, *27*, 1379.
- [228] L. Grgurevic, G. L. Christensen, T. J. Schulz, S. Vukicevic, *Cytokine & Growth Factor Reviews* **2016**, *27*, 105.
- [229] B. Andriopoulos, E. Corradini, Y. Xia, S. A. Faasse, S. Chen, L. Grgurevic, M. D. Knutson, A. Pietrangelo, S. Vukicevic, H. Y. Lin, J. L. Babitt, *Nat Genet* **2009**, *41*, 482.
- [230] A. Dendooven, O. van Oostrom, D. M. van der Giezen, J. Willem Leeuwis, C. Snijckers, J. A. Joles, E. J. Robertson, M. C. Verhaar, T. Q. Nguyen, R. Goldschmeding, *The American Journal of Pathology* **2011**, *178*, 1069.
- [231] R. H. Jenkins, D. J. Fraser, *Am J Pathol* **2011**, *178*, 964.
- [232] K. Sugiura, Y.-Q. Su, J. J. Eppig, *Biology of Reproduction* **2010**, *83*, 997.
- [233] I. M. A. Frota, C. C. F. Leitão, J. J. N. Costa, R. van den Hurk, M. V. A. Saraiva, J. R. Figueiredo, J. R. V. Silva, *Zygote* **2013**, *21*, 270.
- [234] M. Pauk, T. Bordukalo-Niksic, J. Brkljacic, V. M. Paralkar, A. L. Brault, I. Dumic-Cule, F. Borovecki, L. Grgurevic, S. Vukicevic, *Acta Diabetol* **2019**, *56*, 365.
- [235] M. N. Helder, E. Ozkaynak, K. T. Sampath, F. P. Luyten, V. Latin, H. Oppermann, S. Vukicevic, *J Histochem Cytochem.* **1995**, *43*, 1035.
- [236] A. T. Dudley, K. M. Lyons, E. J. Robertson, *Genes Dev.* **1995**, *9*, 2795.

- [237] W. Zarychta-Wisniewska, A. Burdzinska, A. Kulesza, K. Gala, B. Kaleta, K. Zielniok, K. Siennicka, M. Sabat, L. Paczek, *BMC Cell Biology* **2017**, *18*, 13.
- [238] L. David, C. Mallet, M. Keramidas, N. Lamandé, J.-M. Gasc, S. Dupuis-Girod, H. Plauchu, J.-J. Feige, S. Bailly, *Circulation Research* **2008**, *102*, 914.
- [239] A. Desroches-Castan, E. Tillet, C. Bouvard, S. Bailly, *Dev Dyn* **2022**, *251*, 178.
- [240] E. Tillet, S. Bailly, *Frontiers in Genetics* **2015**, *5*.
- [241] L. David, J.-J. Feige, S. Bailly, *Cytokine & Growth Factor Reviews* **2009**, *20*, 203.
- [242] A. M. Blázquez-Medela, M. Jumabay, K. I. Boström, *Obes Rev* **2019**, *20*, 648.
- [243] R. Derynck, E. H. Budi, *Science Signaling* **2019**, *12*, eaav5183.
- [244] M.-C. Ramel, C. S. Hill, *FEBS Letters* **2012**, *586*, 1929.
- [245] A. C. Carreira, G. G. Alves, W. F. Zambuzzi, M. C. Sogayar, J. M. Granjeiro, *Archives of Biochemistry and Biophysics* **2014**, *561*, 64.
- [246] D. Umulis, M. B. O'Connor, S. S. Blair, *Development* **2009**, *136*, 3715.
- [247] K. E. Gregory, R. N. Ono, N. L. Charbonneau, C.-L. Kuo, D. R. Keene, H. P. Bächinger, L. Y. Sakai, *Journal of Biological Chemistry* **2005**, *280*, 27970.
- [248] G. Sengle, N. L. Charbonneau, R. N. Ono, T. Sasaki, J. Alvarez, D. R. Keene, H. P. Bächinger, L. Y. Sakai, *Journal of Biological Chemistry* **2008**, *283*, 13874.
- [249] C. E. S. Spanou, A. P. Wohl, S. Doherr, A. Correns, N. Sonntag, S. Lütke, M. Mörgelin, T. Imhof, J. M. Gebauer, U. Baumann, K. Grobe, M. Koch, G. Sengle, *FASEB J* **2023**, *37*, e22717.
- [250] G. Sengle, R. N. Ono, K. M. Lyons, H. P. Bächinger, L. Y. Sakai, *Journal of Molecular Biology* **2008**, *381*, 1025.
- [251] V. Khattar, J. H. Lee, H. Wang, S. Bastola, S. Ponnazhagan, *FASEB BioAdvances* **2019**, *1*, 180.
- [252] A. Hauburger, S. von Einem, G. K. Schwaerzer, A. Buttstedt, M. Zebisch, M. Schräml, P. Hortschansky, P. Knaus, E. Schwarz, *The FEBS Journal* **2009**, *276*, 6386.
- [253] C. Scheufler, W. Sebald, M. Hülsmeier, *Journal of Molecular Biology* **1999**, *287*, 103.
- [254] B. Tajer, J. A. Dutko, S. C. Little, M. C. Mullins, *Proc Natl Acad Sci U S A* **2021**, *118*, e2017952118.
- [255] M. S. Karim, A. Madamanchi, J. A. Dutko, M. C. Mullins, D. M. Umulis, *PLOS Computational Biology* **2021**, *17*, e1009422.
- [256] D. I. Israel, J. Nove, K. M. Kerns, R. J. Kaufman, V. Rosen, K. A. Cox, J. M. Wozney, *Growth Factors* **1996**, *13*, 291.
- [257] S. C. Little, M. C. Mullins, *Nat Cell Biol* **2009**, *11*, 637.
- [258] J. Greenwald, J. Groppe, P. Gray, E. Wiater, W. Kwiatkowski, W. Vale, S. Choe, *Mol Cell* **2003**, *11*, 605.
- [259] J. Groppe, J. Greenwald, E. Wiater, J. Rodriguez-Leon, A. N. Economides, W. Kwiatkowski, M. Affolter, W. W. Vale, J. C. I. Belmonte, S. Choe, *Nature* **2002**, *420*, 636.
- [260] G. P. Allendorph, M. J. Isaacs, Y. Kawakami, J. C. Izpisua Belmonte, S. Choe, *Biochemistry* **2007**, *46*, 12238.
- [261] M. A. Brown, Q. Zhao, K. A. Baker, C. Naik, C. Chen, L. Pukac, M. Singh, T. Tsareva, Y. Parice, A. Mahoney, V. Roschke, I. Sanyal, S. Choe, *J Biol Chem* **2005**, *280*, 25111.
- [262] A. Moustakas, C.-H. Heldin, *Development* **2009**, *136*, 3699.
- [263] T. D. Mueller, J. Nickel, *FEBS Letters* **2012**, *586*, 1846.
- [264] E. Migliorini, P. Horn, T. Haraszti, S. V. Wegner, C. Hiepen, P. Knaus, R. P. Richter, E. A. Cavalcanti-Adam, *Advanced Biosystems* **2017**, *1*, 1600041.
- [265] F. L. Collins, N. D. Rios-Arce, J. D. Schepper, N. Parameswaran, L. R. McCabe, *Microbiology Spectrum* **2017**, *5*, 10.1128/microbiolspec.bad.
- [266] G. R. Gipson, E. J. Goebel, K. N. Hart, E. C. Kappes, C. Kattamuri, J. C. McCoy, T. B. Thompson, *Bone* **2020**, *140*, 115549.
- [267] J. Nickel, W. Sebald, J. C. Groppe, T. D. Mueller, *Cytokine & Growth Factor Reviews* **2009**, *20*, 367.
- [268] K. Heinecke, A. Seher, W. Schmitz, T. D. Mueller, W. Sebald, J. Nickel, *BMC Biology* **2009**, *7*, 59.
- [269] J. Nickel, T. D. Mueller, *Cells* **2019**, *8*, 1579.
- [270] A. Nohe, S. Hassel, M. Ehrlich, F. Neubauer, W. Sebald, Y. I. Henis, P. Knaus, *J Biol Chem* **2002**, *277*, 5330.
- [271] V. Khodr, P. Machillot, E. Migliorini, J.-B. Reiser, C. Picart, *Biointerphases* **2021**, *16*, 031001.
- [272] S. Ehata, Y. Yokoyama, K. Takahashi, K. Miyazono, *Pathology International* **2013**, *63*, 287.
- [273] S. Ross, C. S. Hill, *The International Journal of Biochemistry & Cell Biology* **2008**, *40*, 383.
- [274] A. Holtzhausen, C. Golzio, T. How, Y.-H. Lee, W. P. Schiemann, N. Katsanis, G. C. Blobe, *FASEB J* **2014**, *28*, 1248.
- [275] B. M. Chacko, B. Y. Qin, A. Tiwari, G. Shi, S. Lam, L. J. Hayward, M. de Caestecker, K. Lin, *Molecular Cell* **2004**, *15*, 813.
- [276] C. S. Hill, *Cold Spring Harb Perspect Biol* **2016**, *8*, a022079.
- [277] X.-H. Feng, R. Derynck, *Annual Review of Cell and Developmental Biology* **2005**, *21*, 659.

- [278] R. Nishimura, K. Hata, T. Matsubara, M. Wakabayashi, T. Yoneda, *The Journal of Biochemistry* **2012**, *151*, 247.
- [279] K. Tzavlaki, A. Moustakas, *Biomolecules* **2020**, *10*, 487.
- [280] L.-Y. Tang, Y. E. Zhang, *Cell & Bioscience* **2011**, *1*, 43.
- [281] K. Miyazono, Y. Kamiya, M. Morikawa, *Journal of Biochemistry* **2010**, *147*, 35.
- [282] G. Sánchez-Duffhues, C. Hiepen, P. Knaus, P. ten Dijke, *Bone* **2015**, *80*, 43.
- [283] J. Sefkow-Werner, P. Machillot, A. Sales, E. Castro-Ramirez, M. Degardin, D. Boturyn, E. A. Cavalcanti-Adam, C. Albiges-Rizo, C. Picart, E. Migliorini, *Acta Biomaterialia* **2020**, DOI 10.1016/j.actbio.2020.07.015.
- [284] B. Mulloy, C. C. Rider, in *Vitamins & Hormones* (Ed.: G. Litwack), Academic Press, **2015**, pp. 63–90.
- [285] L. B. Zimmerman, J. M. De Jesús-Escobar, R. M. Harland, *Cell* **1996**, *86*, 599.
- [286] J. Salbach-Hirsch, M. Rauner, C. Hofbauer, L. C. Hofbauer, *Biological Chemistry* **2021**, *402*, 1415.
- [287] R. Ruppert, E. Hoffmann, W. Sebald, *European Journal of Biochemistry* **1996**, *237*, 295.
- [288] P. C. Billings, E. Yang, C. Mundy, M. Pacifici, *Journal of Biological Chemistry* **2018**, *293*, 14371.
- [289] N. S. Gandhi, R. L. Mancera, *Biochimica et Biophysica Acta (BBA) - Proteins and Proteomics* **2012**, *1824*, 1374.
- [290] W. Wuyts, W. Van Hul, K. De Boulle, J. Hendrickx, E. Bakker, F. Vanhoenacker, F. Mollica, H. J. Lüdecke, B. S. Sayli, U. E. Pazzaglia, G. Mortier, B. Hamel, E. U. Conrad, M. Matsushita, W. H. Raskind, P. J. Willems, *American Journal of Human Genetics* **1998**, *62*, 346.
- [291] A. Superti-Furga, S. Unger, in *GeneReviews®* (Eds.: M. P. Adam, G. M. Mirzaa, R. A. Pagon, S. E. Wallace, L. J. Bean, K. W. Gripp, A. Amemiya), University Of Washington, Seattle, Seattle (WA), **1993**.
- [292] X. Lin, G. Wei, Z. Shi, L. Dryer, J. D. Esko, D. E. Wells, M. M. Matzuk, *Developmental Biology* **2000**, *224*, 299.
- [293] D. Stickens, B. M. Zak, N. Rougier, J. D. Esko, Z. Werb, *Development* **2005**, *132*, 5055.
- [294] D. Swami, J. Aich, B. Bisht, M. K. Paul, in *Advances in Stem Cells and Their Niches* (Ed.: S. Nilsson), Elsevier, **2022**, pp. 97–143.
- [295] M. Fujise, S. Takeo, K. Kamimura, T. Matsuo, T. Aigaki, S. Izumi, H. Nakato, *Development* **2003**, *130*, 1515.
- [296] T. Y. Belenkaya, C. Han, D. Yan, R. J. Opoka, M. Khodoun, H. Liu, X. Lin, *Cell* **2004**, *119*, 231.
- [297] D. J. Bornemann, J. E. Duncan, W. Staatz, S. Selleck, R. Warrior, *Development* **2004**, *131*, 1927.
- [298] C. Han, T. Y. Belenkaya, M. Khodoun, M. Tauchi, X. Lin, X. Lin, *Development* **2004**, *131*, 1563.
- [299] Y. Takei, Y. Ozawa, M. Sato, A. Watanabe, T. Tabata, *Development* **2004**, *131*, 73.
- [300] S. M. Jackson, H. Nakato, M. Sugiura, A. Jannuzi, R. Oakes, V. Kaluza, C. Golden, S. B. Selleck, *Development* **1997**, *124*, 4113.
- [301] N. B. Schwartz, M. S. Domowicz, *Frontiers in Cell and Developmental Biology* **2022**, *10*.
- [302] D. Yan, X. Lin, *Cold Spring Harb Perspect Biol* **2009**, *1*, a002493.
- [303] S. Paine-Saunders, B. L. Viviano, A. N. Economides, S. Saunders, *Journal of Biological Chemistry* **2002**, *277*, 2089.
- [304] T. Inubushi, S. Nozawa, K. Matsumoto, F. Irie, Y. Yamaguchi, *JCI Insight* **n.d.**, *2*, e90049.
- [305] J. R. Meyers, J. Planamento, P. Ebrom, N. Krulewitz, E. Wade, M. E. Pownall, *Developmental Biology* **2013**, *378*, 107.
- [306] W.-J. Kuo, M. A. Digman, A. D. Lander, *Mol Biol Cell* **2010**, *21*, 4028.
- [307] A. Irie, H. Habuchi, K. Kimata, Y. Sanai, *Biochemical and Biophysical Research Communications* **2003**, *308*, 858.
- [308] X. Jiao, P. C. Billings, M. P. O'Connell, F. S. Kaplan, E. M. Shore, D. L. Glaser, *J Biol Chem* **2007**, *282*, 1080.
- [309] C. Mundy, E. Yang, H. Takano, P. C. Billings, M. Pacifici, *Journal of Biological Chemistry* **2018**, *293*, 7703.
- [310] B. Ohkawara, S. Iemura, P. ten Dijke, N. Ueno, *Current Biology* **2002**, *12*, 205.
- [311] S. D. Freeman, W. M. Moore, E. C. Guiral, A. D. Holme, J. E. Turnbull, M. E. Pownall, *Developmental Biology* **2008**, *320*, 436.
- [312] G. H. Olivares, H. Carrasco, F. Aroca, L. Carvallo, F. Segovia, J. Larraín, *Developmental Biology* **2009**, *329*, 338.
- [313] M. C. Fisher, Y. Li, M. R. Seghatoleslami, C. N. Dealy, R. A. Kosher, *Matrix Biology* **2006**, *25*, 27.
- [314] M. Klüppel, T. N. Wight, C. Chan, A. Hinek, J. L. Wrana, *Development* **2005**, *132*, 3989.
- [315] B. Zhao, T. Katagiri, H. Toyoda, T. Takada, T. Yanai, T. Fukuda, U. Chung, T. Koike, K. Takaoka, R. Kamijo, *Journal of Biological Chemistry* **2006**, *281*, 23246.
- [316] D. S. Bramono, S. Murali, B. Rai, L. Ling, W. T. Poh, Z. X. Lim, G. S. Stein, V. Nurcombe, A. J. van Wijnen, S. M. Cool, *Bone* **2012**, *50*, 954.

- [317] T. Miyazaki, S. Miyauchi, A. Tawada, T. Anada, S. Matsuzaka, O. Suzuki, *J. Cell. Physiol.* **2008**, *217*, 769.
- [318] S. A. Khan, M. S. Nelson, C. Pan, P. M. Gaffney, P. Gupta, *American Journal of Physiology-Cell Physiology* **2008**, *294*, C1387.
- [319] P. Miguez, M. Terajima, H. Nagaoka, Y. Mochida, M. Yamauchi, *Biochem Biophys Res Commun* **2011**, *405*, 262.
- [320] D. Al Mahbuba, S. Masuko, S. Wang, D. Syangtan, J. S. Kang, Y. Song, T. W. Shin, K. Xia, F. Zhang, R. J. Linhardt, E. S. Boyden, L. L. Kiessling, *ACS Nano* **2023**, *17*, 7207.
- [321] C. Siverino, S. Fahmy-Garcia, V. Niklaus, N. Kops, L. Dolcini, M. M. Misciagna, Y. Ridwan, E. Farrell, G. J. V. M. van Osch, J. Nickel, *Bioact Mater* **2023**, *29*, 241.
- [322] E. Migliorini, J. Ban, G. Greci, L. Andolfi, A. Pozzato, M. Tormen, V. Torre, M. Lazzarino, *Biotechnology and Bioengineering* **2013**, *110*, 2301.
- [323] M. Kisiel, A. S. Klar, M. Ventura, J. Buijs, M.-K. Mafina, S. M. Cool, J. Hilborn, *PLoS ONE* **2013**, *8*, e78551.
- [324] R. A. A. Smith, S. Murali, B. Rai, X. Lu, Z. X. H. Lim, J. J. L. Lee, V. Nurcombe, S. M. Cool, *Biomaterials* **2018**, *184*, 41.
- [325] N. Sasaki, T. Hirano, T. Ichimiya, M. Wakao, K. Hirano, A. Kinoshita-Toyoda, H. Toyoda, Y. Suda, S. Nishihara, *PLoS One* **2009**, *4*, DOI 10.1371/journal.pone.0008262.
- [326] S. Roy, A. El Hadri, S. Richard, F. Denis, K. Holte, J. Duffner, F. Yu, Z. Galcheva-Gargova, I. Capila, B. Schultes, M. Petitou, G. V. Kaundinya, *J. Med. Chem.* **2014**, *57*, 4511.
- [327] L. E. Tellier, T. Miller, T. C. McDevitt, J. S. Temenoff, *J. Mater. Chem. B* **2015**, *3*, 8001.
- [328] P. Chopra, A. Joshi, J. Wu, W. Lu, T. Yadavalli, M. A. Wolfert, D. Shukla, J. Zaia, G.-J. Boons, *PNAS* **2021**, *118*, DOI 10.1073/pnas.2012935118.
- [329] S. C. Samson, T. Ferrer, C. J. Jou, F. B. Sachse, S. S. Shankaran, R. M. Shaw, N. C. Chi, M. Tristani-Firouzi, H. J. Yost, *PLoS Biology* **2013**, *11*, e1001727.
- [330] Z. Söderlund, A. Ibáñez-Fonseca, S. Hajizadeh, J. C. Rodríguez-Cabello, J. Liu, L. Ye, E. Tykesson, L. Elowsson, G. Westergren-Thorsson, *Commun Biol* **2022**, *5*, 1349.
- [331] U. Freudenberg, Y. Liang, K. L. Kiick, C. Werner, *Advanced Materials* **2016**, *28*, 8861.
- [332] M. I. Neves, M. Araújo, L. Moroni, R. M. P. da Silva, C. C. Barrias, *Molecules* **2020**, *25*, 978.
- [333] A. J. Lepedda, G. Nieddu, M. Formato, M. B. Baker, J. Fernández-Pérez, L. Moroni, *Frontiers in Chemistry* **2021**, *9*.
- [334] J. Chen, T. Sun, Y. You, B. Wu, X. Wang, J. Wu, *Front Cell Dev Biol* **2021**, *9*, 760532.
- [335] A. Wartenberg, J. Weisser, M. Schnabelrauch, *Molecules* **2021**, *26*, 5597.
- [336] H. Sodhi, A. Panitch, *Biomolecules* **2021**, *11*, 29.
- [337] R. Biran, D. Pond, *Advanced Drug Delivery Reviews* **2017**, *112*, 12.
- [338] L. Schirmer, P. Atallah, C. Werner, U. Freudenberg, *Advanced Healthcare Materials* **2016**, *5*, 3157.
- [339] V. Bonito, A. I. P. M. Smits, O. J. G. M. Goor, B. D. Ippel, A. Driessen-Mol, T. J. A. G. Múnker, A. W. Bosman, T. Mes, P. Y. W. Dankers, C. V. C. Bouten, *Acta Biomaterialia* **2018**, *71*, 247.
- [340] L. Schirmer, C. Hoornaert, D. L. Blon, D. Eigel, C. Neto, M. Gumbleton, P. B. Welzel, A. E. Rosser, C. Werner, P. Ponsaerts, B. Newland, *Biomater. Sci.* **2020**, *8*, 4997.
- [341] S. E. Kim, C.-S. Kim, Y.-P. Yun, D. H. Yang, K. Park, S. E. Kim, C.-M. Jeong, J.-B. Huh, *Carbohydrate Polymers* **2014**, *114*, 123.
- [342] S. Yan, L. Feng, Q. Zhu, W. Yang, Y. Lan, D. Li, Y. Liu, W. Xue, R. Guo, G. Wu, *ACS Biomater. Sci. Eng.* **2018**, *4*, 3291.
- [343] X. Xu, A. K. Jha, R. L. Duncan, X. Jia, *Acta Biomaterialia* **2011**, *7*, 3050.
- [344] M. H. Hettiaratchi, L. Krishnan, T. Rouse, C. Chou, T. C. McDevitt, R. E. Guldberg, *Science Advances* **2020**, *6*, eaay1240.
- [345] S. Thanyaphoo, J. Kaewsrichan, *Acta Pharmaceutica* **2016**, *66*, 373.
- [346] R. Y. Kim, B. Lee, S.-N. Park, J.-H. Ko, I. S. Kim, S. J. Hwang, *Tissue Engineering Part A* **2016**, *22*, 801.
- [347] H. S. Yang, W.-G. La, Y.-M. Cho, W. Shin, G.-D. Yeo, B.-S. Kim, *Exp Mol Med* **2012**, *44*, 350.
- [348] Y. Liu, S. Cai, X. Z. Shu, J. Shelby, G. D. Prestwich, *Wound Repair and Regeneration* **2007**, *15*, 245.
- [349] N. R. Johnson, Y. Wang, *Wound Repair and Regeneration* **2015**, *23*, 591.
- [350] J. S. Park, K. Park, D. G. Woo, H. N. Yang, H.-M. Chung, K.-H. Park, *Biomacromolecules* **2008**, *9*, 2162.
- [351] M. Kim, S. E. Kim, S. S. Kang, Y. H. Kim, G. Tae, *Biomaterials* **2011**, *32*, 7883.
- [352] S. Singh, B. M. Wu, J. C. Y. Dunn, *Biomaterials* **2011**, *32*, 2059.
- [353] S. Prokoph, E. Chavakis, K. R. Levental, A. Zieris, U. Freudenberg, S. Dimmeler, C. Werner, *Biomaterials* **2012**, *33*, 4792.
- [354] J. Yu, A. Wang, Z. Tang, J. Henry, B. Lee, Y. Zhu, F. Yuan, F. Huang, S. Li, *Biomaterials* **2012**, *33*, 8062.
- [355] Y. Yao, J. Wang, Y. Cui, R. Xu, Z. Wang, J. Zhang, K. Wang, Y. Li, Q. Zhao, D. Kong, *Acta Biomaterialia* **2014**, *10*, 2739.

- [356] B. S. Conklin, E. R. Richter, K. L. Kreutziger, D.-S. Zhong, C. Chen, *Med Eng Phys* **2002**, *24*, 173.
- [357] W. Wu, R. A. Allen, Y. Wang, *Nat Med* **2012**, *18*, 1148.
- [358] I. Kim, S. S. Lee, S. Bae, H. Lee, N. S. Hwang, *Biomacromolecules* **2018**, *19*, 2257.
- [359] L. Ye, X. Wu, H.-Y. Duan, X. Geng, B. Chen, Y.-Q. Gu, A.-Y. Zhang, J. Zhang, Z.-G. Feng, *Journal of Biomedical Materials Research Part A* **2012**, *100A*, 3251.
- [360] C. Wang, S. Poon, S. Murali, C.-Y. Koo, T. J. Bell, S. F. Hinkley, H. Yeong, K. Bhakoo, V. Nurcombe, S. M. Cool, *Biomaterials* **2014**, *35*, 6776.
- [361] M. T. Koobatian, S. Row, R. J. Smith, C. Koenigsnecht, S. T. Andreadis, D. D. Swartz, *Biomaterials* **2016**, *76*, 344.
- [362] J. J. D. Henry, J. Yu, A. Wang, R. Lee, J. Fang, S. Li, *Biofabrication* **2017**, *9*, 035007.
- [363] D. I. Braghirolli, V. E. Helfer, P. C. Chagastelles, T. P. Dalberto, D. Gamba, P. Pranke, *Biomed. Mater.* **2017**, *12*, 025003.
- [364] U. Freudenberg, A. Zieris, K. Chwalek, M. V. Tsurkan, M. F. Maitz, P. Atallah, K. R. Levental, S. A. Eming, C. Werner, *Journal of Controlled Release* **2015**, *220*, 79.
- [365] H. Chu, J. Gao, C.-W. Chen, J. Huard, Y. Wang, *Proceedings of the National Academy of Sciences* **2011**, *108*, 13444.
- [366] O. Jeon, S.-W. Kang, H.-W. Lim, J. Hyung Chung, B.-S. Kim, *Biomaterials* **2006**, *27*, 1598.
- [367] N. R. Johnson, M. Kruger, K. P. Goetsch, P. Zilla, D. Bezuidenhout, Y. Wang, N. H. Davies, *ACS Biomater. Sci. Eng.* **2015**, *1*, 753.
- [368] M. Younesi, D. M. Knapik, J. Cumsy, B. O. Donmez, P. He, A. Islam, G. Learn, P. McClellan, M. Bohl, R. J. Gillespie, O. Akkus, *Acta Biomaterialia* **2017**, *63*, 200.
- [369] S. Thomopoulos, R. Das, M. J. Silva, S. Sakiyama-Elbert, F. L. Harwood, E. Zampiakos, H. M. Kim, D. Amiel, R. H. Gelberman, *Journal of Orthopaedic Research* **2009**, *27*, 1209.
- [370] S. Kang, J. S. Yoon, J. Y. Lee, H.-J. Kim, K. Park, S. E. Kim, *Carbohydrate Polymers* **2019**, *209*, 372.
- [371] B. Newland, P. B. Welzel, H. Newland, C. Renneberg, P. Kolar, M. Tsurkan, A. Rosser, U. Freudenberg, C. Werner, *Small* **2015**, *11*, 5047.
- [372] B. Newland, H. Newland, F. Lorenzi, D. Eigel, P. B. Welzel, D. Fischer, W. Wang, U. Freudenberg, A. Rosser, C. Werner, *ACS Chem. Neurosci.* **2021**, *12*, 1178.
- [373] M. D. Wood, D. Hunter, S. E. MacKinnon, S. E. Sakiyama-Elbert, *Journal of Biomaterials Science, Polymer Edition* **2010**, *21*, 771.
- [374] K. H. Bae, H. Mok, T. G. Park, *Biomaterials* **2008**, *29*, 3376.
- [375] K. Lee, H. Lee, K. H. Bae, T. G. Park, *Biomaterials* **2010**, *31*, 6530.
- [376] A. A. DeCarlo, M. Belousova, A. L. Ellis, D. Petersen, H. Grenett, P. Hardigan, R. O'Grady, M. Lord, J. M. Whitelock, *BMC Biotechnology* **2012**, *12*, 60.
- [377] P. P. Srinivasan, S. Y. McCoy, A. K. Jha, W. Yang, X. Jia, M. C. Farach-Carson, C. B. Kirn-Safran, *Biomed. Mater.* **2012**, *7*, 024109.
- [378] W. Yang, R. R. Gomes, A. J. Brown, A. R. Burdett, M. Alicknavitch, M. C. Farach-Carson, D. D. Carson, *Tissue Eng* **2006**, *12*, 2009.
- [379] A. K. Jha, W. Yang, C. B. Kirn-Safran, M. C. Farach-Carson, X. Jia, *Biomaterials* **2009**, *30*, 6964.
- [380] M. S. Lord, A. L. Ellis, B. L. Farrugia, J. M. Whitelock, H. Grenett, C. Li, R. L. O'Grady, A. A. DeCarlo, *J Control Release* **2017**, *250*, 48.
- [381] J. Rnjak-Kovacina, F. Tang, J. M. Whitelock, M. S. Lord, *Colloids and Surfaces B: Biointerfaces* **2016**, *148*, 130.
- [382] M. S. Lord, W. Yu, B. Cheng, A. Simmons, L. Poole-Warren, J. M. Whitelock, *Biomaterials* **2009**, *30*, 4898.
- [383] J. S. Pieper, T. Hafmans, P. B. van Wachem, M. J. A. van Luyn, L. A. Brouwer, J. H. Veerkamp, T. H. van Kuppevelt, *Journal of Biomedical Materials Research* **2002**, *62*, 185.
- [384] L. Ling, X. Ren, X. Cao, A. B. M. Hassan, S. Mah, P. Sathiyathan, R. A. A. Smith, C. L. L. Tan, M. Eio, R. M. Samsanraj, A. J. van Wijnen, M. Raghunath, V. Nurcombe, J. H. Hui, S. M. Cool, *Stem Cell Reports* **2020**, *14*, 105.
- [385] M. Mahedia, N. Shah, B. Amirlak, *Plast Reconstr Surg Glob Open* **2016**, *4*, e791.
- [386] G. Nicoletti, M. M. Tresoldi, A. Malovini, M. Visaggio, A. Faga, S. Scevola, *Indian J Plast Surg* **2018**, *51*, 46.
- [387] S. Erbatur, Y. K. Coban, E. N. Aydın, *Int J Burns Trauma* **2012**, *2*, 118.
- [388] A. Gobbi, C. Scotti, G. Karnatzikos, A. Mudhigere, M. Castro, G. M. Peretti, *Knee Surg Sports Traumatol Arthrosc* **2017**, *25*, 2494.
- [389] A. Gobbi, S. Chaurasia, G. Karnatzikos, N. Nakamura, *CARTILAGE* **2015**, *6*, 82.
- [390] A. Gobbi, G. P. Whyte, *Am J Sports Med* **2016**, *44*, 2846.
- [391] M. Marcacci, M. Berruto, D. Brocchetta, A. Delcogliano, D. Ghinelli, A. Gobbi, E. Kon, L. Pederzini, D. Rosa, G. L. Sacchetti, G. Stefani, S. Zanasi, *Clinical Orthopaedics and Related Research®* **2005**, *435*, 96.

- [392] C.-Y. Kuo, C.-H. Chen, C.-Y. Hsiao, J.-P. Chen, *Carbohydrate Polymers* **2015**, *117*, 722.
- [393] X. Yu, G. Qian, S. Chen, D. Xu, X. Zhao, C. Du, *Carbohydrate Polymers* **2017**, *159*, 20.
- [394] M.-E. Han, B. J. Kang, S.-H. Kim, H. D. Kim, N. S. Hwang, *Journal of Industrial and Engineering Chemistry* **2017**, *45*, 421.
- [395] C.-S. Ko, J.-P. Huang, C.-W. Huang, I.-M. Chu, *Journal of Bioscience and Bioengineering* **2009**, *107*, 177.
- [396] M. Bouyer, C. Garot, P. Machillot, J. Vollaire, V. Fitzpatrick, S. Morand, J. Boutonnat, V. Josserand, G. Bettega, C. Picart, *Materials Today Bio* **2021**, *11*, 100113.
- [397] C. Garot, S. Schoffit, C. Monfoulet, P. Machillot, C. Deroy, S. Roques, J. Vial, J. Vollaire, M. Renard, H. Ghanem, H. El-Hafci, A. Decambon, V. Josserand, L. Bordenave, G. Bettega, M. Durand, M. Manassero, V. Viateau, D. Logeart-Avramoglou, C. Picart, *3D-Printed Polymeric Scaffolds with Optimized Architecture to Repair a Sheep Metatarsal Critical-Size Bone Defec*, **2022**.
- [398] E.-C. Kim, S. J. Yoon, K. Noh, D.-W. Lee, *Journal of Nanoscience and Nanotechnology* **2017**, *17*, 143.
- [399] T. B. L. Nguyen, B.-T. Lee, *Tissue Engineering Part A* **2014**, *20*, 1993.
- [400] A. Rajan Unnithan, A. Ramachandra Kurup Sasikala, C. H. Park, C. S. Kim, *Journal of Industrial and Engineering Chemistry* **2017**, *46*, 182.
- [401] C. Manferdini, V. Guarino, N. Zini, M. G. Raucchi, A. Ferrari, F. Grassi, E. Gabusi, S. Squarzone, A. Facchini, L. Ambrosio, G. Lisignoli, *Biomaterials* **2010**, *31*, 3986.
- [402] S. Lepidi, G. Abatangelo, V. Vindigni, G. P. Deriu, B. Zavan, C. Tonello, R. Cortivo, *The FASEB Journal* **2006**, *20*, 103.
- [403] L. Pandis, B. Zavan, G. Abatangelo, S. Lepidi, R. Cortivo, V. Vindigni, *J Biomed Mater Res A* **2010**, *93*, 1289.
- [404] L. Pandis, B. Zavan, F. Bassetto, L. Ferroni, L. Iacobellis, G. Abatangelo, S. Lepidi, R. Cortivo, V. Vindigni, *Microsurgery* **2011**, *31*, 138.
- [405] D. E. Soranno, C. B. Rodell, C. Altmann, J. Duplantis, A. Andres-Hernando, J. A. Burdick, S. Faubel, *American Journal of Physiology-Renal Physiology* **2016**, *311*, F362.
- [406] B. Thierry, F. M. Winnik, Y. Merhi, J. Silver, M. Tabrizian, *Biomacromolecules* **2003**, *4*, 1564.
- [407] J. Gaston, S. L. Thibeault, *Biomatter* **2013**, *3*, e23799.
- [408] S. L. Thibeault, S. A. Klemuk, X. Chen, B. H. Quinchia Johnson, *Journal of Voice* **2011**, *25*, 249.
- [409] X. Jia, Y. Yeo, R. J. Clifton, T. Jiao, D. S. Kohane, J. B. Kobler, S. M. Zeitels, R. Langer, *Biomacromolecules* **2006**, *7*, 3336.
- [410] J. Dienes, S. Browne, B. Farjun, J. Amaral Passipieri, E. L. Mintz, G. Killian, K. E. Healy, G. J. Christ, *ACS Biomater. Sci. Eng.* **2021**, *7*, 1587.
- [411] S. Poveda-Reyes, V. Moulisova, E. Sanmartín-Masiá, L. Quintanilla-Sierra, M. Salmerón-Sánchez, G. G. Ferrer, *Macromolecular Bioscience* **2016**, *16*, 1311.
- [412] P. Kumar, S. Ciftci, J. Barthes, H. Knopf-Marques, C. B. Muller, C. Debry, N. E. Vrana, A. M. Ghaemmaghami, *Journal of Tissue Engineering and Regenerative Medicine* **2020**, *14*, 45.
- [413] T. Majima, T. Irie, N. Sawaguchi, T. Funakoshi, N. Iwasaki, K. Harada, A. Minami, S.-I. Nishimura, *Proc Inst Mech Eng H* **2007**, *221*, 537.
- [414] S. Wu, M. Kuss, D. Qi, J. Hong, H.-J. Wang, W. Zhang, S. Chen, S. Ni, B. Duan, *ACS Appl. Bio Mater.* **2019**, *2*, 4864.
- [415] K.-H. Chang, H.-T. Liao, J.-P. Chen, *Acta Biomaterialia* **2013**, *9*, 9012.
- [416] H. Lagus, M. Sarlomo-Rikala, T. Böhring, J. Vuola, *Burns* **2013**, *39*, 1577.
- [417] D. M. Heimbach, G. D. Warden, A. Luterman, M. H. Jordan, N. Ozobia, C. M. Ryan, D. W. Voigt, W. L. Hickerson, J. R. Saffle, F. A. DeClement, R. L. Sheridan, A. R. Dimick, *J Burn Care Rehabil* **2003**, *24*, 42.
- [418] D. S. Keskin, A. Tezcaner, P. Korkusuz, F. Korkusuz, V. Hasirci, *Biomaterials* **2005**, *26*, 4023.
- [419] S. Andrews, A. Cheng, H. Stevens, M. T. Logun, R. Webb, E. Jordan, B. Xia, L. Karumbaiah, R. E. Guldberg, S. Stice, *Stem Cells Transl Med* **2019**, *8*, 575.
- [420] X. Bai, S. Lü, Z. Cao, B. Ni, X. Wang, P. Ning, D. Ma, H. Wei, M. Liu, *Carbohydrate Polymers* **2017**, *166*, 123.
- [421] Y. J. Park, Y. M. Lee, J. Y. Lee, Y. J. Seol, C. P. Chung, S. J. Lee, *Journal of Controlled Release* **2000**, *67*, 385.
- [422] H. Xu, Y. Yan, S. Li, *Biomaterials* **2011**, *32*, 4506.
- [423] K. C. Butterfield, A. W. Conovaloff, A. Panitch, *Biomatter* **2011**, *1*, 174.
- [424] S. R. Caliari, M. A. Ramirez, B. A. C. Harley, *Biomaterials* **2011**, *32*, 8990.
- [425] R. A. Hortensius, B. A. C. Harley, *Biomaterials* **2013**, *34*, 7645.
- [426] Y. Henrotin, J.-P. Hauzeur, P. Bruel, T. Appelboom, *BMC Res Notes* **2012**, *5*, 407.
- [427] G. C. Ingavle, A. W. Frei, S. H. Gehrke, M. S. Detamore, *Tissue Engineering Part A* **2013**, *19*, 1349.
- [428] S. Sharma, A. Panitch, C. P. Neu, *Acta Biomaterialia* **2013**, *9*, 4618.

- [429] J. Hayder, M. A. Chaouch, N. Amira, M. Ben Mansour, H. Majdoub, F. Chaubet, R. M. Maaroufi, *International Journal of Polymeric Materials and Polymeric Biomaterials* **2018**, *67*, 277.
- [430] M. A. Ruehle, L. Krishnan, S. A. LaBelle, N. J. Willett, J. A. Weiss, R. E. Guldberg, *MRS Communications* **2017**, *7*, 466.
- [431] J. E. Paderi, K. Stuart, M. Sturek, K. Park, A. Panitch, *Biomaterials* **2011**, *32*, 2516.
- [432] T. Douglas, U. Hempel, C. Mietrach, M. Viola, D. Vigetti, S. Heinemann, S. Bierbaum, D. Scharnweber, H. Worch, *Journal of Biomedical Materials Research Part A* **2008**, *84A*, 805.
- [433] K. Stuart, J. Paderi, P. W. Snyder, L. Freeman, A. Panitch, *PLOS ONE* **2011**, *6*, e22139.
- [434] C. Longinotti, *Burns & Trauma* **2014**, *2*, 2321.
- [435] V. Colletta, D. Dioguardi, A. Di Lonardo, G. Maggio, F. Torasso, *J Wound Care* **2003**, *12*, 357.
- [436] S. Thönes, S. Rother, T. Wippold, J. Blaszkiewicz, K. Balamurugan, S. Moeller, G. Ruiz-Gómez, M. Schnabelrauch, D. Scharnweber, A. Saalbach, J. Rademann, M. T. Pisabarro, V. Hintze, U. Anderegg, *Acta Biomaterialia* **2019**, *86*, 135.
- [437] V. R. Driver, L. A. Lavery, A. M. Reyzelman, T. G. Dutra, C. R. Dove, S. V. Kotsis, H. M. Kim, K. C. Chung, *Wound Repair Regen* **2015**, *23*, 891.
- [438] “Dermagen® sur Diabète et Ulcère du pied - Registre des essais cliniques - ICH GCP,” can be found under <https://ichgcp.net/fr/clinical-trials-registry/NCT00521937>, **n.d.**
- [439] M. Cortes, A. T. Baria, N. B. Schwartz, *Development* **2009**, *136*, 1697.
- [440] S. Murali, B. Rai, C. Dombrowski, J. L. J. Lee, Z. X. H. Lim, D. S. Bramono, L. Ling, T. Bell, S. Hinkley, S. S. Nathan, J. H. Hui, H. K. Wong, V. Nurcombe, S. M. Cool, *Biomaterials* **2013**, *34*, 5594.
- [441] R. I. W. Osmond, W. C. Kett, S. E. Skett, D. R. Coombe, *Anal Biochem* **2002**, *310*, 199.
- [442] D. Thakar, E. Migliorini, L. Coche-Guerente, R. Sadir, H. Lortat-Jacob, D. Boturyn, O. Renaudet, P. Labbe, R. P. Richter, *Chem. Commun.* **2014**, *50*, 15148.
- [443] T. F. L. Wishart, F. J. Lovicu, *Cells* **2023**, *12*, 1364.
- [444] F. Kubaski, R. W. Mason, A. Nakatomi, H. Shintaku, L. Xie, N. N. van Vlies, H. Church, R. Giugliani, H. Kobayashi, S. Yamaguchi, Y. Suzuki, T. Orii, T. Fukao, A. M. Montaña, S. Tomatsu, *Journal of Inherited Metabolic Disease* **2017**, *40*, 151.
- [445] T. Kunzke, B. Balluff, A. Feuchtinger, A. Buck, R. Langer, B. Lubber, F. Lordick, H. Zitzelsberger, M. Aichler, A. Walch, *Oncotarget* **2017**, *8*, 68012.
- [446] M. J. Dewey, V. Kolliopoulos, M. T. Ngo, B. A. C. Harley, *Materialia (Oxf)* **2021**, *18*, 101149.
- [447] T. Mckee, “Extracellular matrix composition of connective tissues: systematic review and meta-analysis,” can be found under <https://escholarship.mcgill.ca/concern/theses/6395w9745>, **n.d.**
- [448] N. J. Kuiper, A. Sharma, *Osteoarthritis and Cartilage* **2015**, *23*, 2233.
- [449] S. Bratulic, A. Limeta, F. Maccari, F. Galeotti, N. Volpi, M. Levin, J. Nielsen, F. Gatto, *J Biol Chem* **2022**, *298*, 101575.
- [450] F. Gatto, N. Volpi, H. Nilsson, I. Nookaew, M. Maruzzo, A. Roma, M. E. Johansson, U. Stierner, S. Lundstam, U. Basso, J. Nielsen, *Cell Reports* **2016**, *15*, 1822.
- [451] T. Wang, F. Yang, *Stem Cell Res Ther* **2017**, *8*, 284.
- [452] U. Häcker, K. Nybakken, N. Perrimon, *Nat Rev Mol Cell Biol* **2005**, *6*, 530.
- [453] A. Kleinschmit, T. Koyama, K. Dejima, Y. Hayashi, K. Kamimura, H. Nakato, *Developmental Biology* **2010**, *345*, 204.
- [454] A.-C. Gradilla, I. Guerrero, *Current Opinion in Genetics & Development* **2013**, *23*, 363.
- [455] S. Oberhansl, A. G. Castaño, A. Lagunas, E. Prats-Alfonso, M. Hirtz, F. Albericio, H. Fuchs, J. Samitier, E. Martinez, *RSC Adv.* **2014**, *4*, 56809.
- [456] G. V. Dubacheva, C. Araya-Callis, A. Geert Volbeda, M. Fairhead, J. Codée, M. Howarth, R. P. Richter, *J Am Chem Soc* **2017**, *139*, 4157.
- [457] W. Malaeb, H. F. Bahmad, W. Abou-Kheir, R. Mhanna, *Biomater. Sci.* **2019**, *7*, 4283.
- [458] T. Bürgi, *Nanoscale* **2015**, *7*, 15553.
- [459] C. Vericat, M. E. Vela, G. Benitez, P. Carro, R. C. Salvarezza, *Chemical Society Reviews* **2010**, *39*, 1805.
- [460] Y. Xue, X. Li, H. Li, W. Zhang, *Nature Communications* **2014**, *5*, 4348.
- [461] E. Migliorini, D. Thakar, R. Sadir, T. Pleiner, F. Baleux, H. Lortat-Jacob, L. Coche-Guerente, R. P. Richter, *Biomaterials* **2014**, *35*, 8903.
- [462] H. Otsuka, Y. Nagasaki, K. Kataoka, *Current Opinion in Colloid & Interface Science* **2001**, *6*, 3.
- [463] X.-F. Xiao, X.-Q. Jiang, L.-J. Zhou, *Chinese Journal of Analytical Chemistry* **2013**, *41*, 445.
- [464] R. F. Delgadillo, T. C. Mueser, K. Zaleta-Rivera, K. A. Carnes, J. González-Valdez, L. J. Parkhurst, *PLOS ONE* **2019**, *14*, e0204194.
- [465] D. Thakar, F. Dalonneau, E. Migliorini, H. Lortat-Jacob, D. Boturyn, C. Albiges-Rizo, L. Coche-Guerente, C. Picart, R. P. Richter, *Biomaterials* **2017**, *123*, 24.
- [466] M. Cerruti, S. Fissolo, C. Carraro, C. Ricciardi, A. Majumdar, R. Maboudian, *Langmuir* **2008**, *24*, 10646.

- [467] A.-S. Mertgen, A. G. Guex, S. Tosatti, G. Fortunato, R. M. Rossi, M. Rottmar, K. Maniura-Weber, S. Zürcher, *Applied Surface Science* **2022**, 584, 152525.
- [468] S. S. Perry, X. Yan, F. T. Limpoco, S. Lee, M. Müller, N. D. Spencer, *ACS Appl. Mater. Interfaces* **2009**, 1, 1224.
- [469] M. Müller, S. Lee, H. A. Spikes, N. D. Spencer, *Tribology Letters* **2003**, 15, 395.
- [470] R. Michel, S. Pasche, M. Textor, D. G. Castner, *Langmuir* **2005**, 21, 12327.
- [471] C. Nicosia, J. Huskens, *Materials Horizons* **2014**, 1, 32.
- [472] P. Machillot, C. Quintal, F. Dalonneau, L. Hermant, P. Monnot, K. Matthews, V. Fitzpatrick, J. Liu, I. Pignot-Paintrand, C. Picart, *Adv Mater* **2018**, 30, e1801097.
- [473] C. J. Jones, S. Beni, J. F. K. Limtiaco, D. J. Langeslay, C. K. Larive, *Annu Rev Anal Chem (Palo Alto Calif)* **2011**, 4, 439.
- [474] Susumu. Honda, Yoshikazu. Matsuda, Masaye. Takahashi, Kazuaki. Kakehi, Shigetake. Ganno, *Anal. Chem.* **1980**, 52, 1079.
- [475] S. Honda, *Journal of Chromatography A* **1996**, 720, 183.
- [476] H. Toyoda, T. Nagashima, R. Hirata, T. Toida, T. Imanari, *Journal of Chromatography B: Biomedical Sciences and Applications* **1997**, 704, 19.
- [477] H. Toyoda, K. Shinomiya, S. Yamanashi, I. Koshiishi, T. Imanari, *ANAL. SCI.* **1988**, 4, 381.
- [478] A. D. Easley, T. Ma, C. I. Eneh, J. Yun, R. M. Thakur, J. L. Lutkenhaus, *Journal of Polymer Science* **2022**, 60, 1090.
- [479] E. Migliorini, M. Weidenhaupt, C. Picart, *Biointerphases* **2018**, 13, 06D303.
- [480] K. Singh, C. F. Blanford, *ChemCatChem* **2014**, 6, 921.
- [481] R. P. Richter, K. B. Rodenhausen, N. B. Eisele, M. Schubert, in *Ellipsometry of Functional Organic Surfaces and Films* (Eds.: K. Hinrichs, K.-J. Eichhorn), Springer International Publishing, Cham, **2018**, pp. 391–417.
- [482] I. Reviakine, D. Johannsmann, R. P. Richter, *Analytical Chemistry* **2011**, 83, 8838.
- [483] Y. Abdiche, D. Malashock, A. Pinkerton, J. Pons, *Analytical Biochemistry* **2008**, 377, 209.
- [484] R. Tobias, **n.d.**, 22.
- [485] A. Sales, V. Khodr, P. Machillot, L. Chaar, L. Fourel, A. Guevara-Garcia, E. Migliorini, C. Albigès-Rizo, C. Picart, *Biomaterials* **2022**, 121363.
- [486] J. Sefkow-Werner, J. Le Pennec, P. Machillot, B. Ndayishimiye, E. Castro-Ramirez, J. Lopes, C. Licitra, I. Wang, A. Delon, C. Picart, E. Migliorini, *ACS Appl. Mater. Interfaces* **2022**, 14, 34113.
- [487] C. Kattamuri, K. Nolan, T. B. Thompson, *Biochem J* **2017**, 474, 1093.
- [488] H. Pan, Y. Xia, M. Qin, Y. Cao, W. Wang, *Phys. Biol.* **2015**, 12, 045006.
- [489] B. A. Kerwin, *Journal of Pharmaceutical Sciences* **2008**, 97, 2924.
- [490] S. Sahin, E. van Weeren, H. Zuilhof, L. C. P. M. de Smet, *Applied Surface Science Advances* **2022**, 11, 100271.
- [491] M. Lam, V. Migonney, C. Falentin-Daudre, *Acta Biomaterialia* **2021**, 121, 68.
- [492] N. Zander, D. Pappas, B. Stein, *Oxidation of Polyethylene: A Comparison of Plasma and Ultraviolet Ozone Processing Techniques.*, Defense Technical Information Center, Fort Belvoir, VA, **2009**.
- [493] H. Tan, Y. Tan, K. L. Witte, R. Zuk, G. L. Carricato, S. Lockard, *Fiber-Optic Assay Apparatus Based on Phase-Shift Interferometry*, **2008**, US7319525B2.
- [494] K. L. Witte, H. Persson, S. Choo, R. Zuk, *Amine-Reactive Biosensor*, **2010**, US20100093106A1.
- [495] C. Jurchenko, Y. Chang, Y. Narui, Y. Zhang, K. S. Salaita, *Biophys J* **2014**, 106, 1436.
- [496] F. Boulmedais, B. Frisch, O. Etienne, P. Lavalle, C. Picart, J. Ogier, J.-C. Voegel, P. Schaaf, C. Egles, *Biomaterials* **2004**, 25, 2003.
- [497] S. S. Lee, B. J. Huang, S. R. Kaltz, S. Sur, C. J. Newcomb, S. R. Stock, R. N. Shah, S. I. Stupp, *Biomaterials* **2013**, 34, 452.
- [498] G. Bhakta, A. K. Ekaputra, B. Rai, S. A. Abbah, T. C. Tan, B. Q. Le, A. Chatterjea, T. Hu, T. Lin, M. T. Arafat, A. J. van Wijnen, J. Goh, V. Nurcombe, K. Bhakoo, W. Birch, L. Xu, I. Gibson, H. K. Wong, S. M. Cool, *Spine Journal* **2018**, 18, 818.
- [499] S. Chasan, E. Hesse, P. Atallah, M. Gerstner, S. Diederichs, A. Schenker, K. Grobe, C. Werner, W. Richter, *Advanced Functional Materials* **2022**, 32, 2109176.
- [500] S. Bhattacharyya, L. Feferman, J. K. Tobacman, *Oncotarget* **2017**, 8, 100242.
- [501] S. Nadanaka, M. Ishida, M. Ikegami, H. Kitagawa, *Journal of Biological Chemistry* **2008**, 283, 27333.
- [502] C. M. Willis, M. Klüppel, *J Biol Chem* **2012**, 287, 37042.
- [503] N. Luo, W. Knudson, E. B. Askew, R. Veluci, C. B. Knudson, *Arthritis Rheumatol* **2014**, 66, 1547.
- [504] R. Hua, J. X. Jiang, *Matrix Biology Plus* **2021**, 11, 100063.

## Annex

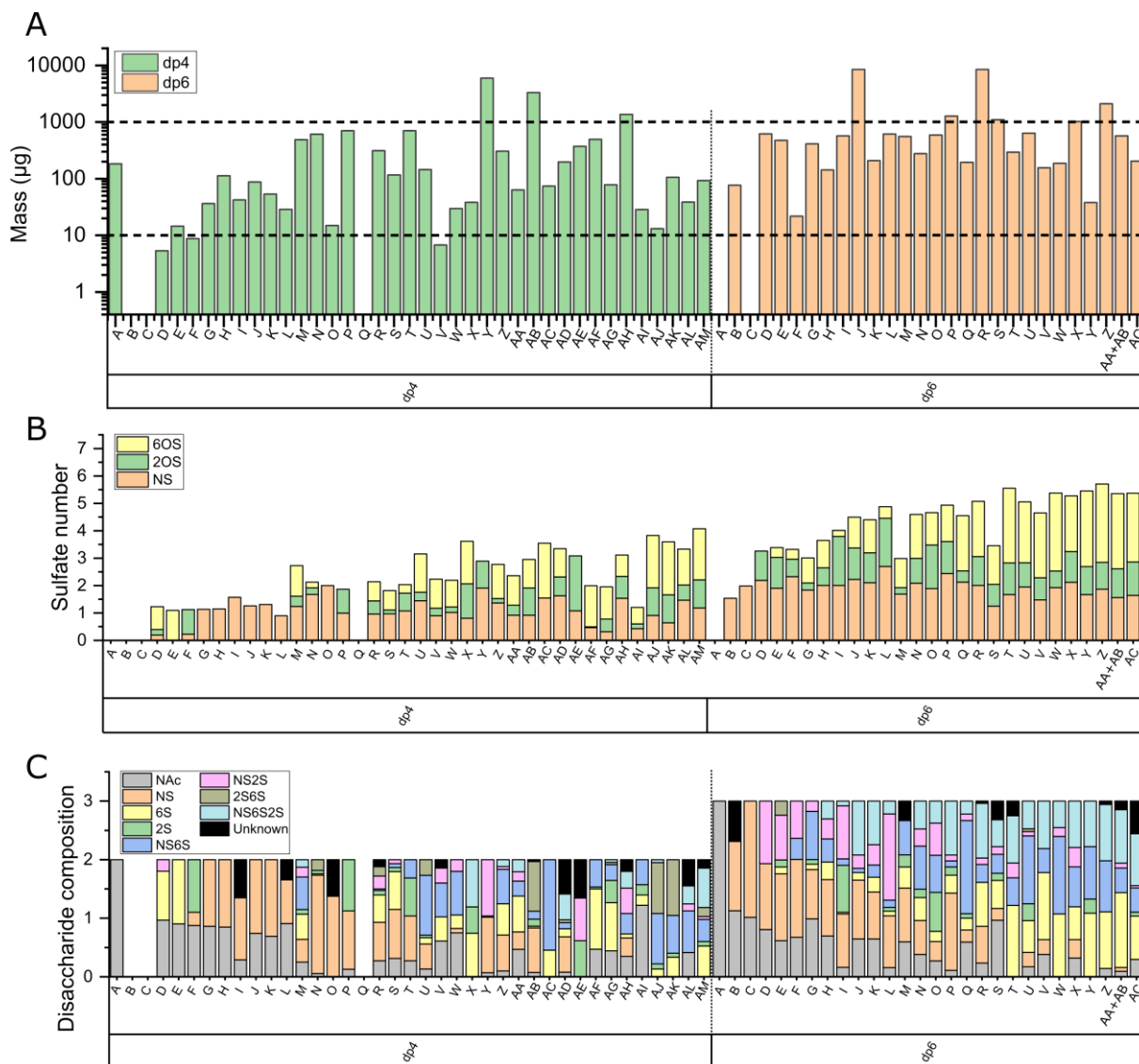


**Figure 40. Characterization of the oligosaccharide library**

**A.** Amounts ( $\mu\text{g}$ ) produced of each oligosaccharide within the library. **B.** Sulfate groups number for each oligosaccharide, classified by their position (NS, 2OS and 6OS). **C.** Composition of the oligosaccharides depicted by their disaccharides constituents:

NAc:  $\Delta\text{UA-GlcNAc}$       NS:  $\Delta\text{UA-GlcNS}$       NS6S:  $\Delta\text{UA-GlcNS6S}$       NS6S2S:  $\Delta\text{UA2S-GlcNS6}$   
 6S:  $\Delta\text{UA-GlcNAc6S}$       2S:  $\Delta\text{UA2S-GlcNAc}$       NS2S:  $\Delta\text{UA,2S-GlcNS}$       2S6S:  $\Delta\text{UA,2S-GlcNAc,6S}$

For mixed compounds, each disaccharide detected is not necessary an integer.

# Sweet but Challenging: Tackling the Complexity of GAGs with Engineered Tailor-Made Biomaterials

Jean Le Pennec, Catherine Picart,\* Romain R. Vivès,\* and Elisa Migliorini\*

**Glycosaminoglycans (GAGs) play a crucial role in tissue homeostasis by regulating the activity and diffusion of bioactive molecules. Incorporating GAGs into biomaterials has emerged as a widely adopted strategy in medical applications, owing to their biocompatibility and ability to control the release of bioactive molecules. Nevertheless, immobilized GAGs on biomaterials can elicit distinct cellular responses compared to their soluble forms, underscoring the need to understand the interactions between GAG and bioactive molecules within engineered functional biomaterials. By controlling critical parameters such as GAG type, density, and sulfation, it becomes possible to precisely delineate GAG functions within a biomaterial context and to better mimic specific tissue properties, enabling tailored design of GAG-based biomaterials for specific medical applications. However, this requires access to pure and well-characterized GAG compounds, which remains challenging. This review focuses on different strategies for producing well-defined GAGs and explores high-throughput approaches employed to investigate GAG–growth factor interactions and to quantify cellular responses on GAG-based biomaterials. These automated methods hold considerable promise for improving the understanding of the diverse functions of GAGs. In perspective, the scientific community is encouraged to adopt a rational approach in designing GAG-based biomaterials, taking into account the in vivo properties of the targeted tissue for medical applications.**

electrostatic interaction depending on sulfation patterns along their chain, GAGs can bind a myriad of proteins, including growth factors (GF), cytokines, and chemokines. Consequently, GAGs can regulate the bioactivity of proteins and their delivery to the surrounding cells, thereby exerting key regulatory roles in many biological processes.<sup>[1–4]</sup> It is well-known that GAG content and fine structural composition vary across tissues and are developmentally regulated.<sup>[5–9]</sup>

For these reasons, the use of GAGs in biomaterials for delivery of GFs in tissue engineering is becoming a common approach.<sup>[10–17]</sup> Over the last decades, a large variety of GAG-based biomaterials has been developed including scaffolds, coatings, microparticles, hydrogels, cryogels, coacervates, or liposomes.<sup>[17,18]</sup> As previously reviewed, the primary applications of GAG-based biomaterials relate to bone, cartilage or tendon regeneration, and wound healing.<sup>[19,20]</sup> Depending on the targeted application, the selection of the biomaterial type must be adapted to the desired properties, including dimensionality

(2D/3D material), mechanical and chemical properties, as well as implantation or injection strategies. The fabrication of GAG-based biomaterials can be achieved through various functionalization approaches to control their shape, viscoelastic properties, cell adhesion properties, degradation properties, and the spatiotemporal release of bioactive molecules such as GFs. The use of GAG-based biomaterials for regenerative medicine applications in combination (or not) with GFs has been exhaustively reviewed.<sup>[17,20,21]</sup> Hachim and co-workers provided a detailed examination of optimal combinations between GFs and GAGs, along with a comprehensive overview of all delivery systems for each type of GF and GAG.<sup>[17]</sup> Strategies for the fabrication of GAG-based hydrogels have been reviewed by Freudenberg and co-workers,<sup>[22]</sup> and those for GAG-based cryogels by Wartenberg and co-workers.<sup>[23]</sup> It is worth noting that several biomaterials featuring identical GAG types have been used for engineering different tissues and exhibited distinct properties. Generally, such property variabilities result from the combination of GAGs and GFs used, which may elicit specific functions related to the targeted tissue, such as vessel or neurite growth, bone formation, or anti-inflammatory effects.<sup>[17]</sup>

## 1. Introduction

Glycosaminoglycans (GAGs) are linear polysaccharides that are major components of the extracellular matrix. Through

J. Le Pennec, C. Picart, E. Migliorini  
 U1292 Biosanté  
 INSERM  
 CEA  
 CNRS EMR 5000 Biomimetism and Regenerative Medicine  
 University Grenoble Alpes  
 Grenoble F-38054, France  
 E-mail: [catherine.picart@cea.fr](mailto:catherine.picart@cea.fr); [elisa.migliorini@cea.fr](mailto:elisa.migliorini@cea.fr)

R. R. Vivès  
 Univ. Grenoble Alpes  
 CNRS, CEA, IBS, Grenoble France  
 E-mail: [romain.vives@ibs.fr](mailto:romain.vives@ibs.fr)

 The ORCID identification number(s) for the author(s) of this article can be found under <https://doi.org/10.1002/adma.202312154>

© 2023 The Authors. Advanced Materials published by Wiley-VCH GmbH. This is an open access article under the terms of the [Creative Commons Attribution-NonCommercial](https://creativecommons.org/licenses/by-nc/4.0/) License, which permits use, distribution and reproduction in any medium, provided the original work is properly cited and is not used for commercial purposes.

DOI: 10.1002/adma.202312154

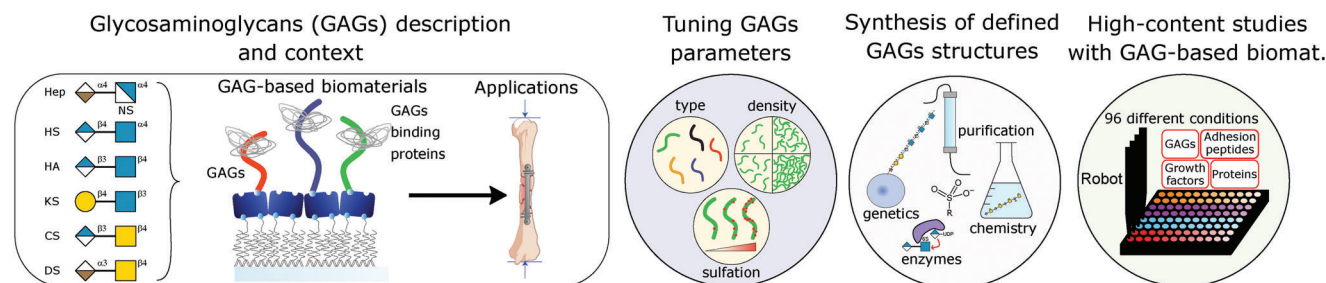


**Figure 1.** Schematic representation of the main topics of the review organized in four chapters to describe GAGs and their use in GAG-based biomaterials, the important parameters that can be tuned when designing a GAG-based biomaterial, the techniques to obtain pure oligosaccharides with defined sulfation, and finally the high-throughput methods available to compare different properties of GAGs for molecular and cellular studies.

Cytotoxicity and the ability to deliver GFs are the most frequently studied parameters of GAG-based biomaterials.<sup>[24–27]</sup> However, the molecular interactions between GAGs and GFs as well as their consequences on cellular responses remain poorly understood. In particular, the biological properties of the GF may depend upon its delivery mode, either in solution as conventionally studied,<sup>[28–32]</sup> or when physically bound to the GAG-based biomaterial. Indeed, the presentation of GFs in a bound form may better mimic the natural conditions, as in the extracellular matrix (ECM) or in the pericellular coat.

A significant challenge for the generation of GAG-based biomaterials is the structural variability of GAGs, which depends on the source, and the requirement for sufficient quantities of well-defined GAGs. Therefore, when designing biomimetic materials for medical applications or to studying the effects of GAGs on cellular responses, it is crucial to consider the structural discrepancies between commercially available GAGs and those found in vivo. Novel methods for producing controlled oligosaccharides in sufficient quantities are therefore needed and are currently under development.

Here, we will focus on immobilized GAGs, which exhibit a greater degree of physiological relevance compared to their soluble counterparts. Improving our understanding of the molecular interactions between GAGs and proteins or GFs is a prerequisite for engineering biomaterials with more advanced functionalities. In this manuscript, we highlight several aspects pivotal for the design of GAG-based biomaterials and their investigation at high content (**Figure 1**). In particular, the type, density, and sulfation of GAGs are highly variable parameters in vivo that depend on the tissue, pathology, or age, and should be considered in the design of biomaterials. To address this, two major issues must be considered: first, the need of methodologies for the synthesis/preparation of well-defined GAG structures, including highly pure, structurally defined oligosaccharides in substantial quantities; second, the implementation of high-throughput techniques to analyze the interactions between GAGs and other biomolecules such as GFs, and to evaluate their impact on cellular responses in vitro. Automated strategies for biomaterial fabrication and cell behavior analysis have recently emerged.<sup>[33,34]</sup> We anticipate that novel high-content methodologies for the study of GAG–GF interactions and the role of GAGs mediated presentation of GFs on cellular responses will emerge and will be further developed.

## 2. GAGs: Structure, Biological Functions, and Biomaterial Applications

### 2.1. The GAG Family

GAGs constitute a family of complex polysaccharides, encompassing heparin (Hep), heparan sulfate (HS), chondroitin sulfate (CS), dermatan sulfate (DS), keratan sulfate (KS), and hyaluronic acid (HA). GAG chains are constituted by the repetition of a disaccharide unit, composed of an amino sugar (either glucosamine or galactosamine) and a hexuronic acid (glucuronic or iduronic acid). The nature of the saccharide constituents defines each GAG type and has been previously reviewed.<sup>[17]</sup> With the exception of HA, these chains are covalently bound to a protein core, forming a proteoglycan (PG) in a well-defined manner. Depending on their protein core, PGs can carry between one to more than a hundred GAG chains of one or different GAG types,<sup>[35]</sup> and can be found in various locations, including the ECM, cell surfaces, the circulation, or even intracellular vesicles.<sup>[36]</sup> GAGs are synthesized directly in the Golgi, starting with the addition of a tetrasaccharide linker to a serine residue (alternatively, threonine or asparagine for KS) of the protein core. Next, they are further elongated and modified by many biosynthesis enzymes.<sup>[9,37–41]</sup> The most crucial modifications involve the transfer of sulfate groups to specific positions of the disaccharide units, which are catalyzed by various sulfotransferase enzymes. By controlling precisely the positions of sulfate groups along the GAG chain, these sulfation enzymes generate a wide array of sulfated saccharide sequences, resulting in tremendous structural diversity. These various combinations of highly negatively charged sulfate groups mediate interactions with a multitude of proteins. A recent extensive literature review unveiled the existence of more than 3400 distinct GAG-binding proteins.<sup>[42]</sup> Through these interactions, GAGs regulate protein activity, structural conformation, interaction with cell receptors, and spatial localization.<sup>[43,44]</sup> Consequently, GAGs govern a large number of biological functions in the organism.<sup>[8]</sup> Mutations of the genes associated to GAG biosynthesis often lead to phenotypic defects.<sup>[9]</sup> This suggests that GAG biosynthesis is highly regulated with evidence indicating the existence of compensatory effects between different GAGs. Notably, alterations of both HS length and sulfation in chondrocytes have been correlated with a strong increase in CS content.<sup>[45,46]</sup> Furthermore, GAGs play pivotal roles in ECM architecture, cohesion, and hydration,

conferring unique mechanical properties of tissues, such as skin, cartilage, synovial fluids, or vitreous humor.<sup>[47]</sup>

## 2.2. Tissue Prevalence, Biological Function of GAGs, and Their Biomaterial Applications

Altogether, the remarkable physical and biological functions of GAGs make them excellent candidates for biomaterial applications, particularly in the field of tissue regeneration (Table 1).<sup>[17–20,22,23,48–50]</sup>

Structurally, GAGs are categorized according to the nature of their saccharide backbone and sulfation patterns. HA, Hep, HS, and KS belong to the glucosaminoglycan subfamily, characterized by a glucosamine-containing disaccharide unit while CS and DS belong to the galactosaminoglycans family since their disaccharide units contain a galactosamine. HA is the structurally simplest GAG, as it is not sulfated and never linked to a PG but synthesized at the cell surface.

As reported in Table 1, except HS which is produced ubiquitously in the body at the cell surface of virtually all cell types, and is present in the ECM of all tissues, the other GAGs are tissue-specific. In particular, Hep has been first extracted from the liver but is also present in the intracellular granules of mast cells, lung arteries, skin, and in the bipotential glial progenitor cells. CS is found attached to aggrecan in cartilage.<sup>[41,51]</sup> KS is predominantly found in the cornea, central and peripheral nervous systems, cartilage, and bone. DS is also widely distributed, notably in skin, blood vessels, heart valves, cornea, tendons, and lungs. HA is abundantly found in soft tissues such as synovial fluid, articular cartilage, skin, vitreous humor, ECM of loose connective tissues and in the umbilical cord.

The functions of GAGs are really vast and summarized in Table 1. Several GAGs (HA, CS, DS, and KS) share the common role of ECM formation, hydration, preservation, and resilience to compression. HA also regulates cell adhesion and motility through interactions with its cell-surface receptors CD44 and RHAMM.<sup>[52,53]</sup> Many studies have reported that HA biological functions vary depending on its molecular weight,<sup>[54]</sup> high molecular weight HA being generally associated with tissue homeostasis and exhibits anti-inflammatory, anti-proliferative, anti-angiogenic, and anti-metastatic activities. Conversely, low molecular weight HA is often considered as an alarm signal related to inflammation, angiogenesis, and metastasis.<sup>[54]</sup> In cartilage, CS is mostly found attached to aggrecan, and confers its elasticity and anti-inflammatory properties to the tissue.<sup>[41,51]</sup> In the nervous system, CS chains serve as cues for guiding neural development and regeneration.<sup>[19,55]</sup> CS, particularly CS-E, plays also a role in angiogenesis.<sup>[56]</sup> DS is involved in various biological functions including wound repair, ECM assembly with collagen fibers, inflammation, anti-coagulation, neural guidance and development, cell proliferation, invasion, and metastasis.<sup>[6,57]</sup> KS contributes to neural guidance, development, and regeneration, notably playing a role in promoting neuron–glial cell interactions, myelination, and axonal repair.<sup>[58]</sup> Hep, beyond its anticoagulant properties, can also inhibit cell proliferation, inflammation, and tumor metastasis.<sup>[59]</sup> HS participates in a wide range of functions, including cell differentiation, tissue morphogene-

sis, cell interactions and proliferation, and interaction with GFs, cytokines, and cell adhesion molecules.<sup>[2,4,60–67]</sup>

Each GAG can exert various biological functions, which are often dictated by their interactions with specific proteins, as described elsewhere.<sup>[68]</sup>

Hep and HA are the most advanced GAGs for biomaterial applications. Indeed, due to its large binding properties, many Hep-based biomaterials have been developed for biomedical applications, particularly in tissue engineering. Medical devices incorporating Hep for its anticoagulant properties have been successfully validated in clinical trials and are now commercially available.<sup>[69]</sup> HA is prevalent in a wide range of cosmetics and is in clinical trials for wound repair using different biomaterials like HA-based sponges,<sup>[70]</sup> or HA-based dermal substitute membranes.<sup>[71,72]</sup> HA-based scaffolds have also been tested in clinics for cartilage repair.<sup>[73–80]</sup>

Various CS-based biomaterials have been developed for a broad range of applications. Notably, a membrane made of bovine tendon collagen and CS-C successfully completed clinical trials and is now commercially available for skin repair of burn victims.<sup>[81,82]</sup> For cartilage repair, CS has already been used in clinical trials and is commercially available, though not as a biomaterial but as an intra-articular injectable solution.<sup>[83]</sup> Alongside, CS-based biomaterials such as hydrogels are currently being developed to repair damaged cartilage.<sup>[77–80,84,85]</sup> There are no HS-based biomaterial under clinical trial, maybe due to the structural diversity of HS and its interaction with numerous proteins, or to the fact that it was rather considered as a secondary product during heparin purification. However, *in vitro* and *in vivo* studies have investigated HS-based biomaterials as listed in Table 1. Application of DS in biomaterials is progressing slowly compared to the other GAGs and Table 1 illustrates emerging developments. Surprisingly, to our knowledge, no KS-based biomaterial has been developed.

## 3. GAGs In Vivo: Importance of Tuning GAG Density, Type, and Sulfation

In tissues, the type, density, length, and sulfation of GAGs are precisely modulated. These parameters directly affect the interactions with bioactive molecules and consequently modify cellular responses. Examples of the variation of these parameters in tissues are shown in Figure 2. Panel A illustrates differences in the distribution of GAG types, as exemplified by distinct localizations of HS and CS in mice eye sections during embryonic development. Panel B depicts variations in the concentration of sulfated GAGs, as in mice growth plate exhibiting well-defined areas with high (dark blue) or low (white) concentrations. Panel C highlights differences of GAG sulfation in tissues. This panel shows glycan fragments detected by MALDI-FT-ICR mass spectrometry in patients with gastric cancer. Some of the glycans detected can be attributed to GAG structures. It is possible to identify a separation between regions containing sulfated or nonsulfated glycans.

### 3.1. Importance of GAG type and Density In Vivo

As seen in Table 1, GAG prevalence varies across tissues and fluids. In animal tissues, the density and distribution of

**Table 1.** Presentation of the structure, location, biological functions, and biomaterial applications of the different GAGs. In the disaccharide unit column are presented both the chemical structure and the representation with the Symbol Nomenclature for Glycans (SNFG). R<sup>2</sup>, R<sup>3</sup>, R<sup>6</sup>, and R indicate H or SO<sub>3</sub><sup>-</sup> groups. Biomaterial applications in green indicate the biomaterials that have already been used in clinical trials for the mentioned application. We specified in light brown which bioactive molecules, such as GFs, have been used in the biomaterials. BMP2/4: Bone Morphogenetic Protein 2/4; FGF2: Fibroblast Growth Factor 2; GDNF: Glial cell line-derived neurotrophic factor; HB-EGF: Heparin-Binding EGF-like Growth Factor; IGF-1: insulin-like growth factor-1; IL-4/-10/-13: Interleukin-4/-10/-13; NGF: Nerve Growth Factor; PDGF-BB: Platelet-Derived Growth Factor -BB; SDF-1 $\alpha$ : Stromal cell-Derived Growth Factor -1 $\alpha$ ; Shh: Sonic Hedgehog; SV: Simvastatin; TGF- $\beta$ 3: Transforming Growth Factor Beta-3; VEGF: Vascular Endothelial Growth Factor.

	Disaccharide unit	Tissue prevalence	Biological functions	Biomaterial applications
Hep	<p> <chem>OC[C@H]1O[C@@H](O[C@H]2[C@@H](O)[C@H](O)[C@@H](O)O[C@H]2O[C@H]1O)[C@H](O)[C@@H](O)[C@H](O)O</chem>             IdoA G1cNS         </p>	Intracellular granules of mast cells <sup>[86]</sup> Lung arteries Liver and skin Bipotential glial progenitor cells	Anti-coagulation Anti-inflammation Anti-proliferation Anti-metastatic	Anti-coagulation <sup>[69]</sup> Anti-inflammation <sup>[87-89]</sup> – IL-4 <sup>[87,88]</sup> IL-13 <sup>[89]</sup> Bone repair <sup>[90-97]</sup> – BMP2 <sup>[90-97]</sup> Wound healing <sup>[98,99]</sup> – FGF2 <sup>[98]</sup> HB-EGF <sup>[99]</sup> Cartilage repair <sup>[92,100,101]</sup> – BMP2 <sup>[92]</sup> TGF- $\beta$ 3 <sup>[100]</sup> Vascular reconstruction <sup>[49,102-117]</sup> – SDF-1 $\alpha$ <sup>[103,104]</sup> VEGF <sup>[102,108-114]</sup> FGF2 <sup>[115,116]</sup> Shh+IL-10 <sup>[117]</sup> Tendon reconstruction <sup>[118-120]</sup> – PDGF-BB <sup>[118-120]</sup> Nerve growth <sup>[121-123]</sup> – GDNF <sup>[121]</sup> NGF <sup>[121-123]</sup> Cancer detection and apoptosis <sup>[124,125]</sup>
HS	<p> <chem>OC[C@H]1O[C@@H](O[C@H]2[C@@H](O)[C@H](O)[C@@H](O)O[C@H]2O)[C@H](O)[C@@H](O)[C@H](O)O</chem>             G1cA G1cNAC         </p>	Basement membranes Cell surface of all cell types ECM of all tissues	Cell differentiation and proliferation Cell-cell interactions Tissue morphogenesis and organ function	Bone repair <sup>[126]</sup> – BMP2 <sup>[126]</sup> Cartilage repair <sup>[127-129]</sup> – BMP2 <sup>[127-129]</sup> Vascular reconstruction <sup>[110,130-133]</sup> – VEGF <sup>[110,130]</sup> FGF2 <sup>[132,133]</sup>
HA	<p> <chem>OC[C@H]1O[C@@H](O[C@H]2[C@@H](O)[C@H](O)[C@@H](O)O[C@H]2O)[C@H](O)[C@@H](O)[C@H](O)O</chem>             G1cA G1cNAC         </p>	Synovial fluid Articular cartilage Skin Vitreous humor ECM of loose connective tissues Umbilical cord	Interactions with GFs, cytokines and cell adhesion molecules Inflammation	Wound healing <sup>[70,137-139]</sup> – HB-EGF <sup>[139]</sup> Cartilage repair <sup>[73-80]</sup> Bone repair <sup>[12,92,140-144]</sup> – BMP2 <sup>[12,92,140,141]</sup> SV <sup>[143]</sup> FGF2 <sup>[144]</sup> Vascular reconstruction <sup>[145-147]</sup> Anti-inflammation <sup>[148,149]</sup> – IL-10 <sup>[148]</sup> Vocal fold repair <sup>[150-152]</sup> Muscle regeneration <sup>[153,154]</sup> Lung tissue model <sup>[155]</sup> – FGF7+FGF10 <sup>[155]</sup> Tendon / ligament repair <sup>[156]</sup> Nerve growth <sup>[157]</sup> Adipose tissue engineering <sup>[158]</sup>
KS	<p> <chem>OC[C@H]1O[C@@H](O[C@H]2[C@@H](O)[C@H](O)[C@@H](O)O[C@H]2O)[C@H](O)[C@@H](O)[C@H](O)O</chem>             Gal G1cNAC         </p>	Cornea Bone Cartilage Central and peripheral nervous system	Corneal ECM assembly for light passage and hydration Resilience to compression Guidance of neural growth and regeneration	

(Continued)

Table 1. (Continued).

	Disaccharide unit	Tissue prevalence	Biological functions	Biomaterial applications
CS		Cartilage Bone Brain Heart valves	Elasticity and anti-inflammatory properties Guidance of neural growth and regeneration Angiogenesis (CS-E)	Wound healing <sup>[82,98,159,160]</sup> – FGF2 <sup>[98]</sup> Cartilage repair <sup>[77-80,84,85]</sup> Bone repair <sup>[126,161-164]</sup> – BMP2 <sup>[126,161,162]</sup> , BMP4, <sup>[163]</sup> PDGF-BB <sup>[164]</sup> Nerve growth <sup>[165,166]</sup> – NGF <sup>[165,166]</sup> Tendon regeneration <sup>[167,168]</sup> – IGF-1/GDF-5 <sup>[168]</sup> Angiogenesis <sup>[131]</sup>
DS		Skin Blood vessels Heart valves Cornea Tendons Lung	Wound repair ECM assembly with collagen Inflammation Anticoagulation Neural guidance and development Cell proliferation, invasion, and metastasis	Reduction of biofilm deposition <sup>[169]</sup> Vascular reconstruction <sup>[170,171]</sup> Bone repair <sup>[97,172]</sup> – BMP2 <sup>[97]</sup> Wound healing <sup>[173]</sup>

GAGs is varying depending on tissue type but also throughout lifetime.<sup>[177,178]</sup> The spatiotemporal distribution of GAGs within tissues is a highly dynamic process, tightly regulated during development, homeostasis, and in response to various physiological and pathological stimuli. It relies on the fine balance between GAG biosynthesis and metabolism, exerting significant influence on tissue-specific mechanical properties, cell signaling, and overall tissue functions. As such, GAGs are intricately involved in tissue patterning, organogenesis, and formation of morphogen gradients (hedgehogs, TGF- $\beta$ , Wnt), which are particularly important in early development.<sup>[61,179-182]</sup> Sulfated GAGs distribution also plays a crucial role in wound healing, where they orchestrate cell migration, proliferation, and differentiation. Additionally, production of HA at the wound site enables the formation of a provisional matrix supporting tissue repair.<sup>[183]</sup> In contrast, alterations in the spatiotemporal distribution of GAGs have been frequently associated with various pathological conditions. For example, in osteoarthritis, an imbalance in the synthesis and degradation of CS leads to the degradation of cartilage ECM, resulting in joint degeneration.<sup>[184]</sup> Similarly, altered HS biosynthesis and/or catabolism have been associated with tumor growth, angiogenesis, and metastasis.<sup>[185-187]</sup>

### 3.2. Importance of Sulfation in GAG-Proteins Interactions

GAGs bind to a multitude of proteins, including growth factors, cytokines, and chemokines.<sup>[43,44,60]</sup> Upon binding, GAGs can trigger different mechanisms regulating protein activity, such as protection from degradation, induction of conformational changes activating the protein function, or formation of complexes with cellular receptors. Protein/GAG interactions are mainly, though not exclusively, of electrostatic nature, involving negatively charged carboxyl and sulfate groups of the polysaccharides and clusters of basic amino acids at the surface of the proteins. Consequently, the binding properties of GAGs are tightly linked to their sulfate density and distribution.<sup>[44,188]</sup> The degree of GAG sulfation varies among GAGs.

Hep is the most sulfated among GAGs, with  $\approx 1.6$  to 3.0 sulfates per disaccharide unit.<sup>[189,190]</sup> HS is less sulfated than Hep (between 0.4 and 2.0 sulfates/disaccharide) and features a distinctive molecular organization, in which non or low sulfated and modified (NAc domains) regions alternate with highly sulfated domains (NS domains).<sup>[38]</sup> CS and DS galactosaminoglycans can be variably sulfated, with different sulfation combinations classified by letters as specific units (A, B, C, D, E, etc., see **Figure 3**).<sup>[191,192]</sup> CS and DS can be distinguished by the nature of their disaccharide unit hexuronic acid, which is glucuronic acid for CS, and iduronic acid for DS.<sup>[9,190]</sup> Of note, DS was first referred to as CS-B, before the classification changed. Finally, KS structure is atypical (a galactose residue replaces the hexuronic acid in the disaccharide unit), for an overall sulfation degree comprised between 0.9 and 1.8 sulfates/disaccharide.<sup>[190]</sup>

However and despite tremendous interest, the vast structural heterogeneity of GAGs and the lack of dedicated tools have constituted severe limitations in the structural and functional characterization of GAGs and GAG/protein interactions.<sup>[200]</sup> The most documented example illustrating the impact of specific GAG motifs on proteins is the role of Hep, which activates

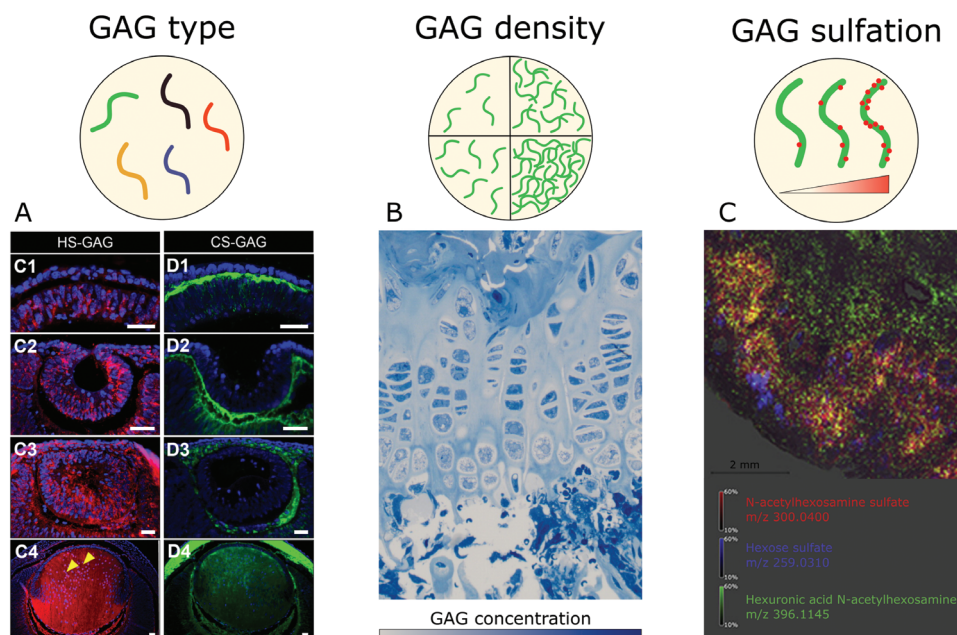


**Figure 2.** Schematic representation of different GAG parameters that naturally vary in animal tissues or cell cultures. A) Immunocytochemical staining of HS and CS in mice eye sections at embryonic days 9.5, 10.5, 11.5 and 14.5. Scale bars are 25  $\mu\text{m}$ . Adapted with permission.<sup>[174]</sup> Copyright 2023, MDPI. B) Toluidine Blue staining representing the density variation of sulfated GAGs in the growth plate of wild-type mice. Adapted with permission.<sup>[175]</sup> Copyright 2017, Elsevier. C) Ion map of *N*-acetylhexosamine sulfate, hexose sulfate, and hexuronic acid *N*-acetylhexosamine glycan fragments detected by MALDI-FT-ICR mass spectrometry in whole tissue sections from a gastric cancer patient shows a separation between areas with sulfated glycans (red and blue) and without nonsulfated area (green). Adapted with permission.<sup>[176]</sup> Copyright 2017, Oncotarget.

Antithrombin III (AT III) by inducing a conformational change of the protein.<sup>[201]</sup> Significant efforts have been dedicated to identifying the precise structure within Hep responsible for mediating this process, and established that AT III bioactivation is highly specific to Hep pentasaccharide sequences featuring a central 3-O sulfated glucosamine.<sup>[202–204]</sup> Compounds exhibiting this sulfation motif are therefore of particular interest for their anticoagulation properties.

Interactions of HS with members of the fibroblast growth factor (FGF) family, notably FGF1 and FGF2, have also been extensively studied. In 1991, two independent research groups demonstrated that cell-surface HS is a coreceptor of FGF2 and is required for the growth factor biological activity.<sup>[1,205]</sup> Subsequent studies highlighted distinct structural features for the binding to these growth factors. The interaction between FGFs and HS requires saccharide motifs of similar size (5–6 sugar

units) and saccharide content (involving *N*-sulfated and 2-*O*-sulfated IdoA residues).<sup>[206,207]</sup> Interestingly, 6-*O*-sulfates were found essential for binding to FGF1, but not to FGF2.<sup>[208,209]</sup> FGF2 activity required the presence of 6-*O*-sulfates and longer saccharide fragments (10–12 sugar units).<sup>[210]</sup> These observations therefore highlighted different structural requirements associated to FGF1 versus FGF2-induced biological responses, providing the first evidence of an uncoupling between HS binding properties and ligand-promoting activities. Structural imaging of the FGF/FGFR/HS complex structure by X-ray crystallography showed that 6-*O*-sulfates contributed to the stabilization of the ternary complex by establishing contact with the FGFR.<sup>[211]</sup> Overall, a wealth of studies also demonstrated the importance of sulfation degree and specific sulfation motifs governing protein/GAG interactions in various biological contexts. These include regulation of the bioactivity of many signaling proteins, including

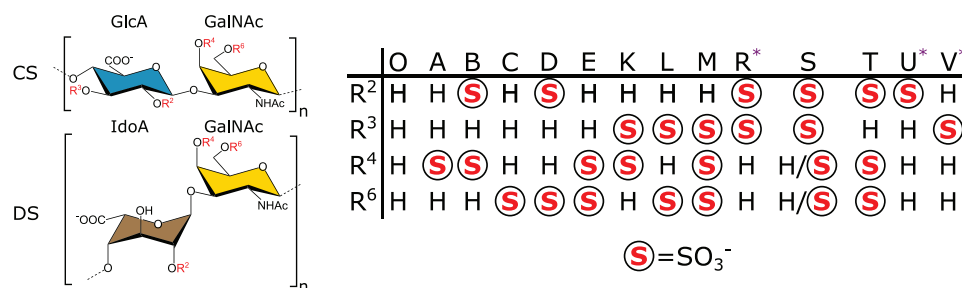


**Figure 3.** Sulfate combinations in CS/DS chains described with the O-, A-, B-, C-, D-, E- main units and the more rare K-,<sup>[193,194]</sup> L-,<sup>[193]</sup> M-,<sup>[193,195]</sup> R-,<sup>[196]</sup> S-,<sup>[197]</sup> T-,<sup>[198]</sup> U-,<sup>[199]</sup> and V-<sup>[199]</sup> units. The star symbol \* indicates a unit that was synthesized but not identified nor extracted from natural source.

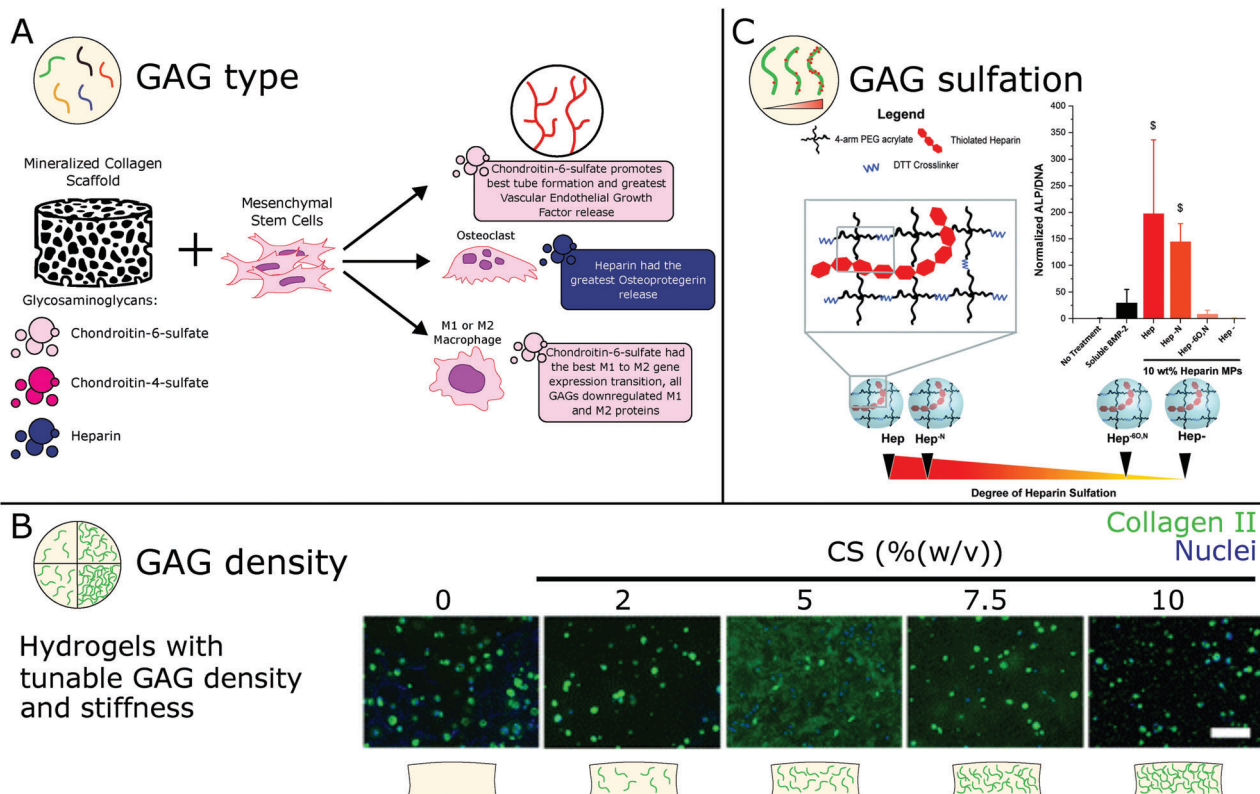


**Figure 4.** Various materials modulating specific GAG parameters to optimize their use for biomedical applications. A) Modulation of GAG type in collagen-GAG scaffolds induces distinct differentiation pathways. Adapted with permission.<sup>[214]</sup> Copyright 2021, Elsevier. B) Modulation of GAG density in hydrogels induces a stronger chondrogenic response for intermediate concentrations of CS, with a more important deposition of collagen II. Scale bar is 200  $\mu\text{m}$ . Adapted with permission.<sup>[216]</sup> Copyright 2017, Springer Nature. C) Modulation of GAG sulfation degree/pattern in microparticles with BMP2 induces sulfation-dependent alkaline phosphatase (ALP) expression. Adapted with permission.<sup>[219]</sup> Copyright 2015, The Royal Society of Chemistry.

cytokines and chemokines, members of the FGF family,<sup>[212]</sup> hepatocyte growth factor (HGF), VEGF, IGFs, and cell membrane receptors and coreceptors.<sup>[8,201]</sup>

In a study by Gama et al., CS-A, C, E, and R (an unnatural GAG, which exhibits the same degree of sulfation as CS-E, but at different positions) tetrasaccharides were compared for their binding affinity to brain-derived neurotrophic factor (BDNF), midkine and FGF1.<sup>[196]</sup> Authors showed that CS-E exhibited the highest affinity with BDNF and midkine, while midkine and BDNF did not bind to CS-R and FGF1 did not bind to any CS. This demonstrates that the binding is not just related to nonspecific charge interactions, but requires specific sulfation patterns. These results therefore support the concept of a “sulfation code” wherein GAGs encode functional information in a sequence-specific manner, akin to DNA, RNA, and proteins.

#### 4. Modulation of GAGs Parameters for Biomaterials Design

Given the inherent variability in GAG type, density, and sulfation profiles, a rational design of biomaterials in relation to the specific *in vivo* attributes of the targeted tissue is critical for biomedical applications. Thus, biomaterial scientists are considering these parameters when engineering GAG-based biomaterials (Figure 4).

#### 4.1. Modulation of GAG Type in Biomaterials

Incorporating GAGs into biomaterials can directly influence stem cell fate by activating some specific cell response, or indirectly by modulating the binding and activity of GFs. Given the distinct structural and functional properties of GAGs, along with their interactions with specific partners at varying affinities, it is expected that each GAG may differently modulate cellular responses.

When considering a biomaterial application, the choice of which GAG to incorporate should be made judiciously to elicit the desired effects (Table 1). Surprisingly, only a limited number of studies have addressed the effect of different GAGs on specific cellular processes. Dewey et al. investigated the effect of various GAGs incorporated into collagen scaffolds on osteogenic differentiation.<sup>[213]</sup> They found that ALP level and BMP2 gene expression, two markers of bone formation, were enhanced on Hep and CS-C scaffolds compared to CS-A scaffolds. Interestingly, CS-C notably increased the expression of SOX9, a marker of chondrogenic differentiation, while Hep markedly enhanced the expression of Osterix, a bone marker. These results therefore indicate that different GAGs may promote the formation of distinct tissues. In another study, Dewey et al. assessed the impact of different GAG types incorporated into collagen scaffolds on endothelial tube formation. They showed that CS-C induced the most robust endothelial tube formation compared to Hep and

CS-A, which was correlated with higher VEGF expression.<sup>[214]</sup> (Figure 4A). All GAGs exhibited anti-inflammatory activities, but CS-C scaffolds led to the most pronounced reduction in IL6 levels, as well as the strongest transition of macrophages from M1 to M2 phenotype. In the same study, Hep showed the best potential to inhibit osteoclastogenesis. In another study, chitosan membranes grafted with various GAGs (HS, Hep, DS, CS-A, CS-C, and HA) were used to investigate their effects on hMSCs adhesion and on osteogenic, adipogenic, and chondrogenic differentiation induced by TGF- $\beta$ .<sup>[215]</sup> Results showed that hMSCs adhered more effectively on HS and HA compared to other GAGs. Furthermore, adipogenic differentiation was predominantly enhanced by HA-chitosan membranes, albeit only at the lowest GAG density. The addition of TGF- $\beta$  to the different GAG-modified chitosan membranes revealed that Hep and HA primarily induced chondrogenic differentiation of MSCs, compared to CS-A. With the aim of developing a biomaterial for tendon tissue engineering, Hortensius et al. engineered collagen-GAG scaffolds via freeze drying with either HA, CS, or Hep.<sup>[168]</sup> They analyzed the cell proliferation and the expression of phenotypic markers in tenocytes cultured in these scaffolds containing IGF-1 growth factor. The authors observed an increase of COL1A2 proliferation marker associated with a decrease in tenascin-C tendon phenotypic marker with Hep, in contrast to HA-scaffolds. Due to the limited amount of studies that compared the role of GAGs on cellular responses, it is, so far, complicated to drive conclusions and to recommend a specific GAG for a specific biomaterial application.

#### 4.2. Modulation of GAG Density in Biomaterials

As previously shown, GAG density is an important parameter for GAG function in vivo. Thus, for designing biomaterials, it is crucial to consider the GAG density of the targeted tissue, since it may impact cells behavior and biological responses, ultimately impacting the tissue regeneration properties of the biomaterial. The control of the GAG density in a biomaterial is complicated since it depends on the way of immobilization of the GAG. In a study by Wang and Yang, methacrylated HS and CS at different densities were incorporated in hydrogels of different stiffness to assess effects on the induction of hMSC chondrogenic differentiation (Figure 4B).<sup>[216]</sup> They observed that chondrogenesis was enhanced with CS compared to HS, particularly in softer hydrogels. The highest neocartilage deposition of collagen types I and II and sulfated GAGs was achieved using intermediate CS concentrations, thus highlighting the importance of precisely regulating GAG density in tissues to induce specific and optimized cellular responses. In another study, collagen-GAG scaffolds were generated via freeze-drying and osteoblasts were cultured on them for seven days.<sup>[217]</sup> Both collagen and GAG concentrations were adjusted to produce different scaffolds, on which cell number and metabolic activity were analyzed. Results showed that the highest metabolic activity and cell number were attained with the highest GAG concentration scaffolds. Another interesting study used PG-mimetic graft copolymers with tunable GAG density.<sup>[218]</sup> Both CS- and Hep-containing graft copolymers successfully delivered FGF-2 to cells, with the Hep low-density copolymer outperforming higher-density counterparts. Such biomaterials

could be of great interest for future investigations into the role of GAG density directly on PG' core protein. Nevertheless, further investigations on GAG density in biomaterials are greatly needed for achieving a more accurate replication of tissue structure and functions.

#### 4.3. Modulation of GAG Sulfation in Biomaterials

Given the importance of GAG sulfation in vivo (see Section 3), the control of sulfation degree and patterns of GAGs in biomaterials is of paramount importance for defining their biological properties (Figure 4C). Cellular studies using CS tetrasaccharide coatings showed that CS-E enhanced neurite outgrowth of different types of neurons including dopaminergic, DRG, and hippocampal neurons.<sup>[196]</sup> This is explained by the ability of CS-E sulfation sequence to recruit specific growth factors to the cell surface, thereby activating downstream signaling pathways. In another study Tellier et al. coated microparticles with either Hep, *N*- or *N*,6-*O*-desulfated Hep or fully desulfated Hep to assess how Hep sulfation pattern regulates BMP2-induced ALP expression in C2C12 cells (Figure 4C).<sup>[219]</sup> The microparticles coated with the most sulfated compounds (Hep and *N*-desulfated Hep), combined with BMP2, elicited enhanced ALP expression compared to soluble BMP2. Conversely, microparticles carrying *N*,6-*O*-desulfated Hep or fully desulfated Hep failed to promote ALP expression with BMP2. This suggests that *N*-sulfation may not be crucial for efficient Hep-mediated BMP2 bioactivity. However, it is worth noting that another study did not support these findings, showing that *N*-sulfation of HS plays a significant role in both the binding and bioactivity of BMP2.<sup>[220]</sup> In this latter study, oligosaccharides of different sizes were used to define the minimum HS oligosaccharide length required for BMP2 binding. SPR competitive binding experiments were then performed to assess the ability of selectively desulfated Hep to compete with surface-bound Hep for binding to BMP2. Results showed that *N*-sulfation is critical for BMP2 binding, followed by 6-*O* and 2-*O* sulfations. C2C12 cells were exposed to BMP2 that had been previously bound to soluble oligosaccharides, and BMP2 bioactivity was assessed by measuring osteogenic gene transcription, ALP activity at 5 days, and mineralization at 12 days. Results further supported the importance of *N*-sulfation. It is worth noting that in this study, the oligosaccharides were presented in solution for in vitro assays, and on a polycaprolactone tube combined with a collagen sponge for in vivo assays. Since GAGs are normally presented via the protein core of PGs, these different presentation modes of the GAG oligosaccharides may influence their interactions with BMP2. Likewise, in the study of Tellier et al., the Hep was neither in the ideal biomimetic conformation, since it was not grafted by its reducing end but was interacting with the microparticles via the multiple thiolation of Hep derivatives. The same group developed a cell coating with layers of biotin and avidin functionalized directly on MSC aggregates, onto which biotinylated Hep were attached, to bind TGF- $\beta$ 1 or FGF2 growth factors.<sup>[221]</sup> In this study, the authors observed that FGF2 loaded on highly sulfated Hep triggered greater proliferation compared to FGF2 loaded on desulfated Hep. With TGF- $\beta$ 1, they observed a significant increase of chondrogenic differentiation, with strong upregulation of collagen II and collagen X gene expression. Interestingly, this

**Table 2.** Comparison of the different methods for the production of defined GAG compounds based on various criteria: simplicity to establish the technique in a laboratory, time-saving characteristics, purity of the produced materials, and control over the structural features of the GAG materials produced, in terms of sulfation and length. The methods are also compared upon a “versatility” criterion that represents their potential applicability in various experimental contexts, such as cell-based assays, whole PG synthesis, or in vivo assays. The two methods in light brown font correspond to straightforward chemical approaches typically used for sulfation modification of large GAG chains. The cell-based biosynthesis method, as the only genetics-based method, is shown with a blue font. The three methods in purple are particularly adapted for the synthesis of GAG-oligosaccharides. Commercial libraries, in black font, have emerged from the development of these other methods.

	Simplicity	Time saving	Purity	Control of GAG structure	Versatility
Chemical desulfation	++	++	-	-	-
Chemical sulfation	++	++	-	-	-
Cell-based biosynthesis	-	-	-	+	++
Chemical synthesis	-	-	+++	+++	+
Chemo-enzymatic synthesis	-	-	+++	+++	+
Purification	+/-	+/-	+	++	+/-
Commercial libraries	+++	+++	+++	+	-

effect was more pronounced with the low-sulfated Hep than with the high-sulfated one, providing further evidence of the crucial role of sulfation. Another study demonstrated that porcine aortic endothelial cell proliferation was more effectively stimulated by collagen hydrogels containing sulfated-HA compared to HA hydrogels, independently of the presence of VEGF<sub>165</sub>.<sup>[222]</sup> Atallah et al. developed injectable hydrogels displaying Hep chains with variable sulfation patterns and observed the proliferation and migration of hMSCs.<sup>[223]</sup> Depending on the Hep sulfation pattern, distinct gradient distributions of platelet-derived growth factor-BB (PDGF-BB) were established, due to different interaction dynamics with the GF. They subsequently observed a slight increase in MSC proliferation and migration for the Hep hydrogels compared to the control, and a significant increase in proliferation and migration for the hydrogels with *N*,6-*O*-desulfated Hep that correlated well with the time-dependent difference in the PDGF-BB gradient formed in the various hydrogels. In a study of Feng et al., the chondrogenic differentiation of hMSCs encapsulated in methacrylated HA-hydrogels was investigated based on the sulfation degree of chemically modified HA.<sup>[224]</sup> After 14 and 28 days of culture in chondrogenic medium with TGF- $\beta$ 1, the expression of aggrecan and collagen II chondrogenic genes was increased in correlation with HA sulfation degree. A similar study compared the chondrogenic differentiation of MSCs encapsulated in PEG-based hydrogels containing CS or its nonsulfated form chondroitin. Surprisingly, they obtained opposite results in relation to GAG sulfation. MSCs in chondroitin hydrogels exhibited significantly greater gene expression of collagen II and aggrecan compared to CS hydrogels after 21 days of culture in chondrogenic medium containing TGF- $\beta$ 1. They even observed a greater early expression of SOX9 on day 7, suggesting that nonsulfated chondroitin materials may promote chondrogenic differentiation more efficiently than CS materials.<sup>[225]</sup> Therefore, the choice of GAG sulfation degree or pattern for biomaterial applications should be carefully considered, depending on the specific tissue targeted for engineering applications. The sulfation pattern of GAGs has been consistently studied for a significant number of growth factors. The development of novel methods for synthesizing defined sulfated GAGs and oligosaccharide structures has made these advances possible.

## 5. Synthesis of Defined Sulfated GAGs and Oligosaccharides

A major challenge for studying GAGs and their mechanisms lies in the preparation of pure and well-characterized GAG materials, with defined length or sulfation patterns. To address this, various strategies can be adopted (Figure 5). We have listed and assessed these strategies (Table 2) based on several key parameters. These include the simplicity and efficiency of their implementation, the degree of purity achieved, and the control of the obtained GAG structures in terms of length, sequence, and sulfation. We have also evaluated them on a “versatility” criterion, by assessing their potential for translation in other research applications, such as cell-based assays, complete proteoglycan synthesis, or in vivo assays necessitating substantial quantities of material.

### 5.1. Specific Desulfation

Methods for specific desulfation of sulfated carbohydrates can use different chemical strategies, including acid-catalyzed desulfation, solvolytic desulfation, alkali-catalyzed desulfation, and desulfation mediated by silylating reagents.<sup>[86,226–228]</sup>

For Hep and HS, chemical treatments have been developed to achieve specific 2-*O*, 6-*O*, or *N*-desulfation and are now commonly used.<sup>[223,229–234]</sup> *N*-desulfation is typically carried out through solvolytic desulfation with dimethyl sulfoxide (DMSO) containing methanol, without depolymerization of HS chains and minimal *O*-desulfation.<sup>[235]</sup> Specific 2-*O* desulfation is generally achieved using sodium hydroxide treatment.<sup>[231]</sup> Although this treatment does not alter other sulfation motifs, it leads to chain depolymerization, resulting in a  $\approx$ 25% reduction of Hep chain molecular weight.<sup>[231]</sup> The 6-*O* specific desulfation is generally performed using *N*-methyl-*N*-(trimethylsilyl)-trifluoroacetamide (MTSTFA) silylating reagent, enabling control of the desulfation degree through temperature and reaction time.<sup>[236,237]</sup> Complete 6-*O* desulfation of Hep results in a loss of  $\approx$ 20% of 2-*O* sulfate groups, without any other structural alteration or depolymerization.<sup>[238]</sup> In contrast, the specific removal of 3-*O* sulfate groups cannot be achieved without affecting other

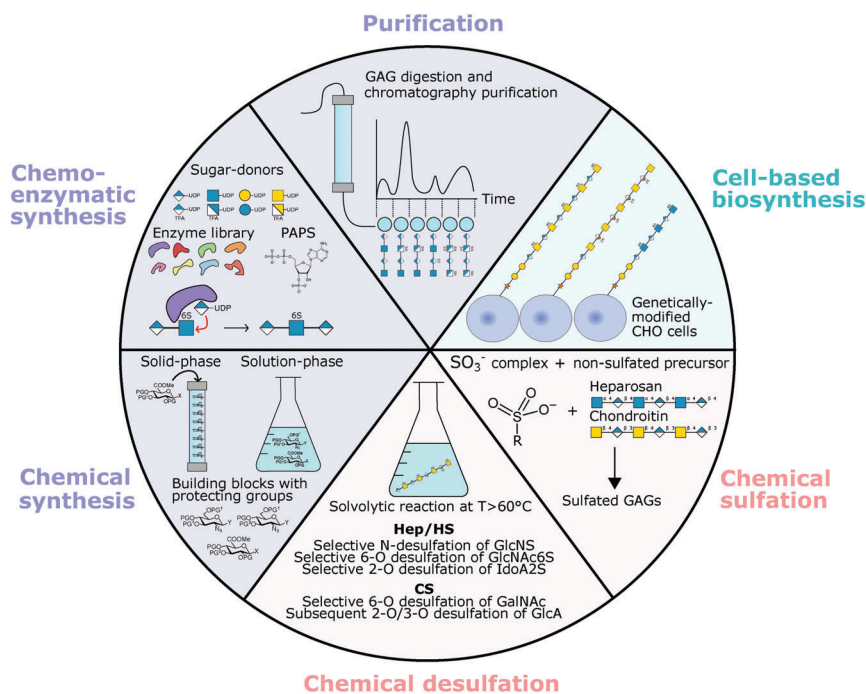


**Figure 5.** Schematic representation of the various methods for the preparation of GAG compounds with defined length, type of sulfation, and sulfation pattern. The two beige-background approaches are commonly used chemical methods for modifying GAG sulfation, using natural sources of polysaccharide. Chemical desulfation consists in using regioselective solvent-based reactions to selectively remove sulfate groups at specific positions. Conversely, chemical sulfation uses  $\text{SO}_3^-$  complexes to add sulfate groups at specific locations on the GAG disaccharide unit. An alternative strategy is the recently reported cell-based biosynthesis approach (shown with a blue background), which involves manipulating CHO cells through knock-in or knock-out of various GAG-biosynthesis genes, to produce cell-surface GAGs with tailored sulfation patterns. The three light purple-background methods are particularly adapted for the synthesis of GAG oligosaccharides. The “purification” approach consists in using a natural source of GAGs. GAG chains are depolymerized with digestion enzymes, and the generated oligosaccharides are purified according to size or charge using chromatography techniques. The chemo-enzymatic synthesis approach is based on the use of recombinant polymerase enzymes with sugar donors to generate oligosaccharide chains or sulfotransferases with 3'-phosphoadenosine-5'-phosphosulfate (PAPS) sulfate donor to introduce sulfate groups at specific positions of the disaccharide motif. Alternatively, full chemical synthesis methods use combinations of monosaccharide or disaccharide building blocks to generate structurally defined oligosaccharides.

sulfation sites. Lyophilization of Hep under extreme alkaline conditions induces selective loss of 2-O and 3-O sulfates, while leaving intact 6-O and N-sulfation.<sup>[239]</sup> These strategies are suitable for examining the overall importance of one type of sulfation, but do not allow the study of precise sulfation sequences. Another strategy for the selective desulfation of HS involves digestion of HS or Hep by sulfatase enzymes.<sup>[240]</sup> Human Sulf1 and Sulf2 (hSulf1 and hSulf2) are the only known extracellular post-synthetic HS modifying enzyme, with a substrate specificity for 6-O sulfation motifs. More precisely, hSulf2 essentially targets HexA(2S)-GlcNS(6S) trisulfated disaccharides, which are then converted into HexA(2S)-GlcNS disaccharides. hSulf2 has been shown to reduce dramatically the FGF1/FGF2-induced proliferation of FGFR1-IIIc-transfected BaF32 cells.<sup>[241]</sup> This result supports further the previously reported requirement of HS 6-O sulfation for promoting the bioactivity of these growth factors.<sup>[210,242]</sup> In addition, the authors showed that hSulf2 differentially regulated FGF1 and FGF2, thereby highlighting the involvement of specific 6-O sulfation pattern in these mechanisms.<sup>[241]</sup> However, this enzymatic desulfation approach is limited by the lack of sulfatases with alternative substrate specificities. The identification of new enzymes may pave the way for the development of novel strategies for preparation of GAG compounds.

Chondroitin, the nonsulfated version of CS can be obtained from the reaction of CS with acidic methanol,<sup>[225,243]</sup> or in DMSO with a small amount of methanol.<sup>[244]</sup> These desulfation methods can also be applied to other GAGs, such as DS or KS.<sup>[232]</sup> For CS, regioselective methods for 4-O and 6-O desulfation have been established.<sup>[245]</sup> The 6-O desulfated CS can be obtained with MT-STFA agent without any depolymerization. A DMSO/methanol-based method was recently reported as an efficient regioselective method for the preparation of 4-O desulfated CS, albeit with some depolymerization. Surprisingly, the conditions used are very similar to the method of Nagasawa et al. for the preparation of chondroitin via global 4-O and 6-O desulfation of CS,<sup>[244]</sup> suggesting that minor protocol modifications may affect the reaction.

## 5.2. Specific Sulfation

An alternative strategy for studying sulfation of GAGs involves the chemical sulfation of nonsulfated precursors such as HA, heparosan (nonsulfated HS), or chondroitin (nonsulfated CS).

For CS, the regioselective sulfation at the C-6 hydroxyl of the GalNAc with limited sulfation at the C-2 hydroxyl of the GlcA can

be achieved using  $\text{SO}_3^-$ -pyridine complex in dimethylformamide (DMF) at 0 °C.<sup>[246,247]</sup>

For HS, chemically sulfated chains can be obtained from the sulfation of heparosan. Effective O-sulfation requires prior N-sulfation of the heparosan chain. First, heparosan must undergo N-deacetylation with NaOH, followed by N-sulfation in  $\text{Na}_2\text{CO}_3$  at 40–50 °C with  $\text{SO}_3^-$ -pyridine complex or  $\text{SO}_3^-$ -trimethylamine complex. The resulting N-sulfated HS can then be regioselectively O-sulfated at the C-6 hydroxyl of the GlcNS, with residual sulfation at the C-2 or C-3 hydroxyls of the GlcA.<sup>[226]</sup> This approach has been used in other studies for sulfation of HA with similar regioselectivity of the C-6 hydroxyl of the GlcNAc, followed by sulfation at the C-4 of the GlcNAc and at the C-2 and C-3 of the GlcA.<sup>[224,248,249]</sup>

### 5.3. Cell-Based Biosynthesis

Due to the complexity of GAG structures, recent research has turned towards producing GAGs using genetically modified cells to avoid complex chemistry or chemoenzymatic steps. Dr. Jeffrey Esko's pioneering work in the 1980s in genetically modifying CHO-K1 cells laid the foundation for the establishment of a comprehensive cell library with specific knock-in (KI) and knock-out (KO) of GAG biosynthesis enzymes. Such a library referred to as the GAGome, has been recently developed by Chen et al. and comprises various cell lines with distinct CS/DS and HS biosynthetic capabilities.<sup>[250]</sup> In total, 28 different genes of biosynthesis enzymes have been targeted to generate cell lines displaying unique GAG structural features. However, while the recovery of GAGs from the cell lysates is feasible, the purity of the samples obtained remains an issue and could be affected by the presence of undesired components. Additionally, GAG-biosynthesis enzymes may not catalyze structural modifications on all available substrates, yielding intravariation in GAG chains with enzyme-processed and -unprocessed domains. Nevertheless, this genetic approach is highly versatile (Table 2) and holds huge potential as it allows for direct cell-based assays, or to synthesize entire PGs and xyloside-primed GAG chains, which can subsequently be used in microarray applications (see Section 6).

### 5.4. Preparation of Well-Defined GAG Oligosaccharides

#### 5.4.1. Purification

While natural GAGs from extractions offer a wide range of structural diversity and physiological relevance, they also exhibit significant structural heterogeneity. Alternatively, libraries of oligosaccharides with defined size and charges can be generated using a combination of different depolymerization and purification strategies. For this, GAG chains are first depolymerized into smaller fragments through enzymatic digestion. Different enzymes can be used, yielding different fragment structures. For example, heparinase III enzyme primarily cleaves HS/Hep in the low-sulfated NAc regions, releasing highly sulfated fragments from the NS domains. GAG samples are then purified by size-exclusion chromatography to separate them by their polymerization degree (dp2, dp4, etc.). The generated oligosaccharides can

be further separated according to charge by various chromatography techniques, such as anion-exchange chromatography or reverse-phase ion-pair liquid chromatography, to isolate fractions with distinct sulfation patterns (see reviews).<sup>[251–253]</sup> However, due to the inherent charge heterogeneity of related oligosaccharides, it is likely to collect fractions comprising coeluting compounds. To improve separation resolution, columns modified with cetyltrimethylammonium salts (CTA-SAX) were used in combination with volatile ammonium bicarbonate salt and enabled distinction of Hep hexasaccharide isomeric structures, which could not be achieved using conventional methods.<sup>[254]</sup> Another advantage of the strategy is the straightforward removal of the volatile ammonium salt through evaporation rather than by dialysis, reducing considerably sample loss and enabling direct coupling to mass spectrometry analysis. Polyacrylamide Gel Electrophoresis (PAGE) has also demonstrated interesting separating properties, achieving resolution of oligosaccharide species that could not be differentiated with conventional chromatography methods. Consequently, oligosaccharide coeluting species obtained by strong-anion exchange high-performance liquid chromatography could be further resolved by PAGE, yielding pure compounds.<sup>[255]</sup> The preparation of oligosaccharide libraries using these purification strategies requires both time and expertise, but is more straightforward and accessible compared to oligosaccharide synthesis approaches (Table 2). However, access to specific oligosaccharide structures is limited to those present in naturally occurring GAGs, by the resolution limits of the available separation techniques, especially for closely related structures and large oligosaccharides. Furthermore, the quantities of oligosaccharides that can be produced remain limited by the scale-up capacities of preparative chromatographies.<sup>[256]</sup> Another general constraint is that selective depolymerization enzymes are available for HS but not for CS. Consequently, libraries of CS oligosaccharides with defined structures still remain very challenging to produce.

#### 5.4.2. Chemo-Enzymatic Synthesis

Chemo-enzymatic synthesis combines chemical reactions with the use of natural GAG-biosynthesis enzymes for oligosaccharide chain elongation and sulfate transfer. Thanks to the unique properties of these enzymes, this approach circumvents the technical challenges of chemical synthesis (see next section) such as regio- and stereo-selectivity, and avoids the need for numerous steps of group protection and deprotection for the transfer of sulfate groups at specific positions.

The activity and functional specificities of a large number of GAG biosynthesis enzymes are well characterized and have facilitated their use for the production of defined oligosaccharides. Elongation enzymes catalyze the transfer of monosaccharide compounds with the adequate glycosidic linkage. These enzymes rely on the presence of uridine diphosphate (UDP) sugar donors such as UDP-GlcNAc, UDP-GlcA, UDP-Glc, UDP-Gal, or UDP-GalNAc. Sulfation enzymes transfer sulfate groups at specific positions using 3'-phosphoadenosine-5'-phosphosulfate (PAPS) as sulfate donor. The order of execution of successive reactions must be carefully designed to be compatible with the enzyme substrate specificities and to improve reaction yields. Various reviews

provide more in-depth information about chemo-enzymatic synthesis and the different aspects of the approach.<sup>[257–260]</sup> While highly effective, the chemo-enzymatic strategy is complex and requires strong expertise in the production of recombinant biosynthesis enzymes, their roles and substrate specificities. Furthermore, the preparation of defined oligosaccharides requires the availability of a wide range of enzymes, sugars and sulfate donors, representing a considerable initial investment. Although complex and time-consuming, this method yields oligosaccharides with exceptional purity and controlled structure. Quantities produced with this approach are suitable for *in vivo* assays, therefore accounting for its versatility potential in Table 2. The enzymatic approach may also be used for sulfation of large GAG polysaccharide chains starting from nonsulfated heparosan or chondroitin, or to increase specific sulfation types in natural GAG samples.<sup>[261,262]</sup>

#### 5.4.3. Chemical Synthesis

The chemical synthesis of GAG oligosaccharides is based on the use of monosaccharides or disaccharides building blocks with protection groups in well-defined positions. Chain elongation is achieved by assembling these building blocks while controlling the stereochemistry of the glycosidic bonds formation and sulfation of specific positions is achieved following de-protection of the targeted groups. The introduction of hexuronic acid moieties is however an additional challenge due to their low reactivity. Chemical synthesis can be carried out either in solution-phase or on-resin (automated solid-phase synthesis) to facilitate the removal of side products after each reaction. More details of the different strategies of chemical GAG oligosaccharide synthesis have been reviewed elsewhere.<sup>[263–265]</sup> The control of the various steps of the process is highly challenging and requires strong expertise in chemistry to properly design the successive reactions. Only a few research groups worldwide have the equipment and skills to achieve the chemical synthesis of large oligosaccharide libraries. However, the purity and the structural control of the chemically synthesized oligosaccharides are excellent.<sup>[266]</sup> Similar to chemo-enzymatic synthesis, quantities obtained are substantial and therefore compatible with *in vivo* assays.

#### 5.4.4. Commercial GAG-Oligosaccharide Libraries

Thanks to the development of the above-mentioned techniques, a wide range of GAG compounds and oligosaccharides with defined length and sulfation pattern are readily accessible through commercial sources (Biosynth, Creative Biolabs, Glycan Therapeutics, Iduron, etc.). Since most of these commercially available compounds are produced using chemical, chemo-enzymatic and to a lesser extent purification approaches, commercial libraries facilitate access to defined oligosaccharide structures with high purity. Although the structural diversity is limited to the available compounds, the repertoire of structures is expanding rapidly and some companies offer custom synthesis service, which may provide a solution to address specific structural requirements. Furthermore, the cost of oligosaccharide compounds is relatively low compared to the time and effort required for the preparation of oligosaccharide libraries.

## 6. Characterization and Quantification of GAGs: From Molecular to Cellular Interactions with GAG-Based Biomaterials Using High Content Tools

As discussed earlier, the extensive functional repertoire of GAGs is intricately linked to their structure and sulfation patterns. This underscores the necessity for precise structural information on naturally occurring GAGs, for tailoring GAG structures in biomaterials to achieve specific biological properties. However, because of their natural diversity and complexity, quantifying and characterizing sulfated GAGs from tissues remains a formidable challenge, greatly impeding the development of new biomaterial applications.

As described above, various biomaterials have been developed to study different parameters of GAG presentation and structure, but only a few studies combine molecular information with cellular responses. Both approaches are time-consuming and complicated to achieve within the same experiment. Compared to genetics and proteomics, the field of glycobiology needs new tools and innovative biomaterials to accelerate and enhance the throughput for both molecular and cellular studies.

In this section, we review the state-of-the-art techniques used for the identification and characterization of GAGs, their sulfation pattern, and GAG-protein interactions, including their binding dynamics. We then present the recent developments using automation to study GAG-growth factor interactions and to quantify cellular responses to GAG-based biomaterials

### 6.1. Quantification of GAGs in Tissues

Quantification of GAGs in tissues can be complex. Determining GAG concentrations in body fluids such as urine plasma and serum is relatively straightforward and can be performed with ultra-high-performance liquid chromatography (UHPLC), coupled with mass spectrometry or fluorescent derivatization detection techniques.<sup>[175,267,268]</sup> In soft and solid tissues, however, assessing GAG content is more complex, and only a few quantitative values of tissue-specific GAG density are available in the literature, especially for human tissues. Various colorimetric assays such as Azure A, toluidine blue, and 1,9-dimethyl-methylene blue (DMMB) enable the quantitative measurement of sulfated GAG content. It is however worth noting that these assays may be biased by other nonsulfated poly-anions such as DNA, RNA, or HA, as well as variations in sulfation degree between GAG samples and standards.<sup>[269,270]</sup> Alternatively, the chemical carbazole assay allows for the recognition of all GAGs except KS, without interference from GAG sulfation.<sup>[270]</sup> All these assays require predigestion of tissue samples and generally a purification step to reduce possible artifacts of the assays caused by chloride ions, or other poly-anions. In clinics, several relatively noninvasive techniques based on MRI or computed tomography (CT) have been developed for the estimation of GAG concentration in cartilage.<sup>[271–274]</sup>

For structural analysis, specific monoclonal GAG-antibodies can be employed on explant tissues to qualitatively evaluate GAG composition, spatial distribution, and sulfation. However, the heterogeneity of GAGs and the unclear epitope recognition

specificities of anti-GAG antibodies limit their use for quantitative measurements.<sup>[55,275,276]</sup> The current gold standard for naturally occurring GAG structural studies is the disaccharide composition analysis, which has been successfully applied to GAGs purified from tissues, requiring only limited material quantities. This is achieved by exhaustive enzymatic GAG chain depolymerization, and analysis of the generated GAG disaccharides using various standard separation techniques (SAX-HPLC, RPIP-HPLC, HILIC, or capillary electrophoresis, etc.) coupled to MS or fluorescent derivatization approaches.<sup>[178,253,277–283]</sup> However, compositional analysis only provides partial structural information. Recent developments in analytical approaches are now offering new solutions to address this issue, enabling detailed structural characterization, up to GAG chain sequencing (for review, see Pérez et al., 2023).<sup>[200]</sup> However, to date, there have been very few reported applications on tissue samples using these emerging technologies.

## 6.2. Immobilization of GAGs on a Support

Advanced screening applications, such as microarrays (see Section 6.4), biosensors, and biomaterials, require immobilization of GAGs on a support, which can be a 2D surface or a 3D scaffold. For this, site-specific conjugation should be preferred over the physio-adsorption of GAGs on a support, since this strategy preserves GAG native structure and therefore its bioactivity and ability to interact with proteins.<sup>[284]</sup> As reviewed by Köwitsch et al. and Gemma et al., GAGs feature multiple reactive groups that can be used for functionalization, such as the saccharide reducing and nonreducing ends.<sup>[285,286]</sup> For biomaterials applications, functionalization through their reducing end is the most effective and straightforward strategy to achieve end-on (single point) attachment of GAGs. This method of immobilization is the most recommended, as it mimics the natural orientation of GAGs on proteoglycans. In the past, hydrazone ligation was a popular method for conjugating the reducing end of GAGs.<sup>[287–289]</sup> However, it was found to be inefficient for long GAG chains and unstable in aqueous solution.<sup>[290]</sup> Functionalization of GAG reducing end through oxime ligation is now favored, as it shows both improved yields and stability.<sup>[291]</sup> Interestingly, a range of oxamine functionalizing agents are commercially available, including oxamine biotin linkers.

In contrast, functionalizing the nonreducing end of GAGs remains challenging with only a few methods available.<sup>[286,292]</sup>

## 6.3. Techniques to Characterize Molecular Interactions

Numerous techniques are available for characterizing molecular interactions. While specific interactions of GAGs with proteins, such as AT III and FGF2, have been demonstrated and extensively studied, the majority of GAG-binding proteins have only been identified by simple screening without a deeper investigation of the interaction dynamics.

Techniques, such as ELISA,<sup>[293,294]</sup> fluorescence binding assays or fluorescence polarization assays,<sup>[295–297]</sup> have been frequently used for studying GAG/protein interactions. However, techniques based on optical biosensors are currently considered most effective.<sup>[298]</sup> Surface plasmon resonance (SPR) is the

reference for measuring kinetics constants, including the association rate constant ( $k_a$  or  $k_{on}$ ), the dissociation rate constant ( $k_d$  or  $k_{off}$ ), and the dissociation equilibrium constant ( $K_D = \frac{k_d}{k_a}$ ). BioLayer Interferometry (BLI) was developed more recently and provides higher throughput capacity. SPR is a flow-operated technique, while BLI operates with analytes in solution in a 96-well plate, agitated at high speed to circumvent mass-transport limitations. SPR has been widely used for the analysis of GAG/protein interactions, revealing complex binding mechanisms, such as positive cooperative interaction of chemokine RANTES to Hep.<sup>[299]</sup> In contrast, there are still relatively few reported studies of GAG/protein interactions using the more recent BLI technique.<sup>[300]</sup> It should be noted that these techniques are not inherently specific to GAGs and their application to GAG-protein interaction studies may necessitate additional precautions. Because of GAG sequence heterogeneity and possible display of multiple protein binding sites on the same polysaccharide chain, GAG-protein interactions rarely correspond to simple interaction models. However, fitting models adapted to this type of interactions are not currently available, and the use of complex fitting models is generally not recommended. Consequently, simple 1:1 interaction models are typically used, which urges for careful consideration of the kinetic parameters obtained.

Quartz-crystal microbalance with dissipation monitoring (QCM-D) technique enables characterization of molecular interactions at surfaces in situ.<sup>[301–304]</sup> However, due to mass transport limitations, QCM-D cannot be generalized for measuring  $k_a$  and  $k_d$  rates. QCM-D can be used to study the crosslinking of GAG chains upon binding to different proteins,<sup>[305]</sup> the conformational change of molecules,<sup>[306]</sup> and the effect of GAG density on molecular interactions.<sup>[307]</sup>

To identify the GAG binding sites on proteins, a technique based on GAG-coated beads has been developed. GAGs are activated with EDC/NHS to form covalent complexes with the protein, which are subsequently proteolyzed. The fragments bound to the GAGs are then analyzed by N-terminal sequencing performed directly on the beads.<sup>[308]</sup>

Several other techniques provide additional information about GAG/protein molecular interactions. The stoichiometry of GAG-protein complexes can be determined using laser light scattering, while Ion Mobility Mass Spectrometry (IMMS) can be used to study complexes shapes. To further investigate the structure of GAG-protein complexes and potential conformational changes, techniques such as X-ray crystallography, NMR, and cryo-EM are the gold standard but are highly challenging. In the literature, only a few structures of GAG-protein complexes have been determined, due to the difficulty of obtaining pure GAG species in large quantities, and propensity of the polysaccharide to induce protein aggregation at high concentrations. In this respect, recent developments in cryo-EM may provide new insights into the structure of GAG-protein complexes.<sup>[309]</sup>

## 6.4. Parallelization of GAG-Protein Molecular Interaction Assays

The last decades have been marked by the development of microarrays to study molecular interactions. Microarrays are particularly adapted for screening interactions between GAGs and growth factors. They can be fabricated on various substrates

including glass, silicon, or plastic. A large number of test sites can be generated by spotting ligands on the microarray surface at specific positions. Chips can include up to several thousand spots. The most common spotting methods are pin-based fluid transfer systems and piezo-based inkjet dispenser systems.<sup>[310–312]</sup> Although originally developed in the 1990s for nucleic acid research, microarrays have been rapidly adapted to the study of other molecules, such as peptides and polysaccharides. The first carbohydrate microarrays were reported in 2002,<sup>[313–316]</sup> and the first GAG-oligosaccharide microarray in 2006.<sup>[317]</sup> GAG compounds are generally spotted on the substrate in an oriented manner by chemical conjugation. The most standard immobilization procedure involves using an NHS-coated substrate to covalently attach amine-tagged oligosaccharides,<sup>[317–322]</sup> though other chemistries including noncovalent attachments have also been used.<sup>[323–325]</sup> The protein or growth factor of interest is then incubated on top of the GAG array, and the interaction can be monitored through fluorescence readout using a microarray scanner, SPR imaging, or mass spectrometry (MS) (Figure 6). The fluorescent detection approach generally requires the use of antibodies or fluorophore/tag (His tag or biotin)-labeled protein, which may in some cases interfere with the protein/GAG interaction. An alternative strategy involves using label-free proteins and assessing binding by SPR imaging. Notably, the Biacore Flex-chip SPR imaging instrument enables measurement of protein binding to biotinylated GAGs spotted onto neutravidin-coated gold chips, or to pyrrole-oligosaccharide electrocopolymerized on gold chips.<sup>[326–330]</sup> MS is another label-free detection method that can be used to analyze various GAGs simultaneously. Interestingly, MS has also been used in combination with glycan arrays to study the functional specificities of glycosyltransferase enzymes for the assembly of oligosaccharides.<sup>[331,332]</sup>

One major advantage of microarrays is the moderate amount of protein required for performing incubation with coverslips or incubation chambers, and screening simultaneously the binding to numerous GAG compounds.<sup>[319,320]</sup> Only a few picomoles of proteins are needed to screen GAG-protein interactions. Furthermore, recent robotic arrays require only femtomolar quantities of GAG for each spot.<sup>[264]</sup> Applications of high-throughput capacity microarrays for GAGs include the study of pathogen or protein interaction networks. For instance, comprehensive investigations have been conducted on the interaction networks of *Leishmania* pathogens and of endostatin with host ECM components, including GAGs. This led to the discovery of new endostatin GAG binding partners, namely CS and DS.<sup>[327,328]</sup> Another notable application of GAG microarrays is the study of biomolecule interactions with various GAG compounds, varying in type, length, and sulfation, to determine the structural features required for binding. In this context, microarrays have been used to analyze the binding of different proteins, including stromal cell-derived factor-1 $\alpha$  (SDF-1 $\alpha$ ), interferon- $\gamma$  (IFN- $\gamma$ ), with different GAGs.<sup>[330]</sup> SDF-1 $\alpha$  exhibited strong binding to Hep, while binding weakly to CS and DS. IFN- $\gamma$  bound to all GAGs, with a preference for Hep, followed by DS and then CS.

Limited access to compounds with defined structures has hindered the development of microarrays featuring sulfation-defined GAG oligosaccharides, but progress in GAG-oligosaccharide synthesis is steadily expanding the repertoire of available compounds. In 2006, the first GAG-oligosaccharide

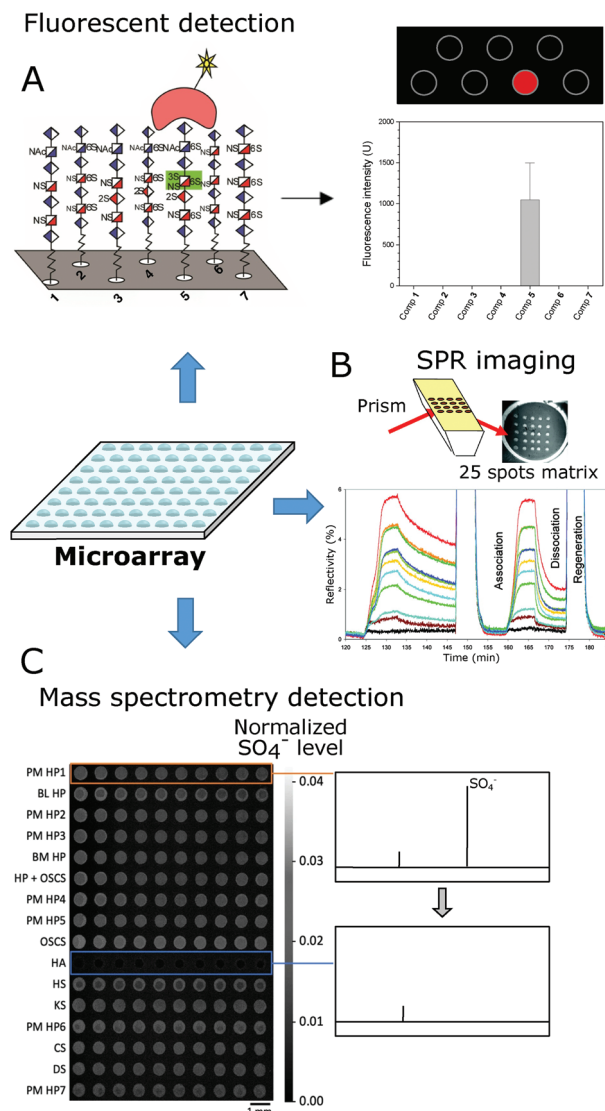


**Figure 6.** Different high-throughput detection methods adapted for microarrays. A) Microarrays can be used for fluorescent detection with a fluorescent protein probe or specific antibodies. Adapted with permission.<sup>[333]</sup> Copyright 2018, Elsevier. B) SPR imaging has also been coupled to microarrays, enabling measurement of binding curves and potential determination of kinetics parameters. Adapted with permission.<sup>[330]</sup> Copyright 2008, American Chemical Society. C) Microarrays coupled with mass spectrometry detection enable analysis of various GAG samples, notably for assessing their sulfation degree. Adapted with permission.<sup>[334]</sup> Copyright 2021, Springer Nature.

microarray featured only 5 different compounds screened for FGF1 binding.<sup>[317]</sup> This number rapidly increased to 12, used for screening the binding of FGF1, FGF2, and FGF4.<sup>[320]</sup> In 2014, Nonaka and coworkers used 14 synthetic oligosaccharides and identified a non-naturally occurring monosaccharide, 2,4-O-disulfated iduronic acid, as a potential inhibitor of CCL20-HS interaction.<sup>[335]</sup> In 2017, Yang et al. used 14 oligosaccharides from their 21 compounds library in a microarray to probe the binding of 3-O-sulfotransferase isoform 1 and AT III.<sup>[321]</sup> During the same year, Zong et al. screened the binding of FGF-2 and

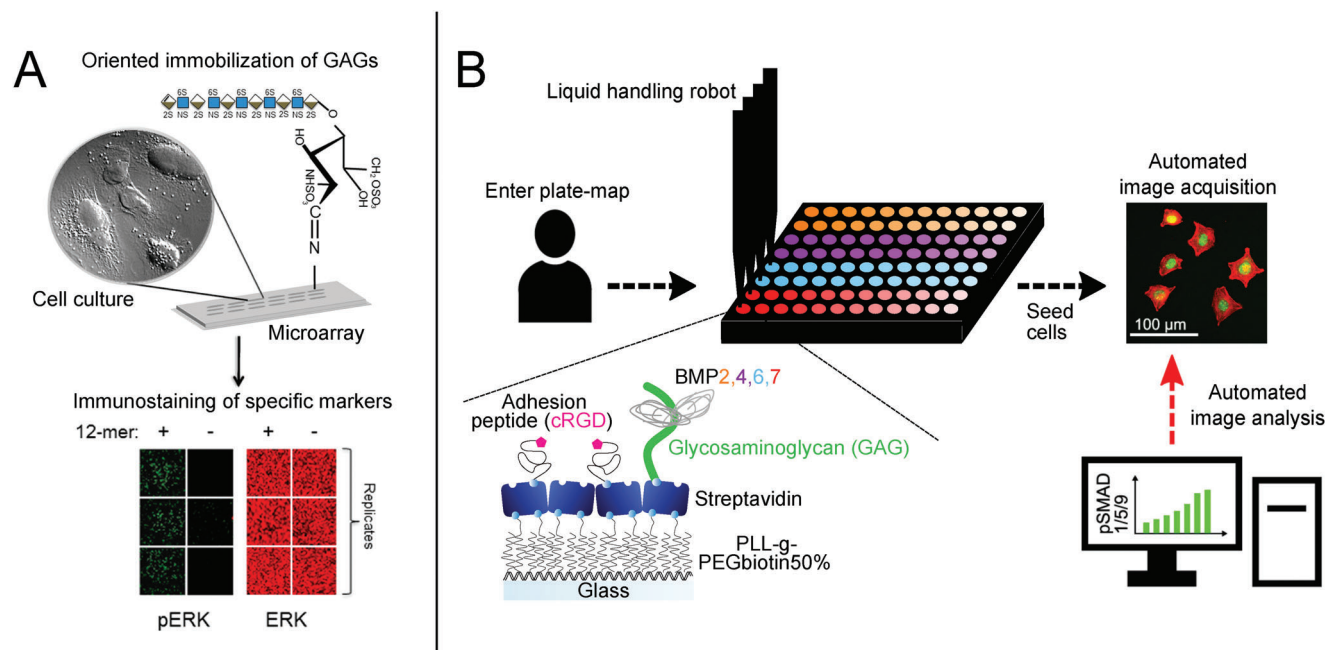


**Figure 7.** High-throughput strategies for studying the in vitro role of GAGs on cells. A) Immobilization of Hep oligosaccharides on a microarray as a support for cell culture. The levels of ERK and pERK were assessed by immunofluorescence after FGF2 stimulation. Adapted with permission.<sup>[340]</sup> Copyright 2016, MDPI. B) Fabrication of GAG-based biomimetic platforms in 96-well plate with liquid-handling robot to study the signaling pathway induced by GAG-bound BMPs. The nuclear pSMAD1/5/9 intensity was measured by immunofluorescence staining with a high-content microscope. A dose-response curve of nuclear pSMAD1/5/9 was established for all BMPs bound to HS. Adapted with permission.<sup>[34]</sup> Copyright 2022, American Chemical Society.

chemokines CCL2, CCL5, CCL7, CCL13, CXCL8, and CXCL10 to 47 synthesized tetrasaccharides.<sup>[322]</sup> More recently in 2021, Chopra et al. characterized the binding of 11 proteins (AT III, HC-II, FGF2,7,9, BMP-2, FGFR-1, RAGE, Stab-2, Nrp-1, HSV-1 gD) to 27 rare 3-O-sulfated hexasaccharides.<sup>[318]</sup> The largest microarray featuring 95 HS structures (94 oligos + Hep) was used by Horton et al. to screen the binding to ATIII, FGF2, IL2 and platelet factor 4.<sup>[319]</sup> Remarkably, they determined the binding affinities ( $K_D$  constants) of AT III with 7 compounds and of FGF2 with 29 compounds.

In another context, microarrays were used to study the crosslinking of lectins to mucin glycans spotted at various surface densities.<sup>[336]</sup> The authors found that lectins such as SBA, WFL, and VVA exhibited valency-dependent binding, while the HPA lectin showed strong avidities regardless of the glycan ligand density. However, the range of densities tested was restricted, due to detection limits of the experimental setup.

Finally, it is worth noting that this technique requires highly specialized equipment, potentially impeding its widespread adoption in research laboratories.

High-throughput alternatives, including microsphere arrays,<sup>[337]</sup> or fluorescent polarization technique,<sup>[338]</sup> have also been used and reviewed.<sup>[264]</sup> Currently, both SPR and BLI systems are undergoing technological developments towards increasing their high-throughput capabilities. Such advances could revolutionize the field, by enabling the analysis of a large number of interactions in a single run, while providing quantitative kinetic information ( $k_{on}$ ,  $k_{off}$ ,  $K_D$ ). These may lead to the generation of large volumes of data, which will require

standardization and new conventions for efficient processing. For instance, the extended Lawrence code for GAGs may be a useful tool for coding and representing disaccharide units and their sulfation.<sup>[8]</sup>

### 6.5. Cellular Studies at High Throughput Using GAG-Based Biomaterials

Given the multitude of parameters (e.g., GAG type, density, and sulfation), automated methods have started to emerge for studies on GAG-based biomaterials. High-throughput readouts are also needed to investigate how GAGs impact cell signaling (Figure 7).

A GAG microarray was used as a platform for a cellular study investigating the binding of chicken hepatocytes to different GAGs.<sup>[339]</sup> This approach identified GlcNAc residues as specific receptors for hepatocyte cell adhesion, independently of the linkage or orientation, while hepatocytes did not bind to galactose or *N*-acetylgalactosamine residues. As reviewed by Puvirajesinghe and Turnbull in 2016, microarrays can also be used to study cellular responses to GAGs.<sup>[340]</sup> For instance, a microarray slide functionalized with different Hep oligosaccharides was incubated in a cell culture dish with HS-deficient 3T3 cells, and the response of these cells to FGF2 was assessed by immunofluorescence staining of total and phosphorylated ERK1/2 markers.<sup>[341]</sup> Results showed the pERK1/2 signal increased with the size of the Hep oligosaccharide printed on the microarray. A 18-mer Hep yielded the strongest pERK1/2 signal compared to 12-mer Hep (Figure 7A). The 2-mer Hep did not elicit

significant signal compared to the negative control. In another study, a cell-based microarray platform was developed to investigate GAG-induced FGF-FGFR signaling.<sup>[342]</sup> For all the FGFs studied, highly sulfated GAGs, especially those containing IdoA like Hep, 2-O desulfated Hep, and DS, were the most effective in inducing FGF-mediated cell proliferation.

More recently, the automation of the fabrication of self-assembled materials in the form of streptavidin-based materials has been developed.<sup>[34]</sup> Such materials deposited in 96-well cell culture microplates can be used for high-content studies of cellular responses. Notably, cells can be cultured on GAG-based biomaterials deposited directly at the bottom of the microplate, and can be stimulated by growth factors adsorbed onto the GAGs (Figure 7B). These materials being built with a basal layer of streptavidin, any type of biotinylated compounds, including GAGs and adhesion peptides, can be subsequently adsorbed. As a proof of concept, these biomaterials were cofunctionalized with HS and an adhesion peptide (RGD). Several proteins from the BMP family were adsorbed on HS at increasing concentrations and their effect on cell differentiation to bone was assessed by following phosphorylated SMAD1/5/9 signaling, using a high content microscope.<sup>[343]</sup> C2C12 cell response to increasing doses of either soluble or adsorbed BMPs on HS allowed determination of EC50 values. C2C12 cells were found to be more responsive to HS-bound BMP2 compared to other HS-bound BMPs. Such biomaterials may be used in the future to study the cellular response to different growth factors, by modulating the experimental conditions: GF presented via different GAGs, modulation of GAG density, and GAG oligosaccharides with distinct sulfation patterns.

## 7. Conclusions and Perspectives

Thanks to their vast biological functions, GAGs are promising candidates for biomedical applications. The design of GAG-based biomaterials is a growing field, with applications in tissue engineering, regenerative medicine, and drug delivery. In this review, we point out the relevance of modulating parameters such as GAGs type, density, and sulfation pattern to engineer tailor-made biomaterials eliciting the desired cellular response and tissue regeneration properties. Given the considerable variability of these parameters amongst tissues and developmental stages, we also encourage the scientific community to correlate these parameters to the *in vivo* conditions of the targeted tissue engineering application, whenever possible. Developments of new strategies for producing structurally defined GAGs have significantly progressed during the past years. However, it is worth noting that efforts have mostly focused on HS and Hep, while other GAGs such as KS have been neglected. Technical limitations pose challenges in various areas of glycobiology, including GAG sample analysis and tissue analysis. However, the emergence of innovative techniques, such as molecular nanopore sequencing and MALDI-FT-ICR mass spectrometry imaging holds the potential to unveil new exciting opportunities in these domains.

Regarding molecular interactions, the development of microarrays has drastically enhanced our ability to identify GAG structures specifically interacting with defined GFs. The development of technologies providing kinetics information (such as SPR or BLI) at high throughput could revolutionize our practices

and understanding of GAGs. Recent addition of automation in the design of GAG-based biomaterials and in the measurement of GAG-GFs or GAG-cell interactions opens new opportunities for conducting parallel tests on different GAGs and experimental conditions.

Altogether, recent developments in the field open new perspectives. First, the use of GAG-based biomaterials presenting GFs bound to the biomimetic matrix may unveil novel cellular processes, in comparison to the soluble delivery of GAGs. Here, in-depth studies of GAG-proteins molecular interactions will be complemented by studies of the effect of GAG-GFs at the cellular level in a biomaterial context. Second, there is a growing need for wider access to methods for producing purified oligosaccharides, within the scientific community. In addition, these methods must be optimized to yield sufficient quantities of material. Third, the complexity and diversity of GAGs, as well as potential modulation of these parameters, will necessitate testing a wide range of conditions within an experiment. However, new developments, including the use of well-defined GAGs, automated fabrication of biomaterials, and automated quantification of molecular and cellular interactions, will significantly facilitate the systematic study of GAG-GF-mediated cellular processes under similar experimental conditions. Therefore, these developments should provide novel insights into the impact of GAG structural features, such as GAG type, density, and sulfation degree, in a given biological function.

Therefore, high content tools will enable to study the complexity and diversity of GAGs, and to gain knowledge on molecular mechanisms, which is currently limited to specific GFs, like AT III or FGF2. We expect that novel methods will be developed in the future to improve the automation of GAG immobilization, the high-throughput quantification of molecular interactions, and the high-content study of cellular readouts.

Regarding their effect on cellular response, only a limited number of high content biomaterials and systems have been developed for such studies. Currently, most systems are using high content microarrays or versatile biomaterials that are compatible with high-throughput immunofluorescence analysis of nuclear translocation of markers. Additionally, the development of high content readouts will be required for analyzing other non-nuclear signaling markers, such as western blot and qPCR equivalent techniques.

Given the large volume of data that will be collected in the future, standardization and conventions will be necessary, as well as the assistance of bioinformaticians for analyzing batches of data.

In summary, GAG-based biomaterials represent a rapidly growing field. We foresee the development of GAG-based biomaterials incorporating well-controlled oligosaccharides and GFs for specific medical applications in the future.

## Conflict of Interest

The authors declare no conflict of interest.

## Keywords

biomaterials, glycosaminoglycans, growth factors, high content, oligosaccharides

Received: November 14, 2023  
Published online:

- [1] A. C. Rapraeger, A. Krufka, B. B. Olwin, *Science* **1991**, 252, 1705.
- [2] A. L. Gray, R. Karlsson, A. R. E. Roberts, A. J. L. Ridley, N. Pun, B. Khan, C. Lawless, R. Luís, M. Szpakowska, A. Chevigné, C. E. Hughes, L. Medina-Ruiz, H. L. Birchenough, I. Z. Mulholland, C. L. Salanga, E. A. Yates, J. E. Turnbull, T. M. Handel, G. J. Graham, T. A. Jowitt, I. Schiessl, R. P. Richter, R. L. Miller, D. P. Dyer, *Cell Rep.* **2023**, 42, 111930.
- [3] T. F. Zioncheck, L. Richardson, J. Liu, L. Chang, K. L. King, G. L. Bennett, P. Fügedi, S. M. Chamow, R. H. Schwall, R. J. Stack, *J. Biol. Chem.* **1995**, 270, 16871.
- [4] L. E. Collins, L. Troeberg, *J. Leukoc. Biol.* **2019**, 105, 81.
- [5] J. Turnbull, A. Powell, S. Guimond, *Trends Cell Biol.* **2001**, 11, 75.
- [6] S. Mizumoto, S. Yamada, *Int. J. Mol. Sci.* **2022**, 23, 7485.
- [7] Q. Wang, L. Chi, *Polymers* **2022**, 14, 5014.
- [8] R. A. Townley, H. E. Bülow, *Curr. Opin. Struct. Biol.* **2018**, 50, 144.
- [9] D. Soares Da Costa, R. L. Reis, I. Pashkuleva, *Annu. Rev. Biomed. Eng.* **2017**, 19, 1.
- [10] L. Ling, X. Ren, X. Cao, A. B. M. Hassan, S. Mah, P. Sathiyathan, R. A. A. Smith, C. L. L. Tan, M. Eio, R. M. Samsonraj, A. J. Van Wijnen, M. Raghunath, V. Nurcombe, J. H. Hui, S. M. Cool, *Stem Cell Rep.* **2020**, 14, 105.
- [11] J. H. Lee, X. Luo, X. Ren, T. C. Tan, R. A. A. Smith, K. Swaminathan, S. Sekar, K. Bhakoo, V. Nurcombe, J. H. Hui, S. M. Cool, *Tissue Eng., Part A* **2019**, 25, 352.
- [12] M. Bouyer, C. Garot, P. Machillot, J. Vollaie, V. Fitzpatrick, S. Morand, J. Boutonnat, V. Jossierand, G. Bettega, C. Picart, *Mater. Today Biol.* **2021**, 11, 100113.
- [13] M. Bouyer, R. Guillot, J. Lavaud, C. Plettinx, C. Olivier, V. Curry, J. Boutonnat, J.-L. Coll, F. Peyrin, V. Jossierand, G. Bettega, C. Picart, *Biomaterials* **2016**, 104, 168.
- [14] S. S. Lee, B. J. Huang, S. R. Kaltz, S. Sur, C. J. Newcomb, S. R. Stock, R. N. Shah, S. I. Stupp, *Biomaterials* **2013**, 34, 452.
- [15] T. Miller, M. C. Goude, T. C. Mcdevitt, J. S. Temenoff, *Acta Biomater.* **2014**, 10, 1705.
- [16] Z. Söderlund, A. Ibáñez-Fonseca, S. Hajizadeh, J. C. Rodríguez-Cabello, J. Liu, L. Ye, E. Tykesson, L. Elowsson, G. Westergren-Thorsson, *Commun. Biol.* **2022**, 5, 1349.
- [17] D. Hachim, T. E. Whittaker, H. Kim, M. M. Stevens, *J. Controlled Release* **2019**, 313, 131.
- [18] A. Köwitsch, G. Zhou, T. Groth, *J. Tissue Eng. Regener. Med.* **2018**, 12, e23.
- [19] R. Menezes, R. Vincent, L. Osorno, P. Hu, T. L. Arinze, *Acta Biomater.* **2022**, 163, 210.
- [20] H. Sodhi, A. Panitch, *Biomolecules* **2021**, 11, 29.
- [21] J. Rnjak-Kovacina, F. Tang, J. M. Whitelock, M. S. Lord, *Adv. Healthcare Mater.* **2018**, 7, 1701042.
- [22] U. Freudenberg, Y. Liang, K. L. Kiick, C. Werner, *Adv. Mater.* **2016**, 28, 8861.
- [23] A. Wartenberg, J. Weisser, M. Schnabelrauch, *Molecules* **2021**, 26, 5597.
- [24] J. J. Lim, T. M. Hammoudi, A. M. Bratt-Leal, S. K. Hamilton, K. L. Kepple, N. C. Bloodworth, T. C. Mcdevitt, J. S. Temenoff, *Acta Biomater.* **2011**, 7, 986.
- [25] W. Malaeb, H. F. Bahmad, W. Abou-Kheir, R. Mhanna, *Biomater. Sci.* **2019**, 7, 4283.
- [26] A. Zieris, R. Dockhorn, A. Röhrich, R. Zimmermann, M. Müller, P. B. Welzel, M. V. Tsurkan, J.-U. Sommer, U. Freudenberg, C. Werner, *Biomacromolecules* **2014**, 15, 4439.
- [27] B. Wang, L. Tan, D. Deng, T. Lu, C. Zhou, Z. Li, Z. Tang, Z. Wu, H. Tang, *Int. J. Nanomed.* **2015**, 10, 3417.
- [28] D. S. Bramono, S. Murali, B. Rai, L. Ling, W. T. Poh, Z. X. Lim, G. S. Stein, V. Nurcombe, A. J. Van Wijnen, S. M. Cool, *Bone* **2012**, 50, 954.
- [29] S. Murali, B. Rai, C. Dombrowski, J. L. J. Lee, Z. X. H. Lim, D. S. Bramono, L. Ling, T. Bell, S. Hinkley, S. S. Nathan, J. H. Hui, H. K. Wong, V. Nurcombe, S. M. Cool, *Biomaterials* **2013**, 34, 5594.
- [30] J. Huegel, C. Mundy, F. Sgariglia, P. Nygren, P. C. Billings, Yu Yamaguchi, E. Koyama, M. Pacifici, *Dev. Biol.* **2013**, 377, 100.
- [31] C. Mundy, E. Yang, H. Takano, P. C. Billings, M. Pacifici, *J. Biol. Chem.* **2018**, 293, 7703.
- [32] E. Migliorini, P. Horn, T. Haraszti, S. V. Wegner, C. Hiepen, P. Knaus, R. P. Richter, E. A. Cavalcanti-Adam, *Adv. Biosyst.* **2017**, 1, 1600041.
- [33] P. Machillot, C. Quintal, F. Dalonneau, L. Hermant, P. Monnot, K. Matthews, V. Fitzpatrick, J. Liu, I. Pignot-Paintrand, C. Picart, *Adv. Mater.* **2018**, 30, 1801097.
- [34] J. Sefkow-Werner, J. Le Pennec, P. Machillot, B. Ndayishimiye, E. Castro-Ramirez, J. Lopes, C. Licitra, I. Wang, A. Delon, C. Picart, E. Migliorini, *ACS Appl. Mater. Interfaces* **2022**, 14, 34113.
- [35] C. L. R. Merry, U. Lindahl, J. Couchman, J. D. Esko, in *Essent. Glycobiol.* (Eds.: A. Varki, R. D. Cummings, J. D. Esko, P. Stanley, G. W. Hart, M. Aebi, D. Mohnen, T. Kinoshita, N. H. Packer, J. H. Prestegard, R. L. Schnaar, P. H. Seeberger), Cold Spring Harbor Laboratory Press, Cold Spring Harbor (NY), **2022**.
- [36] R. V. Iozzo, L. Schaefer, *Matrix Biol.* **2015**, 42, 11.
- [37] M. Kusche-Gullberg, *Curr. Opin. Struct. Biol.* **2003**, 13, 605.
- [38] T. Huneval, R. Wild, Y. Crétinon, R. Sadrir, R. R. Vivès, H. Lortat-Jacob, *Mol. Basel Switz.* **2020**, 25, 4215.
- [39] N. B. Schwartz, N. R. Smalheiser, in *Neurobiology Glycoconjugate*, (Eds.: R. U. Margolis, R. K. Margolis), SpringerPlus, Boston, MA, **1989**, pp. 151–186.
- [40] T. Uyama, H. Kitagawa, K. Sugahara, in *Compr. Glycosci.* (Ed.: H. Kamerling), Elsevier, Oxford, **2007**, pp. 79–104.
- [41] E. Bedini, M. M. Corsaro, A. Fernández-Mayoralas, A. Iadonisi, in *Extracell. Sugar-Based Biopolym. Matrices* (Eds.: E. Cohen, H. Merzendorfer), Springer International Publishing, Cham **2019**, pp. 187–233.
- [42] S. D. Vallet, C. Berthollier, S. Ricard-Blum, *Am. J. Physiol. Cell Physiol.* **2022**, 322, C1271.
- [43] N. S. Gandhi, R. L. Mancera, *Chem. Biol. Drug Des.* **2008**, 72, 455.
- [44] L. Kjellén, U. Lindahl, *Curr. Opin. Struct. Biol.* **2018**, 50, 101.
- [45] V. Bachvarova, T. Dierker, J. Esko, D. Hoffmann, L. Kjellen, A. Vortkamp, *Matrix Biol.* **2020**, 93, 43.
- [46] K. Lidholt, J. L. Weinke, C. S. Kiser, F. N. Lagemwa, K. J. Barne, S. Cheifetz, J. Massagué, U. Lindahl, J. D. Esko, *Proc. Natl. Acad. Sci. USA* **1992**, 89, 2267.
- [47] P. C. Champe, R. A. Harvey, D. R. Ferrier, *Biochemistry*, Lippincott Williams & Wilkins, **2005**.
- [48] M. I. Neves, M. Araújo, L. Moroni, R. M. P. Da Silva, C. C. Barrias, *Molecules* **2020**, 25, 978.
- [49] A. J. Lepedda, G. Nieddu, M. Formato, M. B. Baker, J. Fernández-Pérez, L. Moroni, *Front. Chem.* **2021**, 9, 680836.
- [50] J. Chen, T. Sun, Y. You, B. Wu, X. Wang, J. Wu, *Front. Cell Dev. Biol.* **2021**, 9, 760532.
- [51] J. Martel-Pelletier, S. Kwan Tat, J.-P. Pelletier, *Osteoarthritis Cartilage* **2010**, 18, S7.
- [52] L. Sherman, J. Sleeman, P. Herrlich, H. Ponta, *Curr. Opin. Cell Biol.* **1994**, 6, 726.
- [53] D. Viçetti, E. Karousou, M. Viola, S. Deleonibus, G. De Luca, A. Passi, *Biochim. Biophys. Acta* **2014**, 1840, 2452.
- [54] L. Bohaumilitzky, A.-K. Huber, E. M. Stork, S. Wengert, F. Woelfl, H. Boehm, *Front. Oncol.* **2017**, 7, 242.
- [55] C. P. Mencio, R. K. Hussein, P. Yu, H. M. Geller, *J. Histochem. Cytochem.* **2021**, 69, 61.
- [56] P. Kastana, E. Choleva, E. Poimenidi, N. Karamanos, K. Sugahara, E. Papadimitriou, *FEBS J.* **2019**, 286, 2921.

- [57] J. M. Trowbridge, R. L. Gallo, *Glycobiology* **2002**, *12*, 117R.
- [58] B. Catterson, J. Melrose, *Glycobiology* **2018**, *28*, 182.
- [59] P. Wang, L. Chi, Z. Zhang, H. Zhao, F. Zhang, R. J. Linhardt, *Carbohydr. Polym.* **2022**, *295*, 119818.
- [60] J. Gallagher, *Int. J. Exp. Pathol.* **2015**, *96*, 203.
- [61] X. Lin, *Development* **2004**, *131*, 6009.
- [62] D. Papy-Garcia, P. Albanese, *Glycoconj. J.* **2017**, *34*, 377.
- [63] M. Grunert, V. Nurcombe, S. Cool, *Curr. Stem Cell Res. Ther.* **2008**, *3*, 1.
- [64] B. L. Farrugia, M. S. Lord, J. Melrose, J. M. Whitelock, *J. Histochem. Cytochem.* **2018**, *66*, 321.
- [65] J. L. Dreyfuss, C. V. Regatieri, T. R. Jarrouge, R. P. Cavaleiro, L. O. Sampaio, H. B. Nader, *An. Acad. Bras. Cienc.* **2009**, *81*, 409.
- [66] P. C. Billings, M. Pacifici, *Connect. Tissue Res.* **2015**, *56*, 272.
- [67] F. Gude, J. Froese, D. Manikowski, D. Di Iorio, J.-N. Grad, S. Wegner, D. Hoffmann, M. Kennedy, R. P. Richter, G. Steffes, K. Grobe, *Nat. Commun.* **2023**, *14*, 758.
- [68] D. Hachim, T. E. Whittaker, H. Kim, M. M. Stevens, *J. Controlled Release* **2019**, *313*, 131.
- [69] R. Biran, D. Pond, *Adv. Drug Delivery Rev.* **2017**, *112*, 12.
- [70] M. Mahedia, N. Shah, B. Amirlak, *Plast. Reconstr. Surg. Glob. Open* **2016**, *4*, e791.
- [71] G. Nicoletti, M. M. Tresoldi, A. Malovini, M. Visaggio, A. Faga, S. Scevola, *Indian J. Plast. Surg. Off. Publ. Assoc. Plast. Surg. India* **2018**, *51*, 46.
- [72] S. Erbatur, Y. K. Coban, E. N. Aydin, *Int. J. Burns Trauma* **2012**, *2*, 118.
- [73] A. Gobbi, C. Scotti, G. Karnatzikos, A. Mudhigere, M. Castro, G. M. Peretti, *Knee Surg. Sports Traumatol. Arthrosc.* **2017**, *25*, 2494.
- [74] A. Gobbi, S. Chaurasia, G. Karnatzikos, N. Nakamura, *Cartilage* **2015**, *6*, 82.
- [75] A. Gobbi, G. P. Whyte, *Am. J. Sports Med.* **2016**, *44*, 2846.
- [76] M. Marcacci, M. Berruto, D. Brocchetta, A. Delcogliano, D. Ghinelli, A. Gobbi, E. Kon, L. Pederzini, D. Rosa, G. L. Sacchetti, G. Stefani, S. Zanasi, *Clin. Orthop. Relat. Res.* **2005**, *435*, 96.
- [77] C.-Y. Kuo, C.-H. Chen, C.-Y. Hsiao, J.-P. Chen, *Carbohydr. Polym.* **2015**, *117*, 722.
- [78] X. Yu, G. Qian, Si Chen, D. Xu, X. Zhao, C. Du, *Carbohydr. Polym.* **2017**, *159*, 20.
- [79] M.-E. Han, B. J. Kang, Su-H Kim, H. D. Kim, N. S. Hwang, *J. Ind. Eng. Chem.* **2017**, *45*, 421.
- [80] C.-S. Ko, J.-P. Huang, C.-W. Huang, I.-M. Chu, *J. Biosci. Bioeng.* **2009**, *107*, 177.
- [81] H. Lagus, M. Sarlomo-Rikala, T. Böhling, J. Vuola, *Burns J. Int. Soc. Burn Inj.* **2013**, *39*, 1577.
- [82] D. M. Heimbach, G. D. Warden, A. Luteran, M. H. Jordan, N. Ozobia, C. M. Ryan, D. W. Voigt, W. L. Hickerson, J. R. Saffle, F. A. Declement, R. L. Sheridan, A. R. Dimick, *J. Burn Care Rehabil.* **2003**, *24*, 42.
- [83] Y. Henrotin, J.-P. Hauzeur, P. Bruel, T. Appelboom, *BMC Res. Notes* **2012**, *5*, 407.
- [84] G. C. Ingavle, A. W. Frei, S. H. Gehrke, M. S. Detamore, *Tissue Eng., Part A* **2013**, *19*, 1349.
- [85] S. Sharma, A. Panitch, C. P. Neu, *Acta Biomater.* **2013**, *9*, 4618.
- [86] E. Bedini, A. Laezza, A. Iadonisi, *Eur. J. Org. Chem.* **2016**, *2016*, 3018.
- [87] L. Schirmer, P. Atallah, C. Werner, U. Freudenberg, *Adv. Healthcare Mater.* **2016**, *5*, 3157.
- [88] V. Bonito, A. I. P. M. Smits, O. J. G. M. Goor, B. D. Ippel, A. Driessen-Mol, T. J. A. G. Münker, A. W. Bosman, T. Mes, P. Y. W. Dankers, C. V. C. Bouten, *Acta Biomater.* **2018**, *71*, 247.
- [89] L. Schirmer, C. Hoornaert, D. Le Blon, D. Eigel, C. Neto, M. Gumbleton, P. B. Welzel, A. E. Rosser, C. Werner, P. Ponsaerts, B. Newland, *Biomater. Sci.* **2020**, *8*, 4997.
- [90] S. E. Kim, C.-S. Kim, Y.-P. Yun, D. H. Yang, K. Park, S. E. Kim, C.-Mo Jeong, J.-Bo Huh, *Carbohydr. Polym.* **2014**, *114*, 123.
- [91] S. Yan, L. Feng, Q. Zhu, W. Yang, Y. Lan, D. Li, Yu Liu, W. Xue, R. Guo, G. Wu, *ACS Biomater. Sci. Eng.* **2018**, *4*, 3291.
- [92] X. Xu, A. K. Jha, R. L. Duncan, X. Jia, *Acta Biomater.* **2011**, *7*, 3050.
- [93] M. H. Hettiaratchi, L. Krishnan, T. Rouse, C. Chou, T. C. Mcdevitt, R. E. Guldberg, *Sci. Adv.* **2020**, *6*, eaay1240.
- [94] S. Thanayaphoo, J. Kaewsrichan, *Acta Pharm.* **2016**, *66*, 373.
- [95] R. Y. Kim, B. Lee, Si-N Park, J.-H. Ko, I. S. Kim, S. J. Hwang, *Tissue Eng., Part A* **2016**, *22*, 801.
- [96] H. S. Yang, W.-G. La, Y.-M. Cho, W. Shin, G.-D. Yeo, B.-S. Kim, *Exp. Mol. Med.* **2012**, *44*, 350.
- [97] M. Kisiel, A. S. Klar, M. Ventura, J. Buijs, M.-K. Mafina, S. M. Cool, J. Hilborn, *PLoS One* **2013**, *8*, e78551.
- [98] Y. Liu, S. Cai, X. Z. Shu, J. Shelby, G. D. Prestwich, *Wound Repair Regen.* **2007**, *15*, 245.
- [99] N. R. Johnson, Y. Wang, *Wound Repair Regen.* **2015**, *23*, 591.
- [100] J. S. Park, K. Park, D. G. Woo, H. N. Yang, H.-M. Chung, K.-H. Park, *Biomacromolecules* **2008**, *9*, 2162.
- [101] M. Kim, S. E. Kim, S. S. Kang, Y. H. Kim, G. Tae, *Biomaterials* **2011**, *32*, 7883.
- [102] S. Singh, B. M. Wu, J. C. Y. Dunn, *Biomaterials* **2011**, *32*, 2059.
- [103] S. Prokoph, E. Chavakis, K. R. Levental, A. Zieris, U. Freudenberg, S. Dimmeler, C. Werner, *Biomaterials* **2012**, *33*, 4792.
- [104] J. Yu, A. Wang, Z. Tang, J. Henry, B. Li-Ping Lee, Y. Zhu, F. Yuan, F. Huang, S. Li, *Biomaterials* **2012**, *33*, 8062.
- [105] Y. Yao, J. Wang, Y. Cui, R. Xu, Z. Wang, Ju Zhang, K. Wang, Y. Li, Q. Zhao, D. Kong, *Acta Biomater.* **2014**, *10*, 2739.
- [106] B. S. Conklin, E. R. Richter, K. L. Kreutziger, D.-S. Zhong, C. Chen, *Med. Eng. Phys.* **2002**, *24*, 173.
- [107] W. Wu, R. A. Allen, Y. Wang, *Nat. Med.* **2012**, *18*, 1148.
- [108] I. Kim, S. S. Lee, S. Bae, H. Lee, N. S. Hwang, *Biomacromolecules* **2018**, *19*, 2257.
- [109] L. Ye, X. Wu, H.-Y. Duan, X. Geng, B. Chen, Y.-Q. Gu, Ai-Y Zhang, J. Zhang, Z.-G. Feng, *J. Biomed. Mater. Res., Part A* **2012**, *100A*, 3251.
- [110] C. Wang, S. Poon, S. Murali, C.-Y. Koo, T. J. Bell, S. F. Hinkley, H. Yeong, K. Bhakoo, V. Nurcombe, S. M. Cool, *Biomaterials* **2014**, *35*, 6776.
- [111] M. T. Koobatian, S. Row, R. J. Smith Jr, C. Koenigsnecht, S. T. Andreadis, D. D. Swartz, *Biomaterials* **2016**, *76*, 344.
- [112] J. J. D. Henry, J. Yu, A. Wang, R. Lee, J. Fang, S. Li, *Biofabrication* **2017**, *9*, 035007.
- [113] D. I. Braghirolli, V. E. Helfer, P. C. Chagastelles, T. P. Dalberto, D. Gamba, P. Pranke, *Biomed. Mater.* **2017**, *12*, 025003.
- [114] U. Freudenberg, A. Zieris, K. Chwalek, M. V. Tsurkan, M. F. Maitz, P. Atallah, K. R. Levental, S. A. Eming, C. Werner, *J. Controlled Release* **2015**, *220*, 79.
- [115] H. Chu, J. Gao, C.-W. Chen, J. Huard, Y. Wang, *Proc. Natl. Acad. Sci. USA* **2011**, *108*, 13444.
- [116] O. Jeon, S.-W. Kang, H.-W. Lim, Ji Hyung Chung, B.-S. Kim, *Biomaterials* **2006**, *27*, 1598.
- [117] N. R. Johnson, M. Kruger, K. P. Goetsch, P. Zilla, D. Bezuidenhout, Y. Wang, N. H. Davies, *ACS Biomater. Sci. Eng.* **2015**, *1*, 753.
- [118] M. Yunesi, D. M. Knapik, J. Cumsky, B. O. Donmez, P. He, A. Islam, G. Learn, P. McClellan, M. Bohl, R. J. Gillespie, O. Akkus, *Acta Biomater.* **2017**, *63*, 200.
- [119] S. Thomopoulos, R. Das, M. J. Silva, S. Sakiyama-Elbert, F. L. Harwood, E. Zampakis, H. M. Kim, D. Amiel, R. H. Gelberman, *J. Orthop. Res.* **2009**, *27*, 1209.
- [120] S. Kang, J. S. Yoon, J. Y. Lee, H.-J. Kim, K. Park, S. E. Kim, *Carbohydr. Polym.* **2019**, *209*, 372.

- [121] B. Newland, P. B. Welzel, H. Newland, C. Renneberg, P. Kolar, M. Tsurkan, A. Rosser, U. Freudenberg, C. Werner, *Small* **2015**, *11*, 5047.
- [122] B. Newland, H. Newland, F. Lorenzi, D. Eigel, P. B. Welzel, D. Fischer, W. Wang, U. Freudenberg, A. Rosser, C. Werner, *ACS Chem. Neurosci.* **2021**, *12*, 1178.
- [123] M. D. Wood, D. Hunter, S. E. Mackinnon, S. E. Sakiyama-Elbert, J. *Biomater. Sci., Polym. Ed.* **2010**, *21*, 771.
- [124] K. H. Bae, H. Mok, T. G. Park, *Biomaterials* **2008**, *29*, 3376.
- [125] K. Lee, H. Lee, K. H. Bae, T. G. Park, *Biomaterials* **2010**, *31*, 6530.
- [126] A. A. Decarlo, M. Belousova, A. L. Ellis, D. Petersen, H. Grenett, P. Hardigan, R. O'grady, M. Lord, J. M. Whitelock, *BMC Biotechnol.* **2012**, *12*, 60.
- [127] P. P. Srinivasan, S. Y. Mccoy, A. K. Jha, W. Yang, X. Jia, M. C. Farach-Carson, C. B. Kirn-Safran, *Biomed. Mater.* **2012**, *7*, 024109.
- [128] W. Yang, R. R. Gomes, A. J. Brown, A. R. Burdett, M. Alicknavitch, M. C. Farach-Carson, A. D. D. Carson, *Tissue Eng.* **2006**, *12*, 2009.
- [129] A. K. Jha, W. Yang, C. B. Kirn-Safran, M. C. Farach-Carson, X. Jia, *Biomaterials* **2009**, *30*, 6964.
- [130] M. S. Lord, A. L. Ellis, B. L. Farrugia, J. M. Whitelock, H. Grenett, C. Li, R. L. O'grady, A. A. Decarlo, *J. Control. Release Off. J. Control. Release Soc.* **2017**, *250*, 48.
- [131] J. Rnjak-Kovacina, F. Tang, J. M. Whitelock, M. S. Lord, *Colloids Surf. B: Biointerfaces* **2016**, *148*, 130.
- [132] M. S. Lord, W. Yu, B. Cheng, A. Simmons, L. Poole-Warren, J. M. Whitelock, *Biomaterials* **2009**, *30*, 4898.
- [133] J. S. Pieper, T. Hafmans, P. B. Van Wachem, M. J. A. Van Luyn, L. A. Brouwer, J. H. Veerkamp, T. H. Van Kuppevelt, *J. Biomed. Mater. Res.* **2002**, *62*, 185.
- [134] H. Jiang, R. S. Peterson, W. Wang, E. Bartnik, C. B. Knudson, *J. Biol. Chem.* **2002**, *277*, 10531.
- [135] M. Assunção, C. H. K. Yiu, Ho-Y Wan, D. Wang, D. F. E. Ker, R. S. Tuan, A. Blocki, *J. Mater. Chem. B* **2021**, *9*, 7205.
- [136] C. B. Knudson, *Birth Defects Res. Part C: Embryo Today Rev.* **2003**, *69*, 174.
- [137] C. Longinotti, *Burns Trauma* **2014**, *2*, 162.
- [138] V. Colletta, D. Dioguardi, A. Di Lonardo, G. Maggio, F. Torasso, *J. Wound Care* **2003**, *12*, 357.
- [139] S. Thönes, S. Rother, T. Wippold, J. Blaszkiewicz, K. Balamurugan, S. Moeller, G. Ruiz-Gómez, M. Schnabelrauch, D. Scharnweber, A. Saalbach, J. Rademann, M. T Pisabarro, V. Hintze, U. Anderegg, *Acta Biomater.* **2019**, *86*, 135.
- [140] C. Garot, S. Schoffit, C. Monfoulet, P. Machillot, C. Deroy, S. Roques, J. Vial, J. Voltaire, M. Renard, H. Ghanem, H. El-Hafci, A. Decambron, V. Josserand, L. Bordenave, G. Bettega, M. Durand, M. Manassero, V. Viateau, D. Logeart-Avramoglou, C. Picart, *Adv. Healthcare Mater.* **2023**, *12*, 2301692.
- [141] E.-C. Kim, S. J. Yoon, K. Noh, D.-W. Lee, *J. Nanosci. Nanotechnol.* **2017**, *17*, 143.
- [142] T. B. L. Nguyen, B.-T. Lee, *Tissue Eng., Part A* **2014**, *20*, 1993.
- [143] A. Rajan Unnithan, A. Ramachandra Kurup Sasikala, C. H. Park, C. S. Kim, *J. Ind. Eng. Chem.* **2017**, *46*, 182.
- [144] C. Manferdini, V. Guarino, N. Zini, M. G. Raucchi, A. Ferrari, F. Grassi, E. Gabusi, S. Squarzone, A. Facchini, L. Ambrosio, G. Lisignoli, *Biomaterials* **2010**, *31*, 3986.
- [145] S. Lepidi, G. Abatangelo, V. Vindigni, G. P. Deriu, B. Zavan, C. Tonello, R. Cortivo, *FASEB J.* **2006**, *20*, 103.
- [146] L. Pandis, B. Zavan, G. Abatangelo, S. Lepidi, R. Cortivo, V. Vindigni, *J. Biomed. Mater. Res., Part A* **2010**, *93*, 1289.
- [147] L. Pandis, B. Zavan, F. Bassetto, L. Ferroni, L. Iacobellis, G. Abatangelo, S. Lepidi, R. Cortivo, V. Vindigni, *Microsurgery* **2011**, *31*, 138.
- [148] D. E. Soranno, C. B. Rodell, C. Altmann, J. Duplantis, A. Andres-Hernando, J. A. Burdick, S. Faubel, *Am. J. Physiol.-Ren. Physiol.* **2016**, *311*, F362.
- [149] B. Thierry, F. M. Winnik, Y. Merhi, J. Silver, M. Tabrizian, *Biomacromolecules* **2003**, *4*, 1564.
- [150] J. Gaston, S. L. Thibeault, *Biomatter* **2013**, *3*, e23799.
- [151] S. L. Thibeault, S. A. Klemuk, X. Chen, B. H. Quinchia Johnson, *J. Voice* **2011**, *25*, 249.
- [152] X. Jia, Y. Yeo, R. J. Clifton, T. Jiao, D. S. Kohane, J. B. Kobler, S. M. Zeitels, R. Langer, *Biomacromolecules* **2006**, *7*, 3336.
- [153] J. Dienes, S. Browne, B. Farjun, J. Amaral Passipieri, E. L. Mintz, G. Killian, K. E. Healy, G. J. Christ, *ACS Biomater. Sci. Eng.* **2021**, *7*, 1587.
- [154] S. Poveda-Reyes, V. Moulisova, E. Sanmartín-Masiá, L. Quintanilla-Sierra, M. Salmerón-Sánchez, G. G. Ferrer, *Macromol. Biosci.* **2016**, *16*, 1311.
- [155] P. Kumar, S. Ciftci, J. Barthes, H. Knopf-Marques, C. B. Muller, C. Debry, N. E. Vrana, A. M. Ghaemmaghami, *J. Tissue Eng. Regen. Med.* **2020**, *14*, 45.
- [156] T. Majima, T. Irie, N. Sawaguchi, T. Funakoshi, N. Iwasaki, K. Harada, A. Minami, S.-I. Nishimura, *Proc. Inst. Mech. Eng. [H]* **2007**, *221*, 537.
- [157] S. Wu, M. Kuss, D. Qi, J. Hong, H.-J. Wang, W. Zhang, S. Chen, S. Ni, B. Duan, *ACS Appl. Biol. Mater.* **2019**, *2*, 4864.
- [158] K.-H. Chang, H.-T. Liao, J.-P. Chen, *Acta Biomater.* **2013**, *9*, 9012.
- [159] V. R. Driver, L. A. Lavery, A. M. Reyzelman, T. G. Dutra, C. R. Dove, S. V. Kotsis, H. M. Kim, K. C. Chung, *Wound Repair Regen. Off. Publ. Wound Heal. Soc. Eur. Tissue Repair Soc.* **2015**, *23*, 891.
- [160] Dermagen® sur Diabète et Ulcère du pied – Registre des essais cliniques – ICH GCP, can be found under, <https://ichgcp.net/fr/clinical-trials-registry/NCT00521937>.
- [161] D. S. Keskin, A. Tezcaner, P. Korkusuz, F. Korkusuz, V. Hasirci, *Biomaterials* **2005**, *26*, 4023.
- [162] S. Andrews, A. Cheng, H. Stevens, M. T. Logun, R. Webb, E. Jordan, B. Xia, L. Karumbaiah, R. E. Guldberg, S. Stice, *Stem Cells Transl. Med.* **2019**, *8*, 575.
- [163] X. Bai, S. Lü, Z. Cao, B. Ni, X. Wang, P. Ning, D. Ma, H. Wei, M. Liu, *Carbohydr. Polym.* **2017**, *166*, 123.
- [164] Y. J. Park, Y. M. Lee, J. Y. Lee, Y. J. Seol, C. P. Chung, S. J. Lee, *J. Controlled Release* **2000**, *67*, 385.
- [165] H. Xu, Y. Yan, S. Li, *Biomaterials* **2011**, *32*, 4506.
- [166] K. C. Butterfield, A. W. Conovaloff, A. Panitch, *Biomatter* **2011**, *1*, 174.
- [167] S. R. Caliar, M. A. Ramirez, B. A. C. Harley, *Biomaterials* **2011**, *32*, 8990.
- [168] R. A. Hortensius, B. A. C. Harley, *Biomaterials* **2013**, *34*, 7645.
- [169] J. Hayder, M. A. Chaouch, N. Amira, M. Ben Mansour, H. Majdoub, F. Chaubet, R. M. Maaroufi, *Int. J. Polym. Mater. Polym. Biomater.* **2018**, *67*, 277.
- [170] M. A. Ruehle, L. Krishnan, S. A. Labelle, N. J. Willett, J. A. Weiss, R. E. Guldberg, *MRS Commun.* **2017**, *7*, 466.
- [171] J. E. Paderi, K. Stuart, M. Sturek, K. Park, A. Panitch, *Biomaterials* **2011**, *32*, 2516.
- [172] T. Douglas, U. Hempel, C. Mietrach, M. Viola, D. Vigetti, S. Heinemann, S. Bierbaum, D. Scharnweber, H. Worch, *J. Biomed. Mater. Res., Part A* **2008**, *84A*, 805.
- [173] K. Stuart, J. Paderi, P. W. Snyder, L. Freeman, A. Panitch, *PLoS One* **2011**, *6*, e22139.
- [174] T. F. L. Wishart, F. J. Lovicu, *Cells* **2023**, *12*, 1364.
- [175] F. Kubaski, R. W. Mason, A. Nakatomi, H. Shintaku, Li Xie, N. N. Van Vlies, H. Church, R. Giugliani, H. Kobayashi, S. Yamaguchi, Y. Suzuki, T. Orii, T. Fukao, A. M. Montañó, S. Tomatsu, *J. Inherit. Metab. Dis.* **2017**, *40*, 151.
- [176] T. Kunzke, B. Balluff, A. Feuchtinger, A. Buck, R. Langer, B. Luber, F. Lordick, H. Zitzelsberger, M. Aichler, A. Walch, *Oncotargets Ther.* **2017**, *8*, 68012.

- [177] T. Mckee, Extracellular matrix composition of connective tissues: systematic review and meta-analysis, can be found under <https://escholarship.mcgill.ca/concern/theses/6395w9745>.
- [178] N. J. Kuiper, A. Sharma, *Osteoarthritis Cartilage* **2015**, *23*, 2233.
- [179] M. Cortes, A. T. Baria, N. B. Schwartz, *Dev. Camb. Engl.* **2009**, *136*, 1697.
- [180] U. Häcker, K. Nybakken, N. Perrimon, *Nat. Rev. Mol. Cell Biol.* **2005**, *6*, 530.
- [181] A. Kleinschmit, T. Koyama, K. Dejima, Y. Hayashi, K. Kamimura, H. Nakato, *Dev. Biol.* **2010**, *345*, 204.
- [182] A.-C. Gradilla, I. Guerrero, *Curr. Opin. Genet. Dev.* **2013**, *23*, 363.
- [183] K. L. Aya, R. Stern, *Wound Repair Regen.* **2014**, *22*, 579.
- [184] L. Alcaide-Ruggiero, R. Cugat, J. M. Domínguez, *Int. J. Mol. Sci.* **2023**, *24*, 10824.
- [185] C. Marques, C. A. Reis, R. R. Vivès, A. Magalhães, *Front Oncol* **2021**, *11*, 778752.
- [186] R. R. Vivès, A. Seffouh, H. Lortat-Jacob, *Front. Oncol.* **2014**, *3*, 331.
- [187] R. D. Sanderson, M. Elkin, A. C. Rapraeger, N. Ilan, I. Vlodavsky, *FEBS J.* **2017**, *284*, 42.
- [188] D. Xu, J. H. Prestegard, R. J. Linhardt, J. D. Esko, in *Essentials of Glycobiology*, (Eds.: A. Varki, R. D. Cummings, J. D. Esko, P. Stanley, G. W. Hart, M. Aebi, D. Mohnen, T. Kinoshita, N. H. Packer, J. H. Prestegard, R. L. Schnaar, P. H. Seeberger), Cold Spring Harbor Laboratory Press, Cold Spring Harbor (NY), **2022**.
- [189] L. O. Sampaio, I. L. S. Tersariol, C. C. Lopes, R. I. Bouças, F. D. Nascimento, H. A. O. Rocha, H. B. Nader, *Insights Carbohydr. Struct. Biol. Funct. Transw. Res. Netw. Kerala* **2006**, *37*, 1.
- [190] U. Lindahl, M. Hook, *Annu. Rev. Biochem.* **1978**, *47*, 385.
- [191] C. Malavaki, S. Mizumoto, N. Karamanos, K. Sugahara, *Connect. Tissue Res.* **2008**, *49*, 133.
- [192] F. N. Lamari, N. K. Karamanos, in *Advances in Pharmacology*, Academic, San Diego, CA **2006**, pp. 33–48.
- [193] A. Kinoshita, S. Yamada, S. M. Haslam, H. R. Morris, A. Dell, K. Sugahara, *Biochemistry* **2001**, *40*, 12654.
- [194] K. Higashi, Y. Okamoto, A. Mukuno, J. Wakai, S. Hosoyama, R. J. Linhardt, T. Toida, *Carbohydr. Polym.* **2015**, *134*, 557.
- [195] A. K. Shetty, T. Kobayashi, S. Mizumoto, M. Narumi, Y. Kudo, S. Yamada, K. Sugahara, *Carbohydr. Res.* **2009**, *344*, 1526.
- [196] C. I. Gama, S. E. Tully, N. Sotogaku, P. M. Clark, M. Rawat, N. Vaidehi, W. A. Goddard, A. Nishi, L. C. Hsieh-Wilson, *Nat. Chem. Biol.* **2006**, *2*, 467.
- [197] R. S. Cavalcante, A. S. Brito, L. C. G. F. Palhares, M. A. Lima, R. P. Cavalheiro, H. B. Nader, G. L. Sasaki, S. F. Chavante, *Carbohydr. Polym.* **2018**, *183*, 192.
- [198] N. K. Karamanos, A. Syrokou, P. Vanky, M. Nurminen, A. Hjerpe, *Anal. Biochem.* **1994**, *221*, 189.
- [199] G. Vessella, S. Traboni, D. Cimini, A. Iadonisi, C. Schiraldi, E. Bedini, *Biomacromolecules* **2019**, *20*, 3021.
- [200] S. Perez, O. Makshakova, J. Angulo, E. Bedini, A. Bisio, J. L. De Paz, E. Fadda, M. Guerrini, M. Hricovini, M. Hricovini, F. Lisacek, P. M. Nieto, K. Pagel, G. Paiardi, R. Richter, S. A. Samsonov, R. R. Vivès, D. Nikitovic, S. Ricard Blum, *JACS Au* **2023**, *3*, 628.
- [201] J. D. Esko, J. H. Prestegard, R. J. Linhardt, in *Essent. Glycobiol.*, (Eds.: A. Varki, R. D. Cummings, J. D. Esko, P. Stanley, G. W. Hart, M. Aebi, A. G. Darvill, T. Kinoshita, N. H. Packer, J. H. Prestegard, R. L. Schnaar, P. H. Seeberger), Cold Spring Harbor Laboratory Press, Cold Spring Harbor (NY), **2015**.
- [202] M. Petitou, *Biochimie* **2003**, *85*, 83.
- [203] U. Lindahl, G. Bäckström, M. Höök, L. Thunberg, L. A. Fransson, A. Linker, *Proc. Natl. Acad. Sci. USA* **1979**, *76*, 3198.
- [204] B. Richard, R. Swanson, S. T. Olson, *J. Biol. Chem.* **2009**, *284*, 27054.
- [205] A. Yayon, M. Klagsbrun, *Cancer Metastasis Rev.* **1990**, *9*, 191.
- [206] S. Faham, R. E. Hileman, J. R. Fromm, R. J. Linhardt, D. C. Rees, *Science* **1996**, *271*, 1116.
- [207] M. Maccarana, B. Casu, U. Lindahl, *J. Biol. Chem.* **1993**, *268*, 23898.
- [208] S. Ashikari-Hada, H. Habuchi, Y. Kariya, N. Itoh, A. H. Reddi, K. Kimata, *J. Biol. Chem.* **2004**, *279*, 12346.
- [209] J. Kreuger, M. Salmivirta, L. Sturiale, G. Giménez-Gallego, U. Lindahl, *J. Biol. Chem.* **2001**, *276*, 30744.
- [210] D. A. Pye, R. R. Vives, J. E. Turnbull, P. Hyde, J. T. Gallagher, *J. Biol. Chem.* **1998**, *273*, 22936.
- [211] J. Schlessinger, A. N. Plotnikov, O. A. Ibrahim, A. V. Eliseenkova, B. K. Yeh, A. Yayon, R. J. Linhardt, M. Mohammadi, *Mol. Cell* **2000**, *6*, 743.
- [212] R. El Masri, A. Seffouh, H. Lortat-Jacob, R. R. Vivès, *Glycoconj J* **2017**, *34*, 285.
- [213] M. J. Dewey, A. V. Nosatov, K. Subedi, B. Harley, *RSC Adv.* **2020**, *10*, 15629.
- [214] M. J. Dewey, V. Koliopoulos, M. T. Ngo, B. A. C. Harley, *Materialia* **2021**, *18*, 101149.
- [215] B. E. Uygun, S. E. Stojisih, H. W. T. Matthew, *Tissue Eng., Part A* **2009**, *15*, 3499.
- [216] T. Wang, F. Yang, *Stem Cell Res. Ther.* **2017**, *8*, 284.
- [217] C. M. Tierney, M. J. Jaasma, F. J. O'Brien, *J. Biomed. Mater. Res., Part A* **2009**, *91A*, 92.
- [218] L. W. Place, S. M. Kelly, M. J. Kipper, *Biomacromolecules* **2014**, *15*, 3772.
- [219] L. E. Tellier, T. Miller, T. C. Mcdevitt, J. S. Temenoff, *J. Mater. Chem. B* **2015**, *3*, 8001.
- [220] R. A. A. Smith, S. Murali, B. Rai, X. Lu, Z. X. H. Lim, J. J. L. Lee, V. Nurcombe, S. M. Cool, *Biomaterials* **2018**, *184*, 41.
- [221] J. Lei, E. Trevino, J. Temenoff, *J. Biomed. Mater. Res., Part A* **2016**, *104*, 1817.
- [222] S. Rother, G. Ruiz-Gómez, K. Balamurugan, L. Koehler, K. M. Fiebig, V. D. Galiasso, U. Hempel, S. Moeller, M. Schnabelrauch, J. Waltenberger, M. T. Pisabarro, D. Scharnweber, V. Hintze, *ACS Appl. Biol. Mater.* **2021**, *4*, 494.
- [223] P. Atallah, L. Schirmer, M. Tsurkan, Y. D. Putra Limasale, R. Zimmermann, C. Werner, U. Freudenberger, *Biomaterials* **2018**, *181*, 227.
- [224] Q. Feng, S. Lin, K. Zhang, C. Dong, T. Wu, H. Huang, X. Yan, Li Zhang, G. Li, L. Bian, *Acta Biomater.* **2017**, *53*, 329.
- [225] J. J. Lim, J. S. Temenoff, *Biomaterials* **2013**, *34*, 5007.
- [226] E. Bedini, A. Laezza, M. Parrilli, A. Iadonisi, *Carbohydr. Polym.* **2017**, *174*, 1224.
- [227] L. C. G. F. Palhares, J. A. London, A. M. Kozlowski, E. Esposito, S. F. Chavante, M. Ni, E. A. Yates, *Molecules* **2021**, *26*, 5211.
- [228] R. Takano, *Trends Glycosci. Glycotechnol.* **2002**, *14*, 343.
- [229] Q. Chen, F. Li, H. Wang, C. Bu, F. Shi, L. Jin, Q. Zhang, L. Chi, *Front. Mol. Biosci.* **2022**, *9*, 966754.
- [230] S. Hara, K. Yoshida, M. Ishihara, Process for Producing Desulfated Polysaccharide, and Desulfated Heparin, **2004**, US6809086B2.
- [231] M. Jaseja, R. N. Rej, F. Sauriol, A. S. Perlin, *Can. J. Chem.* **1989**, *67*, 1449.
- [232] K. Nagasawa, Y. Inoue, T. Kamata, *Carbohydr. Res.* **1977**, *58*, 47.
- [233] A. Naggi, B. Casu, M. Perez, G. Torri, G. Cassinelli, S. Penco, C. Pisano, G. Giannini, R. Ishai-Michaeli, I. Vlodavsky, *J. Biol. Chem.* **2005**, *280*, 12103.
- [234] Y. Peng, L. E. Tellier, J. S. Temenoff, *Biomater. Sci.* **2016**, *4*, 1371.
- [235] Y. Inoue, K. Nagasawa, *Carbohydr. Res.* **1976**, *46*, 87.
- [236] M. Matsuo, R. Takano, K. Kamei-Hayashi, S. Hara, *Carbohydr. Res.* **1993**, *241*, 209.
- [237] Z. Ye, R. Takano, K. Hayashi, T.-V. Ta, H. Kato, Y. Kamikubo, Yo Nakahara, K. Kumeda, S. Hara, *Thromb. Res.* **1998**, *89*, 263.
- [238] Y. Kariya, M. Kyogashima, K. Suzuki, T. Isomura, T. Sakamoto, K. Horie, M. Ishihara, R. Takano, K. Kamei, S. Hara, *J. Biol. Chem.* **2000**, *275*, 25949.

- [239] A. Fryer, Y.-C. Huang, G. Rao, D. Jacoby, E. Mancilla, R. Whorton, C. A. Piantadosi, T. Kennedy, J. Hoidal, *J. Pharmacol. Exp. Ther.* **1997**, 282, 208.
- [240] A. Seffouh, R. El Masri, O. Makshakova, E. Gout, Z. E. O. Hassoun, J.-P. Andrieu, H. Lortat-Jacob, R. R. Vivès, *Cell. Mol. Life Sci.* **2019**, 76, 1807.
- [241] A. Seffouh, F. Milz, C. Przybylski, C. Laguri, A. Oosterhof, S. Bourcier, R. Sadir, E. Dutkowski, R. Daniel, T. H. Kuppevelt, T. Dierks, H. Lortat-Jacob, R. R. Vivès, *FASEB J.* **2013**, 27, 2431.
- [242] D. A. Pye, R. R. Vives, P. Hyde, J. T. Gallagher, *Glycobiology* **2000**, 10, 1183.
- [243] T. G. Kantor, M. Schubert, *J. Am. Chem. Soc.* **1957**, 79, 152.
- [244] K. Nagasawa, Y. Inoue, T. Tokuyasu, *J. Biochem.* **1979**, 86, 1323.
- [245] W. Han, Q. Li, Y. Lv, Q. Wang, X. Zhao, *Carbohydr. Res.* **2018**, 460, 8.
- [246] C. Cai, K. Solakylidirim, Bo Yang, J. M. Beaudet, A. Weyers, R. J. Linhardt, F. Zhang, *Carbohydr. Polym.* **2012**, 87, 822.
- [247] K. Nagasawa, H. Uchiyama, N. Wajima, *Carbohydr. Res.* **1986**, 158, 183.
- [248] V. Hintze, S. Moeller, M. Schnabelrauch, S. Bierbaum, M. Viola, H. Worch, D. Scharnweber, *Biomacromolecules* **2009**, 10, 3290.
- [249] S. Vogel, S. Arnoldini, S. Möller, M. Schnabelrauch, U. Hempel, *Sci. Rep.* **2016**, 6, 36418.
- [250] Y.-H. Chen, Y. Narimatsu, T. M. Clausen, C. Gomes, R. Karlsson, C. Steentoft, C. B. Spliid, T. Gustavsson, A. Salanti, A. Persson, A. Malmström, D. Willén, U. Ellervik, E. P. Bennett, Y. Mao, H. Clausen, Z. Yang, *Nat. Methods* **2018**, 15, 881.
- [251] L. E. Pepi, P. Sanderson, M. Stickney, I. J. Amster, *Mol. Cell. Proteomics* **2021**, 20, 100025.
- [252] J. M. Fasciano, N. D. Danielson, *J. Sep. Sci.* **2016**, 39, 1118.
- [253] A. Zappe, R. L. Miller, W. B. Struwe, K. Pagel, *M.Spectrom. Rev.* **2021**, 41, 1040.
- [254] R. L. Miller, S. E. Guimond, M. Shivkumar, J. Blocksidge, J. A. Austin, J. A. Leary, J. E. Turnbull, *Anal. Chem.* **2016**, 88, 11542.
- [255] R. R. Vivès, S. Goodger, D. A. Pye, *Biochem. J.* **2001**, 354, 141.
- [256] K. Robards, D. Ryan, in *Princ. Pract. Mod. Chromatogr. Methods Second Ed.*, (Eds.: K. Robards, D. Ryan), Academic Press, **2022**, pp. 495–513.
- [257] P. L. Deangelis, J. Liu, R. J. Linhardt, *Glycobiology* **2013**, 23, 764.
- [258] J. Liu, R. J. Linhardt, *Nat. Prod. Rep.* **2014**, 31, 1676.
- [259] X. Zhang, V. Pagadala, H. M. Jester, A. M. Lim, T. Q. Pham, A. M. P. Goulas, J. Liu, R. J. Linhardt, *Chem. Sci.* **2017**, 8, 7932.
- [260] X. Zhang, L. Lin, He Huang, R. J. Linhardt, *Acc. Chem. Res.* **2020**, 53, 335.
- [261] X. Xi, L. Hu, H. Huang, Y. Wang, R. Xu, G. Du, J. Chen, Z. Kang, *J. Ind. Microbiol. Biotechnol.* **2023**, 50, kuad012.
- [262] Y. Zhang, Y. Wang, Z. Zhou, P. Wang, X. Xi, S. Hu, R. Xu, G. Du, J. Li, J. Chen, Z. Kang, *Green Chem.* **2022**, 24, 3180.
- [263] N. Karst, R. Linhardt, *Curr. Med. Chem.* **2003**, 10, 1993.
- [264] V. H. Pomin, Xu Wang, *ChemMedChem* **2018**, 13, 648.
- [265] M. Mende, C. Bednarek, M. Wawryszyn, P. Sauter, M. B. Biskup, U. Schepers, S. Bräse, *Chem. Rev.* **2016**, 116, 8193.
- [266] L. Wang, A. W. Sorum, B.-S. Huang, M. K. Kern, G. Su, N. Pawar, X. Huang, J. Liu, N. L. B. Pohl, L. C. Hsieh-Wilson, *Nat. Chem.* **2023**, 15, 1108.
- [267] S. Bratulic, A. Limeta, F. Maccari, F. Galeotti, N. Volpi, M. Levin, J. Nielsen, F. Gatto, *J. Biol. Chem.* **2022**, 298, 101575.
- [268] F. Gatto, N. Volpi, H. Nilsson, I. Nookaew, M. Maruzzo, A. Roma, M. E. Johansson, U. Stierner, S. Lundstam, U. Basso, J. Nielsen, *Cell Rep.* **2016**, 15, 1822.
- [269] Ch Zheng, Me Levenston, *Eur. Cell Mater.* **2015**, 29, 224.
- [270] S. B. Frazier, K. A. Roodhouse, D. E. Hourcade, L. Zhang, *Open Glycosci.* **2008**, 1, 31.
- [271] K. S. Emanuel, L. J. Kellner, M. J. M. Peters, M. J. J. Haartmans, M. T. Hooijmans, P. J. Emans, *Osteoarthritis Cartilage* **2022**, 30, 650.
- [272] W. Ling, R. R. Regatte, G. Navon, A. Jerschow, *Proc. Natl. Acad. Sci. USA* **2008**, 105, 2266.
- [273] D. Mittelstaedt, D. Kahn, Y. Xia, *Quant. Imaging Med. Surg.* **2016**, 6, 648.
- [274] E. M. Shapiro, A. Borthakur, A. Gougoutas, R. Reddy, *Magn. Reson. Med.* **2002**, 47, 284.
- [275] Y. Ito, M. Hikino, Y. Yajima, T. Mikami, S. Sirko, A. Von Holst, A. Faissner, S. Fukui, K. Sugahara, *Glycobiology* **2005**, 15, 593.
- [276] P. Pothacharoen, K. Kalayanamitra, S. S. Deepa, S. Fukui, T. Hattori, N. Fukushima, T. Hardingham, P. Kongtawelert, K. Sugahara, *J. Biol. Chem.* **2007**, 282, 35232.
- [277] J. C. Silva, M. S. Carvalho, X. Han, Ke Xia, P. E. Mikael, J. M. S. Cabral, F. C. Ferreira, R. J. Linhardt, *Glycoconj. J.* **2019**, 36, 141.
- [278] J. E. Turnbull, R. M. Miller, Y. Ahmed, T. Puvirajasinghe, S. E. Guimond, *Methods Enzymol.* **2010**, 480, 65.
- [279] H. Toyoda, A. Kinoshita-Toyoda, S. B. Selleck, *J. Biol. Chem.* **2000**, 275, 2269.
- [280] Y. Song, F. Zhang, R. J. Linhardt, *J. Histochem. Cytochem.* **2021**, 69, 121.
- [281] D. Pál, G. Tóth, S. Sugár, K. D. Fügedi, D. Szabó, I. Kovalszky, D. Papp, G. Schlosser, C. Tóth, T. Tornóczky, L. Drahos, L. Turiák, *Int. J. Mol. Sci.* **2023**, 24, 7050.
- [282] D. R. Studelska, K. Giljum, L. M. McDowell, L. Zhang, *Glycobiology* **2006**, 16, 65.
- [283] L. Turiák, G. Tóth, O. Ozohanics, Á. Révész, A. Ács, K. Vékey, J. Zaia, L. Drahos, *J. Chromatogr. A* **2018**, 1544, 41.
- [284] N. Altgärde, E. Nilebäck, L. De Battice, I. Pashkuleva, R. L. Reis, J. Becher, S. Möller, M. Schnabelrauch, S. Svedhem, *Acta Biomater.* **2013**, 9, 8158.
- [285] A. Köwitsch, G. Zhou, T. Groth, *J. Tissue Eng. Regener. Med.* **2018**, 12, e23.
- [286] E. Gemma, O. Meyer, D. Uhrin, A. N. Hulme, *Mol. BioSyst.* **2008**, 4, 481.
- [287] H. Ichijo, N. Sugiura, K. Kimata, *Polymers* **2013**, 5, 254.
- [288] T. Mori, T. Kodaera, H. Yoshimine, Y. Yakuta, N. Sugiura, K. Kimata, Y. Okahata, *Chemistry* **2012**, 18, 7388.
- [289] E. Saesen, S. Sarrazin, C. Laguri, R. Sadir, D. Maurin, A. Thomas, A. Imberty, H. Lortat-Jacob, *J. Am. Chem. Soc.* **2013**, 135, 9384.
- [290] J. Kalia, R. T. Raines, *Angew. Chem. Int., Ed. Engl.* **2008**, 47, 7523.
- [291] D. Thakar, E. Migliorini, L. Coche-Guerente, R. Sadir, H. Lortat-Jacob, D. Boturyn, O. Renaudet, P. Labbe, R. P. Richter, *Chem. Commun.* **2014**, 50, 15148.
- [292] C. Przybylski, V. Bonnet, R. R. Vivès, *Chem. Commun.* **2019**, 55, 4182.
- [293] J. A. Eble, *J. Vis. Exp.* **2018**, 15, 57334.
- [294] P. C. Billings, E. Yang, C. Mundy, M. Pacifici, *J. Biol. Chem.* **2018**, 293, 14371.
- [295] Z. Nikolovska-Coleska, R. Wang, X. Fang, H. Pan, Y. Tomita, P. Li, P. P. Roller, K. Krajewski, N. G. Saito, J. A. Stuckey, S. Wang, *Anal. Biochem.* **2004**, 332, 261.
- [296] S. Köhling, J. Blaszkiewicz, G. Ruiz-Gómez, M. I. Fernández-Bachiller, K. Lemmnitzer, N. Panitz, A. G. Beck-Sickingler, J. Schiller, M. T. Pisabarro, J. Rademann, *Chem. Sci.* **2019**, 10, 866.
- [297] C. Yung-Chi, W. H. Prusoff, *Biochem. Pharmacol.* **1973**, 22, 3099.
- [298] E. Migliorini, M. Weidenhaupt, C. Picart, *Biointerphases* **2018**, 13, 06D303.
- [299] R. R. Vivès, R. Sadir, A. Imberty, A. Rencurosi, H. Lortat-Jacob, *Biochemistry* **2002**, 41, 14779.
- [300] C. Laguri, R. Sadir, E. Gout, R. R. Vivès, H. Lortat-Jacob, in *Glycosaminoglycans Methods Protocol*, (Eds.: K. Balagurunathan, H. Nakato, U. Desai, Y. Saijoh), SpringerPlus, New York, NY, **2022**, pp. 121–137.
- [301] H. J. Kwon, C. K. Bradfield, B. T. Dodge, G. S. Agoki, Study of fluid and mass adsorption model in the QCM-D sensor for characteriza-

- tion of biomolecular interaction. Proceedings for COMSOL conference: 6561, **2009**.
- [302] S. Vogt, M. Kelkenberg, T. Nöll, B. Steinhoff, H. Schönherr, H. Merzendorfer, G. Nöll, *Analyst* **2018**, *143*, 5255.
- [303] L. D. Lozeau, M. W. Rolle, T. A. Camesano, *Colloids Surf. B: Biointerfaces* **2018**, *167*, 229.
- [304] L. Oldak, Z. Lukaszewski, E. Gorodkiewicz, *J. Pharm. Biomed. Anal.* **2022**, *212*, 114640.
- [305] E. Migliorini, D. Thakar, J. Kühnle, R. Sadir, D. P. Dyer, Y. Li, C. Sun, B. F. Volkman, T. M. Handel, L. Coche-Guerente, D. G. Fernig, H. Lortat-Jacob, R. P. Richter, *Open Biol.* **2015**, *5*, 150046.
- [306] S. Attili, R. P. Richter, *Soft Matter* **2013**, *9*, 10473.
- [307] C. Zapp, B. B. Minsky, H. Boehm, *Front. Physiol.* **2018**, *9*, 1022.
- [308] R. R. Vivès, E. Crublet, J.-P. Andrieu, J. Gagnon, P. Rousselle, H. Lortat-Jacob, *J. Biol. Chem.* **2004**, *279*, 54327.
- [309] G. Künze, D. Huster, S. A. Samsonov, *Biol. Chem.* **2021**, *402*, 1337.
- [310] M. J. Heller, *Annu. Rev. Biomed. Eng.* **2002**, *4*, 129.
- [311] S. Russell, L. A. Meadows, R. R. Russell, *Microarray Technology in Practice*, Academic, San Diego, CA **2008**.
- [312] Ed.: M.-Y. Lee, *Microarray Bioprinting Technology*, Springer International Publishing, Cham, **2016**.
- [313] S. Fukui, T. Feizi, C. Galustian, A. M. Lawson, W. Chai, *Nat. Biotechnol.* **2002**, *20*, 1011.
- [314] S. Park, I. Shin, *Angew. Chem., Int. Ed.* **2002**, *41*, 3180.
- [315] D. Wang, S. Liu, B. J. Trummer, C. Deng, A. Wang, *Nat. Biotechnol.* **2002**, *20*, 275.
- [316] W. G. T. Willats, S. E. Rasmussen, T. Kristensen, J. D. Mikkelsen, J. P. Knox, *Proteomics* **2002**, *2*, 1666.
- [317] J. L. De Paz, C. Noti, P. H. Seeberger, *J. Am. Chem. Soc.* **2006**, *128*, 2766.
- [318] P. Chopra, A. Joshi, J. Wu, W. Lu, T. Yadavalli, M. A. Wolfert, D. Shukla, J. Zaia, G.-J. Boons, *Proc. Natl. Acad. Sci. USA* **2021**, *118*, e2012935118.
- [319] M. Horton, G. Su, L. Yi, Z. Wang, Y. Xu, V. Pagadala, F. Zhang, D. A. Zaharoff, K. Pearce, R. J. Linhardt, J. Liu, *Glycobiology* **2021**, *31*, 188.
- [320] C. Noti, J. L. De Paz, L. Polito, P. H. Seeberger, *Chemistry* **2006**, *12*, 8664.
- [321] J. Yang, Po-H Hsieh, X. Liu, W. Zhou, X. Zhang, J. Zhao, Y. Xu, F. Zhang, R. J. Linhardt, J. Liu, *Chem. Commun.* **2017**, *53*, 1743.
- [322] C. Zong, A. Venot, X. Li, W. Lu, W. Xiao, J.-S. L. Wilkes, C. L. Salanga, T. M. Handel, L. Wang, M. A. Wolfert, G.-J. Boons, *J. Am. Chem. Soc.* **2017**, *139*, 9534.
- [323] J. Y. Hyun, J. Pai, I. Shin, *Acc. Chem. Res.* **2017**, *50*, 1069.
- [324] S. Park, J. C. Gildersleeve, O. Blixt, I. Shin, *Chem. Soc. Rev.* **2013**, *42*, 4310.
- [325] E. L. Shipp, L. C. Hsieh-Wilson, *Chem. Biol.* **2007**, *14*, 195.
- [326] M. Fais, R. Karamanska, S. Allman, S. A. Fairhurst, P. Innocenti, A. J. Fairbanks, T. J. Donohoe, B. G. Davis, D. A. Russell, R. A. Field, *Chem. Sci.* **2011**, *2*, 1952.
- [327] M. Fatoux-Ardore, F. Peysselon, A. Weiss, P. Bastien, F. Pralong, S. Ricard-Blum, *Infect. Immun.* **2014**, *82*, 594.
- [328] C. Faye, E. Chautard, B. R. Olsen, S. Ricard-Blum, *J. Biol. Chem.* **2009**, *284*, 22041.
- [329] R. Karamanska, J. Clarke, O. Blixt, J. I. Macrae, J. Q. Zhang, P. R. Crocker, N. Laurent, A. Wright, S. L. Flitsch, D. A. Russell, R. A. Field, *Glycoconj. J.* **2008**, *25*, 69.
- [330] E. Mercey, R. Sadir, E. Maillart, A. Roget, F. Baleux, H. Lortat-Jacob, T. Livache, *Anal. Chem.* **2008**, *80*, 3476.
- [331] L. Ban, N. Pettit, L. Li, A. D. Stuparu, Li Cai, W. Chen, W. Guan, W. Han, P. G. Wang, M. Mrksich, *Nat. Chem. Biol.* **2012**, *8*, 769.
- [332] M. Shipp, R. Nadella, H. Gao, V. Farkas, H. Sigrist, A. Faik, *Glycoconj. J.* **2008**, *25*, 49.
- [333] D. Xu, K. Arnold, J. Liu, *Curr. Opin. Struct. Biol.* **2018**, *50*, 155.
- [334] A. L. Hook, J. Hogwood, E. Gray, B. Mulloy, C. L. R. Merry, *Commun. Chem.* **2021**, *4*, 67.
- [335] M. Nonaka, X. Bao, F. Matsumura, S. Götze, J. Kandasamy, A. Kononov, D. H. Broide, J. Nakayama, P. H. Seeberger, M. Fukuda, *Proc. Natl. Acad. Sci. USA* **2014**, *111*, 8173.
- [336] K. Godula, C. R. Bertozzi, *J. Am. Chem. Soc.* **2012**, *134*, 15732.
- [337] E. W. Adams, J. Ueberfeld, D. M. Ratner, B. R. O'keefe, D. R. Walt, P. H. Seeberger, *Angew. Chem.* **2003**, *115*, 5475.
- [338] S. Maza, M. Mar Kayser, G. Macchione, J. López-Prados, J. Angulo, J. L. De Paz, P. M. Nieto, *Org. Biomol. Chem.* **2013**, *11*, 3510.
- [339] L. Nimrichter, *Glycobiology* **2004**, *14*, 197.
- [340] T. Puvirajesinghe, J. Turnbull, *Microarrays* **2016**, *5*, 3.
- [341] T. M. Puvirajesinghe, Y. A. Ahmed, A. K. Powell, D. G. Fernig, S. E. Guimond, J. E. Turnbull, *Chem. Biol.* **2012**, *19*, 553.
- [342] E. Sterner, L. Meli, S.-J. Kwon, J. S. Dordick, R. J. Linhardt, *Biochemistry* **2013**, *52*, 9009.
- [343] A. Sales, V. Khodr, P. Machillot, L. Chaar, L. Fourel, A. Guevara-Garcia, E. Migliorini, C. Albigès-Rizo, C. Picart, *Biomaterials* **2022**, *121363*.



**Jean Le Pennec** is a Ph.D. candidate in Biomaterials Science applied to Biology at the University Grenoble Alpes, France. He received in 2019 an engineering degree with specialization in Biomedical Engineering at the Grenoble Institute of Technology as well as a Master degree in Nanosciences and Nanotechnologies at the University Grenoble Alpes. He subsequently began his doctoral research at the University Grenoble Alpes under the supervision of Dr. Elisa Migliorini and Dr. Romain Vivès. His current research focuses on exploring the role of GAGs in the regulation of Bone Morphogenetic Protein 2 signaling using biomaterials.



**Catherine Picart** is research director, head of the Biology and Biotechnology for Health Joint Research Unit (INSERM/CEA/UGA). She also leads the “Biomimetism and Regenerative Medicine (BRM)” research team (EMR BRM 5000, CNRS/CEA/UGA). She was senior member of the Institut Universitaire de France (IUF) (2016-2021). Her research is focused on tissue engineering, biomaterials, medical devices, drug delivery, molecular and cellular biophysics. She received the CNRS Silver medal in 2016 and the Emilia Valori Prize from the French Academy of Science in 2019. Over the past 10 years, she was the PI of 4 ERC grants.



**Romain Vivès** is a CNRS Research director at the Institute of Structural Biology, Grenoble, France. After completing a PhD at the University of Manchester (UK) on the role of heparan sulfate (HS) in the modulation of the response to bFGF, and a post-doctoral fellowship on the interaction of HS with HIV envelope glycoprotein gp 120 (university of Grenoble-Alpes, France), he obtained a tenured position at CNRS in 2002. His research interests are the structural analysis of Glycosaminoglycan (GAG) structure and characterization of GAG/protein interactions, the biosynthesis and post-synthesis mechanisms regulating GAG structure and function and amongst them, the study of SULF extracellular endosulfatases. Romain Vivès is presently coordinator of the GLyco@Alps network (21 research laboratories in interdisciplinary glycosciences).



**Elisa Migliorini**, CNRS researcher since 2017, is working at BRM team at CEA-Grenoble (France) since 2020. Actually PI of national and international grants in 2015 she obtained the Marie-Sklodowska-Curie postdoctoral fellow working in Max-Planck Institute, Stuttgart, Germany after 2.5 years of post-doctorate between Grenoble and San Sebastian, Spain. Since the Ph.D. (obtained in 2012 at the University of Trieste, Italy) she focused her studies at the interface between cells and substrates. She now aims to design biomaterials with controlled chemical functionalization and mechanical properties able to mimic selected aspects of the extracellular matrix presentation of growth factors and glycosaminoglycans.